# The Application of Environmental Magnetism to Archaeological Prospection

Neil Terrington Linford

*Department of Earth Sciences*
*University College London*

Thesis submitted for the degree of Doctor of Philosophy

# *Abstract*

*Magnetic survey is the most widely used shallow geophysical technique for the location of archaeological activity in the United Kingdom but is often discounted from use within alluviated landscapes. Results presented in this thesis from fluxgate gradiometer surveys conducted over an alluviated flood plain near the village of Yarnton, Oxfordshire, UK, demonstrate a wide variation of magnetic response between adjacent sites. This suggests a more complicated relationship between the rock magnetic properties of underlying archaeological sediments and the resultant magnetic anomalies recorded during surface magnetometer surveys. This study aims to investigate this relationship further and determine the influence of post-depositional mineral dissolution in water logged soils; a factor that together with increased alluvial overburden, has often been cited as an explanation for disappointing magnetic results over similar sites. A wide ranging study has been conducted including geophysical surveys, environmental magnetic analysis of archaeological sediments recovered during excavation and experimental work to investigate the influence of burning. Initial, rapid determination of isothermal magnetic parameters, such as susceptibility, has been complemented, for selected samples, by more detailed hysteresis measurements and thermomagnetic variation over a temperature range from 20 to 973K. Interpretation of the resulting data has been assisted through the development of semi-quantitative numerical models to describe the complex magnetic mixtures present. The results, including over 20ha (20,0000m$^2$) of geophysical survey and the analysis of more than 500 samples, demonstrate the important role of fire for magnetic enhancement and also provides evidence, under suitable conditions, for more esoteric biogenic mechanisms. The main conclusions reached suggest archaeological features magnetised before the onset of flood plain conditions may still be detected through geophysical survey, particularly if more sensitive, caesium vapour magnetometers are applied. In addition, semi-quantitative unmixing models allow both the thermal history of burnt sediments to be estimated and provide a means for identifying biogenically enhanced samples.*

# *Table of contents*

# *Additional Material (inside rear cover)*

Canti, M. G. and Linford, N. T., (2000). The effects of fire on archaeological soils and sediments: temperature and colour relationships. *Proceedings of the Prehistoric Society,* **66**:385-395.

Linford, N. T. and Canti, M. G., (2001). Geophysical evidence for fires in antiquity: preliminary results from an experimental study. *Archaeological Prospection,* **8**:211-225.

# *List of tables*



# *List of figures*

# *Dedication*

*To my wife Jennifer who could not give a fig for geophysics but understood its importance to me; also to my brother Paul, who shared the fruit so generously.*

# *Chapter 1*

## *1.0 Introduction*

The impetus for this study began during the geophysical survey of agricultural land destined for gravel extraction, between the villages of Yarnton and Cassington to the north of Oxford, UK. This initial geophysical survey including magnetic, electromagnetic and earth resistance techniques was conducted by the author and colleagues from the Ancient Monuments Laboratory, English Heritage, in advance of archaeological excavation and recording of the threatened area by the Oxford Archaeological Unit. Despite the disappointing results of the geophysical survey, the subsequent excavation revealed a wealth of multi-period archaeological activity buried beneath a modest depth of overburden well within the range of the instruments deployed.

Undeterred, the geophysical survey was extended throughout the area of Somerton-Radley river terrace gravel threatened by extraction utilising mainly magnetic techniques as these had proved most successful on this and other similar sites. This wider survey programme proved to be far more encouraging with excellent results recorded over a number of sites in close proximity to other less fruitful areas. Again, the subsequent excavation revealed considerable archaeological activity but confirmed a degree of subjectivity within the geophysical data. For example, on specific sites magnetic anomalies related to prehistoric features had been successfully identified yet abundant later activity had apparently failed to produce a detectable geophysical signature.

The current study aims to reveal the dominant processes of magnetic mineral enhancement within the archaeological horizons and the relative influence of geological, archaeological and post-depositional factors. The considerable variation in magnetic response recorded by the geophysical survey will be investigated through the analysis of the magnetic properties of the underlying sediments and soils. In addition, the study aims to revise the limitations on magnetic prospection for archaeological

activity in light of the recent availability of high sensitivity alkali-vapour field magnetometers. Three distinct approaches have been applied to resolve this problem:

(1) The characterisation of magnetic mineralogy of archaeological sediments in comparison to natural sub/top soils
(2) Numerical modelling of the predicted magnetometer response from excavated features
(3) Quantification of anthropogenic magnetic enhancement through the use of fire determined from actualisitic field experiments

*1.1 Background*

Buried archaeological features have been located prior to excavation through the application of surface magnetic surveys for many years (Clark 1990). However, whilst the techniques and instrumentation used for such surveys have advanced rapidly, the processes by which archaeological sediments acquire and maintain their characteristic magnetic signatures are still not fully understood. Often the potential success of magnetic survey is gauged from the geological substrate of the site (David 1995) and may take little account of more subtle mechanisms, such as the production of biogenic magnetism or the effects of post-depositional mineral alteration - particularly within seasonally waterlogged environments. Indeed, when considering the influence of waterlogged conditions on the apparent decrease of magnetic susceptibility of soils, Graham and Scollar 1976 (pp25-26) stated that :

> *It might be of some pedological interest to investigate these observations in detail, but there appears to be no archaeological application at first glance.*

Certainly, the complex interaction of naturally occurring pedogenic processes with the influence of anthropogenic activity in antiquity is difficult to quantify - particularly when post-depositional alteration may well account for much of the resultant magnetisation. However, the extreme sensitivity of common iron minerals to environmental conditions in soils and sediments has been widely established throughout a range of related disciplines and utilised for the construction of proxy environmental

records (e.g. Thompson and Oldfield 1986, Maher and Thompson 1995 and Verosub and Roberts 1995). Coupled with the high potential for archaeological preservation within alluviated landscapes and a growing threat to these environments from modern development a more sober evaluation of Graham and Scollar's statement is justified.

The identification of magnetic minerals (mainly iron oxides) through traditional methods of sample analysis, such as X-ray diffraction (XRD), is limited due to the low concentration typically found within soils and sediments. In addition, the minerals of interest are often poorly crystalline / amorphous, extremely small or in close physical association with other bulk mineral phases (for example haematite coating of quartz grains in sand). Cornell and Schwertmann (1996) provide a summary of appropriate techniques for the characterisation of iron oxides and the limitations of these techniques with regard to specific mineral systems. In particular, more advanced analytical techniques, such as Mössbauer spectroscopy, offer a greater sensitivity to iron minerals but are constrained by the both the availability and cost of suitable equipment to conduct a large scale study.

Rock magnetic measurements, however, are extremely sensitive to minute concentrations of magnetic minerals due to their highly diagnostic magnetic behaviour (e.g. Dunlop 1986, Maher 1988) and can be applied to determine both the mineralogy and grain-size distribution of a sample (e.g. Collinson 1983). In addition, with modern equipment measurements can be made rapidly on a range of bulk samples without the need for extensive preparation procedures. Indeed such measurements, including susceptibility and acquisition of isothermal/anhysteretic remanence after exposure to a laboratory field, may be applied to classify a large sample set into a series of distinct groups sharing a diagnostic magnetic behaviour. These groups may be further investigated through more detailed analysis of representative samples applying a much wider range of analytical techniques such as full hysteresis data and thermomagnetic analysis.

The quantitative characterisation of samples containing a mixture of magnetic minerals is important for two reasons. First, the combination and concentration of magnetic minerals present will reflect the competing magnetic enhancement mechanisms that have led to the magnetisation of the sample. This may reveal evidence for the

environmental conditions under which the magnetisation developed and perhaps the more direct influence of anthropogenic activity through, for example, the deliberate use of fire. Secondly, once the degree and concentration of magnetisation has been established for a particular feature type, limitations for the identification of similar features through surface magnetic survey may be estimated through an appropriate forward model. This is of particular importance as the sensitivity of available field instrumentation improves to the point where more subtle magnetic anomalies may be detected and related to often very small archaeological features such as individual post-holes (e.g. Faßbinder and Stanjek 1993).

*1.2 Aims of the current study*

The principle aim of the project is to investigate the relationship between the magnetic mineralogy of archaeological sediments and the resultant magnetic anomalies recorded during surface magnetometer surveys. It is hoped that this will establish the influence of anthropogenic activity over competing magnetic enhancement mechanisms and the effects of post depositional alteration of magnetic minerals.

- The initial aim of this research was to obtain magnetometer data from the study area and compare the recorded anomalies with the mineral magnetic properties of subsequently excavated archaeological features. This comparison includes similar feature types from a range of archaeological periods and activities. The influence of post-depositional mineral alteration was addressed by comparison of sites from a recent flood plain (Chapter 5) to areas of higher ground developed over a fundamentally uniform geological substrate (Chapter 4).

- The second aim was to use rapid room temperature magnetic measurements to identify diagnostic groups of magnetic behaviour within all the recovered samples. More detailed measurements were then applied to representative samples to better determine both the mineral type and grain size distribution present.

- As environmental samples are seldom composed of a single magnetic mineral of consistent grain size an additional aim of the project was to develop a semi-quantitative interpretation of the data through a linear unmixing model. Such models attempt to match the complex magnetic behaviour of a sample with a linear combination of empirical data drawn from a range magnetic minerals of known grain size (Chapter 6).

- A particular aim of the study was to determine the influence of deliberate burning, through both laboratory and field experiments, on the magnetisation of sediments and the extent to which magnetic measurements may provide an accurate thermal history for a burnt sediment or soil. Magnetic enhancement through the deliberate use of fire has long been recognised but to date only limited attempts have been made to quantify the influence of this mechanism. In addition, the identification of burnt sediments is of particular significance for the interpretation of archaeological features when visual analysis proves inconclusive (Chapter 7).

- Finally, it was hoped that the results of the mineral magnetic studies could be combined with the excavation data to produce numerical models of the expected magnetometer anomalies. These models were then compared to the recorded field data and for very weak anomalies, that failed to be detected by the fluxgate gradiometer survey, the likelihood of detection with more sensitive instrumentation was assessed (Chapter 6).

### *1.3 An overview of relevant magnetic theory*

Magnetism covers a wide range of physical phenomena and has been a subject of fascination to scientists for many centuries. Indeed it was the ancient Chinese who first marvelled at the behaviour of lodestone in the Earth's magnetic field and began an interest in the magnetic properties of geological materials that continues to this day. The fundamental basis of magnetic behaviour arises from the charged electrons and numerous texts provide a detailed description of solid state magnetism (e.g. Kittel 1976, Crangle 1970, Jakubovics 1994). Theory of

relevance to rock magnetic studies is treated within more specific geological literature (e.g. Stacey and Banerjee 1974, Collinson 1983, Tarling 1983, O'Reilly 1984, Thompson and Oldfield 1986, Butler 1992, Dunlop and Özdemir 1997).

This chapter provides a review of the relevant magnetic theory and will, for brevity, make reference to literature cited above. Consideration will be given both to the atomic basis of magnetism and the macroscopic properties of solids from initial susceptibility to the numerical determination of hysteresis behaviour. Where appropriate direct comparison will be made between theoretical estimates of magnetic parameters, empirical experimental measurements and alternative phenomenological models. This chapter provides much of the underlying theory supporting the interpretation of rock magnetic parameters discussed throughout the thesis particularly the quantitative analysis described in Chapter 6.

### *1.3.1 Diamagnetism*

All material exhibits diamagnetism that can be explained from the classical model of a charged electron in orbit around an atomic nucleus. Lenz's law states that a current will be induced when the flux through an electrical circuit is changed and that this current will be in the opposite direction to the flux change. Thus any moving electron within an applied magnetic field $\boldsymbol{B}$ will produce a finite current around the nucleus equivalent to a magnetic moment opposite to the applied field. Such an electron moving within a field $\boldsymbol{B}$ will experience a Lorentz force causing a gyroscopic effect and the precession of the electron orbit about $\boldsymbol{B}$. The superposition of a number of electrons with charge $e$ and mass $m$ leads to their precession at the *Larmor angular frequency* (Bohm 1951; p443):

$$\omega = eB/2m \tag{1.1}$$

The Larmor precession of the electrons is equivalent to an electric current loop that will in turn lead to a magnetic moment equal to the product of this current and the area of the loop in opposition to the applied field $\boldsymbol{B}$.

The majority of non-iron bearing minerals, water and most plastics are purely diamagnetic and thus exhibit a weak, negative susceptibility $\chi_{dia}$ (e.g. Thompson and Oldfield 1986; Table 3.4). Whilst the diamagnetic component seldom dominates the combined paramagnetic and ferromagnetic susceptibility of environmental samples an appreciable diamagnetic signal may result at high temperatures or applied fields. This may occur either from the plastic/glass components of the specimen holder or more directly from diamagnetic minerals such as quartz that may be found in abundance within the sample.

### *1.3.2 Paramagnetism*

Paramagnetism occurs in materials that contain atoms with unpaired electrons, where the spin and orbit of these unpaired electrons produces an atomic magnetic moment. Due to the relatively large distance between atoms with unpaired electrons there is no interaction between the atomic magnetic moments and thus no moment in the absence of an applied field. In the presence of an applied field $\boldsymbol{B}$ the atomic magnetic moments are partially aligned resulting in a small, positive susceptibility $\chi_{para}$ several orders of magnitude greater than $\chi_{dia}$ at ambient temperatures (e.g. Dunlop and Özdemir 1997; Table 2.2).

A classical derivation of $\chi_{para}$ can be achieved by consideration of the Zeeman energy due to the torque on each atomic moment $\mu_{para}$ caused by the field $\boldsymbol{B}$ (Kittel 1976; pp438-440). The average magnetic moment in a sample is therefore related to the average angle of alignment of the magnetic moments $\mu_{para}$ with the applied field $\boldsymbol{B}$. Following a statistical approach and assuming that only thermal perturbations will prevent the alignment of magnetic moments with $\boldsymbol{B}$ then according to the Maxwell-Boltzmann energy distribution law the paramagnetic susceptibility can be shown to be

$$\chi_{para} = \frac{\mu_0 n(\mu_{para})^2}{3kT} = \frac{C}{T} \tag{1.2}$$

where $\mu_0$ is the permeability of free space, $n$ is the total number of magnetic moments per unit volume, $k$ is the Boltzmann constant and $T$ the absolute temperature. This reduces to Curie's law where $C$ is the Curie constant.

The variation of paramagnetic susceptibility with temperature is important for the interpretation of thermomagnetic data from samples that contain a mixed magnetic mineralogy including a significant paramagnetic component. The increase of $\chi_{para}$ as T $\rightarrow$ 0K predicted by Eqn (1.2) often results in a characteristic low temperature susceptibility curve where the paramagnetic component may completely dominate the response of other magnetic phases.

### *1.3.3 Mean Field Theory of ferromagnetism*

Experimental results demonstrate that many substances retain both a remanent magnetisation $M_R$ in the absence of an applied field and will also saturate in comparatively modest applied fields. These substances behave as if a coupling of atomic moments has occurred and are described generally as ferromagnets. The arrangement of electron spins and magnetic moments need not be entirely parallel and a more complex interaction between two opposing sublattice orientations may occur. Figure 1.1 introduces more precise terminology describing the resulting magnetisations due to simple ferromagnetic, simple antiferromagnetic, ferrimagnetic and canted antiferromagnetic order. Such behaviour is found within compounds of the transition

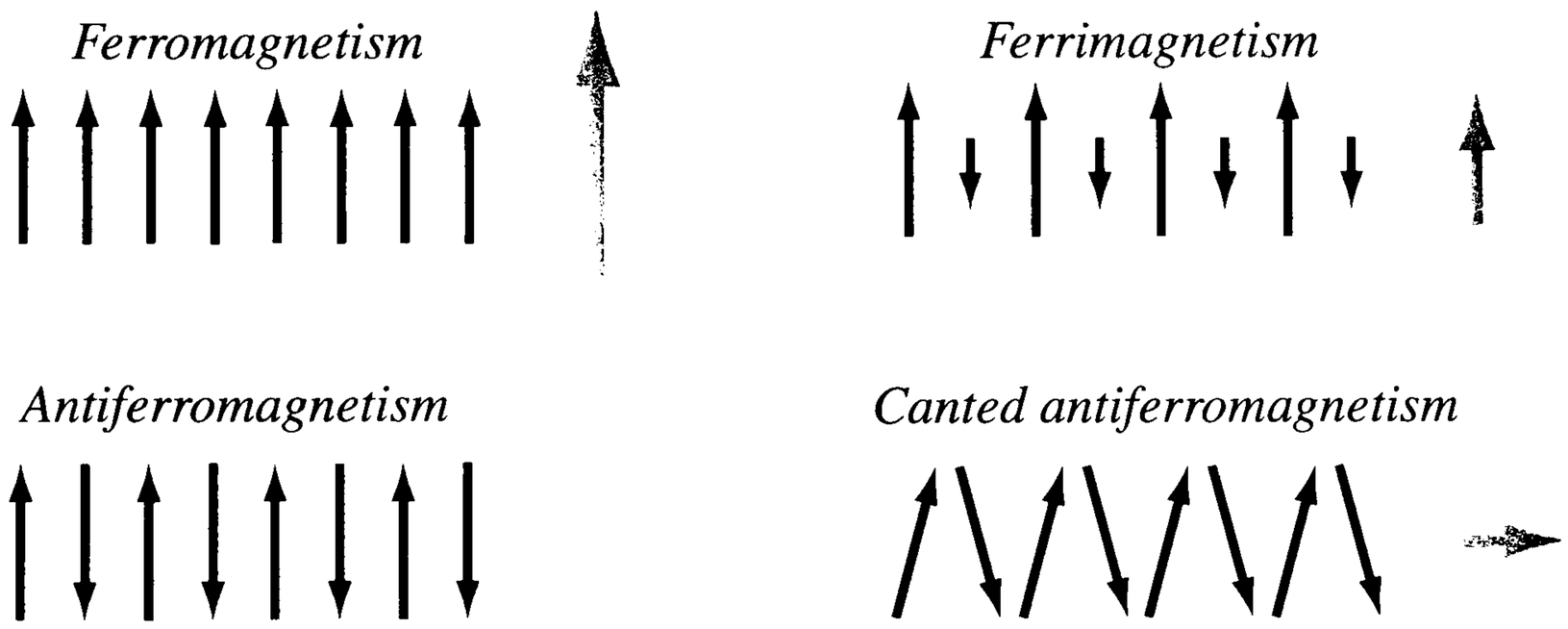


***Figure 1.1*** *Arrangement of electron sublattice spins showing the relative direction and magnitude of the net magnetisation as a shaded arrow.*

metals, particularly the oxides of iron, nickel and cobalt, where the coupling of electrons occurs via intermediate oxygen atoms and results in two, opposed sublattice magnetisations (§1.3.7).

### *1.3.4 Mean Field Theory of ferrimagnetism*

Much of the experimental behaviour of ferromagnets can be explained through *mean field theory* a powerful modern day equivalent of the molecular field theory developed by Pierre Weiss in 1907. The mean field theory assumes that every ion experiences an effective magnetic field due to the mean field produced by all the other electron spins. This mean interaction field $B_E$ can be described as

$$B_E = \lambda M \tag{1.3}$$

where $\lambda$ is assumed to be a temperature independent constant and $M$ is the magnetisation.

In the ferrimagnetic case two sublattices $A$ and $B$ exist with the second magnetic moment, $M_B$, antiparallel to the stronger $M_A$ lattice resulting in a reduced total magnetisation (Figure 1.1). The total mean fields are then described by

$$B_A = B_0 - \lambda_{AA} M_A - \lambda_{AB} M_B \tag{1.4A}$$

$$B_B = B_0 - \lambda_{AB} M_A - \lambda_{BB} M_B \tag{1.4B}$$

Where $\lambda_{AA}$ is the mean field interaction constant for the $A$ electron spins with $A$ sublattice, $\lambda_{AB}$ is the interaction constant for the $A$ spins with the $B$ sublattice etc. and $\lambda_{AA} \neq \lambda_{BB}$.

Above the ferrimagnetic Curie point $T_C$ the magnetisation of each sublattice will behave as a paramagnet with a separate Curie constant. However below $T_C$ a ferrimagnetic *Néel temperature* exists at which non-zero values of the sublattice magnetisations $M_A$ and $M_B$ can occur for zero applied field. As the $A$ and $B$ sites of the sublattice are not equivalent the resulting temperature dependent magnetisation $M_A(T)$ will not be the negative image of $M_B(T)$ and the combined magnetisation of ferrimagnetic material will depend upon the values of the lattice interaction constants $\lambda_{AA}$, $\lambda_{AB}$ and $\lambda_{BB}$. The differing thermal behaviour of the sublattice magnetisations results in the distinctive behaviour and classification of ferrimagnetic material (*cf* Dunlop and Özdemir 1997; Fig. 2.7).

### *1.3.5 Mean Field Theory of antiferromagnetism*

In the antiferromagnetic case the two sublattices have equal magnitude, opposing spins resulting from a body centred cubic (bcc) crystal lattice of atoms *A* on the corner sites and atoms *B* on the body positions. The nearest neighbours of any atom *A* will always be atoms of *B* and vice versa leading to a mean interaction field for spin *A* described by

$$B_A = -\lambda_{AA} M_A - \lambda_{AB} M_B \tag{1.5}$$

where $M_A$ and $M_B$ are the magnetisations of the two sublattices of *A* and *B* spins. The mean field constant describing the interaction between the *A* spins and the *B* spins is given by $\lambda_{AA}$ and $\lambda_{AB}$ respectively. The antiparallel orientation of the two sublattices is implied by the negative contribution of the two mean field constants. When the two sublattice orientations are perfectly opposed there will be no observable magnetisation $M_S$. However, many natural magnetic minerals have slightly canted sublattice magnetisations that results in a weak, but observable $M_S$.

As the lattice sites are equivalent the interaction field for the B spins will be

$$B_B = -\lambda_{BA} M_A - \lambda_{BB} M_B \tag{1.6}$$

where $\lambda_{AB} = \lambda_{BA}$ and $\lambda_{AA} = \lambda_{BB} = \lambda_{ii}$

Spontaneous ordering of the sublattices occurs at the *Néel Temperature*, where $T_N = C(\lambda_{AB} - \lambda_{ii})$. Below $T_N$ both sublattice magnetisations $M_A$ and $M_B$ are non zero in zero applied field were as above $T_N$ the combined magnetisation behaves as a paramagnet.

### *1.3.6 Susceptibility below the Néel temperature*

The susceptibility below $T_N$ is dependent upon the direction of the applied field with respect to the sublattice magnetisation. First consider the application of field parallel to the $M_A$ sublattice magnetisations and thus antiparallel to the $M_B$. In this case the spins of the antiparallel $M_B$ sublattice must be rotated through 180° to align with the applied field and will require a considerable quantity of thermal energy to assist this rotation.

If the applied field is perpendicular to the sublattice magnetisation a torque exists that attempts to rotate the $M_A$ and $M_B$ which is opposed by the mean field interaction, resulting in a *perpendicular susceptibility* $\kappa_\perp$. In principle, applying a field parallel to the sublattice magnetisation will (unless the field is very great) result in no net magnetisation. However, above *0K* thermal energy allows small rotations of $M_A$ and $M_B$ to occur and the parallel susceptibility, $\kappa_{||}$ will increase smoothly with temperature to $T_N$ and the susceptibility of a polycrystalline sample will be a 2:1 ratio of perpendicular and parallel orientations.

In a strong enough parallel field *spin flopping* may occur where the two sublattices rotate through 90° to become perpendicular to the applied field. Spin flopping may also occur spontaneously in zero applied field due to the magnetocrystalline anisotropy of the crystal lattice (§1.4.1). In this case $M_A$ and $M_B$ may assume preferred *easy axis* directions within the crystal at different temperatures. On passing through specific transition temperatures the sublattice magnetisations will change direction to a new easy axis within the crystal. For example the *Morin Transition* ($T_{Morin}$) of haematite occurs at around 258K below which the sublattice magnetisations are pinned parallel to the *c*-axis of the inverse spinel crystal structure. Above $T_{Morin}$ the sublattice spins flop perpendicular to the *c*-axis allowing a greater freedom of movement and a canted antiferromagnetic order to occur resulting in a diagnostic increase of $M_S$.

### *1.3.7 Exchange and superexchange interactions*

Whilst the molecular field theory provides a simple, qualitative description of co-operative magnetic phenomenon it is evident from experimental results above $T_C$ that a more detailed explanation is necessary. This is provided through the quantum mechanical *exchange interaction* describing co-operative behaviour between neighbouring atoms with overlapping electron orbits. The exchange interaction results from the fact that all electrons are considered identical and must obey the Pauli exclusion principle that prohibits electrons shared between two atoms in overlapping orbitals from having the same quantum numbers.

For the iron oxides that are of interest to the current study the metal cations are too distant from one another to allow the direct overlap of electron orbits. In this case the

exchange mechanism occurs through overlap with the oxygen ions that provide a link between nearest neighbour cations referred to as *indirect* or *super* exchange. A useful qualitative description is given by O'Reilly 1984 who considers the indirect exchange interaction between $Fe^{3+}$ and $Fe^{2+}$ cations sited on the tetrahedral and octahedral sites of a spinel oxide via a shared oxygen anion.

## *1.4 Macroscopic magnetic properties*

Whilst the preceding section has examined the properties of magnetic materials at an atomic level an appreciation of macroscopic behaviour is required to understand the observed hysteresis of iron oxides relevant to this study. The following section provides a review of the underlying theory and presents simplified numerical models to predict the behaviour of macroscopic magnetic material.

### *1.4.1 Magnetocrystalline anisotropy*

The magnetisation of crystalline solids is observed to be anisotropic and may be highly stable over significant periods of time for certain materials. Without this anisotropy techniques of palaeomagnetic dating would fail and magnetic materials would be of little use as recording materials. This anisotropy arises from the crystal structure of the material that presents certain preferred "easy directions" of magnetisation that will lead to the reduced energy of the crystal in an external field. This results in a specific *magnetocrystalline anisotropy* for a particular material that occurs through a combination of physical mechanisms:

*Dipolar anisotropy* Any atomic dipole coherently coupled with other atoms through an exchange interaction will experience the dipolar field of its nearest neighbour that will influence its orientation (O'Reilly 1984; pp42-44).

*Single ion anisotropy* The orbital motion of an electron around the nucleus of an ion is often quenched by the crystal electric field arising from neighbouring ions in a solid. However, if incomplete quenching occurs an energy penalty will be incurred if the orientation of the orbital motion is rotated away from the preferred crystal axes.

*Exchange anisotropy* The exchange energy (§1.3.7) depends critically upon the degree of overlap between the anion and cation electron orbitals. Any external field will rotate the coherent magnetisation vectors of the electron spins producing a rotation of the magnetisation away from a position of minimum exchange energy. Due to the weak interaction of atomic dipoles it is, in fact, the exchange anisotropy that provides the observed pseudo-dipolar coupling of magnetic material (Dunlop and Özdemir 1997; pp38).

### *1.4.2 Magnetocrystalline anisotropy constants*

The mechanisms detailed above may be combined into a single expression to describe the anisotropy energy per unit volume of a crystal structure with uniaxial symmetry

$$E_{anis} = E_0 + K_{U1} \sin^2 \theta + K_{U2} \sin^4 \theta ... \tag{1.7}$$

where $\theta$ is the angle between the magnetisation and the unique crystal symmetry axis. The constants $K_{U1}$, $K_{U2}$... define both the magnitude of the anisotropy and their sign indicates the preferred easy direction. Positive values result when the easy direction lies along $\theta = 0°$ and negative values when the unique plane ($\theta = 90°$) is favoured.

For most theoretical calculations it is acceptable to disregard terms of $K_{U2}$ and above (e.g. Winklhofer et al. 1997). However, some of these coefficients of $K_U$ may vary independently with temperature as crystal structure contracts resulting in diagnostic transition temperatures for the magnetic properties of many magnetic materials, such as the Verwey transition of magnetite at 120K (Verwey and Haayman 1941, §3.3.10).

### *1.4.3 Shape anisotropy*

At the macroscopic level a grain of magnetic material may be envisaged as a series of microscopic dipoles originating from the atomic magnetic moments. If the material is considered to be uniformly magnetised in one direction then the poles of adjacent atomic moments will cancel each other out. However, at the surface of the body, uncompensated poles will occur that produce the familiar macroscopic magnetic field often demonstrated by shaking iron filings over a piece of paper above a bar magnet. This external field is in opposition to the polarised atomic moments within the body and

gives rise to an internal component described as the *demagnetising field,* $\boldsymbol{H}_d$. The magnitude of $\boldsymbol{H}_d$ is equal to the product of the uniform internal magnetisation $\boldsymbol{M}$ and a demagnetising factor $N$ that describes the geometrical arrangement of the uncompensated poles.

$$\overline{H}_d = -N\overline{M} \tag{1.8}$$

where the minus sign indicates that $\boldsymbol{H}_d$ is always in opposition to $\boldsymbol{M}$.

Spherical bodies simply have $N = \frac{1}{3}$, however, non-spherical bodies are more complicated and the demagnetising factor will depend on a number of subcomponents related to the direction of the internal magnetisation (e.g. O'Reilly 1984; pp58-61).

The presence of the opposing demagnetising field gives rise to a *magnetostatic self energy* per unit volume of

$$E_{self} = -\tfrac{1}{2}\mu_0 \overline{MH}_d \tag{1.9}$$

This energy results in a strong *shape anisotropy* that will influence the direction of magnetisation in non-spherical bodies. For example, it is difficult to magnetise a thin needle shaped crystal in any direction other than its long axis.

### *1.4.4 Magnetic domains*

One curious experimental observation that remains to be explained is how a ferromagnetic body may have zero magnetisation below the Curie temperature. It was Weiss who first suggested the concept of magnetic *domains* where the magnetisation in a crystal divides into a number of sub regions. The ferromagnetic order exists within each domain but the direction of magnetisation varies between neighbouring domains allowing the magnetic self energy of the crystal as a whole to be reduced. However, it is important to remember that overall energy of the crystal will be due to a combination of all the terms discussed above that will limit the subdivision of magnetic material into a series of infinitely small domains. For example, the anisotropy energy associated with rotating the magnetisation of a domain away from an easy axis in a crystal may well exceed the reduction of self energy to be gained from the subdivided domains resulting in an equilibrium state based on a finite number of domains. Thus, to

overcome the competing terms of exchange and anisotropy energy the reversal of magnetisation between two adjacent domains may occur over a large number of atomic spins, rotated by a small angular degree from its neighbour forming a line of spins, called a *Bloch wall*.

Theoretical calculations can be made for a particular material based on estimates of the anisotropy constant and the size and geometry of the body under consideration. For example, Butler and Banerjee (1975) have calculated the domain energy of magnetite and estimate that a cubic grain will remain as a *single domain* until it exceeds a threshold of ~0.08$\mu$m. Above this threshold it becomes more energetically favourable for the grain to divide into two or more domains. This state is often referred to as *pseudo-single domain* as the magnetic behaviour of the system is similar to a single domain particle with uniform magnetisation. Once a cubic crystal of magnetite exceeds a grain length of ~1.0$\mu$m it will behave as a true *multidomain* system with the number of domains restricted only by the minimisation of the energy terms discussed above and the influence of crystal lattice defects that may restrict the movement or creation of Bloch walls.

### *1.5 Numerical models of hysteresis*

The term *hysteresis* is derived from the Greek *"to lag behind"* and is used to describe ferromagnetic behaviour that depends critically on the previous exposure of the material to a magnetic field. This behaviour can be derived from micromagnetic numerical models that accurately represent the physical magnetisation process. Such models aim to find a local minimum of the free energy associated with a particle, or system of particles, for the conditions of temperature and applied field under consideration. However, the derived local free energy minima may not, necessarily, represent a global minimum that leads to a non-reversible magnetisation function with applied field referred to as *magnetic hysteresis*.

The majority of minerals of interest to this study demonstrate hysteresis parameters that vary widely with particle size over the range of grain sizes commonly encountered under natural conditions. Within this range three distinct modes of behaviour are

identified related to the domain state of the magnetisation within the particle and the balance between its energy and the thermal environment in which the hysteresis observations are made. With increasing grain size these are: superparamagnetic (SP), single domain (SD) and multidomain (MD) and each case is considered separately below comparing the theoretical hysteresis parameters with observed measurements from known size minerals.

### *1.5.1 Single domain hysteresis*

Micromagnetic theory defines the free energy as the sum of six contributing sources (e.g. Stoner and Wohlfarth 1948, Jiles and Atherton 1986, Brown 1963), however, it is acceptable to consider only four terms, *Exchange energy, Anisotropy energy*, *Magnetostatic self energy* and *Magnetostatic energy due to an external field* when constructing an elementary numerical model (e.g. Fabian et al. 1996, Tauxe et al. 1996). Starting from the same consideration of energy terms made for the derivation of initial susceptibility the energy of a single magnetic particle with uniaxial anisotropy orientated at an angle $\phi$ from the axis of the applied field $H$. On application of $H$, the magnetisation of the particle $M_S$ will rotate to an equilibrium angle $\theta$ that represents an energy minimum for the system. At some critical magnitude of the applied field $H_C$ the anisotropy energy of the particle will be overcome and the magnetisation vector will reverse its orientation with respect to its initial state. The energy required for this reversal, per unit volume of the particle, is given by

$$E = K_U \sin^2\theta - \mu_0 M_S H \cos(\phi - \theta) \tag{1.10}$$

and the necessary applied field is found at values of $H_C$ and $\theta$ where

$$\frac{dE}{d\theta} = 2K_U \sin\theta\cos\theta - M_S H \sin(\phi - \theta) = 0 \tag{1.11}$$

and

$$\frac{d^2E}{d\theta^2} = 2K_U \cos(2\theta) + M_S H \cos(\phi - \theta) = 0 \tag{1.12}$$

In this case the anisotropy constant $K_U$ has been simplified to a single variable and represents the sum of all relevant anisotropy energies. Note that for SD theory this is the sole factor influencing the hysteresis parameters of the model and will reflect both the crystal structure of the mineral system under consideration and the self energy associated with the volume of the grains.

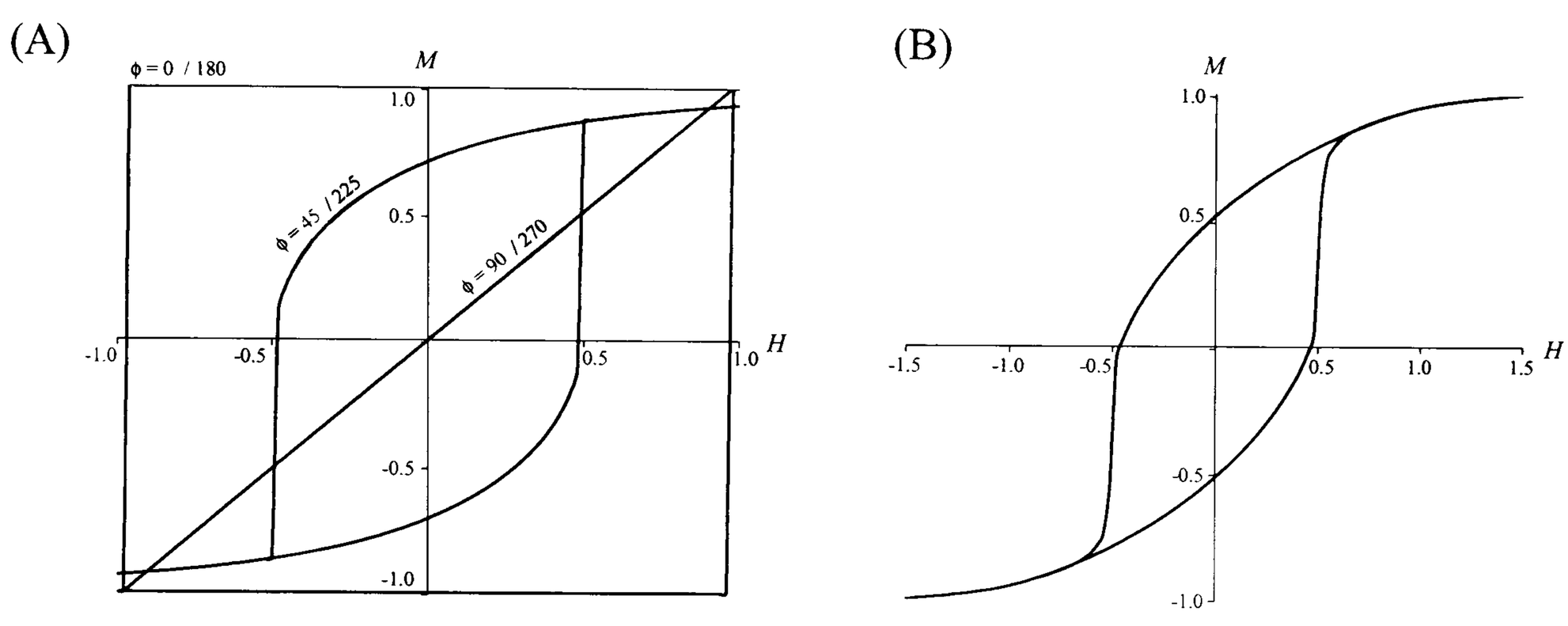


***Figure 1.2*** *(A) hysteresis curves for individual particles with the field applied at an angle $\phi$ to the easy axis of 0°, 45° and 90°. (B) bulk hysteresis curve calculated from a randomly orientated assemblage of particles.*

Figure 1.2 shows individual hysteresis loops calculated for particles whose magnetisation lies along easy directions of $\phi = 0, 45°$ and $90°$ and bulk hysteresis of an assemblage of randomly orientated particles approximating a true ferrimagnetic material. It should be noted that the shape of the hysteresis loop for an assemblage of particles is governed by the crystalline anisotropy, $K_U$, when the particles are all assumed to be spherical and the shape anisotropy reduces to a constant term. For real materials the anisotropy terms will be more complex and critically dependent on the shape of the individual grains giving rise to the experimentally observed variation of hysteresis parameters with grain size (e.g. Day et al. 1977).

### *1.5.2 Superparamagnetic hysteresis*

Superparamagnetic particles (SP) are characterised by the equivalence that exists

between the energy terms of the particles in an applied magnetic field and the thermal energy of the environment in which the measurements are observed. For magnetite at ambient temperatures SP behaviour is observed for particles with diameter <0.03μm (Butler and Banerjee 1975) and gives rise to increased initial susceptibility and the absence of irreversible hysteresis parameters.

Conceptually, SP particles may be treated in an identical manner to the single domain (SD) case discussed above. However, the energy required to reverse a magnetisation initially lying along a crystallographic easy direction is derived from the thermal energy determined by Maxwell-Boltzmann statistics for the mean measurement temperature *T*. Thus, depending upon the ambient temperature an individual SP particle of volume *v* will have to wait for a specific *relaxation time* $\tau$ before sufficient thermal energy becomes available to enable its rotation into the applied field described by Néel (1949) as

$$\tau^{-1} = f_0 \exp^{-\left(\frac{K_U V}{kT}\right)} \qquad (1.13)$$

where $f_0$ = the attempt frequency, $K_u$ = uniaxial anisotropy constant and $k$ = Boltzmann's constant ($10^{-23}$ $JK^{-1}$). Strictly, equation (1.13) is only valid for uniaxial grains (*ie* grains with a single crystallographic easy axis) aligned parallel to the applied field under conditions of zero field. This is, of course, paradoxical as conditions of zero field preclude the identification of an applied field direction for the magnetisation of the individual grains to align themselves with. However, it is assumed that eqn. (1.13) will still be valid for the application of weak fields such as those used by susceptibility meters (Dearing et al. 1996a).

The variation of energy barriers associated with particles whose easy axes are not parallel to the applied field can be accounted for by substituting an effective anisotropy constant, $K_{eff}$ over the uniaxial case (Chantrell et al. 1991) of the order $10^4$ $Jm^{-3}$ for magnetite. The value of $f_0$ is a matter of some debate, although work by Dickinson et al (1993) suggests a range for iron oxides from $10^{11}$ to $10^{12}$.

If a steady field is applied to a population of identical, non-interacting SP particles over an observation period greater than the relaxation time predicted by equation (1.13) the majority of these particles will gain sufficient thermal energy to realign themselves parallel to the field. If the available thermal energy is reduced by cooling the sample under investigation the relaxation time for particles of a given volume will increase eventually exceeding the experimental measurement period and SD behaviour will be observed.

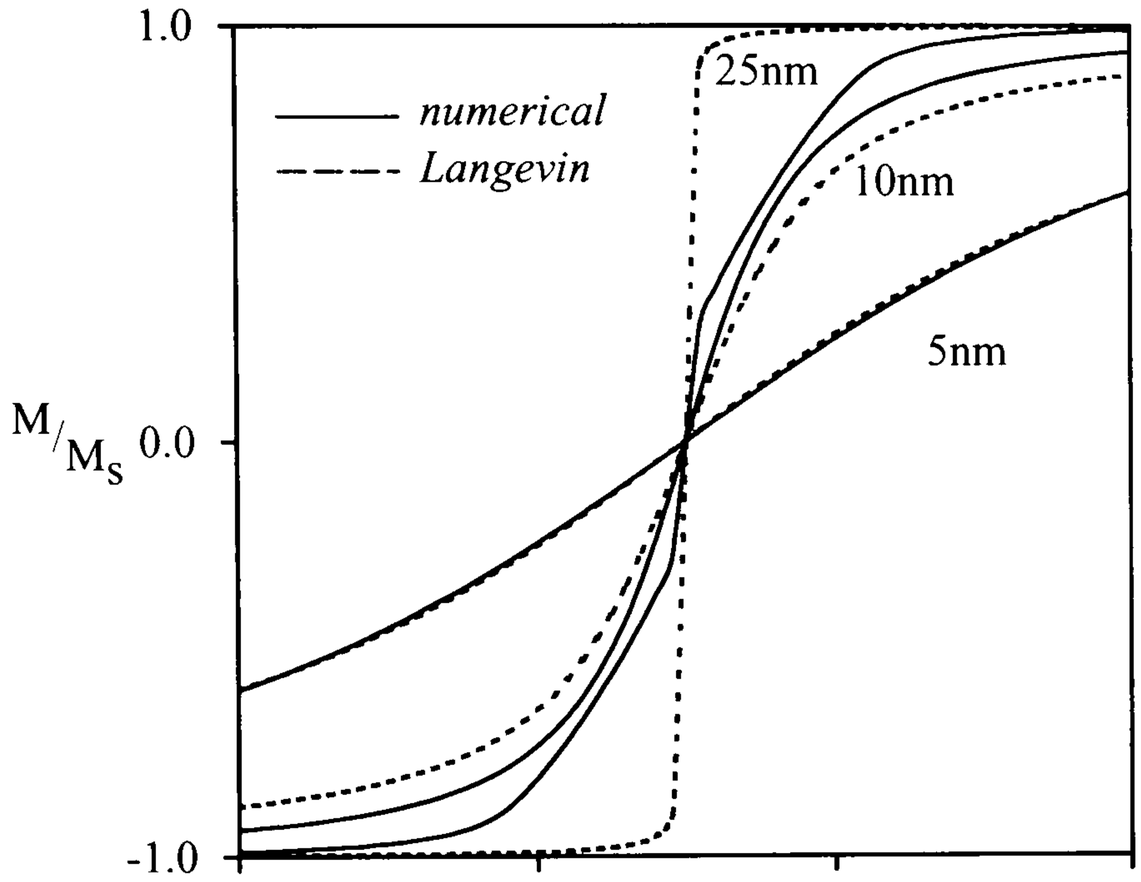


***Figure 1.3*** *Superparamagnetic hysteresis calculated for spherical particles with diameters of 5, 10 and 25nm. The solid curve shows the numerical results calculated from an assemblage of randonly orientated grains and the dashed curve indicates the equivalent Langevin approximation.*

Figure 1.3 shows the calculation of SP hysteresis for a population of 100 cubic grains with $M_s = 4.5 \times 10^5$ Am$^{-1}$, $K_{eff} = 1.4 \times 10^4$ Jm$^{-3}$ and $T = 300$K, values assumed appropriate for magnetite (*cf* Tauxe et al. 1996; Figure 3d) together with results calculated for the same grain sizes using the *Langevin function*

$$\frac{M}{M_S} = N\left(\coth\gamma - {}^{1}\!/\!_{\gamma}\right) \tag{1.14}$$

where $N$ = number of moments in the population and $\gamma = (M_S B v) / kT$.

The Langevin equation describes the magnetisation of a paramagnetic gas and gives rise to the term *superparamagnetic* for any material exhibiting similar magnetic behaviour.

Whilst the Langevin function is often applied to model superparamagentic behaviour of minerals such as magnetite, Figure 1.3 demonstrates that the equivalence between this function and the numerical model only holds for cubic grains less than ~8nm. Above this grain size the anisotropy energy exceeds the thermal energy and the magnetisation behaviour deviates significantly from the Langevin function.

### *1.5.3 Multi domain hysteresis*

The consideration of multi-domain hysteresis is more complicated as numerical models must take account of the energy terms associated with the creation, movement and reversal of the individual domain walls. For a real system the number of domains will be so great that numerical models have only recently become practical to provide an insight to this complex process. Much of the hysteresis behaviour of multi domain particles will be governed by crystal lattice defects that will inhibit the movement of domain walls in certain regions leading to *domain wall pinning*. The resulting hysteresis is often observed to increase towards saturation in a series of steps, due to the energy associated with the creation and movement of individual domains, producing a distinctive pattern of micro-coercivity often described as a *Barkhausen Staircase*.

As a result of the complexities of the multi domain case descriptions of the resulting hysteresis process are either presented in general qualitative terms (e.g. O'Reilly 1984; pp73-6), restricted to a simple two domain model (e.g. Dunlop and Özdemir 1997, Stacey and Banerjee 1974) or require extensive numerical simulation beyond the scope of the current discussion (e.g. Williams and Dunlop 1995). The subject is, however, of particular interest with regard to determining the fidelity of secular palaeomagnetic vectors recovered from pseudo-single / multi domain geological fabrics (e.g. Winklhofer et al. 1997).

### *1.5.4 Other phenomenological hysteresis models*

The complexity associated with numerical modelling has led to the investigation of a number of phenomenological hysteresis models. The majority of these models are based on fitting a mathematical function with appropriate parameters to empirical data and extrapolating unknown data from these algorithms. For example, *Preisach models* may be constructed from isothermal remanence data for a material and used to estimate

additional hysteresis parameters (Mayergoyz 1986, Hejda and Zelinka 1990, Hejda et al. 1994, Del Vecchio 1980, Kadar and Della Torre 1987, Della Torre and Kadar 1987, Roberts et al. 2000).

Perhaps of greater interest are phenomenological hysteresis models based on algorithms whose parameters may be varied to describe experimental observations of real magnetic minerals. Robertson and France (1994) examined the application of cumulative log Gaussian (CLG) functions as a numerical analogue for the acquisition of isothermal remanent magnetisation (IRM). The normalised gradient of IRM acquisition curves can be approximated by a log normal Gaussian function of the form:

$$\frac{\Delta IRM(B)}{\Delta B} = \frac{M_{RS}}{DP\sqrt{2\pi}} \exp - \left[ \frac{((\log(B) - \log(B_{1/2}))^2}{2(DP)^2} \right] \tag{1.15}$$

where $M_{RS}$ is the remanent saturation magnetisation and $B_{½}$ and $DP$ (both expressed on a $\log_{10}$ scale) are parameters that describe the mean value and the standard deviation of the log Gaussian distribution. From a physical perspective $B_{½}$ is approximately equal to coercivity of remanence, $H_{CR}$, the field required to reduce the saturation isothermal remanence to zero. $DP$ represents the distribution of apparent coercivities within the sample.

The CLG model does not differentiate the IRM behaviour of individual mineral systems (e.g. magnetite from haematite) other than through the chosen values for the mean remanent coercivity and dispersion parameter, $DP$. Despite the limitations of the model statistically rigorous fits to experimental data have been achieved (e.g. Stockhausen 1998) allowing the IRM acquisition curve of samples to be expressed in terms of a series of individual components representing a mixture of source minerals.

A similar approach for modelling hysteresis loop data has been applied by von Dobeneck (1996) based on the hyperbolic *sech* and *tanh* functions. The hysteresis loop is first decomposed from a standard sigmoid curve to the auxiliary pair of remanent and induced magnetisation curves (Rivas et al. 1981) which may be approximated by hyperbolic *sech* and *tanh* functions respectively. In this case the ferromagnetic hysteresis loop $\sigma^{\pm}_{fs}(B)$ may be modelled by:

$$\sigma_{fs}^{\pm}(B) = \sigma_{ihs}(B) \pm \sigma_{rh}(B) \approx \sigma_s \tanh(tB) \pm \sigma_{rs} \sec h(sB) \qquad (1.16)$$

where $\sigma_{ihs}$ and $\sigma_{rs}$ are the decomposed induced and remanent magnetisation curves. The shape of the modelled loop is controlled by the two coercivity coefficients $t$ and $s$.

### *1.5.5 Comparison with empirical data*

Figure 1.4 demonstrates a series of best-fit hysteresis models following von Dobeneck (1996) in comparison to the experimental hysteresis data for a variety of minerals given in Peters (1995). The parameters required by eqn. (1.16) to generate the model hysteresis data are summarised in Table 1.1. Initially, a single component theoretical model was used to generate the model hysteresis data by varying the values of $\sigma_{s,}$ $\sigma_{rs}$, $t$ and $s$ within physically acceptable limits (e.g. $\sigma_s, \sigma_{rs}, t$ and $s \geq 0$).

However, when this procedure resulted in a poor fit to the experimental data, an additional model composed of two linearly combined independent components was used (shaded cells in Table 1.1). In both cases, the best-fit variables were established by a downhill Simplex algorithm (Press et al. 1988). The results demonstrate that the hysteresis model provides a good fit to experimentally derived data even when there has been no attempt to calibrate the numerical model to the specific laboratory instrumentation used to obtain the empirical data. It is of interest to note that the statistically weakest fit to the experimental data was obtained for the two samples of haematite, the highest coercivity mineral examined. This suggests that the algorithm is best suited to the modelling of mid to low coercivity minerals.

Figures 1.5 shows data calculated from the magnetite model by extending the parameters of $\sigma_{rs}$ and $t$ determined in Table 1.1. A reasonable fit between the model data and coercivity parameters ($(B_0)_C$ and $(B_0)_{CR}$) of known size titanomagnetites is found that allows the tentative variation of $\sigma_{rs}$ and $t$ with physical grain diameter, $d$ [$\mu m$] to be suggested. Assuming a constant value for the saturation magnetisation of magnetite, $\sigma_s = 90.0$ [$Am^2kg^{-1}$], a relationship of $\sigma_{rs} \propto d^{-0.35}$ and $t \propto \log(d)$ appears to hold.

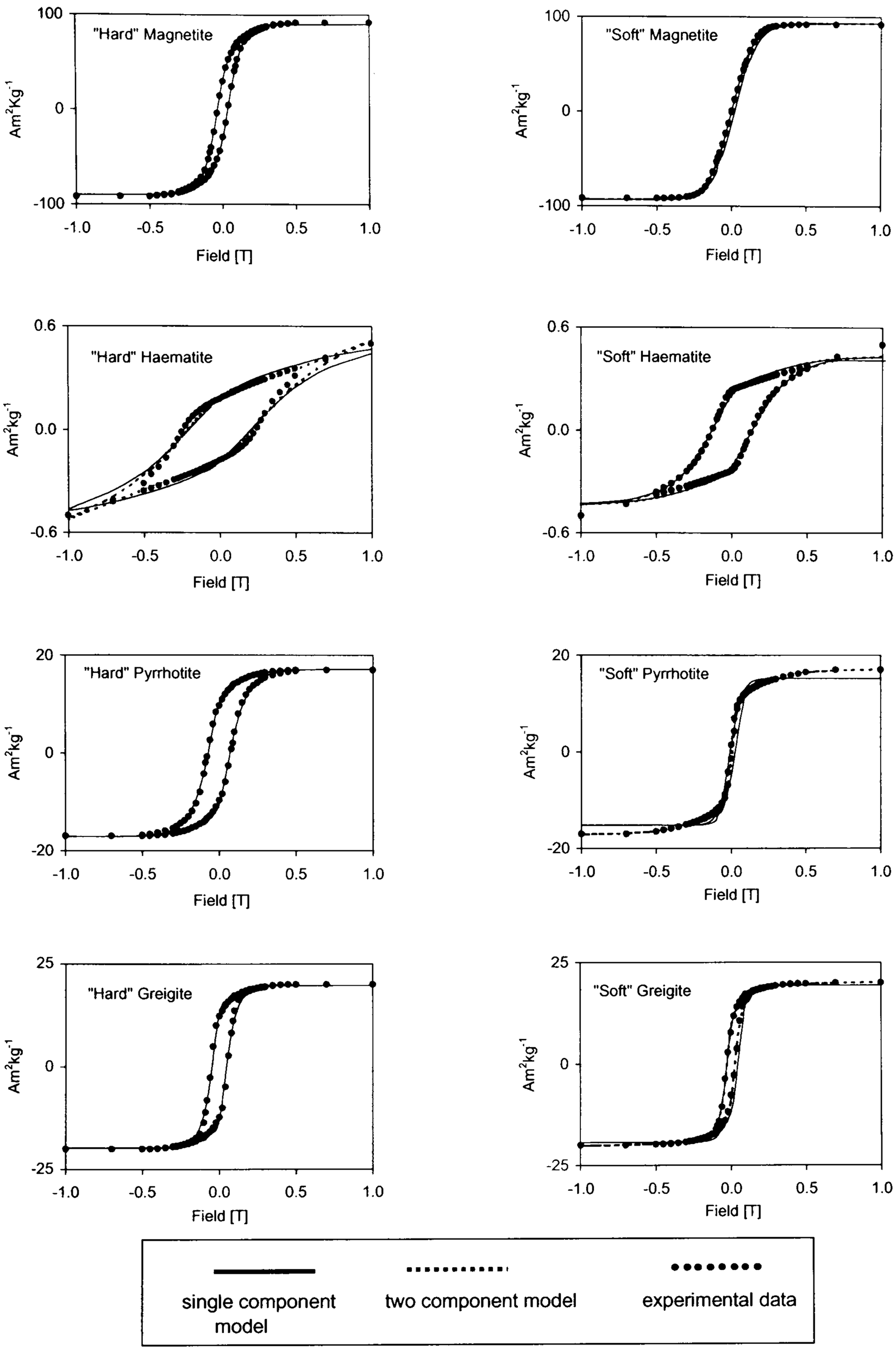


***Figure 1.4*** *Comparison between numerical model data calculated with Eqn. (1.16) and empirical hysteresis results for a range of magnetic minerals. Parameters for the various models are given in Table 1.1.*

***Table 1.1*** *Parameters used by Eqn. (1.16) to model empirical hysteresis data from a range of magnetic minerals together with the $R^2$ coefficient indicating the agreement between the two data sets (for an exact fit $R^2 = 1.0$). Shaded cells indicate best-fit data calculated from a two component model.*

| | $\sigma_s$ [$Am^2kg^{-1}$] | $\sigma_{rs}$ [$Am^2kg^{-1}$] | $t$ | $s$ | $R^2$ |
|---|---|---|---|---|---|
| *"Hard" Magnetite* | 90.0 | 31.1 | 8.1 | 19.4 | 0.9996 |
| | 93.3 | 0.4 | 6.8 | 16.2 | 0.9962 |
| *"Soft" Magnetite* | 36.6 | 0.4 | 6.8 | 16.2 | 0.9996 |
| | 56.7 | 0.0 | 6.8 | 16.2 | |
| *"Hard" Haematite* | 0.5 | 0.2 | 1.4 | 6.4 | 0.988 |
| | 0.4 | 0.2 | 2.7 | 6.4 | 0.994 |
| | 0.002 | 0.0 | 1.1 | 2.6 | |
| *"Soft" Haematite* | 0.4 | 0.2 | 2.7 | 6.4 | 0.993 |
| | 0.4 | 0.2 | 2.7 | 6.4 | 0.994 |
| | 0.002 | 0.0 | 1.1 | 2.6 | |
| *"Hard" Pyrrhotite* | 17.1 | 10.3 | 5.8 | 13.9 | 0.9989 |
| | 15.2 | 1.3 | 13.3 | 31.9 | 0.9938 |
| *"Soft" Pyrrhotite* | 10.4 | 1.6 | 26.9 | 64.6 | 0.9999 |
| | 6.6 | 0.16 | 3.0 | 7.1 | |
| "Hard" Greigite | 19.8 | 12.8 | 9.3 | 22.2 | 0.9978 |
| | 19.3 | 8.4 | 12.7 | 30.6 | 0.9993 |
| "Soft" Greigite | 18.1 | 8.7 | 13.7 | 32.9 | 0.9996 |
| | 2.0 | 0.0 | 2.0 | 4.9 | |

Correlation of the model magnetisation data generated from Eqn. (1.16) following the above grain size relationship ($0 < d > 50\mu$m) to the empirical $M_{RS}/M_S$ values reported by Day et al. (1977) is less successful and shows a considerable deviation for larger, multi-domain grains (Figure 1.5(A)).

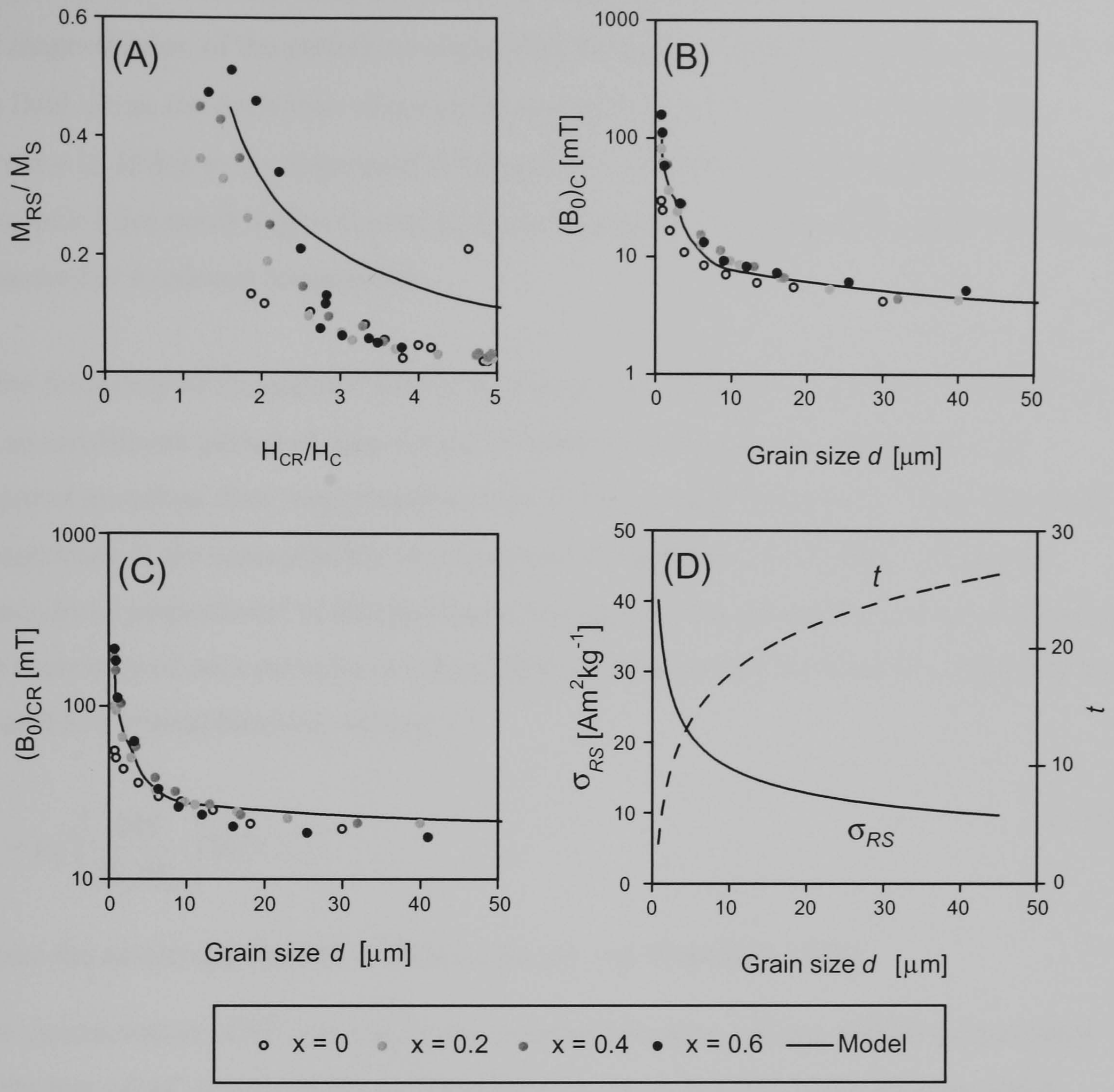


***Figure 1.5*** *(A) Comparison between model data (Eqn. (1.16)) and empirical measurements for known grain size (titano)magnetite reported by Day et al 1977. The relationship between the apparent grain size and the parameters of the model, $\sigma_{RS}$ and t, was determined through a best fit model to the empirical $(B_0)_C$ and $(B_0)_{CR}$ data shown in (B) and (C). The resulting variation of model parameters with grain size is shown in (D).*

*1.6 Frequency dependence of susceptibility*

The discussion of superparamagnetic hysteresis §1.5.2 demonstrates that at ambient temperatures many fine-grained particles will obtain sufficient thermal energy to realign their magnetisation along the direction of an applied magnetic field. The stability of such particles has already been described through their relaxation time, $\tau$, calculated from eqn. (1.13). If an alternating field is applied to such a particle at a frequency less

than $\tau^{-1}$ (for the ambient temperature $T$) sufficient thermal energy will be available for the magnetisation of the particle to align itself through the forward and reverse cycles of the field. From the definition of magnetic susceptibility, $\chi = {}^{M}/_{H}$, it is seen that the increase in $M$ due to the alignment of SP particles with the applied field $H$ will result in susceptibilities much higher than in equivalent systems in a stable single domain state measured at a reduced temperature.

If the frequency of the applied field is increased until it begins to exceed $\tau^{-1}$ there will be an insufficient period of time for the SP particles to receive the thermal energy required to realign their magnetisation with $H$ before the field reverses. Thus for a given temperature $T$, the susceptibility of a system of SP particles will exhibit a *frequency dependence* proportional to distribution of relaxation times within the system. Assuming the coercivity of such particles is independent of volume then the relaxation time can be related to a critical blocking volume $V_b$

$$V_b = \mu_0^{-1}\left(\frac{2kT}{H_k M_S}\right)\ln(\tau f_0) \tag{1.17}$$

where the anisotropy field $H_k = 2.09H_c$ (Stoner and Wohlfarth 1948).

The concentration of SP material below a certain blocking volume will be proportional to the loss of AC susceptibility measured at two (or more) critical frequencies and is often expressed in terms of the percentage loss of susceptibility at the higher measurement frequency:

$$\chi_{FD\%} = \frac{\chi_{low} - \chi_{high}}{\chi_{low}} \tag{1.18}$$

For environmental samples $\chi_{FD\%}$ seldom exceeds a maximum limit of 15% (e.g. Thompson and Oldfield 1986) when measured at the commonly applied frequencies of $\chi_{low} = 0.47$ kHz and $\chi_{high} = 4.7$ kHz available with the Bartington susceptibility bridge (§3.1.3). A number of both theoretical (e.g. Stephenson 1971, Eyre 1997, Worm 1998) and phenomenological (e.g. Dearing et al. 1996a) models may be used to predict the variation of frequency dependence for different mineral types.

### *1.7 Grain interactions*

The above discussion of hysteresis models has assumed an assemblage of individual particles at a sufficient distance from one another to avoid any interaction between the respective magnetostatic fields of near neighbours. However, experimental data often demonstrates a considerable deviation from theoretical behaviour such as a reduction in the expected values of $(B_0)_C$ and $M_{RS}/M_S$ for SD material and the onset of remanent magnetisation within SP sized particles (e.g. Davis and Evans 1974, Maher 1988, Hayashi et al. 1997, Lees 1997, Fiorani et al. 1997, Dormann et al. 1998). This may be explained by the presence of an interaction field, $H_{int}$, between near neighbours that results in more complex magnetisation behaviour (e.g. Wohlfarth 1958, Fearon et al. 1990). The presence of interacting particles within a magnetic system may be determined experimentally by analysing the cross over of IRM/ARM acquisition curves and subsequent DC or AF demagnetisation (e.g. Wohlfarth 1958, Cisowski 1981, Hejda et al. 1994). For non-interacting, SD particles the rate of acquisition and the rate of demagnetisation will be identical and the two normalised curves will cross at a value of 0.5, often referred to as the *Wohlfarth R ratio*. Values of $R < 0.5$ indicate strongly interacting particle systems.

# *Chapter 2*

## *2.0 Introduction*

This chapter introduces the most commonly encountered naturally occurring magnetic minerals found within environmental samples and discusses the pedogenic and biological processes by which these minerals may form. Diagnostic magnetic properties of the minerals are also considered with reference to the underlying theoretical basis of magnetic phenomena discussed in Chapter 1.

## *2.1 Naturally occurring iron minerals and their formation in soil*

Iron is not only one of the most stable elements, but also one of the most common elements in the earth as a whole and the fourth most abundant element in the earth's crust. Common iron bearing minerals include olivine, pyroxenes, amphiboles, biotite, numerous clay minerals, magnetite, haematite, goethite and ilmenite. Whilst these minerals may occur as direct detrital components within surface sediments and soils it is the iron bearing minerals within the earth's crust, including mafic silicates, iron sulphides, carbonates, oxides and certain clay minerals, that are more directly involved in the geochemical cycle of iron.

### *2.1.1 Lithogenic and pedogenic magnetic minerals in the soil*

The primary source of iron for soil minerals (Table 2.1) occurs through the weathering of silicate and sulphide minerals from the lithosphere. Generally, under conditions including the presence of $O_2$, $H_2O$ and a pH >2 the released $Fe^{2+}$ will oxidise to $Fe^{3+}$ and be immediately hydrolysed to form $Fe^{3+}$ oxides and oxyhydroxides (Cornell and Schwertmann 1996). As the maturity of a soil increases only the most stable lithogenic iron minerals will remain (e.g. Ilmenite) with the released $Fe^{2+}$ forming secondary pedogenic iron minerals that are more susceptible to extraction with a strong reductant such as sodium dithionite. The ratio of extractable secondary iron minerals to the total iron content can provide an indication to the maturity of the soil.

***Table 2.1*** *Summary of commonly occurring iron minerals.*

| *Mineral* | *Composition* | *Crystal structure* | *Magnetic properties*[1] | *Curie / Néel Temperature [°C]* | *Susceptibility* $\chi \times 10^{-6}$ [$m^3kg^{-1}$] | *Saturation magnetisation* $M_S \times 10^3$ [$Am^{-1}$] |
|---|---|---|---|---|---|---|
| Goethite | $\alpha$FeOOH | orthorhombic | *AFM* | 80 -120 | 0.4-1.0 | ~2 |
| Haematite | $\alpha Fe_2O_3$ | Hexagonal / rhombohedral | *canted AFM* | 675 → 695 | 0.7 – 3.83 | ~2.5 |
| Lepidocrocite | $\gamma$FeOOH | orthorhombic | *Para* | -196 | 0.7 | *N/A*[2] |
| Ferrihydrite | $Fe_5O_7(OH).4H_2O$ | hexagonal | *SPM* | -248 → -158 | *not reported* | *N/A*[2] |
| Titanomagnetite | $Fe_{3-x}Ti_xO_4$ | cubic inverse spinel | *Ferri* | 150 | 339 | 125 |
| Maghaemite | $\gamma Fe_2O_3$ | cubic/tetragonal inverse spinel | *Ferri* | 591 → 675 | $400 \times 10^{-6}$ | 380 |
| Magnetite | $Fe_3O_4$ | cubic inverse spinel | *Ferri* | ~580 | $285\text{-}1232 \times 10^{-6}$ | 480 |
| Pyrrhotite | $Fe_7S_8$ | monoclinic/cubic | *Ferri* | 315 → 320 | $5.7\text{-}67.5 \times 10^{-6}$ | 80→90 |
| Greigite | $Fe_3S_4$ | cubic inverse spinel | *Ferri* | ~330 | $\sim 100 \times 10^{-6}$ | 138 |

[1] *At room temperature (AFM = antiferromagnetic, Para = paramagnetic, SPM = Superparamagnetic, Ferri = ferrimagnetic)*
[2] *Unable to hold a remanence at room temperature*

As divalent iron has a much higher mobility than the trivalent state, minerals with a high Fe(II):Fe(III) ratio are the least stable under oxidising conditions and the most vulnerable to weathering at ambient temperatures. Other factors affecting the liberation of iron during weathering are temperature, water regime, pH, Eh and (micro)biological activity. Thus the rate of weathering will increase with temperature in the presence of water but become inhibited under arid conditions (e.g. Tite and Linington 1975). Variation of pH is particularly important as protolysis provides an essential mechanism for the disruption of crystal structures. Both pH and Eh are often controlled locally by microbial activity, although the redox potential is largely determined by the relative position of the water table that, in turn, may provide a fundamental constraint to the distance over which the oxidised Fe state may be transported. In addition, any process favouring an increase in microbial activity, such as the concentration of C, N, $O_2$ raised pH and temperature will also have an important impact on the local alteration of minerals.

Iron bearing minerals also play an important role in the biosphere where despite much lower concentrations they are constituents of many essential compounds utilised for respiration by plants and animals. It is a combination of their ubiquity and extreme sensitivity to environmental conditions that accounts for the importance of iron minerals to the study of both present and past environments where the biosphere and lithosphere meet, in recent soils and sediments. In particular, this study is concerned with the perturbation of environmental conditions through anthropogenic activity in antiquity and the record this has left in the variation of commonly magnetic iron minerals.

A complicating factor in the identification of soil iron minerals is the poor crystal structure that develops under conditions of low temperature and the presence of crystallisation inhibitors. This often results in physically small crystals with rough surfaces with many pores and structural defects, hampering their identification through X-ray crystallography. In this respect, the widely varying magnetic properties of iron minerals may provide the most suitable means for their identification. The following discussion together with Table 2.1 provides a summary of the most common iron minerals found in soils, typical conditions of formation and their distinctive physical attributes. In general, the basic structural unit for all iron oxides and hydroxides is an octahedron. Each Fe ion is then surrounded by either six oxygen (O) atoms or a

combination of oxygen (O) and hydroxide (OH) ions that form layers arranged in either a hexagonal close packed arrangement (termed $\alpha$ phases) or cubic close packed (termed $\gamma$ phases). Tetrahedral interstices exist between the O or OH ions in adjacent planes and in magnetite and maghaemite additional Fe may be present at these sites (Schwertmann and Taylor 1977).

#### *2.1.1.1 Goethite ($\alpha$ FeOOH)*

*(named after the poet and amateur mineralogist J. W. von Goethe)*

Collectively, the hydrous iron oxides (including goethite, ferrihydrite and feroxhyte) have been generally referred to as *limonite*: a somewhat imprecise term necessitated by the often amorphous nature of these weathering products that has hampered more precise distinction through X-ray diffraction. More recent advances in experimental procedures have improved the discrimination of these minerals and goethite has emerged as an important constituent of soils and sediments in temperate climates due to its high thermodynamic stability. Soil goethite may occur either through the oxidation and hydrolysis of lithogenic minerals containing $Fe^{2+}$ (e.g. iron silicates, carbonates and sulphides) or by microbial reduction of existing $Fe^{3+}$ oxides such as ferrihydrite. Due to its ubiquity throughout temperate climates and in the absence of haematite it is goethite that accounts for the yellow to rust-brown colour of many temperate soils.

The magnetic properties of goethite are summarised in Table 2.1 (Collinson 1983, Creer 1962, Banerjee 1970, Thompson 1986). The addition of impurity ions to the crystal lattice considerably lowers $T_N$ resulting in the common application of thermal demagnetisation to remove any spurious magnetisation held by this mineral (Collinson 1983). In addition, a weak superimposed ferromagnetism coexists in the crystal structure due, apparently, to a defect moment with a Curie temperature that coincides with $T_N$ (Dunlop and Özdemir 1997). High coercive forces are typical for this mineral (e.g. Thompson 1986) and may lead to the presence of goethite being neglected if laboratory measurements are made in applied fields <1T (France 1997).

At temperatures above 200°C goethite dehydrates to form either haematite or maghaemite dependent upon the reaction temperature and conditions (O'Reilly 1984; p20). The extremely fine (15-20nm), needle-like form of the original goethite crystals is

preserved through this thermal transition generally resulting in alteration products beneath the superparamagnetic threshold (Dunlop and Özdemir 1997; p74).

*2.1.1.2 Haematite ($\alpha Fe_2O_3$)*
*(from the Greek Αιματιτης = "blood like")*

Despite possessing a similar thermodynamic stability to goethite the occurrence of haematite predominates in warmer climates where it typically forms bright red soils. However, haematite rarely occurs as the sole iron oxide within a soil and is closely associated with goethite where the ratio between the two minerals is often determined by highly localised environmental conditions. Haematite forms either directly from the dehydration and internal reorganisation of ferrihydrite or through the thermal decomposition of most other iron oxides and oxy-hydroxides. The reaction kinetics of the former mechanism are determined largely by the ambient temperature and pH (Cornell and Schwertmann 1996; pp327-9) with increasing temperature favouring the production of haematite over goethite. At low temperatures haematite forms the ultimate pseudomorphic end product following the oxidisation of magnetite and when the original crystal structure of the magnetite is preserved the final mineral is referred to as *martite*.

Haematite has similar magnetic properties to goethite (Table 2.1) but is distinguished through its crystal lattice (Eggleton et al. 1988; pp154-7), higher Curie temperature, increased susceptibility of haematite (Dankers 1978) and generally lower coercive forces.

At ambient temperatures the dipolar and single-ion anisotropy of haematite both have significant magnitudes but opposite signs. However, on cooling between –10 to -15°C the relative magnitudes of the two anisotropy terms alter to the point that the net anisotropy is reversed and the easy axis of the crystal structure is changed. The resulting antiferromagnetic *spin flop* (§1.3.6) causes both the sublattice magnetisations to be pinned along the *c*-axis with a loss of spin canting and an abrupt fall of $M_S$. The point at which this discontinuity occurs is called the *Morin transition* (Morin 1950) and it is noted that both increased Ti substitution of the crystal lattice and decreased particle size suppress this phenomenon.

### *2.1.1.3 Lepidocrocite ($\gamma FeOOH$)*

*(from the Greek Λεπης = "scale", "flake" and κροκος = "saffron-coloured")*

Although not recognised as a common constituent of soil, lepidocrocite has been identified over a range of macroclimatic conditions particularly within redoxomorphic environments where seasonal variations between reducing and oxidising conditions occur (Cornell and Schwertmann 1996). When present, lepidocrocite is readily apparent due to its bright orange colour and forms via the temporary production of $Fe^{2+}$ through anaerobiosis of a waterlogged soil followed by rapid oxidisation when oxygen is available again during the dry season. Lepidocrocite seldom forms from an $Fe^{3+}$ system and although the exact process is not fully understood it would appear that greenish-blue $Fe^{(2+,\ 3+)}$ hydroxysalts "green rusts" provide an essential precursor (Taylor and McKenzie 1980). In calcareous soils the production of lepidocrocite is inhibited in favour of goethite but the two minerals are often found together in noncalcareous conditions. Indeed lepidocrocite is metastable relative to goethite and both laboratory experiments and field samples suggest a gradual transformation via solution of the former mineral to the latter. However, the kinetics of this reaction are somewhat slow and it seems likely that lepidocrocite will remain stable for at least pedogenic time spans (Schwertmann and Taylor 1972).

Under conditions favourable for the production of lepidocrocite (e.g. a seasonally waterlogged soil) the mineral often forms a rhizoconcretion around plant roots, or decaying organic matter, in association with goethite. Typically, goethite predominates close to the root system where increased pressure of $CO_2$ favours this mineral with the more visibly obvious lepidocrocite forming slightly further away. Lepidocrocite is seldom found evenly distributed throughout the soil profile.

The crystal structure of lepidocrocite has a layer like structure with sheets of $Fe(O,OH)_6$ octahedra linked by hydrogen bonds resulting in relatively weak magnetic interactions with a Néel temperature 77K (Table 2.1; Murad and Schwertmann 1984). Furthermore, it has been suggested that the degree of crystallinity provides an environmental indicator for the predominant rate of oxidation with much less crystalline forms produced under conditions of rapid oxidation (Schwertmann 1988). Above the Néel temperature the ferrimagnetic ordering of the lattice is disturbed resulting in paramagnetic behaviour

and thus lepidocrocite is unable to retain a saturation magnetisation but exhibits a susceptibility similar to goethite (Thompson and Oldfield 1986; Table 3.4).

Much of the importance of lepidocrocite stems from its dehydration to strongly magnetic maghaemite at relatively low temperatures of ~250°C depending on the particle size (Schwertmann and Taylor 1979). This makes it an important precursor for anthropogenic magnetic enhancement and also a possible indicator for the thermal history of soils and sediments (e.g. Stanjek 1987, Marmet et al. 1999). One peculiar aspect of this thermal transformation has been observed when the alteration takes place in a magnetic field and at sufficient temperature to further invert the maghaemite to haematite. Under these conditions the final remanence of the haematite often develops at a considerable angle (up to 180°) from the initial chemical remanence formed during the alteration of lepidocrocite to maghaemite (Özdemir and Dunlop 1993). Such a mechanism may well be significant, from an archaeomagnetic point of view, when the deliberate repeated use of fire occurs on a soil containing lepidocrocite. Here the fidelity of the resulting chemical / thermo remanence may well be strongly dependent on the source of the remanence carrying minerals.

#### *2.1.1.4 Ferrihydrite ($Fe_5O_7(OH).4H_2O$)*

This poorly ordered $Fe^{3+}$-hydroxide is highly unstable and is typically found in young, reductomorphic soils where the transformation to more stable oxides has been inhibited. The crystal structure of ferrihydrite is not particularly well understood but is similar to haematite consisting of hexagonal-close-packed layers of $O^{2-}$, $OH^-$, and $H_2O$ with $Fe^{3+}$ occupying the octahedral positions (Chukrov et al. 1973, Eggleton et al. 1988). Ferrihydrite often forms close to the surface of the soil where the presence of organic matter and oxygen favours the production of this mineral over goethite. An increase in the concentration of organic material and the rapid oxidation of $Fe^{2+}$ will impede the formation of crystalline iron oxides and promote the development of metastable ferrihydrite (Schwertmann et al. 1986). Thus ferrihydrite is likely to occur as the initial iron mineral in many organic rich archaeological deposits (e.g. rubbish pits) where, during the site formation process, the conditions would prove ideal for its formation. Typically, ferrihydrite forms small spherical particles with a diameter of ~3-7nm

(Schwertmann and Taylor 1977) that may be closely associated with decaying plant litter (e.g. Meng et al. 1997).

Little is known about the precise magnetic properties of ferrihydrite (Table 2.1) due to its poorly ordered crystal structure. Magnetic ordering has been observed at 4.2K (Murad and Johnston 1987) and a Néel temperature of 25-115K has been suggested by Murad 1988). Ferrihydrite forms naturally as ultrafine particles with blocking temperatures in the range of 25-115 K and thus at room temperature the mineral is always superparamagnetic and unable to carry any form of remanence.

### *2.1.1.5 Feroxyhyte ($\delta$' FeOOH)*

Feroxyhyte is a similar, poorly understood iron oxyhydroxide sharing the same crystal structure as ferrihydrite but with a more random distribution of Fe ions throughout the lattice (Eggleton et al. 1988). It has been reported in two soils formed over basalt under conditions of heavy rainfall (Parfitt et al. 1988) but is otherwise largely absent from the literature (Schwertmann and Taylor 1977). Coey (1988) suggests that the magnetic structure is a planar antiferromagnet with moments aligned parallel to the *c* axis and a net magnetisation arising from either ordered vacancies in the lattice or the reduced dimension of the crystallites in the *c* direction. It is of interest to note that feroxyhyte exhibits a strong saturation magnetisation of 15 $Am^2kg^{-1}$ (Coey 1988) and thus could contribute significantly to the magnetisation of soils, if present. However, it is not clear whether the reported saturation magnetisation was derived from synthetic $\delta$FeOOH or naturally occurring feroxyhyte ($\delta$' FeOOH). Cornell and Schwertmann (1996) report that due to the poor crystallinity and small particle size naturally occurring feroxyhyte will be superparamagnetic at ambient temperatures and thus unable to carry a remanence.

As with ferrihydrite the most important role of feroxyhyte is primarily as an intermediate, metastable mineral that provides a source of iron for alteration to more crystalline oxide forms through a variety of inorganic and biological mechanisms.

### *2.1.1.6 Maghaemite ($\gamma Fe_2O_3$)*

Maghaemite is found widely in tropical and subtropical soils but has also been identified in the soils of more humid climates (Van der Marel 1951, Schwertmann and Heinmann 1959, Faßbinder 1994). It may well occur throughout the soil profile but often accumulates close to the surface (LeBorgne 1955, Singer and Fine 1989, Singer et al. 1995). Cornell and Scwertmann (1996) suggest two possible pathways for the formation of maghaemite from either the aerial oxidation of lithogenic magnetite or the thermal alteration of intermediate iron oxyhydroxides. The first mechanism results in Ti rich maghaemite with virtually no substitution by Al. The second mechanism occurs either directly through the dehydration of lepidocrocite at ~250°C or from goethite or ferrihydrite in the presence of organic matter. As lepidocrocite is seldom found in the (sub)tropical soils where maghaemite is abundant goethite or ferrihydrite are the most likely precursors of the mineral under these conditions. The presence of organic matter is important to insure that the goethite does not oxidise on heating before it dehydroxylates to maghaemite. Soils containing maghaemite often demonstrate a positive relationship with the concentration of corundum ($\alpha Al_2O_3$) that is identified as a high temperature alteration product of Al compounds. This latter observation together with the high degree of Al substitution of the resulting maghaemite provides further proof that the soil has undergone substantial heating supporting the hypothesis of formation from Al rich goethite.

In more temperate climates maghaemite has also been found with other direct evidence of burning such as an association with charcoal and haematite. Indeed, a number of authors (e.g. Tite and Mullins 1971) identify maghaemite as the principle iron oxide produced through anthropogenic activity (particularly burning) and have identified it in soil samples from a number of archaeological sites.

Whilst sharing the same chemical formula as haematite, maghaemite is distinguished through its crystal structure that is similar to magnetite and results in much enhanced magnetic properties (Table 2.1). This cubic inverse spinel structure contains a number of vacancies and the precise distribution of these remains controversial (Eggleton et al. 1988). Maghaemite is ferrimagnetic at ambient temperatures and particles with a diameter larger than 10nm across are completely magnetically ordered. Smaller

particles are considered to be superparamagnetic (Coey and Khalafalla 1972) but may aggregate to form ordered interparticle magnetic coupling or superferromagnetism (Mørup et al. 1980, Jolivet and Tronc 1988).

The Curie temperature of maghaemite is difficult to ascertain due to the thermal alteration of this mineral to haematite reported at temperatures between 250-900°C (Dunlop and Özdemir 1997; p59). Estimates have therefore been obtained by measuring $T_C$ for various degrees of Na or Al substituted maghaemites and then extrapolating the results back for the unsubstituted phase (Table 2.1; Maxwell et al. 1949, Michel et al. 1951, Özdemir and Banerjee 1984).

#### *2.1.1.7 Magnetite ($Fe_3O_4$)*

*(named after the ancient Cretan shepherd Magnes who allegedly found himself unable to move after the nails in his sandals and ferrule of his staff became strongly attracted to the rocks on Mount Ida, where he tended his sheep)*

In petrology, the word magnetite has been used to describe practically all magnetic minerals that can be extracted with a hand magnet from a powdered specimen (Nagata 1961; p78). In reality these "magnetites" cover a range of minerals whose chemical properties represent a ternary system between the metallic oxides FeO, $Fe_2O_3$ and $TiO_2$ variously substituted with small quantities of MnO, MgO, $Al_2O_3$, and $V_2O_3$. Figure 2.1 shows a graphical representation of this ternary system that encompasses many of the important soil magnetic minerals, such as magnetite, maghaemite and haematite reviewed more extensively in this section.

Until comparatively recently the presence of magnetite in soil was assumed to be due entirely to lithogenic sources with no evidence for pedogenic formation. However, there is now considerable evidence for both inorganic and biologically mediated mechanisms for the pedogenic formation of this mineral. The discovery of magnetite in a wide range of biota including bacteria and higher organisms (e.g. Lowenstam 1962, Blakemore 1975, Towe and Moench 1981) led to the suggestion that under suitable conditions these may provide a significant source of soil magnetite. Faßbinder et al. (1990) identified biogenic magnetite in soil from Bavaria derived from magnetotactic bacteria active

within the soil fuelling the lively debate to determine the source of soil magnetite (e.g. Banerjee 1988).

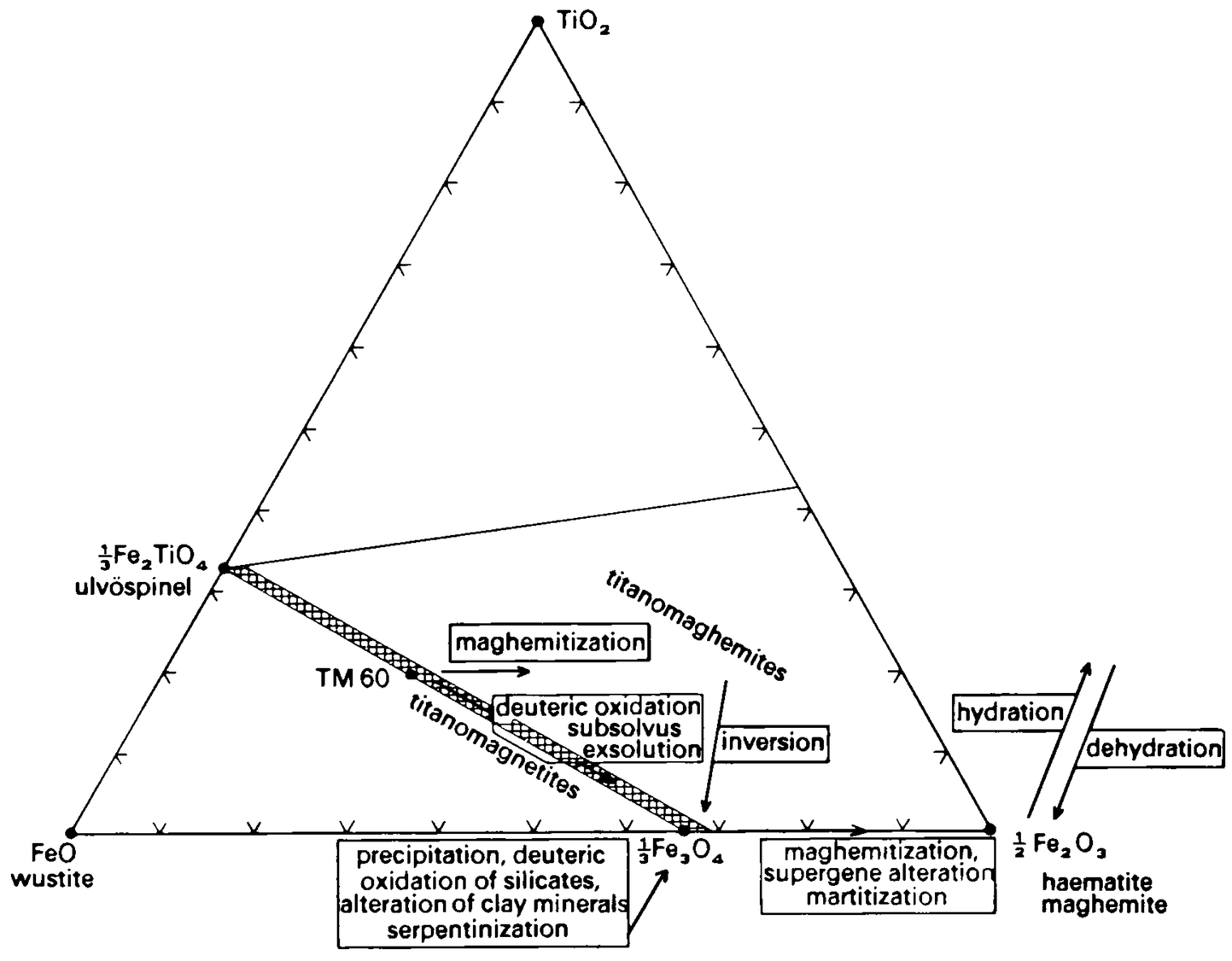


***Figure 2.1*** *Ternary diagram showing common oxide compounds containing mixtures of $Fe^{2+}$, $Fe^{3+}$ and $Ti^{4+}$ (redrawn from O'Reilly 1984; Figure 2.1).*

A number of authors have demonstrated the inorganic synthesis of magnetite through the precipitation of $Fe^{2+}/Fe^{3+}$ solutions under neutral to alkaline conditions at room temperature (e.g. Tamaura et al. 1983, Taylor 1984, Maher and Taylor 1988). However, Maher and Taylor (1988) have suggested that the inorganic neoformation of magnetite may proceed via an intermediate microbiologically induced mechanism producing $Fe^{2+}$ to react with an existing Fe oxide such as ferrihydrite. At ambient temperatures fine grained magnetite will be metastable and will eventually oxidise to maghaemite over a period of approximately 2000 years. Therefore, the presence of ultrafine magnetite in a soil suggests either a comparatively recent or ongoing neoformation process.

Magnetite shares a cubic inverse-spinel crystal structure similar to maghaemite with a slightly longer cell dimension that should allow well defined crystals of the two minerals to be distinguished through X-ray diffraction. Below its Curie temperature of ~580°C magnetite is ferrimagnetic with the two different cation sites of the crystal structure forming antiparallel magnetic sublattices. The differing magnitude of the

sublattice magnetisations results in the observed ferrimagnetism of magnetite at ambient temperatures. Above ~120K the $Fe^{2+}$ and $Fe^{3+}$ sites of the octahedral B sublattice are disordered and the electrons are thermally delocalised between the two ions accounting for the high electrical conductivity of magnetite. Below this temperature an ordered arrangement of the $Fe^{2+}$ and $Fe^{3+}$ ions occurs together with a slight distortion of the crystal lattice from cubic to monoclinic symmetry. The electron hopping between the neighbouring B sublattice ions is also inhibited resulting in a reduced electrical conductivity known as the *Verwey transition* (Verwey and Haayman 1941).

The distortion of the lattice symmetry at the Verwey transition temperature $T_V$ does not alter the saturation magnetisation but greatly affects the single-ion anisotropy of the $Fe^{2+}$ sites. This changes from a large positive value at $T < T_V$ to a negative value for $T > T_V$ and alters all the magnetic properties that depend upon crystalline anisotropy, such as remanent coercivity, susceptibility and coercive force. The abrupt change in these magnetic properties at $T_V$ for larger grains of magnetite provides a unique means for identifying the presence of magnetite (e.g. Muxworthy 1999).

At ambient temperatures magnetite exhibits the most enhanced magnetic behaviour of the common soil iron minerals with a high initial susceptibility (Table 2.1; Maher 1988, Parry 1981, Dunlop 1986, Rahman et al. 1973, Day et al. 1977, Bailey and Dunlop 1983, Parry 1965, Dankers 1978, Hartstra 1982, Peters and Thompson 1998). Both the magnetic hysteresis and $M_S(T)$ properties of magnetite are extremely similar to maghaemite that often leads to great difficulty in distinguishing the two minerals.

### *2.1.1.8 Titanomagnetite ($Fe_{3-x}Ti_xO_4$)*

Increasing substitution of Fe by Ti in the magnetite lattice produces a range of single phase titanomagnetites distinguished from magnetite by a lower $T_C$ and absence of magnetic changes associated with the Verwey transition. Titanomagnetites generally occur within rapidly cooled basaltic lava and may be present in soils developed over appropriate igneous geology. Partial oxidation results in a *titanomaghaemite* where the degree of oxidation need not, necessarily, be complete (O'Reilly 1984; p14, Brown and O'Reilly 1999).

### *2.1.1.9 Pyrite and Marcasite ($FeS_2$)*

*(Pyrite from the Greek πυρτης = "fire")*

Pyrite is the most common iron sulphide and has, in the past, been used as a fire making stone. Due to its brassy yellow colour and occurrence as flecks or granular masses in rocks it is often referred to as *"Fool's Gold"*. It is found in igneous rocks, coals, slates and grey clays such as the Gault clay of south east England. Marcasite (white iron pyrites) is similar to pyrite but forms at lower temperatures and is commonly found as framboidal nodules in limestones and clays, especially chalk (e.g. Sawolowicz 1993). Pyrite has a cubic crystal structure and is paramagnetic at ambient temperatures with a Néel temperature of 2 to 3K (von Dobeneck et al. 2002). Conversion to pyrrhotite occurs if pyrite is heated to >743°C (Faßbinder 1994). Biogenic sources have also been reported (Mann et al. 1990, Donald and Southam 1999).

### *2.1.1.10 Pyrrhotite ($Fe_7S_8$)*

*(from the Greek πυρροτης = "fire coloured")*

Considered to be a rare mineral in soils and young sediments pyrrhotite is distinguished from pyrite due to its enhanced magnetic properties. These vary widely dependent upon the dominant crystal structure in a sample with the monoclinic arrangement being the more magnetic than the cubic form. Due to a mixture of the two forms being found in many natural samples magnetic properties cover a wide range of reported values (Table 2.1; Faßbinder et al. 1990, Dunlop and Özdemir 1997, Menyeh and O'Reilly 1991, Clark 1984, Dekkers 1988, Bleil and Petersen 1982, Schwarz 1975).

### *2.1.1.11 Greigite ($Fe_3S_4$)*

Greigite was considered to be a relatively rare mineral but occurs quite commonly in anoxic, sulphate reducing sediments (e.g. Dell 1972, Snowball 1991, Snowball and Thompson 1988, Snowball and Thompson 1990, Krs et al. 1991, Roberts 1995). Pedogenic greigite was first reported by Stanjek et al. (1994) who described the presence of ultrafine black crystals ranging in size between 5-50nm. Biomineralisation of greigite has also been reported (Mann et al. 1990) and both inorganic and biologically mediated mechanisms for the formation of this mineral seem plausible.

Greigite is the sulphide counterpart of magnetite and shares the same inverse spinel crystal structure. This results in a ferrimagnetic electron arrangement but with a lower saturation magnetisation and susceptibility compared to magnetite (Table 2.1; Spender et al. 1972, Hoffman 1992, Vandenberghe et al. 1991, Peters 1995). However, due to the limited number of studies conducted on this mineral the full variation of susceptibility, particularly with grain size, is unknown. The Curie point of greigite cannot be determined directly as greigite undergoes a thermal transformation to pyrrhotite at 327°C (Skinner et al. 1964, Krs et al. 1992).

### *2.1.1.12 Siderite ($FeCO_3$)*

*(from the Greek σιδερος = "iron")*

A low temperature hydrothermal mineral common within carbonate sediments and various sulphides siderite is paramagnetic at room temperature. It is unstable on exposure to air at room temperature and will oxidise more rapidly to haematite via magnetite or maghaemite if heated to 300°C. Although unable to retain a remanence at ambient temperatures siderite has a moderate initial susceptibility of $\sim 100 \times 10^{-6}$ $m^3kg^{-1}$ (Thompson and Oldfield 1986). A Néel temperature of 38K has been suggested from studies of low temperature magnetisation (von Dobeneck et al. 2002).

### *2.1.1.13 Silicates (including sheet silicate clay minerals)*

The presence of $Fe^{2+}$, $Fe^{3+}$ or $Mn^{2+}$ cations results in paramagnetic behaviour in many silicate minerals (e.g. Thompson and Oldfield 1986; Table 3.4). Whilst some silicates have been reported to exhibit ferromagnetic behaviour (Dunlop and Özdemir 1997; p80) there is a high degree of variation between samples and most clay minerals fail to demonstrate any magnetic order above ~20 K (Coey 1988; pp454-6). The importance of this group of minerals lies more with their ubiquity than their magnetic properties as they represent an important iron source for thermal alteration to more magnetic phases.

### *2.1.1.14 Ilmenite ($FeTiO_3$)*

This is considered to be an extremely stable iron mineral and the ultimate end member of the haematite-ilmenite solid solution series $Fe_{2-y}Ti_yO_3$ ($0 < y < 1$). Found mainly in

igneous rocks it is only likely to occur as a detrital mineral in soils and sediments. It has a crystal arrangement similar to corundum but with the alternating layers of Fe and Ti cations.

Ilmenite is antiferromagnetic below its Néel temperature of 55K and paramagnetic above this temperature. However, considerable variation of the magnetic properties has been reported for other members of the solid solution series in the composition range between $0.51 \leq y \leq 0.78$ (Westcott-Lewis and Parry 1971). In particular, the Curie point falls with increasing $y$ resulting in magnetic behaviour similar to haematite for partially Ti substituted members (e.g. Butler 1992; Figure 2.10).

#### *2.1.1.15 Vivianite ($Fe_3(PO_4)_{2.8}H_2O$)*

This octahydrophosphate mineral, named after the English mineralogist F. G. Vivian, occurs in phosphorus-rich, reducing environments, such as sedimentary iron ores and peat bogs and is often found in association with organic remains such as bones or shells. It has a monoclinic crystal structure with single $Fe(II)O_6$ octahedra (A site) and isolated pairs of edge-shared Fe(II) octahedra (B site) which are linked together by phosphate groups. Vivianite has a characterisitic deep blue colour and exhibits two low temperature transitions due to paramagnetic (12.4K) and antiferromagnetic (9.6K) transitions (Grodzicki and Amthauer 2000).

### *2.1.2 Atmospheric sources*

The atmosphere may contain significant quantities of particulate matter and provide a means of transport over substantial distances, particularly within volcanic terranes. The main sources include particulate emissions of ferro-magnesium minerals during volcanic eruptions and wind erosion of arid environments (e.g. Chester et al. 1984). A growing interest has developed in more recent industrial and combustion emissions associated with the burning of fossil fuel that produces highly diagnostic magnetic spherules (e.g. Hunt et al. 1984). Generally, the concentration of these spherules in young sediments, soils and peat bogs is attributed to a massive increase in the combustion of fossil fuels following the industrial revolution. However, at a more localised scale historical iron smelting and smithing will produce similar characteristic spherules that may be indicative of such activity in archaeological sediments.

Extraterrestrial particles, derived from meteorites entering the earth's atmosphere have been proposed as a more exotic source for the abundance of spherules noted above. However, it is generally accepted that the supply of such particles will be highly localised and only likely to be of significance in regions remote from other forms of terrigenous input (Thompson and Oldfield 1986; p126).

### *2.1.3 Biological sources*

It is only comparatively recently that the importance of biogenic magnetic minerals has been recognised and the field developed as a distinct area of research (e.g. Kirschvink et al. 1985; Dunlop and Özdemir 1997, Frankel and Blakemore 1991). However, the biochemical production of iron minerals extends across a wide range of organisms, spanning both the plant and animal kingdoms, that are now recognised as significant mechanisms for the concentration, enhancement and diagenesis of magnetic minerals in surface sediments and soils where the lithosphere and biosphere meet (e.g. Maher and Hounslow 1999, Donald and Southam 1999).

Sources for such biomagnetic minerals include the controlled precipitation of durable iron oxide "teeth" by molluscs for grazing organic material from rocks to the discovery of biologically induced magnetite and greigite in a range of bacteria and the central nervous systems of higher organisms. Explanations for the presence of such highly controlled biominerals in birds and fish have concentrated upon their use as a navigational aid providing a biological "compass" to follow the earth's magnetic field (e.g. Diebel et al. 2000). This hypothesis has been extended to include magnetotactic bacteria that produce highly ordered chains of morphologically unique magnetite or greigite crystals (§2.2.2). Presumably, such bacteria benefit from the ability to navigate vertically in the soil section to obtain the ideal anaerobic conditions under which they thrive in response to varying climatic conditions. Limited studies of live magnetotactic bacteria confirm this complex motile response to applied magnetic fields and suggest a possible diurnal periodicity of movement between oxidising/reducing zones of the sediment (Blakemore and Blakemore 1991, Thompson and Oldfield 1986, Hesse and Stolz 1999, Popa and Nealson 2003).

However, this cannot explain the advantage to these organisms of growing a continuous chain of magnetic material over the more energetically efficient production of a single crystal. Furthermore, the discovery of soil bacteria containing magnetosomes (e.g. Faßbinder et al. 1990, Stanjek et al. 1994) has questioned how magnetotaxis, or indeed flagella, may be of adaptive advantage where motility is severely restricted due to the absence of a sufficiently aquatic environment (Williams 1990, Blakemore and Blakemore 1991). Thus, without any obvious navigational advantage an explanation for the persistence of magnetosomes within such bacteria is difficult to find. Perhaps, the latent magnetotaxis provides a control against catastrophic environmental change, such as rapid flooding, or alternatively the magnetic moment may provide an aid to stability against Brownian motion within their immediate soil-pore environment (B. Moskowitz pers. comm.).

Whilst the majority of reactions involving iron minerals in the soil occur at the microbial level it should be remembered that iron is also essential for many higher organisms. For example, most animals including humans utilise iron in the porphyrin like molecule *heme* that combines with *globulin* peptides to support oxygen transport around the body for respiration. Further non-heme molecules include enzymes such as peroxidase (oxidation by $H_2O_2$), catalase (decomposition of $H_2O_2$) and cytochromes that control redox processes. This dependency upon iron compounds for the metabolism of both plants and animals results in the need to develop effective storage mechanisms for iron in protein molecules such as *ferritin* (animals) or *phytoferritin* (plants). This protein contains ~23% Fe and from Mössbauer spectra electron diffraction data has been determined to have crystal structure similar to ferrihydrite (Towe and Moench 1981, Bauminger and Nowik 1989; Laulhere and Briat 1993; Wong et al. 1998). Indeed, it has been suggested a significant proportion of soil ferrihydrite may be derived from such biological sources.

Quantitative estimates suggest that total iron contents as a percentage of dry matter are in the range 0.01 – 0.2% for animals, 0.005 – 0.025% for tree leaves and ~0.2% for bacteria (Murad and Fischer 1988). However, long term observations of a beech forest in the Solling area of West Germany (Mayer and Heinrichs 1980) revealed higher concentrations of Fe in the leaf litter beneath the trees (0.06%) and in the humus layer of the soil (L horizon, 0.5%, Oh horizon, 1.0%). From these observations it is suggested

that whilst the concentration of Fe in the biomass is comparatively low (with respect to the topsoil) the extremely high turnover rate of the biomass will exert a significant influence over the reactions of iron minerals within the soil.

*2.2 Enhancement mechanisms*

The investigation of magnetic enhancement mechanisms has been a matter of some debate since LeBorgne (1955) proposed a number of pedogenic enhancement mechanisms producing secondary ferrimagnetic oxides in soil. This process of pedogenic ferrimagnetic mineral enrichment is of direct relevance to the formation of many archaeological sites where sediment accumulating in cut features is derived directly from local topsoil (although not necessarily from topsoil contemporary with the construction of the feature). Additional factors, such as the use of fire in antiquity or the concentration of organic matter in a rubbish pit or post-hole may also influence the enhancement of iron oxides in archaeological features.

Pedogenic, secondary iron oxides develop in the soil through a diverse range of both inorganic and biologically mediated mechanisms. These mechanisms are of great interest as they are influenced directly by the common soil forming factors and lead to the formation of specific mineral phases or distributions within a soil section. In turn, these factors are directly linked to environmental and climatic conditions; thus the magnetic minerals in a soil may well provide a proxy record of past environments.

The term *enhancement mechanism* has been applied to describe any mechanism or process that results in an increase in the magnetic properties of a soil. In this respect the terminology is comparatively vague as it fails to distinguish entirely pedogenic processes from those directly influenced by anthropogenic activity, such as the sustained and deliberate use of fire. However, a firm distinction between the two classes is often misleading and they should, perhaps, be considered in combination.

*2.2.1 Pedogenic processes*

Iron is present in the majority of rocks forming the earth's crust and may be released by weathering during pedogensis. The main source of soil Fe originates from silicates

where the ion is predominately bound in the divalent (reduced) state that is then released either through protolysis, from protons made available from dissolved $CO_2$, oxidation or a combination of the two mechanisms (Schwertmann and Taylor 1977). The resulting $Fe^{3+}$ will hydrolyze immediately on contact with water forming metastable FeOOH compounds. Redissolution of these iron oxides is unlikely as soil pH seldom falls to a low enough value to permit this reaction to proceed. However, whenever microbial activity limits the availability of $O_2$ a reductive reaction may occur liberating $Fe^{2+}$ for reoxidation to new mineral forms.

The formation of a soil may, therefore, be described directly through a series of factors that, to varying degrees, influence the cycling of soil Fe between various mineral phases. The most stable phase formed may be determined from thermodynamic considerations and will depend on the concentration of $Fe^{2+}$ / $Fe^{3+}$, pH, Eh and $H_2O$ activity in the specific environment. These soil forming factors may be subdivided initially into separate processes that lead to the *neoformation* of magnetic minerals in the soil and those that simply enrich the concentration of such material inherited from the parent lithology. In general, however, five main environmental factors may be identified that account for the pedogenic enhancement of soil:

1. *Lithology - determining the type and concentration of material inherited from the parent rock*

2. *Topography - influencing the local hydro-geological conditions and the stability of the resulting soils to erosion*

3. *Biota - the principle factor that distinguishes soils from sediments derived from a similar parent lithology*

4. *Time - the ongoing nature of the development of soil*

5. *Climate - an important factor at a regional scale.*

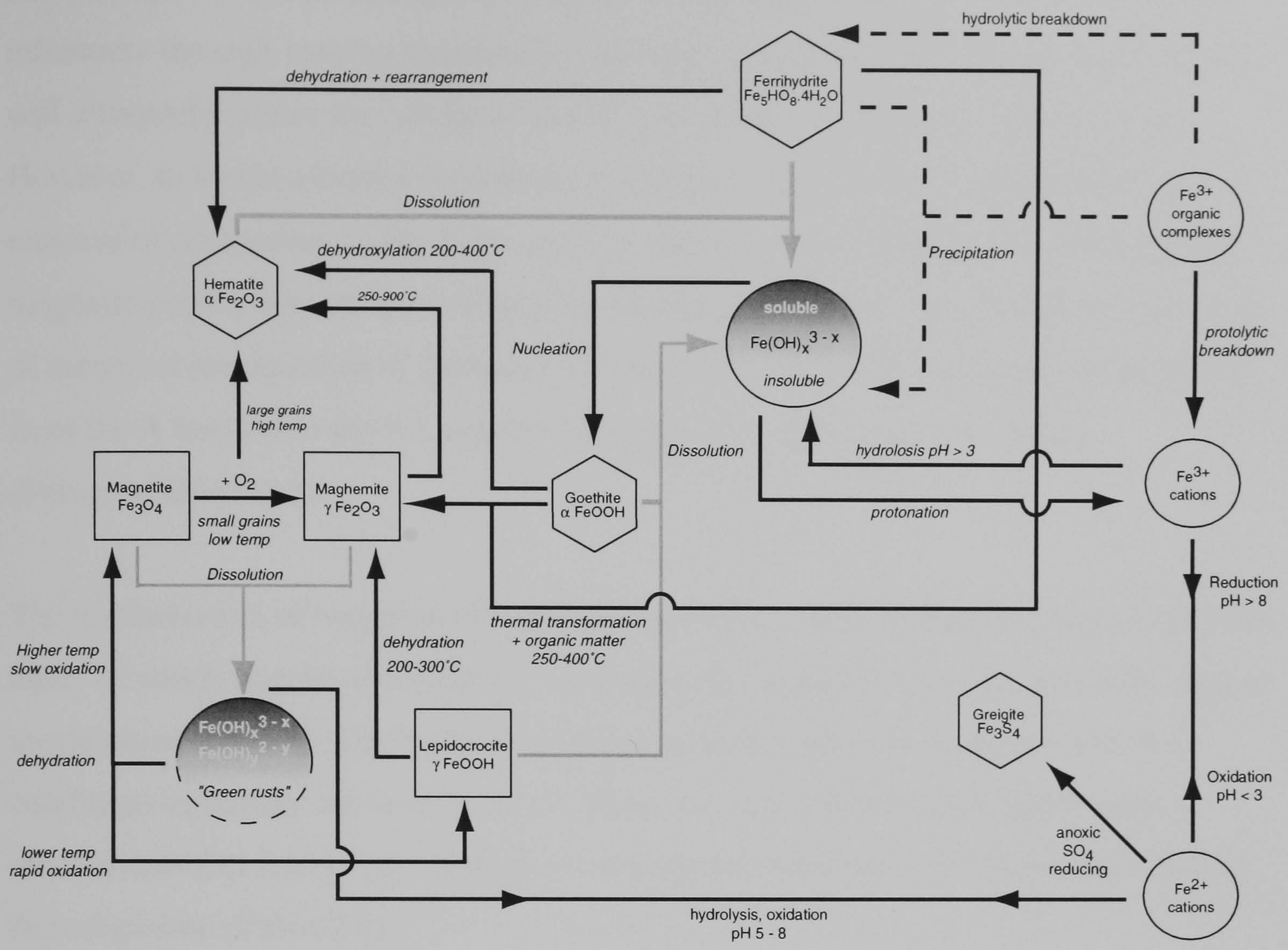


***Figure 2.2*** *Summary diagram showing pathways for the inorganic formation of iron minerals. Many of the conditions necessary for these processes may be controlled either directly or indirectly by (micro)biological mechanisms.*

The magnetic enhancement of a soil progresses when the above factors result in carbonate dissolution that establishes favourable conditions for the formation of ferrimagnetic mineral phases. For example, the addition of organic material to a soil and action of soil biota leads to the production of both $CO_2$ and $H^+$ leading to a reduced pH, increased calcite dissolution and the weathering of silicates where these are available from the parent lithology. This in turn produces an enrichment of the concentration of magnetic minerals inherited from the parent lithology in the soil. With time, the depth of soil development will increase moderated by both the topography of the region and surface flora that will influence the downwards erosion of soil from exposed slopes.

An understanding of the influence of climate over pedogenesis represents, perhaps, the ultimate goal of many earth scientists attempting to establish patterns of past climatic change from proxy records held within soil columns (e.g. Nawrocki et al. 1996, Maher

and Thompson 1995, Dearing et al. 1996b). In this respect, climate exerts two major influences through varying temperature and rates of precipitation. Higher temperatures will ultimately reduce the solubility of $CO_2$ and decrease the dissolution of calcite. However, in wetter climates increased precipitation will lead to the dissolution and removal of carbonates. In the latter case, as with the action of biota, the enrichment of magnetic phases derived from the parent lithology will ensue. Another important result of increased precipitation is the translocation of clay minerals, including ferrimagnets, from the A horizon to the B horizon where they are often fixed into visibly distinguishable bands.

The neoformation of magnetic minerals proceeds via a more complex series of reactions many of which may be either directly or indirectly moderated through (micro)biological mechanisms. Figure 2.2 provides a graphical summary of these processes and the conditions necessary for them to occur. However, it is useful to distinguish those mechanisms that lead to the enrichment of magnetic minerals from those that result in their depletion (Table 2.2).

***Table 2.2*** *Summary of factors influencing the enrichment or depletion of magnetic susceptibility*

| | | *Controlling factor* |
|---|---|---|
| *Enrichment* | Fe oxide + $e^- \rightarrow Fe^{2+}$ | surface area, microbial activity |
| | $Fe^{2+}$ + ferrihydrite → magnetite | inorganic (near neutral pH) or (micro)biological |
| *Depletion* | Magnetite + $e^- \rightarrow Fe^{2+}$ | surface area, microbial activity |
| | $Fe^{2+} + O_2 \rightarrow$ maghaemite | pH, sorption of clay minerals |
| | Magnetite + $O_2 \rightarrow$ maghaemite | Availability of $O_2$, crystal size and surface coating |

### *2.2.2 Microbial*

Microorganisms play an important role in the transformation of Fe mineral phases in the soil both through the chemical reduction of Fe and also at a structural level within clay minerals (e.g. Kostka et al. 1999). Indeed, the microbial reduction of Fe oxides is recognised as the most important mechanism in the cycling of soil Fe leading to the formation of characteristic *redoxomorphic* soils that occur throughout the world. Generally, microbial activity is restricted to the near surface where sufficient biomass and $O_2$ occurs to allow metabolism to take place. However, purely anaerobic strains of bacteria have recently been discovered (e.g. Lovley 1987, Lovley et al. 1987). Lowenstam (1981) suggested a subdivision into two categories of biomineralisation.

#### *2.2.2.1 Biologically Induced Mineralisation (BIM)*

This term is used to describe the transformation of Fe phases through *extracellular* activity. Principally, it includes the metabolic oxidation of organic matter by iron reducing bacteria, resulting in the liberation of electrons that require a suitable electron acceptor in the immediate soil environment. In the absence of $O_2$ and at a redox potential of approximately +0.1V, $Fe^{3+}$ may act as the acceptor for these electrons. It is postulated that the electron transfer occurs via an enzyme excreted by the bacterial cell that is in close association with the surface of the Fe oxide. The resultant $Fe^{2+}$ may then precipitate from solution directly to a solid phase such as siderite, vivianite, iron sulphide or as an amorphous "green rust". Other mixed $Fe^{2+}$ / $Fe^{3+}$ phases will form under certain conditions of decreasing pH and Eh with ferrihydrite being a common product due to its formation at a higher redox potential than other iron oxides (e.g. Schwertmann and Taylor 1977). Indeed there is considerable evidence for the microbial formation of ferrihydrite spherules in close association with decaying leaf litter (Meng et al. 1997).

Perhaps of greater interest is the production of magnetite by a variety of BIM-type microorganisms under anaerobic conditions. Many of these organisms reduce $Fe^{3+}$ indirectly, relying on the fermentation of organic matter as their principle mode of metabolism. However, more recently identified strains of bacteria, such as GS-15, have demonstrated metabolism through the complete oxidation of organic compounds to $CO_2$

utilising $Fe^{3+}$ as the sole electron acceptor (e.g. Lovley et al. 1987, Stolz et al. 1990, Frederickson et al. 1998). Laboratory experiments demonstrate that, as noted above, magnetite may not be the only stable mineral phase to be formed and a comparatively minor alteration to the immediate environment may produce either siderite or vivianite (Lovley 1991, Bell et al. 1987). The production of magnetite is favoured under conditions of high pH and an adequate source of both $Fe^{2+}$ and $Fe^{3+}$ from the metabolism of organic matter (e.g. Gibbs-Eggar et al. 1999). Magnetite crystals produced by GS-15 are either round or oval and have a diameter of 10-50nm with many falling below the superparamagnetic threshold for magnetite of ~30nm. Furthermore, Bazylinski (1991) suggests that biomineralisation by iron reducing bacteria will be copious potentially producing 1Kg of magnetite to obtain enough energy for the growth of 10g of cell material compared with the 200mg of magnetite found within the magnetotactic bacterial cells.

*2.2.2.2 Biologically Controlled Mineralisation (BCM)*
*(also referred to as Boundary Organised (Bio)Mineralisation BOB or BOM)*

This most enigmatic source of magnetic biominerals was only recognised comparatively recently by Blakemore (1975) but has rapidly created an expanding field of research encompassing a wide variety of disciplines (e.g. Stolz et al. 1990). These bacteria are distinguished by their ability to control the biomineralisation of magnetic material in highly ordered chains of crystals known as *magnetosomes* within the cell structure. Since the initial discovery similar bacteria containing magnetosomes have been revealed in a diverse range of environments from marine sediments to soils and archaeological features.

All such bacteria fall within the phylogenetic classification of *Eubacteria* rather than *Archaebacteria*, have a Gram negative type of cell wall[1] and cover the full range of morphological forms: coccoid (spherical), bacilli (rod-shaped) and spirilla (helical). Current sampling methods of live bacteria have only recovered motile organisms that all

[1] The Gram stain technique is used to classify bacteria and relies on the differential ability of bacterial cells to retain dye stains. The ability to retain the dye (Gram positive) is due to the presence of an extra lipoprotein membrane outside the cytoplasmic membrane of the bacteria. Gram negative bacteria do not have this membrane and may have other physiological differences from morphologically similar Gram positive bacteria. Named after Hans Christian Joachim Gram (1853 - 1938).

share an aversion to atmospheric levels of oxygen and prefer either anaerobic or microaerobic conditions.

In contrast to BIM type bacteria discussed in the previous section, BCM bacteria metabolise organic matter via either $O_2$ under microaerobic conditions (e.g. *Aquaspirillum magnetotacticum*) or $NO_2$ under anaerobic conditions (e.g. strain MV-1). It should be noted that the production of magnetosomes is highly controlled within the cell structure of the microorganism. Thus the magnetic minerals produced are less susceptible to the influence of the extracellular environment and apparently demonstrate a highly organised range of morphologies (e.g. Sparks 1991, Bazylinski et al. 1994). In general the resulting magnetic crystals all fall within the single domain size range for magnetite (35-100nm) and are often elongated ("bullet" shaped) to increase the magnetic moment. Such morphologies are unlikely to form inorganically due to the increased magnetotactic self energy associated with the elongated form. This has led several authors to speculate that similar elongated crystals of magnetic minerals in sediments represent "magneto-fossils" originally produced by magnetotactic bacteria (e.g. Kirschvink and Chang 1984, Petersen et al. 1986, Chang et al. 1987, Vali et al. 1987, Stolz et al. 1990, Snowball 1994). Indeed, Borradaile (1994) has proposed an archaeomagnetic dating technique for masonry buildings based on the viscous remanent properties of the magnetosomes within the original limestone.

Production of magnetite by BCM bacteria similar to *Aquaspirillum magnetotacticum* has also been reported in the more oxygenated A horizon of soil (Faßbinder et al. 1990, Faßbinder and Stanjek 1993). However, magnetotactic bacteria producing iron sulphides of similar morphology and size have also exist (e.g. Heywood et al. 1990, Diaz Ricci and Kirschvink 1992) both in marine environments (Farina et al. 1990, Mann et al. 1990) and soils (Stanjek et al. 1994).

### *2.2.3 Enhancement through burning*

There is considerable evidence from both laboratory and field studies that natural and deliberate fires enhance topsoil magnetisation (e.g. LeBorgne 1960b, LeBorgne 1960a, Tite and Mullins 1971, Schwertmann and Taylor 1972, Dunlop 1972, Mullins 1974,

Longworth and Tite 1977, Mullins 1977, Longworth et al. 1979, Rummery et al. 1979, Oldfield et al. 1981, Rummery 1983, Stanjek 1987, Oldfield 1991, Kletetschka and Banerjee 1995, Marshall 1998, Marmet et al. 1999, Morinaga et al. 1999). Some debate surrounds the relative importance of this mechanism due to the expected frequency and intensity of natural fires that will depend on both climate and vegetation. For example, the comparatively low temperature required for the conversion of lepidocrocite to maghaemite (§2.1.1.3) would, perhaps, provide a significant enhancement mechanism wherever this mineral is found in abundance. However, the occurrence of lepidocrocite is limited to poorly drained soils, favouring wetter climates where natural burning episodes may well be expected less frequently (Thompson and Oldfield 1986; p75).

In addition, much of the experimental work has been conducted under controlled laboratory conditions where both comparatively high temperatures (350-700°C) and near perfect redox conditions (hydrogen or nitrogen atmosphere followed by air) could be obtained (e.g. Mullins 1974, Tite and Linington 1975, Graham and Scollar 1976). Whilst these experiments certainly illustrate the potential enhancement due to burning it is questionable how often such conditions would occur through both natural causes, such as forest fires, or due to deliberate human activity, either domestic or industrial. Chapter 7 examines these issues in an archaeological context through a series of field experiments and the laboratory heating of samples under more controlled conditions.

One intriguing aspect of the debate surrounding enhancement through fire is the possible contribution of biogenic sources of Fe to wood ash. A number of studies demonstrate that archaeological deposits of ash often exhibit an enhanced magnetic susceptibility (e.g. Hamilton et al. 1986, McClean and Kean 1993, Boucher 1996, Peters et al. 1999a, Peters et al. 1999b) and McClean and Kean (1993) propose that this magnetisation may well arise from the enhancement, through burning , of iron proteins within the wood fuel itself. Whilst there is certainly much evidence for iron uptake by plants (e.g. Murad and Fischer 1988, Laulhere and Briat 1993) this is generally concentrated in the form of the iron storage protein, phytoferritin, in the leaves and seeds of the plants rather than the heartwood that forms the most common fuel source. Indeed the presence of phytoferritin in plant leaves has recently been proposed as a Fe source to explain the seasonal magnetic enhancement of Chinese loess deposits (e.g. Meng et al. 1997 but see also Maher 1999 and Meng et al. 1999).

Recent laboratory determinations of the magnetic susceptibility of ash derived from a range of tree species and habitats revealed a wide range of enhancement with volume susceptibilities in the range $\kappa = 1.0 - 101.7 \times 10^{-5}$ from initial samples of unburnt wood with a negligible susceptibility (M. A. Cole pers. comm.). However, a considerable mass of wood was required to produce the enhanced ash (samples from 120 - 682g) and estimates based on the average of the range of tree species investigated suggests ~12.4Kg of wood are required to raise the susceptibility of a non-magnetic soil matrix forming a 1m x 1m hearth to a depth of 1cm by $1 \times 10^{-5}$. Thus significant enhancement through wood ash alone is likely to occur only through the repeated use of a hearth or the concentration of waste ash in a rubbish pit.

In addition, the influence of modern particulate pollution is difficult to assess as recent environmental studies have shown that trees intercept airborne particulate pollutants. Whilst the majority of this uptake is temporary, with the particles concentrated on the leaf surfaces, the heartwood tissue is capable of absorbing various trace metals. Obviously, the recent increase in such airborne pollutants may well account for the considerable magnetic susceptibility of more recent wood ash noted above.

*2.2.4 Anthropogenic influence*

Studies by Tite and Mullins (1971) following a suggestion of LeBorgne (1960b) concluded that thermal alteration through domestic and semi-industrial fires was the dominant enhancement mechanism of relevance to archaeological magnetism. The mechanism proposed by LeBorgne involves the heating of haematite in the presence of organic matter resulting in a reduction to magnetite at a peak temperature of 550-600°C and the subsequent oxidation to maghaemite. Under laboratory conditions magnetite should normally oxidise directly back to haematite. However, Stacey and Banerjee (1974) have proposed that the presence of other ions, such as sodium, aluminium or magnesium may fill vacancies in the magnetite cubic crystal lattice stabilising this arrangement and thus favouring oxidation to maghaemite.

The conditions proposed by Le Borgne are readily available through the deliberate use of fire where initial reducing conditions will prevail during the combustion of the fuel due to increased competition for available oxygen and the production of carbon

monoxide. This was confirmed through limited field experiments (LeBorgne 1960b, LeBorgne 1960a). When the fuel is spent, predominantly oxidising conditions will return and the abundance of the common metal ions noted above within most soils will ensure the production of a stable maghaemite. Perhaps the most pertinent question surrounding this mechanism is the ability of domestic fires to produce the significant temperatures required for the enhancement of common iron oxides such as haematite and goethite and this topic is considered in greater detail in Chapter 7.

Since this initial work, the introduction of more sensitive magnetometers has identified magnetic anomalies arising from unburnt features some distance from sites of concentrated archaeological occupation. Much debate surrounds the origin of this magnetism and recent research indicates the importance of both inorganic (e.g. Maher and Taylor 1988) and biologically controlled (e.g. Faßbinder and Stanjek 1993) production of magnetite in soils and sediments. Detailed studies of these various enhancement mechanisms indicates characteristic mineral-type and grain-size dependencies which, it is hoped, will result in the quantification of competing systems in archaeological samples.

Several mechanisms have been proposed to account for the strong magnetisations that are observed in some archaeological sediments (Faßbinder and Stanjek 1993; Faßbinder et al. 1990; McClean and Kean 1993; Stanjek et al. 1994) and may be related to either the direct or more subtle intervention of anthropogenic activity in antiquity. These mechanisms can be divided into two main groups; those that enhance or concentrate the magnetic minerals within a sediment and those that align the *in situ* magnetic material to produce a semi-permanent Natural Remanent Magnetisation (NRM) (§2.3). Many of these mechanisms have a characteristic mineralogical and grain-size dependence which may be identified through the application of suitable rock magnetic techniques and interpretation procedures. A summary of significant anthropogenic processes resulting in magnetic enhancement is shown in Figure 2.1.

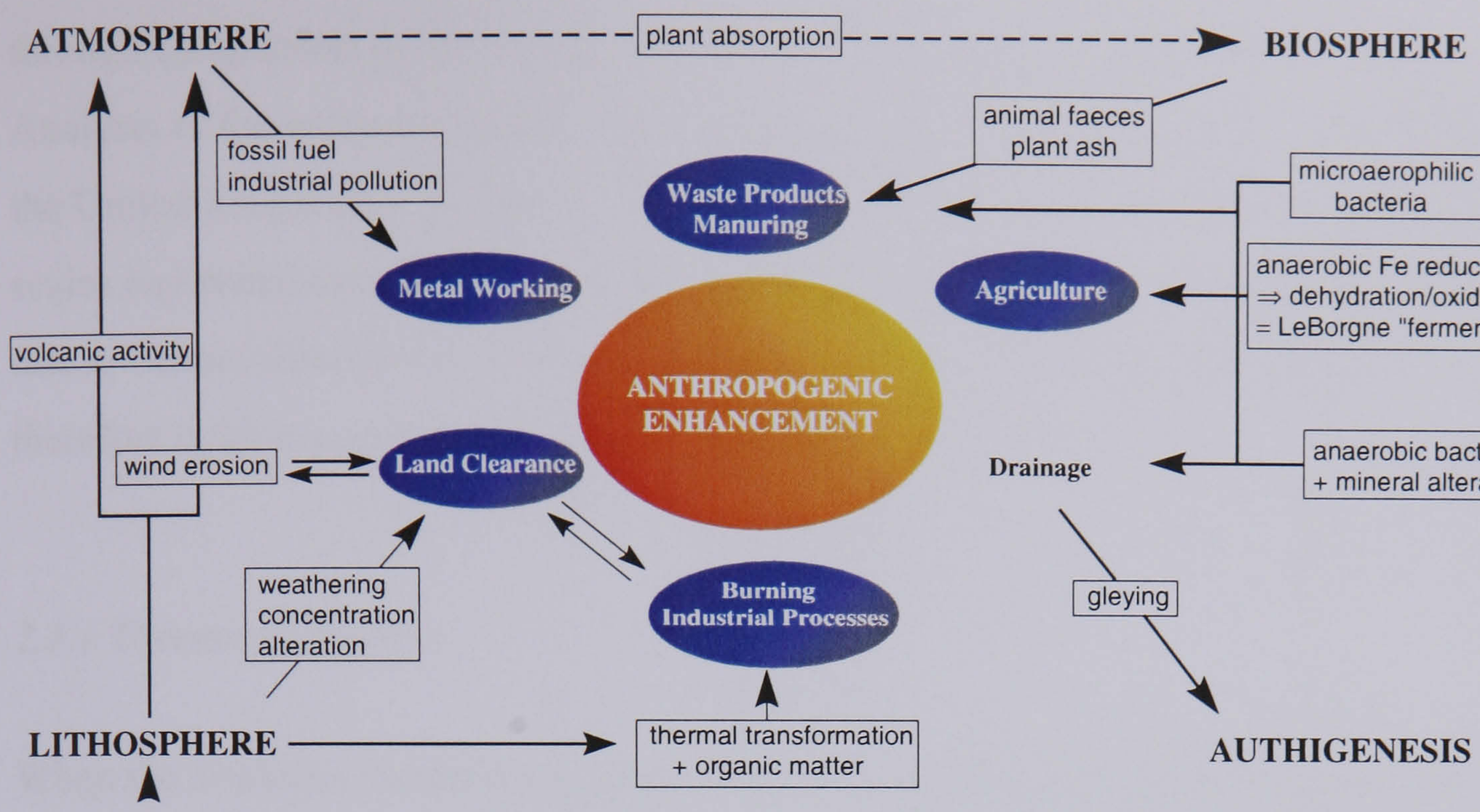


***Figure 2.3*** *Summary diagram showing the major mechanisms for anthropogenic enhancement.*

It should also be noted that whenever a natural pedogenic susceptibility contrast is evident between the topsoil and subsoil horizons then a magnetic anomaly may well occur simply through the construction of a cut feature such as a ditch. The feature will form a gravity trap that will slowly become silted with enhanced topsoil material washed from the surface into the bottom of the ditch producing a detectable susceptibility contrast. Figure 2.4 demonstrates this principle through the theoretical fill of a ditch-type anomaly derived from the admixture of a thin 0.2m layer of enhanced topsoil ($\kappa = 30 \times 10^{-5}$) overlying a less magnetic subsoil ($\kappa = 10 \times 10^{-5}$).

## *2.3 Formation and Retention of NRM*

The magnitude of magnetometer anomalies produced by magnetised archaeological features consists of two components: that *induced* by the inherent susceptibility of the material in the earth's magnetic field and the *remanent* component produced by the alignment of individually magnetised particles along a preferred axis of orientation. The direction of the induced component will be determined by the current ambient field and this will combine with the remanent component to produce the resultant magnetisation. In general, the remanent component will form along the ambient direction of the earth's field at the time the feature was formed and may provide a means for dating the activity

through comparison of the remanent magnetisation with a suitable calibration curve. Analysis of the archaeomagnetic calibration curve produced by Clark et al. (1988) for the United Kingdom (e.g. Figure 5.34(D)) demonstrates that over archaeological time scales any remanent component will not vary significantly from the induced component due to current direction of the Earth's magnetic field. The two components will therefore combine and increase the total magnetisation of the feature.

### *2.3.1 Thermoremanence*

When the available thermal energy exceeds the macroscopic magnetic energy of a particle (§1.5.2) the magnetisation will realign with the current ambient field. The precise temperature at which this process occurs, known as the *unblocking temperature*, varies with the mineral type and size and shape of the crystal involved but many studies confirm that the reorientation of magnetisation may begin at relatively low temperatures and remain stable over considerable periods of time, at ambient temperatures (e.g. Blanco-Mantecón and O'Grady 1999, Lowrie 1990, Winklhofer et al. 1997, Dunlop and Argyle 1997). After the particles fall below their unblocking temperature the resultant magnetisation remains aligned in the direction of the ambient field producing a *thermo remanent magnetisation (TRM)*. The process of TRM acquisition has been investigated in great detail with the aim of recovering high fidelity records of palaeo and archaeo magnetic secular variation (e.g. Collinson 1983, O'Reilly 1984, Butler 1992, Dunlop and Özdemir 1997). For suitable archaeological samples, such as hearths or pottery kilns, TRM provides a means of physical dating by comparing the direction of the acquired magnetisation to a local calibration curve. This curve has been constructed from known age features that record an unique archaeological event, the point at which the features was last heated to above the unblocking temperature (Tarling 1983, Clark et al. 1988, Batt 1997, Creer et al. 1983).

### *2.3.2 Detrital remanence*

During the deposition of the constituent grains during the formation of a sediment magnetic particles will, under certain conditions, rotate and align with the ambient magnetic field. This process, referred to as *detrital (depositional) remanent*

*magnetisation (DRM)* is largely controlled by the size, shape and rate of deposition within the sedimentary environment (e.g. Butler 1992; pp66-74, Roy and Park 1972, Shcherbakov and Shcherbakova 1987, Levi and Banerjee 1990, Saarinen 1999). The process of DRM alignment will occur for as long as the sediment remains plastic and the motion of individual particles is not inhibited by contact with surrounding grains. Thus the time at which the DRM becomes stable, known as the *lock-in time*, may extend over a considerable period since the initial deposition of material.

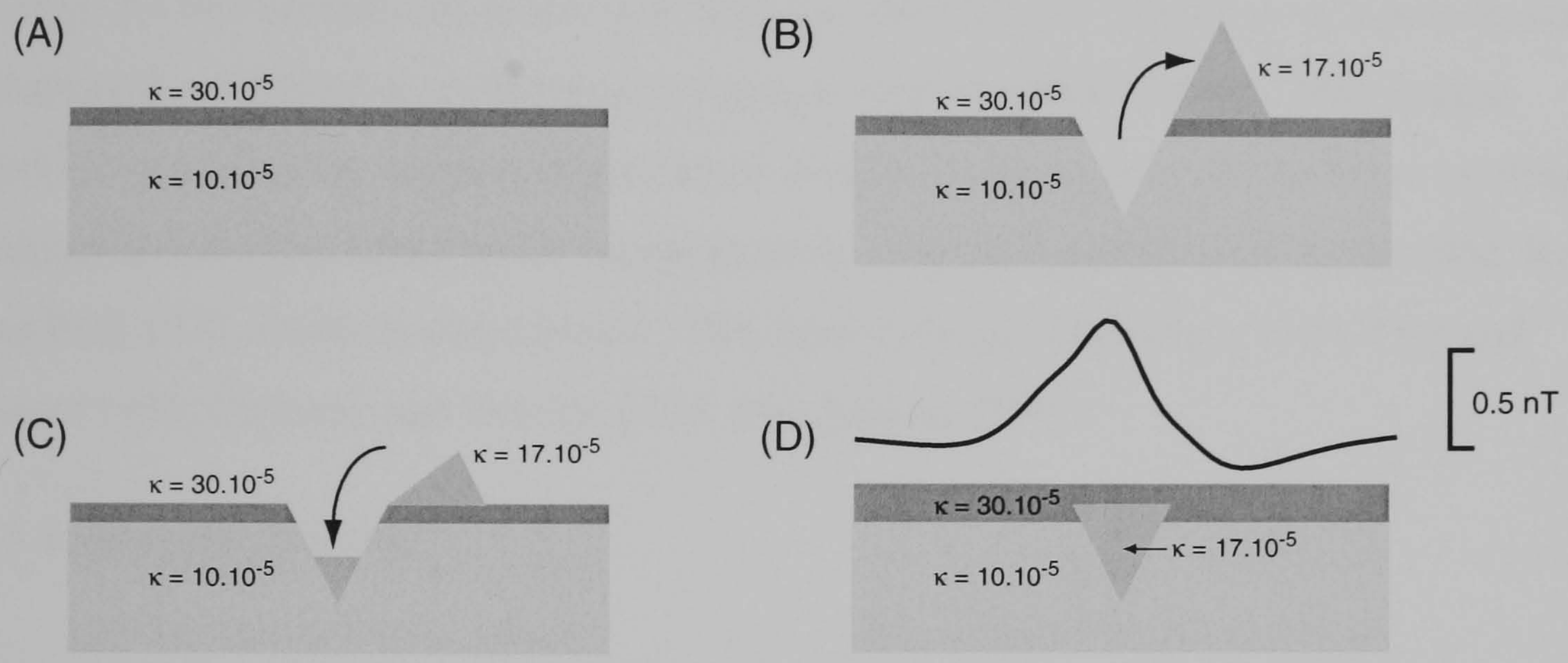


***Figure 2.4*** *Formation of a magnetic anomaly at a theoretical site (A) with a thin layer of moderately enhanced topsoil 0.2m thick overlying a less magnetic subsoil. Creation of a 1m deep 'V' shaped ditch (B) assumes the admixture of the excavated soil on the surface that subsequently silts back into the ditch (C). The final gradiometer anomaly (D) has been calculated for the buried ditch assuming an additional 0.2m of topsoil has accumulated over the original ground surface and an instrument sensor height of 0.2m.*

Laboratory experiments also demonstrate the ability of sedimentary grains to realign with a varying ambient field direction following initial deposition (e.g. Verosub 1977). This acquisition of *post-depositional remanent magnetisation (pDRM)* is important within sediments containing extremely fine particles subject to thermal agitation by Brownian motion or environments disturbed by bioturbation through, for example, burrowing worms. Many recent archaeological sediments provide an accurate record of the ambient field direction and results are often used to obtain an archaeomagnetic date (e.g. Nöel and Thistlewood 1989, Tarling 1983, Ellis and Brown 1998).

### *2.3.3 Chemical remanence*

The formation of a magnetic mineral through either the alteration of an existing mineral

or precipitation from solution provides a similar mechanism to TRM for the alignment of magnetisation vectors with the ambient field. In this case, it is the volume of the new mineral that alters rather than an increase in thermal energy and the process is controlled by a critical *unblocking volume*. During the initial stages of alteration/precipitation the volume of the new crystal is so small that even ambient temperatures will provide sufficient energy for the alignment of magnetisation along the direction of the ambient field. At some point the crystal will pass through its critical unblocking volume and the magnetisation will remain locked-in unless there is an increase in the available thermal energy. As this mechanism relies on a chemical alteration or formation of a new crystal structure it is referred to as *chemical remanent magnetisation (CRM)*. CRM is most likely to occur during the post-depositional diagenesis of magnetic minerals in existing sediments and often forms as an overprint to the original (p)DRM (e.g. Creer 1962, Roy and Park 1972, Dekkers and Linssen 1989, Snowball and Thompson 1990, Pick and Tauxe 1991, Özdemir and Dunlop 1993, McClelland 1996).

### *2.3.4 Magnetic Viscosity*

As noted above (§2.3.1), extremely fine magnetic particles will be above their unblocking temperature at ambient temperatures and the magnetisation of such particles is able to realign with an applied field within a short time scale, a process known as *magnetic viscosity*. A more detailed discussion of the theory behind this phenomenon has been given in §1.6 but it is noted that suitably fine particles (generally with a diameter $<0.03\mu m$) are common within soil and archaeological sediments (e.g. Dearing et al. 1996a, Peters and Thompson 1999). Graham and Scollar (1976) draw attention to the fact that a concentration of such fine magnetic particles in an archaeological deposit will align with the ambient magnetic field in a reasonably short period of time ($10^9$s for spherical magnetite particles with a radius of 34nm) resulting in an additional component of remanent magnetisation.

In addition, Graham and Scollar defined a *viscosity constant,* $V_C$ that describes the percentage increase in magnetisation of a substance after exposure to a laboratory magnetic field of 2mT for 100 seconds. Typical values for soils fell within a range of 3 - 6% and the authors further calculated that an increase in magnetisation of 45% would occur for a value of $V_C$ = 5% over a time period of 100 - $10^3$ seconds. Thus the

calculation of remanent magnetisation from archaeological features should allow for the magnetic viscosity of the soil to avoid underestimating the magnitude of the resultant anomaly.

*2.4 Long term mineralogical effects of Fe-redox processes in periodically flooded soils*

The reduction of Fe(III) oxides to dissolved, adsorbed and solid Fe(II) phases is discussed by van Breemen (1988a) with particular regard to the periodic or long-term flooding of soils (van Breemen 1988b). Two processes of particular importance under such conditions are: *ferrolysis*, the cyclic displacement of adsorbed cations by Fe(II) and the segregation of iron oxides due to redox processes.

Ferrolysis begins with the reduction of iron oxides providing $Fe^{2+}$ ions that exchange with $Ca^{2+}$ and $Mg^{2+}$ cations within the clay fraction. These displaced cations together with the anions separated during the production of $Fe^{2+}$ are removed from the soil by percolation and diffusion and in the short term, will not be replaced through the weathering of primary minerals. Subsequent aeration of the soil results in the oxidation of the exchangeable $Fe^{2+}$ to less soluble $Fe^{3+}$ oxy-hydroxides and its replacement by less stable $H^+$ in base anions. The $H^+$ will subsequently be replaced by Al that again may be displaced by $Fe^{2+}$ arising from reduction during further flooding incidents leading to the partial dissolution of clay minerals and an increase in soil chlorites. Over an extended period of time ferrolysis will lead to a more silty, highly acidic soil and an increased concentration of ferric hydroxides.

Seasonally waterlogged soils, or *gleys*, are generally identified through the separation between brown/red horizons containing concentrations of $Fe^{3+}$ oxides and adjacent grey/green/blue/black where solid $Fe^{2+}$ predominates. The formation of these layers arises from the higher solubility of many $Fe^{2+}$ compounds that results in a higher mobility and translocation within the soil section. As with ferrolysis, the process begins with the reduction of $Fe^{3+}$ to $Fe^{2+}$ through microbial action (e.g. Ottow and Glathe 1971, Kostka et al. 1999) accelerated by the absence of $O_2$ and the presence of organic matter as an energy source for the bacteria. Translocation of the liberated $Fe^{2+}$ will then occur through either diffusion or mass flow until the $Fe^{2+}$ is immobilised. Immobilisation may occur through either the precipitation of solid $Fe^{2+}$ compounds (high pH, concentration of sulphide), the adsorption of $Fe^{2+}$ by clay or $Fe^{3+}$ oxides or the direct oxidation to $Fe^{3+}$

following the reintroduction of $O_2$ during subsequent dry periods together with possible bacterial catalysis under acidic conditions (Fischer 1988).

The effect of repeated waterlogging on a soil is to lead to a concentration of fine grained, iron oxides of poor crystallinity that hampers precise identification. However, both goethite and lepidocrocite occur widely in such hydromorphic soils with lepidocrocite forming distinctive bright orange mottles around root tubers following the rapid oxidation of mixed $Fe^{2+}/Fe^{3+}$ hydroxides "green rusts" (§2.1.1). Ferrihydrite may also be present as an intermediary phase in soils undergoing frequent redox cycling but is difficult to identify in low concentrations. Magnetite and maghaemite despite being typical products of the slow oxidation of $Fe^{2+}/Fe^{3+}$ hydroxides are rarely found in hydromorphic soils due to the more rapid kinetics of the oxidation reaction.

The effect of prolonged gley conditions would appear to reduce the magnetic susceptibility of a waterlogged soil through the preferential dissolution of fine superparamagnetic iron oxides such as magnetite or maghaemite (Thompson and Oldfield 1986; pp81-82). In addition, the degree of magnetic iron oxide depletion depends upon the local soil environment that may well be moderated by surface vegetation over comparatively short periods of time. For example, Dearing et al. (1995) report results from similar soils collected under stands of deciduous oak and pine that showed that the latter species produced a marked reduction in the subsoil magnetic properties. This depletion correlated with an increase in both the acidity and concentration of organic matter beneath the pine that may well account for enhanced microbial oxidation of $Fe^{3+}$ to $Fe^{2+}$. It seems likely that increased levels of microbial activity within waterlogged soils would account for the poor survival of fine ferromagnetic material as opposed to their apparent persistence in lacustrine and marine sediments (e.g. Oldfield et al. 1981).

### *2.5 Occurrence of iron sulphides in terrestrial soils*

The occurrence of magnetic iron-sulphide minerals is not uncommon within marine anoxic sulphate reducing sediments, particularly in the presence of organic matter (e.g. Berner 1971, Roberts and Turner 1993) and it is possible that such conditions may be

supported on waterlogged terrestrial sites. The most stable iron sulphide found under these conditions is the paramagnetic mineral pyrite, which is the ultimate product of a well-defined chemical pathway beginning with the formation of intermediate ferrimagnetic sulphides such as mackinawite, pyrrhotite and greigite. This process begins with the production of $H_2S$ through the reduction of sulphate by anaerobic bacteria utilising organic matter within the sediment as an energy source. Ferrous ions, produced either by bacterial or inorganic decomposition of detrital iron minerals, will then react to form a series of metastable iron sulphides resulting in the formation of pyrite. The amount of iron sulphide formed is critically controlled by the availability of reactive iron compounds, the concentration of dissolved sulphate and the presence of organic matter for the bacterial reduction of $H_2S$.

The survival of greigite within soil is comparatively rare (Stanjek et al. 1994) and will result from a phase of arrested diagenesis where the metastable ferrimagnetic iron sulphides survive and the ultimate formation of pyrite has not yet occurred. This may be due to the reduced availability of $H_2S$ that is unable to freely permeate through the fine-grained sediment (*cf.* Roberts and Turner 1993) or the absence of sufficient organic matter for bacterial respiration. The presence of greigite dominating the magnetic properties of a sample may be supported by high values of coercivity and (s)$IRM_{2.5T}/\chi$, distinctive high-temperature thermomagnetic curves and the unique acquisition of gyro or rotational remanent magentisation (e.g. Hilton 1990, Snowball and Thompson 1990, Snowball 1991, Snowball and Thompson 1992, Roberts and Turner 1993, Roberts 1995, Roberts et al. 1996, Snowball 1997a, Snowball 1997b).

# *Chapter 3*

## *3.0 Methodology and qualitative analysis*

The repeatability, calibration and error estimation of both field and laboratory measurements are considered in this chapter and suitable limits for their sensitivity are suggested. Where possible, comparison between parameters for the same samples with differing instrumentation and measurement techniques is presented. In addition, the relationship between magnetic parameters and qualitative identification of magnetic mineralogy and domain states is also discussed.

## *3.1 Geophysical survey*

A range of geophysical techniques was applied during this study including magnetic, earth resistance, electromagnetic (EM) and ground penetrating radar (GPR) (Table 3.1). Of these magnetic survey, using both gradiometer and total field instruments, proved the most successful with trials of both EM and GPR producing less fruitful results.

All geophysical survey data are presented as false colour greyscale images with low/negative values plotting as dark tones of grey to black and high/positive values plotting as tones of grey to white. A histogram scale bar is included with each figure to illustrate the mapping of data values to shades of grey. Additional representations of each data set were used during interpretation.

### *3.1.1 Fluxgate gradiometry*

Geoscan FM36 fluxgate gradiometers were used for the majority of the magnetic survey. The two vertically aligned fluxgates in these instruments are separated by 0.5m and record the local gradient of the vertical component of the earth's magnetic field. In practice, the lower sensor is held approximately 0.2-0.3m above ground but, through a mechanical modification to the instrument handle, this may be lowered to increase the magnitude of recorded anomalies.

Whilst the correct units of magnetic gradient are (nano)Tesla / metre unless the field is of constant gradient then such units will only be correct for an infinitesimally small sensor separation (R. Walker pers. comm.). Thus the convention of recording data in terms of the relative difference in magnetic flux density between the two sensors, measured in nano Tesla (nT), is adopted throughout this study.

Data were collected at the sample intervals describe in Table 3.1 along parallel N-S orientated traverses separated. Post acquisition processing of the data was kept to a minimum but included the statistical zero-mean adjustment of each traverse to minimise heading errors due to the directional sensitivity of the fluxgate gradiometer. Intense magnetic responses from surface iron objects were removed with a 2m × 2m thresholding median filter (Scollar et al. 1990; pp491-492) and any additional numerical processing is discussed with respect to the specific data set (Chapters 4 and 5).

Geoscan FM36 gradiometers allow data to be recorded to a theoretical sensitivity of 0.1nT. However, in practise this sensitivity will be compromised by thermal fluctuations in the mu-metal cores of the fluxgates and noise from the instrument electronics. The standard deviation of noise test results (Figure 3.1(A)) suggests a more realistic sensitivity of ~0.5nT. In addition, the sensitivity may be further reduced by motion error induced by the operator carrying the instrument over rough terrain (§3.1.6).

### *3.1.2 High sensitivity caesium-vapour magnetometers*

Renewed interest in geophysical survey over weakly magnetised sites has arisen, partly, from the wider availability of high sensitivity caesium-vapour field magnetometers. Initially, such instrumentation was derived from aeromagnetic sensors beyond the financial means of many archaeological survey groups (e.g. Ralph et al. 1968, Becker 1995). However, the introduction of affordable field instruments offering enhanced sensitivity over fluxgate gradiometers has encouraged the increased use of such magnetometers (e.g. Cole et al. 1999).

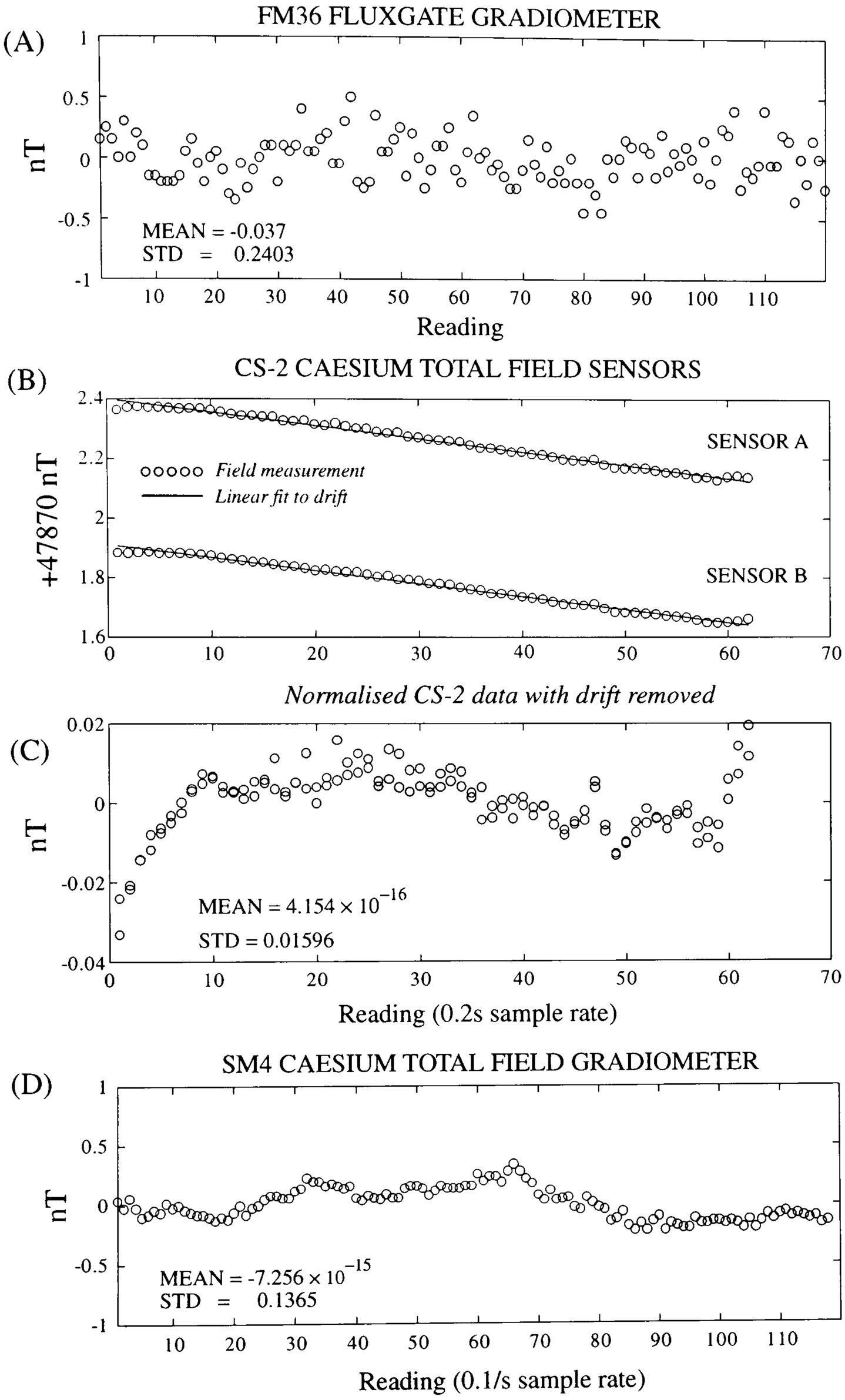


***Figure 3.1*** *Experimental determination of instrument noise for three stationary field magnetometers. (A) Geoscan FM36 fluxgate gradiometer, (B) uncorrected Scintrex CS-2 total field sensors, (C) CS-2 sensors following a linear correction for diurnal drift and (D) Scintrex SM4 total field gradiometer.*

Caesium vapour magnetometers obtain a sensitivity of up to 0.001nT (Becker 1995) through measuring the Larmor frequency (§1.3.1) of electrons in the ambient magnetic

field by means of a semi-transparent optically pumped cell (Telford et al. 1976; pp78-80). For optimum operation the angle between the optical axis of the measurement cell and the ambient magnetic field, known as the *tumble angle*, should not be less than 0-10° to avoid the dead zone of the instrument sensors (Scintrex 1996; p77). The two total field sensors may be configured either as a vertical gradiometer with a separation of between 0.5m to 2.0m, or as a single total field sensor referenced, for diurnal drift, to the second sensor at a fixed base station. In practice, except during periods of sun-spot activity (e.g. Ratcliffe 1970), diurnal drift is approximately linear and may be removed from survey data by adjusting each instrument traverse to a zero-mean. Thus the base station may be better employed as a second data collecting sensor (J. Faßbinder pers. comm.).

High sensitivity surveys in this study were collected with Jörg Faßbinder of the Bayerischen Landesamtes für Denkmalpflege, München, using two Scintrex CS-2 sensors mounted on a non-magnetic cart recording the total ambient magnetic field. The horizontal separation between the sensors was 0.5m and they were positioned ~0.15m above the ground surface. Figure 3.1(C) shows a comparison of stationary instrument noise tests that suggests anomalies <0.01nT should be detected by this instrument. For comparison, data collected with the more affordable Scintrex SM4 Caesium vapour magnetometer is also shown (Figure 3.1(D)) and demonstrates how this latter instrument is compromised by proximity of the control electronics and batteries.

In theory, the response of a total field instrument will be greater than that of a differential vertical gradiometer due to the inclination of the earth's magnetic field (approximately 68° from horizontal in the UK) and the subtraction of the signal from the upper and lower sensors. The vertical component decreases in magnitude with latitude towards the equator as the inclination of the Earth's magnetic field becomes horizontal. The effect of subtracting the two sensors in a gradiometer configuration will decrease with increasing vertical separation but may still be significant in instruments such as the Geoscan FM36 with a 0.5m separation (Figure 3.2(A)).

In addition, horizontal distributions of enhanced magnetisation/susceptibility are likely to be misinterpreted in gradiometer data as the constant gradient anomaly recorded will

be set to a negligible background value after zero-mean adjustment of the instrument traverse. Figure 3.2(B) demonstrates the response to such a horizontal distribution for vertical gradiometer and total field instruments respectively. Note how the gradiometer response (broken line in Figure 3.2(B)) is defined by the rapid change in gradient at the edge of the target.

Following the correction for heading errors both gradiometer and total field data are presented as a distribution in mean nano-Tesla (nT) around a nominal zero mean whose total magnitude will vary with the soil conditions at the site and the strength of the earth's ambient magnetic field.

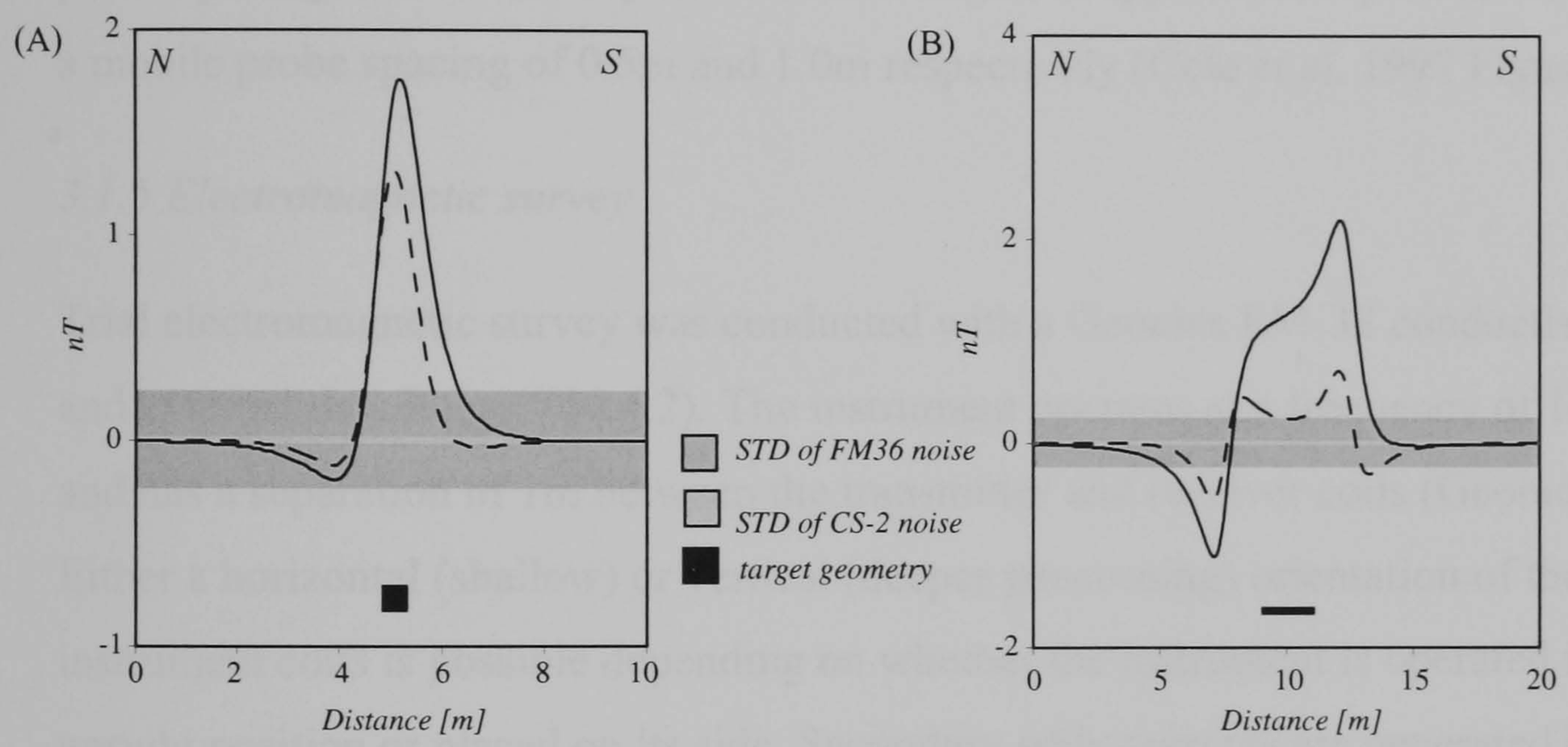


***Figure 3.2*** *Theoretical variation of the total induced magnetic field (solid line) and gradient of the vertical component for two sensors separated by 0.5m (broken line). In the first model (A) the target feature is a 0.5m cube with a volume susceptibility contrast of $\kappa = 10 \times 10^{-5}$ (SI). The second model (B) shows a similar magnetic contrast for a 2.0m square laminar sheet of thickness 0.2m. A field magnitude of 55000nT, inclination = 68° and declination = 0° was assumed for both models. The target was 0.75m below the instrument sensors. Empirically derived noise limits from Figure 3.1 are also shown on the figure.*

### *3.1.3 Topsoil magnetic susceptibility survey*

Magnetic susceptibility data were collected both as a reconnaissance survey technique to identify areas of increased anthropogenic enhancement and from the stripped topsoil surface of selected sites prior to excavation. The reconnaissance surveys were conducted along linear transects where ~100g soil samples were collected at 15m intervals for subsequent laboratory measurement following the procedures described in §3.3.1 below. Details of *in situ* volume susceptibility measurements for topsoil and

stripped excavation surface surveys are provided in Table 3.1. The use of such measurements is well documented (e.g. Clark 1990; pp104-105, Dearing 1994; pp25-26) and the limitations with regard to depth of penetration have also been investigated (Lecoanet et al. 1999).

### *3.1.4 Earth resistance survey*

Earth resistance measurements (Table 3.1) were made using the twin-electrode configuration and a mobile probe spacing of 0.5m or 1.0m (Clark 1990; pp44-46). The use of a multiplexor system allowed the simultaneous acquisition of data at the two mobile probe spacings and an increased sample interval for the shallow 0.5m mobile probe spacing. The sensitivity to resistance targets is approximately 0.75m and 1.5m for a mobile probe spacing of 0.5m and 1.0m respectively (Cole et al. 1997 Figure 7).

### *3.1.5 Electromagnetic survey*

Trial electromagnetic survey was conducted with a Geonics EM-38 conductivity meter and external data logger (§4.4.2). The instrument operates at a frequency of 14.2KHz and has a separation of 1m between the transmitter and receiver coils (Geonics 1992). Either a horizontal (shallow) or vertical (deeper penetrating) orientation of the instrument coils is possible depending on whether the instrument is operated in an upright position or placed on its side. Secondary eddy currents are generated by the primary transmitter signal within any conductive bodies close to the instrument and a combination of these two components is detected at the receiver coil. The received signal may then be separated into an in phase and quadrature component, with respect to the primary signal, that under typical field conditions are found to be proportional to the conductivity and magnetic susceptibility of the subsurface respectively (Scollar et al. 1990; pp541-6, Cole et al. 1995, Linford 1998).

### *3.1.6 Sampling intervals, errors and noise*

Repeated measurement of a given quantity subject to some form of random error or "noise" will produce a normal or Gaussian distribution about the mean of the observations (Topping 1972). As the distribution of these errors will, with respect to the true value $x_0$, be both positive and negative the sum of the error made on a repeated measurement will tend to zero and the arithmetic mean of the measurements will tend to

$x_0$. In practise, geophysical field observations may be improved by *stacking* repeated measurements at the same sample station to reduce noise. However, when the instruments are continuously in motion it is not possible to repeat measurements at the same sample station and only a single measurement is recorded. The situation is partially improved with caesium vapour magnetometers where the instrument electronics allow considerable oversampling along the traverse at an effective sample interval <0.1m that may later be interpolated to the desired sample interval by summing a number of adjacent readings.

***Table 3.1**; Summary of geophysical instrumentation and field methodology (1ha = 10,000m$^2$)*

| *Survey type* | *Instrument* | *Area* | *Sampling interval & Parameters* | *Comments* |
|---|---|---|---|---|
| *Magnetic* | Geoscan FM36 | 35ha | 0.25m × 1.0m | Standard reconnaissance sampling interval |
| | | 0.5ha | 0.25m × 1.0m + lowered sensor + sample averaging | High sensitivity methodology for weakly magnetised sites |
| | Scintrex CS-2 | 1.5ha | 0.5m × 0.5m | High sensitivity caesium vapour magnetometer |
| *Magnetic Susceptibility* | Bartington MS2 + MS2D field loop | 4 ha | 15m × 15m | Additional transects were also measured from topsoil samples |
| | Randall MS meter + search loop* | 1ha | 0.5m × 0.5m | Trial survey of stripped excavation surfaces |
| *Earth resistance* | Geoscan RM15 + MPX15 | 2ha | 0.5m × 1.0m<br>1.0m × 1.0m | 0.5m mobile probe spacing (shallow)<br>1.0m mobile probe spacing (deeper penetrating) |
| *Electromagnetic* | Geonics EM38 | 0.5ha | 0.5m × 1.0m | Trial survey of both in-phase (susceptibility) and quadrature phase (conductivity) |
| *GPR* | Pulse Ekko 1000 | n/a | 0.05m | Inconclusive trial of GPR with 450Mhz centre frequency antenna |

**Equivalent to the Bartington MS2 system*

Similarly, whilst the resolution and identification of anomalies increases with a closer spaced sample interval (e.g. Schmidt and Marshall 1995) there are practical limitations imposed by both the data logger memory of the Geoscan FM36 and the time required to collect closely spaced instrument traverses. At Yarnton a rectangular sampling grid with measurements at 0.25m intervals along parallel NS traverses separated by 1.0m was used for the reconnaissance fluxgate gradiometer surveys. For more detailed high sensitivity surveys conducted with both the fluxgate and the caesium vapour instruments the distance between traverses was reduced to 0.5m.

In practise, the minimum dimensions of an anomaly likely to be detected by a survey are given by the *Nyquist frequency*, defined as half the sample interval (Schmidt and Marshall, 1995). For the above sample intervals this will be 0.5m and 0.25m for the reconnaissance fluxgate and high sensitivity surveys respectively. However, under field conditions the signal recorded by any geophysical instrument will be a sum of the anomaly due to the target body and a combination of various systematic and random noise terms. These will vary dependent upon the geophysical technique and the particular instrument in use but in general will include the following:

*Instrument Noise* An intrinsic limit to sensitivity is imposed by the electronic components of the instrument itself and has been discussed in §3.1.1 and §3.1.2.

*Motion induced noise* Most modes of geophysical data acquisition are either semi-continuous (e.g. magnetometer surveys) or conducted rapidly between sample stations (e.g. earth resistance). This may lead to additional sources of noise due to the gait of the operator. The topography of the terrain may also induce an additional anomaly if the height of the instrument above the ground surface can not be held level.

*Heading errors* Magnetometers are often sensitive to the orientation of the ambient field including both the direction of the Earth's magnetic field and any component due to acquisition equipment itself. The term is derived from aeromagnetic surveys where the errors are largely due to changes in the induced magnetisation of the aircraft with direction (J. Milsom pers. comm.). For terrestrial surveys heading errors are most likely to occur with modular magnetometer systems where the instrument sensors may be influenced by location of external battery packs and console electronics, either worn by

the operator on a harness (e.g. Scintrex SM-4) or mounted on a cart system (e.g. Scintrex CS-2). In addition, fluxgate gradiometers become highly sensitive to the orientation of the Earth's magnetic field if the two sensors are not maintained in an accurate vertical alignment. When heading errors do occur, they may be eliminated by altering data from each traverse to a zero mean at the possible expense of removing genuine anomalies running parallel to the survey traverses.

*Thermal drift* Fluxgate instruments are often prone to a degree of thermal drift due to a combination of the Barkhausen effect in the mu-metal cores of the sensors (§1.5.3) and the expansion/contraction of the sensor housings. This may be minimised by avoiding rapid changes of temperature before data acquisition.

*Position errors* Geophysical survey data are generally assumed to be collected from a regular rectangular survey grid with a known sample interval. Any deviation from this sample interval during acquisition may lead to the target anomalies being misrepresented in the final data set, particularly for small features close to the sample interval of the survey.

Figure 3.3 illustrates the influence of varying levels of simulated noise on a range of different sample intervals assessed over the theoretical response from a 10m square enclosure ditch containing a central group of four small 0.5m square pits. Resolution of the anomalies from the four closely spaced pit features is only possible when the separation between parallel instrument traverses is reduced to 0.5m. However, with the addition of Gaussian noise approaching the peak magnitude of the target anomalies (~2nT) this resolution is lost.

It is of interest to compare the theoretical response of the 0.25m × 1.0m and 0.5m × 0.5m as both have a similar sample density per unit area and thus will fill the limited memory capacity of the FM36 instrument at a similar rate. However, the reduced interval between the survey transects for the 0.5m × 0.5m will require approximately twice as long to collect in the field. The memory of the FM36 can hold 14,400 readings and supports a maximum baud rate that requires approximately 15 minutes to complete the transfer of data to an external computer. In practice, reducing the sample interval may often double the amount of time required to survey a given area when both the


***Figure 3.3*** *The influence of random Gaussian distributed random noise on model data calculated over a range of target features with a susceptibility contrast of* $\kappa = 10 \times 10^{-5}$ *from the background.*

additional time required to acquire the data and more frequent downloads to an external computer are considered.

Under conditions of low noise (<1nT) the 0.5m × 0.5m sample interval demonstrates a greater resolution of the target anomalies but this advantage is rapidly lost as the noise component increases. Due to the increased rate of data acquisition at a 1.0m traverse interval this sample interval is recommended under typical field conditions over weakly magnetised features.

Reducing the sample interval to 0.5m × 1.0m would, of course, halve the memory requirement for the same unit area and increase the rate of field acquisition. However, analysis of the theoretical data demonstrates that a penalty in resolution will occur in the case of both the noise free and noise inclusive models (Figure 3.3).

## *3.2 Sediment Sampling*

### *3.2.1 Bulk soft sediments*

Sediment samples were collected in 10cc polystyrene containers free of magnetic impurities with a tapered entry aperture rim and an exhaust hole for expelled air in the base. Flush fitting lids provide a final sample with an outer diameter identical to a standard 1 inch rock drill core. Soft or friable sediments may therefore be sampled *in situ* with reduced risk of deforming the material during the sampling procedure. All samples were stored in air-tight containers and initial measurements were made as soon as possible following recovery to avoid alteration due to oxidation and drying (Crockford and Willett 1995a, Crockford and Willett 1995b). Loose sand and gravel were secured within the sample containers by tightly wrapping the sample in food grade self-adhesive plastic film to prevent mechanical movement during measurement.

Excavated archaeological features were identified by a unique feature number and were recorded in section including the identification of each specific layer of soil/sediment, referred to as a context, identified by a universal context number applied throughout each site. Individual samples collected from such features also received a unique sample number and their location, with respect to the observed context layers, is shown overlaid upon section drawings of the relevant features (Chapters 4 and 5). For clarity, on these

drawings feature, context layer and sample numbers are contained within square, circle or diamond shaped outlines respectively.

### *3.2.2 Orientated samples*

Samples from suspected thermoremanent features were collected following the method described in Clark et al. 1988 where a nylon button is attached to an *in situ* bulk sample and a fiducial mark added. When appropriate, samples were consolidated with a 15% solution of Poly Vinyl Acetate (PVA) in acetone prior to measurement in a low speed spinner magnetometer (§3.3.4). Soft sediments selected for measurement of a detrital remanent magnetisation were sampled following the procedure outlined in §3.2.1 and a fiducial mark was added to the sample container for subsequent orientation. In both instances, the orientation of the fiducial mark was made relative to absolute north determined in the field with a gyro-theodolite.

### *3.2.3 Rock magnetic sub-samples*

Rock magnetic measurements of hysteresis, low temperature magnetisation and frequency dependence of susceptibility (determined with the Lakeshore susceptometer) required ~100mg sub-samples to be prepared from the bulk sediments. These sub-samples were air dried at room temperature and subsequently ground to a fine powder in a pestle and mortar. The sample could then be packed in a pharmaceutical gelatin capsule with an approximate volume of 1cc for measurement.

## *3.3 Laboratory measurements and qualitative analysis*

A number of authors have investigated the variation of room temperature magnetic parameters for a range of magnetic minerals of known grain size and composition. Many excellent summaries of this work are available (e.g. Stacey and Banerjee 1974, Tarling 1983, Thompson and Oldfield 1986, O'Reilly 1984, Dekkers, 1988, Dekkers and Linssen 1989, Butler 1992, Dunlop and Özdemir 1997, Peters and Thompson 1998) and all demonstrate the considerable overlap of magnetic parameters that exist for differing mineral types. Therefore, any attempt to identify magnetic minerals based on a single magnetic parameter is unrealistic and an approach using a combination or ratio of parameters is required.

Table 3.2 provides a summary of the laboratory instrumentation and operating parameters discussed in greater detail in this section. Throughout the study, sample storage, preparation and measurement was conducted in ways designed to reduce the possible alteration of sediments through oxidation and drying (e.g. Walden 1999). In addition, measurements were made in ascending order of magnitude of the required laboratory field, starting with the determination of initial susceptibility.

### *3.3.1 Initial low field magnetic susceptibility*

This quantity is defined as the *reversible* susceptibility and is measured by the application of a weak inducing field (Table 3.2; Figure 3.4(D)). In this study all bulk sediment samples were measured with a Bartington Instruments MS2 susceptibility meter and MS2B 10cc laboratory coil on the $0.1 \times 10^{-5}$ (SI) sensitivity range following calibration with a known susceptibility sample of a paramagnetic salt. Linear drift between measurements was corrected following a procedure adapted from Dearing (1994) and each reported value represents an average of at least three measurements. In addition, the paramagnetic contributions of the plastic sample holder and sample packing material were determined and the effects subtracted from the final reading. The mass of each sample was determined after air drying following the completion of all rock magnetic measurements.

The Bartington MS2B laboratory coil is calibrated to provide an accurate determination of volume susceptibility for a 10cc sample. Thus the volume susceptibility of a sample will be misrepresented should the actual measurement volume vary from this figure. However, empirical measurements of varying volumes of a known susceptibility paramagnetic salt demonstrate that measurement error is <3% for sample volumes of ≥3.9cc (Dearing 1994: pp22). All samples within this study met this volume requirement.

For consistency, all initial susceptibility measurements made with the Bartington meter are given in dimensionless units of *volume susceptibility*, κ. These data were subsequently reduced to *mass specific susceptibility*, $\chi$, with units of $m^3kg^{-1}$ through division of the volume specific susceptibility by the density of the sample calculated from the final air-dried mass of each sample. The accuracy of the Bartington meter, when correctly calibrated, is given by the manufacturer as equal to the minimum

sensitivity of $0.1 \times 10^{-5}$. However, in practice the repeatability of measurements was never worse than $0.3 \times 10^{-5}$ and therefore the most probable fractional error was calculated to be better than 4% for samples with $\kappa > 10 \times 10^{-5}$ and to increase to an unacceptable level (>20%) for samples with $\kappa < 1 \times 10^{-5}$. Mass specific measurements will be subject to additional error due to the experimental determination of the sample density from the mass (<0.01%) and any variation from the assumed 10cc volume.

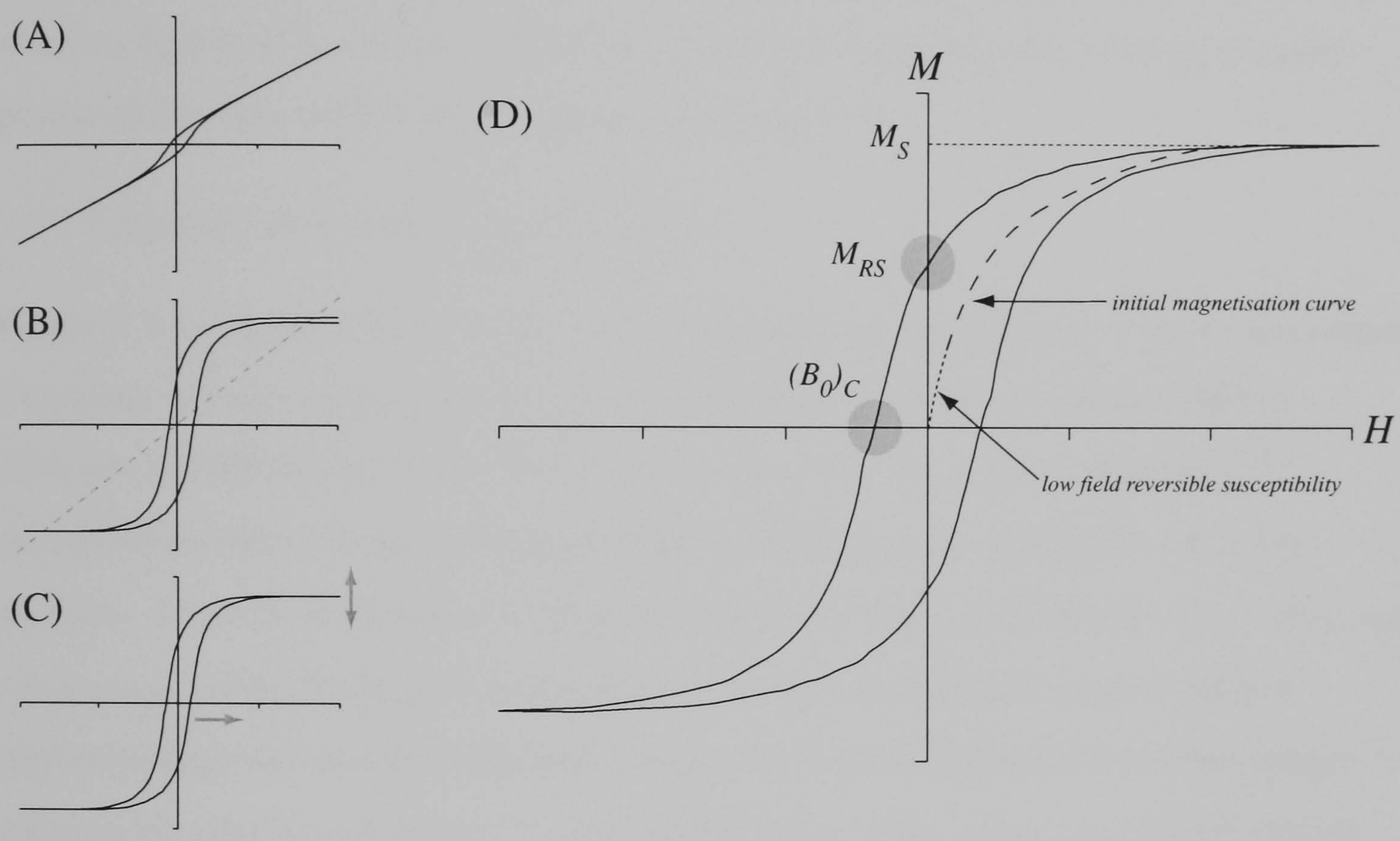


***Figure 3.4*** *Graphical depiction of hysteresis loop data processing and definition of key parameters. The paramagnetic component (A) is subtracted to the ferri/ferro magnetic hysteresis loop (B) that is then corrected for instrumental errors such as the non-closure of the outer branches and symmetry about the origin (C). The resulting hysteresis loop (D) is described by the key parameters $M_S$, $M_{RS}$ and $(B_0)_C$. Note the initial susceptibility calculated from the reversible, linear portion of the curve.*

The mass specific susceptibility of magnetic minerals covers a wide range of values and a considerable overlap between individual mineral types occurs due to variation with grain size and composition (e.g. Maher 1988). Discrimination is further complicated in environmental samples by the typically low concentrations of ferrimagnetic material encountered (<0.01%) and the often significant contribution of dia- and para- magnetic material such as sand or clay. However, as Dearing (1994) suggests, the susceptibility of environmental samples with $\chi \leq 2 \times 10^{-8}$ [$m^3kg^{-1}$] may, in general, be attributed to the

contribution of the paramagnetic clay fraction alone since in such samples the presence of significant secondary ferrimagnetic minerals is unlikely.

The susceptibility of secondary ferrimagnetic material is more complicated as background values will be heavily influenced by the parent geology (Dearing et al. 1996b). For the Yarnton study site average topsoil mass specific magnetic susceptibility varied between ~$20 \times 10^{-8}$ [$m^3kg^{-1}$] on the floodplain and ~$30 \times 10^{-8}$ [$m^3kg^{-1}$] for the raised gravel terrace. Thus susceptibility values greater than these average figures are likely to represent more significant concentration of ferrimagnetic material, possibly produced through anthropogenic enhancement (§2.2.4).

### *3.3.2 Frequency dependence of susceptibility*

Figure 3.5(A) demonstrates the theoretical variation of susceptibility with measurement frequency for superparamagnetic spherical magnetite particles of radius 0.009 to 0.016$\mu m$ calculated following Worm (1998). Note that the initial steep decay of susceptibility becomes approximately linear for frequencies >500Hz for very fine particles. Thus the difference between the dual frequency measurements, $\kappa_{FD} = \kappa_{LF(470Hz)} - \kappa_{HF(4700Hz)}$, of the Bartington meter may be used to estimate the concentration of superparamagnetic material within the sample. It is often normalised to a percentage value of the total low frequency susceptibility, $\kappa_{FD\%} = (\kappa_{LF} - \kappa_{HF}) / \kappa_{LF}$. Many studies demonstrate that $\kappa_{FD\%}$ for environmental samples will fall within a range of 0→ 20% limiting the confident determination of frequency dependence to samples with $\kappa > 10 \times 10^{-5}$.

For comparison the frequency dependent susceptibility of a limited number of samples was determined at room temperature between 0.04→4kHz on a Lakeshore Cryotonics 7130 AC Susceptometer. The manufacturer claims a sensitivity of $2 \times 10^{-8}$ (SI) at an applied field of magnitude 80 $Am^{-1}$ identical to the Bartington meter. Figure 3.5(B) shows the frequency dependence of susceptibility for a sample containing a high concentration of superparamagnetic particles. The percentage frequency dependence was calculated from this and other similar curves by analysis of the difference in susceptibility between 0.4 and 4.0kHz. In addition, to determine the error associated with a calculation based on just two measurements the frequency dependence was also

estimated from the slope of a linear fit to eight data points between the same frequencies.

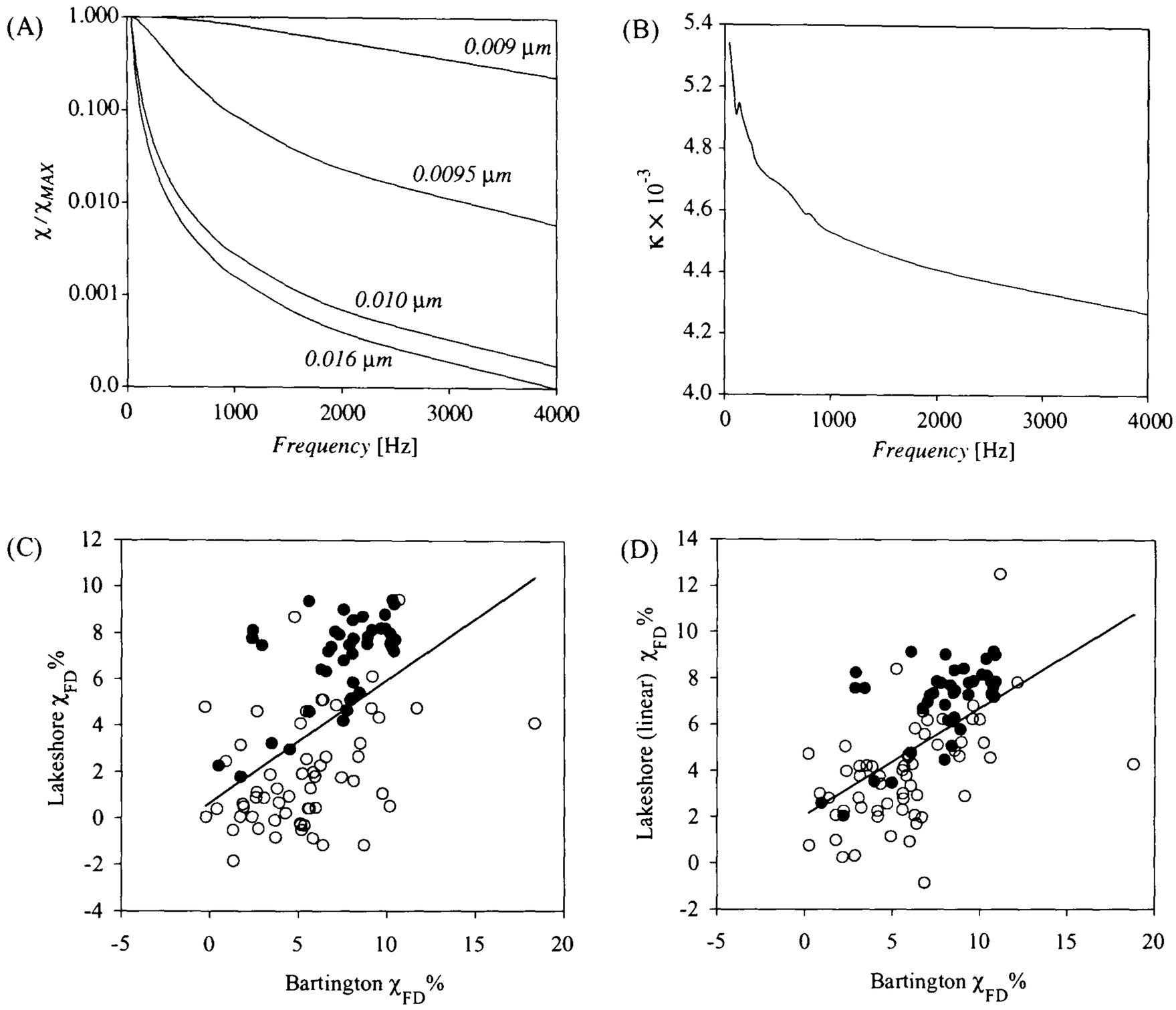


***Figure 3.5****(A) Theoretical variation of normalised susceptibility for spherical magnetite particles of radius 0.009 to 0.016μm (Worm 1998). (B) Typical environmental sample measured over the same frequency range. Comparison of frequency dependence measured with the Bartington and Lakeshore instruments at frequencies of 0.4 and 4kHz is shown in (C) and for a linear best fit (least squares regression) to the Lakeshore data in (D). Solid/open symbols denote samples with $\kappa_{LF} > 30 \times 10^{-5}$ / $\kappa_{LF} < 30 \times 10^{-5}$ respectively.*

The correlation between the Lakeshore dual-frequency and linear-fit values and values derived from the Bartington system are shown in Figures 3.5(C) and 3.5(D). In both figures samples with $\kappa > 30 \times 10^{-5}$ are distinguished from weaker samples by plotting as a solid symbol. Whilst an apparent linear relation between the Lakeshore and Bartington $\kappa_{FD}$% is suggested by this data there is a considerable degree of scatter (least squares regression coefficient $R^2 = \sim 0.3$) that may, in part, be due to the non-homogeneous

nature of the sediments and the different volume of sample required by the two instruments. It is of interest to note that the weaker samples consistently plot below the best-fit linear trend line suggesting the Bartington meter underestimates the frequency dependence of these samples. This is not entirely surprising as such weak samples are likely to contain a considerable concentration of paramagnetic material, diluting the response due to superparamagnetic particles (Worm 1998). The presence of titanomagnetite within the samples may also complicate the comparison of frequency dependence as synthetic samples of this mineral have been shown to exhibit a strong field dependence that may vary between instrumentation (Jackson et al. 1998). Recent research suggests that the applied field used by some Bartington meters varies in magnitude between the two measurement frequencies (de Wall and Worm 1999).

*3.3.3 High/Low temperature susceptibility*

A Geofyzika KLY-2 Kappabridge susceptometer with CS-3 cryostat and furnace was used to determine the variation of susceptibility over a temperature range of -196 →700°C for selected ~100mg powder sub-samples. The measurements were made in an 720Hz alternating field with a magnitude of 300Am$^{-1}$ to a sensitivity of ~$1 \times 10^{-7}$ (SI) after correction for the diamagnetic contribution of the empty cryostat or furnace. Redox conditions in the high temperature furnace were partially controlled through the supply of a continuous blanket of argon gas over the sample to exclude oxygen. However, it proved impossible to completely avoid the chemical alteration of organic rich sediments.

Comparison of susceptibility between the Bartington MS2 meter and the Kappabridge is hampered by the differing applied measurement fields. Studies made on magnetically soft titanomagnetites demonstrate that irreversible hysteresis behaviour begins in low magnitude AC fields resulting in a considerable quadrature susceptibility and field dependence of the in-phase (initial) susceptibility (Jackson et al. 1998).

The Curie or Néel temperatures for many common minerals may be used to identify a specific mineral through the abrupt change in magnetic behaviour that will occur (e.g. Table 1.1, Orlicky 1990). However, the loss of susceptibility due to a weak ferrimagnetic mineral within a paramagnetic clay matrix may be difficult to detect and in this case the variation of a laboratory induced IRM (held only by the ferrimagnet)

would prove a more suitable means of identifying the specific mineral (e.g. Lowrie 1990).

In theory, the Curie or Néel temperatures of a mixture of different magnetic minerals should be readily distinguished from thermo-magnetic curves. However, chemical alteration on heating may often mask the true Curie/Néel temperature of the original mineral phase. In certain cases the recognition of such chemical alterations may itself prove diagnostic for the identification of thermally unstable magnetic phases such as greigite (e.g. Snowball 1997) and lepidocrocite (e.g. Marmet et al. 1999). It has also been suggested that the thermo-magnetic behaviour of (Ti substituted) maghaemite may be differentiated from magnetite through the presence of an initial Curie temperature just above 600°C followed by the subsequent alteration to haematite producing a secondary Curie temperature of ~675°C and a significantly reduced susceptibility on cooling (Özdemir and Banerjee 1984, Walden et al. 1999; Fig 11.8(b)).

Progressive thermal demagnetisation of an orientated sample subjected to varying laboratory fields along orthogonal axes allows the resulting magnetisation to be expressed in terms of the three field-related coercivity classes. France (1997) has adapted this method for the discrimination of goethite from haematite by thermally demagnetising an IRM created in a laboratory field in excess of 1T. This IRM is initially subjected to a DC 400mT field orthogonal to the original magnetisation that will result in distinct "low" (<400mT) and "high" coercivity magnetisations along the orthogonal sample axes. Determination of the high coercivity mineral present may then be made through the decay of IRM with temperature as the Néel temperature of goethite (~120°C) is considerably lower than that of haematite (~675°C). This technique may also be adapted for low temperature measurement by cooling the sample in liquid nitrogen (-196°C) and recording the variation of IRM on warming to ambient. In this case goethite will distinguish itself through a characteristic increase in remanence on warming back to room temperature (Dekkers 1988).

In practical terms, the thermomagnetic analysis of remanent magnetisation will be dependent upon the grain size of the material present, as very fine grained material will not retain a stable remanence - even at room temperature. Thus the use of in field magnetic parameters, such as saturation magnetisation or susceptibility, may well prove

more suitable under these circumstances. Furthermore, for organic rich sediments it is good experimental practice to retain part of the sample for repeat measurement of inflection points identified within an initial high temperature run. This procedure will allow reversible Curie/Néel temperatures to be distinguished by heating to the specific inflection point and allowing the sample to cool. Chemical alteration of the constituent minerals will be distinguished by the non-reversible nature of these curves.

### *3.3.4 Natural Remanent Magnetisation (NRM) and the Köenigsberger ratio*

Orientated field samples were measured with an Agico JR-5A spinner magnetometer mounted in a triple-axis system of Helmholtz coils to null the static ambient field (e.g. Collinson 1983; pp121-130). The magnitude and direction of any remanent magnetisation present is determined by automatically rotating the sample through six independent measurement positions to a claimed sensitivity of $2.4 \times 10^{-6}$ $Am^{-1}$.

Whilst the identification of magnetic minerals can not be directly inferred from either of these parameters the presence of a significant NRM within a sample may well provide additional evidence for the dominant domain state of the remanence carriers. Samples dominated by the grain-grain interaction of fine viscous particles will demonstrate an NRM orientated with the current ambient field at the site that will be easily removed through low field AF demagnetisation in peak fields of 5mT or less (Collinson 1983, Tarling 1983). A more stable NRM orientated at a differing angle to the ambient field indicates the presence of a single or multi domain mineral that has acquired a remanence through one of the mechanisms discussed in §2.2.

Continuous AF demagnetisation may also reveal a diagnostic coercivity spectrum for a sample related to the mineral type and grain size distribution. In practice the peak demagnetising field of laboratory equipment is only suitable for the removal of NRM held by low coercivity minerals such as magnetite or maghaemite. Samples retaining a significant NRM following demagnetisation to 200mT must therefore contain a high coercivity mineral such as haematite or goethite.

### *3.3.5 Demagnetisation of NRM*

Spurious components of Viscous Remanent Magnetisation (VRM) were removed from NRM samples through step-wise, triple-axis alternating field demagnetisation using a D-Tech D2000 microcomputer controlled coil system producing a peak demagnetising field of 200mT.

The presence of a viscous component is of importance due to the common occurrence of fine-grained ferrimagnetic minerals within soils and archaeological sediments (e.g. Linford 1994, Cole et al. 1995, Peters and Thompson 1999). This results in a significant component of Viscous Remanent Magnetisation (VRM) that may, under certain circumstances, be utilised as a means of physical dating (e.g. Heller and Market 1973, Borradaile 1994, Borradaile 1996, Borradaile and Brann 1997, Borradaile et al. 1999, Borradaile 1999). However, of greater significance is the contribution such a VRM will make to the magnetisation of a buried feature that may often equal or exceed the induced component (e.g. Graham and Scollar 1976, Eder-Hinterleitner et al. 1995).

### *3.3.6 Anhysteretic Remanent Magnetisation (ARM)*

Anhysteretic (free from hysteresis) remanence is imparted by subjecting a sample to a strong alternating field gradually decreased to zero in the presence of a small, steady field. Laboratory ARM was induced along a single direction in each bulk sample using a D-Tech D2000 AF demagnetisation system (§3.3.5) in peak 199mT AF field superimposed over a 0.05mT steady state field. The maximum 200mT AF field of this instrument was not applied to allow for the complete demagnetisation of ARM from samples if necessary. The ARM was measured in a JR5-A spinner magnetometer (§3.3.4) along the axis of the applied laboratory magnetisation using a single position sample holder and control software written by the author.

AF demagnetisation of the ARM was conducted following the procedure detailed in §3.3.5 along the axis of the laboratory induced field.

The acquisition of ARM is dependent upon the coercivity and domain state of the remanence carrier with the highest values reported for single domain magnetite (e.g. Gillingham and Stacey 1971, Johnson et al. 1975, Schmidbauer and Schembera 1987,

Dunlop and Argyle 1997). For a sample containing a broad spectrum of coercivities the ARM will depend on the magnitude of both the peak AF field and the steady state field. To facilitate the comparison of ARM data collected under differing experimental conditions the magnetisation value may be normalised by the magnitude of the steady state field resulting in a final determination with dimensions of mass specific susceptibility, $m^3kg^{-1}$, that is referred to as *anhysteretic susceptibility*, $\chi_{ARM}$ (King et al. 1982).

Taken as an individual parameter $\chi_{ARM}$ will be proportional to the concentration of remanence-carrying material in a sample. However, empirical measurements of minerals of known grain-size minerals demonstrate that a biplot of $\chi$ against $\chi_{ARM}$ provides a rapid means for establishing the relative grain-size and concentration of magnetite assemblages (e.g. Dankers 1978) that may be successfully applied to environmental samples (e.g. Banerjee et al. 1981, King et al. 1982, Dalan and Banerjee 1996). In addition, the latter biplot distinguishes high coercivity minerals such as haematite from magnetite (Banerjee et al. 1981; Fig. 3).

Stepwise AF demagnetisation of $\chi_{ARM}$ reveals a diagnostic coercivity spectrum for common magnetically soft minerals and indicates the greatest degree of variation occurs on application of a -40mT AF field (Peters and Thompson 1998; Figure 1). The latter authors also note the distinctive $\chi_{ARM}$ behaviour demonstrated by greigite and show that a biplot of $\chi_{ARM}$(-40mT)/$\chi_{ARM}$ against IRM(-100mT)/saturation IRM provides a reasonable distinction between this mineral and samples of magnetite, titanomagnetite and pyrrhotite. More detailed coercivity spectrum analysis may be obtained by applying the steady field through only a narrow window of the demagnetising field. By incrementing this window the partial Anhysteretic Remanence (*pARM*) of a sample may be defined over a spectrum of demagnetising AF fields where the relative magnitude of each pARM will be proportional to the concentration of material in the sample within this window of coercivity.

### *3.3.7 Isothermal Remanent Magnetisation (IRM)*

Isothermal remanence is acquired by a sample following exposure to a steady field at a given temperature (usually room temperature). Following the determination of ARM, bulk samples were subjected to a single axis 2.5T pulse field and subsequent

measurement of the induced forward acquisition field in a manner analogous to the ARM measurements (§3.3.6). The sample was then reversed (with respect to the initial induced field) and subjected to incremental back fields to a maximum of 1.0T. All laboratory fields were generated with an ASC PMU-10 pulse magnetiser with appropriate coils for the desired magnitude of field. The digital display of the pulse magnetiser allows the charging voltage to be set to within ±0.5V of the desired capacitor load resulting in a ±1.7mT error in the pulse field.

Additional IRM measurements were made on selected sub-samples during the determination of hysteresis parameters discussed in §3.3.8.

The stepwise acquisition of IRM is highly diagnostic of both mineral type and dominant grain-size (e.g. Thompson 1986). For all but the very highest coercivity minerals IRM is found to saturate within readily available laboratory fields of 1-2.5T and this maximum value is often referred to as *saturation remanent magnetisation* ((s)IRM). However, it should be noted that the coercivity of remanence of goethite, a mineral commonly encountered within temperate soils, often exceeds 5T and it will not be saturated in the laboratory fields applied during this study (e.g. Lowrie and Heller 1982, Thompson 1986). A broadly linear relationship is found for natural samples when (s)IRM is plotted on a bilogarithmic scale against volume susceptibility ($\kappa$). Both indicate the concentration of magnetic material present (e.g. Thompson and Oldfield 1986; Figure 4.8). Empirical measurements on samples of known grain-size magnetite demonstrate that the ratio of (s)IRM/$\chi$ provides a concentration independent estimate of granularity (e.g. Thompson and Oldfield 1986; Figure 4.9).

In addition, the ratios of reverse field measurements normalised by (s)IRM can also be used to identify the dominant coercivity class. Backfield ratios of -30, -100, and –300mT have been applied following saturation in a 2.5T field to distinguish the contribution of low coercivity minerals such as (titano)magnetite from mid to high coercivity minerals such as haematite and goethite. The contribution of high coercivity minerals was investigated further through a backfield ratio of -1000mT and the -300mT backfield ratio is also presented as the widely adopted *S* ratio (e.g. Stober and Thompson 1979, Hilgenfeldt 2000):

$$S_{-300mT} = 0.5 \times \left(1 - \frac{IRM_{-300mT}}{(s)IRM}\right) \tag{3.1}$$

This normalised parameter is found to vary between 0 for samples dominated by high coercivity minerals and 1 for low coercivity minerals.

Both IRM and ARM (§3.3.6) demonstrate a strong grain size dependency for specific mineral types (e.g. Thompson and Oldfield 1986; Figure 4.10, Gillingham and Stacey 1971, Johnson et al. 1975, Oldfield 1994) and may be used to identify a dominant grain size by comparison with the behaviour of known size synthetic material (e.g. Banerjee et al. 1981, King et al. 1982, Thompson 1986). Such tests may be applied simply to identify stable remanence carriers from multi domain (MD) particles (e.g. Lowrie and Fuller 1971) or combined with susceptibility data for the identification of a narrow grain size range, (e.g. King et al. 1982, Oldfield 1994, Walden et al. 1999; Figure 7.3).

### *3.3.8 Hysteresis*

Magnetic hysteresis is the term used to describe the lag between the magnetisation of ferromagnetic material and the external inducing field. It is generally measured through exposure of a sample to a cyclic external field producing a graph of sample magnetisation with the form of a symmetric loop. In this study, selected sub-samples were measured on a Princeton MicroMag Vibrating Sample Magnetometer (VSM) to determine forward acquisition of IRM, back-field IRM and in-field hysteresis in steps of 5mT to ±1.0T. This instrument has a sensitivity of $2 \times 10^{-8}$ $Am^2$ and may be operated with an additional furnace between room temperature and 927°C. Room temperature measurements were made on ~100mg sub-samples (§3.2.3) mounted in a pharmaceutical gelatin capsule ("gelcap") held within a plastic drinking straw.

Hysteresis data were treated numerically following von Dobeneck (1996) involving the interpolation of the magnetisation values to a symmetric distribution of applied fields, centring correction of the loop about the origin and calculation of the paramagnetic/diamagnetic contribution from the approach to saturation at high-fields. Figure 3.4 illustrates the application of the above procedure to data from a representative sample and indicates the standard hysteresis parameters of Saturation Magnetisation ($M_S$), Remanent Saturation Magnetisation ($M_{RS}$) and Coercive Force ($B_C$) that may be extracted from the loop. Analysis of back-field IRM curves provided a

value for the Coercivity of Remanence ($B_{CR}$), defined as the field necessary to reverse half the saturated magnetisation of the sample.

One advantage of the high temperature measurement of hysteresis parameters for the determination of Curie points over measurement with the Kappabridge (§3.3.3) is the increased sensitivity for weakly magnetic samples. This may prove particularly useful for samples consisting of a low concentration of ferri/ferro magnetic material heavily diluted in a paramagnetic matrix.

Hysteresis behaviour demonstrates a strong mineral-type and grain-size dependence that may be used to identify the dominant magnetic mineralogy within a sample (e.g. Day et al. 1977, Dankers 1978, Clark 1984, Dunlop 1986, Schmidbauer and Schembera 1987, Worm and Markert 1987, Dekkers 1988, Argyle and Dunlop 1990, Snowball 1991, Brown and O'Reilly 1996, Peters and Thompson 1998, Keller and Schmidbauer 1999). Indeed the study of synthetic known size (titano)magnetites by Day et al. 1977 remains a fundamental aid to determining the domain state of magnetic material by comparison through the $(B_0)_{CR}/(B_0)_C$ against $M_{RS}/M_S$ biplot proposed by these authors. However, such interpretation may be flawed if a mixture of magnetic minerals is present or if the material is not limited to a narrow grain-size range. For example, the presence of SP material within a sample will simultaneously lower the value of $(B_0)_C$ and increase $M_S$. This will lead to samples plotting to the bottom right of the Day biplot and may well lead to the misidentification of the domain state. In addition, it is essential to correct hysteresis loop data for the presence of any paramagnetic component as this too will lead to a misleading increase of $M_S$ that may be significant in more weakly magnetised environmental samples.

### *3.3.9 Mössbauer spectroscopy*

A Ranger Scientific Mössbauer spectrometer was used with a $^{57}$Co source to examine valency state and bonding of $^{57}$Fe within a limited number of samples (e.g. Frankel and Blakemore 1991, Cranshaw et al. 1985). However, despite the success reported by other authors for similar environmental samples (e.g. Longworth and Tite 1977, Longworth et al. 1979) the concentration of iron minerals was apparently too low to produce useful results.

### *3.3.10 Low Temperature magnetisation*

The temperature dependence of magnetisation for selected samples was measured continuously at 5K intervals through a cycle of exposure to a 2.5T pulse field at room temperature, cooling to 20K, reapplication of the 2.5T field at 20K and warming back to 300K. The measurements were made with a Quantum Design Magnetic Property Measurement System (MPMS) model 5S or XL. Both instruments have been modified to provide a near zero-field environment in the vicinity of the sample (~200-300$\mu$T) and utilise a reciprocating-sample option to increase the sensitivity for weak samples (Jackson and Marvin 1998)[1].

Sediments suspected to contain biogenic magnetite were measured using a modified zero-field/in-field cooling cycle described by Moskowitz (1993) for the identification of intact chains of magnetosomes. Samples were initially cooled from room temperature to 20K in zero-field before the application of a 2.5T pulse field that was then removed to allow zero-field measurement in 5K intervals on warming from 20-300K. The sample was then cooled again from 300-20K in a steady 2.5T field before a repeat zero-field measurement cycle on warming back to room temperature.

The variation of low temperature magnetisation or susceptibility may often identify a diagnostic transition due to the presence of a specific mineral. Perhaps the most widely recognised of these occurs close to the *Verwey transition,* $T_V$, of magnetite at ~120K, below which the cubic symmetry of the octahedral sublattice is slightly distorted to a monoclinic arrangement and magnetite converts from a semiconductor to an insulator (Verwey and Haayman 1941). Electron hopping between neighbouring $Fe^{2+}$ and $Fe^{3+}$ sites occurs above 120K and the cation sites become interchangeable, resulting in the equivalence of all <100> crystallographic directions in the perfectly cubic lattice. This transition greatly affects the single-ion anisotropy constant, $K_1$, of the $Fe^{2+}$ B lattice ions that are now constantly switching to and from the $Fe^{3+}$ state. $K_1$ is large and positive below 120K but becomes negative as electron hopping occurs above the Verwey transition resulting in a much reduced crystalline anisotropy and abrupt changes in remanent magnetisation, susceptibility and coercive force. The magnitude of these

---

[1] Measurements were also made on two similar instruments in the Department of Physics and Astronomy, UCL and at the Royal Institution. Both instruments had a 7T magnet that is difficult to fully quench and so the measurements were made in a constant 10mT field following a saturating field of 5T.

changes are found to vary with both the grain-size, oxidation and degree of substitution within the magnetite (e.g. Maher 1988; figure 4, Özdemir et al. 1993, Moskowitz et al. 1998, Muxworthy 1999).

Whilst a diagnostic loss of susceptibility may be detected in samples dominated by magnetite in practice this effect is often masked by the presence of a considerable paramagnetic fraction that increases significantly as $T \rightarrow 0$K (§1.3.2, Richter and van der Pluijm 1994). This may be overcome by measuring low temperature magnetisation (in zero field) that will be dominated by ferri/ferro magnetic components. Inflections within these curves may be further enhanced by taking the first derivative, $^{dM}/_{dT}$, of the experimental magnetisation curve.

Due to the temperature dependence of viscous behaviour (e.g. Blanco-Mantecón and O'Grady 1999, Liu et al. 1998) the unblocking spectra of very fine material may be revealed by cooling to the point where the grains enter the single-domain, non-viscous state. Experimentally, the unblocking spectra may be determined by analysing either the increase in susceptibility or the loss of remanence imparted at a low temperature (20K) on warming the sample back to ambient.

The interpretation of low temperature susceptibility/magnetisation data will be further complicated by the variation of the viscosity parameter with external factors such as temperature and the magnetic field (e.g. Tejada et al. 1993, Godhino et al. 1994 Schumann and Jahn 1995, Crew et al. 1998). In addition, the presence of grain-grain interactions (§1.7) and loss of remanence due to domain wall relaxation in multi-domain grains will further complicate the estimation of grain size distributions from magnetic viscosity data.

Unblocking spectra at high temperatures may also be used to estimate the grain size of more stable PSD/SD material (e.g. Krs et al. 1990). However, in addition to mineral specific phase changes, chemical alterations may further complicate the interpretation of such data.

### *3.3.11 Chemical dissolution methods*

The increased ratio of surface area to volume that occurs with fine-grained particles renders such material far more susceptible to chemical dissolution with reagents such as dilute hydrochloric acid or citrate bicarbonate dithionite (CBD). These techniques are generally employed for the chemical "cleaning" of palaeomagnetic rock samples to remove any spurious contribution to the NRM that may arise from sources such as the haematite coating around constituent sand grains (e.g. Collinson 1983; pp353-6). The major limitation of chemical dissolution techniques for rock samples is the porosity of the material that may lead to the uneven dissolution of magnetic minerals throughout the fabric. However, finely powdered environmental samples do not suffer from this disadvantage and chemical treatment may be used to dissolve increasingly soluble particles as the length of exposure or chemical reagent is strengthened (e.g. Hunt et al. 1995, Singer et al. 1995, Oorschot and Dekkers 1999). Whilst such data do not directly relate to the grain-size distribution of the sample, magnetic measurements of susceptibility or remanence parameters made throughout the exposure to the chemical reagent may well prove to be a useful proxy, particularly for the inter-comparison of samples from a similar source geology.

## *3.4 Interpretation of magnetic mixtures*

The success of the magnetic techniques for mineral characterisation discussed in §3.3 relies heavily upon the domination of the sample magnetically by a single mineral phase. This is clearly unrealistic for environmental samples that may often contain a mixture of ferri/ferro magnetic minerals further complicated by their dilution within a soil matrix dominated by para and dia magnetic material. Indeed, the conflicting magnetic contribution from a typical environmental sample will, in many cases, lead to the misidentification of the mineral phase and domain state / grain-size distribution present.

However, the qualitative identification of magnetic mixtures can be obtained from the analysis of a number of the measurement techniques discussed in this chapter:

### *3.4.1 Low temperature measurements*

The differing behaviour of paramagnetic and superparamagnetic material at low temperature allows these components to be identified from either low temperature susceptibility or remanence measurements. Indeed the theoretical variation of paramagnetic susceptibility with temperature (§1.3.2) may be employed to estimate and remove the paramagnetic contribution from experimental data (e.g. Hrouda et al. 1997, Richter and van der Pluijm 1994).

### *3.4.2 High temperature measurements*

From a qualitative stance the variation of magnetic parameters at high temperature allows the relative contribution of differing mineral phases to be assessed. However, this relies upon the constituent minerals of the mixture exhibiting discrete, non-overlapping thermal behaviour with well separated Curie/Néel points or alteration temperatures.

### *3.4.3 Hysteresis data*

Both in-field hysteresis and remanence measurements may indicate magnetic mixtures due to the presence of minerals with widely differing coercivities (e.g. Thompson 1986, Roberts et al. 1995, Tauxe et al. 1996). Interpretation is largely qualitative and must be based on the shape of the entire curve rather than an individual parameter or ratio derived from the data. In addition, the linear component of high field hysteresis may be used to estimate the concentration of paramagnetic material within a sample (§3.3.8). A semi-quantitative interpretation of such data is proposed in Chapter 6.

***Table 3.2*** *Magnetic parameters and ratios used during this study*

| *Parameter or Ratio* *(superscripts refer to instrumentation used)* | *Units of measurement* | *Comments* |
|---|---|---|
| $\chi^{1,2}$ | $[m^3kg^{-1}]$ | Mass specific magnetic susceptibility induced in a reversible $80Am^{-1}$ field. Proportional to concentration of ferrimagnetic minerals. |
| $\chi_{FD}{}^{1,3}$ | $[m^3kg^{-1}]$ | Frequency dependence of susceptibility calculated at two (0.47 or 4.7kHz)[1] or more[3] excitation frequencies. Loss of susceptibility with frequency indicates superparamagnetic material (Worm 1998). |
| $NRM^4$ | $[Am^2kg^{-1}]$ | Natural Remanent Magnetisation due to the preferential orientation of magnetic material in a sample. |
| Q | *dimensionless ratio* | Köenigsberger ratio of NRM to induced magnetisation. |
| $\chi_{ARM}{}^{4,5}$ | $[m^3kg^{-1}]$ | Anhysteretic Remanent Magnetisation produced by an AC demagnetising field (max. 199mT) in the presence of a steady field (0.05mT). Proportional to the concentration of fine stable single domain particles (King *et al* 1982). This parameter is normalised against the intensity of the steady field. |
| $\chi_{ARM\ x\,mT}{}^{4,5}$ | *dimensionless ratio* | Removal of $\chi_{ARM}$ acquired in a 199mT field by incremental AF demagnetisation to a peak field of $x$ mT. An initial field of $x$ = -40mT was used to indicate the ratio of 'soft' to 'hard' ARM. Additional values were used to investigate grain-grain interactions and establish the Median Destructive Field ($MDF_{ARM}$) which reduces $\chi_{ARM}$ to half of its initial value. |
| $(s)IRM_{+x\,mT}{}^{4,6,7}$ | $[Am^2kg^{-1}]$ | Isothermal Remanent Magnetisation (IRM) after exposure to incremental pulse fields $x$ from 0.001-1.8T. The coercivity spectrum can be derived from the gradient of the resulting IRM acquisition curve. $IRM_{1.8T}$ saturates the majority of magnetic material and is proportional to the ferrimagnetic concentration above the SD threshold. |
| $S_{-x\,mT}{}^{4,6,7}$ | *dimensionless ratio* | Ratio of $IRM_{+1.8T}$ to reverse fields of $x$ = -30, -100, -300 and -1000mT represented as $(IRM_{1.8T} - IRM_{-x\,mT}) / (2 \times IRM_{1.8T})$ for the discrimination of high/low coercivity mineral assemblages. Additional values of $x$ = 0.001 - 1.8T were applied to determine grain-grain interactions and the coercivity of remanence, $H_{CR}$. |

*Continued overleaf*

| | | |
|---|---|---|
| R | *Dimensionless ratio* | Wholfarth's 'R' ratio determined from IRM acquisition and demagnetisation curves normalised by (s)IRM. A value of $R = 0.5$ is expected for a SD assemblage and $R < 0.5$ indicates the presence of significant grain-grain interactions. |
| $\chi_{ARM}/\chi$ [1,4,5] | *dimensionless ratio* | This ratio can indicate the presence of finer stable single domain grain sizes. |
| $IRM_{+1.8mT}/\chi$ [1,4,6] | $[Am^{-1}]$ | Indicative of both mineralogy and dominant grain-size. However, mixtures of mineral types and concentrations will produce ill-defined results (e.g. both paramagnetic and superparamagnetic material will lower the value of this ratio). |
| $IRM_{+1.8mT}/\chi_{ARM}$ [4,5,6] | $[Am^{-1}]$ | Lower values of this ratio may be indicative of finer stable single domain grain sizes. |
| $M_S(B_{\pm 1.0T})$ [7] | $[Am^{-1}]$ | Measurement of the in field magnetisation $M_S$ produces characteristic hysteresis loops for ferrimagnetic material. For a sample of mixed mineralogy the resulting data represents a complex superposition of individual loops due to the composite minerals and grain size populations. |
| $H_C/H_{CR}$ *vs* $M_S/M_R$ [7] | *dimensionless ratios* | Values for the in field saturation ($M_S$) remanent magnetisation ($M_R$) and coercive force ($H_C$) determined from the hysteresis loop may be combined with the remanent coercivity ($H_{CR}$) to indicate the apparent grain-size/micro-structure of the sample (Day et al. 1977). |
| $IRM_{+x\ mT}(B, T_{10\text{-}350\ K})$ [8] | $[Am^{-1}]$ | Low temperature variation of IRM (or $\chi$) indicates the blocking temperature distribution of superparamagnetic material within a sample. Crystal lattice reorganisation may also prove diagnostic for specific mineral types (e.g. Verwey transition of magnetite). |
| $M_S(T_{300\text{-}900\ K})$ [7] | $[Am^{-1}]$ | High temperature variation of $M_S$ (or $\chi$) reveals high coercivity unblocking spectra and mineral identification through determination of Curie temperatures. Non-reversible thermomagnetic behaviour may also be indicative of mineral type through characteristic chemical alteration temperatures. |

Instrumentation:

[1] *Bartington MS2 AC susceptibility meter + dual frequency MS2B sensor*
[2] *Geophysica Kappabridge KLY2*
[3] *Lakeshore susceptometer*
[4] *Geophysica JR5A spinner magnetometer*
[5] *DTech AF demagnetiser*
[6] *Pulse magnetiser*
[7] *Princeton MicroMag VSM + high temperature furnace*
[8] *Quantum Design MPMS*

# *Chapter 4*

## *4.0 Results from the raised gravel terrace*

Geophysical surveys conducted on sites from the raised gravel terrace are reported here together with an analysis of the rock magnetic measurements conducted on samples from archaeological features revealed through subsequent excavation. In this respect, different feature types have been described in terms of the magnitude of magnetic response, their degree of discrimination from the background magnetic response of the site and the apparent success of magnetic techniques for the location of archaeological activity.

## *4.1 Introduction to the study area*

The study area consists of approximately 200ha of mainly agricultural land lying between the villages of Yarnton and Cassington in the Upper Thames Valley 5km north of the city of Oxford, UK (Figure 4.1). Planning permission for the extraction of aggregates was granted prior to the firm establishment of developer funded provision for archaeological investigations (PPG16 1990). However, due to the considerable research potential of the area, English Heritage funded a series of excavations undertaken by the Oxford Archaeological Unit (OAU) and provided more direct specialist scientific advice and assistance such as geophysical survey.

### *4.1.1 Archaeological background*

The threatened area lies mainly within the floodplain of the river Thames but also encompasses higher ground over the raised gravel terrace. In general, the identification of archaeological activity on the gravel terrace has been facilitated through the presence of substantial cropmark evidence (Featherstone and Dyer 1994) and surface artefact scatters visible in the modern plough soil. Initial excavation by the OAU on one of these cropmark sites at Worton Rectory Farm demonstrated the rich archaeological potential of the area through the discovery of Iron Age, Roman and Saxon settlements and a scatter of Neolithic and Bronze Age pits (Hey 1993b, Hey 1993a).

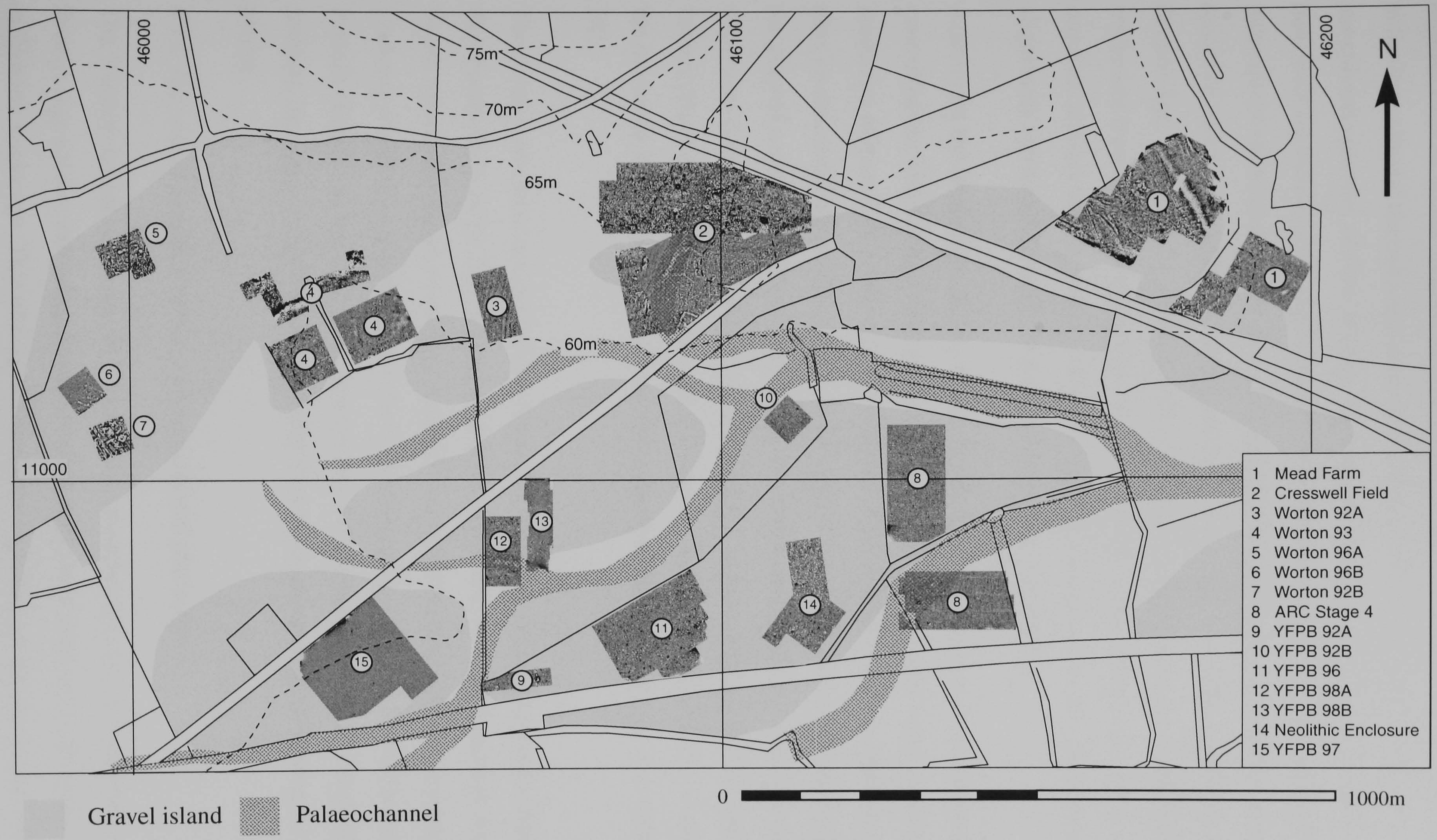


***Figure 4.1*** *Plan of the study area showing the location of geophysical surveys and geomorphology.*

Identification of archaeological activity on the floodplain proved more complicated due to the later alluvial deposits that obscure the formation of cropmarks. However, the unexpected recovery of flint, Bronze Age pottery sherds and burnt stone scatters during field walking indicated the significance of the floodplain for prehistoric settlement. Subsequent excavation, based on a 2% random trial trenching, revealed an exceptional record of continuous domestic settlement from the middle Neolithic to the end of the Bronze Age. This activity included both short-stay encampments and more permanent settlement represented by groups of circular buildings surrounding water holes with the domestic activity woven within a complex ritual landscape of burials, pit and posthole alignments and a rare example of a Neolithic funerary enclosure.

Activity on the floodplain was dominated by the course of former palaeochannels that controlled the habitability, communication and import of materials throughout the landscape (Figure 4.1). Even today, the degree of preservation varies widely between sites on the raised gravel islands and those close to or within the former channels, where the alluvial cover affords an extraordinary level of protection. Environmental data from these sites charts the gradually changing landscape from the early Neolithic when the former channels flowed freely through a relatively dry landscape of dense woodland to the increased water levels and tree clearance that had developed by the first millennium BC.

The rising water level undoubtedly terminated permanent occupation on the floodplain that slowly shifts to the higher ground of the raised gravel terrace. Abundant Anglo-Saxon activity on the gravel terrace supports this hypothesis with little contemporary evidence revealed on the floodplain itself. However, Iron Age and Roman activity extends throughout the study area representing the gradual onset of the floodplain or, perhaps, the improved control of the water flow through canalisation during the Roman period.

### *4.1.2 The role of geophysical survey in an alluvial landscape*

The Yarnton record is unusual as it provides a complete account of Neolithic and Bronze Age society extending from individual settlement sites across an entire prehistoric landscape. This totality continues through later phases of activity on the site that result in an extraordinary, ever changing picture of habitation in

response to environmental change. However, the recording of such a large area presents a considerable challenge where geophysical survey should provide a means to place individual sites within the context of a wider archaeological landscape.

Unfortunately, alluvial landscapes have long been recognised as a challenging test for geophysical survey and the success of individual techniques is often highly variable (e.g. Clark 1992). Indeed, initial disappointing results from the floodplain might well have curtailed the use of geophysics within the study area. However, the excellent results from the gravel terrace sites led to a more critical re-examination of the floodplain data and provided considerable insight into the use of geophysical methods within alluviated landscapes.

*4.1.3 The influence of geology and soils*

The success of geophysical techniques, particularly magnetic survey, is critically dependent upon the underlying geology and the soils that have developed over a site. Previous survey results may provide some guide to the success of such techniques over similar substrates (e.g. David 1995) and for magnetic surveys the regional variation of soil magnetic susceptibility may also provide a useful insight (Dearing et al. 1996b).

The Yarnton project area lies over a substrate of Oxford Clay and Kellaways Beds that outcrops between deposits of post-glacial river gravels and more recent alluvium (Institute of Geological Sciences 1972). Throughout this region the gravels are arranged in a series of terraces and, following the classification of Sandford (1924), both flood plain deposits and the second raised (Summertown-Radley) terrace occur within the project area. Due to the lateral movement of the Thames southward down the dip-slope of the underlying Jurassic strata, the Summertown-Radley terrace forms a large, gently sloping surface to the N of the current river course (Richardson et al. 1946; pp118-9). The boundary between the Summertown-Radley terrace and the flood plain gravel is often indistinct, although in the Yarnton-Cassington area it would appear to approximately follow the 60m contour recorded by the Ordnance Survey. Buried palaeochannels cross the floodplain and these are partially visible during wet weather through the pooling of surface water. Alluvium extends gradually from the former river channels and forms wide lake-like expanses with outcrops of the floodplain gravel occurring as slightly raised islands. A variety of soils are found over the project area

(Soil Survey of England and Wales 1983) but are mainly clayey soils belonging to the Thames and Kelmscot Associations developed over the alluvium and are affected by seasonal waterlogging. Finer loamy soils of the Badsey 1 Association are found over the gravel terrace deposits surrounding the village of Cassington.

Despite the generally low magnetic susceptibility of the gravel and the underlying clay, results from a number of topsoil susceptibility surveys over the raised terrace demonstrate that under suitable conditions sufficient iron minerals are available for significant magnetic enhancement to occur. Much lower susceptibilities have been recorded from the soils developed over the floodplain and it is likely that the seasonally waterlogged nature of these soils has led to considerable gleying of iron minerals.

A far greater impediment to magnetic survey has been the wide scatter of ferrous detritus found principally upon the floodplain. Colloquial evidence suggests that this material is derived from the former railway line which used clinker from the north midlands pottery industry for track-bedding. These were later incorporated into the topsoil by ploughing following the closure of the railway. More recent ferrous detritus is derived from the commercial processing of organic waste on the site by the current land owner. It is evident that much of the waste received by this plant is contaminated with domestic ferrous rubbish, that is screened from the organic fraction and spread over the remaining agricultural land. The results from the two coincident magnetic surveys of Cresswell Field (§4.3.1), conducted before and after the waste processing site was established, clearly illustrate the detrimental impact this change of landuse has had on the quality of the magnetic survey data.

*4.2 Results from the raised gravel terrace*

The geophysical survey results are presented as grey scale images superimposed over the base OS map data. Topsoil susceptibility values are presented as either greyscale images or a bar graph when the data has been measured from a transect of soil samples. All grey scale images include a histogram scale key indicating the distribution of data in the plot and the mapping of a specific value to a particular tone of grey between black (low or negative values) and white (high or positive values). Each geophysical data set is also accompanied by a graphical interpretation plan summarising significant

(A)




(B)

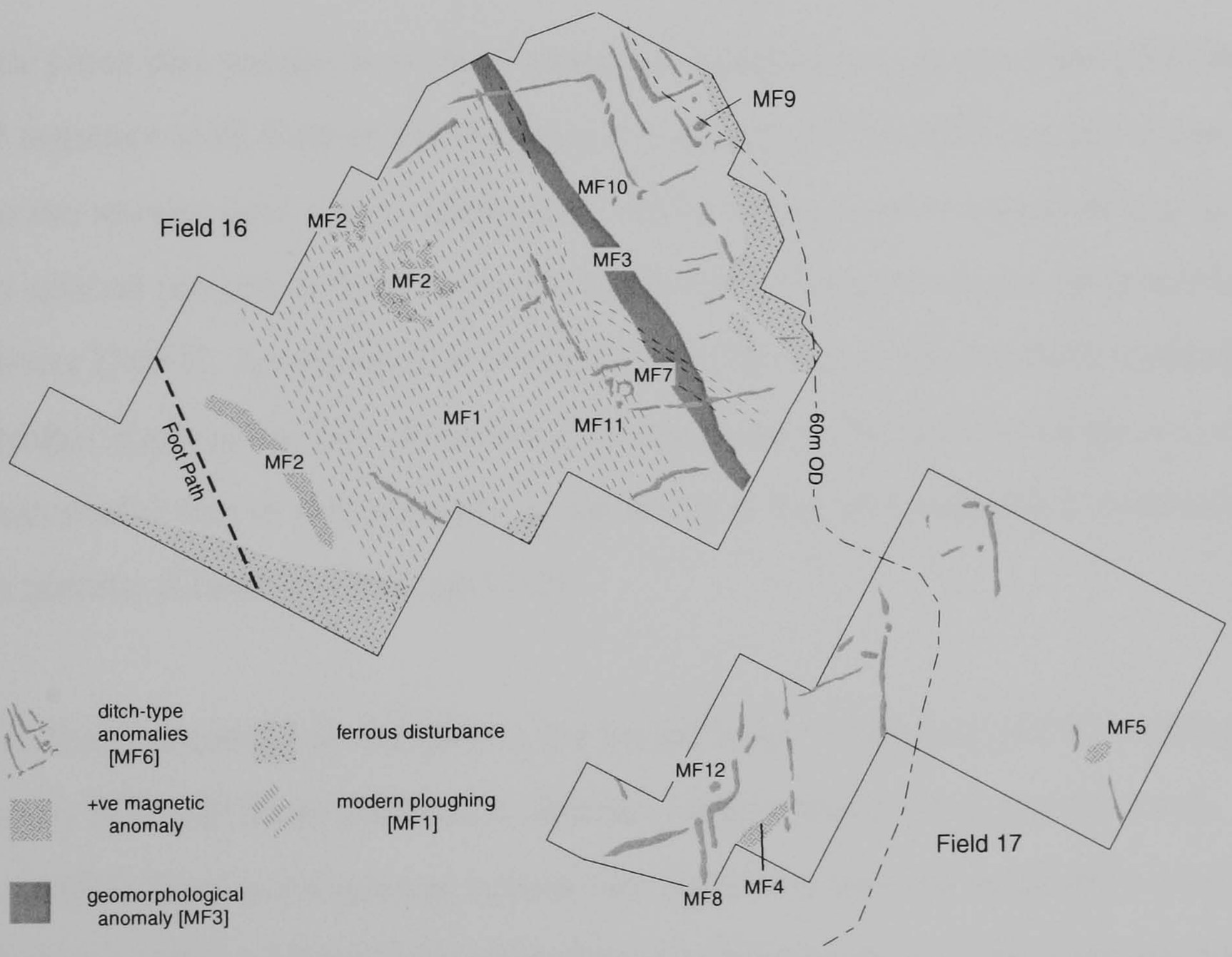


***Figure 4.2*** *(A) Greytone image of fluxgate gradiometer data from Mead Farm together with (B) a graphical summary of significant anomalies.*

anomalies discussed in the following text. The location of specific features selected for magnetic mineral analysis are also shown together with sections of these features indicating the position and archaeological context of the recovered samples.

### *4.2.1 Yarnton Mead Farm*

Despite lying beyond the area threatened by gravel extraction it was considered prudent to examine the probable continuation of settlement activity revealed at Yarnton Mead Farm associated with an Anglo-Saxon burial ground identified at NGR SP 4759 1141. The survey was conducted over two of the fields (OAU numbers 16 and 17) covered by the field-walking programme, which are divided by an unmetalled access track leading to a tunnel beneath the railway line. The area available for survey in field 16 was affected by extensive tree planting immediately north of the railway and following the course of the access road. The saplings in this area were spaced far enough apart to permit survey to take place but considerable interference was noted from the ferrous staples securing rodent protection around each plant.

Disturbance from this source is evident along the margins of the greytone plot shown in Figure 4.2 together with further interference caused by the Mead Farm buildings adjacent to the survey grid. Other anomalies likely to be of more recent origin include the closely spaced pattern of linear plough marks [MF1] and evidence of possible quarry activity [MF2]. An attempt to remove the influence of the modern agricultural pattern through application of a directional cosine filter in the time domain was only partially successful due to the common orientation of the archaeological anomalies with the plough pattern (Geosoft 1997; pp51-2).

The most striking anomaly in the plot is the broad linear response [MF3] running approximately NW-SE from the Manor House towards the railway access track. Curiously, [MF3] does not continue across this trackway into the adjacent survey area suggesting that it either ends at this point or turns sharply on a course towards the railway line. Similar anomalies have been noted throughout the project area and the majority of these are coincident with geological boundaries between either the gravel and underlying clay or, perhaps, deposits of colluvial overburden. In this case, the

geological survey suggests a boundary with the clay following the 60m OD contour and returning to the E in field 17 (*cf* Figure 4.1; Institute of Geological Sciences 1972). However, [MF3] follows a contour line slightly below 60m and does not appear to continue into field 17. The absence of a distinctive magnetic anomaly and the apparent change in soil type in field 17 suggest the transition from gravel to clay occurs along the corridor of unsurveyed land following the course of the railway access track.

An additional anomaly [MF5], found in the E of field 17, is also suspected to be of geomorphological origin and is similar to magnetic responses recorded during the Worton 1993 survey discussed below (§4.4.1; Figure 4.11).

Anomaly [MF3] partially obscures a network of less intense ditch-type responses [MF6] that are concentrated in the NE of the survey area and apparently continue N beyond the current field boundaries. A similar group of linear anomalies E of the trackway probably form a continuation of [MF6] and it seems reasonable to interpret the entire network as a series of boundary ditches enclosing a relic field system of possible Saxo-Norman date (*cf* Taylor 1975). Whilst [MF6] may well represent a phase of activity contemporary with the excavated Anglo-Saxon field enclosure ditches revealed at the Yarnton Saxon Site (Hey 1991) the geophysical evidence is not entirely conclusive.

A subtle circular anomaly [MF7] is discernible within the network of the field system and it is difficult to ascertain whether this response is associated with the Anglo-Saxon field system [MF6] or represents an earlier phase of activity on the site. The dimensions and magnetic response of [MF7] are more reminiscent of a pre-historic funerary monument than Anglo-Saxon domestic activity, such as a sunken featured building (see §4.3.1).

Despite the recovery of a high density of surface artefacts in the vicinity of the pond in the eastern field few significant anomalies are evident beyond the apparent continuation of the field system [MF6]. A quite intense double linear anomaly [MF8] is evident in the S of field 17. However, sub-surface soil samples recovered by auger suggested that the highly magnetic fill of the underlying feature may be associated with recent contamination from the cinder covering of the adjacent trackway.

Several discrete positive anomalies [MF9-12] occur within the data which, from their dimensions may possibly represent sunken-featured buildings (*cf* David 1994). However, the isolated nature of their distribution would suggest that they represent later Saxon activity at the site based around individual farmstead tofts.

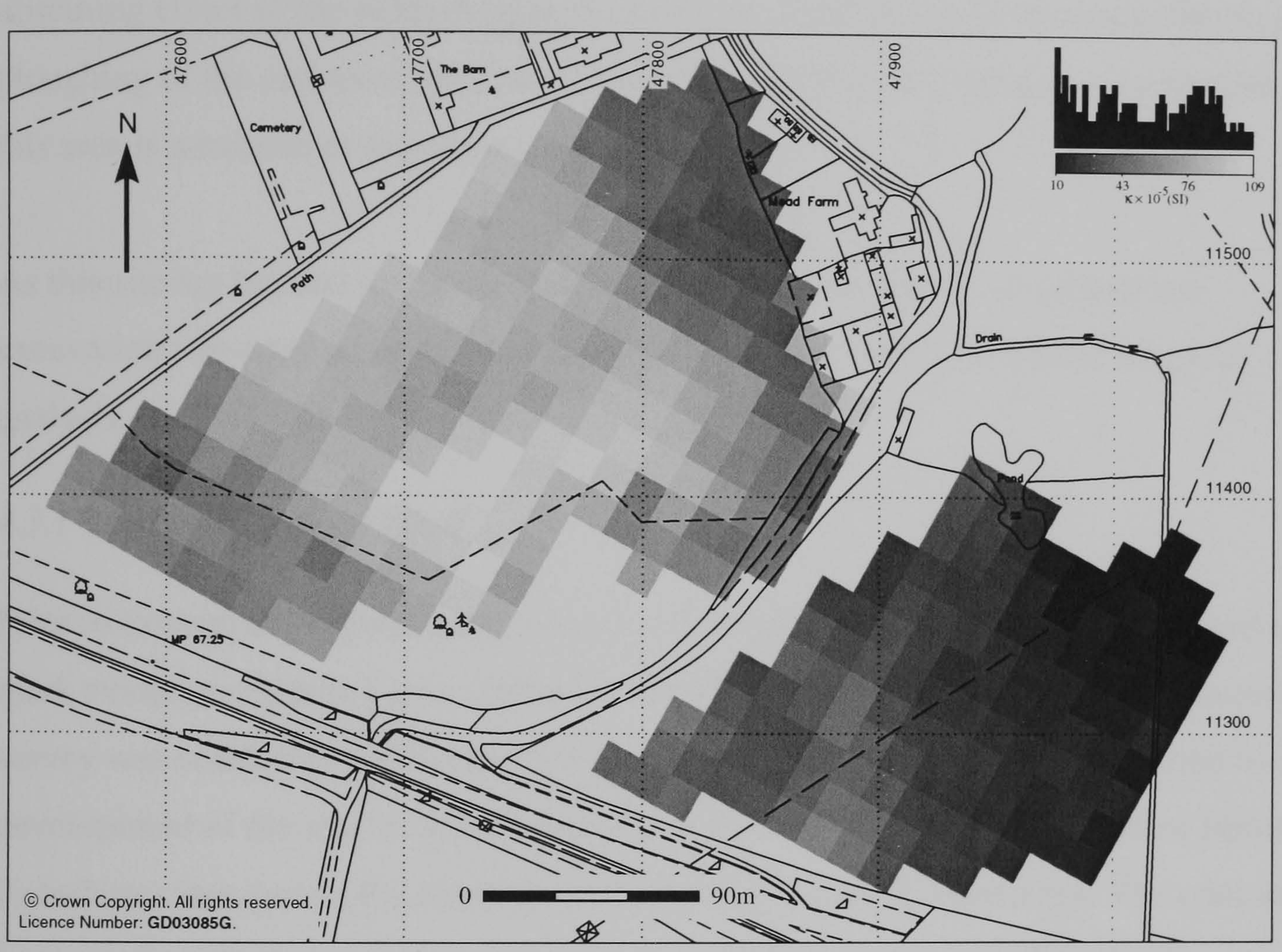


***Figure 4.3*** *Topsoil susceptibility survey at Mead Farm.*

### *4.2.2 Topsoil Magnetic Susceptibility*

A topsoil magnetic susceptibility survey was conducted at a 15m sample interval over the area covered by the magnetometer survey (Figure 4.3). Susceptibility declines to the E and N of anomaly [MF3] following the apparent boundary between the gravel and clay. The differing magnetic properties of the two soil types may explain why despite the similar agricultural regime across the survey area the pattern of modern ploughing has only appeared in field 16. Such patterns are generally caused by the magnetic contrast between raised plough ridges of soil and the air-filled furrows. However, when the magnetic susceptibility of the soil is low the resulting anomalies are often too subtle

to be discerned. A further influence of current land use is seen in the vicinity of the recorded burial ground in the S of field 16 where the arable land gave way to grass, suppressing susceptibility values recorded through the vegetation in this area.

It is of interest to note that the area of highest susceptibility fails to correlate with any significant concentration of gradiometer anomalies. Whilst this may be due to the obscuring effect of the modern plough pattern or to the complete truncation by recent ploughing of the causative features, it would appear that the enhanced susceptibility in this area is unrelated to archaeological activity.

As this site lay beyond the area threatened by gravel extraction no subsequent excavation was conducted to allow the recovery of samples for mineral magnetic analysis.

*4.3.1 Yarnton Cresswell Field*

Prior to excavation a gradiometer survey was conducted over an area of indistinct crop mark evidence occurring on a slight rise within Cresswell Field. Further gradiometer survey was conducted following the excavation but this data was compromised by the development of the site for gravel working and an increased concentration of ferrous disturbance hampering the identification of subtle magnetic anomalies. The contrast between the two data sets was so great that an additional area of fallow land encompassing part of the original survey area was resurveyed to examine the extent of the ferrous disturbance. This produced almost identical results to the original data set and confirmed that the ferrous litter must have been introduced since this date; possibly as a by-product from the adjacent organic waste processing activity. The combined fluxgate gradiometer data is shown in Figure 4.4 together with a graphical summary of significant magnetic anomalies.

Superficial anomalies within the data include the response to both the modern plough pattern (extant at the time of the 1995 survey) and underlying evidence for a system of former ridge and furrow agriculture [CW1] which corroborates the NS orientation of former agricultural patterns determined through aerial photography.

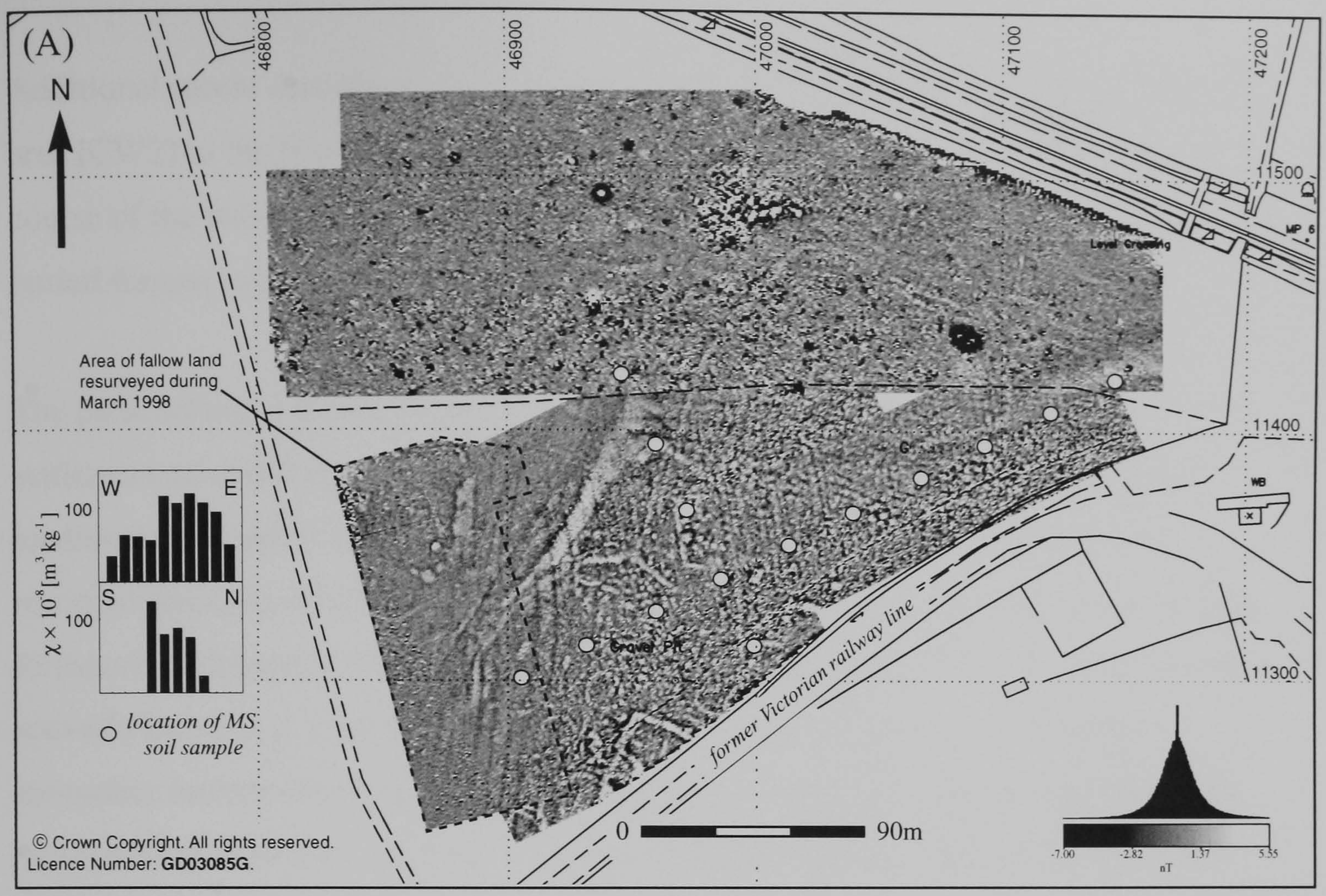


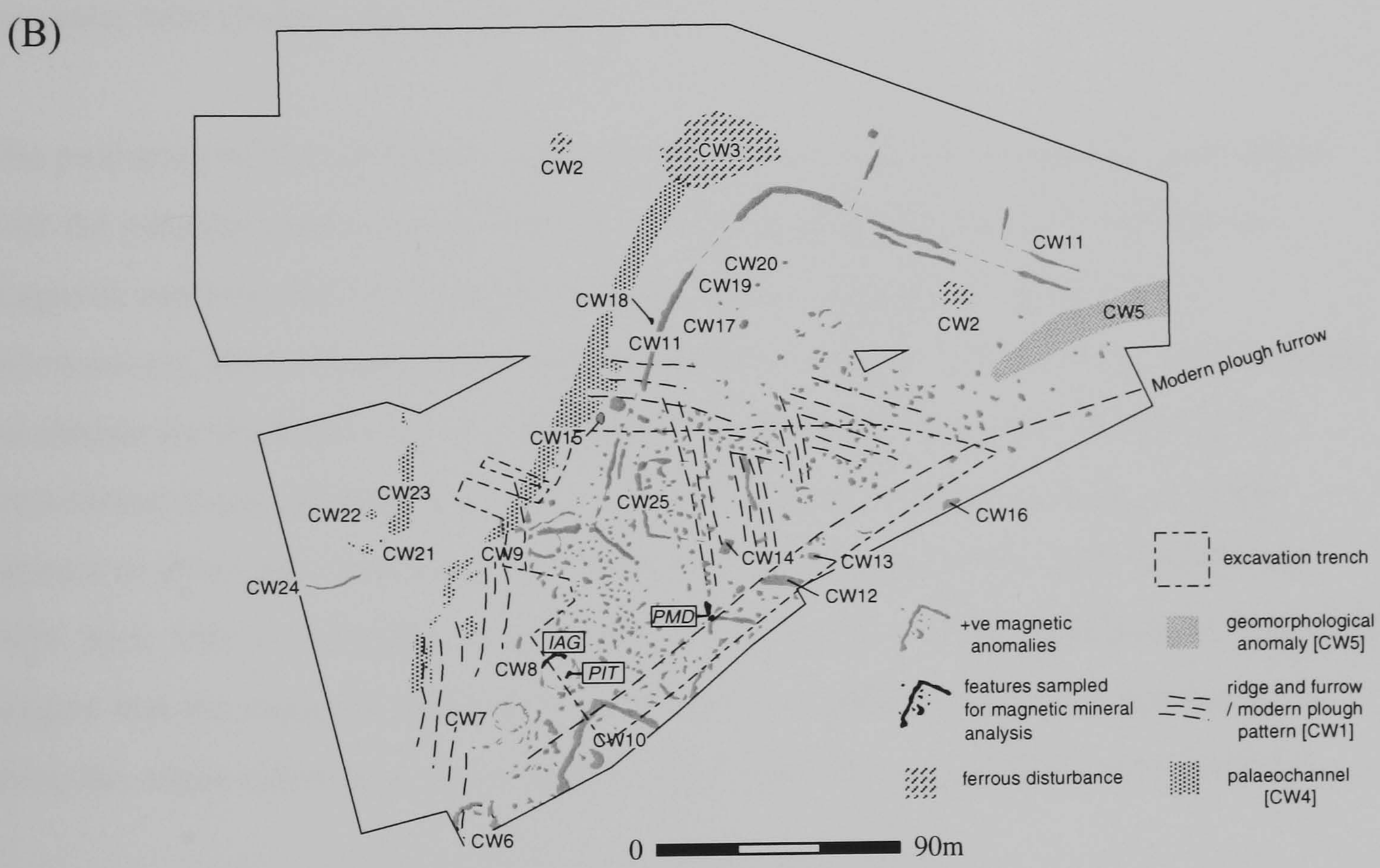


***Figure 4.4*** *(A) Greytone image of fluxgate gradiometer data from Cresswell Field together with (B) graphical summary of significant anomalies.*

Additional recent disturbance is associated with the telegraph poles crossing the survey area [CW2] to the N and a highly magnetic response [CW3] located within the apparent course of the palaeochannel [CW4]. The intense nature of [CW3] suggests it represents buried ferrous material, possibly abandoned agricultural machinery.

The palaeochannel [CW4] appears to represent a boundary to the multi-period settlement revealed at the site that all anomalies, with exception of the presumed medieval ridge and furrow plough pattern respect. Similar anomalies have been recorded throughout both the project area and at other fluvial sites in association with former river channels although determining the precise cause of the response has often proved elusive (*e.g.* Linford 1994, Cole 1995). Possible explanations for these anomalies include the accumulation of sediment with an anomalously high magnetic susceptibility within the channel or the development of a (p)DRM (§1.5.2) as water borne magnetic minerals settle from suspension and align themselves with the ambient magnetic field (Butler 1992, pp66-74).

The proximity of the settlement activity to the most pronounced anomaly associated with the palaeochannel may well account for the local concentration of enhanced magnetic material derived from the occupation into the channel depression. Alternatively, this section of the channel may have offered more suitable, lower energy, conditions for the formation of a (p)DRM. This latter mechanism may explain the intermittent nature of these anomalies through varying turbidity conditions which appears to effect the stability of the (p)DRM formation process (*cf* Ellis and Brown 1998, Rees 1961). Certainly, geophysical survey results from the floodplain (Chapter 5) suggest that the magnetic anomalies associated with palaeochannels at this site form along the edges rather than in the more deeply scoured centre of the former channel.

A diffuse magnetic anomaly [CW5] is found to the E of the site where the settlement activity is apparently much reduced. Due to the surrounding topography this anomaly is unlikely to represent a former palaeochannel and no corroborative evidence is found in the AP record. However, it is possible that [CW5] represents a geomorphological feature, possibly a discontinuity between the gravel and underlying clay.

A series of more significant anomalies [CW6-10] appear to represent a number of enclosure ditches and hut circles that, with the exception of [CW6] and [CW7] were all confirmed through subsequent excavation to be of Iron Age date. The largest of these [CW10] appears to form part of a rectangular enclosure continuing beyond the survey area into the course of the Victorian railway. Note the significant magnitude of response (approximately 10nT) arising from the north-eastern section of this [CW10], suggesting the inclusion of highly enhanced material from a semi-industrial process, such as pottery production or metal working (*cf* David and Payne 1993).

A linear ditch-type anomaly [CW11] apparently forms part of a field system or an incomplete enclosure extending to the N where it continues as a more subtle response. Along elements of its course [CW11] appears as a double linear anomaly although it is difficult to determine whether this represents a more significant causative feature, such as the drainage ditches surrounding a former trackway, or a recut of the original ditch system.

Anomaly [CW12] was revealed to be a Roman ditch infilled with later Saxon occupation debris possibly associated with [CW13 and CW14] that were identified as sunken feature buildings (SFB) of the same period. A further SFB was identified at [CW15] although this anomaly is confused by the superimposition of the response from the adjacent palaeochannel. Due to the distinctive response of the SFBs the location of further similar features may be tentatively proposed beyond the excavation area at the location of anomalies [CW16-19]. One of these responses [CW18] lies beyond the postulated enclosure ditch [CW11] together with [CW15] which suggests [CW11] predates the Saxon activity, possibly representing a Roman field boundary.

A further group of diffuse magnetic anomalies [CW21-23] W of the palaeochannel may also be indicative of settlement activity related to a subtle curvi-linear response [CW24]. However, the presence of the diffuse anomaly [CW23] is more suggestive of a geomorphological origin (see results from Worton 1993, §4.4.1).

The excavation did reveal a number of Anglo-Saxon timber buildings represented as a series of post hole features that are not indicated by a magnetic response within the fluxgate data. This is not entirely surprising as the magnetic response generated by a

post-hole is often quite subtle (*e.g.* Faßbinder and Stanjek 1993) unless the site has suffered a catastrophic destruction phase through fire and the subsequent *in situ* burning of individual timbers (e.g. Thompson and Oldfield 1986; p84). However, it is surprising that concentrated domestic activity within the timber buildings has not produced a greater degree of magnetic enhancement. This suggests that recent plough damage may have truncated the buried occupation surface.

Anomaly [CW25] was found to represent a rectangular post-Medieval enclosure abutting a NS field boundary that failed to produce a discernible magnetic response. Again, the palimpsest of superimposed strongly magnetic anomalies both within and surrounding the enclosure, together with the orientation of the field boundary along the same alignment as the ridge and furrow may have obscured the identification of significant anomalies related to this phase of activity.

### *4.3.2 Topsoil magnetic susceptibility*

Topsoil samples were recovered at 30m intervals along the two orthogonal traverses (Figure 4.4(A) inset bar graphs). There is little apparent correlation between the values of enhanced topsoil magnetic susceptibility and the concentration of magnetic anomalies revealed by the magnetometer survey. However, the values do appear to fall over areas associated with the palaeochannel to the N and W of the site. Overall, the topsoil susceptibility values are high with respect to those recorded on the floodplain which may well be due to the influence of recent ploughing redistributing occupation enhanced material into the modern plough soil.

In addition, during the 1995 survey it was noted that a concentration of magnetic slag-type debris was distributed throughout the topsoil over the site. Two samples of this material were recovered for subsequent identification (D. Starley and K. Eckstein pers. comm.). One of the samples ($\chi = 997 \times 10^{-8}$ $m^3kg^{-1}$) was probably a smithing slag but may well be related to the track bedding material incorporated into the Victorian railway line (§4.1.3). The second sample ($\chi = 38 \times 10^{-8}$ $m^3kg^{-1}$) was identified as river worn haematite and would be potentially viable as an ore, although no evidence for the extraction of iron was found at the site.

### *4.3.3 Mineral magnetic analysis*

Samples were collected from three accessible features including the circular gully ditch of an Iron Age sub-circular enclosure (IAG), an Iron Age pit-fill (PIT) and a Post-Medieval enclosure ditch (PMD) (Figure 4.5). All three features produced magnetic anomalies that are readily identifiable within the fluxgate gradiometer survey (*cf* Figure 4.4) although the Post Medieval enclosure ditch varies quite markedly in the magnitude of its response.

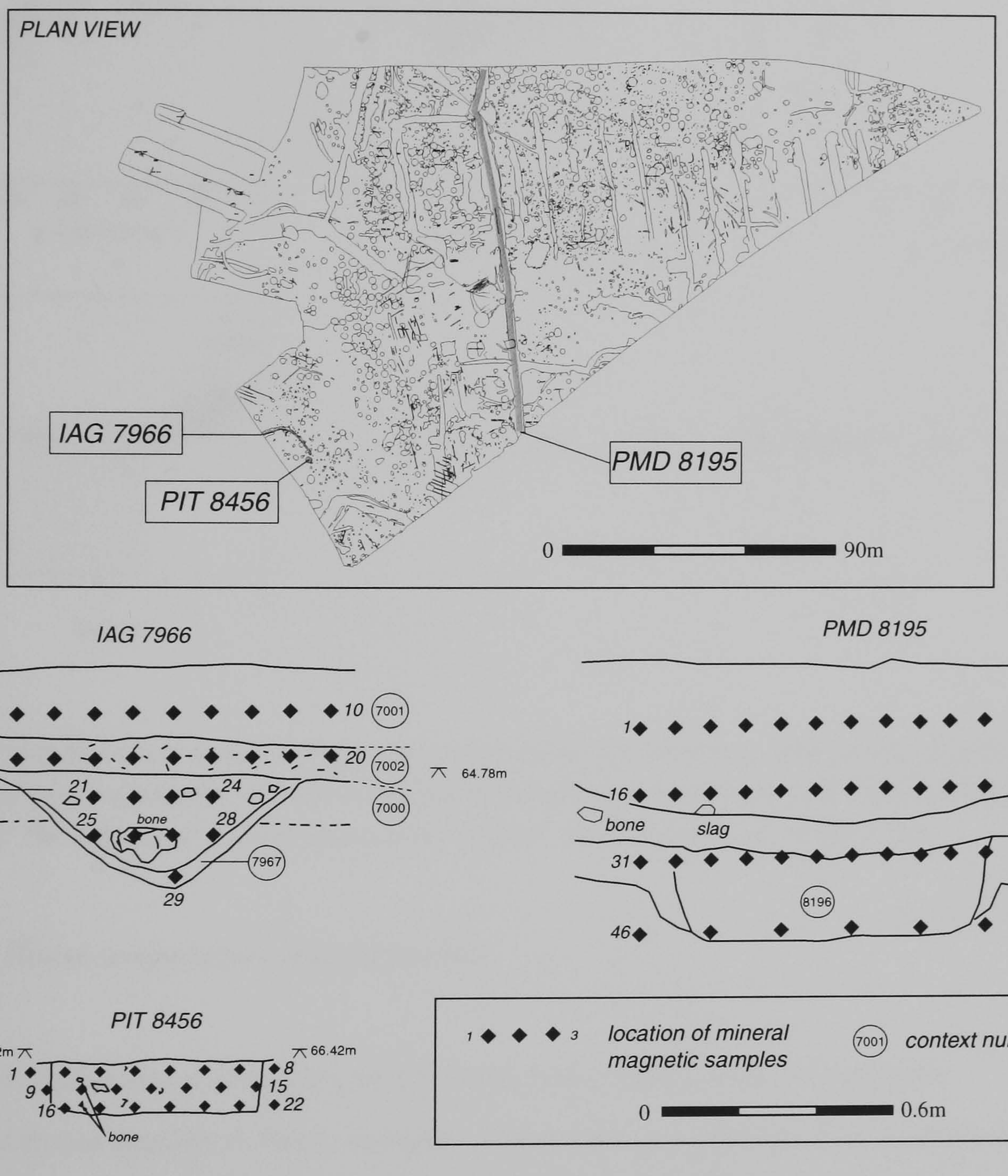


***Figure 4.5*** *Plan view of the features recorded during the excavation of the Cresswell Field site together with sections drawn through those features selected for the collection of mineral magnetic samples. The sections show the location of the recovered samples and context layers identified in the field.*

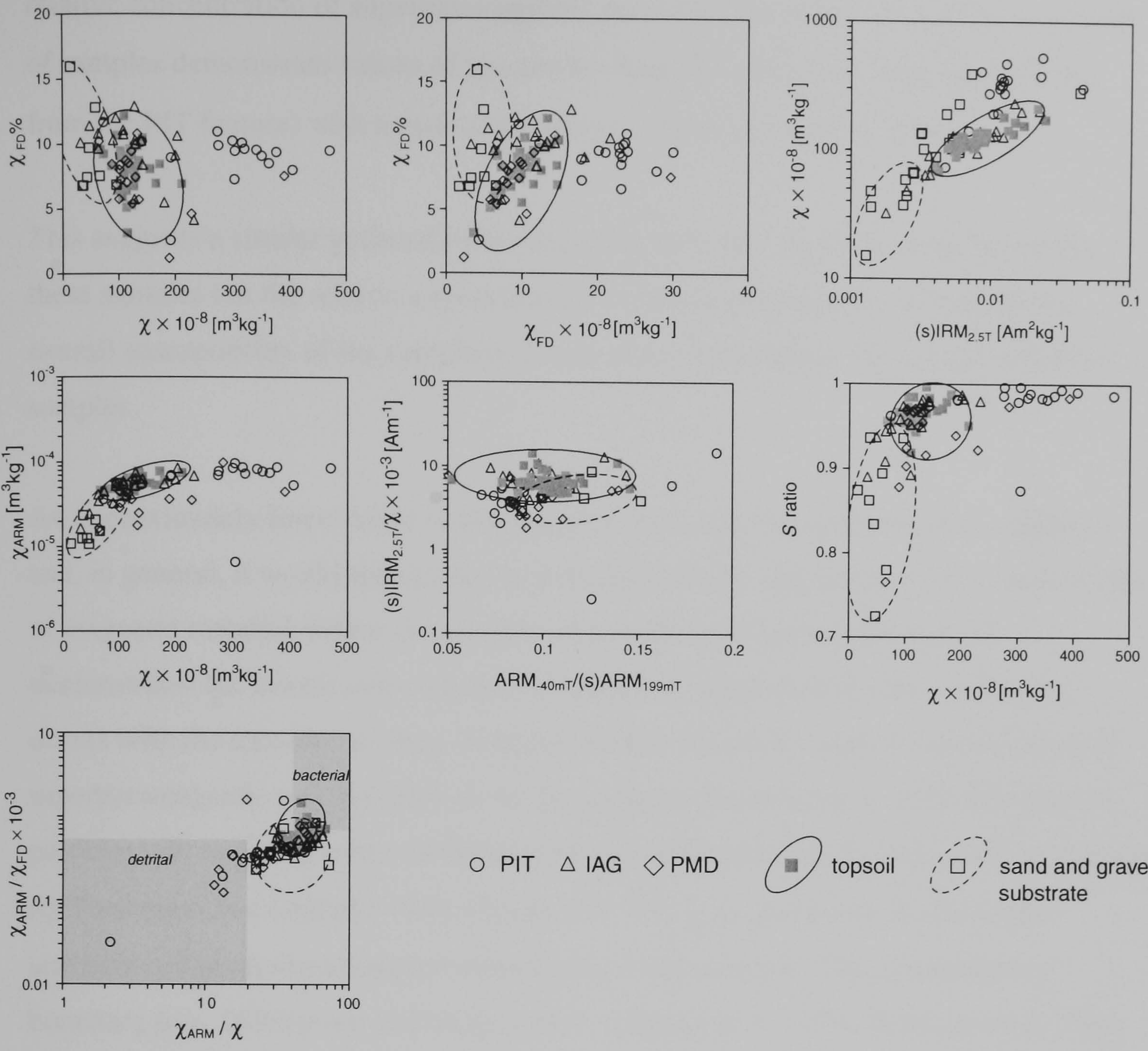


***Figure 4.6*** *Selected room temperature magnetic parameters and ratios displayed as a series of bi-plot graphs for the samples recovered from Cresswell Field. Envelopes indicate the range of values from topsoil and subsoil contexts at this site.*

### *4.3.3.1 Room temperature measurements*

Figure 4.6 provides a summary of the room temperature suite of magnetic measurements applied to these samples. These data are presented as a series of biplots with envelopes representing the range of values recorded from both topsoil and subsoil samples. The results demonstrate high values of initial susceptibility (average $\chi = 180 \times 10^{-8}$ $m^3kg^{-1}$) and frequency dependence of susceptibility (average $\chi_{FD\%} = 9.3\%$) suggesting a concentration of superparamagnetic material. Samples falling within the envelope of values expressed by the topsoil demonstrate an approximately linear increase of $\chi_{FD\%}$ with $\chi_{FD}$ suggesting a variation of both the average grain size and

relative concentration of superparamagnetic particles (Dearing et al. 1996a). A number of samples demonstrate values of $\chi_{FD}$ greater than the topsoil envelope (particularly from the PIT feature) with a more constant $\chi_{FD\%}$ of approximately 10%.

This suggests a similar grain size distribution of very fine magnetic material within these samples but the relative concentration of superparamagnetic particles to the overall susceptibility of the sample is greater than that of either the topsoil or subsoil samples.

An approximately linear trend is also apparent between susceptibility and (s)$IRM_{2.5T}$ and, in general, it would appear that both parameters are indicative of the concentration of magnetic material within the samples. As would be expected, the subsoil demonstrates the lowest concentration of magnetic minerals but some overlap still occurs with the topsoil envelope. Samples with an enhanced relative concentration of superparamagnetic material plot above the apparent linear trend as these fine grained particles will make a greater contribution to susceptibility than to isothermal remanence (*cf* Thompson and Oldfield 1986; Figure 4.7). The $\chi_{ARM}$ parameter is also highly sensitive to fine grained material close to the single domain / superparamagnetic boundary (*e.g.* Gillingham and Stacey 1971, Johnson et al. 1975, Banerjee et al. 1981, King et al. 1982, Schmidbauer and Schembera 1987, Oldfield 1994, Dunlop and Argyle 1997) and plotted against susceptibility it provides a partial discrimination of the topsoil from the subsoil samples. Again, high susceptibility samples plotting beyond the top/subsoil envelopes have relatively constant values of $\chi_{ARM}$ suggesting their magnetic behaviour is dependent upon an increased concentration of superparamagnetic material opposed to a reduced average grain size of the particles present.

Plotting the anhysteretic demagnetisation of (s)$ARM_{-199mT}$ in a –40mT alternating field against the concentration independent parameter (s)$IRM_{2.5T}/\chi$ produces little discrimination between the sample types. This suggests that the ARM behaviour of the samples is largely due to magnetically "soft" minerals with coercivities less than 40mT.

The contribution of minerals with coercivities greater than 300mT is illustrated by the biplot of susceptibility versus the $S_{300mT}$ ratio. This biplot distinguishes the majority of

the subsoil samples that in general demonstrate that "hard" magnetic minerals with coercivities >300mT contribute >10% of the total magnetisation of the samples. In contrast, such high coercivity material contributes <5% of the magnetisation of the topsoil and feature fill samples and less than 2% of the samples apparently containing a high concentration of superparamagnetic material.

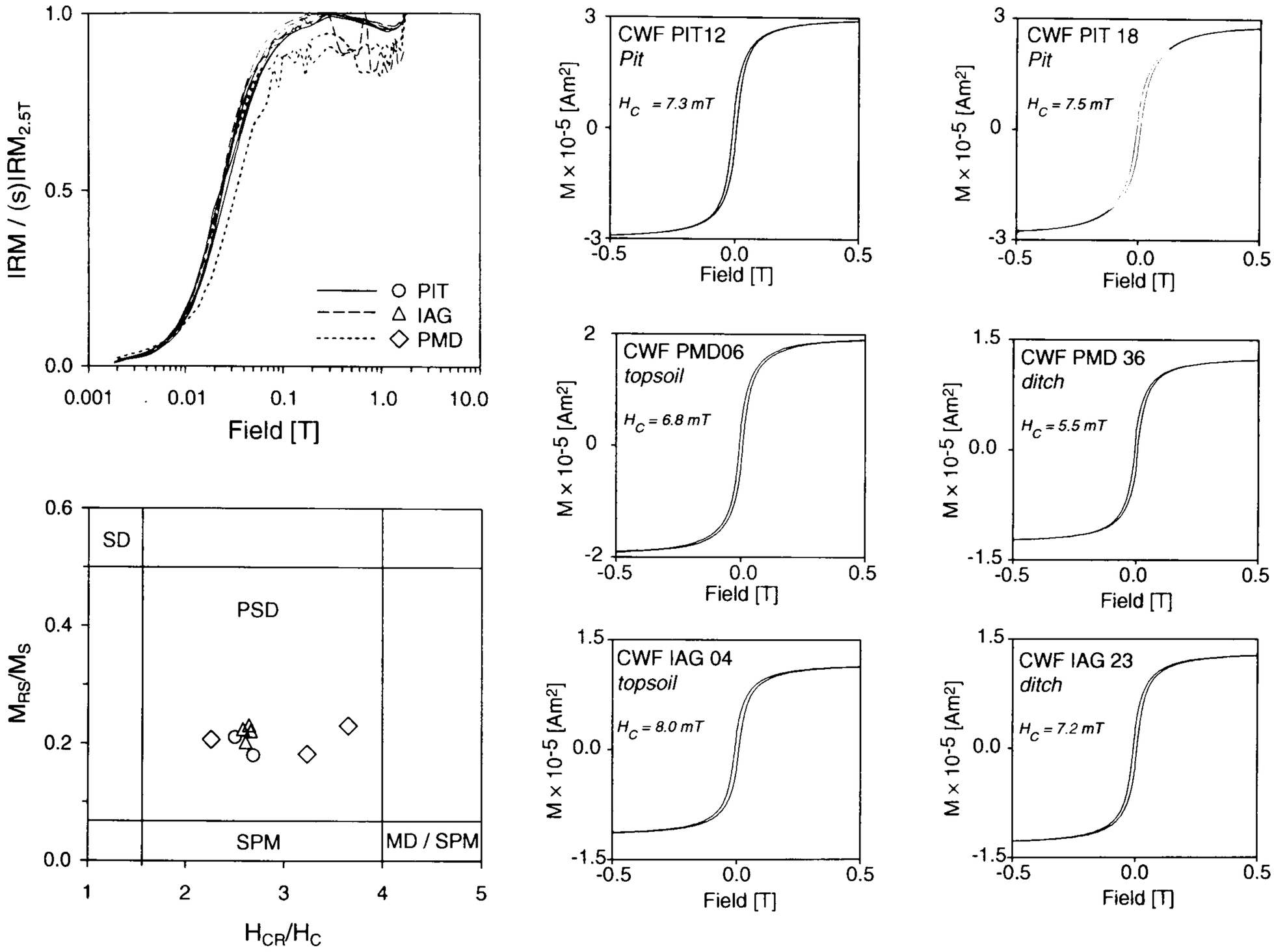


***Figure 4.7*** *Summary of the IRM acquisition and selected hysteresis behaviour for the Cresswell Field samples. Ferrimagnetic minerals dominate the hysteresis loops of these samples and a paramagnetic component is only visible at high applied fields.*

Due to the highly controlled nature of the fine grain sized material characteristic of bacterial enhancement Oldfield (1999) suggests a logarithmic biplot of $\chi_{ARM}/\chi$ versus $\chi_{ARM}/\chi_{FD}$ to investigate the fine-viscous/superparamagnetic 'tail' of such fine grained assemblages. Both these latter ratios are highly sensitive to fine grained material on the superparamagnetic/single domain boundary and comparison with empirical data, where the presence or absence of bacterial enhancement has determined through alternative means, may indicate the importance of this enhancement mechanism. In this case, the majority of samples from all three features plot with moderate values for both ratios

(Figure 4.6) suggesting an intermediate assemblage between the fine-viscous contribution from detrital sources and the more highly controlled SSD behaviour of sediments dominated by magnetosomes (*cf* Oldfield 1999; Figure 7.3).

*4.3.3.2 IRM acquisition and hysteresis*

Figure 4.7 summarises acquisition of isothermal remanence curves and hysteresis data for 9 of the Cresswell Field samples. IRM acquisition curves are similar for both the topsoil and fill from the three different features. These curves show a rapid saturation of IRM in comparatively low applied fields with >50% of the overall saturation remanence obtained following application of a 30mT field and full saturation is reached by 300mT. The apparent loss of IRM at high fields from ~0.5→1.0T is consistent for all of the measured samples until saturation is regained in fields approaching the maximum of 1.8T. Theoretically, for single domain material the acquisition of IRM should be cumulative with applied field and such behaviour would not be expected, even if the applied magnetic field proved unstable at high fields. However, after application of a high field, the MicroMag VSM uses a software controlled feedback loop to modify the current in the magnet until the Hall probe sensor close to the sample obtains a final set point of zero (M. Jackson pers. comm.). The control software is designed to avoid any over or under shoot of the zero field set point, although, in practice the actual field will oscillate around a number of descending intermediary set points until the final field is achieved.

Whilst the magnitude of the oscillating fields is quite small (no more than a few mT) samples containing a significant proportion of very fine / viscous particles will be sensitive to the stabilisation history of the field that, in effect, will superimpose a small pseudo-alternating field demagentisation over the initial IRM. In addition, the period of time between the application of the IRM field and the measurement of the sample will increase with the magnitude of the applied field as the approach to the zero field requires more intermediary set points. This will allow highly viscous particles to thermally unblock before measurement suppressing the apparent IRM further. The gradual return to saturation as the field approaches a maximum value of 1.8T may be explained by the presence of high coercivity minerals that begin to contribute to IRM in these increased fields.

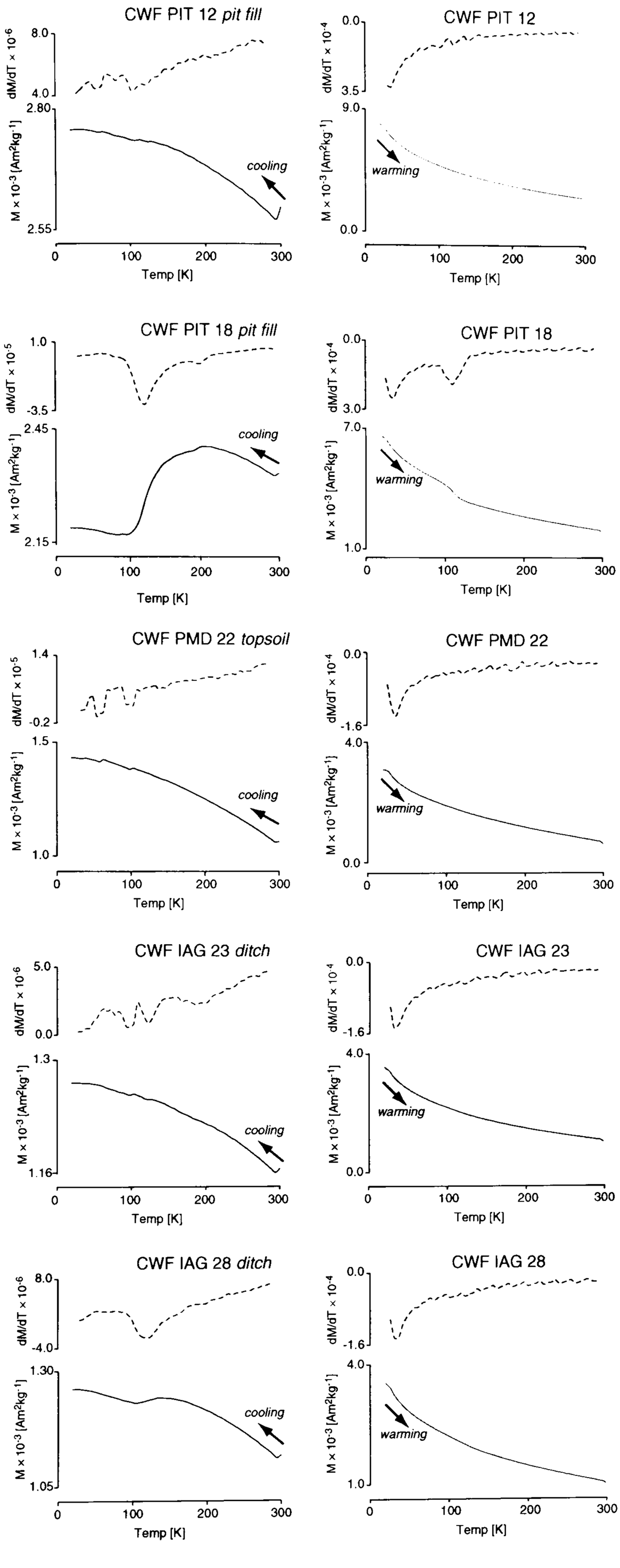


***Figure 4.8*** *Low temperature behaviour of samples from Cresswell Field. Cooling curves are plotted separately from warming curves due to the differing magnitude of the two data sets and the first differential of each curve is also shown (dashed line) to aid the identification of subtle inflections.*

Full hysteresis loops are shown for 6 of the samples, including two from the topsoil context together with a summary of hysteresis parameters from all of the samples presented as a biplot of $H_{CR}/H_C$ vs $M_{RS}/M_S$ following Day et al. (1977) (Figure 4.7). All of the hysteresis loops are presented following the subtraction of the paramagnetic component calculated from the high field slope of the raw data (§3.3.8).

The residual ferrimagnetic loops are highly similar with low coercivities in the range of $H_C$ = 5.0 to 8.0 mT and saturation reached by 500mT. The resulting Day plot shows that all the samples fall within the envelope of hysteresis parameters reported for pseudo single domain magnetite. There is no convincing evidence for the presence of any high coercivity material from the hysteresis loops although such a phase would, if present, be difficult to distinguish through in field measurements. However, both the IRM acquisition data and backfield remanence measurements to a maximum field of 2.5T suggest a persistent tail of unsaturated material remains within the samples, particularly from the PMD feature, that fails to fully saturate even after exposure to a 1.0T reverse field. This may well indicate the presence of a high-coercivity, detrital mineral such as goethite.

*4.3.3.3 Low temperature thermomagnetic behaviour*

The variation of saturation magnetisation with temperature measured in zero field is shown in Figure 4.8 for five selected samples: PIT 12, PIT 18, PMD 22, IAG 23 and IAG 28. Two separate curves are plotted for each sample the first showing the variation of a 2.5T magnetisation acquired at 300K cooled to 20K (cooling curve) and the second the decay of a subsequent 2.5T magnetisation applied at 20K on warming back to 300K (warming curve). The two curves have been plotted separately to allow detail within the lower intensity cooling curve to be identified. In addition, both cooling and warming curves are shown together with their rate of change of slope, *dM/dT* that often allows slight inflections within the curves to be identified.

The most striking low temperature behaviour is shown by sample PIT 18 that undergoes a considerable loss of room temperature acquired magnetisation on cooling through the Verwey transition at ~120K. It would appear that the magnetic behaviour of this sample is largely dominated by the presence of magnetite that, from the distinct nature of the

Verwey transition, is likely to be in a single rather than a multi domain state (Muxworthy 1999). On warming, the Verwey transition is still evident together with a gradual loss of the magnetisation acquired after exposure to a 2.5T field at 20K that may well indicate the thermal unblocking of superparamagnetic material that is only able to retain a magnetisation at low temperatures.

The low temperature curves of the other samples appear more uniform and exhibit a gradual increase of magnetisation on cooling to 20K, similar to that reported for the mineral goethite (*e.g.* Dekkers 1988). Only sample IAG 28 provides evidence for a minor inflection at the Verwey transition although the *dM/dT* curves for all the samples demonstrate some form of irregularity at approximately 120K.

.

*4.3.3.4 High temperature thermomagnetic behaviour*

Samples PIT 18 and PMD 22 represent two distinct patterns of thermomagnetic behaviour reflecting the constituent iron minerals present (Figure 4.9). Initial heating of PIT 18 produces a slight increase of $\chi$ between room temperature and ~100°C consistent with the unblocking of a fine grained ferrimagnetic mineral. No variation of $\chi$ is discernible from 100 to ~275°C until a linear decrease occurs before a very slight inflection at ~440°C. The rate of decrease is reduced between 410 and 500°C when a rapid loss of $\chi$ occurs to a Curie temperature of 580°C, consistent with the presence of magnetite. Repeat experiments conducted on fresh portions of PIT18 demonstrate that the thermomagnetic behaviour is fully reversible during heating between room temperature and 350°C, suggesting the loss of $\chi$ between 275 and 440°C is due to minerals with Curie temperatures distributed across this range (Figure 4.10).

The reversible nature of the heating curve to 350°C dispels an explanation of the thermomagnetic behaviour due to the inversion of minerals such as maghaemite to heamatite (e.g. Fine et al. 1989, Liu et al. 1999) or the production of maghaemite through the dehydration of lepidocrocite (e.g. Marmet et al. 1999). However, a similar loss of magnetisation on heating is reported for synthetic titanomaghaemite that inverts to magnetite at ~400°C (*cf* Dunlop and Özdemir 1997: Figure 3.12). The absence of a peak in the PIT 18 heating curve at this temperature due to this inversion may be

explained by a mixture of titanomaghaemite and magnetite with the contribution to $\chi$ of the latter mineral decreasing markedly on approach to the magnetite Curie temperature.

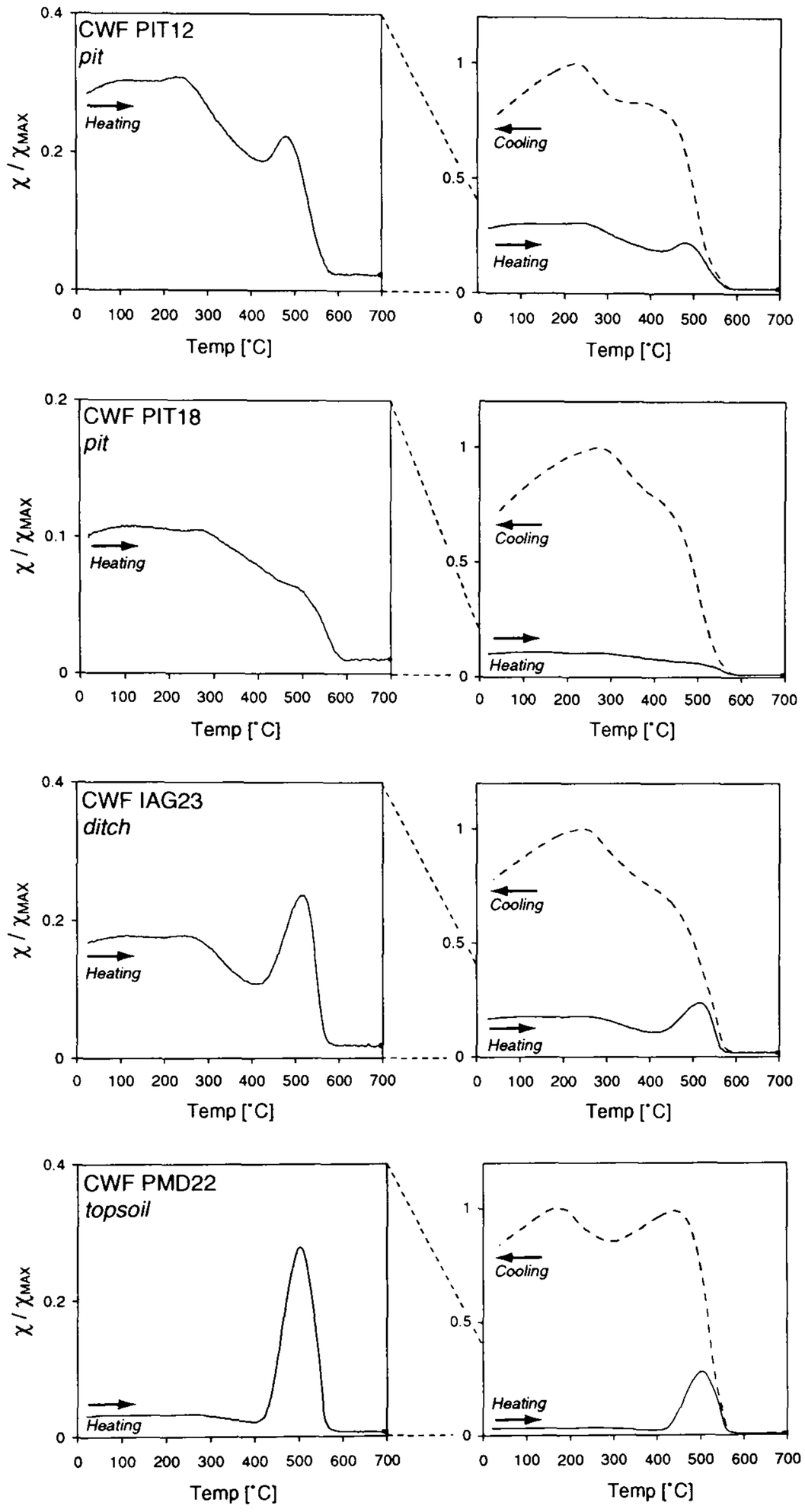


***Figure 4.9*** *Variation of high temperature susceptibility for selected samples from Cresswell Field. The heating and cooling curves are plotted separately for each sample.*

The cooling curve suggests the inversion of iron minerals to magnetite continues on heating to 700°C and a rapid increase in $\chi$ only occurs below the Curie temperature of magnetite. Whilst this latter chemical inversion will occur most readily under reducing conditions, promoted by the combustion of organic material, heating a fresh portion of the sample in an inert argon atmosphere suppressed the maximum $\chi$ value relative to the

unheated sample. This suggests the magnetite produced at high temperatures is susceptible to oxidation on cooling to a less magnetic mineral, such as maghaemite, that has been widely reported to be the final product of similar soil heating experiments (e.g. Tite and Mullins 1971, Mullins 1977). The susceptibility peak at 280°C, on cooling, may then be explained by the Curie temperature of a substituted maghaemite with a significant proportion of very fine grained particles that become thermally blocked on the return to room temperature. A sample of PIT 18 previously heated to 700°C demonstrates near reversible thermomagnetic behaviour when reheated from room temperature to 300°C in an inert atmosphere (Figure 4.10). The slight increase of $\chi$ on cooling may indicate the reduction of (titano)maghaemite formed during the initial heating to (titano)magnetite.

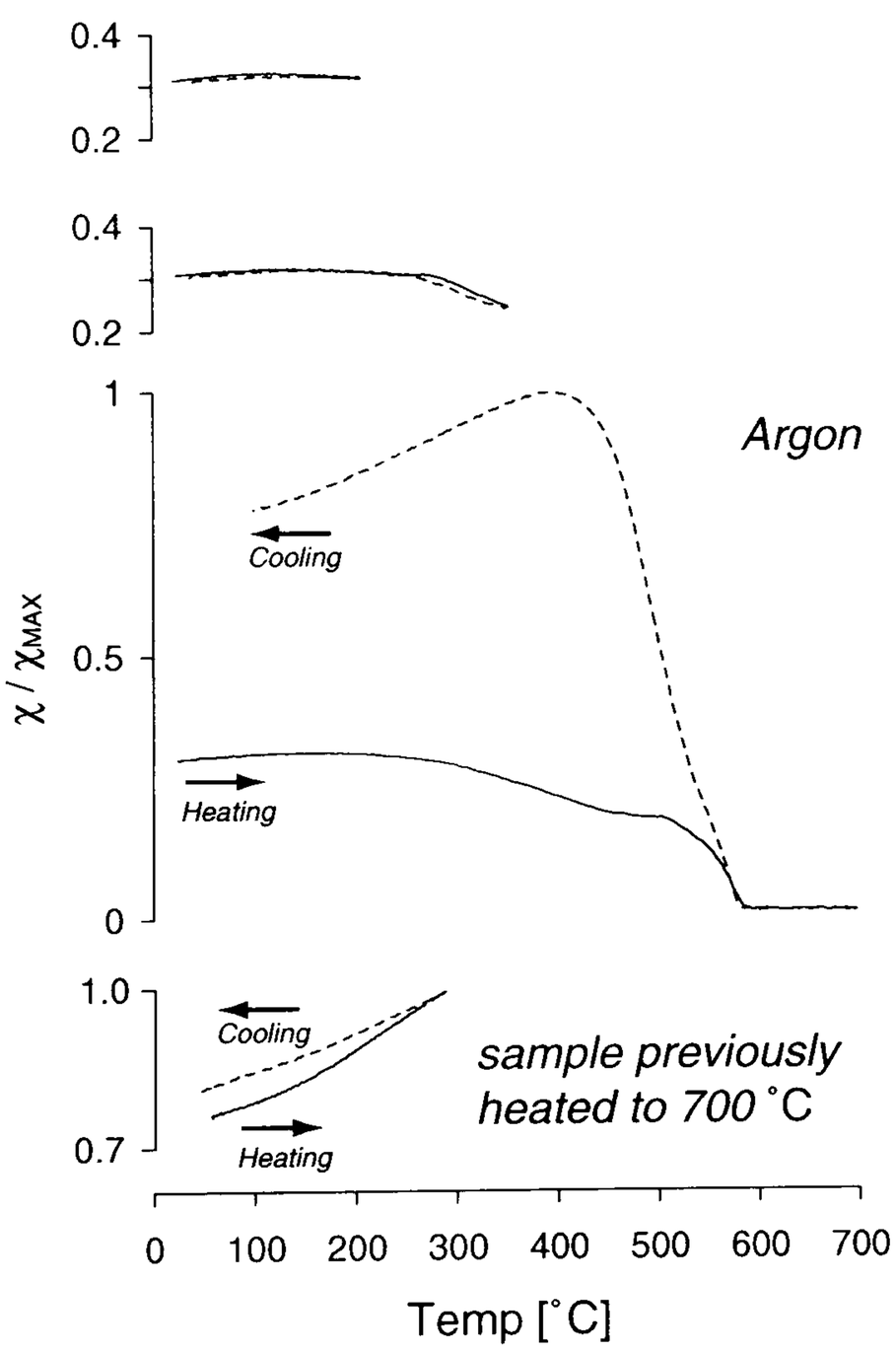


***Figure 4.10*** *Repeat heating experiments conducted on fresh portions of sample CWF PIT 18.*

On heating from room temperature to ~410°C sample PMD22 is highly similar to PIT 18 and demonstrates an identical linear loss of $\chi$ from 280°C (Figure 4.9). However, above 410°C the susceptibility increases markedly to a peak at 500°C until it decays,

equally rapidly, to a Curie temperature of ~580°C. Again, the results suggest the production of magnetite on heating. However, the prominence of the peak in $\chi$ at ~500°C indicates the alteration of a more significant proportion of low susceptibility minerals. The cooling curve demonstrates a rapid increase in $\chi$ to a peak at 450°C after passing back through the 580°C magnetite Curie temperature. A slight loss of $\chi$ is evident on cooling to 300°C that may be attributed to the oxidation of magnetite to (titano)maghaemite before a second peak is obtained at ~180°C. This latter peak occurs at a significantly lower temperature than that found on the cooling curve of PIT 18 and may well indicate the unblocking spectra of very fine grained particles that decay from this peak back to room temperature.

The remaining two samples, PIT 12 and IAG 23 demonstrate intermediate behaviour between that described in detail above and inflections in the heating and cooling curves occur at broadly similar temperatures (Figure 4.9). A slight peak in $\chi$ on heating at ~500°C is evident for both samples, but this is not nearly so pronounced as that created on heating PMD22. The peak in $\chi$ on cooling may also be significant as both PIT 12 and IAG23 show a peak at ~250°C, similar to the behaviour of PIT 18.

### *4.4.1 Worton November 1992 and November 1993*

Geophysical surveys were conducted to the S of the shrunken medieval village[1] at Worton Rectory Farm (Figure 4.11). The surveys lie over the boundary between the floodplain and second gravel terrace and encompass a series of linear earthworks and possible building platforms in the pasture field SW of the modern farm. The land is currently divided into a series of four fenced paddocks separated by an open land drain with a considerable degree of ferrous interference along the paddock fences and modern farm buildings. This interference has degraded the apparent quality of the data collected close to the farm buildings in comparison to the data from the open paddocks.

However, despite this interference a number of anomalies have been resolved that are believed to be mainly geomorphological in origin, possibly related to the interface between either the terrace gravel and the underlying clay or the clay and the floodplain

[1] A settlement where previous house sites are now unoccupied, but often visible as earthworks, crop or soil marks. Individual buildings from the original settlement often survive in use to the present day, such as the farmhouse at Worton.


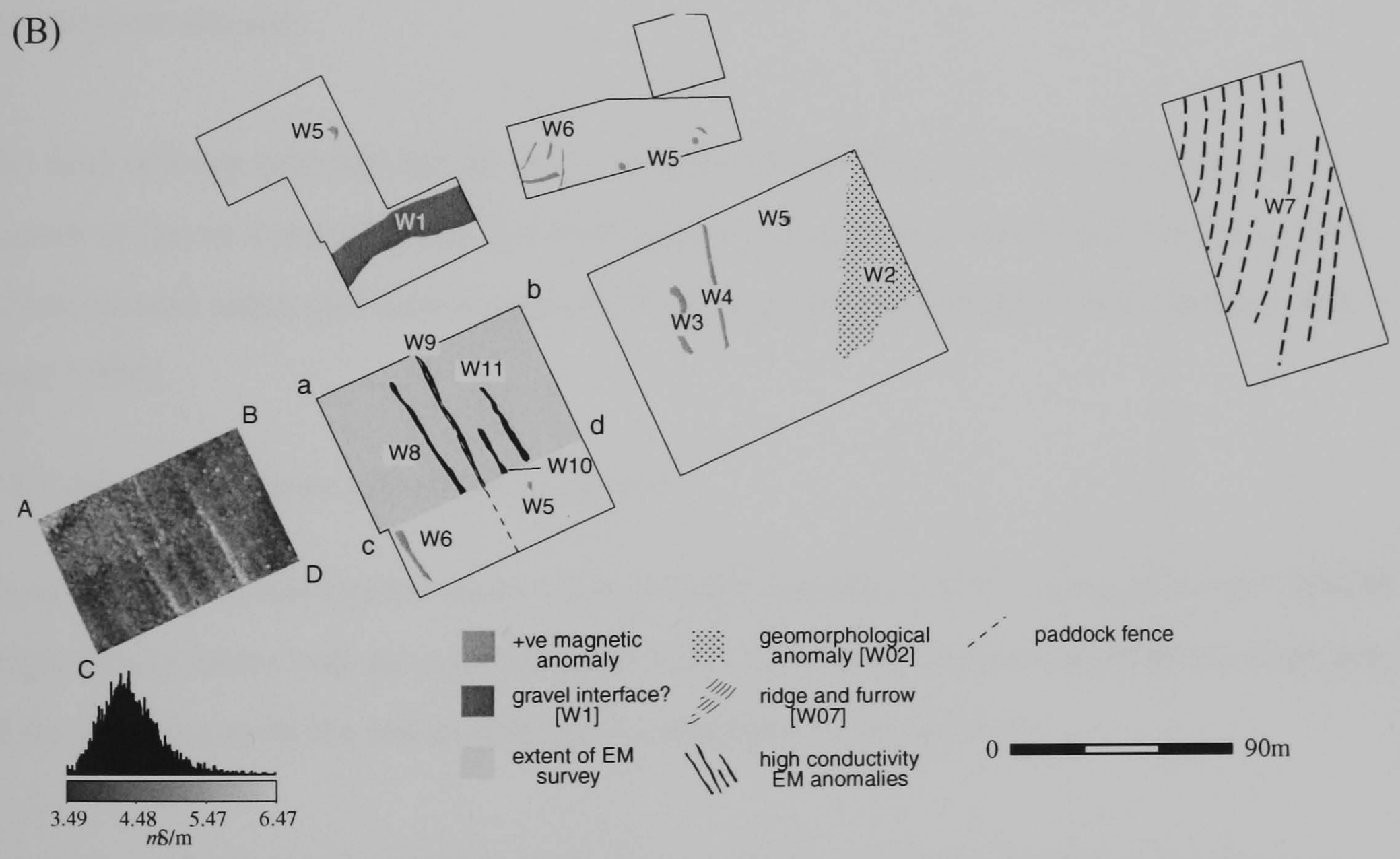


***Figure 4.11*** *(A) Greytone image of fluxgate gradiometer survey conducted at Worton Rectory Farm together with (B) a graphical summary of significant anomalies. A greytone image of the trial EM data survey, ABCD, is shown offset from its actual location (abcd).*

alluvium (Institute of Geological Sciences 1972). These include a broad magnetic response [W1] similar to anomalies recorded in both the Mead Farm and Cresswell Field data sets that does not appear to the W of the field drain suggesting the geological interface turns sharply to the N at this point. A more amorphous anomaly [W2] is similar to the response of former palaeochannels detected throughout the project area but as there is no other evidence for such a feature in this area it seems more likely that the response is due to an isolated clay pocket.

Of greater archaeological significance are the two linear anomalies [W3] and [W4] which possibly represent former field boundary ditches. However, these follow a different alignment to the linear anomalies associated with the topographic features identified by the electromagnetic survey discussed below. A number of tentative pit-type [W5] and interrupted linear anomalies [W6] are also evident but a more confident interpretation of these is hampered by the concentration of near-surface ferrous material littered over the site.

The area of magnetic survey SE of the modern farm (Worton 1992A) reveals only a pattern of linear anomalies [W7] which appears to represent additional evidence for a NS orientated ridge and furrow identified from aerial photographs (Featherstone and Dyer 1994).

*4.4.2 Electromagnetic conductivity survey*

Conductivity measurements were made at a 1m sample interval using a Geonics EM38 conductivity meter and an external data logger to record the quadrature phase response of the instrument in the horizontal coil orientation mode (§3.1.5).

Data was collected from a 60m × 90m grid over the visible earthworks and shows an area of interference that correlates with similar, presumably modern, disturbance in the magnetometer plot (Figure 4.11(B)). Of greater interest are the high conductivity linear anomalies [W8-11] running NS across the survey area. Whilst [W9] is caused by interference from the paddock fencing, anomalies [W8], [W10] and [W11] represent the extension of the ditch features visible on the ground. As there is no indication of similar anomalies running in the EW direction it seems reasonable to suggest that these are

conduits discharging water into the drain to the S of the site. The high conductivity nature of their response is, most probably, due to the accumulation of water within more moisture retentive humus buried in the base of these former ditches.

### *4.4.3 Topsoil magnetic susceptibility*

A topsoil susceptibility survey was conducted at a 15m sample interval using a Bartington MS2 meter and field search loop (Figure 4.12) over a limited area due to instrument failure. The results show a comparatively low degree of topsoil enhancement in the vicinity of the earthwork anomalies. Comparison with results from Mead Farm (§4.2.1) suggest that the low values encountered are typical for soils developed over the clay substrate. The significance of the slight enhancement along the E edge of the survey is difficult to ascertain and fails to correlate with any anomalies in either the magnetometer or conductivity data.

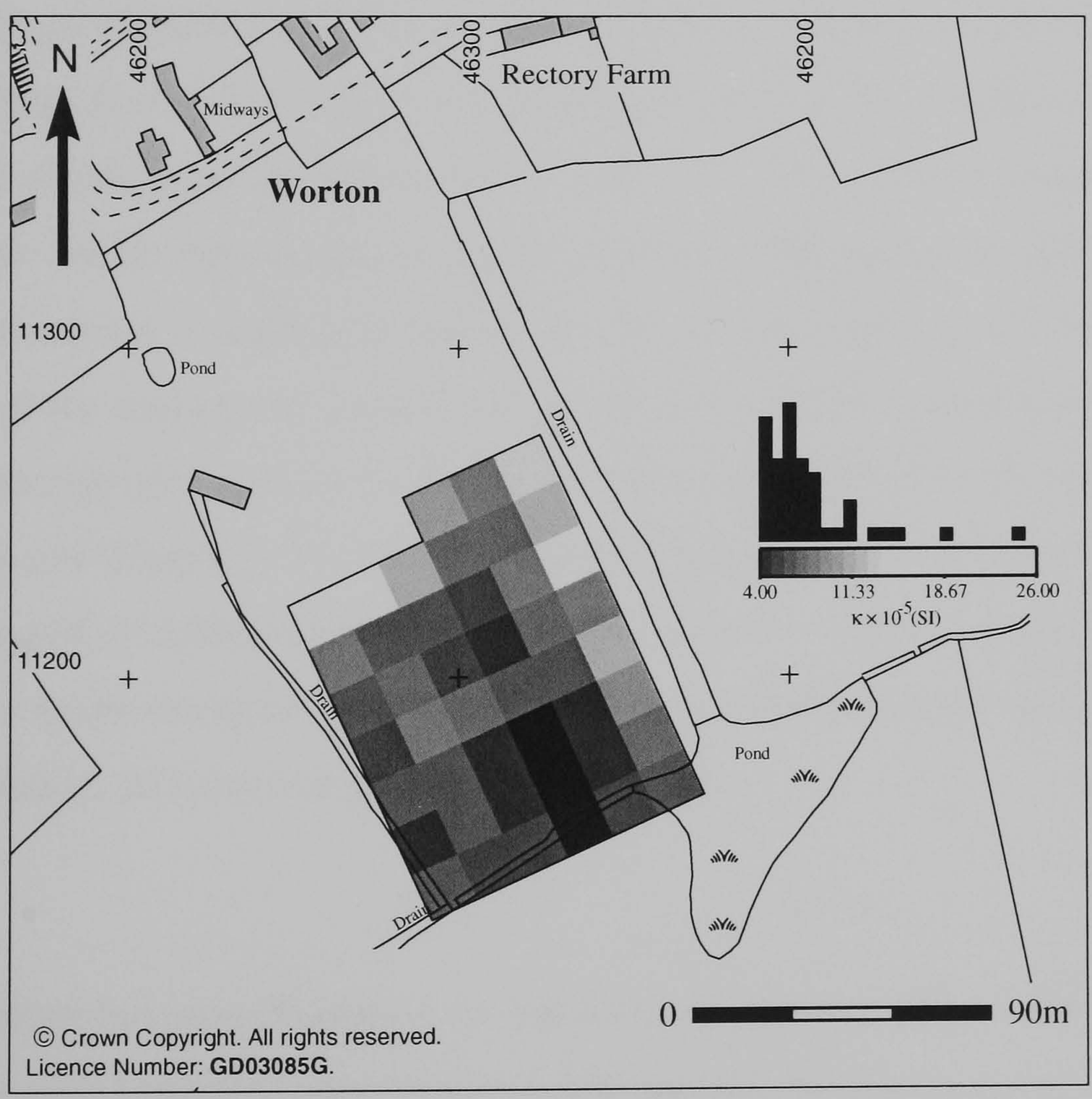


***Figure 4.12*** *Topsoil susceptibility survey at Worton Rectory Farm.*

Laboratory determination of soil samples collected from a NS traverse across the magnetometer grid E of the modern farm fall within a range of 18-33 $\times 10^{-8}$ $m^3kg^{-1}$ and are apparently enhanced with respect to the volume susceptibility field loop readings recorded over the paddock area (Figure 4.11 inset). Whilst this may represent increased pedogenic enhancement of soil susceptibility over the arable land it is more likely that the field loop measurements, made through short grass, have been partially suppressed by this vegetative cover (*cf* Cole et al. 1995).

### *4.5.1 Worton 1996*

Two areas E of Worton Rectory Farm (Figure 4.13) were investigated during June 1996 as part of an ongoing collaborative research project comparing high sensitivity caesium magnetometer data to the results from more routinely applied fluxgate instrumentation. It was hoped that the application of high sensitivity magnetometers would aid the identification of anomalies from weakly magnetic features such as the Anglo-Saxon timber buildings revealed during excavation at both the Yarnton Saxon site and Cresswell Field. Just such a feature was suspected due E of Worton Rectory Farm where aerial photography (Featherstone and Dyer 1994) has located a rectilinear anomaly with similar dimensions to the other timber buildings surrounded by an extensive palimpsest of additional cropmarks. An initial fluxgate gradiometer survey in the vicinity of the rectangular cropmark (Site B) successfully located a corroborative magnetic anomaly although the quality of the data was impaired by the over-grown nature of the site (Figure 4.13). The landowner kindly agreed to remove this vegetation and also allowed an additional survey to be conducted over more open ground to the N used as horse paddocks (Site A) whilst the clearance work was in progress. This latter area also contains an extensive pattern of cropmarks.

*Site A*

The results from this area (Figures 4.13 and 4.14) are dominated by a 20m wide band of intense disturbance running approximately EW through the SE corner of the survey [W11]. Analysis of a stacked XY traceplot representation of this data suggests that this disturbance is caused by a quantity of near-surface ferrous material that may possibly represent a recent rubbish dump. However, no evidence of surface disturbance was observed in the paddock during the survey and no cropmark anomaly is discernible in

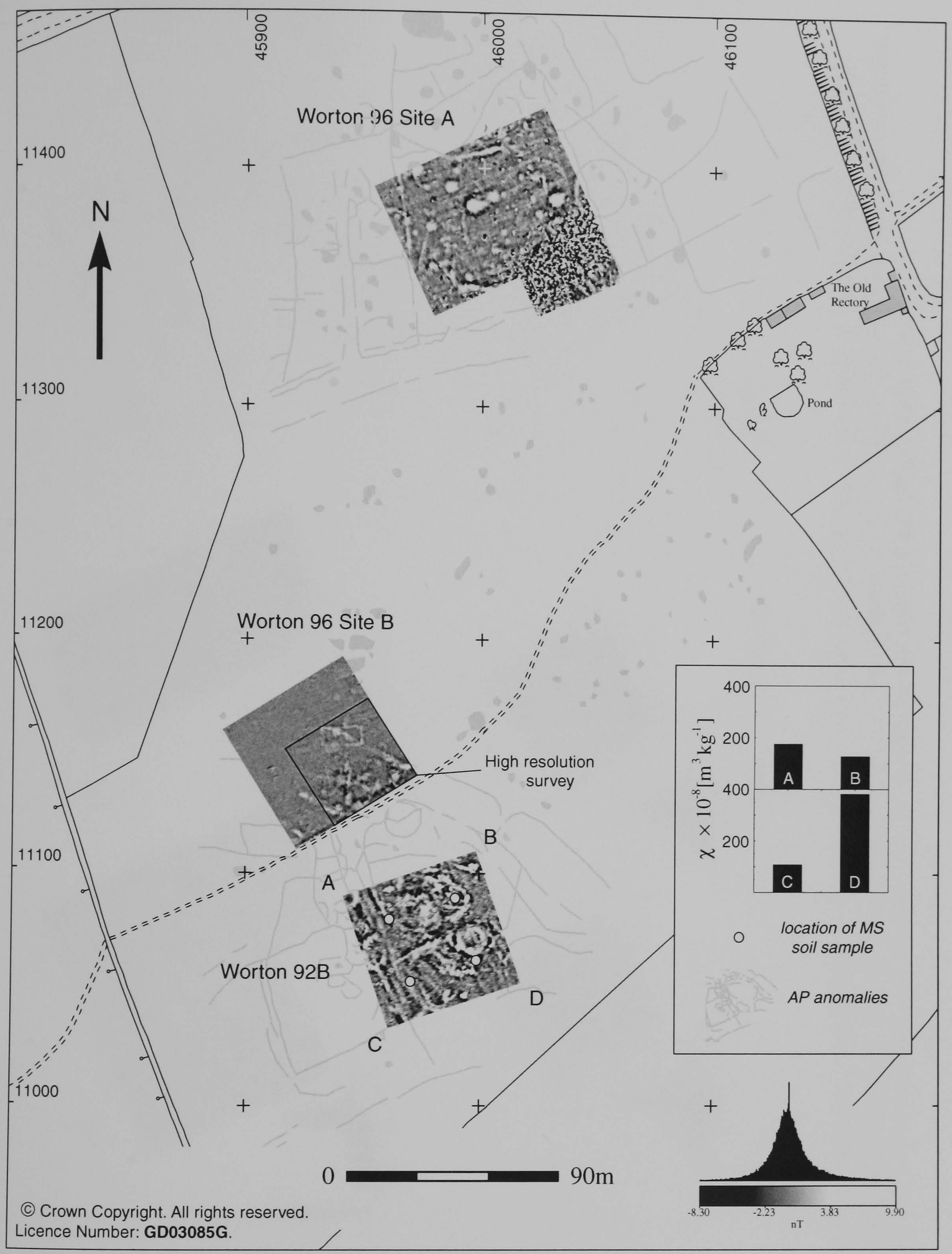


***Figure 4.13*** *Greytone images of the fluxgate gradiometer data from Worton 1992 and Worton 1996 (Sites A and B) superimposed over the crop mark anomalies identified from aerial photography (AP).*

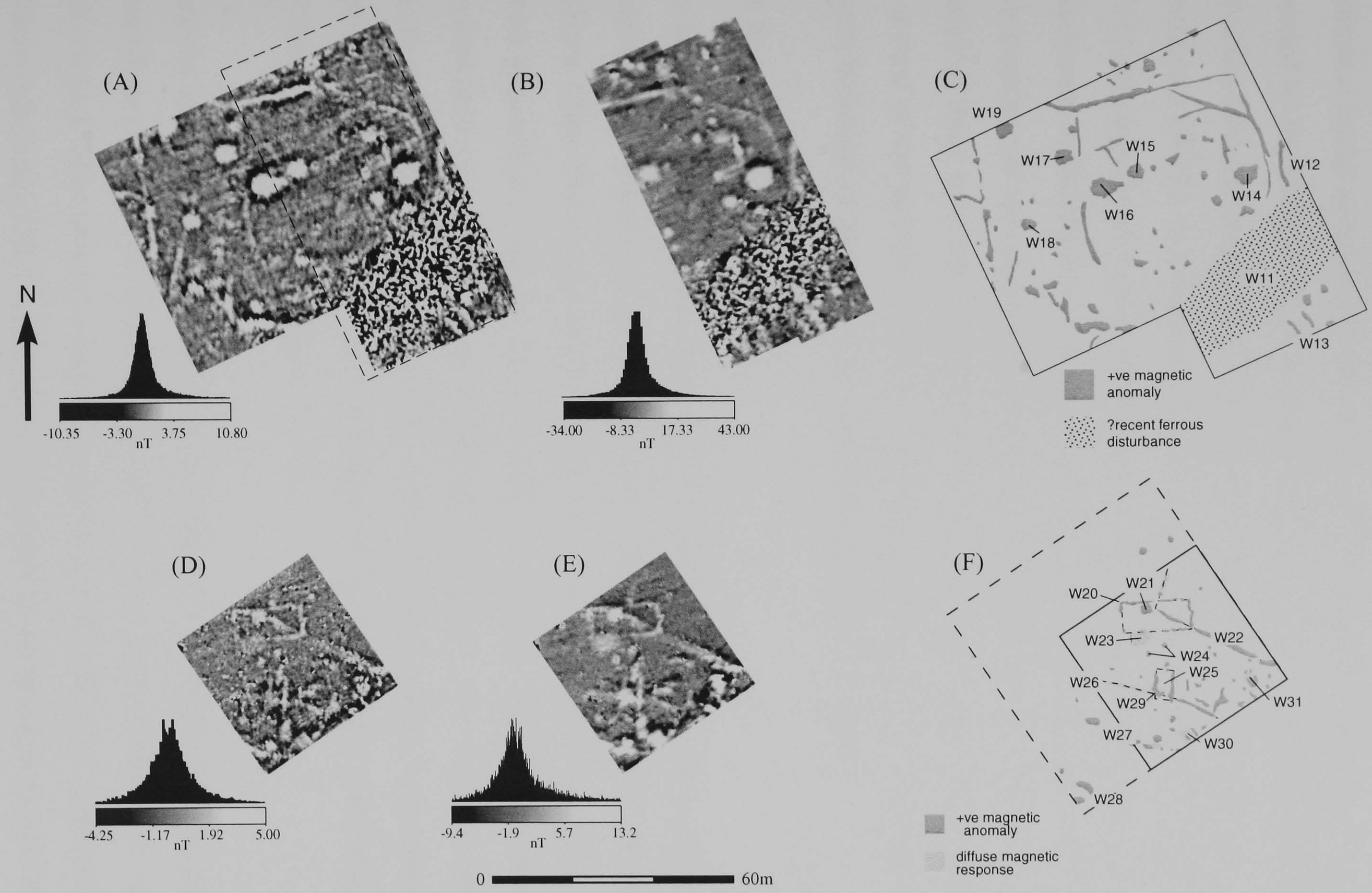


***Figure 4.14*** *(A) High resolution fluxgate gradiometer data from Worton 1996 Site A with (B) the corresponding caesium data and (C) a graphical summary of significant anomalies. Results from Worton 1996 Site B are shown in the lower part of the figure (D) high resolution fluxgate gradiometer data, (E) corresponding caesium data and (F) graphical summary of significant anomalies.*

aerial photographs taken in 1968. This would suggest that the disturbance is relatively recent.

Additional linear anomalies within this area correspond to the pattern of cropmarks recorded by the 1968 aerial photograph (AP) and include a curvilinear portion of the distinctive circular cropmark [W12] which is, unfortunately, affected by the band of disturbance [W11]. A portion of the double linear anomaly [W13] is also visible S of [W11] although the change in orientation evident in the AP data is masked by this latter disturbance. A distribution of discrete positive anomalies are also found to correlate with a number of sub-rectangular cropmark patterns identified from the AP. Whilst the smaller of these may represent a scatter of pits the magnitude of response demonstrated by several of the anomalies [W14-19] is reminiscent of results recorded over sunken feature buildings at Barrow Hills, Radley (Bartlett forthcoming).

*Site B*

The initial survey of this site (Figure 4.13) covered a 60m × 60m area prior to the removal of the vegetation and readings were collected at a standard sample resolution of 0.25m × 1.0m. The results of this survey have been severely curtailed by the much denser population of thistles to the N of the area which required the magnetometer to be elevated above the height of the vegetation, attenuating the magnetic response of the data to the N. However, despite these constraints the survey has successfully located a number of significant anomalies including [W20] that appears to be half of the rectilinear cropmark identified in the AP.

Once the precise location of the cropmark had been established on the ground a more detailed survey was conducted over a 40m × 40m area from which the vegetation had been cleared. This latter area was surveyed with both a fluxgate gradiometer and a high resolution Scintrex CS-2 caesium magnetometer at an identical sample interval of 0.25m × 0.5m. Results from the two detailed surveys are shown in Figure 4.14 and demonstrate a broad agreement between the two instrument types with the outline of the Saxon building appearing as a rectangular anomaly [W20] in both data sets. The outline of the ditch in the high-resolution data suggests a less continuous response with some correlation between discrete magnetic pit-type anomalies and the location of excavated timber-pits.

The building also contains an additional pit-type response [W21] and a linear ditch-type anomaly [W22] that enters from the SE corner of the survey and appears to alter direction as it exits to the N. Subsequent excavation revealed that [W21] corresponds to the location of a large pit, post-dating the construction of the timber building and [W22] to the course of a Roman field boundary ditch, not associated with the later Saxon activity.

A diffuse area of magnetic disturbance [W23] appears on both plots producing a greater magnitude of response in the total field data and is related to an earlier sunken feature building cut by the timber building. Two pit-type anomalies [W24] to the S are prominent in both the detailed data shown in Figure 4.14 and in the initial data shown in Figure 4.13 and are likely to contain a highly enhanced magnetic fill. Further activity is evident to the south of the survey and the faint outline of a second rectangular anomaly [W25] may be tentatively proposed. This latter anomaly coincides with a presumably Roman ditch-type response [W26] running parallel to [W22] which is replicated in the AP evidence. Additional cropmark anomalies correlate with indistinct magnetic responses [W27] and [W28] in the S of the survey area.

Anomalies [W29], [W30] and [W31] all demonstrate a strong response particularly evident within the total field data. Whilst these anomalies may well represent a series of pits an interpretation as further sunken feature buildings cannot be entirely discounted.

*4.5.2 Mineral magnetic analysis*

Samples were collected from four features revealed during the excavation of the Saxon timber building at Worton Rectory Farm (Site A).The resulting excavation trench (Figure 4.15) allowed three features to be sampled in section and additional samples to be collected from the topsoil stripped surface and sand and gravel substrate (NAT). A section through the timber building slot-trench was sampled in detail (SXB) including what was believed to be the position of one of the original timber post settings. Less detailed sampling was made through sections of two pit features (PIT25 and PIT48) together with samples from the Roman ditch (RD) predating the Saxon occupation at the site. The identification of unique context boundaries within the sections was

hampered by the nature of the feature fills that contained a high concentration of sand and gravel that was often difficult to distinguish from the highly similar underlying substrate.

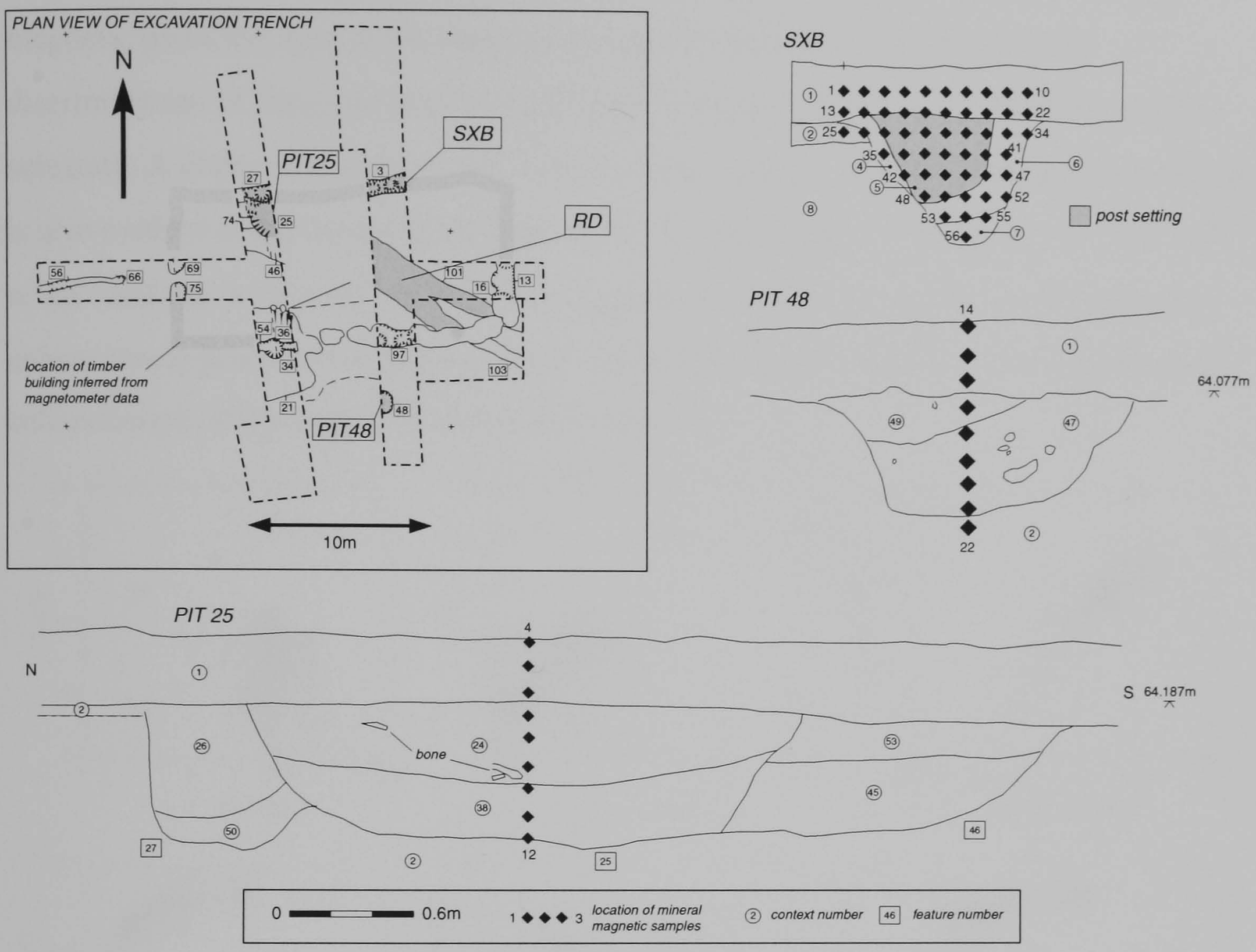


***Figure 4.15*** *Plan view of the features recorded during the excavation of the Saxon Building found at the Worton 1996A site together with sections drawn through those features selected for the collection of mineral magnetic samples. The sections show the location of the recovered samples and context layers identified in the field.*

### *4.5.2.1 Room temperature measurements*

Selected bi-plots drawn from the room temperature measurements are shown in Figure 4.16. The variation of magnetic behaviour for the different archaeological feature fills is illustrated together with envelopes indicating the range of values exhibited by samples of topsoil and the natural sand and gravel substrate recovered from this site. The discrimination of the sand and gravel substrate samples is clearly achieved from consideration of $\chi$ alone and is also reflected in the suppressed values of (s)$IRM_{2.5T}$ from this context layer. The envelope enclosing the sand and gravel substrate is also

found to include a number of samples collected from the edge of the feature fill context layers within the excavated sections and these samples may well represent a mixture between the two classes of behaviour. Analysis of the frequency dependent data suggests the feature fill / topsoil samples contain a higher concentration of very fine magnetic particles close to the superparamagnetic transition reflected by the discrimination of these samples through higher values of $\chi_{FD}$ compared to the natural substrate. A distinction between the topsoil and a number of extreme feature fill samples is also evident in the susceptibility data with the latter samples exhibiting $\chi > 100 \times 10^{-8}$ $m^3kg^{-1}$ and $\chi_{FD} > 10 \times 10^{-8}$ $m^3kg^{-1}$. This suggests a significant difference between the enhancement processes occurring within the archaeological features and the pedogenic enhancement of the topsoil developed over the site.

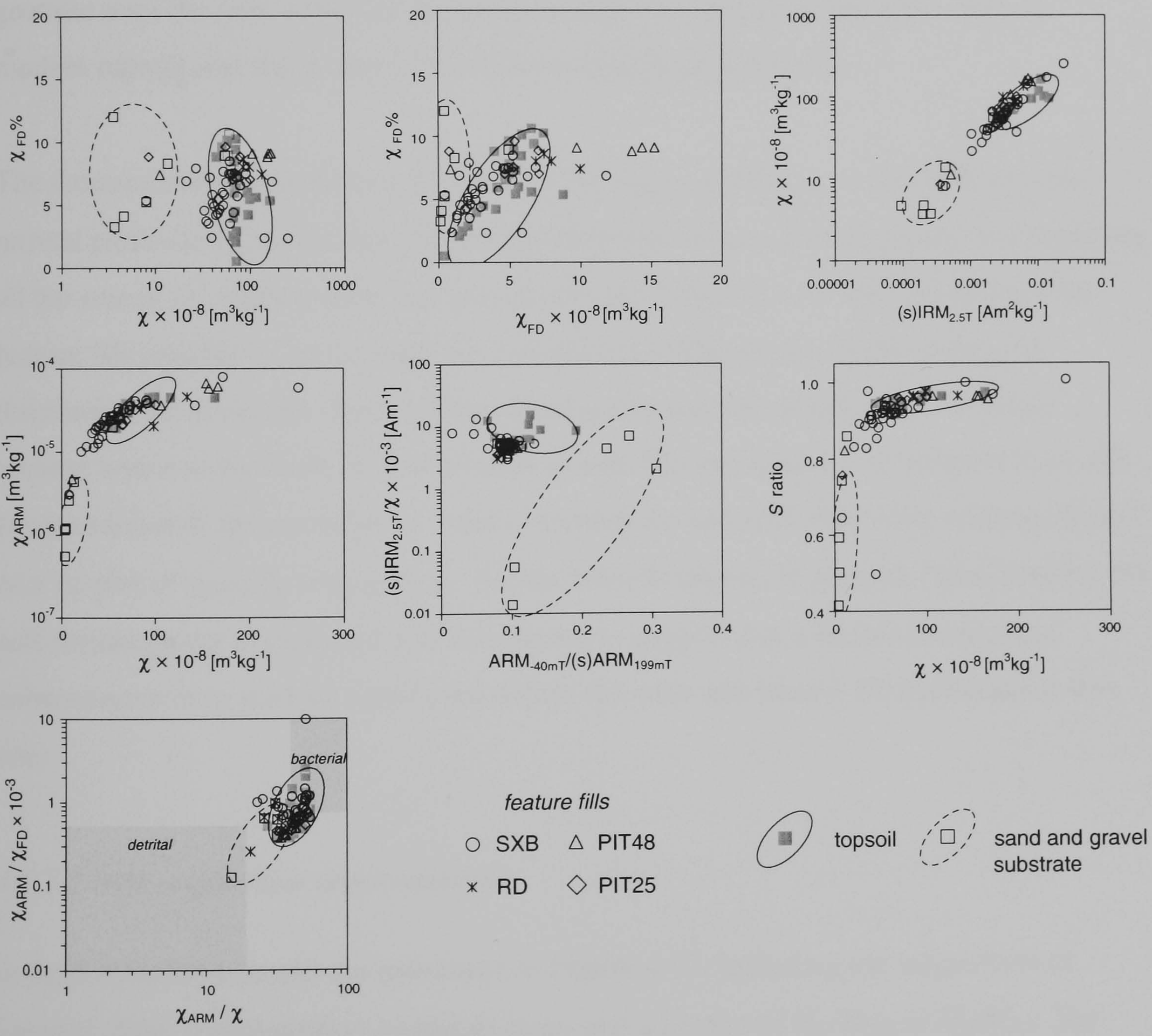


***Figure 4.16*** *Selected room temperature magnetic parameters and ratios displayed as a series of bi-plot graphs for the samples recovered from the Saxon timber building excavated at the Worton 1996A site. Envelopes indicate the range of values from topsoil and subsoil contexts at this site.*

The importance of superparamagnetic particles is further illustrated by the concentration independent $\chi_{ARM}$ ratio that again separates the natural context from the topsoil and feature fill samples. Further distinction of the feature fill samples from the topsoil context is achieved when $\chi_{ARM}$ is plotted against $\chi$ that, in comparison to reported results of these ratios from a series of synthetic samples of magnetite, would suggest that the feature fills contain a higher concentration of very fine grain material (*cf* King et al. 1982). Coercivity data, represented by the $\chi$ *vs* $S_{-300mT}$ biplot, indicates a significant separation between magnetically "harder" natural samples ($S_{-300mT}$ <0.8) and the much "softer" behaviour of the topsoil and feature fill samples ($S_{-300mT}$ >0.9). This would suggest a distinction between the magnetic minerals within the natural context, that indicates the presence of hard antiferromagnetic phases, such as haematite or goethite over the soft, very fine grained particles that appear to dominate both the modern topsoil and the primary fill of the archaeological features.

The concentration independent bi-plot of $ARM_{-40mT}/(s)ARM_{199mT}$ *vs* $(s)IRM_{2.5T}/\chi$ has proved particularly successful at distinguishing the various context groups and separates all bar one of the natural sand and gravel samples. Separation of the topsoil from the feature fill samples is not so clear but certainly provides an acceptable degree of discrimination given the often ambiguous classification of samples from adjacent context layers in the field. It is of interest to note that the majority of samples from this site plot towards the envelope of values reported for bacterial magnetite when presented on a bi-plot of $\chi_{ARM}/\chi$ *vs* $\chi_{ARM}/\chi_{FD}$. As this latter bi-plot is, in general, influenced by the soft ferrimagnetic component it is reasonable to suggest that a bacterial source of enhancement may well be significant within the soils and feature fill sediments at this site.

*4.5.2.2 IRM acquisition and hysteresis*

In field hysteresis results are presented in Figure 4.17, including the acquisition of forward IRM, representative hystersis loops and a bi-plot of $H_C/H_{CR}$ *vs* $M_S/M_{RS}$. The majority of samples demonstrate similar IRM acquisition curves to the samples recovered from the Cresswell Field site with a very rapid increase in magnetisation at low fields. Approximately half the total value is obtained in a forward field of 20mT

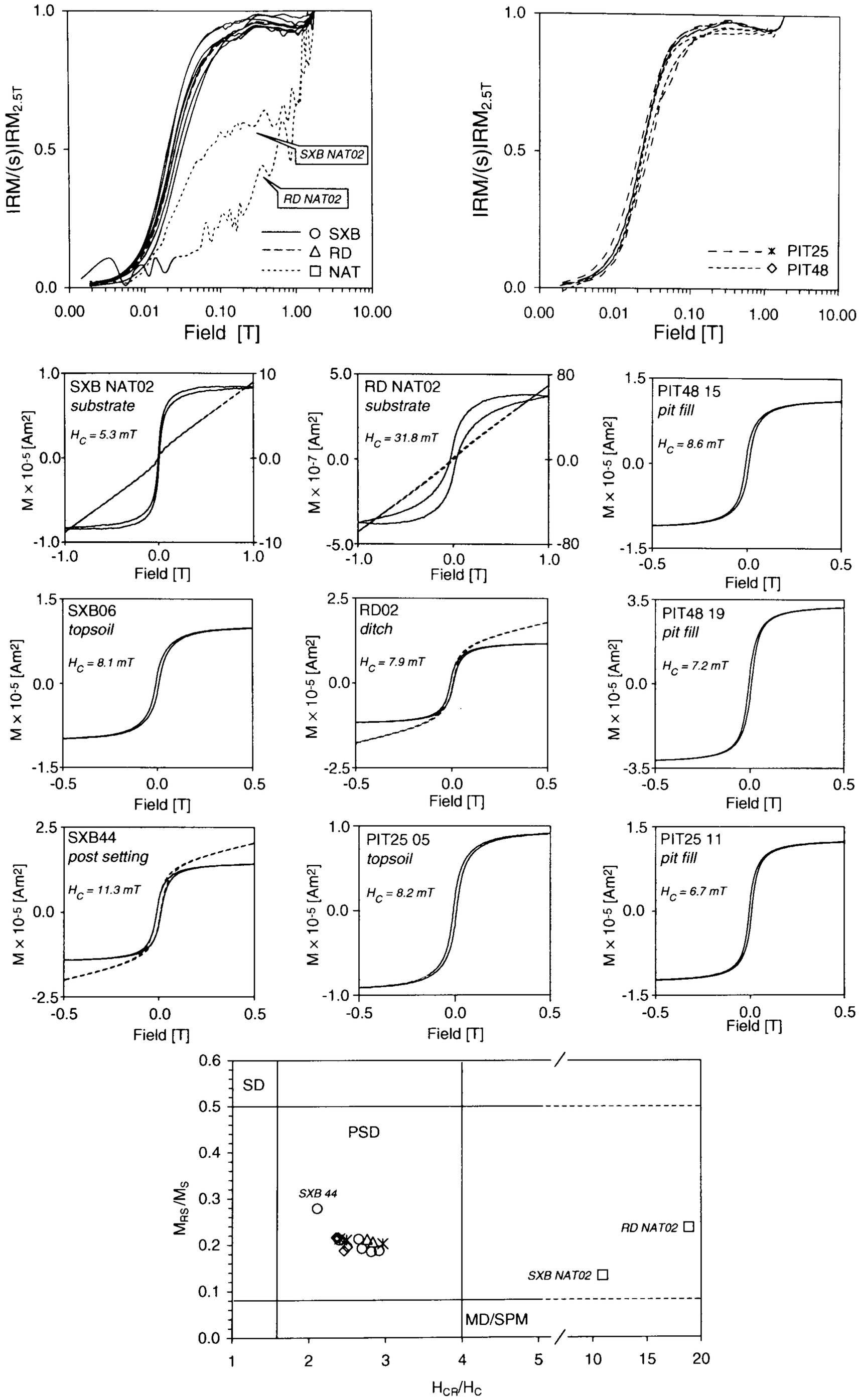


***Figure 4.17*** *Summary of the IRM acquisition and selected hysteresis behaviour for the samples recovered from the Saxon timber building excavated at the Worton 1996A site. Where hysteresis loops contain a significant paramagnetic component the uncorrected data is shown (dashed line) superimposed over the underlying ferrimagnetic loop (solid line).*

and full saturation by ~200mT. Again, a slight 'sag' in the IRM acquisition curves occurs at high fields due, perhaps, to the presence of viscous material as discussed in §4.3.3.2 above. The samples also show a rapid increase of magnetisation in very high fields, between 1.0 and 1.8T, suggesting the presence of a high coercivity mineral such as haematite or goethite.

The two samples of the underlying sand and gravel substrate demonstrate quite different IRM acquisition behaviour with increased noise due to their low magnetisation. The most extreme sand and gravel sample (RD NAT02) acquires negligible magnetisation in low fields and requires a 500mT field to obtain half of the maximum laboratory IRM. The increase of IRM in high fields is approximately linear with no indication of an approach to saturation, indicative of the dominance of high coercivity minerals. Sample SXB NAT02 demonstrates an intermediate behaviour for IRM acquisition with a more rapid increase in magnetisation in low fields to RD NAT02. Indeed, the curve reaches a partial saturation by ~200mT before a high field behaviour similar to RD NAT02 ensues between 0.5 to 1.8T, suggesting a mixed mineralogy between that of the feature fills and the underlying sand and gravel substrate.

In field hysteresis loops show a similar distinction between the sand and gravel substrate, topsoil and feature fill contexts. Samples from the latter two groups demonstrate a small paramagnetic component superimposed over a low coercivity, ferrimagnetic loop that reaches saturation in by 500mT. When combined with the corresponding remanent coercivity data the majority of these samples fall within a tight group on the $H_{CR}/H_C$ *vs* $MR_S/M_S$ bi-plot within the envelope of values reported for pseudo single domain magnetites (Day et al. 1977). One outlier from this group, SXB44 from the post setting, suggests the possible presence of biogenic SD magnetite (*cf* Faßbinder and Stanjek 1993).

In contrast, the two samples of natural sand and gravel are dominated by a paramagnetic response with a magnetisation at 1.8T at least an order of magnitude greater than the underlying saturation magnetisation of the ferrimagentic loop. Both ferrimagnetic loops are constricted, or 'wasp waisted', around the origin and do not reach saturation within the maximum ±1.0T field applied. The apparent closure of the upper and lower branches of these loops at ±1.0T is due to the data processing algorithm applied

(§3.3.8). From the forward IRM data it would seem unlikely that the minerals giving rise to this behaviour would saturate in fields less than ±2.5T and if goethite is indeed a dominant mineral then saturation may not occur until a field of >20T is applied (Thompson 1986).

Sample SXB NAT02 would appear to demonstrate an intermediate hysteresis behaviour between that of the toposoil/feature fill samples and the extreme 'wasp waisted' loop of RD NAT02. Differences are apparent in the coercivity of the ferrimagnetic loops, the degree of closure in high fields and the overall magnitude of the sample magnetisation. However, both natural samples when plotted on the $H_{CR}/H_C$ *vs* $MR_S/M_S$ bi-plot, fall well beyond the values of these two ratios reported for magnetite due mainly to much increased values of $H_{CR}$ compared with the topsoil and feature fill samples.

*4.5.2.3 Low temperature results*

Figure 4.18 shows the variation of low temperature magnetisation for five samples selected from the Saxon building site samples. All five curves demonstrate a gradual increase of $M_S$ on cooling from room temperature to 20K. As the measurements were made in zero field and the increase in $M_S$ is approximately linear, rather than $^1/_T$, it is unlikely that the variation is due to any paramagnetic component within the samples and may be due to the presence of goethite (e.g. Dekkers 1988). This interpretation would concur with the hysteresis data that indicates a high coercivity component within the samples (Figures 4.16 and 4.17).

.

Analysis of the *dM/dT* data derived from the cooling curves reveals a possible Verwey transition in the topsoil sample SXB06 between 118-124K. Data from the other three samples fails to reveal this transition although inflections do occur within the *dM/dT* cooling curves at approximately 100K. The rate of change of slope from room temperature to 100K is either approximately linear (SXB06, PIT25 11) or consists of a more rapid decrease from 300 to ~225K followed by a constant rate of decay between 225 to 100K (SXB44, RD02 and PIT48 19). Between ~100K and 20K *dM/dT* demonstrates a slight peak at ~75K that possibly represents the blocking temperature of very fine superparamagnetic particles in the samples.

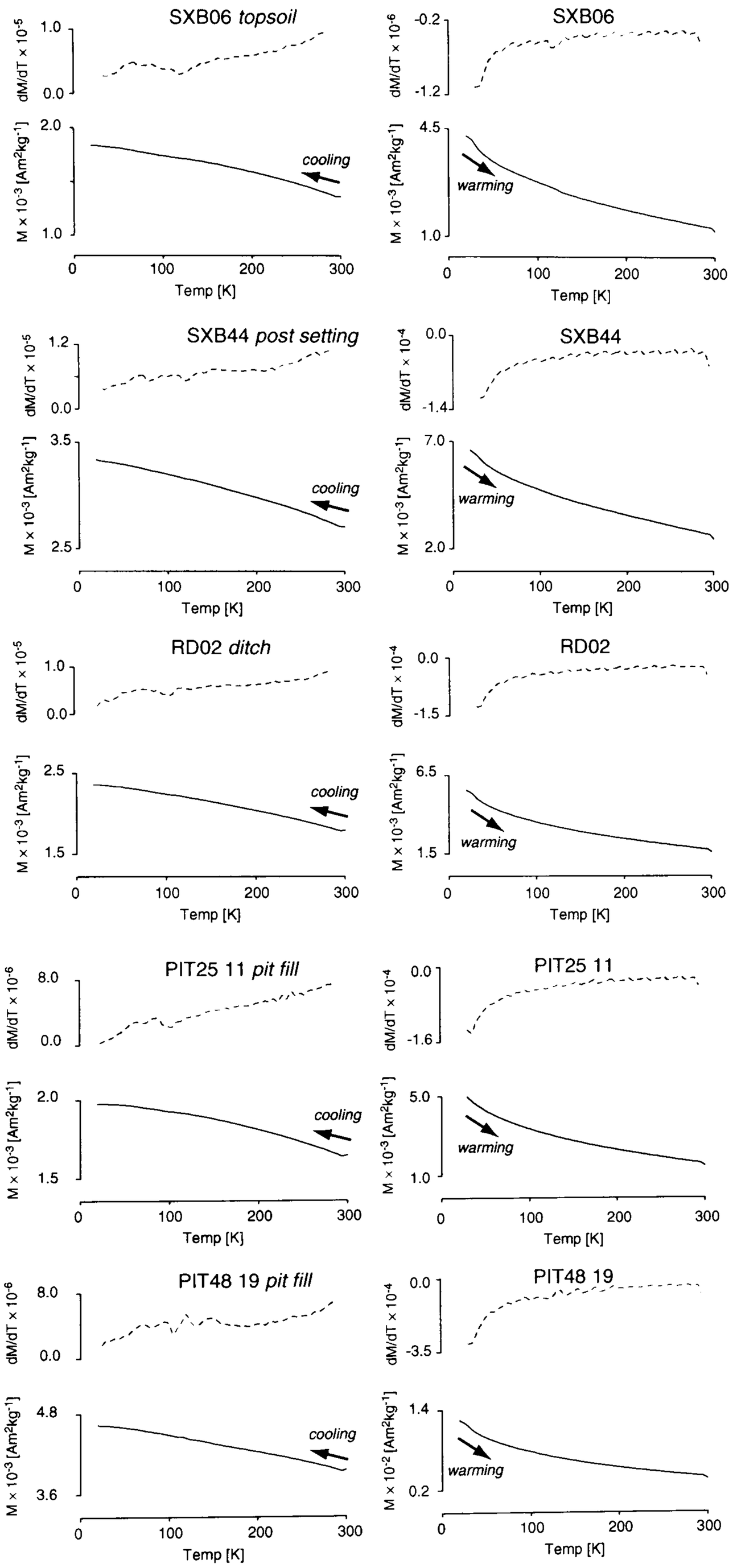


***Figure 4.18*** *Low temperature behaviour of selected samples recovered from the Saxon timber building excavated at the Worton 1996A site. Cooling curves are plotted separately from warming curves due to the differing magnitude of the two data sets and the first differential of each curve is also shown to aid the identification of subtle inflections.*

The *dM/dT* warming curves are more uniform between the five samples and show a rapid decay of $M_S$ from 20K to approximately 100K. Again, this is thought to represent the unblocking of magnetisation held by fine superparamagnetic particles until a more linear loss of $M_S$ sets in above 100K to room temperature.

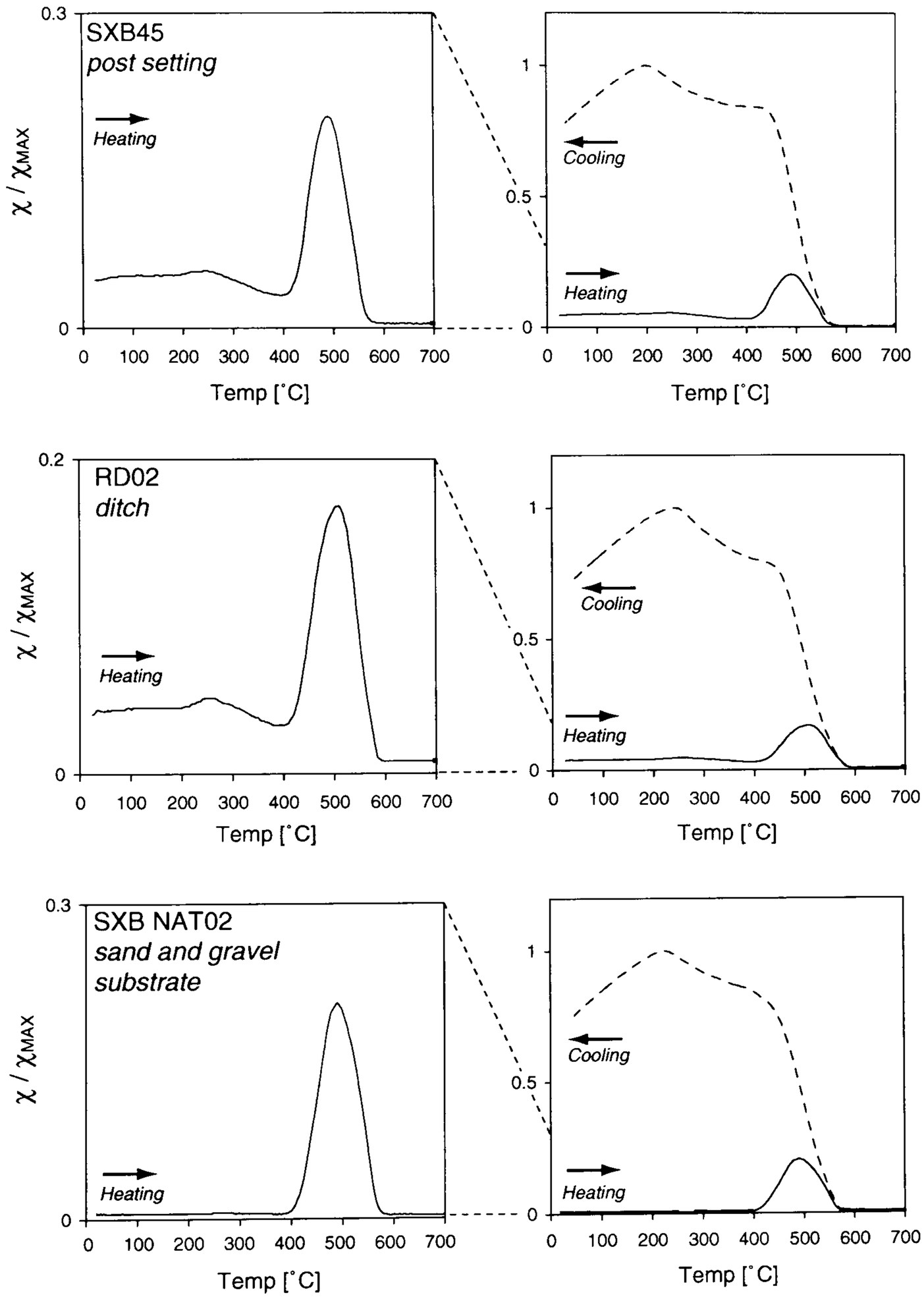


***Figure 4.19*** *Variation of high temperature susceptibility for selected samples from the Worton 1996A site. The heating and cooling curves are plotted separately for each sample.*

*4.5.2.4 High temperature thermomagnetic analysis*

The variation of $\chi$ from room temperature to 700°C was conducted on 3 samples, SXB45, RD02 and NAT02, from the Worton 1996A site (Figure 4.19). The heating curve is again plotted separately from the cooling curve to allow the identification of subtle inflections. The two feature fill samples, SXB45 and RD02, behave in a similar manner with little or no variation of $\chi$ between room temperature and ~250°C where a slight increase, possibly due to the inversion of lepidocrocite to maghaemite, is evident. A gradual loss of $\chi$ occurs above 250°C to ~400°C, that may be attributed to the range of Curie temperatures of (titano)maghaemite, either newly formed from the chemical alteration noted at 250°C or present as a constituent mineral phase in the unheated sample. A rapid increase in $\chi$ then begins at 400°C reaching a peak at 500°C before falling, equally rapidly, to the magnetite Curie temperature of ~580°C.

The cooling curves of these two samples are highly similar to the behaviour of CWF PIT12 and CWF IAG23 being dominated by the continued alteration of weakly magnetic iron minerals to magnetite. Below 575°C inflections are found in the much enhanced cooling curve at ~450 and ~200°C that may again be interpreted as the oxidation of magnetite to maghaemite and blocking spectra of these newly formed, fine grained minerals respectively.

The behaviour of the sand and gravel sample, SXB NAT02, is similar but may be distinguished from the feature fill samples on heating from room temperature to 400°C. In this case, the initial value of $\chi$ prior to heating is negligible and little variation is evident in the heating curve before the rapid alteration of weakly magnetic iron minerals at 500°C. This data suggests the behaviour of all samples following heating to at least 500°C is determined by the chemical alteration of weakly magnetic iron minerals that would appear to be present in similar concentrations in all of the context types. Consequently, the identification of ferrimagnetic material is only visible on heating where the presence of (titano)maghaemite or magnetite may be determined.

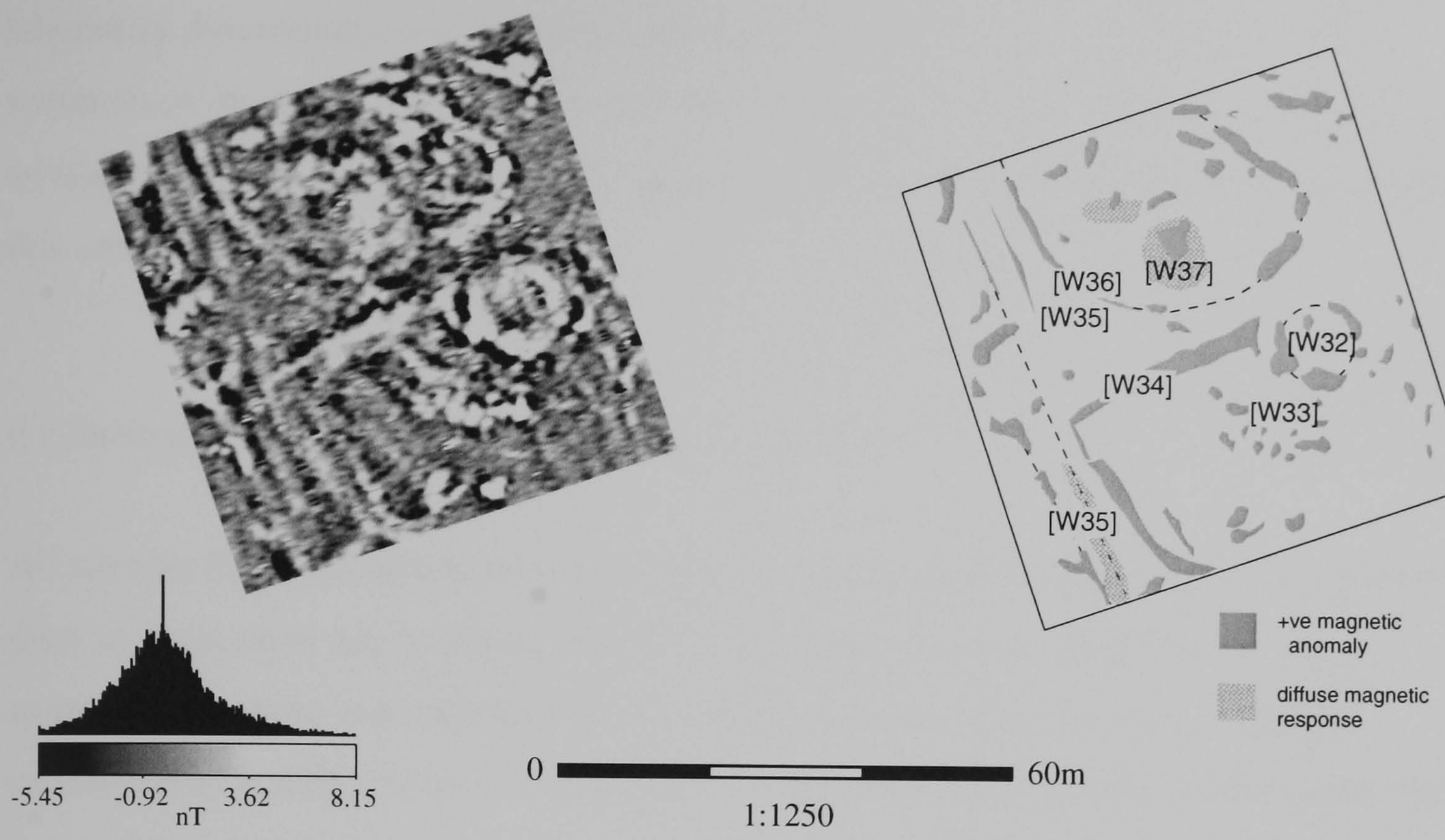


***Figure 4.20*** *Greytone image of fluxgate gradiometer data from Worton 1992 (A) together with a summary of significant anomalies (B).*

### *4.6.1 Worton 1992*

During March 1992 a 60m × 60m trial fluxgate gradiometer survey was conducted over the agricultural land to the S of Worton 1996 Site B to assess the geophysical response of the project area (Figure 4.20). Although this area has never been tested through excavation the survey reveals a palimpsest of strong magnetic anomalies which replicate the fine detail evident in the cropmark data (Figure 4.13). A circular anomaly [W32] is adjacent to a series of pit-type responses [W33] that correlate with the position of an apparent enclosure within the cropmark data. Two sides of a larger enclosure [W34] are found to the W where they adjoin a number of linear anomalies [W35] forming a large rectangular enclosure revealed by the cropmark data beyond the limit of the geophysical survey.

A third enclosure evident in the cropmark data to the N correlates with anomaly [W36]. Both the datasets show a large sub-circular anomaly within the enclosure that the magnetic data resolves into a pit-type anomaly surrounded by a more diffuse magnetic response [W37].

Four topsoil samples were recovered from the centre of each 30m survey square for the laboratory determination of magnetic susceptibility. Figure 4.13 (inset) shows the variation of magnetic susceptibility and the considerable enhancement that has occurred within the square containing [W32], suggesting more intense occupation activity within this area.

### *4.7 Summary of results from the raised gravel terrace*

All sites on the raised gravel terrace produced a good magnetic response when surveyed prior to excavation and a strong correlation between anomalies identified in the geophysical survey and subsequently excavated features. The degree of magnetic enhancement is reflected in the behaviour of samples recovered from these features that, in general, demonstrates an unambiguous separation of the underlying sand and gravel substrate from the feature fills and topsoil layers. Whilst the magnetic parameters of the topsoil overlap with many of the feature fills some distinction is evident in the apparent grain size distribution. For example, samples from pit-type features demonstrate an increased concentration of very fine grained, superparamagnetic material and samples from the timber post setting appear to be dominated by single domain magnetite. These distinctions are more clearly evident within the thermomagnetic data, particularly the variation of high temperature susceptibility, where the pronounced loss of $\chi$ on heating to 300°C differentiates many of the feature fills from both the topsoil and the sand and gravel substrate.

# *Chapter 5*

## *5.0 Flood plain sites*

The distribution of geophysical survey sites over the flood plain is shown in Figure 4.1 where the magnetic response was far more subdued than the raised gravel terrace sites. As the majority of gravel extraction for the Yarnton Cassington project area was planned for the flood plain large scale archaeological excavations were conducted allowing the recovery of mineral magnetic samples from a wide range of features found on these sites. However, a number of sites were only available for excavation following the removal of topsoil.

### *5.1.1 ARC Stage 4*

This 4ha survey was the first to be conducted within the project area and both the fluxgate gradiometer and earth resistance data sets produced quite disappointing results (Figures 5.1, 5.2 and 5.3). Modern ferrous disturbance has hampered the identification of weak magnetic anomalies throughout this area particularly in the vicinity of the overhead electricity supply stanchion [ARC1]. However, a number of tentative magnetic anomalies have been identified including a series of negative linear responses [ARC 2]; pit-type responses at [ARC 3 - 7] and very weak curvilinear anomalies at [ARC 8], [ARC 9] and [ARC 10] that may be associated with occupation activity. The linear negative anomalies [ARC 2] follow an orientation similar to the modern plough pattern revealed by the earth resistance survey (see below) and may be due to the same source. These latter anomalies are less evident on the small scale plots reproduced in Figure 5.1.

In the southern area, the magnetic survey revealed a broad magnetic anomaly indicating the course of a former palaeochannel [ARC 11] which contains a negative linear anomaly that correlates with the location of the Oxford Archaeological Unit (OAU) evaluation trench 23 excavated in advance of the geophysical survey [ARC 12]. This latter response suggests the anomaly due to the palaeochannel possibly arises from a (?detrital) remanent component that has been disturbed by the excavation and back-

(A)

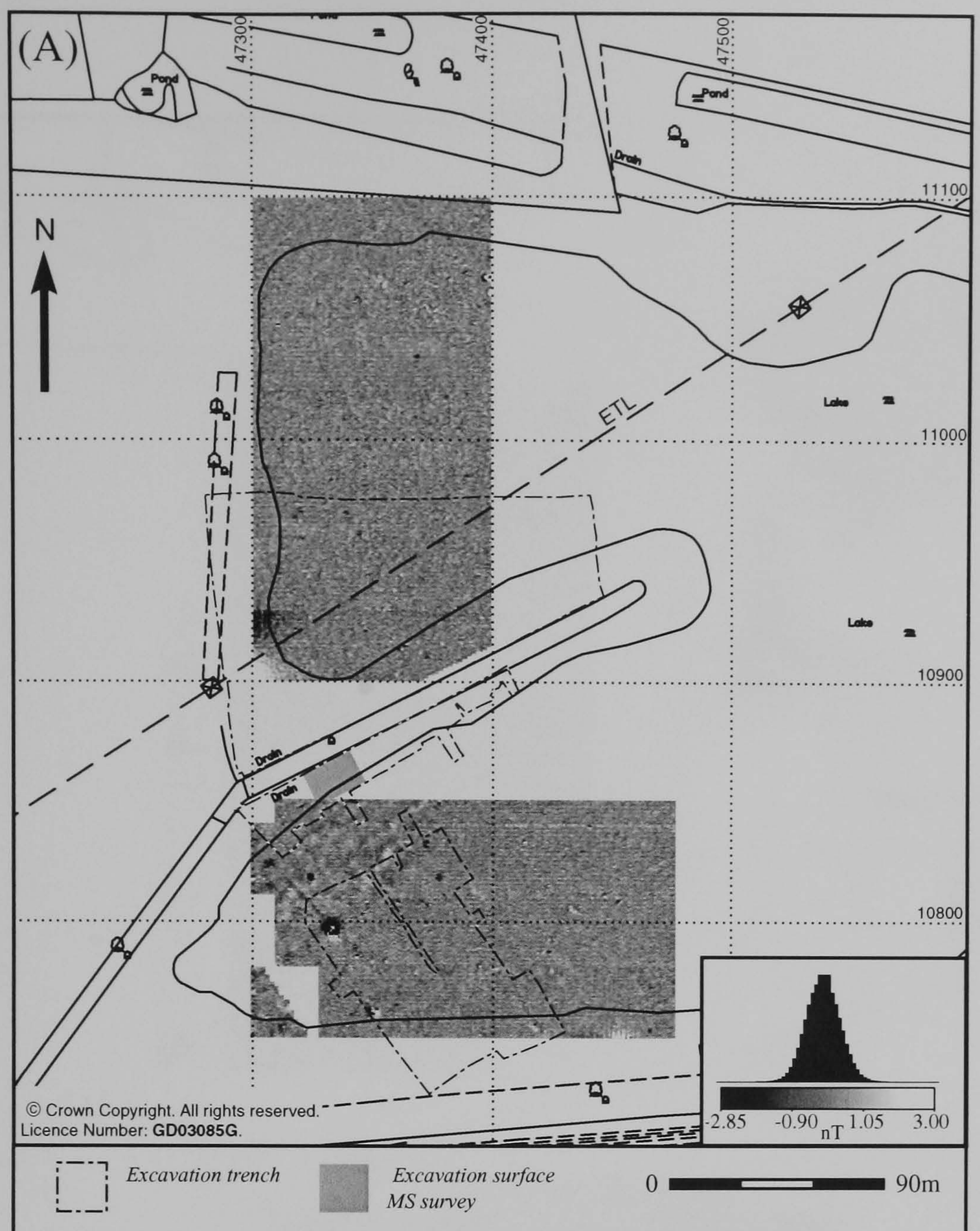


(B)

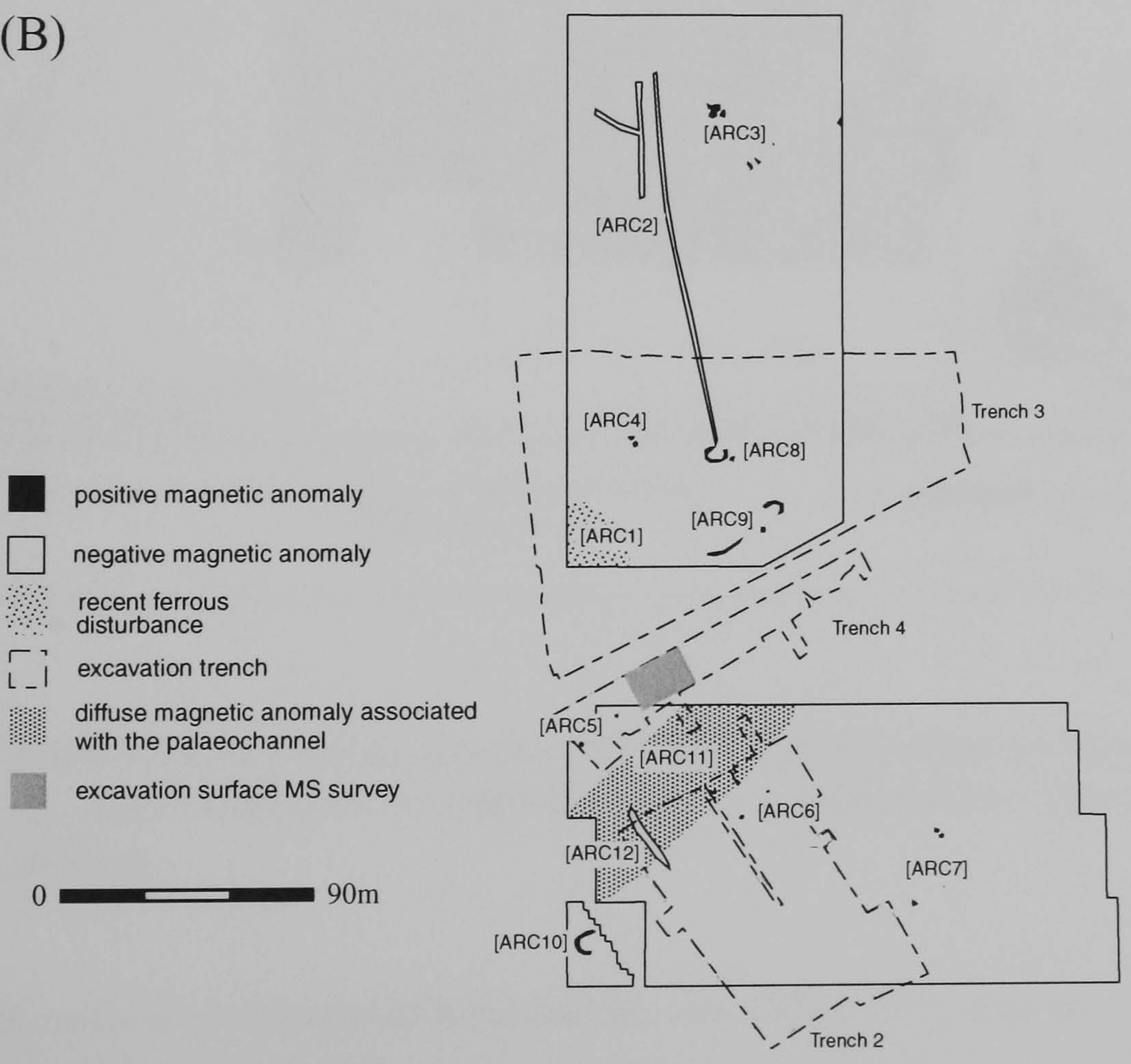


***Figure 5.1*** *(A) Greytone image of fluxgate gradiometer data from ARC Stage 4 together with (B) a summary of significant anomalies.*

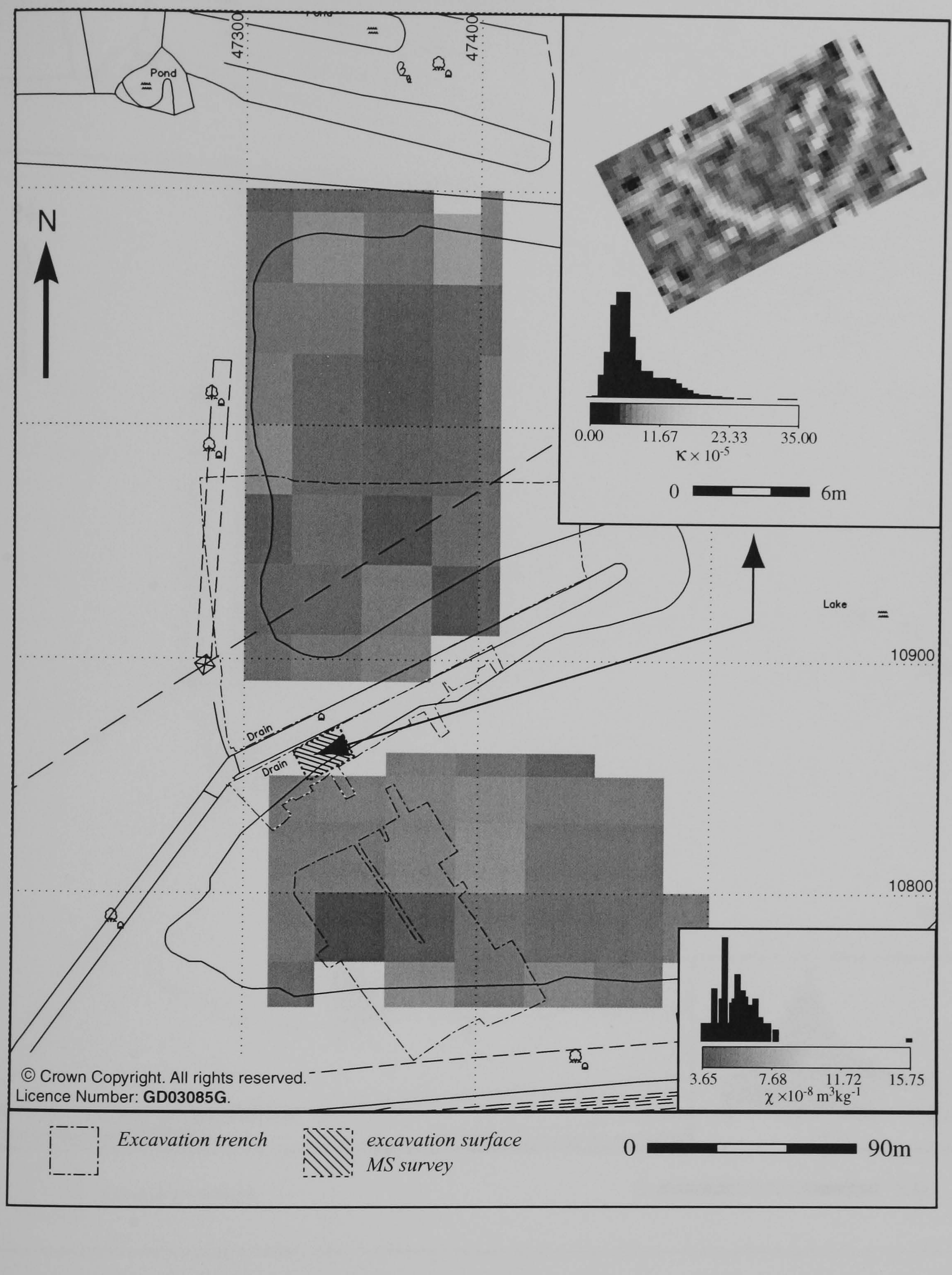


***Figure 5.2*** *Topsoil susceptibility data for ARC Stage 4. The inset greytone image shows the results of a high resolution susceptibility survey conducted over the topsoil stripped excavation surface.*

filling of the evaluation trench (*cf* Ellis and Brown 1998). This area also contains a number of discrete negative circular anomalies due to modern ferrous disturbance that have not been included within the interpretation plan.

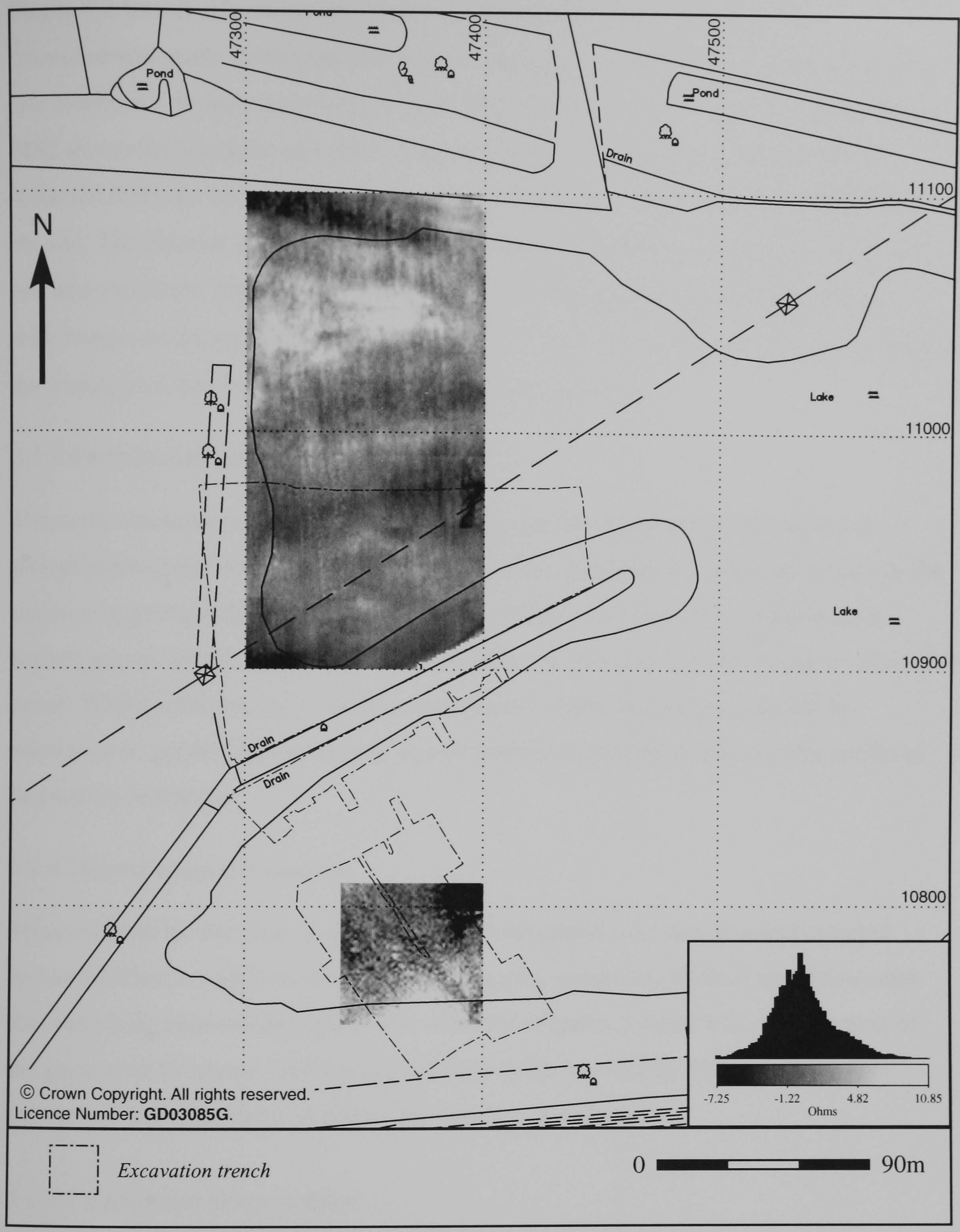


***Figure 5.3*** *Greytone image of earth resistance data collected over ARC Stage 4.*

*5.1.2 Topsoil magnetic susceptibility*

Topsoil magnetic susceptibility results (Figure 5.2) demonstrate the uniformly low level of enhancement that has occurred. The majority of recorded readings are $\chi < 10 \times 10^{-8}$ $m^3kg^{-1}$ and there are no significant concentrations of raised readings within the data set.

Figure 5.2 (inset) also shows the results of the high-resolution susceptibility measurements made during the subsequent excavation of the site over the location of a late Neolithic / Bronze Age circular ditch. The survey was conducted with a Bartington MS2 susceptibility meter and 20cm diameter field search loop with measurements collected from the excavation surface following the removal of overlying topsoil from the site. The circular ditch is cut by a later Roman ditch and also contains a number of pits and tree throw features. The susceptibility of these features is slightly enhanced with respect to the sand and gravel substrate ($\kappa$ = ~10 to 20 × $10^{-5}$) and clearly identifies the majority of the features identified during excavation.

### *5.1.3 Earth resistance survey*

The earth resistance survey (Figure 5.3) reveals an NS orientated pattern of recent plough marks superimposed over a lower frequency variation of resistance related to the underlying geomorphology. The distribution of high resistance areas represents near surface gravel islands surrounded by more moisture retentive concentrations of alluvial cover. Whilst such data may indicate areas more suitable for past occupation no anomalies of greater archaeological significance could be identified from the results of this survey technique.

### *5.1.4 Mineral magnetic analysis*

Three excavation trenches, Sites 2, 3 and 4 were opened over this area and samples recovered from a variety of features including pits, postholes, ditches, tree throws and the underlying natural sand and gravel substrate (Figures 5.4 and 5.5). The location of the excavated Neolithic / Bronze Age circular ditch covered by the topsoil magnetic susceptibility survey (§5.1.2; Figure 5.2 inset) is also shown.

#### *5.1.4.1 Isothermal measurements*

Selected biplots of isothermal parameters and ratios are shown in Figure 5.6 and demonstrate low magnetic susceptibility ($\chi < 10 \times 10^{-8}$ $m^3kg^{-1}$) for the majority of samples. A few pit / posthole samples do exceed the envelope of $\chi$ values recorded by the underlying sand and gravel, including 4005 with $\chi > 100 \times 10^{-8}$ $m^3kg^{-1}$, but in general this parameter fails to separate the archaeological sediments from the underlying substrate. Values for $\chi_{FD}$ lie between 0 and $6 \times 10^{-8}$ $m^3kg^{-1}$ with the majority

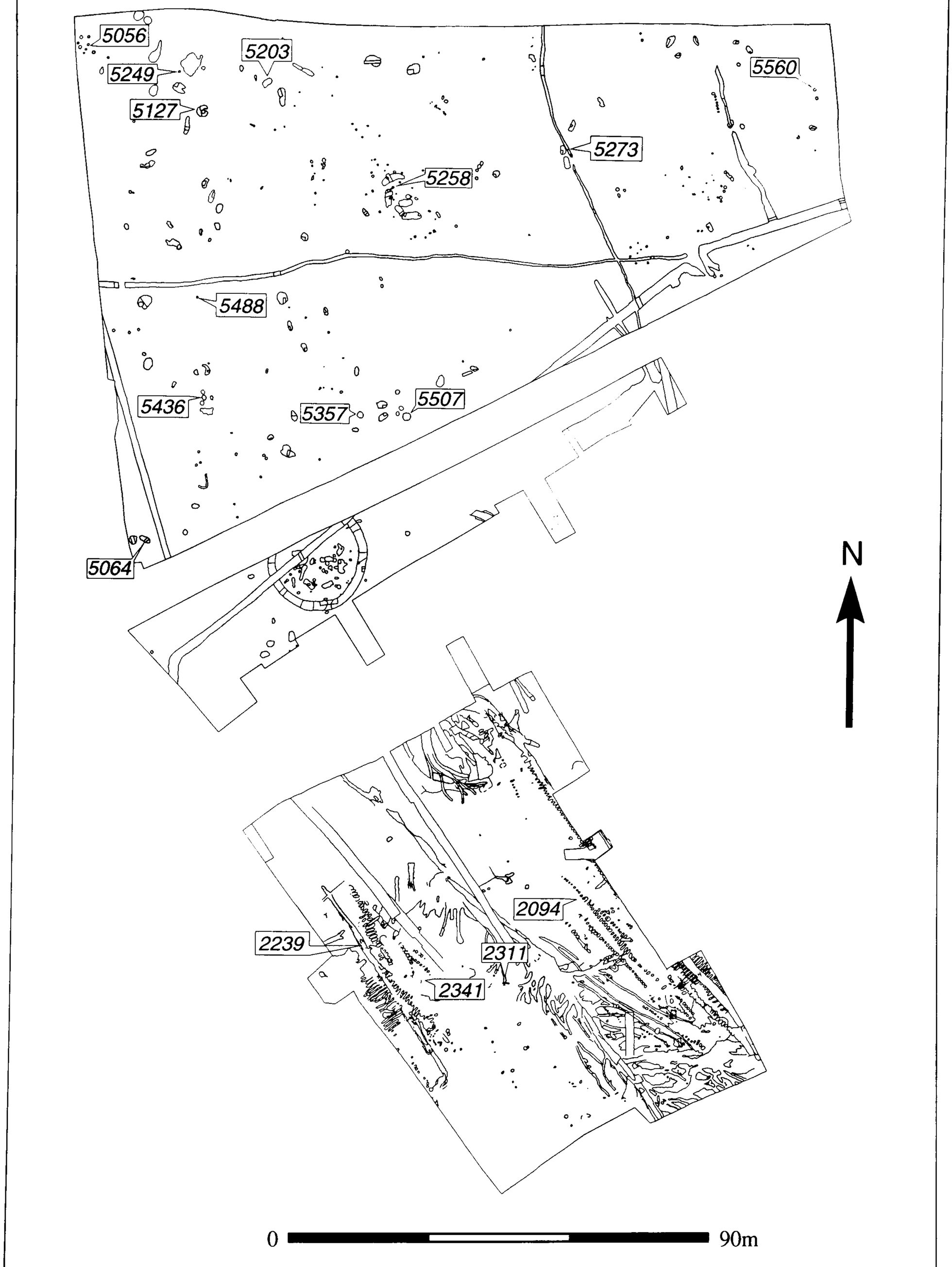


***Figure 5.4*** *Plan view of the features recorded during the excavation of ARC Stage 4 sites 2, 3 and 4.*

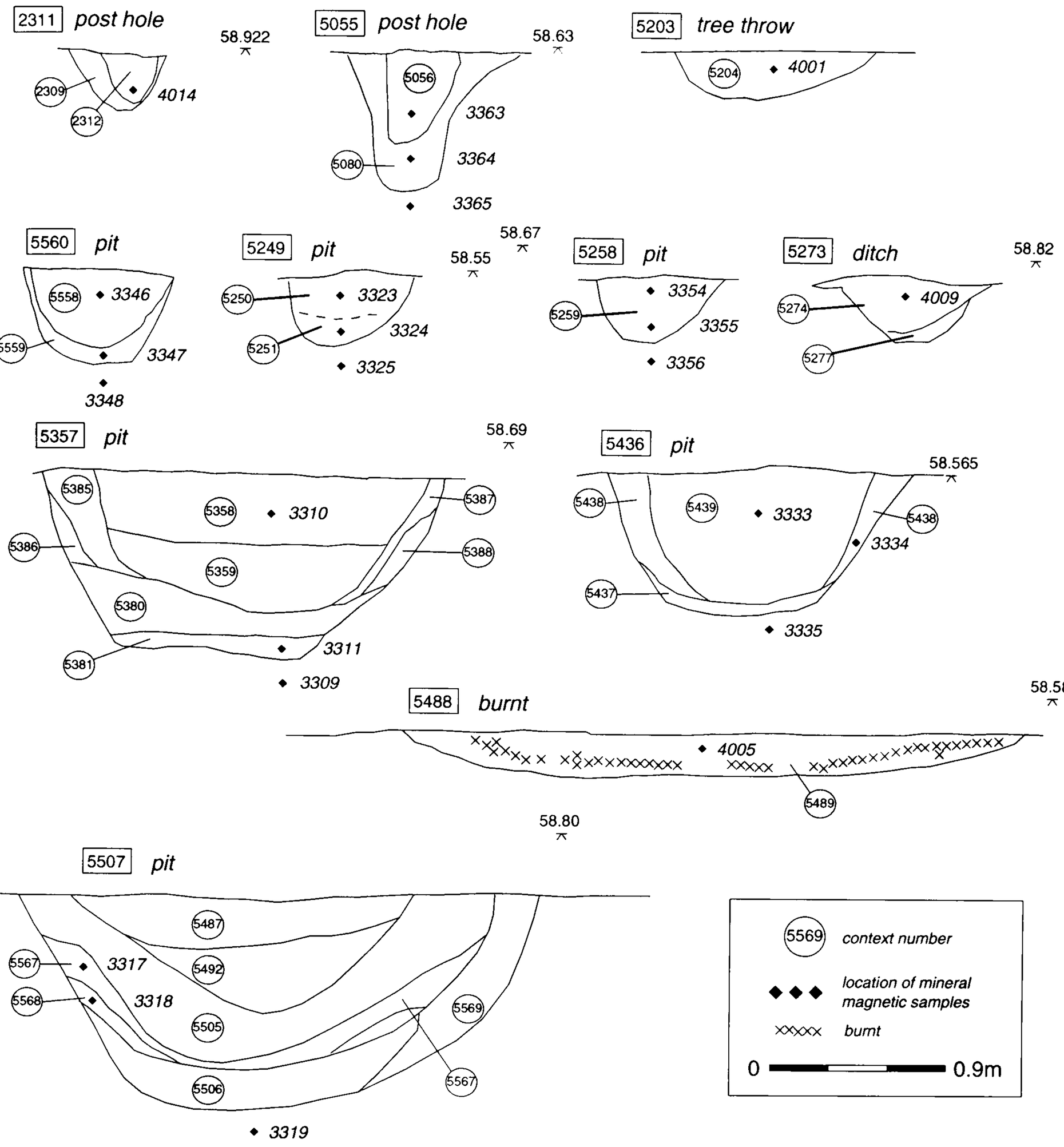


***Figure 5.5*** *Sections drawn through features selected for the collection of mineral magnetic samples from ARC Stage 4 sites 2, 3 and 4 (Figure 5.4). The sections show the location of the recovered samples and the context layers identified in the field.*

of samples, including the sand and gravel, recording $\chi_{FD} < 2 \times 10^{-8}$ $m^3kg^{-1}$. Such low values, close to the noise level of the susceptibility meter, questions the fidelity of the normalised $\chi_{FD\%}$ ratio for the weaker samples. Despite this reservation, values of $\chi_{FD\%}$ are less than 10%, suggesting very fine grained superparamagnetic particles are unlikely to dominate the magnetic properties of these samples.

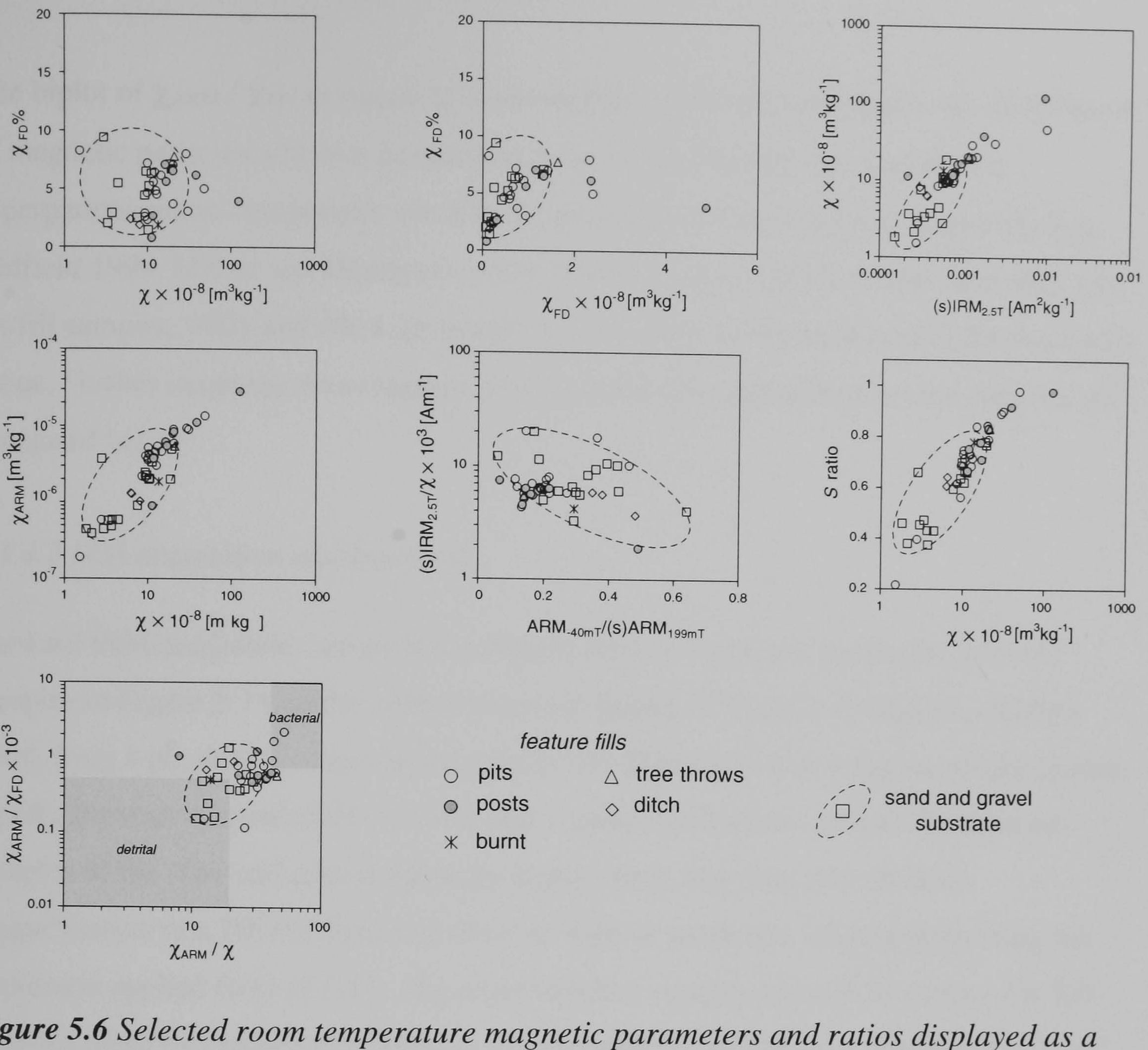


***Figure 5.6*** *Selected room temperature magnetic parameters and ratios displayed as a series of bi-plot graphs for the samples recovered from ARC Stage 4 sites 2, 3 and 4. An envelope showing the approximate range of these parameters for samples of the natural sand and gravel substrate is also illustrated.*

A greater discrimination between the archaeological samples and the natural substrate is obtained from the laboratory induced magnetisation parameters (S)$IRM_{2.5T}$, $\chi_{ARM}$ and the IRM backfield *S* ratio. When plotted against $\chi$ all three of these parameters distinguish a greater number of pit/post hole samples from the envelope of the sand and gravel substrate. In addition, the majority of natural samples fall within an less magnetised, higher coercivity group. The majority of feature fills are also tightly grouped on a biplot of (S)$IRM_{2.5T}/\chi$ *vs* $ARM_{-40mT}$/(S)ARM despite falling with the wide envelope of values encompased by the natural samples. This latter biplot is largely concentration independent and is more sensitive to the type and magnetic grain-size distribution of minerals present within the sample, suggesting the grouping of the feature fills represents a distinct process of magnetic enhancement compared to the pedogenic enhancement of the underlying substrate.

The biplot of $\chi_{ARM}$ / $\chi_{FD}$ *vs* $\chi_{ARM}$ / $\chi$ is also highly sensitive to the grain size distribution of magnetic particles within a sample and may, in the absence of a significant superparamagnetic component, identify the presence of fine, biogenic magnetite (e.g. Oldfield 1999, Maher and Hounslow 1999, Snowball et al. 2002). In this case only two pit-fill samples, 0001 and 4015, lie within the envelope of bacterial values for these two ratios. Further magnetic investigation of these latter two and other selected samples are discussed below.

*5.1.4.2 IRM acquisition and hysteresis*

Forward IRM acquistion curves and infield hysteresis loops are shown for selected samples in Figure 5.7 together with a summary biplot of $H_{CR}/H_C$ *vs* $M_{RS}/M_S$. Sample 4005, from a pit, demonstrates an extremely soft IRM curve that acquires magnetisation rapidly from an induced field of 10mT and is fully saturated by 100mT. In contrast, samples of the sand and gravel substrate acquire only less than 30% of their magnetisation in a 100mT field and show no sign of saturation when approaching the maximum applied field of 1.8T. The other selected samples have IRM curves that fall between these two extremes of behaviours and show evidence for a mixture of a "soft" magnetic component, that accounts for the majority of the magnetisation acquired in induced fields less than 200mT, together with a higher coercivity mineral that slows the approach to saturation in higher fields.

Mixed magnetic mineralogies are also evident within the ferrimagnetic hysteresis loops with many of the samples (e.g. 0001, 4004, 5246, 4012, 5358, 4000 and 4016) demonstrating a restricted "wasp waist" open branches that often do not close within the maximum applied field of 1T. However, this behaviour is by no means universal and a number of samples (e.g. 4005 and 4014) suggest the presence of a low coercivity ($H_C$ = 5 to 6mT) mineral that produces a fully saturated (ferrimagnetic) loop in fields of 0.5T together with a less dominant paramagnetic fraction. These latter samples, when plotted on a biplot of $H_{CR}/H_C$ *vs* $M_{RS}/M_S$, fall within the envelope of values reported for pseudo single domain (titano)magnetite (Day et al. 1977) and may well be dominated by a similar mineralogy. Hysteresis loops showing evidence of a mixed mineralogy, including samples of the natural sand and gravel, plot beyond the values of the $H_{CR}/H_C$

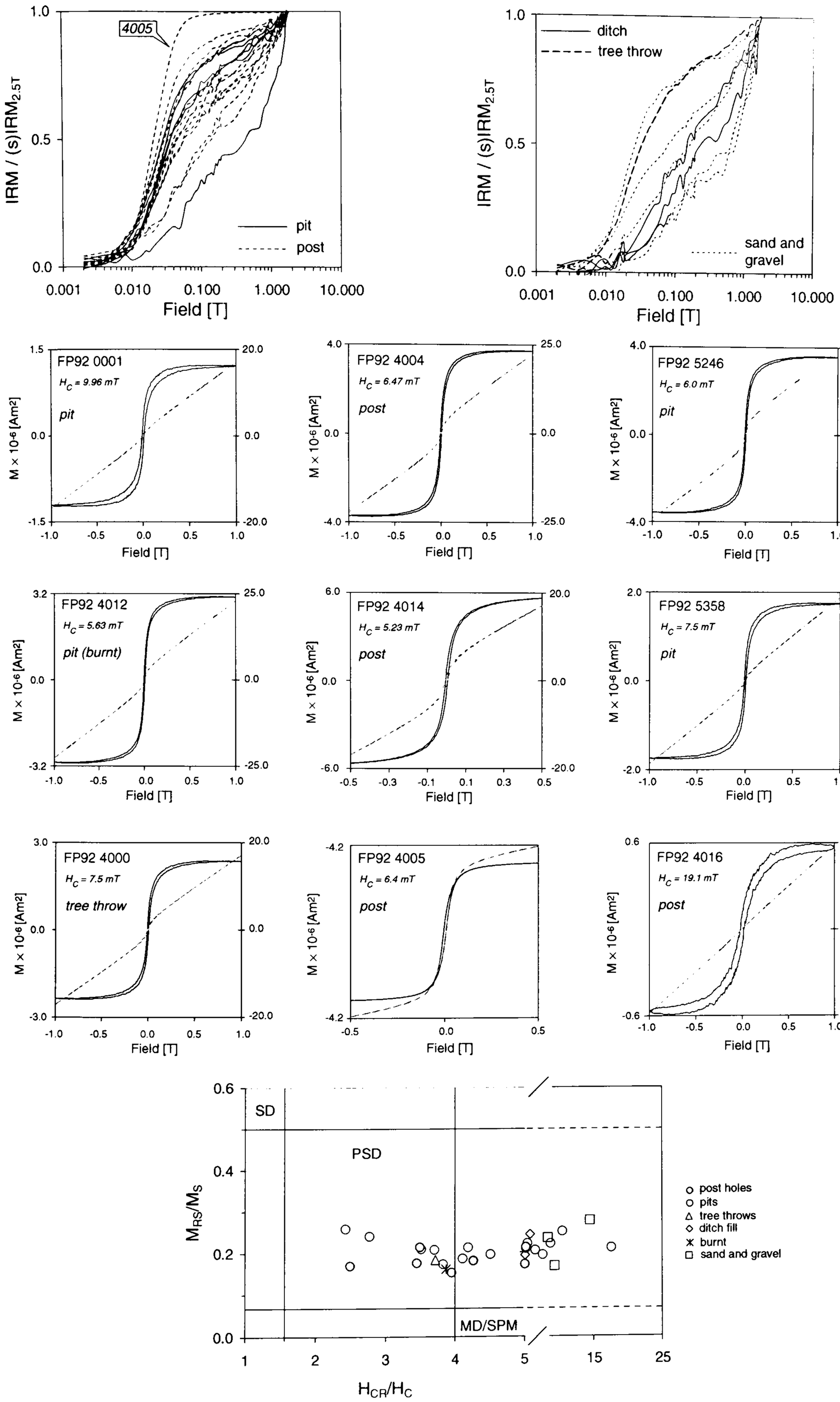


***Figure 5.7*** *Summary of the IRM acquisition and hysteresis behaviour for samples from ARC Stage 4 sites 2, 3 and 4. Where hysteresis loops contain a significant paramagnetic component the uncorrected data is shown (dashed line) superimposed over the underlying ferrimagnetic loop (solid line). Where necessary, the paramagnetic component is plotted against a second scale axis (right hand side of figure).*

and $M_{RS}/M_S$ ratios reported for (titano)magnetite ($H_{CR}/H_C > 5$) confirming the presence of a high coercivity component.

*5.1.4.3 Low temperature magnetisation*

The low temperature variation of a magnetisation acquired in a 2.5T field at 300K subsequently cooled to 20K is shown in Figure 5.8 for 5 of the 14 measured samples. This figure also shows the variation of a second magnetisation applied in a similar field at 20K on warming back to ambient. The cooling curves, with the exception of sample 4005, are all very similar and show an approximately linear increase of magnetisation on cooling to 20K. The magnetisation of sample 4005 also increases in a linear manner during cooling from 300 to ~150K, before a more rapid rise occurs between 150 to ~50K below which the magnetisation levels to a more gentle plateau.

From analysis of the hysteresis loops (Figure 5.7) it can be seen that the paramagnetic component of sample 4005 (calculated from the highfield slope of the hysteresis loop) is similar to the other samples from this site (sample 4005 $\kappa_{para} = 1.61 \times 10^{-5}$ compared to a range of $\kappa_{para} = 0.76 \rightarrow 2.87 \times 10^{-5}$ for the 29 samples measured for hysteresis from this site). However, the ferrimagnetic component of sample 4005 is of the same order of magnitude as the paramagnetic contribution and apparently dominates the response of the cooling curve. Whilst the linear increase found within the majority of the other samples may well be due to the more significant paramagnetic component a $^1/_T$ variation would, perhaps, be more expected from magentic theory (§1.3.2). This suggests that the linear increase on cooing is either due to the ferrimagnetic ordering of paramagnetic minerals on cooling or, more likely, the dominance of detrital goethite as the remanence carrying mineral within these samples as the saturation magnetisatioin of this mineral is reported to increase on cooling (e.g. Dekkers 1988).

A greater degree of interpretation may be extracted from the first differential, $^{dM}/_{dT}$, of the cooling curves. All of the samples contain an initial inflection on cooling from 273 to ~245K that, despite having been air dried at room temperature prior to measurement, may be due to mechanical dislocation within the sample as constituent water freezes to form ice crystals. The $^{dM}/_{dT}$ then show little variation until an inflection occurs within

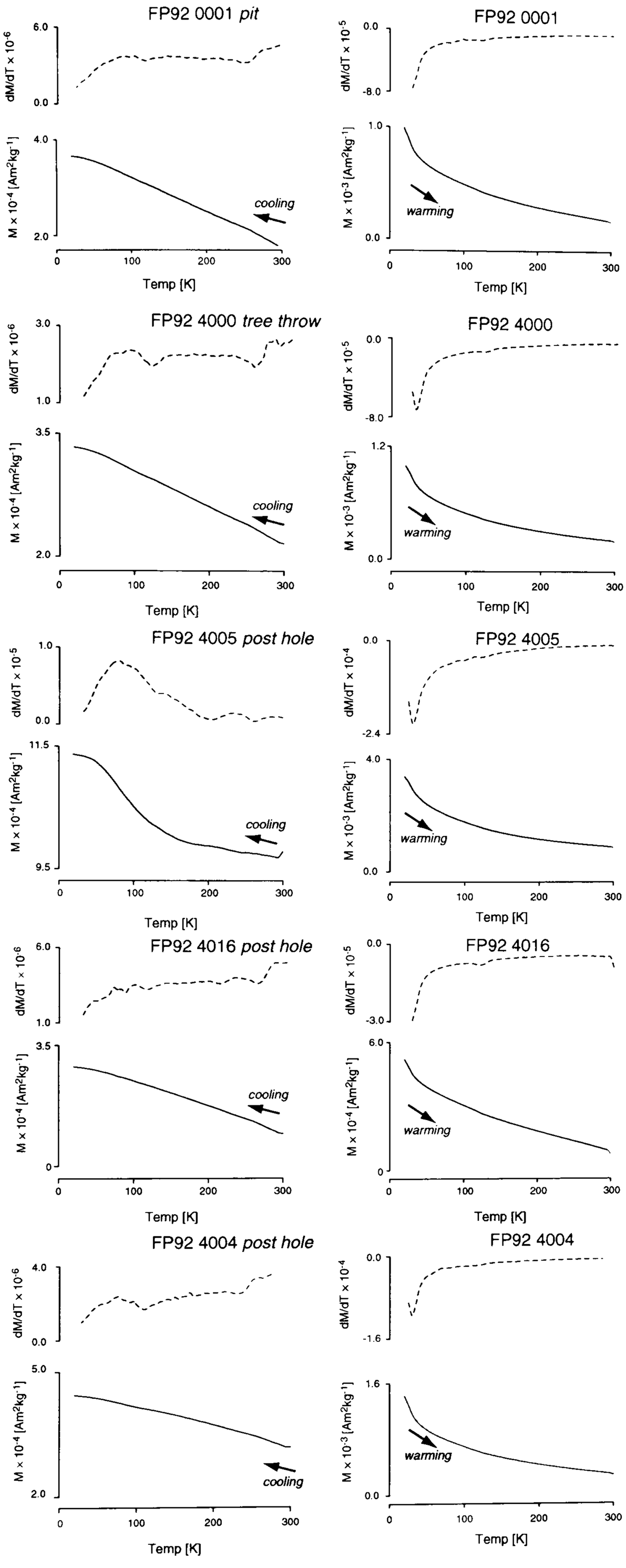


***Figure 5.8*** *Low temperature behaviour of samples from ARC Stage 4 sites 2, 3 and 4. Cooling curves are plotted separately from warming curves due to the differing magnitude of the two data sets and the first differential of each curve is also shown (dashed line) to aid the identification of subtle inflections.*

all the samples at ~120K followed by a gentle rise through a peak value at ~80K and decay towards zero gradient as the samples reach a low temperature saturation at the minimum measurement temperature. This anomaly is clearly evident within many of the $^{dM}/_{dT}$ curves (e.g. 4000, 4005 and 4004) but may also be identified on close inspection of data from the apparently weaker samples.

The coincidence of this low temperature inflection with the expected temperature of Verwey transition suggests fine magnetite crystals may account, in part, for the magnetisation of these samples. In addition, the recovery of magnetisation below this transition may be indicative of the unblocking spectra of these fine grained minerals, that is particularly pronounced in sample 4005.

Warming curves are also highly similar for all of the samples and the magnetisation acquired at 20K follows an approximately $^{1}/_{T}$ decay as the temperature returns to ambient, possibly due to the varying susceptibility of the paramagnetic component noted above. Again, the first derivative of the warming curve proves useful for the identification of subtle features including a rapid loss of magnetisation between 20 and ~100K that almost obscures a minor inflection at ~120K. The initial inflection may well be due to low temperature ferrimagnets disordering to a paramagentic state and the second provides additional evidence for the Verwey transition of magnetite.

*5.1.4.4 High temperature thermomagnetic data*

Figure 5.9 shows the variation of magnetic susceptibility from ambient to 700°C for four selected samples. Again, the much lower magnitude heating curve is plotted separately to aid the interpretation of the data. The sample of natural sand and gravel substrate (4017) shows very little variation on heating beyond a slight increase at approximately 500°C and an apparent magnetite Curie temperature at 580°C. However, the cooling curve for this sample shows a massive degree of enhancement, recovering susceptibility rapidly on cooling from ~550°C to an initial peal centred at ~350°C before the curve passes through a second peak just above 100°C. This behaviour suggests the presence of relatively non-magnetic iron minerals in the unheated sample that are thermally altered to a ferrimagnetic form on heating to 700°C.

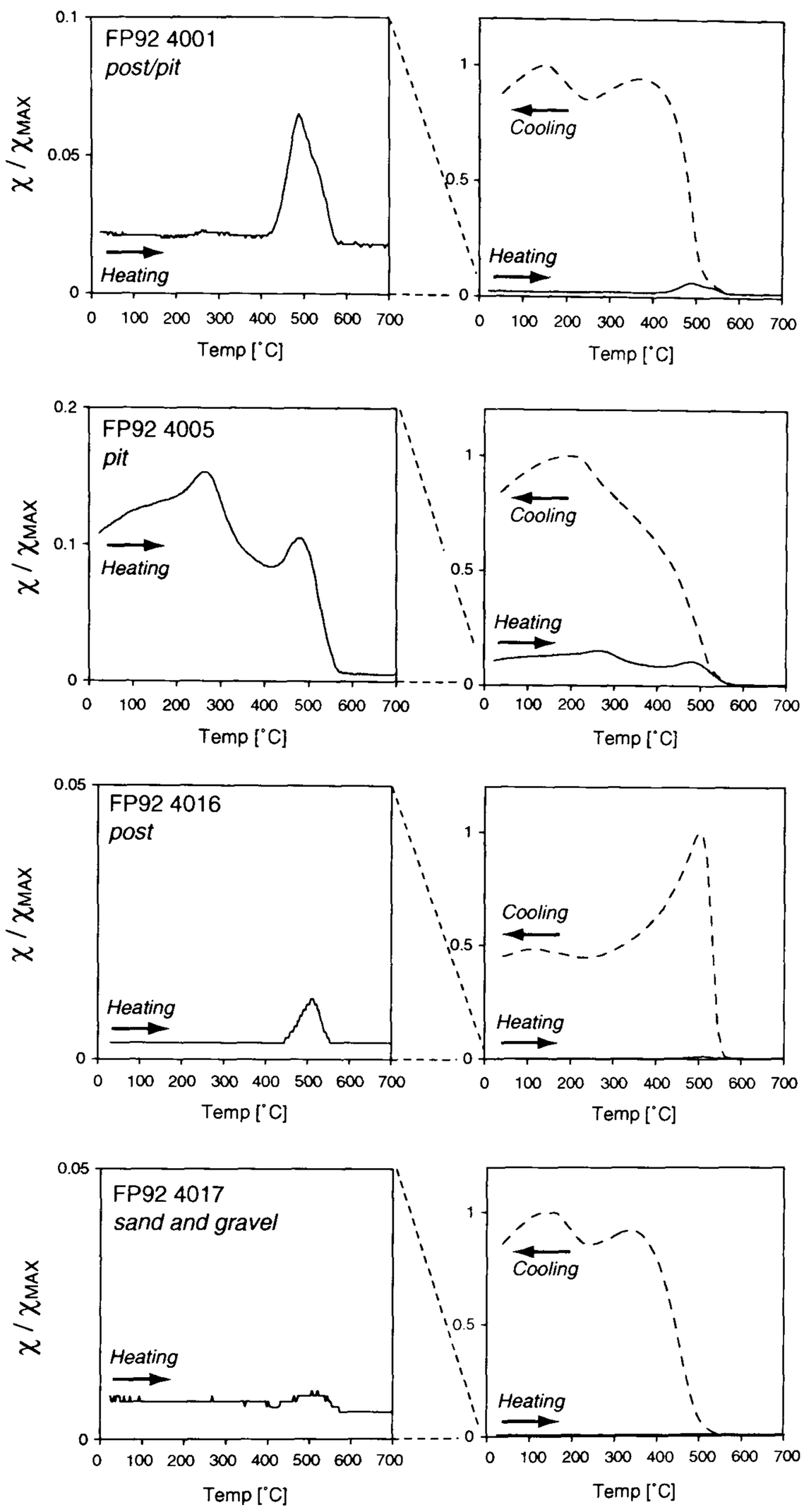


***Figure 5.9*** *Variation of high temperature susceptibility for 4 samples selected from ARC Stage 4 sites 2, 3 and 4. The heating and cooling curves are plotted separately for each sample.*

In addition, the heating curve indicates that either this alteration only occurs at temperatures greater than 580°C or that the newly formed ferrimagnetic minerals are produced above their Curie temperture (e.g. maghaemite). The low temperature data from sample 4017 (not shown in Figure 5.8 but highly similar to sample 4016) suggest the presence of goethite and it is possible that the absence of organic material within the sand and gravel substrate influences the dissociation of this mineral to an intermediate

form on heating (§2.1.1 and §7.6). The recovery of susceptibility below 550°C may suggest the fomation of a substituted magnetite from this intermediate mineral at high temperatures that rapidly oxidises to maghaemite, accounting for the loss of of $\chi$ at ~200°C, with a fine grain size distribution represented by a possible distribution of unblocking temperatures from 200°C to ambient.

Sample 4016, recovered from a post hole, shows a similar heating curve to 4017 with the exception of a more pronounced alteration to magnetite centred on 500°C . The cooling curve too shows a more rapid increase of $\chi$ below ~550°C and a substantial loss of susceptibility between a peak at 500°C and ambient. This suggests the newly formed magnetite produced at high temperatures is oxidising back to a mixture of maghaemite and haematite lowering the overall susceptibility of the sample. The post/pit feature 4001 also demonstrates a more pronounced alteration to magnetite on heating at 500°C but in this case the cooling curve is most similar to 4017, perhaps, due to a reduced organic content within the sample.

Finally, sample 4005 demonstrates a much lower degree of thermal enhancement than the other samples and shows evidence for both a rapid loss of $\chi$ at ~280°C and the formation of magnetite above 400°C proceeding to a Curie temperature at 580°C. The low temperature data for this sample suggests the presence of a very fine grained ferrimagnetic component that may well be due to the presence of maghaemite produced through previous thermal enhancement of the sample. This might explain the initial loss of $\chi$ on heating due, perhaps, to the dissociation of the maghaemite to haematite above 250°C followed by the partial alteration of the intermediate haematite to magnetite from 400°C. Again, more considerable enhancement occurs either on heating above 580°C or through increased oxidation during subsequent cooling. The cooling curve itself has a similar form to samples 4001 and 4017 but with the absence of a such a pronounced intial "shoulder" on regaining $\chi$ below the magnetite Curie temperature. This suggests a mixture of some previously burnt material together with unenhanced sand and gravel from the underlying substrate.

(A)

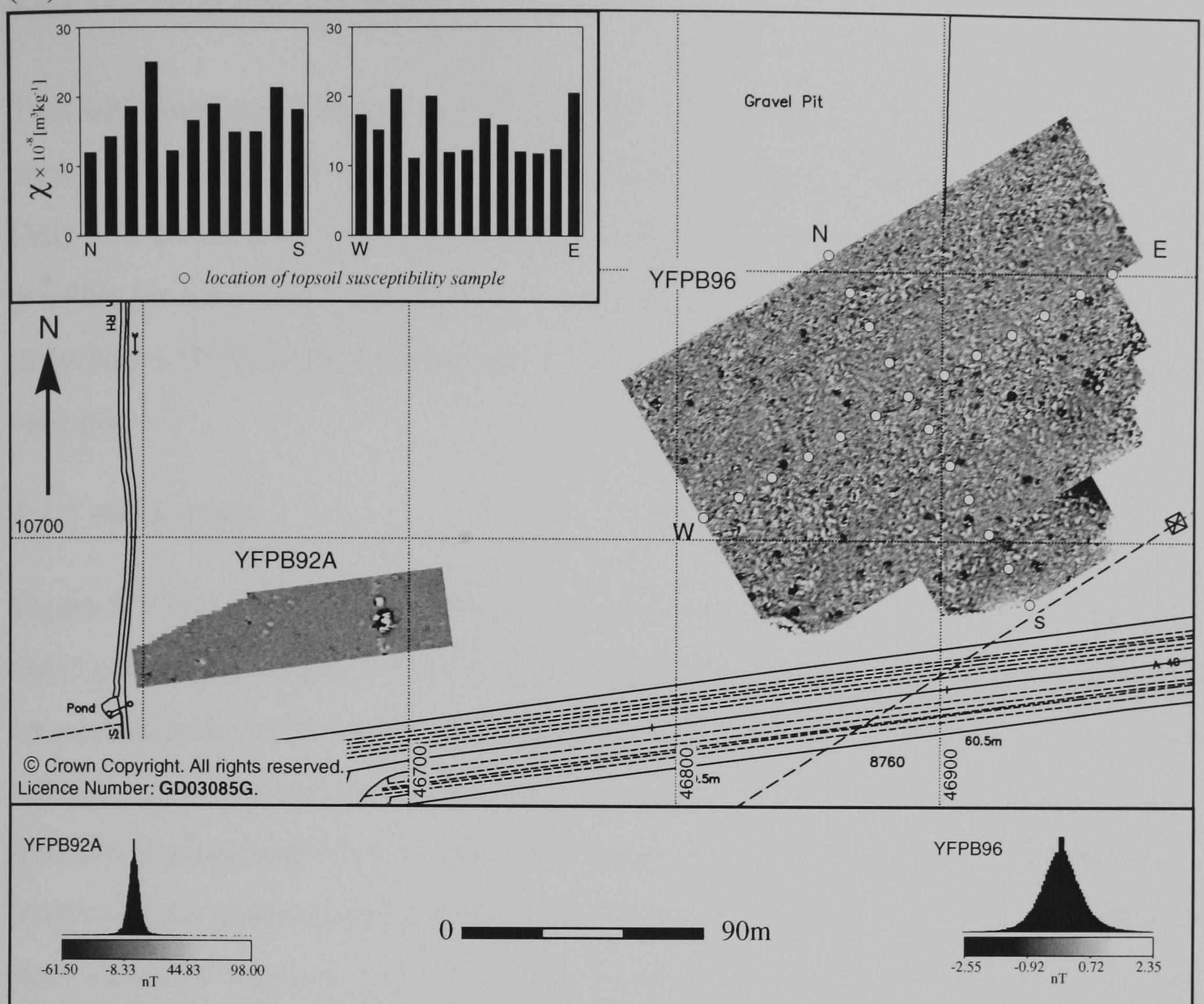


(B)

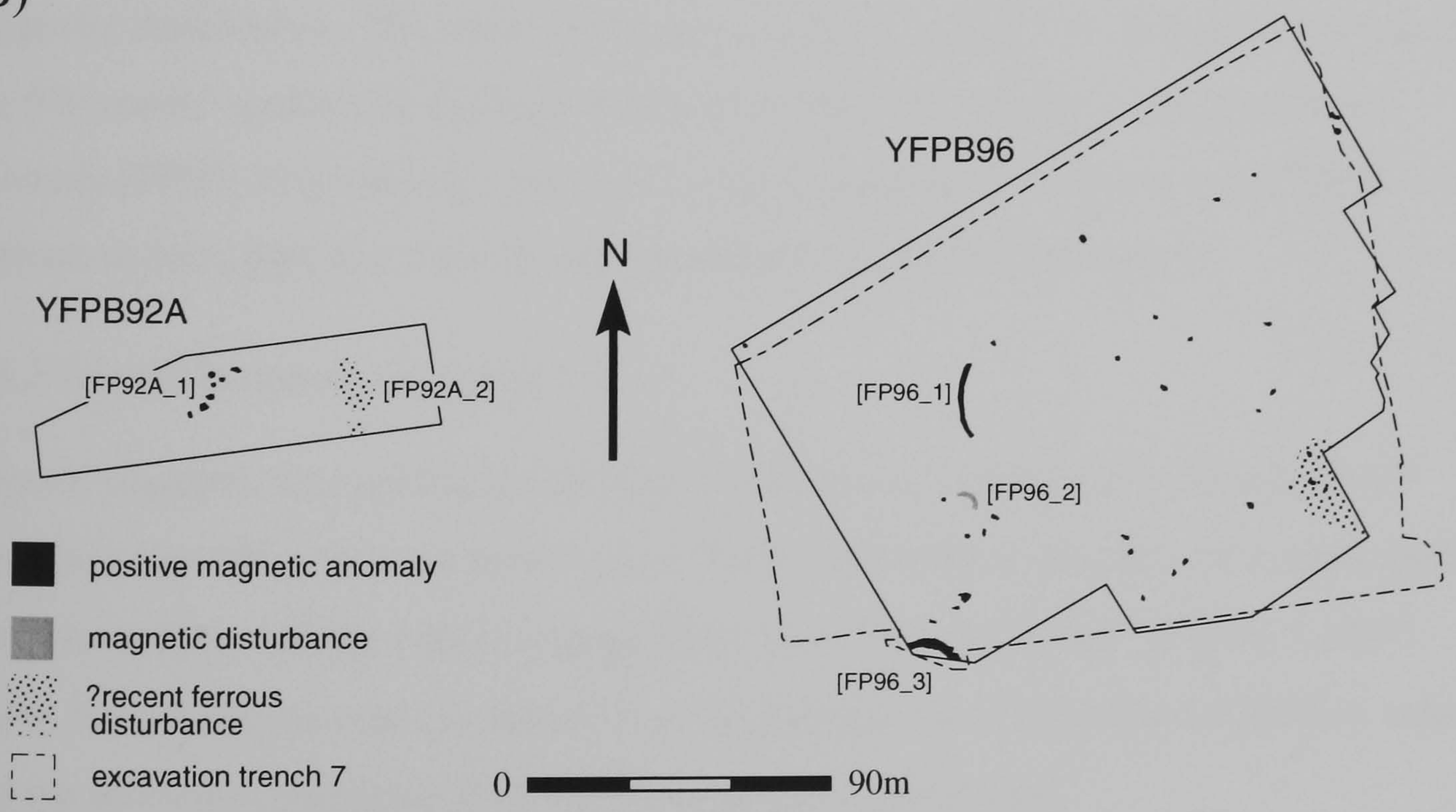


***Figure 5.10*** *(A) Greytone image of fluxgate gradiometer data from sites YFPB92A and YFPB96 together with (B) graphical summary of significant anomalies. The inset bar chart shows topsoil susceptibility values for samples collected along the indicated transects over the YFPB96 survey area.*

### *5.2.1 YFPB92A and YFPB92B*

Two additional small scale fluxgate gradiometer surveys, YFPB92A and YFPB92B were conducted on the edge of palaeochannels crossing the flood plain (Figure 4.1). Only YFPB92A produced significant anomalies (Figure 5.10) that include a scatter of possible pit-type responses [FP92A_1] and an area of presumably recent ferrous disturbance [FP92A_2]. Unfortunately, no subsequent excavation of the survey area took place.

### *5.3.1 YFPB 1996*

Figure 5.10(A) also shows the results from the 4ha survey conducted in advance of OAU excavation trench 7. Identification of weak magnetic anomalies is again hampered by a combination of recent ferrous detritus and track bedding clinker from the former railway line incorporated into the modern topsoil. Disturbance from an electricity transmission line stanchion is also evident in the SE area of the survey. Despite this interference a scatter of pit-type responses, shown graphically on Figure 5.10(B), has been identified together with two linear anomalies [FP96_1 ] and [FP96_2]. The latter anomaly is associated with a number of pit-type responses and forms a general area of magnetic disturbance. The most significant anomaly revealed by this survey is found in the SW corner against the drainage ditch at the edge of the field. This curvilinear anomaly [FP96_3] produced a relatively high magnitude of response (~2nT) and appears to form part of a circular ditch truncated by the field boundary.

### *5.3.2 Topsoil magnetic susceptibility*

Topsoil magnetic susceptibility was assessed from two orthogonal transects of soil samples collected across the survey area. Values from these samples were again quite uniform and low falling within a range from 10 to 20 $\times 10^{-8}$ $m^3kg^{-1}$ (Figure 5.10(A) inset). No correlation could be found from the distribution of topsoil susceptibility values and the anomalies identified from the fluxgate gradiometer data.

### *5.3.3 Mineral magnetic analysis*

Figure 5.11 shows a plan view of features excavated from OAU trench 7 covering the majority of the YFPB96 survey area. Section drawings are also shown on Figure 5.11 where multiple samples have been recovered from the same feature. The excavation

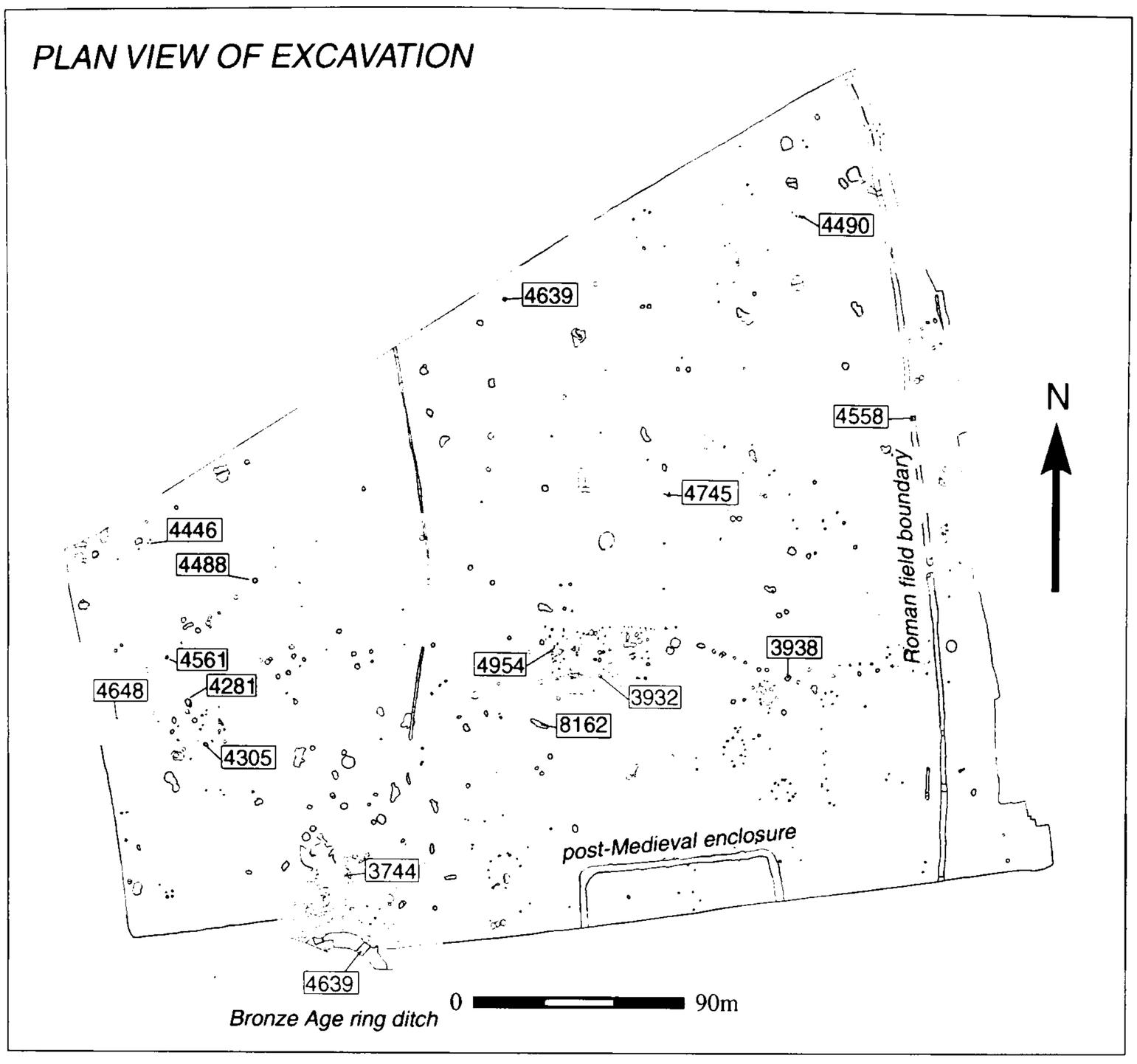


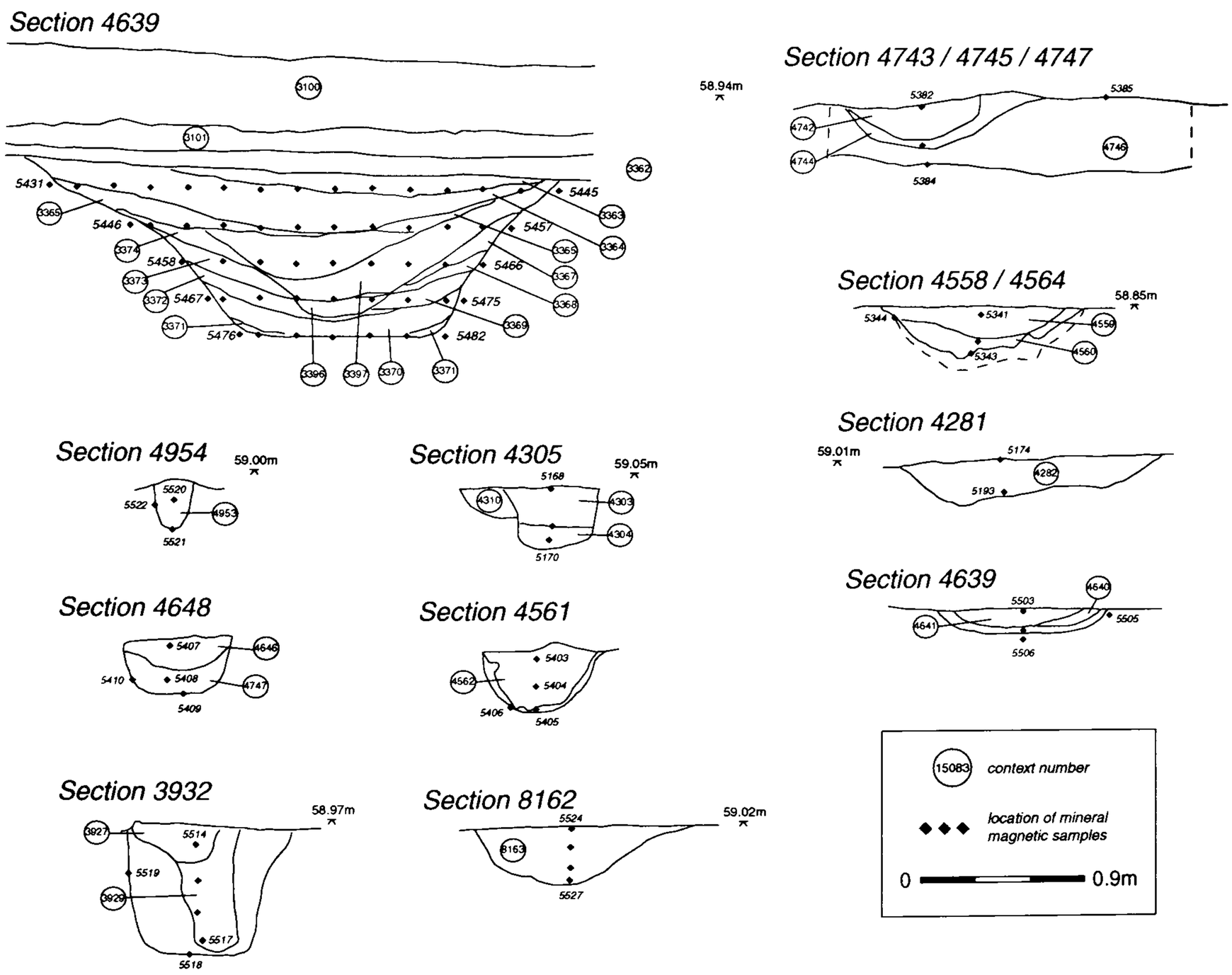


***Figure 5.11*** *Plan view of the features recorded during the excavation of YFPB96 together with sections drawn through those features selected for the collection of mineral magnetic samples. The sections show the location of the recovered samples and the context layers identified in the field.*

reveals a wealth of archaeological activity including timber buildings revealed through distributions of post hole features, a scatter of pits and both boundary and enclosure ditches. It is of interest to note that only the Bronze Age ring ditch produced a detectable magnetic anomaly during the initial geophysical survey and both the Roman field boundary ditch and the rectilinear post-Medieval enclosure failed to be located prior to excavation.

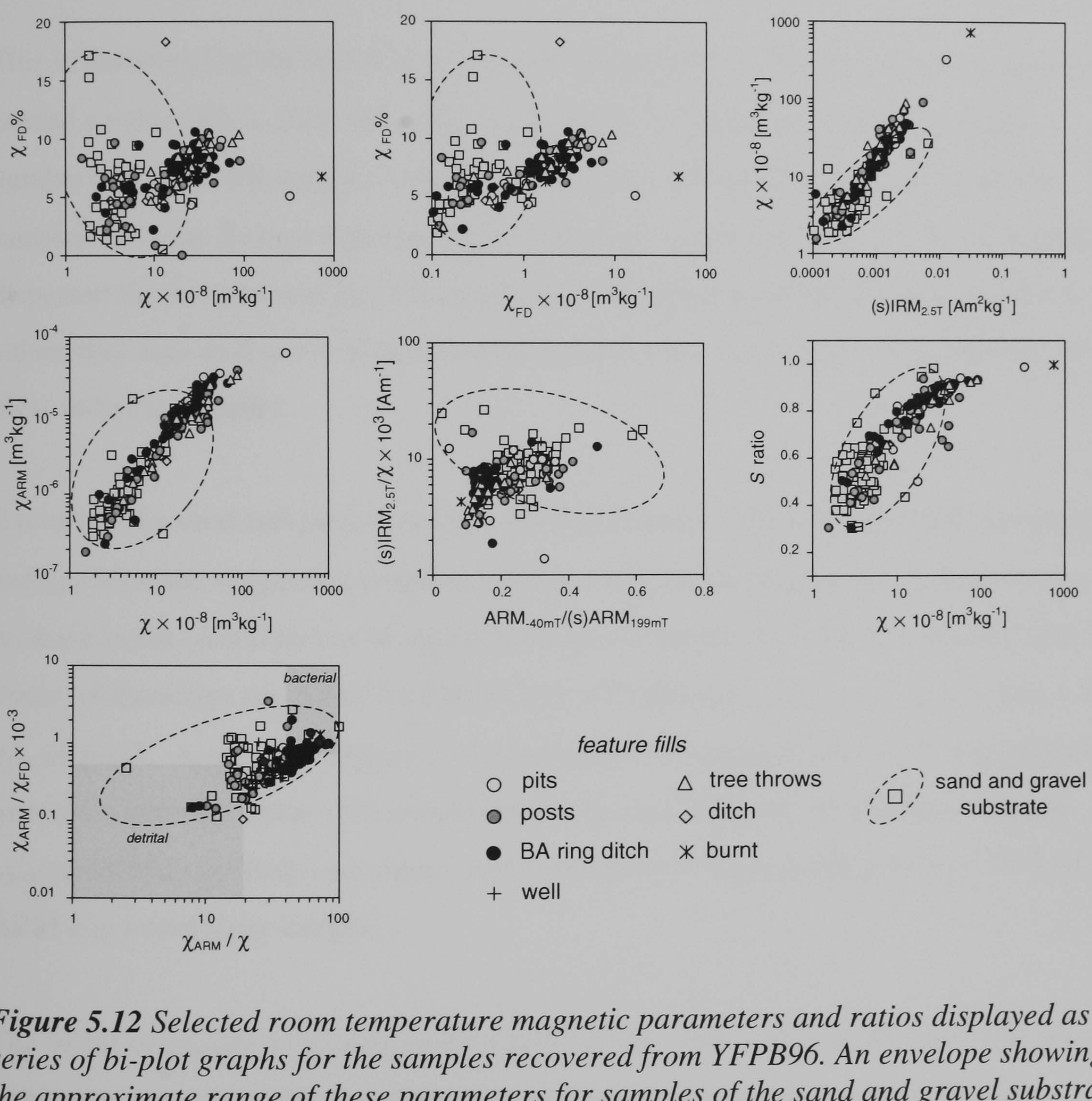


***Figure 5.12*** *Selected room temperature magnetic parameters and ratios displayed as a series of bi-plot graphs for the samples recovered from YFPB96. An envelope showing the approximate range of these parameters for samples of the sand and gravel substrate is also illustrated.*

*5.3.3.1 Isothermal measurements*

Biplots illustrating the isothermal behaviour of all samples recovered from the YFPB96 site are shown in Figure 5.12. Samples are distinguished by feature type and are plotted together with an envelope encompassing the behaviour of the underlying sand and

gravel substrate (see symbol key, Figure 5.12). No topsoil samples were recovered from this site as this material was removed mechanically in preparation for gravel extraction prior to the excavation of the site. In general, the envelope of values exhibited by the sand and gravel also includes many of feature fill samples suggesting little differential magnetic enhancement has occurred over the site. However, on closer inspection it can be seen that the majority of the sand and gravel samples fall within a less dispersed group with the envelope expanded by a limited number of outlying samples.

This is illustrated by the biplot of $\chi$ *vs* $\chi_{FD}\%$ where few of the sand and gravel samples exceed a value of $\chi = 10 \times 10^{-8}$ $m^3kg^{-1}$, separating the underlying substrate from a number of feature fill samples including posts, pits, tree throws, burnt material and samples from the Bronze Age ring ditch. Values for $\chi_{FD}\%$ are, however, more widely dispersed for the sand and gravel samples encompassing a limited number of extreme values that may well prove to be erroneous due to the extremely low susceptibility of these outlying samples.

Excluding the sand and gravel samples, an approximately linear relationship between $\chi$ and $\chi_{FD}\%$ exists, suggesting magnetic enhancement of the feature fills is related to an increase in the concentration of superparamagnetic material within the samples. Similar linear relationships are found for biplots of $\chi$ *vs* (s)$IRM_{2.5T}$, $\chi$ *vs* $\chi_{ARM}$, $\chi$ *vs S* ratio and $\chi_{FD}$ *vs* $\chi_{FD}\%$ . Again, this suggests a concentration of magnetically "soft", fine grained material within the feature fill samples that is further reflected in the biplot of $ARM_{40mT}$/(s)ARM *vs* $(s)IRM_{2.5T}/\chi$ where, for the majority of feature fill samples, ~80% of the ARM has a coercivity <40mT.

The biplot of $\chi_{ARM}/\chi$ *vs* $\chi_{ARM}/\chi_{FD}$ demonstrates the wide scatter of the sand and gravel samples together with the discrimination of a number of post holes from the other feature fill samples. However, the majority of samples, both feature fill and underlying substrate, fall between the two envelopes of behaviour reported for bacterial and detrital sources. This may well be due to the presence of a more complicated mixture of magnetic material within the samples, including both high coercivity minerals and superparamagnetic particles that the biplot cannot adequately discriminate.

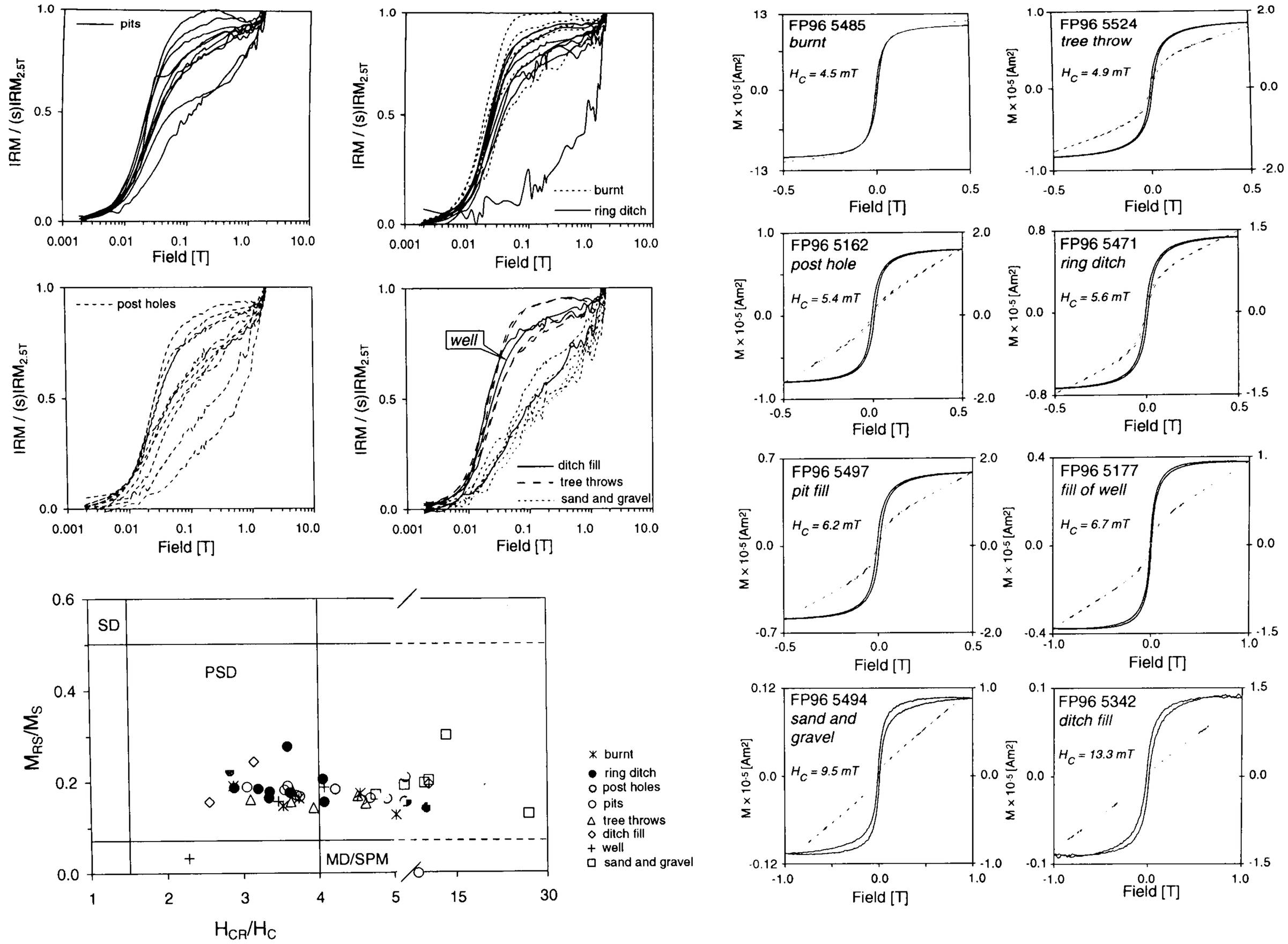


***Figure 5.13*** *Summary of the IRM acquisition and hysteresis behaviour for samples from YFPB96. Where hysteresis loops contain a significant paramagnetic component the uncorrected data is shown (dashed line) superimposed over the underlying ferrimagnetic loop (solid line). If necessary, the paramagnetic component is plotted against a second scale axis (right hand side of figure).*

*5.3.3.2 IRM acquisition and hysteresis*

A total of 56 samples were selected from YFPB96 for more detailed measurements of IRM acquisition and hysteresis parameters summarised in the plots shown in Figure 5.13. For clarity the IRM acquisition curves have been plotted separately for differing feature types to discriminate the charactersitic acquisition behaviour of the samples. For example, the sand and gravel substrate show a slow acquisition of IRM in low fields with only 50% of the total magnetisation acquired in a 100mT field. In addition, the sand and gravel curves demonstrate a change of slope between 100 to 500mT and fail to reach saturation in the maximum applied field of 1.8T. This suggests the sand and gravel samples contain a small quantity of ferrimagnetic minerals, accounting for the low field behaviour, together with a high coercivity mineral.

A number of the feature fill samples demonstrate IRM behaviour similar to the sand and gravel substrate curves. It is possible that these samples were either recovered from sand and gravel lenses formed within ditch-type features or from the bottom/edge of a cut feature where the distinction between feature fill and underlying natural was difficult to ascertain.

In contrast, the majority of feature fill samples, including pits, post holes, burnt material, tree throws and samples from the Bronze Age ring ditch demonstrate IRM acquisition behaviour dominated by "soft" ferrimagnetic material. Comparitively low applied fields, of between 20 to 30mT, are required for these samples to obtain 50% of their total IRM and the samples are almost entirely saturated by 100mT. Many of the samples then demonstrate a viscous "sag" in IRM acquisition between 0.5 to 1.0T and the presence of a high coercivity phase towards the maximum applied field.

Figure 5.13 also shows a selection of 8 hysteresis loops that demonstrate the range of magnetic behaviour encountered in samples recovered from this site. The uncorrected, paramagnetic component is shown as a broken line together with the underlying ferrimagnetic hystersis loop. As with the IRM acquisition curves two extremes of hysteresis behaviour may be identified, typified by burnt material (e.g. FP96 5485) and samples of the underlying sand and gravel substrate (e.g. FP96 5494). The burnt material contains a low coercivity ($H_C$ < 5mT), ferrimagnetic component of similar

magnitude to the paramagnetic contribution. In contrast, the sand and gravel samples show "wasp-waisted" hysteresis loops with increased coercivities ($H_C$ > 10mT) together with a dominant paramagnetic component with a saturation magnetisation approximately one order of magnitude greater than the ferrimagnetic contribution. The restricted shape of the sand and gravel loops about the origin together with the open branches in higher fields is suggestive of a mixture of high and low coercivity minerals. Samples from the other feature types show behaviour that falls between these two extremes with intermediate values of $H_C$ and a varying paramagnetic component. Ratios of $H_{CR}/H_C$ vs $M_{RS}/M_S$, determined from the ferrimagnetic hysteresis loops, presented on a Day plot discriminate the sand and gravel substrate from the majority of feature fill samples. However, a number of posts, ditch fills and even burnt sediments also plot with the sand and gravel samples suggesting a degree of admixture with the underlying substrate has occurred. Given the strong response of the Bronze Age ring ditch within the surface magnetometer survey it is not surprising that all samples from this feature are separated from the sand and gravel. Again, both the ring ditch samples and a number of samples from the range of other feature types fall within the envelope of values reported for pseudo-single domain magnetite (Day et al. 1977).

*5.3.3.3 Low temperature magnetisation*

A total of 18 samples were selected for low temperature measurements and the results of six representative cooling/warming curves are shown in Figure 5.14. The behaviour of the feature fill samples, with the exception of burnt material, is quite similar and shows a gradual increase in $M_S$ on cooling from 300 to 20K consistent with the presence of goethite. These samples also show evidence for a subtle Verwey transition within the $^{dM}/_{dT}$ cooling curve suggesting the presence of magnetite. Warming curves demonstrate either a significant fine grained, superparamagnetic component gradually unblocking from 20K or the low temperature ordering of paramagnetic phases.

Samples of the sand and gravel substrate show an increase of $M_S$ on cooling but less convincing evidence for a Verwey transition. This suggests, perhaps, that the presence of magnetite is associated with the development of secondary ferrimagnetic minerals

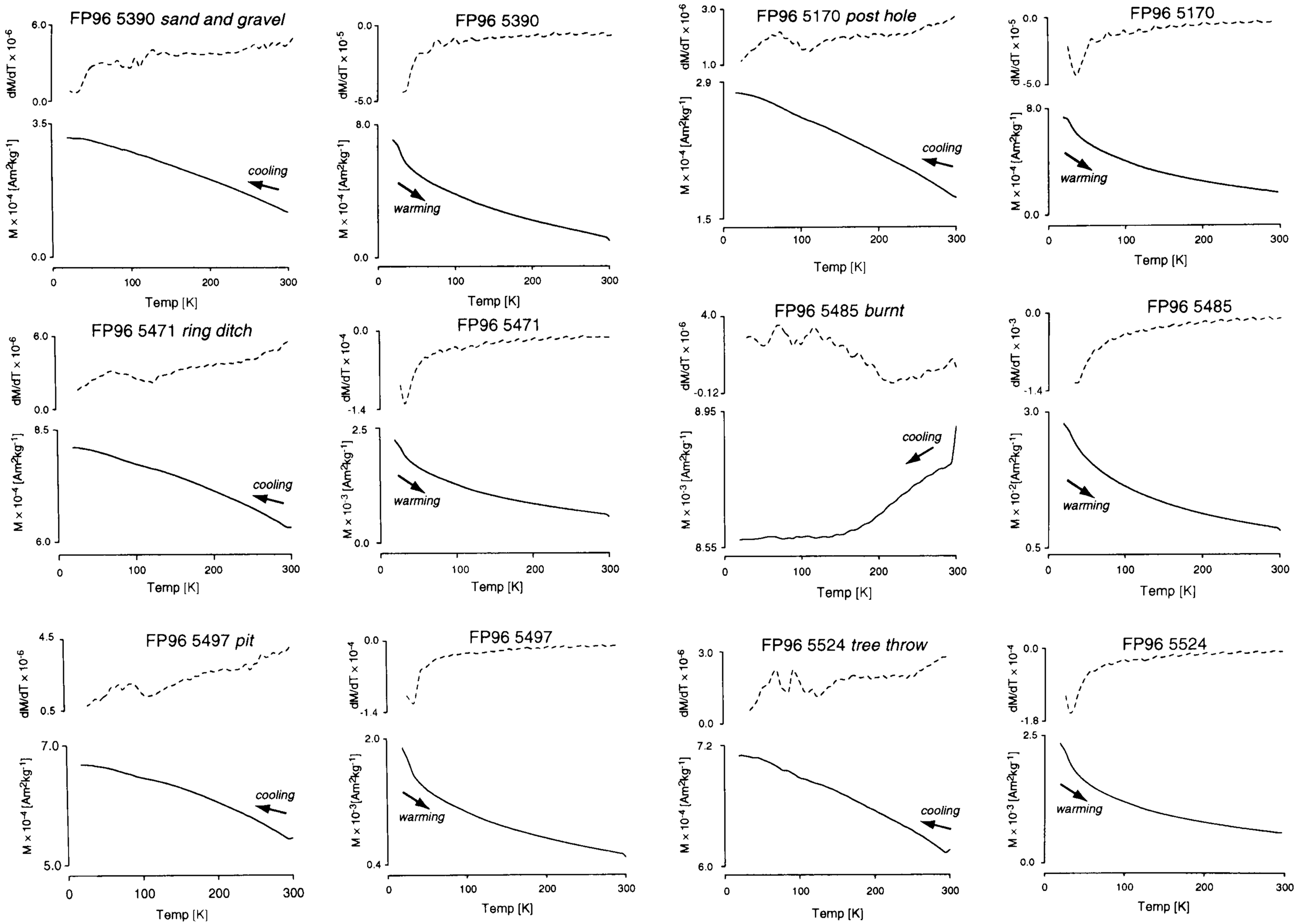


***Figure 5.14*** *Low temperature behaviour of samples from YFPB96. Cooling curves are plotted separately from warming curves due to the differing magnitude of the two data sets and the first differential of each curve is also shown (dashed line) to aid the identification of subtle inflections.*

within the archaeological features rather than as an inhertited detrital component. Sample FP96 5485, recovered from a burnt feature, shows an extraordinary, approximately linear loss of $M_S$ on cooling from 300 to ~150K. Such behaviour is unlikely to be due to a Verwey type transition as it occurs at too high a temperature and despite its dominance on cooling, no similar anomaly appears within the warming curve. It seems more likely that this behaviour is explained by a significant superparamagnetic component that loses magnetisation on cooling before reaching its blocking temperature. At 20K the majority of this material is below the relevant blocking temperature and the gradual loss of magnetisation on warming is proportional to the thermal unblocking spectra of this superparamagnetic component

.

*5.3.3.4 High temperature thermomagnetic data*

Four samples selected for high temperature analysis of the variation of magnetic susceptibility are shown in Figure 5.15. All four samples demonstrate an approximately hundred fold increase in susceptibility on heating to 700°C, suggesting low intial concentrations of ferrimagnetic minerals. Two of the samples, 4137 and 5370, show a similar behaviour on heating with a slight increase in $\chi$ occurring at ~220°C that falls on heating above 250°C before a more pronounced alteration at ~500°C that would appear to indicate the production of magnetite due to the 580°C Curie temperature. The remaining two samples are similar but do not show the initial increase in $\chi$ above 200°C and have less pronounced "magnetite" peaks at 500°C.

The cooling curves are more uniform and show the rapid recovery of $\chi$ below 580°C before reaching a peak value between 100 to 200°C. Below this peak the susceptibility falls slightly on cooling to room temperature perhaps due to the thermal blocking of very fine grain material or stress relaxation within stoichiometric magnetite grains. Three of the samples show evidence for a more pronounced inflection within the cooling curve at ~220°C and it is unclear whether this represents the unblocking/relaxation mechanism discussed above or, perhaps, the Curie temperature of maghemite created during the heating cycle.

The heating data is of particular interest with regard to samples 4137 and 5219 that were recovered from features directly associated with secondary evidence for burning, such

as distinctive red colouration or the presence charcoal/ash. The high degree of magnetic enhancement that occurs after laboratory heating suggests that either the initial heating event failed to reach a sufficient temperature for significant magnetic enhancement to occur (>400°C) or more thermally stable ferrimagnetic minerals were formed during the initial heating (§7.3.3).

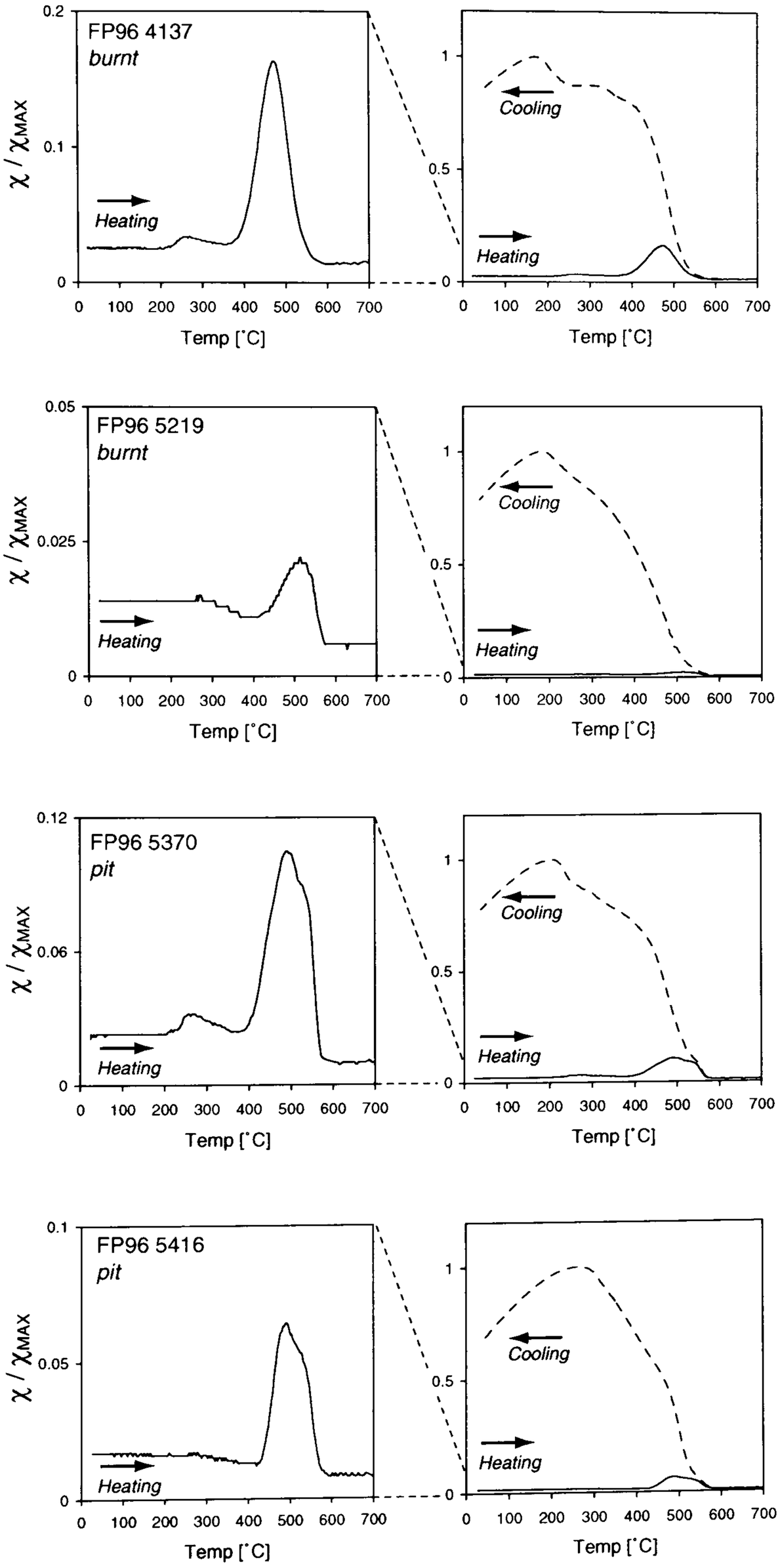


***Figure 5.15*** *Variation of high temperature susceptibility for 4 samples selected from YFPB96. The heating and cooling curves are plotted separately for each sample.*

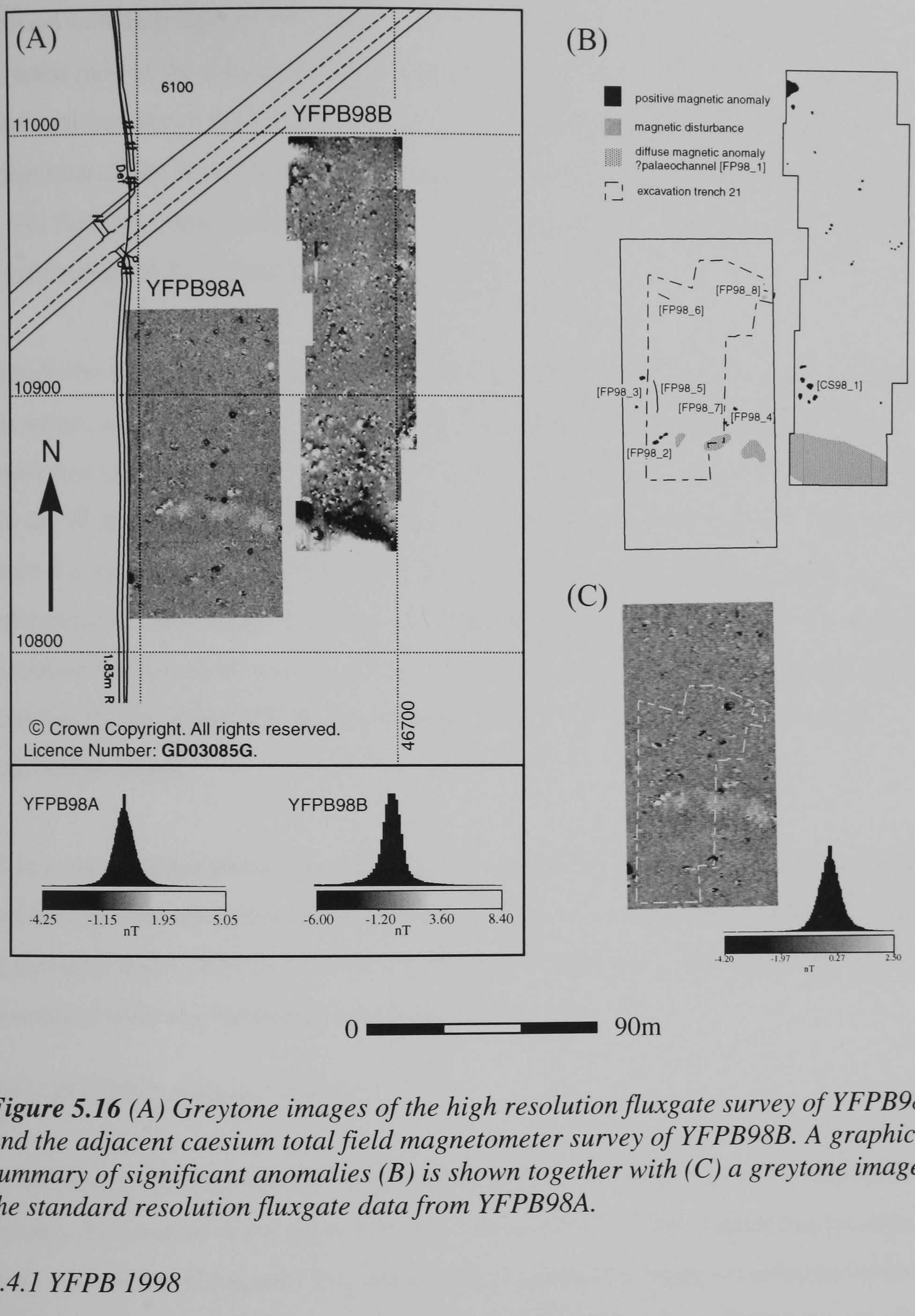


***Figure 5.16*** *(A) Greytone images of the high resolution fluxgate survey of YFPB98A and the adjacent caesium total field magnetometer survey of YFPB98B. A graphical summary of significant anomalies (B) is shown together with (C) a greytone image of the standard resolution fluxgate data from YFPB98A.*

### *5.4.1 YFPB 1998*

An area of 60m × 120m encompassing the proposed location of trench 21 was initially surveyed with a Geoscan FM36 fluxgate gradiometer utilising the standard sample interval of 0.25m × 1.0m and instrument sensor height (Figure 5.16(C)). Given the poor results recorded over the flood plain, the same area was resurveyed with identical instrumentation at a revised sample interval of 0.25m × 0.5m and with reading averaging over 16 individual observations applied at each measurement station (Figure 5.16(A)). Whilst the

revised sampling regime considerably slowed data acquisition it was hoped that the signal to noise ratio of the data would be much improved and allow more subtle anomalies to be distinguished above the background soil noise (Schmidt and Marshall 1995). The magnitude of the recorded anomalies was further amplified by reducing the height of the lower fluxgate sensor to within 0.05m of the ground surface through a minor mechanical modification of the instrument carrying handle.

Results from the magnetic data demonstrate the high density of ferrous detritus present. However, a diffuse positive anomaly was identified in both the standard and high resolution data sets related to the course of the palaeochannel [FP98_1] (Figure 5.16(B)). To the W of this anomaly three discrete positive anomalies [FP98_2] are evident, which from the magnitude of their response (>10nT standard resolution data), could be interpreted as thermoremanent in origin. Subsequent excavation revealed the underlying causative features to be a series of burnt tree throw bowls. Other pit-type anomalies are found at [FP98_3] and [FP98_4] just beyond the area covered by the subsequent excavation trench.

Two more tentative linear anomalies are found at [FP98_5] and [FP98_6] but these failed to correlate with any subsequently excavated features. In addition, two areas of magnetic disturbance were identified, [FP98_7] and [FP98_8], however only [FP98_7] was associated with any significant archaeological activity.

*5.4.2 YFPB98A resistivity Survey*

In addition to the magnetic survey a limited earth resistance survey was undertaken to identify the position of the palaeochannel and its relation to the magnetic anomalies. This was conducted at 0.5m and 1.0m mobile probe separations using the instrumentation and procedure described in following §3.1.4. The data identifies three distinct ranges of earth resistance values visible as discrete statistical distributions in the histogram grey scale keys of Figures 5.17(A) and 5.17(B). These distributions apparently relate to the varying response of the high resistance gravel islands, intermediate values along the edge of the palaeochannel and a central, low resistance anomaly following the deepest course of the former channel.

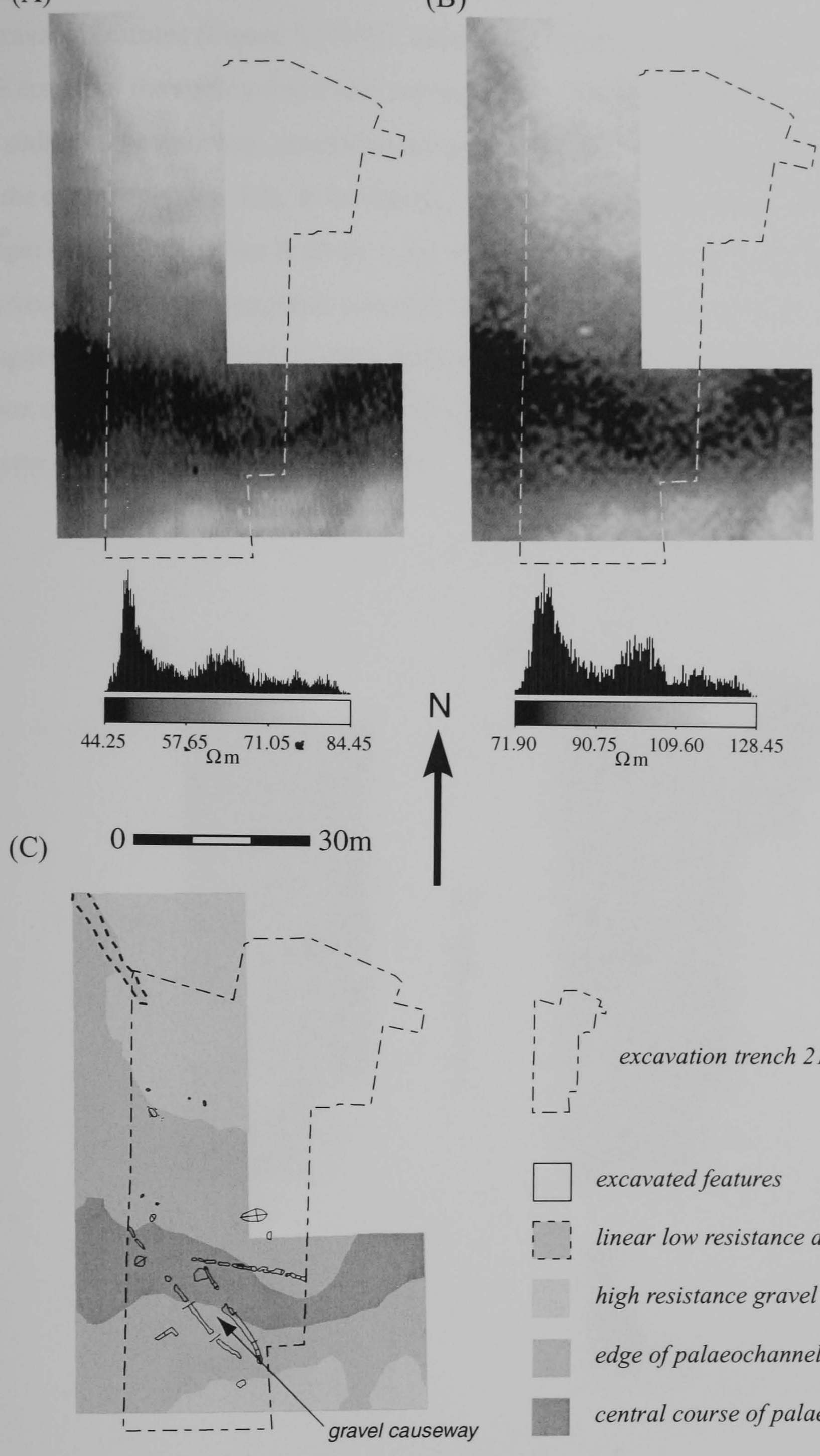


***Figure 5.17*** *Greyscale images of the 0.5m (A) and 1.0m (B) mobile probe spacing earth resistance data from YFPB98A together with a summary of significant anomalies (C). The location of excavation trench 21 and the features revealed are also shown.*

No correlation was observed between earth resistance anomalies and subsequently excavated features (Figure 5.17(C)). However, a subtle linear anomaly was detected in the NE corner of the survey that could not be identified where it entered the excavation trench. In addition, the magnetic anomalies associated with the palaeochannel appear, with respect to the earth resistance data, to be situated on the southern edge of the water course. The origin of these anomalies is likely to be a depositional remanent magnetisation (DRM) formed when detrital magnetic minerals settle from suspension and align with the ambient magnetic field. The stability of the DRM process will depend upon the turbidity of the water course which may well favour shallow edges rather than the faster flowing central course of the channel (e.g. Rees 1961).

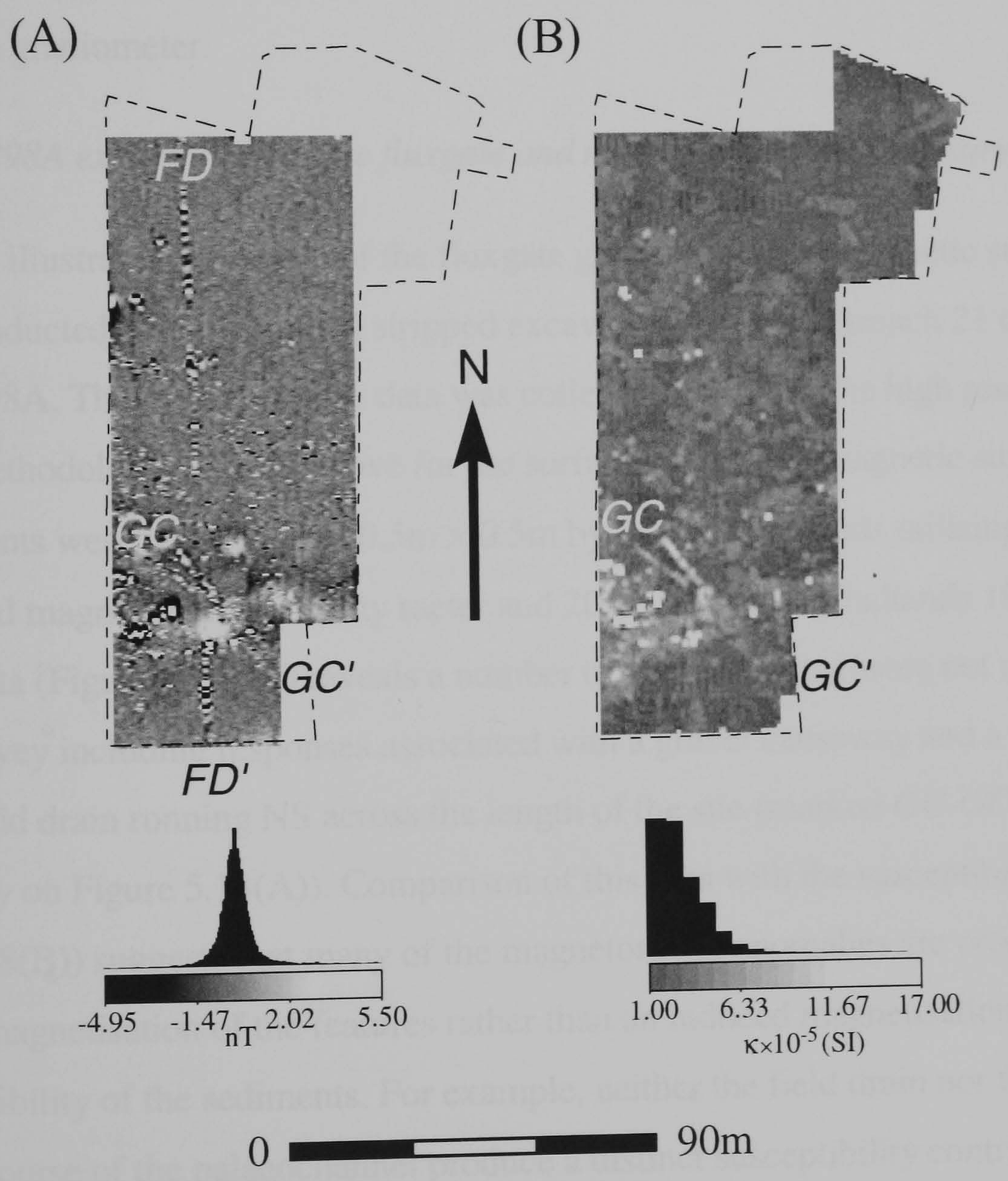


***Figure 5.18*** *Greytone images of (A) the fluxgate gradiometer data and (B) the magnetic susceptibility survey both conducted over the topsoil stripped excavation surface of YFPB98A.*

### *5.4.3 Caesium magnetometer survey of YFPB98B*

A high resolution caesium magnetometer survey was conducted over ~1ha to the E of site 21 using the instrumentation and sample intervals described in §3.1.2 (Figure 5.16(A)). Due to the timing of the survey it was not possible to extend the adjacent excavation trenches to examine significant anomalies within the data. However, a tentative interpretation is provided (Figure 5.16(B)), indicating the course of the palaeochannel and a scatter of pit-type responses distinguishable from the litter of near surface ferrous detritus. Of particular interest are the group of intense (>10nT) anomalies [CS98_1] immediately N of the palaeochannel that may well indicate the location of thermoremanent features similar to the burnt tree throws revealed in the adjacent gradiometer survey conducted over site 21. Note how the total field magnetometer records a far more intense anomaly over the course of the palaeochannel than the rather diffuse response produced by the fluxgate gradiometer.

### *5.4.4 YFPB98A excavation surface fluxgate and magnetic susceptibility surveys*

Figure 5.18 illustrates the results of the fluxgate gradiometer and magnetic susceptibility surveys conducted over the topsoil stripped excavation surface of trench 21 opened over site YFPB98A. The magnetometer data was collected following the high resolution fluxgate methodology detailed above for the surface survey and magnetic susceptibility measurements were collected at a 0.5m × 0.5m by Adrian Challands utilising a TR Systems Ltd magnetic susceptibility meter and 20cm field coil (Challands 1998). The fluxgate data (Figure 5.18(A)) reveals a number of anomalies that were not evident in the surface survey including responses associated with a gravel causeway and a modern ceramic field drain running NS across the length of the site (marked *GC-GC'* and *FD-FD'* respectively on Figure 5.18(A)). Comparison of this data with the susceptibility results (Figure 5.18(B)) suggests that many of the magnetometer anomalies are produced by the remanent magnetisation of the features rather than an induced magnetisation arising from the susceptibility of the sediments. For example, neither the field drain nor the alluvium along the course of the palaeochannel produce a distinct susceptibility contrast in Figure 5.18(B), however, both are easily discernible in the fluxgate data (Figure 5.18(A).

The magnetic response of the gravel causeway is of interest as it would appear to be either constructed from a higher susceptibility material than the channel deposits or have had

magnetically enhanced topsoil compacted along its course during use. Furthermore, both surveys provide evidence for a second, slightly weaker, linear anomaly to the west of the excavated gravel causeway, suggesting a previous alignment of the crossing.

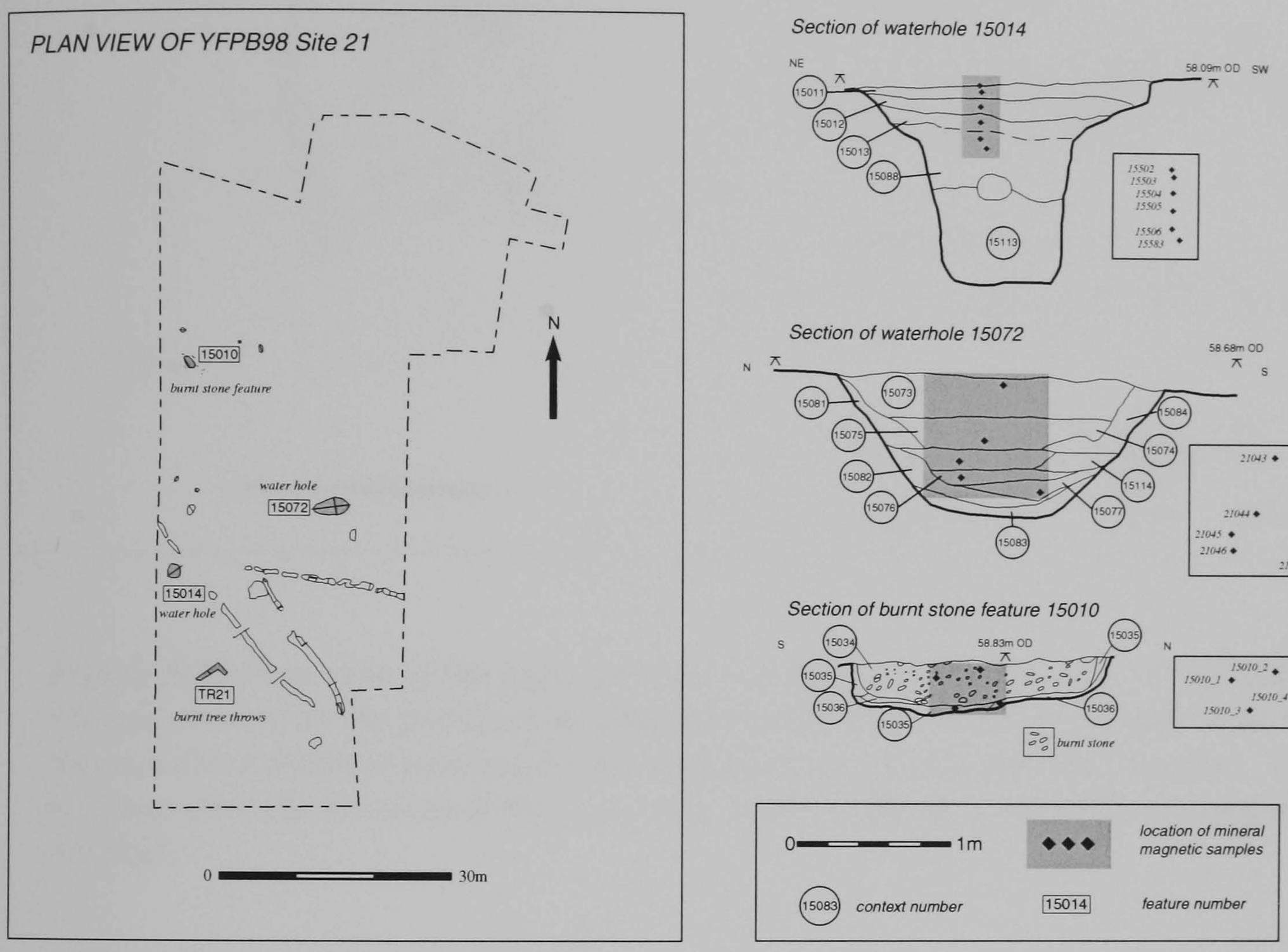


***Figure 5.19*** *Plan view of the features recorded during the excavation of YFPB98 Site 21 together with sections drawn through those features selected for the collection of mineral magnetic samples. The sections show the location of the recovered samples and the context layers identified in the field.*

### *5.4.5 Mineral magnetic measurements*

Samples were recovered from three separate trenches, Site 21, 4A and 4C during the 1998 excavation (Figures 5.19, 5.20 and 5.21). However, only Site 21 was covered by the geophysical survey prior to excavation. The resulting samples from all three trenches represent a range of different feature types including in-filled waterholes, pits, post holes, a Roman field boundary ditch and a number of burnt features.

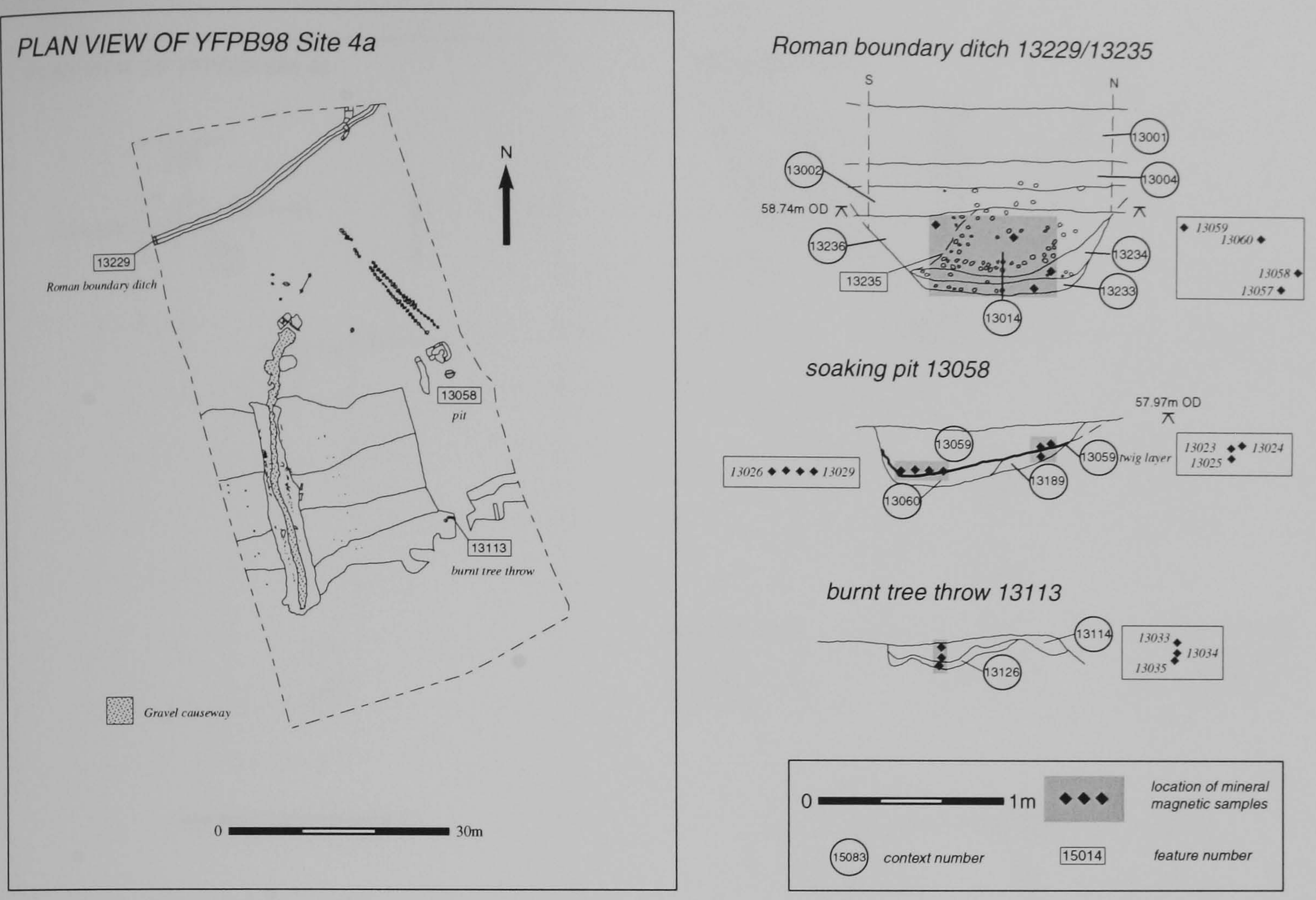


***Figure 5.20*** *Plan view of the features recorded during the excavation of YFPB98 Site 4A, not covered by the previous geophysical survey, together with sections drawn through those features selected for the collection of mineral magnetic samples. The sections show the location of the recovered samples and the context layers identified in the field.*

*5.4.5.1 Isothermal measurements*

Figure 5.22 shows biplots for selected isothermal parameters and demonstrates the considerable magnetic enhancement of the burnt features, reflected particularly in values of $\chi$ and (s)$IRM_{2.5T}$. Note also how sample 16092, recovered from an ash filled pit (Figure 5.21), plots closer to the samples of burnt material than the other features. Despite the high values of $\chi$ from the burnt features these samples are not distinguished by particularly high values of $\chi_{FD\%}$. Indeed the majority of the burnt features fall within a range of $\chi_{FD\%}$ between 5 to 10%, similar to many of the other feature types. Whilst this may suggest a similar grain-size distribution of very fine grained magnetic particles throughout all feature types the susceptibility of the un-burnt features is extremely low ($\chi < 10 \times 10^{-8}$ $m^3kg^{-1}$) resulting in a much increased sensitivity of the $\chi_{FD\%}$ parameter to the noise level of the instrumentation.

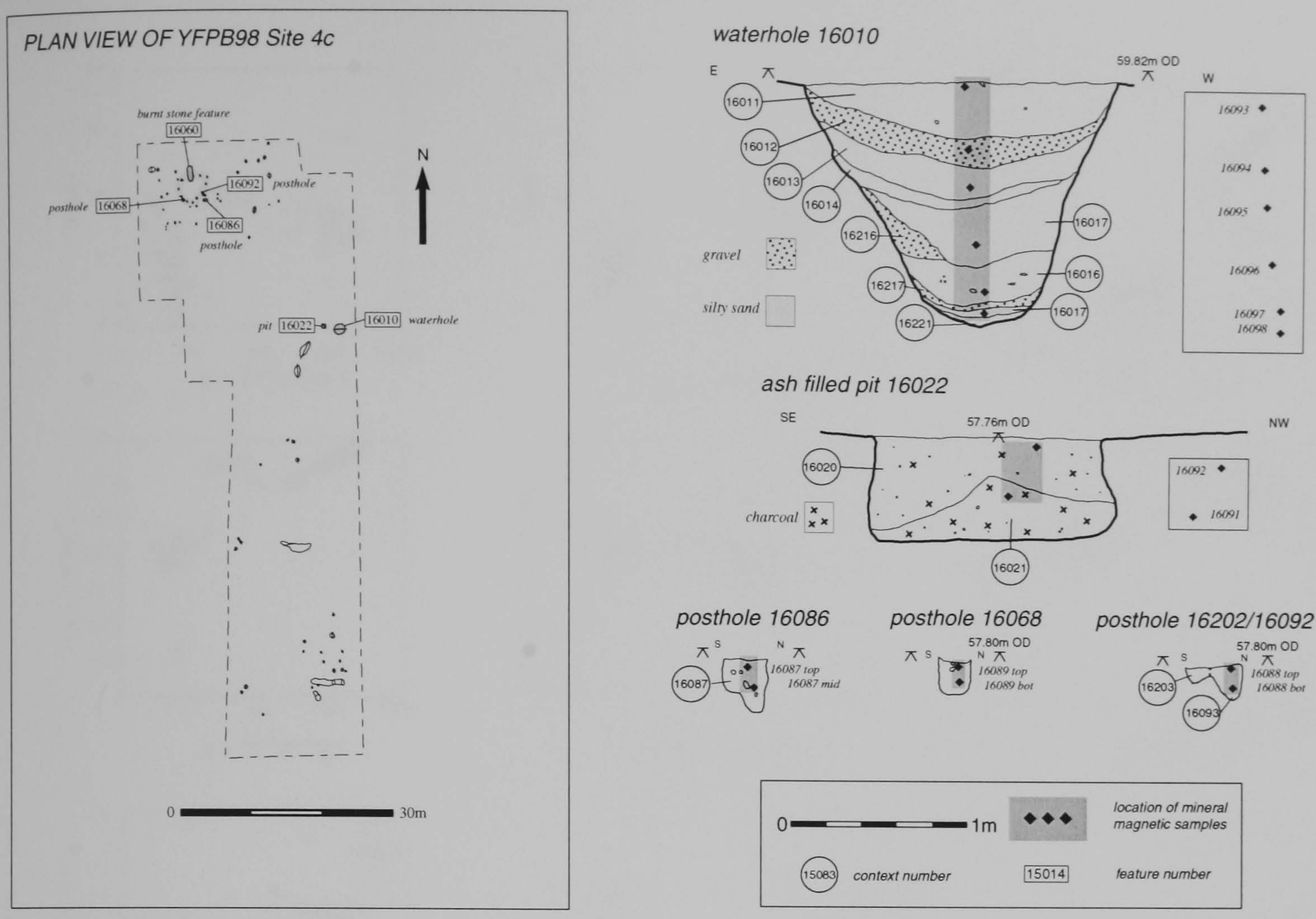


***Figure 5.21*** *Plan view of the features recorded during the excavation of YFPB98 Site 4C, not covered by the previous geophysical survey, together with sections drawn through those features selected for the collection of mineral magnetic samples. The sections show the location of the recovered samples and the context layers identified in the field.*

The biplot of (s)$IRM_{2.5T}$ vs $\chi$ clearly distinguishes the burnt features, in terms of both the magnitude and the steeper slope of the apparent linear relationship between the two parameters for the burnt features ($\chi$ increasing more rapidly than (s)$IRM_{2.5T}$). This again suggests an increased concentration of very fine grained magnetic particles within the burnt material that is also reflected by extremely high values of $\chi_{ARM}$, $ARM_{-40mT}$ and the *S* ratio. The biplot of $\chi$ vs $\chi_{ARM}$ also isolates samples of alluvium and the upper fill of the Roman boundary ditch, due to their low values of $\chi_{ARM}$. This may well indicate a magnetic signature for the alluvium that began to in-fill extant features from the late Iron Age / Roman transition as the area changed from dry landscape to a seasonal floodplain. The alluvium also demonstrates a wide scatter of values for the concentration independent (s)$IRM_{2.5T}/\chi$ ratio, possibly due to the influence of instrumental noise on the extremely low values of $\chi$ rather than a reflection of any true magnetic variation.

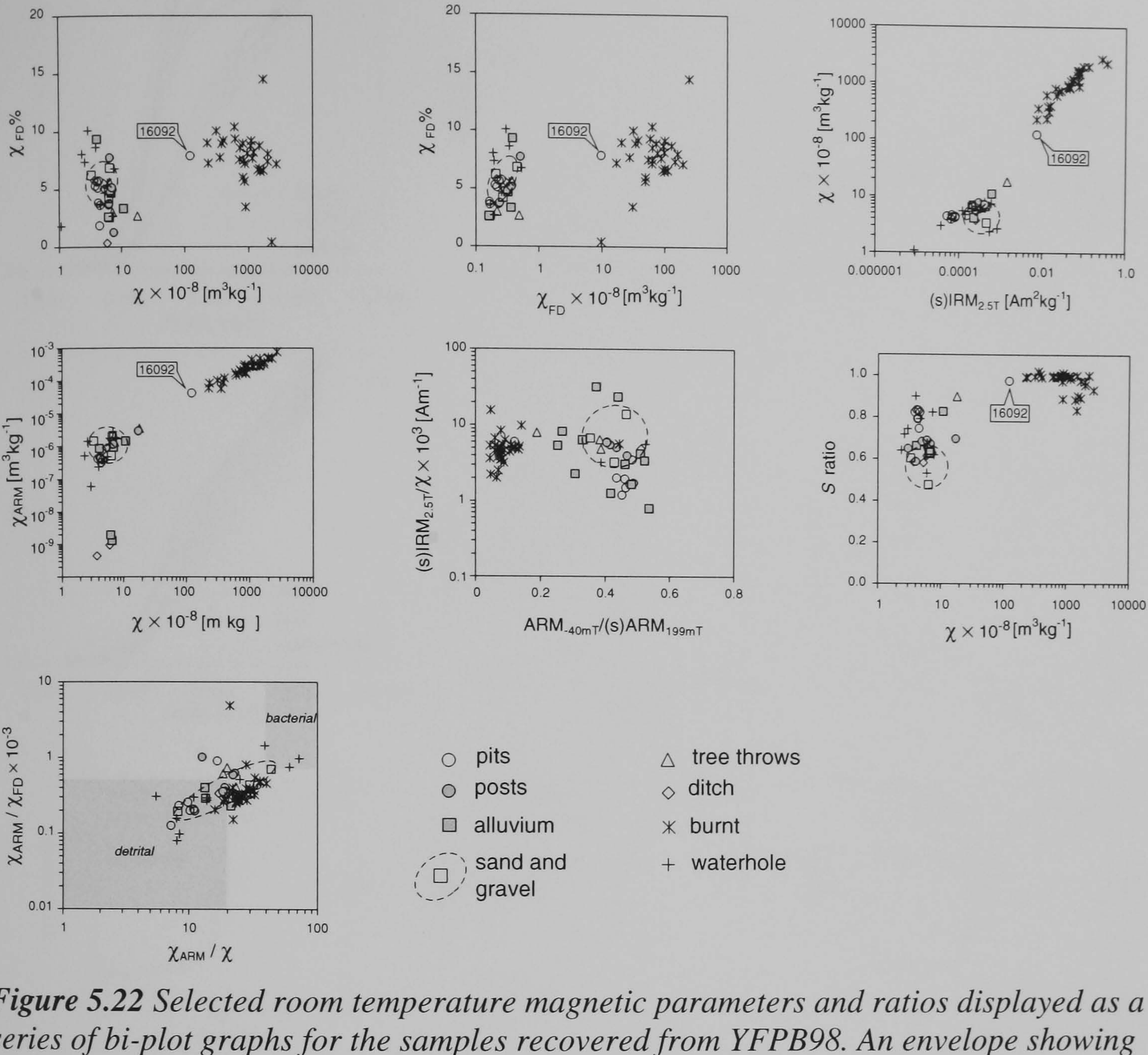


***Figure 5.22*** *Selected room temperature magnetic parameters and ratios displayed as a series of bi-plot graphs for the samples recovered from YFPB98. An envelope showing the approximate range of these parameters for samples of the sand and gravel substrate is also illustrated.*

The high concentration of very fine grained, superparamagnetic material within the burnt features possibly negates the use of the $\chi_{ARM}/\chi$ vs $\chi_{ARM}/\chi_{FD}$ ratios for determining single-domain sized magnetite associated with bacterial magnetosomes for these samples (Snowball et al. 2002). However, three of the (unburnt) samples from a waterhole feature do fall within the envelope of values reported for bacterial magnetite and the feature may well have provided the anaerobic conditions under which these organisms thrive (e.g. Frankel and Blakemore 1991).

*5.4.5.2 Hysteresis*

Forward IRM acquisition curves demonstrate the similarity of response shown by the burnt features that all rapidly reach saturation in an applied field of ~50mT (Figure

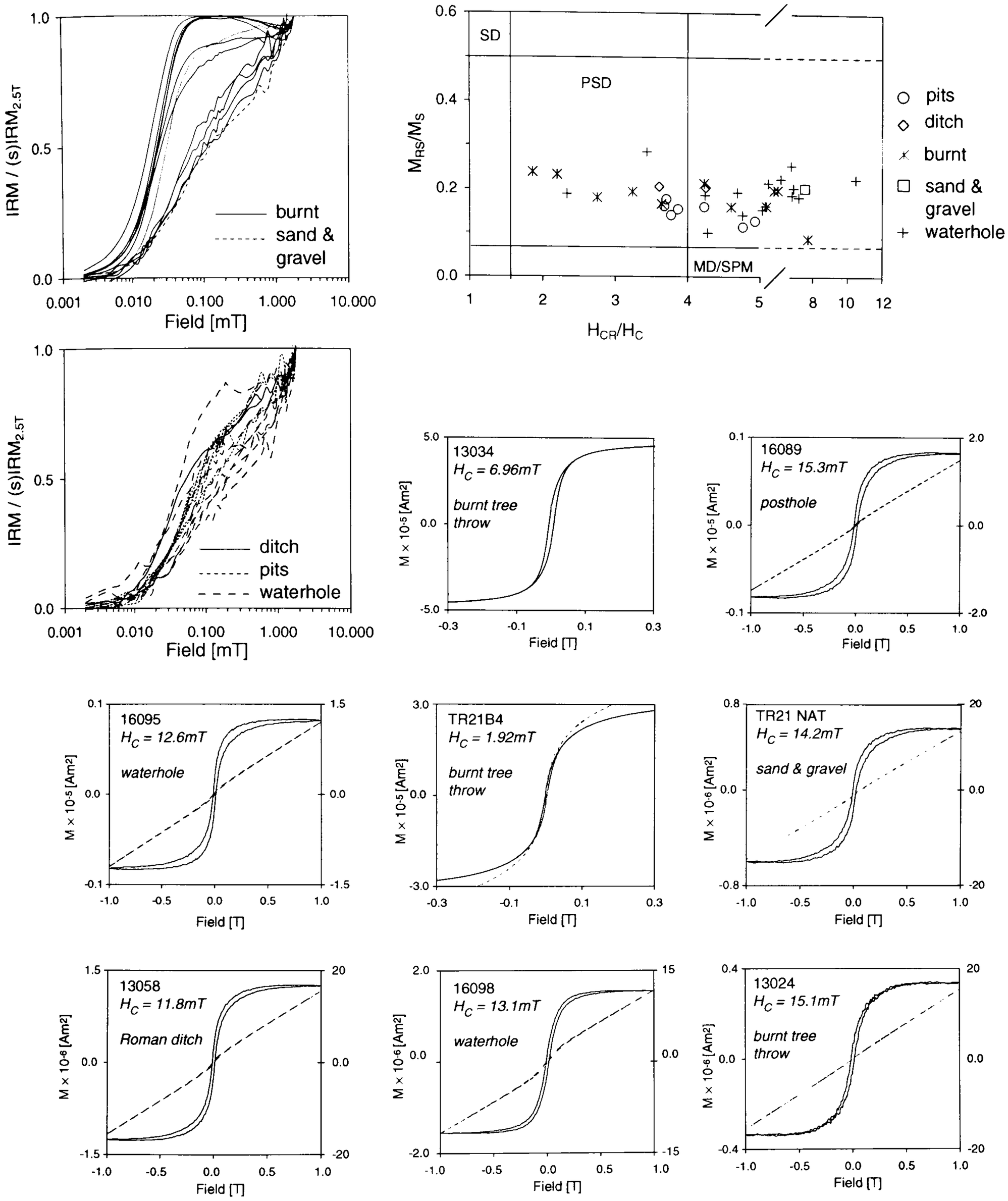


***Figure 5.23*** *Summary of the IRM acquisition and hysteresis behaviour for samples from YFPB98. Where hysteresis loops contain a significant paramagnetic component the uncorrected data is shown (dashed line) superimposed over the underlying ferrimagnetic loop (solid line). If necessary, the paramagnetic component is plotted against a second scale axis (right hand side of figure).*

5.23). The viscous "sag" of IRM in fields >200mT is also evident in many of the burnt samples as is the recovery of IRM when approaching the highest applied field due, most probably, to the presence of a high coercivity mineral such as goethite. A number of the burnt samples reach only 90% saturation within a 50mT field and then follow a linear acquisition of IRM to the maximum applied field. These latter samples most likely

represent a mixture of burnt material and higher coercivity minerals, due, perhaps, to admixture with the underlying sand and gravel substrate. Samples recovered from the other feature types, including the natural substrate, lie within an envelope of apparently two-phase behaviour. This begins with a relatively rapid acquisition to 50% of the final (s)IRM obtained in fields of ~100mT followed by a more gradual, linear increase towards the maximum applied field. Again, these latter curves may be interpreted as representing a mixture of both low and high coercivity material.

In field hysteresis loops for the burnt samples show a strong, low coercivity ($H_C <$ 10mT) ferrimagnetic component with very little paramagnetic contribution (e.g. samples 13034 and TR21B4). Despite this dominant, soft ferrimagnetic phase, the Day biplot of $H_{CR}/H_C$ vs $M_{RS}/M_S$ shows that the burnt samples are scattered over a range of values including the range of values expected for pseudo-single domain magnetite. This suggests that a mixture of magnetic minerals may be present including a higher coercivity component. Hysteresis loops from the unburnt features are more obviously derived from mixtures of magnetic minerals and demonstrate a strong paramagnetic component. Underlying ferrimagnetic loops are either "wasp-waisted" (e.g. samples 16089, 16095 and TR21 NAT) or show a more regular shaped loop whose branches fail to close below 500mT (e.g. 16098 and 13024). Again, a plausible interpretation would appear to be a mixture of low coercivity (possibly superparamagnetic) ferrimagnets and magnetically "hard" antiferromagnets inherited from the sand and gravel substrate.

*5.4.5.3 Low temperature magnetisation*

The variation of magnetisation on cooling to 20K and warming back to ambient is shown in Figure 5.24 for selected samples. A number of the burnt samples, demonstrate an unusual loss of room temperature acquired magnetisation on cooling to 20K (e.g. TR21B4 and 13034). However, this does not appear to be uniquely diagnostic of burnt sediments as some of the other burnt samples fail to demonstrate this behaviour (e.g. 16091). Analysis of the gradient, $^{dM}/_{dT}$, of the cooling curves suggests that burnt samples are more likely to show an apparently linear variation of gradient with no indication of the low temperature inflection at ~110K found in many of the unburnt samples (e.g. 16089 and 16095 but also present in 15010_1 that did come from an allegedly burnt feature). Below this inflection the unburnt samples show a smooth increase of $^{dM}/_{dT}$

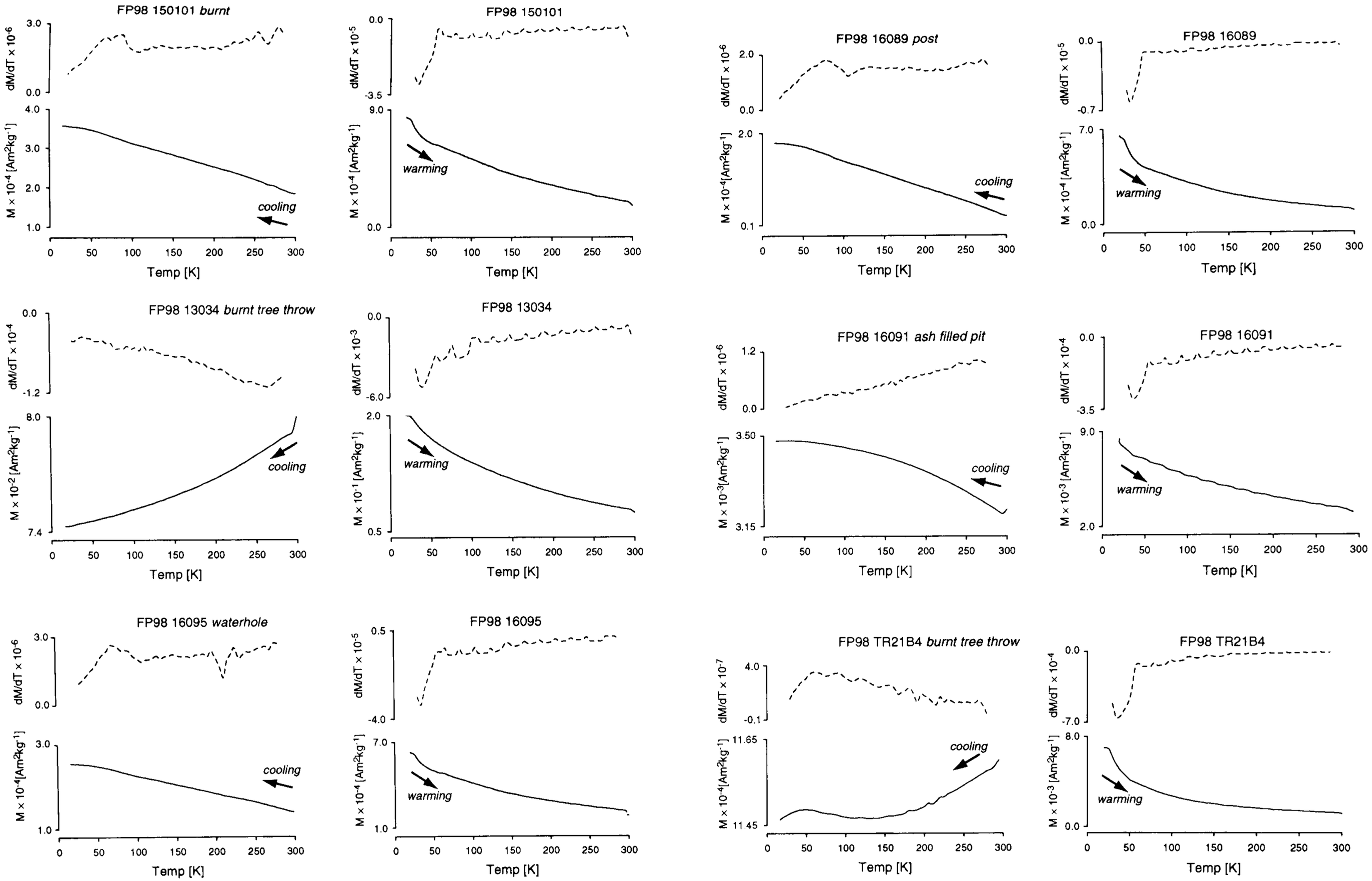


***Figure 5.24*** *Low temperature behaviour of samples from YFPB98. Cooling curves are plotted separately from warming curves due to the differing magnitude of the two data sets and the first differential of each curve is also shown (dashed line) to aid the identification of subtle inflections.*

through a peak at ~75K before declining towards 0 as the sample is cooled to 20K. This inflection may well represent a Verwey transition, due to the presence of magnetite, below which the unblocking spectra of very fine grained material is possibly indicated by the smooth curve through the ~75K peak that appears in many of the curves from unburnt samples.

Variation of the magnetisation acquired at 20K on warming back to room temperature appears to contain little directly interpretable information. However, many of the samples from both burnt and unburnt features show a distinct change in the gradient of the warming curve between 55-60K.

*5.4.5.4 High temperature variation of magnetic susceptibility*

The variation of $\chi$ with temperature between 40 to 700°C is shown for three selected samples, two burnt tree throw features (TR214A and 13034) and a pit (Figure 5.25). Both the burnt tree throw samples behave in a similar manner on heating with a slight peak occurring at ~300°C followed by a rapid loss of $\chi$ that continues to ~450°C. A slight inflection in the curve then appears above 450°C before a rapid loss of $\chi$ reflecting a magnetite Curie temperature of 560°C for TR214A and 580°C for 13034. These curves suggest both burnt samples contain a significant proportion of maghaemite that begins to dissociate to ?haematite above 300°C before this intermediate mineral is reduced to magnetite between 400 and 500°C, accounting for the reduced loss of $\chi$ through this latter temperature range. The more pronounced loss of $\chi$ from the magnetite "peak" at 500°C for sample 13034 suggests a lower degree of previous enhancement through burning for sediment from this feature.

The cooling curves demonstrate the continued reduction to form magnetite that reaches a peak value at approximately 500°C for both burnt tree throw samples. Below this temperature the cooling curves differ with 13034 showing an almost linear loss of $\chi$ from 500°C to room temperature were as TR214A demonstrates a step-like increase in $\chi$ between 300 to 250°C. In both cases the magnetite formed at high temperatures is likely to oxidise to maghaemite/haematite on cooling once any organic matter in the

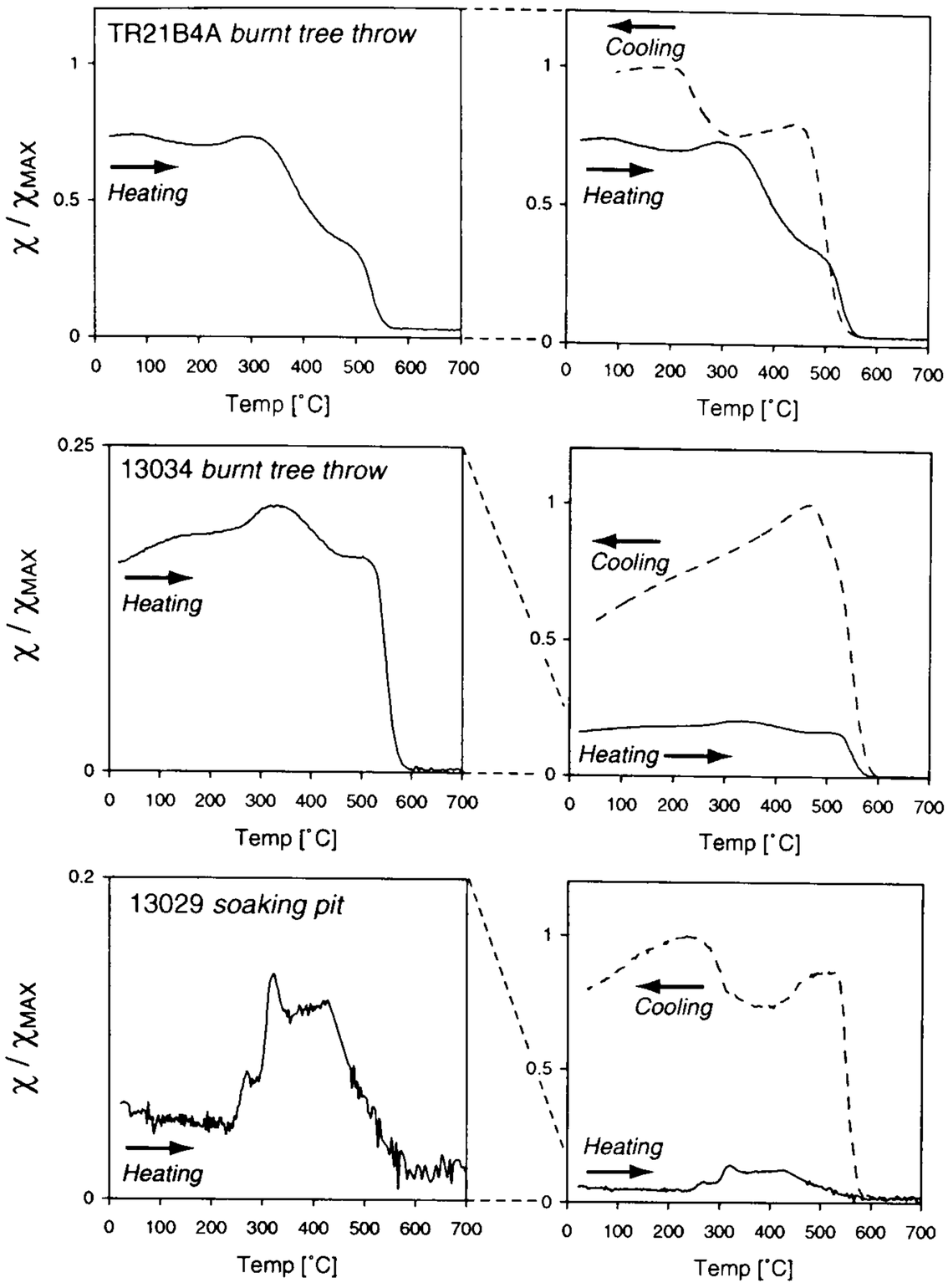


***Figure 5.25*** *Variation of high temperature susceptibility for 3 samples selected from YFPB98. The heating and cooling curves are plotted separately for each sample.*

samples has been fully combusted. The differing behaviour during this cooling phase may be indicative of the degree of initial enhancement possibly indicating that sample TR21B4A was exposed to temperatures beyond 500°C (*cf* Figures 7.4, 7.5 and 7.6).

An additional unburnt sample, 13029, recovered from a possible soaking pit demonstrates a very low degree of enhancement prior to laboratory heating. Indeed, the heating curve for this sample is quite weak but shows a rapid increase in $\chi$ from 220°C before decreasing from ~450°C to an apparent magnetite Curie temperature at ~580°C. On cooling, $\chi$ is regained below this Curie temperature and reaches an initial peak between 550-450°C. A slight fall is then seen before a peak value is obtained at 280°C followed by a slight loss on cooling back to room temperature. This data suggests sample 13029 has not been previously exposed to temperatures >200°C and still contains iron minerals that undergo thermal alteration to more magnetic phases, apparently magnetite, above this temperature. The majority of magnetic enhancement occurs above the magnetite Curie temperature and results in a massively increased $\chi$ on

cooling from 700°C. The cooling curve is then similar to sample TR21B4A and demonstrates the apparent oxidation of the high temperature magnetite to ?maghaemite as the sample returns to room temperature.

### *5.5.1 Neolithic enclosure, YFPB95 Site 5*

Sections of a Neolithic enclosure ditch were revealed during the invasive 2% trial trenching evaluation conducted by the OAU over the floodplain. Subsequent fluxgate gradiometer survey of ~0.9ha of this area revealed a rectilinear anomaly [NE1] truncated by the modern field boundary to the E (Figure 5.26(A)). Interpretation of the data from this site is hampered by the extremely weak magnetic response of the feature and the plethora of ferrous detritus incorporated into the topsoil from the organic waste processing site. Thus, it is impossible to discern whether discontinuities along the course of [NE1] represent entrances into the enclosure or a variation in the magnetic response.

Few significant anomalies have been identified within the enclosure other than a group of pit-type responses [NE2] obscured by more recent ferrous litter (Figure 5.26(B)). A tentative linear anomaly [NE3] is found just beyond the enclosure to the N running parallel to the course of the enclosure ditch that may, possibly, represent a recut of this feature. Activity beyond the enclosure is limited to a scatter of possible pit-type anomalies to the N ([NE4] and [NE5]) and S ([NE6] and [NE7]). However, no morphological identity is suggested by these groups and it seems equally likely that these anomalies may relate to less significant geomorphological or tree throw features. An earlier attempt to locate the Neolithic enclosure was erroneously positioned to the N of the evaluation trench but revealed a negative linear anomaly [NE8] that fell beyond the subsequent excavation trench 5.

### *5.5.2 Magnetic susceptibility survey of the Trench 5 excavation surface*

Following the successful mapping of archaeological features through magnetic susceptibility measurements made over part of the Stage 4 excavation surface (§5.1.2), a similar survey was commissioned to cover the Neolithic enclosure site. The survey was conducted with a Randall susceptibility meter and search loop by an external contractor,

Adrian Challands, who has kindly made the data available for analysis in this thesis (Figure 5.27; Challands 1995).

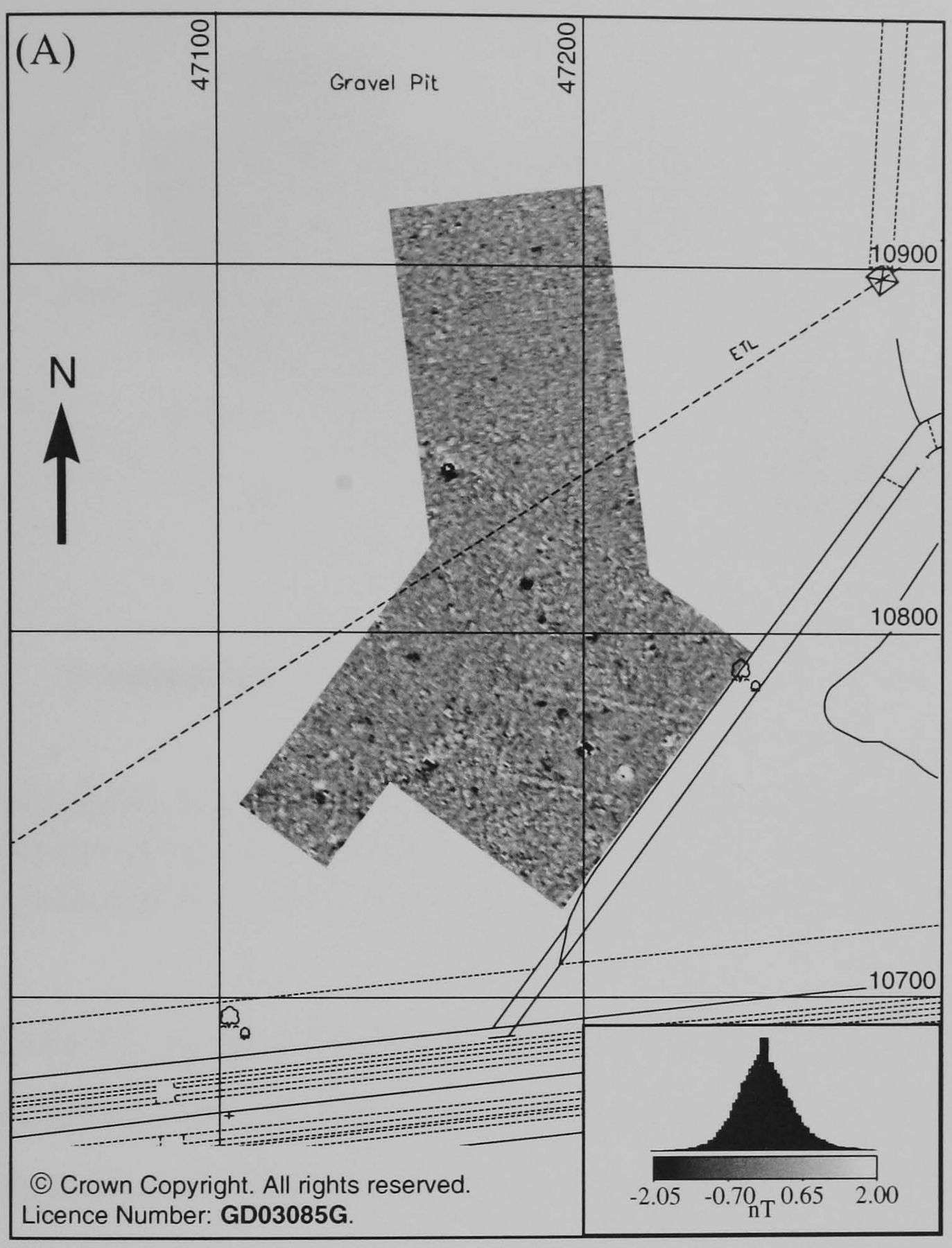


***Figure 5.26*** *(A) Greytone image of the fluxgate gradiometer data collected over the Neolithic enclosure site together with (B) a graphical summary of significant anomalies. The location of the subsequent excavation, Trench 5, is also shown.*

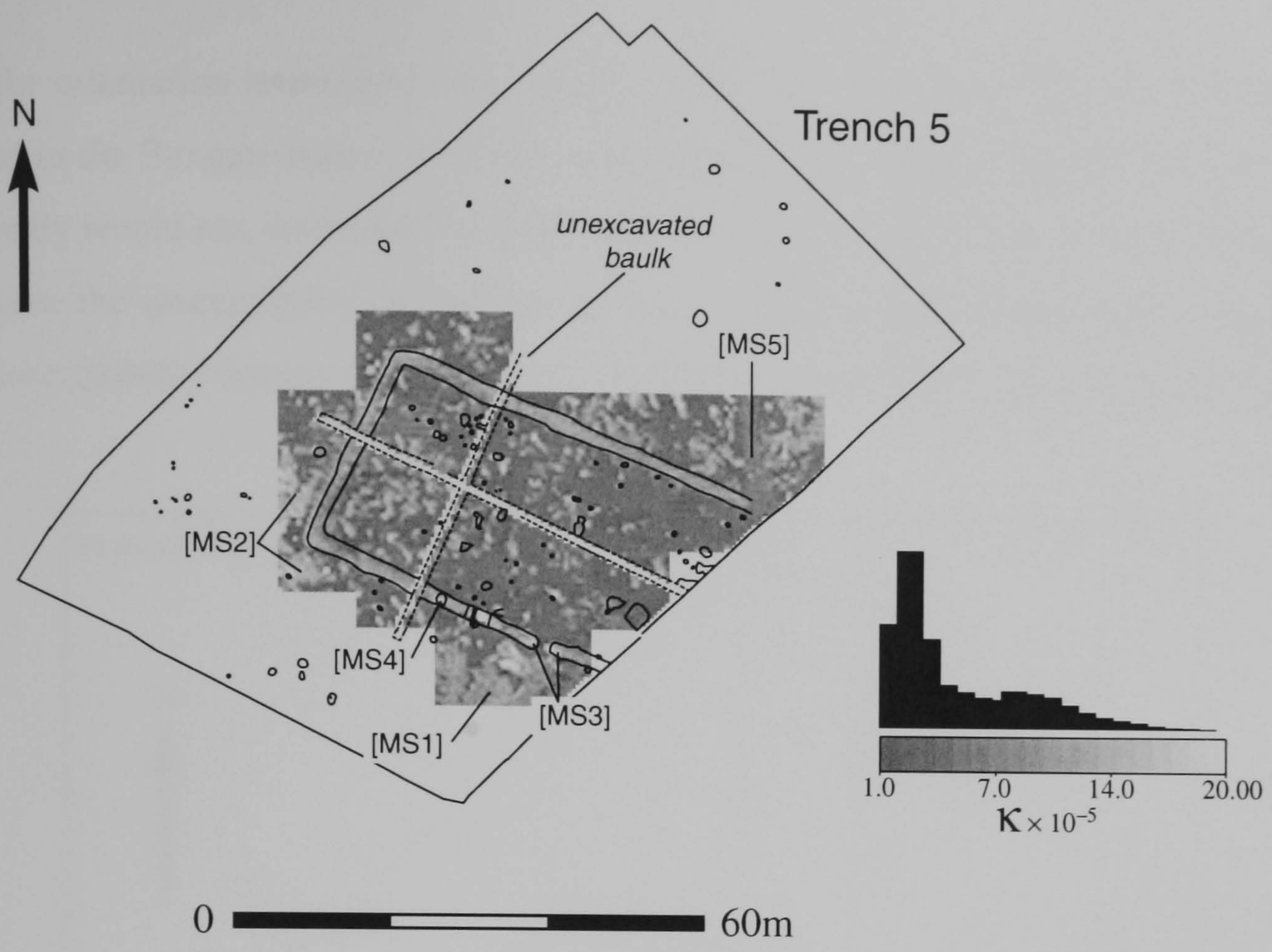


***Figure 5.27*** *Magnetic susceptibility survey conducted over the topsoil stripped excavation surface of the Neolithic enclosure, Trench 5. The figure also shows features subsequently revealed by excavation including the location of the enclosure ditch.*

Due to extremely dry weather conditions, difficulty was encountered with evenly removing topsoil from the site and some areas of enhanced A/B horizon soils remained producing enhanced readings in the magnetic susceptibility survey ([MS1], [MS2]). However, most of the excavation surface was successfully stripped back to the natural sand and gravel. This latter substrate has extremely low susceptibility in contrast to the fill of the Neolithic enclosure ditch that has produced the highest readings recorded in the survey area. The magnetic enhancement appears to be concentrated in the NW part of the ditch, possibly suggesting a focus of activity within the enclosure. The ditch terminals found at the apparent entrance to the enclosure [MS3] also demonstrate an enhanced susceptibility as does the remains of a pit-feature [MS4] cut into the course of the southern course of the ditch. The magnetic response of other cut features is more variable with little obvious correlation between their location and areas of enhanced susceptibility.

A NS orientated section of Roman ditch [MS5] was detected as an area of moderate susceptibility cut into an area of magnetically enhanced (burnt?) sand and gravel. Unfortunately, the location of this ditch is not recorded on the supplied excavation plan

but the orientation is similar to the negative linear anomaly [NE8] (Figure 5.26(B)) found in the fluxgate survey N of the excavation trench. Whilst a negative magnetic anomaly would not, necessarily, be identified as a ditch section the variable contrast between the susceptibility of cut features and occupation enhanced subsoils revealed by the susceptibility survey suggests such interpretations should be revised on certain sites.

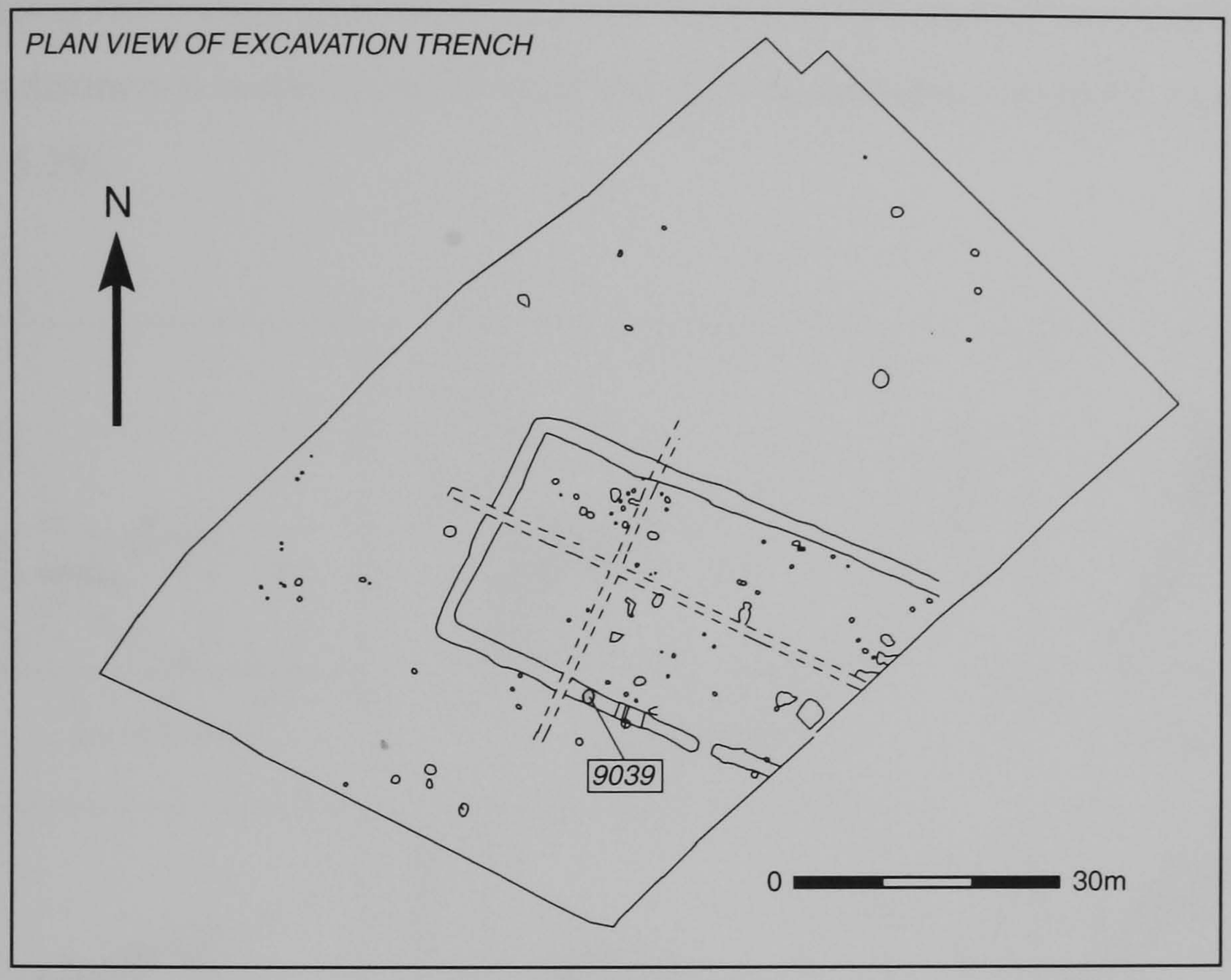


***Figure 5.28*** *Plan view of the features recorded during the excavation of the Neolithic enclosure, YFPB95 Site 5 together with a section showing the detailed location of the mineral magnetic samples and relevant context layers.*

### *5.5.3 Mineral magnetic results*

Figure 5.28 shows the location of samples collected through a section of the Neolithic ditch believed to be a funerary enclosure. The samples were made over a regular grid and include the topsoil, all context layers identified within the section of the ditch and the surrounding natural substrate. A further classification between the upper fill and the more gravel rich lenses accumulating at the bottom of the ditch section has been made and this distinction is illustrated through the room temperature magnetic measurements (Figure 5.29).

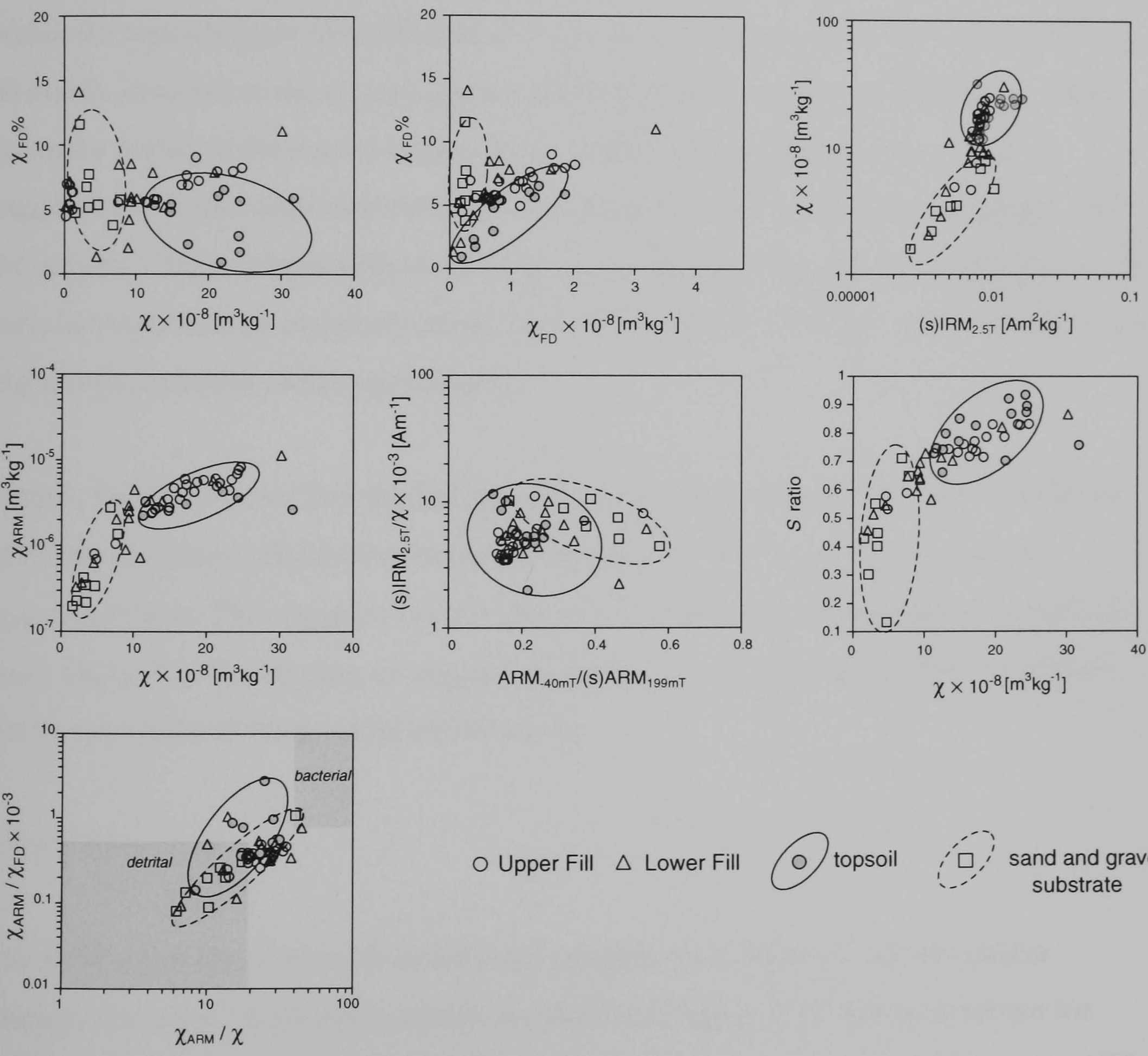


***Figure 5.29*** *Selected room temperature magnetic parameters and ratios displayed as a series of bi-plot graphs for the samples recovered from the Neolithic enclosure. An envelope showing the approximate range of these parameters for samples of both the topsoil and the sand and gravel substrate is also illustrated.*

*5.5.3.1 Isothermal measurements*

In general, the topsoil and upper fill samples demonstrate a higher susceptibility than the natural sand and gravel substrate with samples from the lower fill of the ditch falling between these two groups (Figure 5.29). The frequency dependence of susceptibility is quite scattered and only the topsoil samples, with higher values of $\chi$, demonstrate a convincing near-linear relationship between $\chi_{FD}$ and $\chi_{FD\%}$.

Three of the biplots, *(s)IRM$_{2.5T}$* vs $\chi$, $\chi$ vs $\chi_{ARM}$ and $\chi$ vs *S ratio* further illustrate the differing magnetic properties of the topsoil/upper fill from the natural samples. In each case the data suggests an increased concentration of very fine grained magnetic material within the topsoil/upper fills reflected as an increase in $\chi$, $\chi_{ARM}$ and the S ratio that are all highly sensitive to the effective grain size distribution. Values of (s)IRM$_{2.5T}$, whilst generally higher in the topsoil/upper fill, are relatively constant for these contexts suggesting a similar total concentration of magnetic minerals. This would suggest that the apparent linear relationship between $\chi$, $\chi_{ARM}$ and the S ratio for the topsoil/upper fill samples represents an increasing proportion of fine grained material within opposed to a higher concentration of ferrous minerals.

Despite the presence of fine grained particles none of the samples falls fully within the envelope of values exhibited by bacterial magnetite when plotted on a $\chi_{ARM}/\chi$ vs $\chi_{ARM}/\chi_{FD}$ biplot. This suggests that the material is either superparamagnetic or, perhaps more likely, that the mixture of magnetically hard detrital minerals within the samples skews the values of these ratios on this biplot.

*5.5.3.2 Hysteresis*

The IRM acquisition curves from selected samples representing a vertical profile through the centre of the ditch section are shown in Figure 5.30 and demonstrate the similar behaviour of the topsoil and fill contexts to the natural substrate. The topsoil/fill samples are generally "softer", acquiring IRM more rapidly in low fields, but all samples fail to reach saturation by 1.8T suggesting the presence of a significant hard detrital mineral.

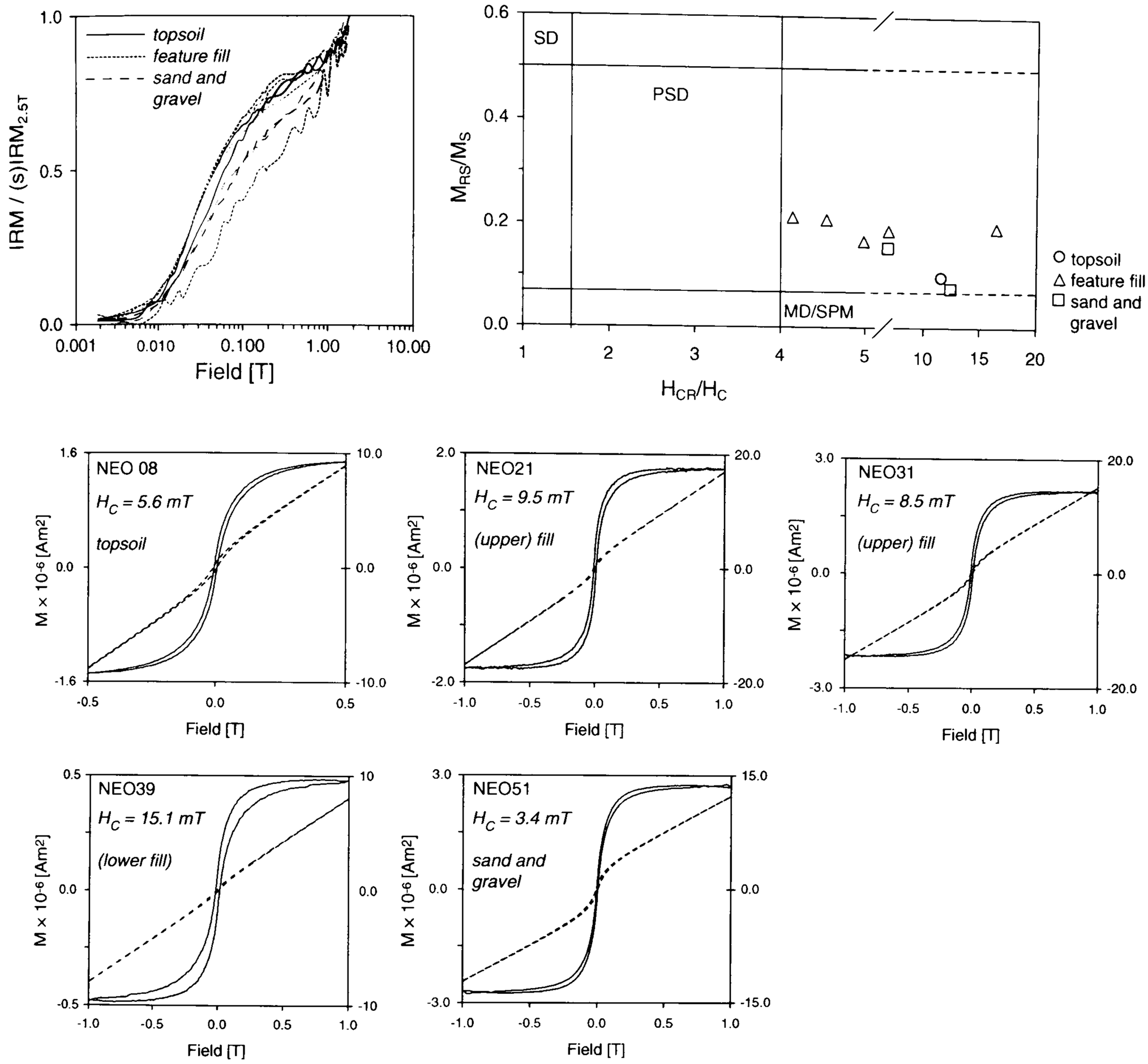


***Figure 5.30*** *Summary of the IRM acquisition and hysteresis behaviour for samples from the Neolithic Enclosure. Where hysteresis loops contain a significant paramagnetic component the uncorrected data is shown (dashed line) superimposed over the underlying ferrimagnetic loop (solid line). If necessary, the paramagnetic component is plotted against a second scale axis (right hand side of figure).*

In field hysteresis data for the same samples are again highly similar and are dominated by a paramagnetic component that largely obscures the underlying ferrimagnetic loops. All of these loops appear to be "wasp-waisted" and exhibit an increasing degree of constriction around the origin with depth through the ditch section. Whilst such wasp-waisted loops may be due to a mixture of superparamagnetic material within the samples the extreme values of $H_{CR}/H_C$ and the unsaturated IRM acquisition curves

suggests this behaviour is due to the presence of a high coercivity mineral such as goethite (Muttoni 1995, Roberts et al. 1995, Tauxe et al. 1996).

It is of interest to note that the discrimination between the topsoil/upper fill samples and the underlying natural substrate is not so well defined within the hysteresis data than the selected biplots of isothermal parameters and ratios. This may well be due to the adverse contribution of the paramagnetic component to the in-field data or suggest the importance of very fine grained material to which both $\chi_{ARM}$ and the *S* ratio are highly sensitive.

*5.5.3.3 Thermomagnetic data*

Results from a single low temperature experiment (NEO 31) are presented together with the high temperature variation of $\chi$ for samples NEO 08, NEO 31 and NEO 45 (Figure 5.31). The low temperature sample shows a gradual increase in the magnetisation imparted at room temperature on cooling to 20K, consistent with the presence of goethite. Although the cooling curve is apparently devoid of any inflections the change of slope, $^{dM}/_{dT}$, suggests the presence of a slight Verwey transition (*cf* Figure 4.8). The loss of magnetisation imparted at 20K on warming back to 300K demonstrates a change in slope at approximately 50K that may well be due to the low temperature ordering of the paramagnet component.

The high temperature variation of $\chi$ for NEO 31 is highly similar to the other ditch fill sample NEO 45. Both exhibit little change on heating to 300°C where a slight drop in $\chi$ precedes the production of a highly magnetic mineral at a peak of 500°C with a Curie temperature of ~580°C that suggests the formation of magnetite. The cooling curves demonstrate a high degree of enhancement with a slight inflection at ~450°C before a peak value of $\chi$ is found just above 200°C, possibly due to the oxidation of magnetite to maghaemite on cooling and the blocking of fine grained material. The sample of topsoil, NEO 08, is distinguished through the presence of an additional $\chi$ peak on heating to ~280°C, possibly due to the formation of maghaemite from lepidocrocite present within the gleyed surface soils (Marmet et al. 1999). This newly formed mineral decays rapidly on heating to 400°C before the production of magnetite begins at ~450°C. The

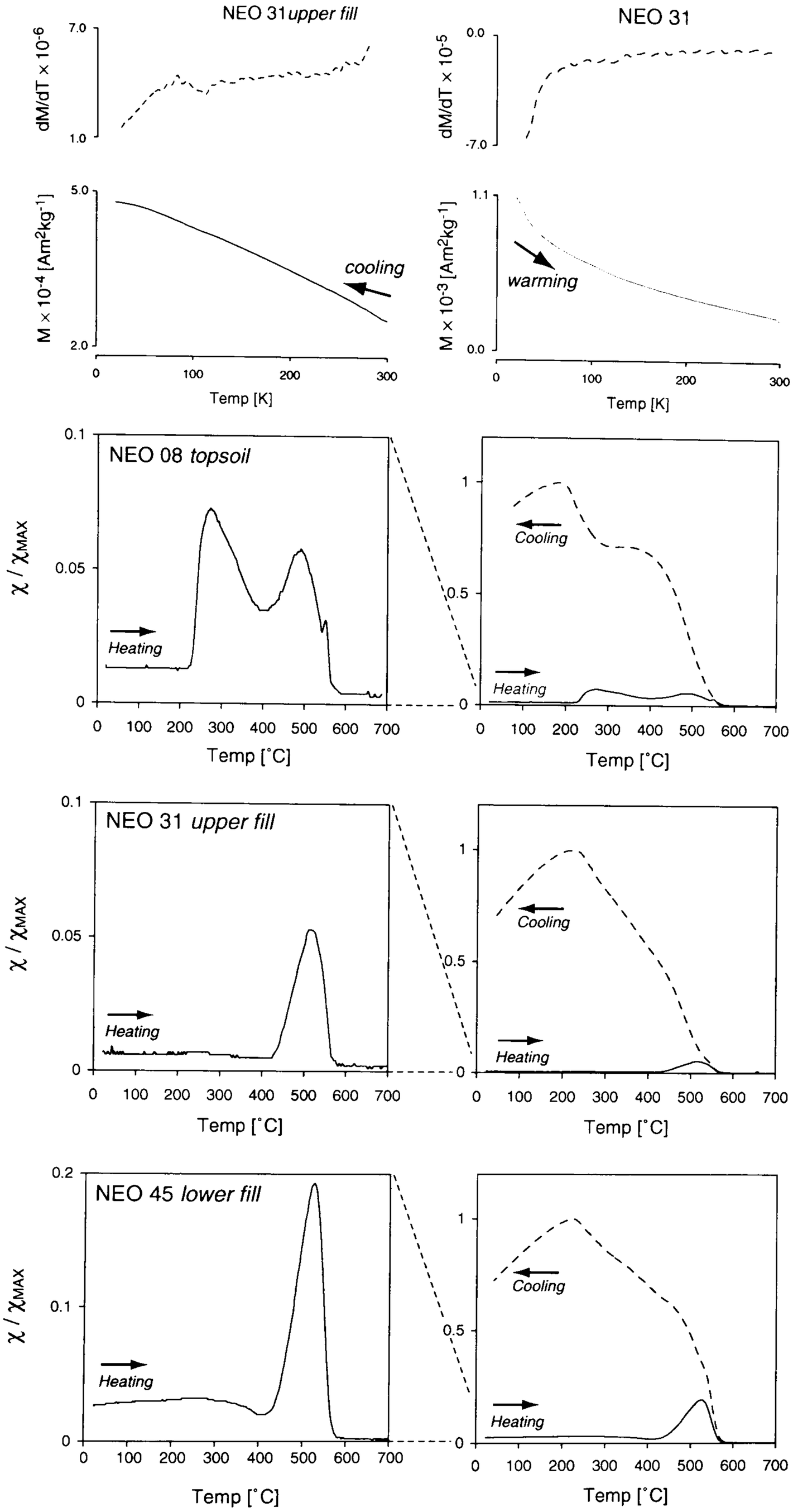


***Figure 5.31*** *Thermomagnetic behaviour of samples from the Neolithic enclosure. The low temperature variation of a single sample (NEO31) was measured together with the high temperature variation of susceptibility of this and two additional samples. Cooling curves are plotted separately from warming curves due to the differing magnitude of the two data sets and for the low temperature magnetisation the first differential of each curve is also shown (dashed line) to aid the identification of subtle inflections.*

degree of enhancement on cooling is similar to samples NEO 31 and NEO 45, however, a more pronounced high temperature "shoulder" between 450 and 300°C exists before the peak at 250°C attributed to the oxidation of maghaemite occurs. It is unclear whether the absence of the heating peak at 250°C in the ditch fills provides evidence for the previous thermal history of these sediments. Certainly, Neolithic funerary practice often involved ritual cremation and it is therefore likely that the fill of the enclosure ditch may well contain burnt topsoil derived from this activity.

### *5.6.1 YFPB 1997*

A fluxgate gradiometer survey was conducted over ~3ha in advance of OAU excavation trench 25. The previous trial trench evaluation survey had identified an important Bronze Age boundary ditch within this area that apparently divided occupation related activity from the ritual landscape. The results from this survey are shown in Figure 5.32(A) that illustrates the extremely quiet nature of this site with the majority of the readings falling within ±0.5nT of the zero mean. Identification of significant archaeological anomalies so close to the noise level of the fluxgate instruments was therefore severely hampered and the data contains a number of linear artefacts due to the characteristics of individual instruments and operator gaits.

However, three tentative linear anomalies have been identified (Figure 5.32(B)) including the course of the NS post medieval field boundary which is represented as a series of aligned high intensity responses [FP97_1], possibly caused by ferrous rubbish that has accumulated along its course. The course of this field boundary along a similar orientation is still extant to the S of the A40. Two additional very subtle linear anomalies [FP97_2] and [FP97_3] were located and correlate with the position of a Bronze Age ditch identified during the trial trench evaluation.

### *5.6.2 Mineral magnetic results*

Samples were collected from a variety of features including pits, a waterhole and various phases of ditch cuts (Figure 5.33). Initial evaluation trenches had revealed a wide variation in the depth of alluvial cover over the site that increased in depth to the south. To investigate the influence of this varying alluvial cover one of the more substantial boundary ditches, containing only abraded Bronze Age pottery sherds, was

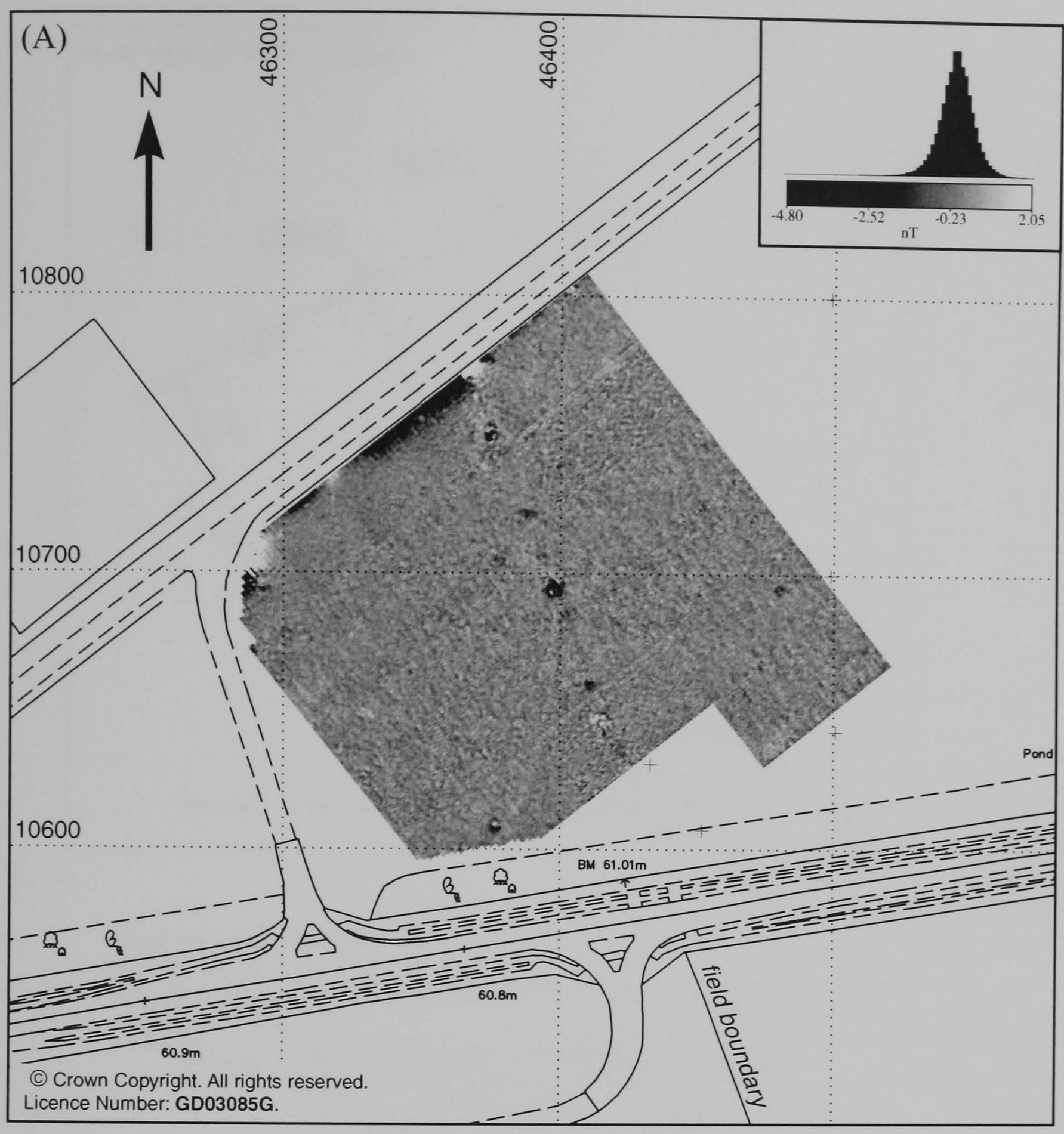


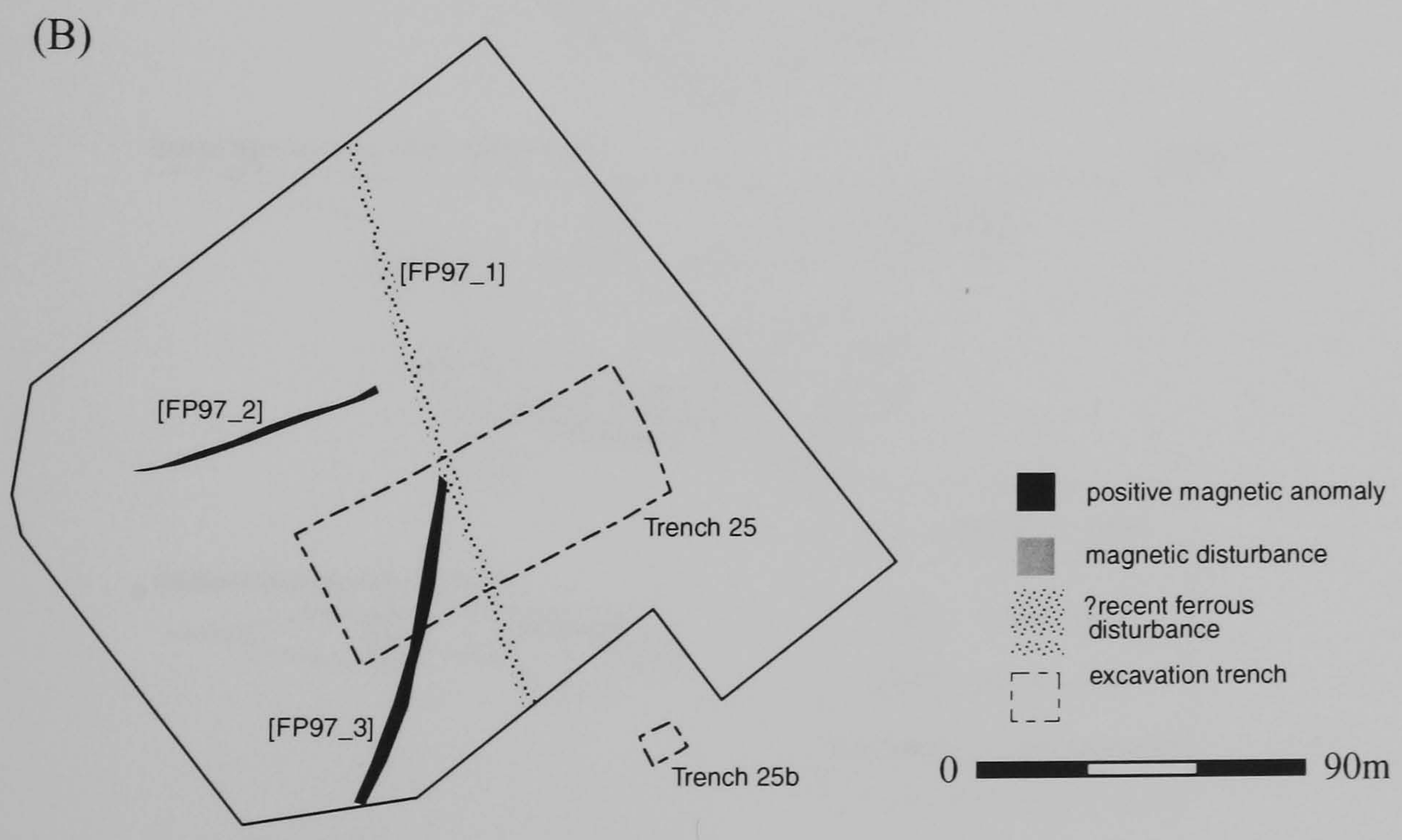


***Figure 5.32*** *(A) Greytone image of the fluxgate gradiometer data collected over YFPB97 together with (B) graphical summary of significant anomalies.*

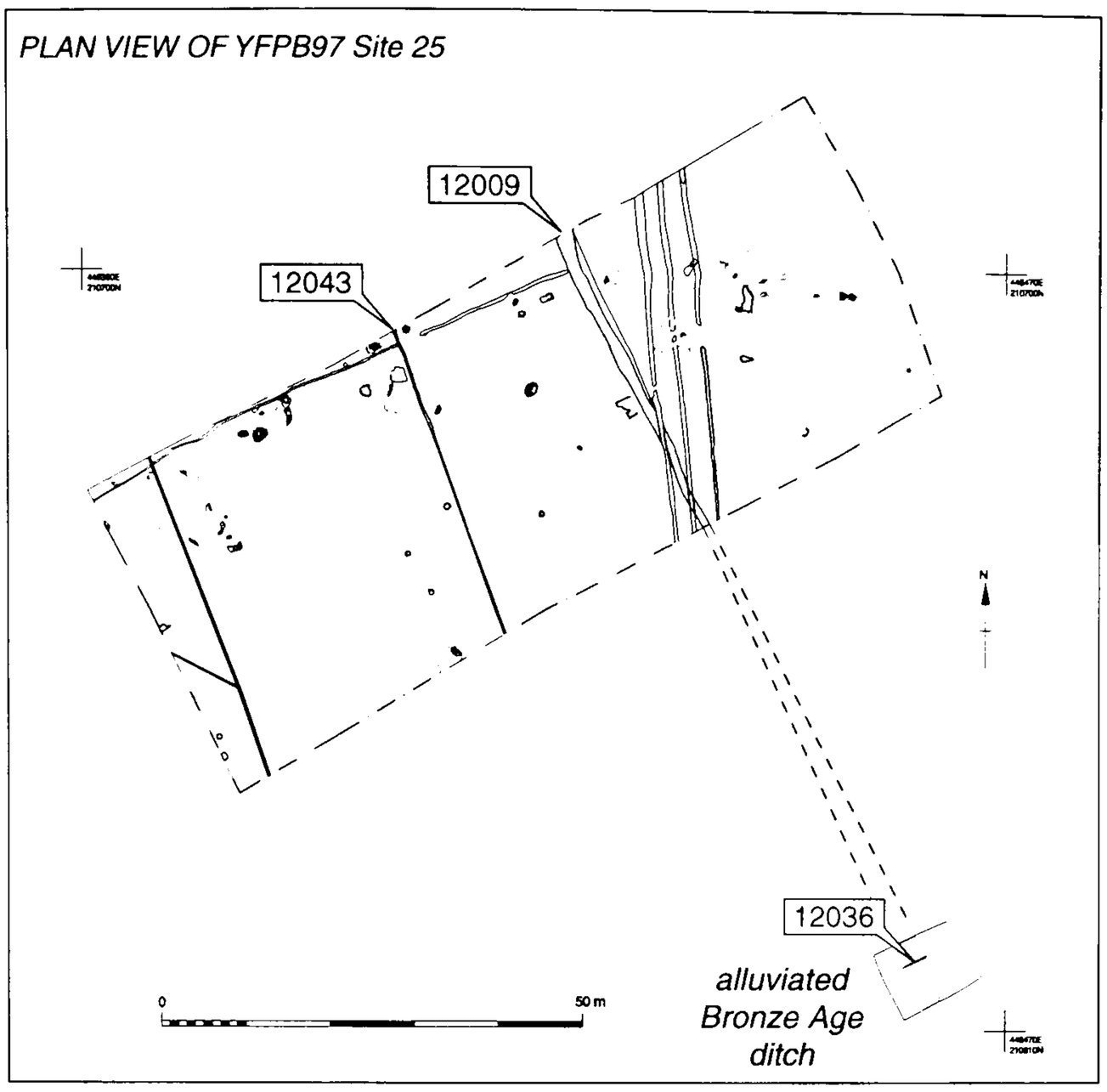


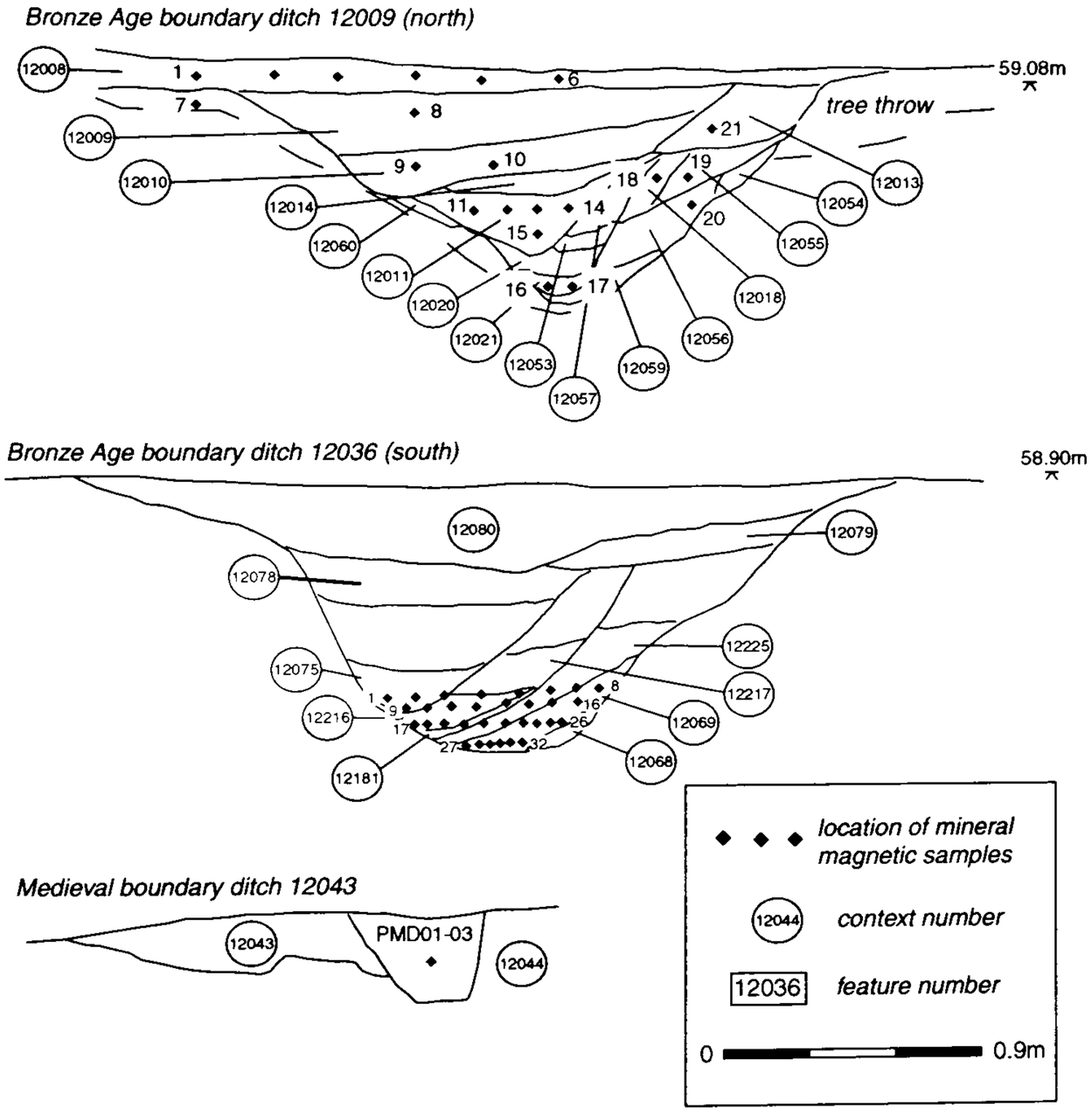


***Figure 5.33*** *Plan view of the features recorded during the excavation of YFPB97 together with sections drawn through those features selected for the collection of mineral magnetic samples. The sections show the location of the recovered samples and the context layers identified in the field.*

sampled both to the N where the top of the feature lay close to the modern ground surface and further to the S where the ditch was sealed by a substantial layer of overburden. The southern section of this ditch contained a black, organic rich fill at the base of the feature that when sampled was found to have a susceptibility and apparently stable NRM. A second cut of this ditch was made, revealing a similar organic rich basal fill, and orientated samples were recovered to facilitate the archaeomagnetic dating of the sediment.

Magnetic extracts were also kindly prepared by Dr M. Hounslow, from the organic rich ditch sediment following Hounslow and Maher (1996) and Hounslow and Maher (1999).

*5.6.2.1 Natural Remanent Magnetisation*

Field observations with a Bartington MS susceptibility meter and `F` probe confirmed the enhanced magnetic properties of the organic rich layer found at the bottom of the initial cut of the alluviated ditch. Therefore, prior to conducting any further magnetic measurements, the NRM of these samples was determined and found to be both consistent and highly stable during AF demagnetisation. To confirm the fidelity of this NRM a second section, 12036, was cut through this feature (approximately 1m to the N) to allow the more concentrated sampling of the organic rich layer that provided the most stable magnetisation.

Figure 5.34 summarises the NRM data recovered from this ditch section and shows, for a representative sample, the presence of a single magnetisation vector that remains stable during AF demagnetisation up to a 50mT peak field. Above 50mT the initial intensity of NRM is reduced to ~25% and almost completely removed by 80mT. The mean direction of all stable magnetisation vectors (Inc = 70.6°, Dec = 3.4, $\alpha$-95 = 2.0) recovered from the 20 samples is shown superimposed over the archaeomagnetic calibration curve for the UK (Clark et al. 1988a) and suggests a date of 127 to 97 BC at a 68% confidence level (167 to 85 BC at a 95% confidence level). This is in good agreement with the radiocarbon determinations from two samples, OxA-10707 and OxA-10708 of the organic material that produced calibrated dates of cal BC 360 to 1 and cal BC 390 to 90 respectively (A. Bayliss pers. comm.).

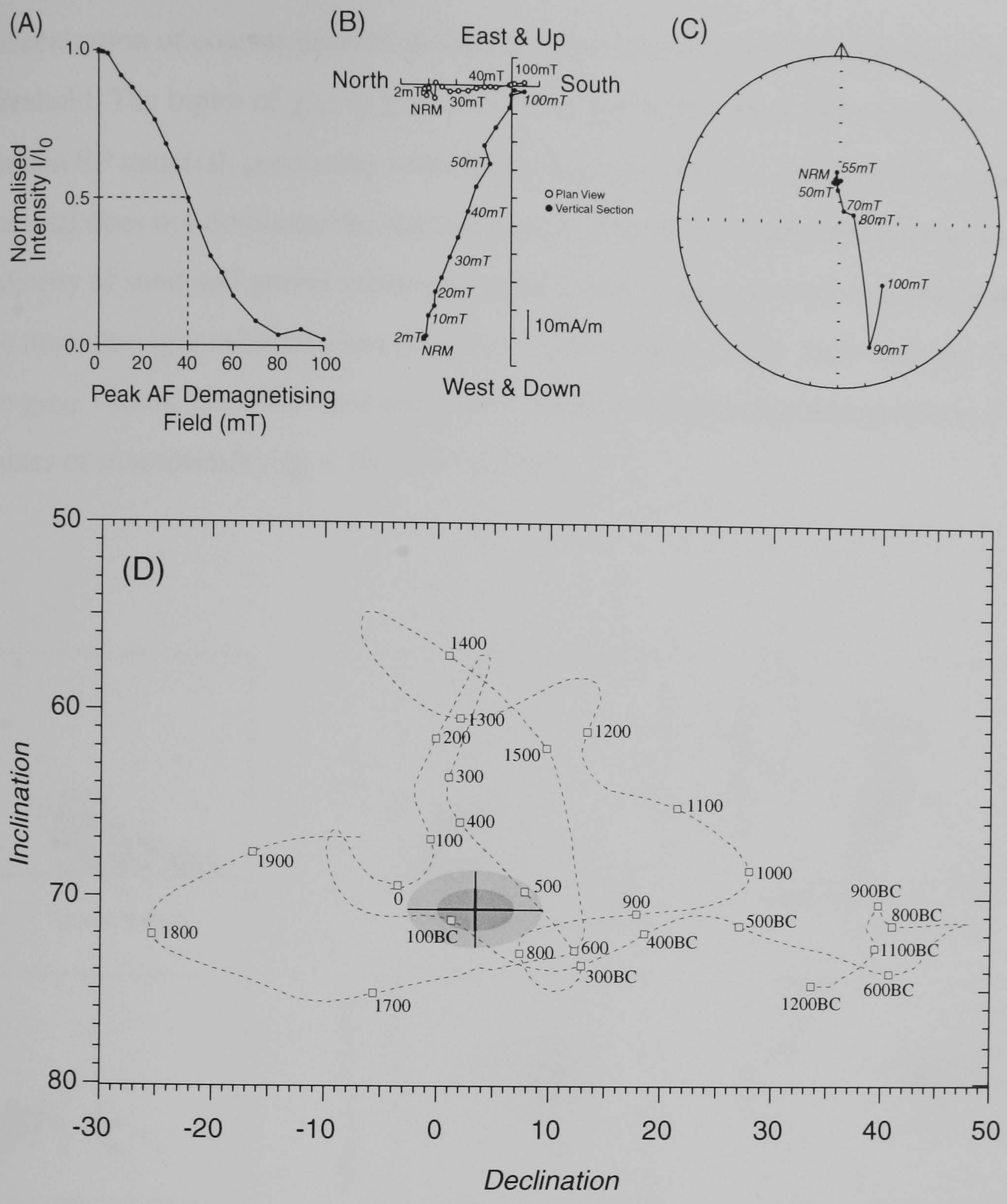


***Figure 5.34*** *NRM data for samples collected from the organic rich layer at the base of the alluviated ditch (section 12036). AF demagnetisation behaviour is shown for a single representative sample (BAS230) including (A) the loss of intensity and stability of remanence represented as both Zijderveld (B) and stereonet (C) projections. The lower figure (D) shows a graphical representation of the mean calculated from all samples superimposed over the UK archaeomagnetic calibration curve. The data suggests a date of 97BC to 127BC cal at the 68% confidence limit (85BC to 167BC cal at the 95% confidence limit)(after Clark et al. (1988b)).*

### *5.6.2.2 Isothermal measurements*

A wide range of initial susceptibilities are found within the samples recovered from this site and again the sand and gravel substrate produce some of the lowest values, $\chi < 10 \times 10^{-8}$ $m^3kg^{-1}$ (Figure 5.35). Samples from the base of the alluviated boundary ditch demonstrate the highest values of $\chi$ and lowest values of $\chi_{FD\%}$ suggesting an increased

concentration of coarser grained magnetic material above the superparamagnetic (SP) threshold. The biplot of $\chi_{FD}$ vs $\chi_{FD\%}$ confirms that whilst these latter contexts do indeed contain SP material, producing some of the highest values of $\chi_{FD}$, this fine grained material does not dominate the magnetic properties of the ditch fill samples. Indeed, the majority of sand and gravel substrate samples have a $\chi_{FD\%}$ greater than the majority of the more strongly enhanced samples from ditch section 12036. However, the fidelity of the $\chi_{FD\%}$ values, from the sand and gravel substrate, is questionable given the low values of susceptibility ($\chi < 10 \times 10^{-8}$ $m^3kg^{-1}$).

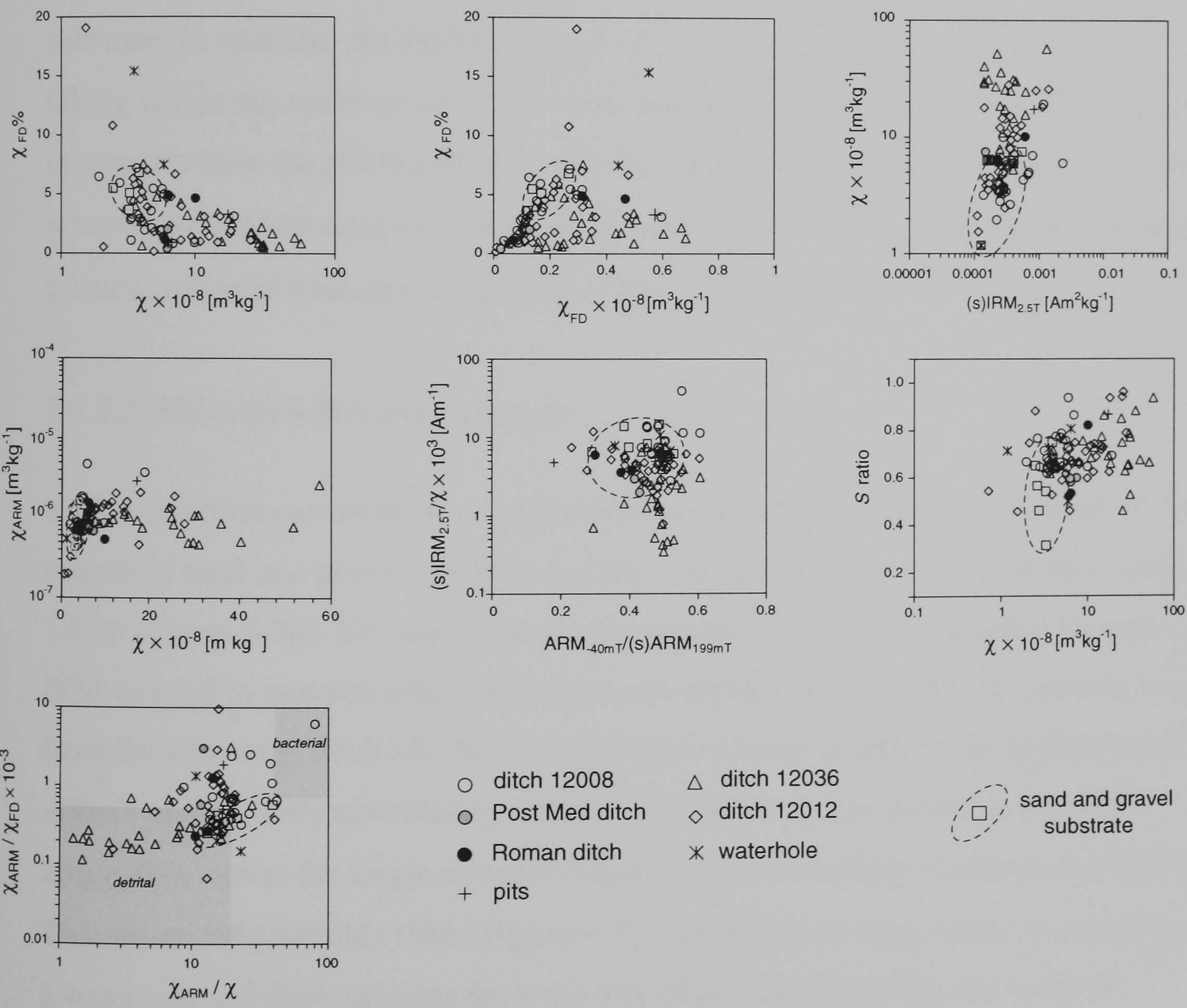


***Figure 5.35*** *Selected room temperature magnetic parameters and ratios displayed as a series of bi-plot graphs for the samples recovered from YFPB97 site 25. An envelope showing the approximate range of these parameters for samples of the sand and gravel substrate is also illustrated.*

Values of saturation magnetisation do not distinguish the feature fills from samples of the underlying substrate. However, a linear relationship between (s)IRM$_{2.5T}$ and $\chi$ is found for weaker samples that apparently fails for the more strongly enhanced ditch fills (*cf* Figure 5.29) that are distinguished through higher values of $\chi$ alone. This does not appear to be related to an increased concentration of superparamagnetic particles as values of $\chi_{FD\%}$ are uniformly low for these samples.

A similar linear correlation is found between $\chi$ and $\chi_{ARM}$ for the weaker samples and again as $\chi$ increases this relationship breaks down. Both the ARM$_{-40mT}$/(s)ARM vs (s)IRM$_{2.5T}$ / $\chi$ and $\chi$ vs *S* ratio biplots suggest that many of the feature fills contain an increased concentration of magnetically softer minerals compared to the sand and gravel substrate. In addition, the biplot of $\chi_{ARM}$ / $\chi$ vs $\chi_{ARM}$ / $\chi_{FD}$ shows only one sample falling within the envelope of values expected for biogenic magnetite with the majority of samples from the alluviated ditch section 12036 demonstrating values similar to those reported for detrital sources. Indeed these latter samples show some of the lowest $\chi_{ARM}$ / $\chi$ values reported from any of the sites within the study area.

*5.6.2.3 IRM acquisition and hysteresis*

IRM acquisition curves show a range of behaviour between extremes defined by the sample of sand and gravel substrate and the samples from the alluviated ditch section 12036 (Figure 5.36). The sand and gravel samples demonstrate a gradual increase of IRM and fail to saturate within the maximum applied field of 1.8T. In contrast, samples from the alluviated ditch fill show a very rapid increase in IRM from applied fields of ~20mT and are fully saturated by 100mT. This behaviour is similar to the IRM acquisition curves for single-domain magnetite (grain diameter 0.63$\mu$m) reported by Thompson and Oldfield (1986; Figure 4.3). Samples from other features, including pits, a waterhole and ditch sections from the less alluviated part of the site to the N, demonstrate intermediate behaviour between these two extremes and generally provide evidence for either mixed mineral phases or bimodal grain-size populations.

Hysteresis loops measured from selected samples show the presence of a strong paramagnetic component. The underlying ferrimagnetic loops from features to the N of

the site (e.g. BAN14 and 10104nlr) are highly similar to the "wasp-waisted" loops produced by the sand and gravel substrate (e.g. BANNAT02).

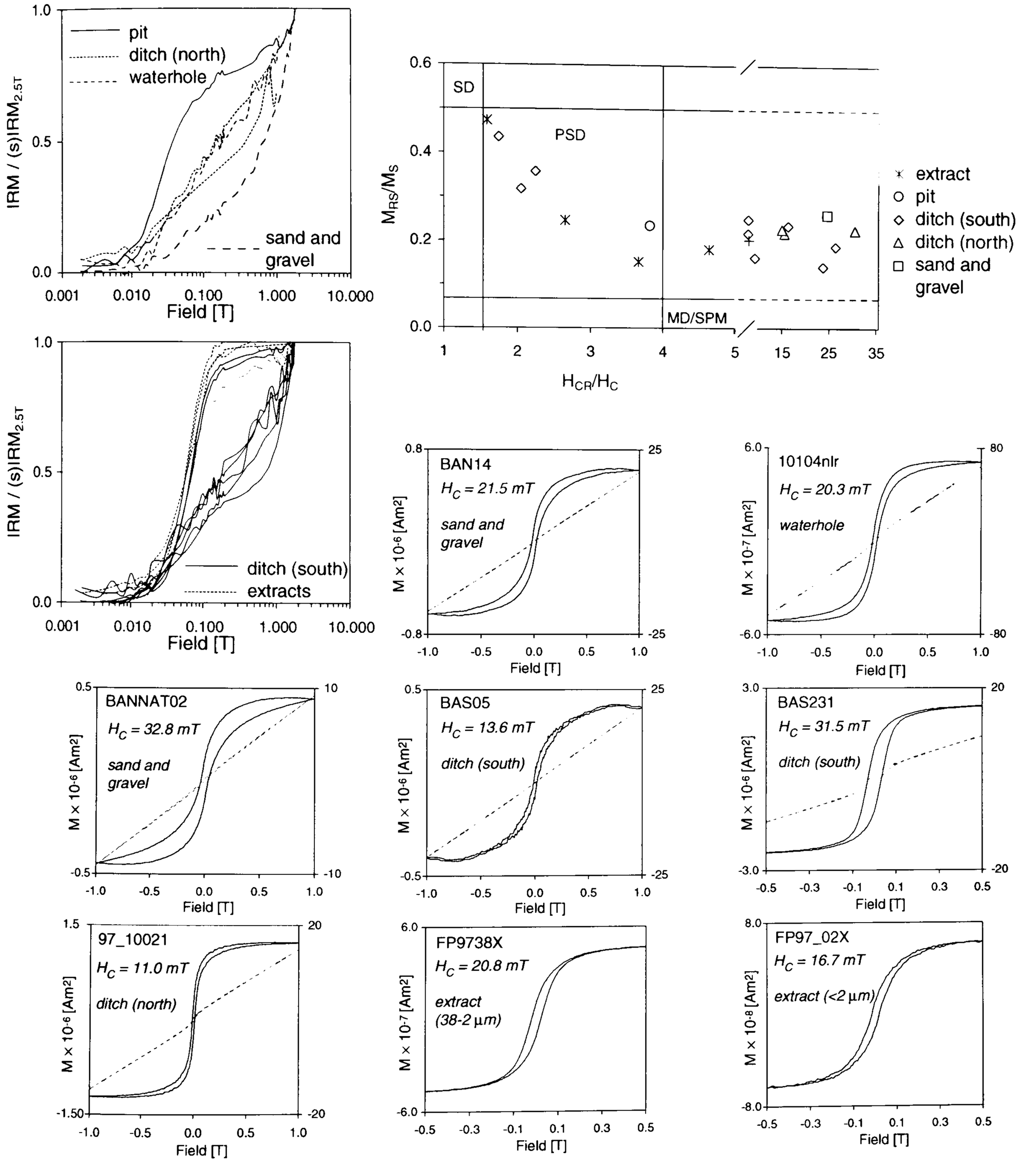


***Figure 5.36*** *Summary of the IRM acquisition and hysteresis behaviour for samples from the YFPB97 site 25. Where hysteresis loops contain a significant paramagnetic component the uncorrected data is shown (dashed line) superimposed over the underlying ferrimagnetic loop (solid line). If necessary, the paramagnetic component is plotted against a second scale axis (right hand side of figure).*

Samples from the alluvium overlying the organic rich deposit to the S (e.g. BAS05) are dominated by an extremely strong paramagnetic component that, once removed, reveals an extremely weak ferrimagnetic loop. However, samples from the organic rich layer (e.g. BAS231) whilst still containing a significant paramagnetic contribution reveal ferrimagnetic loops similar to those expected from single-domain magnetite. Hysteresis loops from the magnetic extract are also shown for two physical size fractions, <2$\mu$m and 2-38$\mu$m (FP97_02X and FP97_38X respectively). It is of interest to note that the coercivity of the loops decreases from the bulk sample through to the finest <2$\mu$m extract, suggesting the extraction procedure has successfully concentrated increasingly finer grain-sized material within the two fractions.

*5.6.2.4 Low temperature magnetisation*

Cooling and warming curves for 6 samples are shown in Figure 5.37. The two samples from features excavated to the N of the site, PMD01 and RD03, are very similar showing a gradual increase in $M_S$ on cooling from 300 to 20K. A slight change in slope is evident within the $^{dM}/_{dT}$ curves below 100K but neither curve demonstrates the presence of a wholly convincing Verwey transition. The warming curves are again mostly featureless but do show evidence for a slight change in slope at very low temperatures that may well be due to the presence of paramagnetic minerals with Néel temperatures less than 30K. Samples from the alluviated ditch to the S, BAS29, BAS33, BAS230 and BAS232, are also quite similar but the gradient of the cooling curves provides more convincing evidence for a Verwey transition at ~120K suggesting the presence of magnetite.

*5.6.2.5 Thermomagnetic analysis*

Three samples were selected for high temperature thermomagnetic analysis including a Roman ditch fill from the N of the site RD03, a sample of alluvium BAS05 and a sample from the organic rich fill of the ditch to the S BAS230 (Figure 5.38). In addition, sample RD03 was reheated following the initial experiment to verify the nature of the magnetic minerals on heating to 700°C.

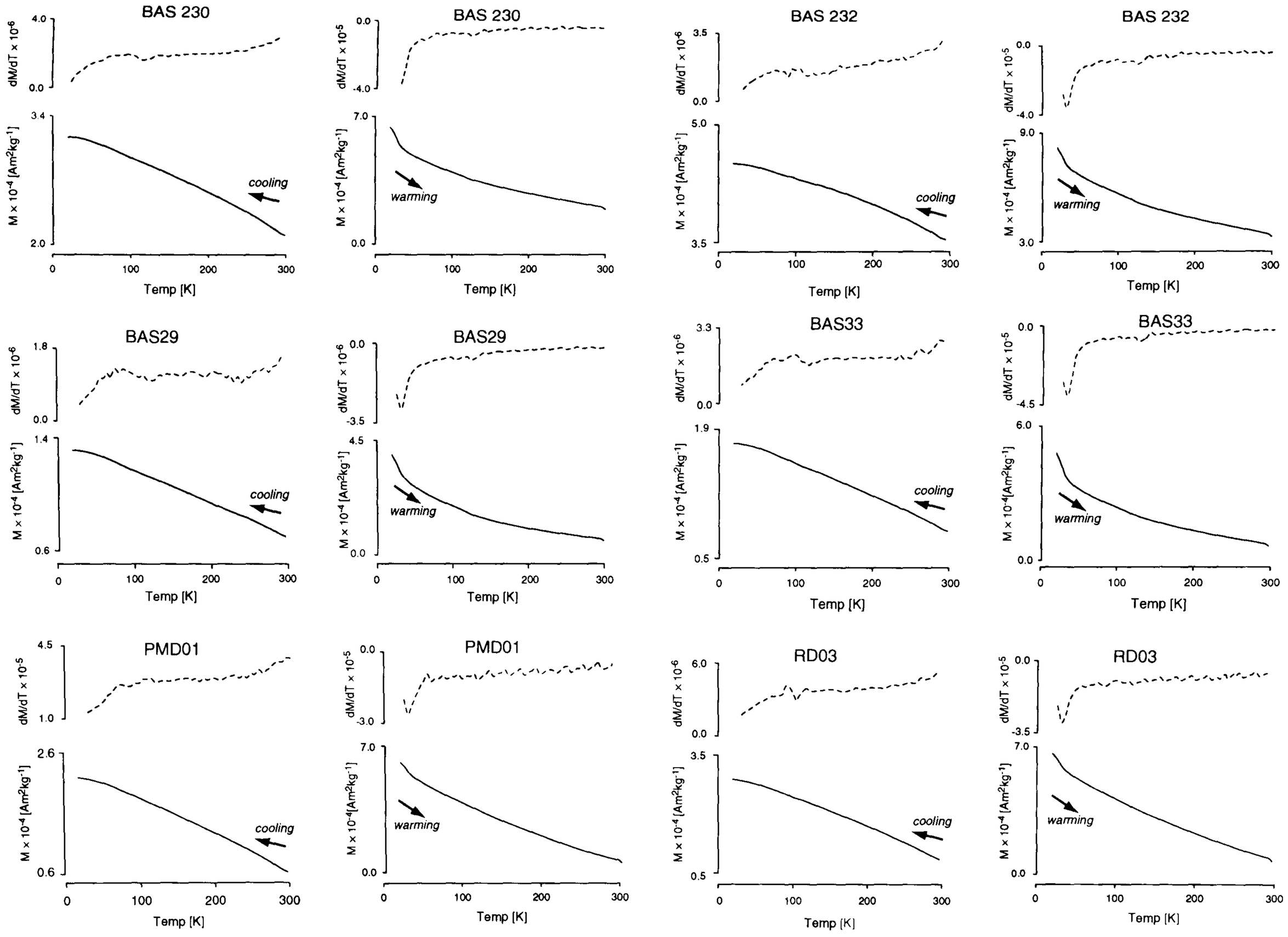


***Figure 5.37*** *Low temperature behaviour of samples from YFPB97. Cooling curves are plotted separately from warming curves due to the differing magnitude of the two data sets and the first differential of each curve is also shown (dashed line) to aid the identification of subtle inflections.*

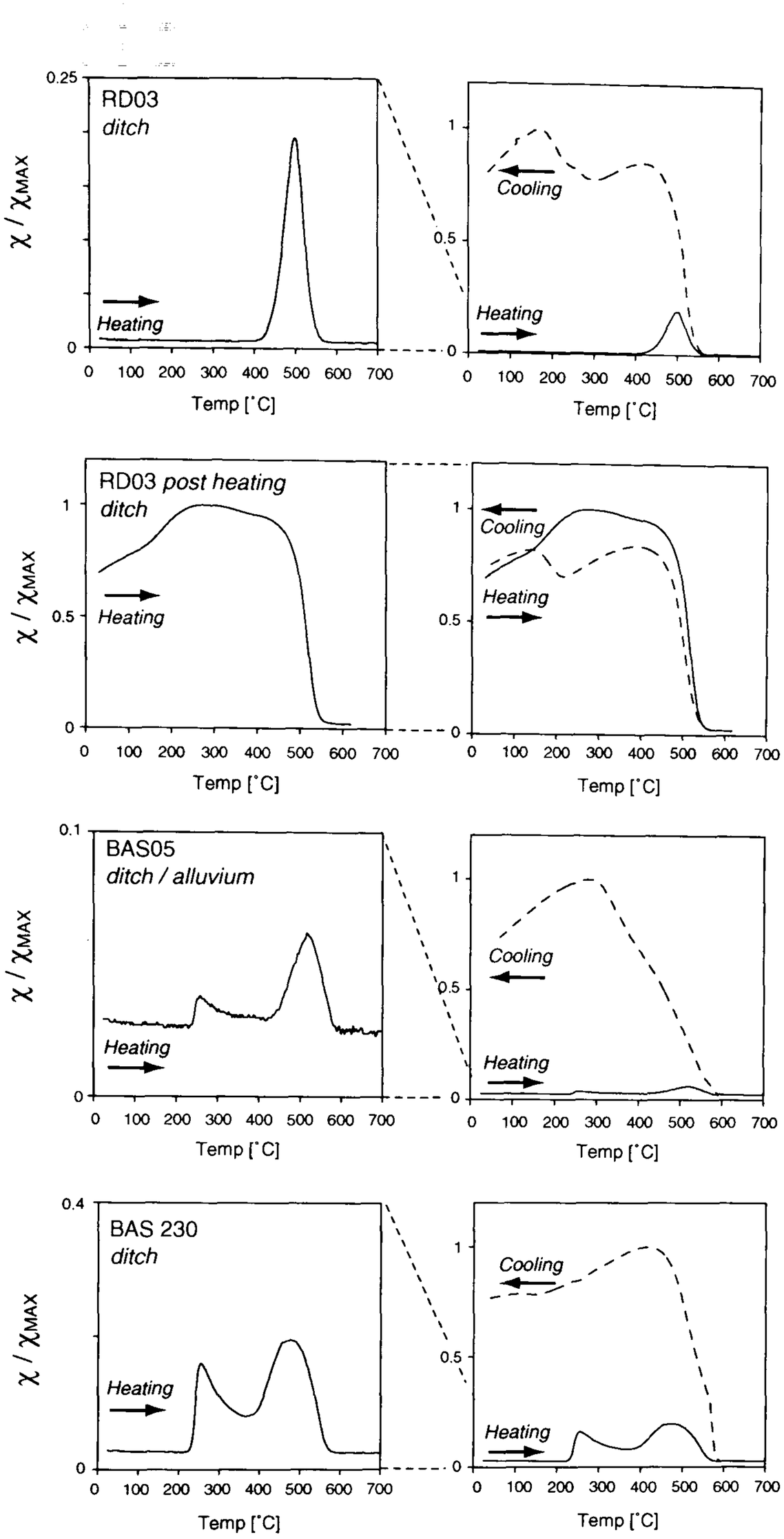


***Figure 5.38*** *Variation of high temperature susceptibility for 3 samples selected from YFPB97. The heating and cooling curves are plotted separately for each sample.*

On heating, the two samples from the alluviated ditch, BAS05 and BAS230, show an initial low temperature alteration at ~230°C that decays on heating above 250°C before a second, more intense, alteration occurs reaching a peak at 500°C. The initial peak may well be due to the dehydration of lepidocrocite to maghaemite (e.g. Özdemir and Banerjee 1984, Marmet et al. 1999) followed by a more complete alteration of iron minerals (on heating to 500°C) to magnetite, inferred from a 580°C Curie temperature. The greater prominence of the initial alteration peak in BAS230 suggests the mineral undergoing thermal alteration is more likely to be formed under the anoxic/anaerobic conditions found in the organic rich layer at the bottom of this ditch section. This may

well account for the absence of any low temperature alteration in the more aerated Roman ditch section to the N of the site (sample RD03) that demonstrates only the high temperature "magnetite" peak on heating.

Cooling curves from all three samples confirm the high degree of magnetic enhancement that occurs on heating to 700°C, apparently through the alteration of iron minerals within the samples to magnetite. The recovery of $\chi$ is quite rapid below 580°C for samples RD03 and BAS230, reaching an initial peak at ~450°C, but is more gentle for BAS05 that does not reach a peak value until 300°C. Below the initial peak in the cooling curve both BAS05 and BAS230 gradually lose susceptibility on cooling back to room temperature. However, RD03 shows a second, slightly higher susceptibility peak at ~150°C suggesting, perhaps, a mixture of both magnetite and maghaemite that regains $\chi$ after cooling below a sub 300°C Curie temperature.

Reheating sample RD03 to 600°C demonstrates a slight increase in $\chi$ until ~200°C and a 560°C Curie temperature that suggests the sample is dominated by the presence of magnetite. The cooling curve has a similar shape to that of the fresh sample and has a lower susceptibility than the heating curve until <100°C where the curves are highly similar. This suggests a largely repeatable cycle of magnetite formation on heating followed by partial, although not necessarily complete, oxidation to maghaemite as the sample cools.

*5.6.2.6 Magnetic extracts*

Magnetic extracts from the >38μm and the <38μm fractions, recovered from sample BAS230, were prepared for analysis by scanning/transmission electron microscopy respectively (SEM/TEM). Elemental analysis was conducted on both instruments through energy dispersive X-ray (EDAX) techniques. Sample BAS230, from the organic rich lower layer of the alluviated ditch section 12036, was chosen for magnetic extraction due to the apparent domination of single domain ferrimagnetic material suggested by the hysteresis data for this material (e.g. BAS231, Figure 5.36).

Results from the >38μm extract contained a range of rather curious magnetic particles that appeared to by intimately associated with organic material. The SEM analysis shown in Figure 5.39(A) suggests the ferrimagnetic material has directly replaced

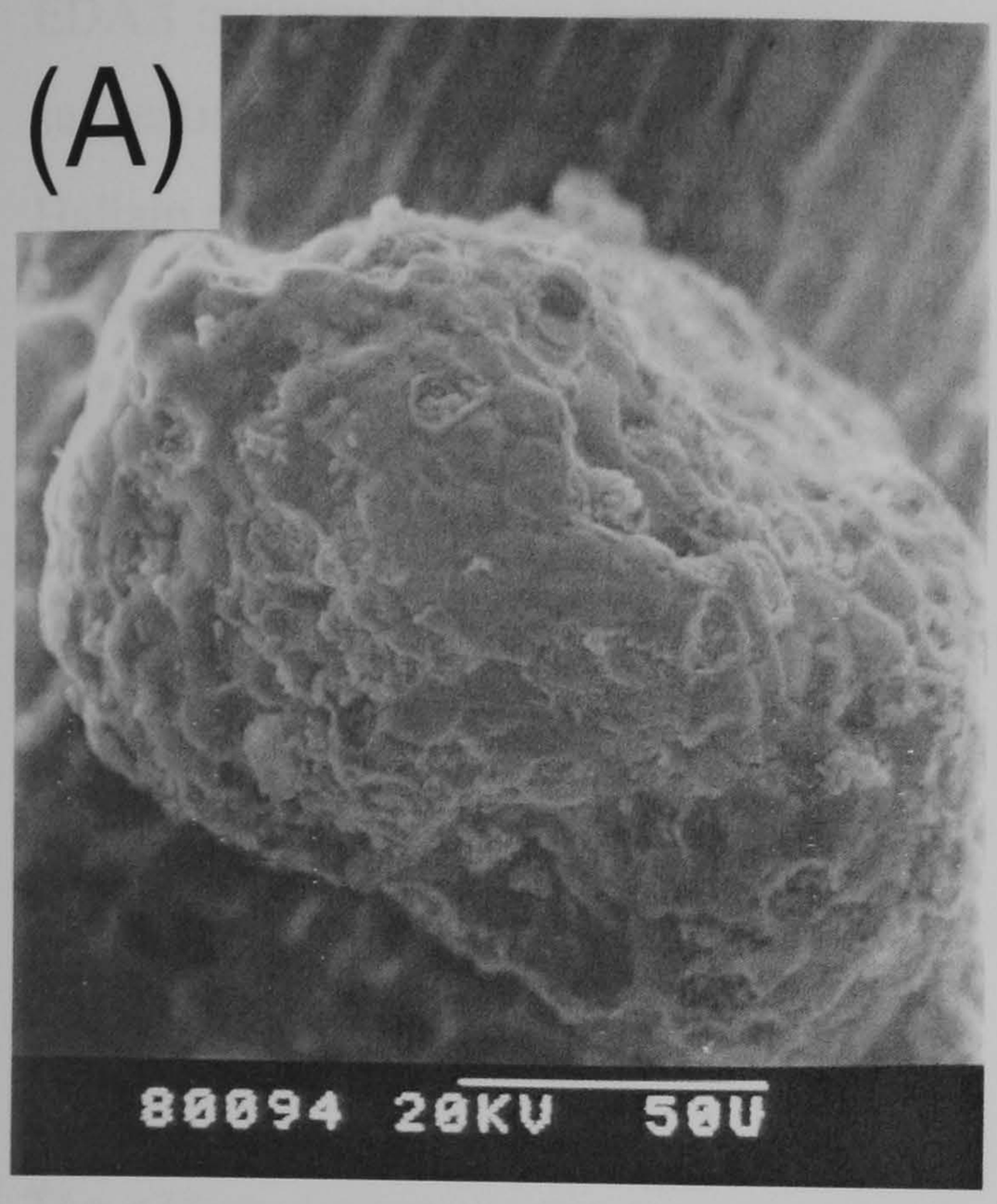


***Figure 5.39*** *(A) Scanning Electron micrograph of an organic particle partially replaced by greigite found in the >38μm magnetic extract prepared from sample BAS230. Transmission electron micrographs produced from the <38μm extract revealed the presence of both (B) an amorphous Fe/S (?greigite) component together with (C) characteristic bacterial magnetosomes some of which are apparently still preserved within intact chains (D).*

organic material preserving considerable detail within the plant remains. In addition, EDAX analysis of these ferrimagnetic particles revealed the presence of Fe, S and O suggesting the presence of both greigite[1] and magnetite (e.g. Dell 1972, Hilton 1990, Hallam and Maher 1994, Stanjek et al. 1994, Roberts et al. 1996, Snowball and Torii 1999). It is possible that the close association with organic matter indicates a biogenic origin for the ferrimagnetic material with the decayed plant material acting as a food source (e.g. Heywood et al. 1990, Mann et al. 1990, Bazylinski 1991, Diaz Ricci and Kirschvink 1992, Stanjek et al. 1994, Hesse and Stolz 1999). Similar occurrences of iron sulphide coupling with organic material have been reported from anaerobic soils (Snowball 1997, Snowball and Torii 1999) including one instance were greigite was identified as the principle corrosion product on an iron sword in a leather scabbard (Fell and Ward 1998).

The <38μm fine magnetic extract contained particles that could only be resolved through TEM analysis including some sub-crystalline/amorphous material that appeared to be very fine grained greigite from the EDAX data (Figure 5.39(B)). However, the sample also contained ferrimagnetic material with both a distinctive size and morphology, mainly "bullet" and "hexagonal" shaped crystals, highly similar marine magnetite magnetosomes (Figure 5.39(C); M. Hounslow pers. comm.). Indeed, a number of these crystals appeared, possibly, to be preserved in chains (Figure 5.39(D)) similar to observations made on modern magnetotactic bacterial cultures (e.g. Blakemore 1975, Towe and Moench 1981, Vali et al. 1987, Frankel and Blakemore 1991, Sparks 1991, Bazylinski et al. 1994). However, Hesse (1994) suggests the apparent arrangement of the crystals within intact chains may result from the extraction procedure itself.

Additional low temperature experiments following Moskowitz et al. (1993) were performed on the bulk sample and the two size fractionated magnetic extracts (Figure 5.40). The experiment involved applying a 2.5T field at 20K and measuring the decay of (s)IRM, in zero field, on warming back to 300K after first cooling the sample to 20K in either zero field (ZFC) or an applied field of 2.5T (FC). Moskowitz et al. (1993) found a preferential orientation of whole-cell magnetosomes along the easy axes of the

[1] Thermal demagnetisation of NRM/IRM to further distinguish the iron sulphide phase was not attempted due to the plastic sampling cylinders used and the rapid alteration of the samples on exposure to air.

crystal most closely parallel to the applied field when field cooled through the Verwey transition. This led to a considerable increase in low temperature (s)IRM compared to the zero field cooled samples until warmed through the Verwey transition where the dependence on field cooling was lost.

In this case all three samples show a subtle Verwey transition most evident in the $^{dM}/_{dT}$ and only the bulk sample demonstrates a considerable difference between the ZFC/FC low temperature (s)IRM. However, the difference in behaviour between the ZFC and FC curves continues above the Verwey transition suggesting the differing low temperature (s)IRM may be due, perhaps, to the preferential ordering of paramagnetic phases on cooling through their relevant Néel temperatures. The results of these experiments suggest either few intact chains survive or that the biogenic magnetite does not dominate the sample.

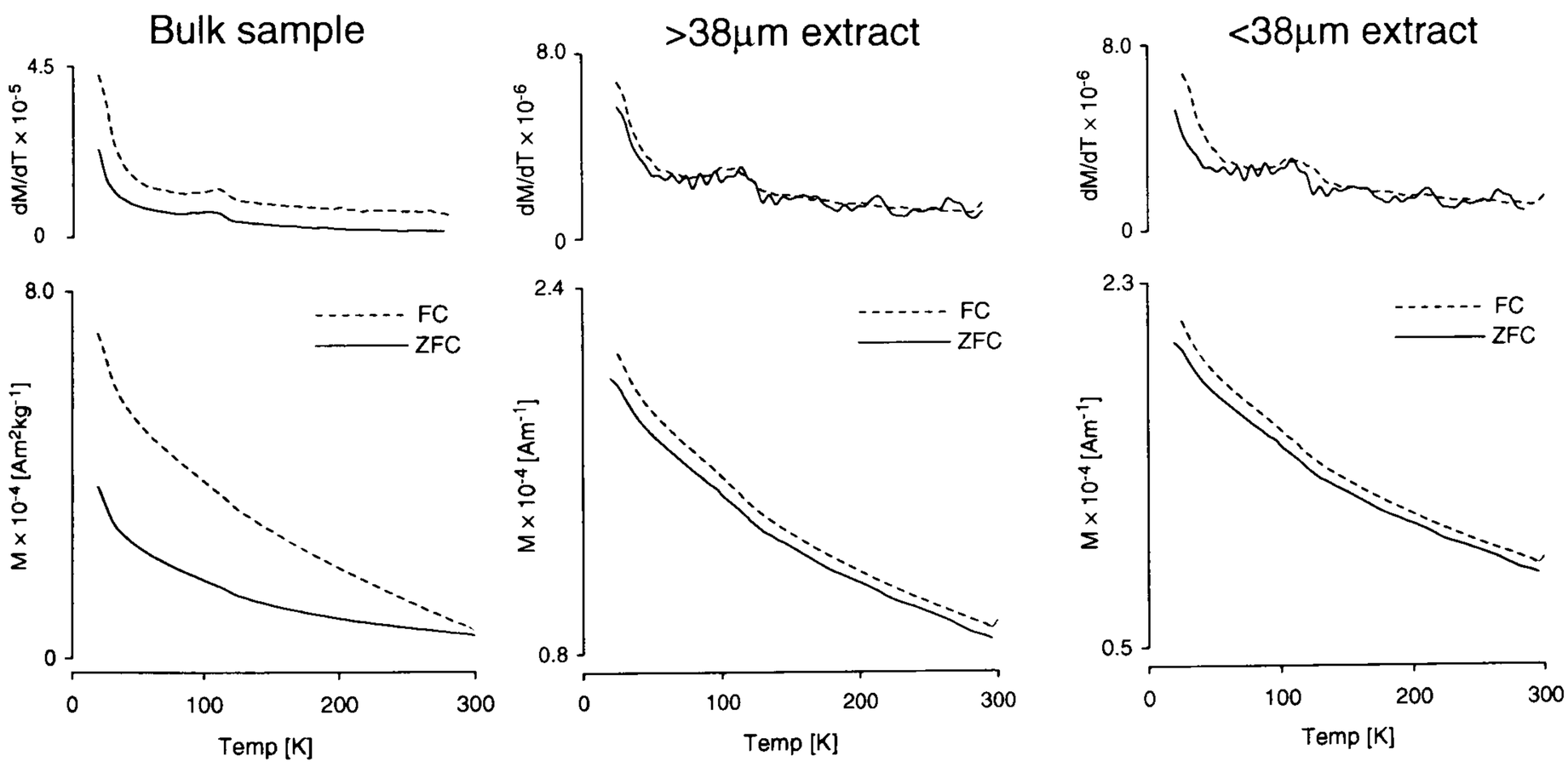


***Figure 5.40*** *Low temperature zero field cooled (ZFC; solid line) and field cooled (FC; dashed line) curves measured on both the bulk sample and magnetic extracts of BAS230 to determine the presence of intact chains of magnetosomes. The first differential of each curve is also shown to enable the identification of subtle inflections.*

### *5.6.3 Significance of the NRM carrier*

The occurrence of greigite or biogenic magnetite within terrestrial, archaeological features or soils is not unique but remains comparatively rare (Faßbinder et al. 1990, Faßbinder and Stanjek 1993, Stanjek et al. 1994). This may well be due to the generally aerated conditions within terrestrial soils that would not favour the preservation of

greigite. But could equally be due to the limited investigation of organic rich features where magnetic enhancement mechanisms would favour the production of both greigite and magnetite through microbially moderated enhancement mechanisms. In this respect, the presence of the two latter minerals suggests their formation in the alluviated ditch must have occurred under anoxic conditions. Thus the late Iron Age archaeomagnetic date obtained from the sediment would appear to represent the onset of more waterlogged conditions on the floodplain that concurs with the shift of both permanent domestic and ritual activity to the raised gravel terrace found from this period within the archaeological record.

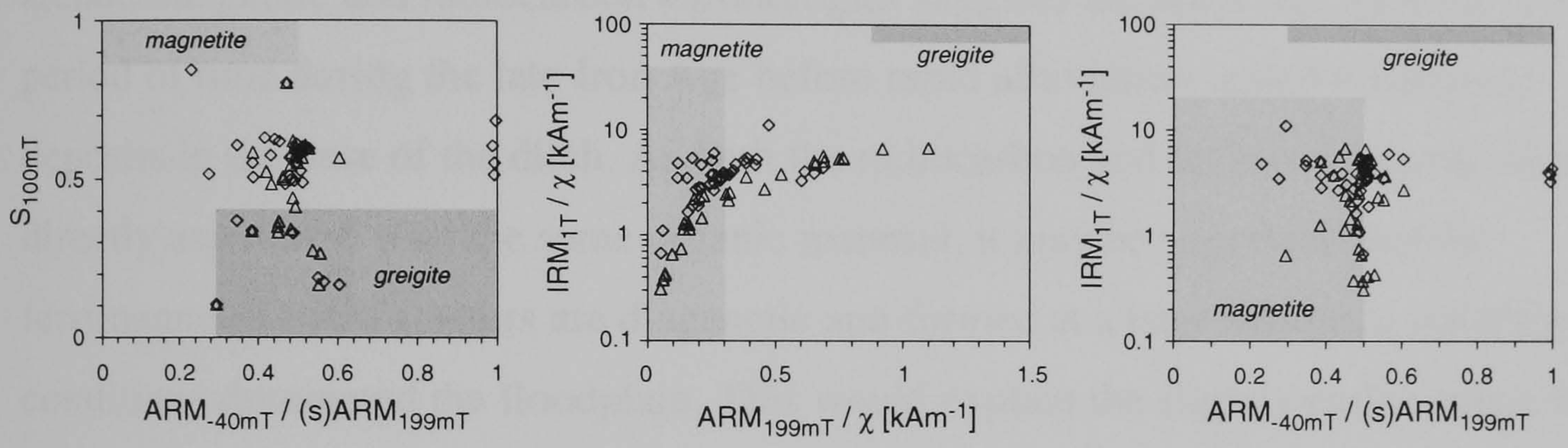


***Figure 5.41*** *Samples from the alluviated ditch section 12036 presented as biplots of magnetic parameters and ratios selected for their ability to distinguish magnetite from greigite. Shaded boxes show the expected behaviour for samples dominated by these two minerals.*

Determining the NRM carrying mineral is complicated as samples from the alluviated ditch produce values intermediate between greigite and magnetite for magnetic ratios identified for their ability to separate these two minerals (Figure 5.41; Peters and Thompson 1998, Maher et al. 1999). In addition, the Mean Destructive Field[2] determined during the NRM measurements ranged from 18.9 to 54.3mT with an average value of 38.9mT. As the majority of NRM is also removed in an AF demagnetising field of 80mT this would suggest that greigite is a more dominant NRM than magnetite in these samples. However, a degree of sample variability is also evident, for example BAS205 recorded the lowest MDF (18.9mT) and is completely demagnetised in a 45mT AF field, suggesting magnetite as a more likely remanence carrier.

[2] The Mean Destructive Field (MDF) is defined here as the magnitude of AF demagnetising field required to remove 50% of the original NRM.

The thermomagnetic data is, perhaps, more useful as this confirms the presence of a Verwey transition within both the >38μm and <38μm magnetic extracts (Figure 5.40). However, none of the bulk samples show the characteristic loss of susceptibility on heating that would be expected from the dissociation of greigite from 320 to 350°C (Figure 5.38; Snowball 1991), although this may be masked by the alteration of non-ferrimagnetic minerals (e.g. lepidocrocite) above 220°C.

Therefore it seems most likely that the magnetisation is carried by a combination of both greigite and biogenic magnetite that were formed in response to local environmental change at the onset of floodplain conditions. The correlation between the archaeomagnetic and radiocarbon chronologies suggests the ditch was open for a short period of time during the late Iron Age before rapid alluviation sealed the organic deposits in the base of the ditch. As both the radiocarbon and archaeomagnetic dates are directly associated with the same organic material, it may be suggested that the ferrimagnetic NRM carriers are diagenetic and formed at a later date once waterlogged conditions dominated the floodplain. This would explain the slightly earlier range for the radiocarbon determination and suggests that the archaeomagnetic date represents a *terminus post quem* for the ditch.

### *5.7 Summary of results from the flood plain sites*

Magnetometer surveys conducted over the flood plain sites produced a diverse range of results that often failed to identify the location of underlying archaeological features. Poor results such as these may be encountered over unfavourable geology or sites covered by deep alluvial overburden. However, in this case, given both the quality of magnetic response from adjacent sites on the raised gravel terrace and the limited alluvial overburden revealed by subsequent excavation, neither explanation seems wholly acceptable. Of even greater intrigue is the success of the magnetometer survey in identifying ritual prehistoric features, such as the Neolithic funerary enclosure and the Bronze Age ring ditch. As both these features were found in close proximity to other later features of similar, if not greater dimensions, it seems strange that only the prehistoric archaeology produced a detectable magnetic response.

Mineral magnetic measurements on samples recovered from a range of archaeological

features confirmed the wide variation of magnetic properties suggested by the magnetometer survey. However, a magnetic contrast between the majority of archaeological features and the surrounding sand and gravel substrate was also revealed. The magnetic enhancement mechanisms active on the flood plain also appear to be similar to those on the raised gravel terrace sites with strongly magnetic samples often being associated with an increased concentration of fine grained, superparamagnetic material.

Additional, unexpected magnetic enhancement was also revealed under the more heavily alluviated areas of the flood plain where organic remains had become buried under microaerobic to anoxic conditions. This has led to the formation of both inorganic iron sulphides and bacterial magnetosomes within the sediments associated with the organic material that retain a stable remanent magnetisation. The archaeomagnetic date obtained from these sediments, when combined with radiocarbon age determinations from the same organic material, allows an enhanced interpretation of the site chronology to be proposed in good agreement with the gradual shift of settlement activity to higher ground revealed by the archaeological record.

# *Chapter 6*

## *6.0 Semiquantitative analysis*

The aim of this chapter is to explore methods of semiquantitative analysis for the treatment of the magnetic data discussed qualitatively in the preceding chapters. For the mineral magnetic data the goal is to describe the magnetic behaviour of each sample in terms of a simplified distribution of known grain size synthetic minerals. Whilst such distributions are unlikely to model the precise mineralogy of the samples, it is hoped that common mineral assemblages may indicate dominant enhancement mechanisms within similar samples.

In addition, results from excavation are combined with the mineral magnetic results to produce models of the geophysical anomalies expected from identified features. The model anomalies are then compared with field data from the magnetometer surveys to assess the limitations of applied instrumentation for the location of archaeological remains within an alluvial environment.

## *6.1 Unmixing mineral magnetic data*

Environmental samples are rarely dominated by a single magnetic phase and are more likely to consist of a mixture of secondary ferromagnetic material, detrital parent material (often antiferromagnetic minerals such as goethite or haematite) and weakly magnetic matrix minerals such as diamagnetic quartz grains or paramagnetic clays. The complexity of these mixtures considerably hampers the interpretation of magnetic measurements made on environmental samples and even relatively straight forward parameters, such as magnetic susceptibility, will often vary widely due to the precise mineral phases present and the physical grain size of this material.

Such complex situations can, however, be modelled in terms of a mixture of pre-defined components whose sum magnetic behaviour is identical to the properties of the sample under consideration. The only constraints being the relevance of the pre-defined

components, or end-members, to the samples under consideration and that they behave in a linear, additive manner with respect to the physical parameters under analysis.

### *6.1.1 Sediment source studies*

Many magnetic parameters used within this study are well suited for use within such unmixing models, particularly when the end-member data set may be drawn from material with a direct relevance to the interpretation of the environmental system. For example, fluvial catchment studies may often be well defined in terms of the source geologies and soils entering the head of the catchment before concentration in downstream sediments. Providing the source geologies and soils can be suitably well defined (e.g. Lees 1999) and offer a distinct variation in the magnetic parameters used within the model, considerable success has been achieved (e.g. Stott 1986, Yu and Oldfield 1989, Shankar et al. 1994, Peters 1995, Foster et al. 1998). However, the success of such sediment-source models is often determined by the ability to fully identify the catchments within the end-member data set and this may be constrained in more complex situations, limiting the effective number of end-member components that may be used (Lees 1999).

### *6.1.2 Known grain-size magnetic component unmixing*

Perhaps a more challenging application of unmixing models is the interpretation of samples in terms of an end-member data set drawn from well defined magnetic minerals of known composition and grain size. This approach may be used to determine the dominant mineral phase within a sample (e.g. Thompson 1986) or suggest an apparent mixture of the end-member components that would give rise to the equivalent magnetic behaviour of the sample under investigation.

Due to the similar behaviour of many magnetic minerals, for example magnetite and maghaemite, and quite subtle variations that may occur due to relatively minor variations in composition the precise determination of mineral types and concentrations is unrealisitic. Further constraints may be encountered through the reported non-additivity of some

components due, in part, to grain interactions within certain material (Lees 1997). However, the description of a sample in terms of an apparent magnetic mixture may often allow a more informed interpretation by classifying the most likely mineral types and grain-size populations present. This may, for example, distinguish the contribution and relative concentration of extremely fine-grained secondary ferrimagnetic minerals from antiferromagnetic detrital parent material.

### *6.1.3 Apparent magnetic mineralogy from unmixing models*

The adoption of similar ill-defined problems is not without precedent in geophysics. For example, earth resistance measurements are given in terms of "apparent resistivities", representing an integration of the true subsurface resistivity by the spatial sensitivity of the particular electrode array in use (e.g. Telford et al. 1976, Scollar et al. 1990). Furthermore, for multi-electrode configurations, iterative algorithms may be employed to yield more complex forward models of the subsurface, again in terms of apparent resistivities (e.g. Loke and Barker 1996b). It is accepted that the apparent resistivities do not, necessarily, provide the resistivity of the subsurface but indicate the envelope of possible values. Where *a priori* knowledge of the local geology exists, perhaps from boreholes or a local exposure, suitable constraints may be added to the forward modelling procedure based on laboratory determinations for the resistivity parameters of the known geological units. A best-fit model to the field measurements may then be calculated taking account of these known resistivities and any additional constraints, such as the maximum depth to interfaces between the geological units (e.g. Loke and Barker 1996a).

In this respect the application of unmixing models to magnetic measurements may be similarly constrained by the use of appropriate end-member data sets. Where these end-members are drawn from well characterised synthetic or natural samples of known composition, the resulting model mixture may be considered as an "apparent magnetic mineralogy", analogous to the apparent resistivities discussed above. Whilst such apparent magnetic mineralogies are unlikely to fully represent the precise mineralogy of an individual sample, they will greatly facilitate the interpretation of a suite of samples

through comparison of both the normalised distribution and concentration of the resulting end-members.

### *6.1.4 Description of complex magnetisation data through unmixing models*

In addition, many magnetic measurements, such as IRM curves or hysteresis loops, involve the acquisition of densely sampled data points and much useful information is contained within subtle variations in the shape of these curves (e.g. Robertson and France 1994, Roberts et al. 1995, Tauxe et al. 1996, Kruiver et al. 2001). Yet, when interpreting this data the majority of this information is ignored and the sample reduced to a characterisation based on a limited selection of key values or ratios. For example, the ubiquitous biplot of $H_R/H_{RS}$ *vs* $M_S/M_{RS}$ suggested by Day et al. 1977 is determined from only 3 points of the measured hysteresis loop ($H_R$,, $M_S$ and $M_{RS}$) and a single point from the backward coercivity curve ($H_{CR}$). Admittedly, parameters such as $H_{CR}$ may often be derived through interpolation from a number of regularly spaced backfield values on either side of the actual value that would produce zero magnetisation. However, information contained within the shape of the curve is still lost during this interpretation procedure.

A number of successful studies involving the unmixing of such data have been reported and include the use of IRM curves (e.g. Thompson 1986, Robertson and France 1994, Stockhausen 1998, Kruiver et al. 2001), hysteresis loops (e.g. von Dobeneck 1996, Peters 1995, Rivas et al. 1981) and more extensive analysis through first order differential curves (e.g. Roberts et al. 2000). These studies differ mainly in the end-member data sets chosen as the basis for the unmixing model as both mathematical proxies (e.g. Robertson and France 1994, von Dobeneck 1996, ) and data from well characterised natural or synthetic samples (e.g. Thompson 1986, Peters 1995) have been used. Whilst reducing the shape of a complex hysteresis loop to a discrete number of proxy parameters allows the wider inter-comparison of samples a direct relationship between the unmixing model and coercivity classes / grain size of "real" magnetic minerals may often prove more useful for interpretation in terms of environmental systems.

An alternative approach for large numbers of samples is to apply an unmixing model to a suite of the more rapid magnetic measurements, such as magnetic susceptibility and selected backfield coercivity ratios. Whilst this is unlikely to yield an apparent magnetisation for the individual samples to the same detail as the more involved measurements, the behaviour of typical or extreme samples may be used as the basis of an end-member data-set. For example, in the present study samples of topsoil and subsoil could be readily identified in the field and combined with samples from archaeological contexts demonstrating highly distinct magnetic behaviour (e.g. burnt sediments, feature fills, sand and gravel substrate). Unmixing the entire data set in terms of these selected end-members allows ambiguous sample classifications from the field to be identified and the competing influence of pedogenic and anthropogenic enhancement mechanisms to be assessed.

A similar approach to sample classification may be made using multivariate statistical techniques such as principle components or cluster analysis (Lees 1999). However, the groups suggested by such statistical techniques may not relate directly to an individual sample type unlike the key samples that should be identified within the end-member data set of an unmixing model. This more limited group of end-member samples could then be investigated in greater detail applying more extensive analytical techniques such as preparing magnetic extracts for electron microscopy (§5.6.2.6).

## *6.2 Mathematical basis of the unmixing model*

### *6.2.1 Linear programming*

Eqn. (6.1) summarises the mathematical basis of linear programming for unmixing $n$ magnetic parameters, $p_1$ to $p_n$, of a real sample in terms of a predefined data set of $m$ end-members. In this case, the solution is represented by a single row matrix of $m$ components, $a_1$ to $a_m$, that indicates the contribution of each of the individual end-members. The known value of the $n$ parameters of the model under consideration is represented by an $m \times n$ matrix with a row, $x_{i,1}$ to $x_{i,n}$, for each of the end-members. Multiplication of the solution matrix by the end-member data matrix results in a forward model predicting the value of

the *n* parameters based on the sum of the relative contribution of each of the end-members defined by the solution matrix.

$$(a_1, a_2, a_3 \ldots \quad a_m) \begin{pmatrix} x_{1,1} & x_{1,2} & x_{1,3} \ldots & x_{1,n} \\ x_{2,1} & \ldots & \ldots & \ldots \\ x_{3,1} & \ldots & \ldots & \ldots \\ x_{m,1} & \ldots & \ldots & \ldots \end{pmatrix} = \left( \sum_{i=1}^{m} a_i x_{i,1}, \sum_{i=1}^{m} a_i x_{i,2} \sum_{i=1}^{m} a_i x_{i,3} \ldots \quad \sum_{i=1}^{m} a_i x_{i,n} \right) \tag{6.1}$$

The quality of fit between the predicted forward model and the real data is assessed through the sum of the squared differences, $R$ or $R^2$, between the sample data and the predicted model normalised by the sum of the squared values of the sample data (Eqn (6.2)).

In practice values of $R$ greater than 0.999 represent an acceptable fit between the forward model and the sample data with a value of 1 representing perfect agreement.

$$R = 1 - \frac{\sum_{j=1}^{n} \left( p_j - \sum_{i=1}^{n} a_i x_{i,j} \right)}{\sum_{j=1}^{n} \left( p_j^2 \right)} \tag{6.2}$$

However, it should be noted that the value of $R$ returned by Eqn. 6.2 does not provide a measure of either the quality or uniqueness of the resultant magnetic model. This might often be subject to additional constraints, such as determining the best-fit solution utilising the minimum number of end-member components. In addition, the error between individual data and model points are, in this case, rarely independent and unlikely to fulfil the Gaussian distribution required by least mean squares theory.

### *6.2.2 Optimisation algorithms*

Providing the end-member data set represents the full magnetic behaviour of the samples under consideration, the success of the unmixing model will largely depend on the ability of the numerical algorithm employed to minimise the "cost" function representing the mis-fit between model parameters and the real sample data. With ill-defined problems, such as that presented by the unmixing of magnetic measurements, many local minima will exist within the cost function and it is essential that the optimisation algorithm searches the entire

parameter space to determine the best legal solution. A variety of optimisation algorithms have been applied to similar problems and more recently genetic algorithms have been found to offer advantages with ill-defined problems (e.g. Goldberg 1989, Eder-Hinterleitner et al. 1995). These latter algorithms adopt an optimisation strategy similar to the biological process of genetic evolution.

In this case, the parameters to be optimised represent information to be encoded into a mathematical "gene". A process of evolution then begins from an initial population of possible solutions where two randomly chosen "parent" genes are combined to produce two new "offspring" solutions. The survival of a particular element of each gene is determined by genetic crossover operators, governed by the fitness of the original parent and a degree of random mutation. The quality of the offspring solutions is then tested by the cost function and the process continued, slowly eliminating the poorest solutions from the gene pool, until the optimisation conditions for the algorithm are met.

Whilst genetic algorithms are often computationally expensive, the population of genes rapidly grows to encompass the entire solution space examining the possibility of minima existing some distance from the starting solution. In addition, the mutation terms are effective in avoiding self-reinforcing local minima in which other optimisation techniques, such as downhill Simplex algorithms, may become trapped. A more recent approach (Carter-Stiglitz et al. 2001) has explored the optimisation of the mixture model through single value decomposition of Eqn. (6.1) (Press et al. 1988, pp60-71) providing a better determination for the uniqueness of the solution.

To test the stability of the solution each optimisation algorithm was restarted using the final convergence of the initial, randomly seeded model.

### *6.2.3 Selection of End Member data sets*

To test the robustness of the unmixing models a series of end-member data sets were defined from a variety of sources including previously reported parameters for minerals of known composition and grain-size and mathematical models (§1.5).

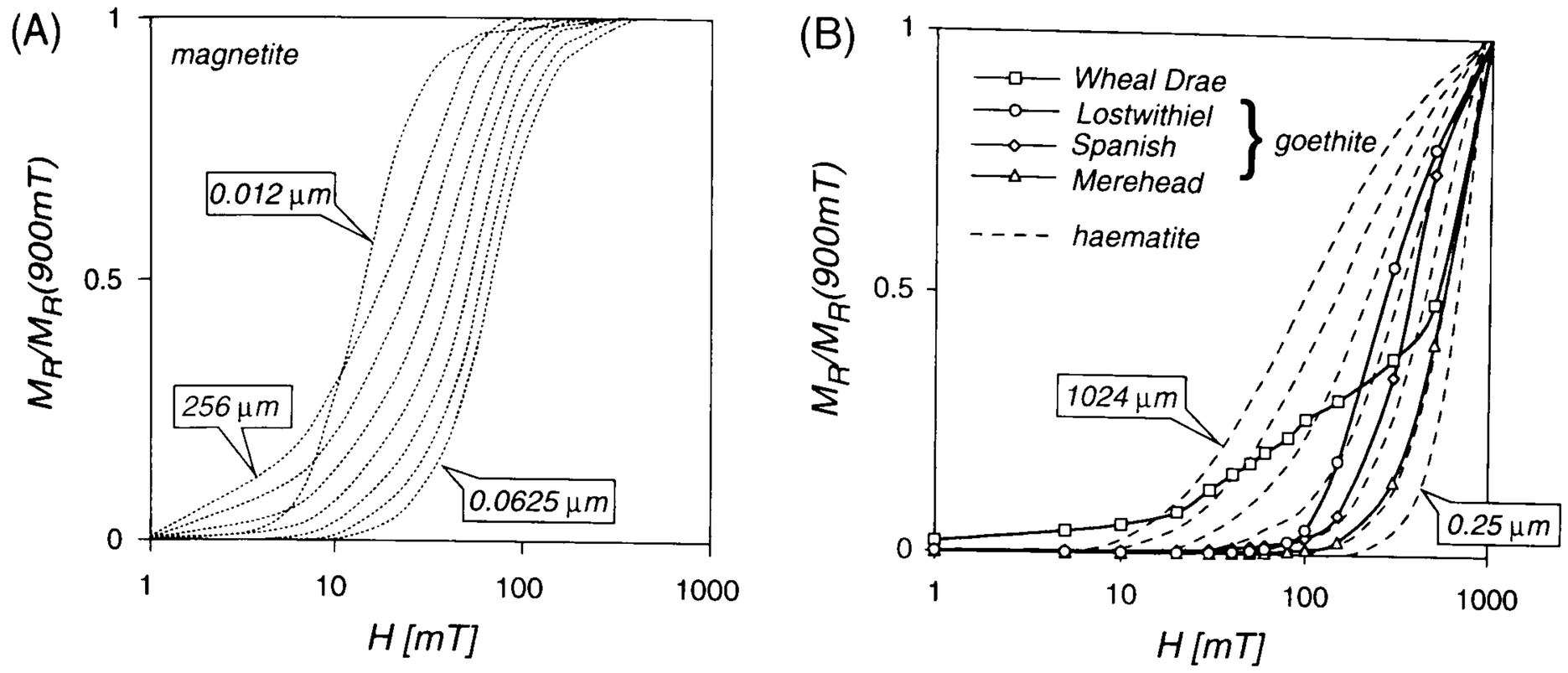


***Figure 6.1*** *Forward IRM acquisition curves of known grain size magnetite (A) and (B) haematite samples used in the end member data set of the unmixing model. Data from four natural samples of goethite are also included that fall within the envelope of haematite behaviour for the applied fields available to this study.*

*6.2.3.1 Forward IRM acquisition curves*

Published forward IRM curves in fields from 1 to 900mT are available for both magnetite and haematite covering a grain-size range from 0.012 to 256µm and 0.25 to 1024µm respectively (e.g. Thompson 1986, Maher 1988). This data set covers the full range of domain states for magnetite including three superparamagnetic components with grain diameters <0.03µm (Figure 6.1(A)). Despite being superparamagnetic (SPM) Eqn. (1.13) predicts that even the finest magnetite end-member will hold a magnetic remanence over the time period of the IRM measurements ($\tau$ = ~27.5s). However, it is possible that part of this remanence will be due to grain interactions in these synthetic samples and SPM material in environmental samples may well fail to retain IRM in a similar manner.

Whilst the antiferromagnetic mineral haematite may well be present within many of the samples collected during this study, there is considerable evidence from the low temperature experiments for the presence of goethite. The IRM acquisition curves of four natural samples of goethite of unconfirmed purity are presented in Figure 6.1(B) together with the envelope of curves from the published haematite data (dashed lines). With the

exception of the sample from Wheal Drae, St Just[1], Cornwall, UK, the normalised goethite IRM curves fall entirely within the haematite envelope, suggesting the IRM behaviour of the two minerals is similar within fields less than 1T. However, a slight deviation between the reported values of $\chi$ and $M_S$ is evident for haematite and goethite (Table 2.1) that may lead to a misrepresentation of the true concentration of antiferromagnetic minerals within the unmixing models. Given the similar ambiguity that exists between magnetite and maghemite the adoption of the haematite end-member data was considered to be a reasonable compromise to achieve a representative "apparent magnetisation" from the unmixing model.

*6.2.3.2 Hysteresis loops*

Data from a number of known grain size, synthetic samples of magnetite were used for the end-member data set covering a range of grain sizes from 0.05 to 40μm (Solheid and Jackson 2001). Additional hysteresis data encompassing both superparamagnetic (0.005, 0.01 and 0.015μm) and large multi-domain (256μm) grain sizes were then calculated from the numerical hysteresis model discussed in §1.5.2 and the phenomenological model proposed in §1.5.4 respectively. This latter model was found to provide a reliable fit to the empirical data above a grain size of approximately 0.75μm.

More difficulty was experienced in obtaining suitable end-member data from known grain-size hard minerals such as haematite and goethite. A single sample of synthetic haematite of grain size 0.5μm (Solheid and Jackson 2001) was combined with published hysteresis data from a sample of magnetically "hard" and "soft" natural haematite whose coercivity parameters suggest approximate grain size of 1.0μm and 100μm respectively (Peters 1995, Kletetschka and Wasilewski 2002).

[1] Little is known of St Justus (Just) other than his apparent martyrdom in AD 1140 and that he is patron of two Cornish parishes in Penwith and Roseland (Farmer 1992).

## *6.3 Results of the unmixing analysis*

A generic unmixing model was constructed as a series of MatLab functions that produces a best-fit model of the sample data in terms of the supplied end-member components. The contribution of individual end-members is constrained to be greater than or equal to zero.

### *6.3.1 Synthetic mixtures*

Five trial mixtures of synthetic iron oxides were prepared to investigate the practicalities of producing accurate mixtures with iron oxide concentrations analogous to those found in soils and archaeological sediments. The mixtures were prepared from a combination of commercially available magnetite and haematite powders with an average grain size of 0.2μm and 0.5μm respectively. These were then prepared into a slurry with distilled water and disaggragated in an ultrasonic bath to produce an even distribution of the iron oxide throughout the sample. These mixtures were then used to test the unmixing algorithm and end-member data sets in terms of the ability to detect both the relative contribution and absolute concentration of material within each sample.

#### *6.3.1.1 Unmixing IRM acquisition curves*

IRM acquisition curves contain information related to the mineral phase, grain size and relative concentration of each phase within the sample. However, the dominant nature of strongly magnetic minerals, such as magnetite, may often mask the presence of more weakly magnetic components. Figure 6.2 shows the results of unmixing IRM curves from the five synthetic mixtures against the known grain-size magnetite and haematite end-member data set. Whilst the models do not produce an exact fit to the experimental data the misfit is reasonable given the degree of noise present (e.g. sample SM01) and the inter calibration error inherent between the end-member data measured with a pulse magnetiser/spinner magnetometer and the synthetic mixtures measured on a VSM.

The models demonstrate an extreme sensitivity to presence of magnetite that dominates the shape of the IRM acquisition curve and masks the presence of the weaker haematite component. However, both the grain-size and the relative concentration of the magnetite

component are accurately reflected by the IRM unmixing model. The inability to detect the presence of haematite is disappointing due, perhaps, to the limited applied fields used during this study (maximum of 1.8T). For comparison, Kruiver et al. (2001) report a much greater degree of success separating goethite from titanomagnetite in samples where the hard magnetic component is clearly distinguished within the IRM acquisition curve measured to 2.5T and accounts for at least 50% of the total (s)IRM.

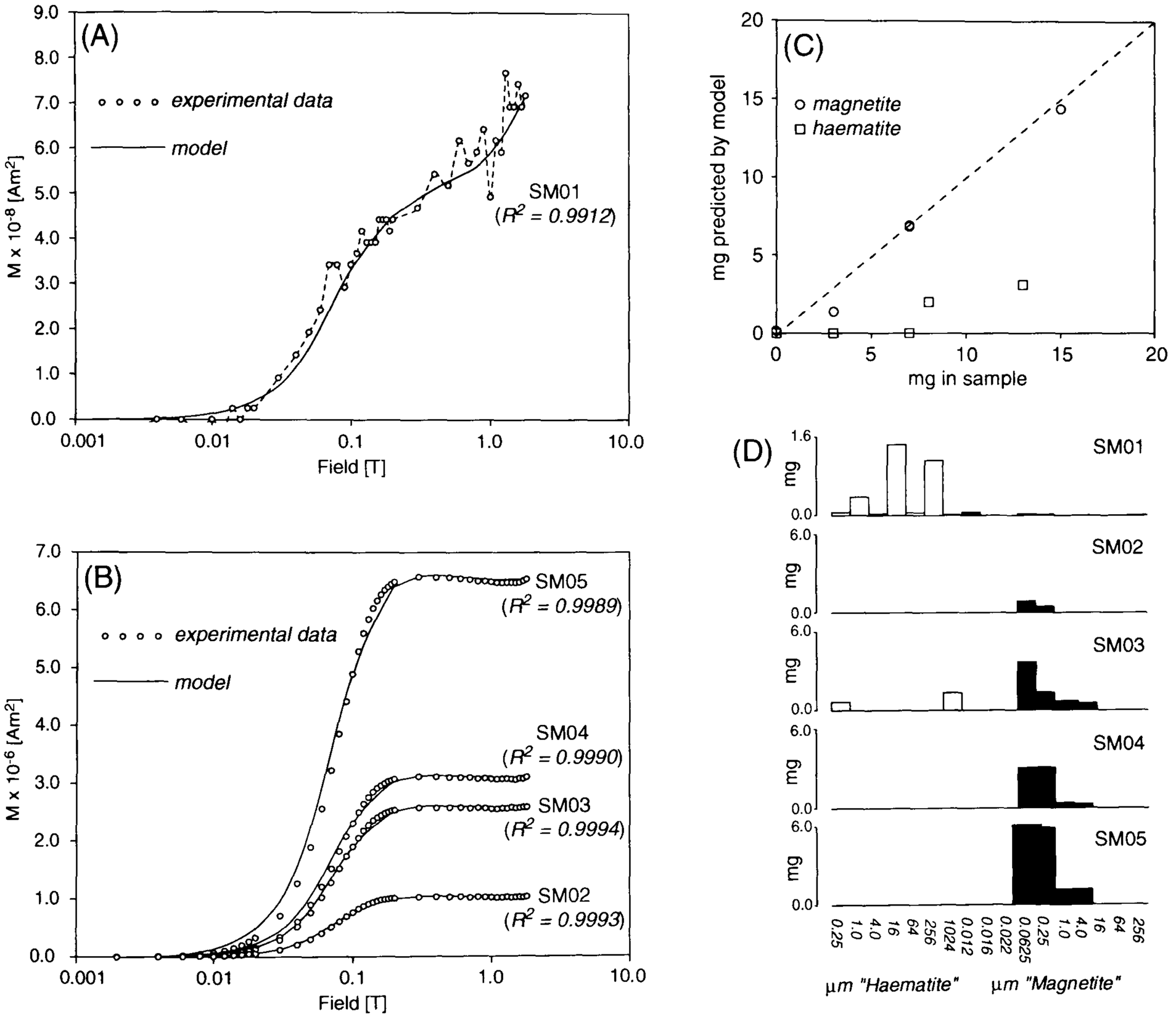


***Figure 6.2*** *Results of the unmixing model based on IRM acquisition curves (A) and (B) for the five mixtures of synthetic magnetite and haematite. Results from the weakest sample, SM01, are, for clarity, shown separately in (A). The total concentrations of magnetite / haematite predicted by the model are plotted against the actual concentrations (C) together with barcharts (D) illustrating the apparent grain size distribution present.*

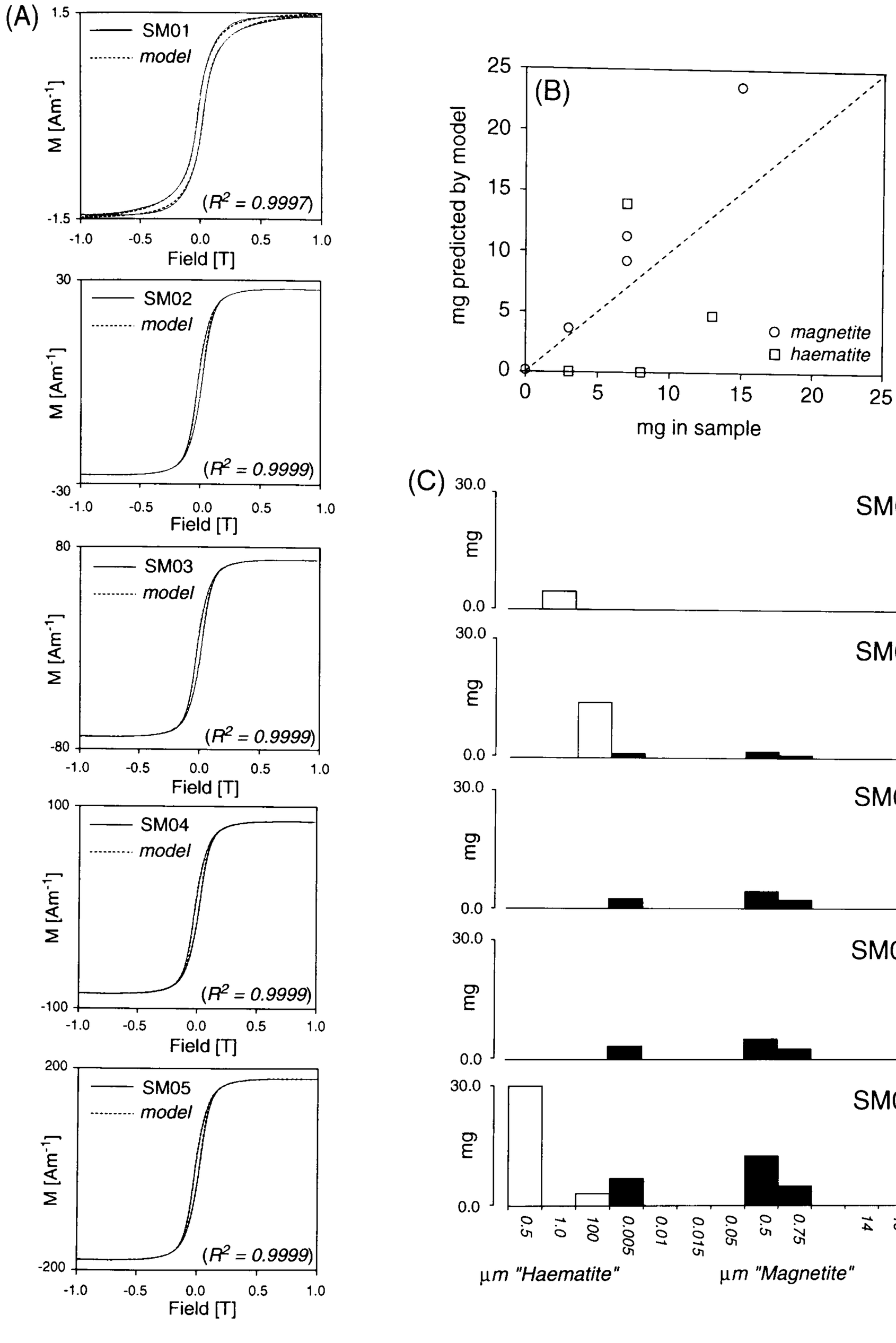


***Figure 6.3*** *(A) Results of the unmixing model based on hysteresis loops for the five mixtures of synthetic magnetite and haematite together with (B) a comparison of predicted/actual concentrations of magnetite / haematite and (C) barcharts illustrating the apparent grain size distribution present.*

Even sample SM01, containing only synthetic haematite, produced an extremely noisy IRM curve and a corresponding unmixing model that correctly identified the mineral phase but not the apparent grain-size. The use of high field IRM data, for example to 4.5T, may well prove more successful for the identification of high coercivity minerals due to the greater influence of these components on the high field IRM curve above the remenant saturation of magnetite.

An attempt to improve the discrimination of the hard component through the inclusion of magnetic susceptibility failed to improve the unmixing model. This is, perhaps, unsurprising as the variation of susceptibility for the individual end-member components is similar to the variation of $M_{RS}$, with the exception of the superparamagnetic grain-sized magnetite, that was not present within the synthetic mixtures.

*6.3.1.2 Unmixing hysteresis loops*

A second unmixing model was constructed using hysteresis loop data from the five synthetic mixtures and the end-member data described in §6.2.3.2. Figure 6.3 shows the results of this model and the generally good fit to the experimental data. Again, the magnetite component in samples SM02, SM03 and SM04 has dominated the hysteresis behaviour and rendered the model insensitive to haematite at the concentrations included within the synthetic samples. However, the model has correctly identified the dominant grain size of the magnetite within the synthetic samples and indicated the presence of a significant superparamagnetic component. Whilst the average grain size of the synthetic magnetite used in the samples was reported to be 0.2μm, the low temperature magnetisation data apparently support the presence of such fine grained material within the sample (Figure 6.4). The concentration of magnetite within the samples is slightly over predicted by the model and that may well be due to the combination of empirical measurements with numerically derived data for the superparamagnetic grain sizes within the end-member data set.

Sample SM01 should contain only haematite although it is evident from both the "wasp-waisted" shape of the hysteresis loop and the low temperature magnetisation data (Figure 6.4) that the synthetic iron oxide contains trace quantities of magnetite.

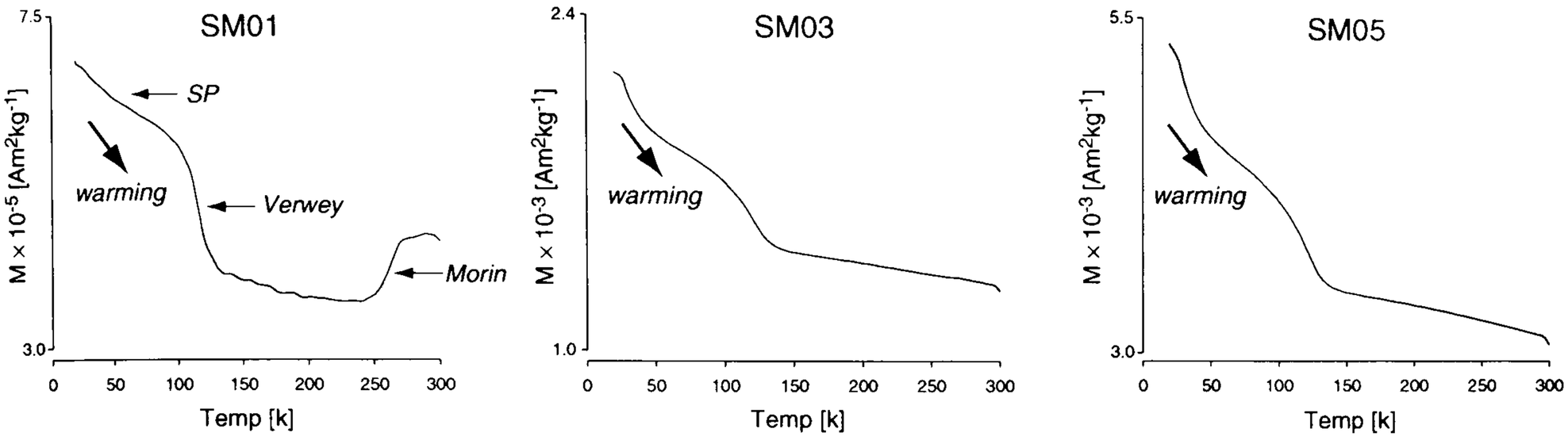


***Figure 6.4*** *Variation of low temperature magnetisation from 20 to 300K measured in zero field following the application of a 2.5T field at 20K for three of the synthetic mixture samples. The synthetic "haematite" SM01 shows evidence for both Verwey and Morin transitions indicating a mixture of magnetite and haematite. A Verwey transition is also evident in the synthetic magnetite (SM05) and the intermediate mixtures (e.g. SM03) of both synthetic iron oxides. A steep decay of low temperature magnetisation from 20 to ~ 50K occurs in all the synthetic mixture samples due to the presence of a superparamagnetic component.*

### *6.3.2 Comparison of optimisation algorithms*

Figure 6.5(A) shows a comparison of the final error function generated by an IRM acquisition curve unmixing model using a genetic algorithm (Houck et al. 1995) and a more commonly used *Golden section*[2] *(or Golden Rule)* search and parabolic interpolation algorithm (e.g. Forsythe et al. 1976). Whilst both algorithms produce acceptable fits to the experimental data ($R > 0.999$), for a number of samples the genetic algorithm produces model parameters that offer a superior fit to the sample data (points plotting above the 45° line of equality). Comparison of the final models shows a strong correlation between both

[2] This algorithm is based on sampling a function $f(x)$ between an interval of 3 points of $x = A$, $B$ and $C$ where the mid-point $B$ is a minima between $A$ and $C$. The position of $B$ is determined by a ratio of $1:\tau$ between $A$ and $C$ where the value of $\tau$ is given by the *Golden section* defined as the point of division along a line where the ratio of the longer section to the whole is identical to the ratio of the two subdivided sections. The golden section ratio is thought to hold special aesthetic qualities in art and architecture and has a value of 1:1618. If $f(x)$ behaves more reasonably a parabolic interpolation through $A$, $B$ and $C$ may be employed with the new mid-point determined from the minima of the best-fit parabola.

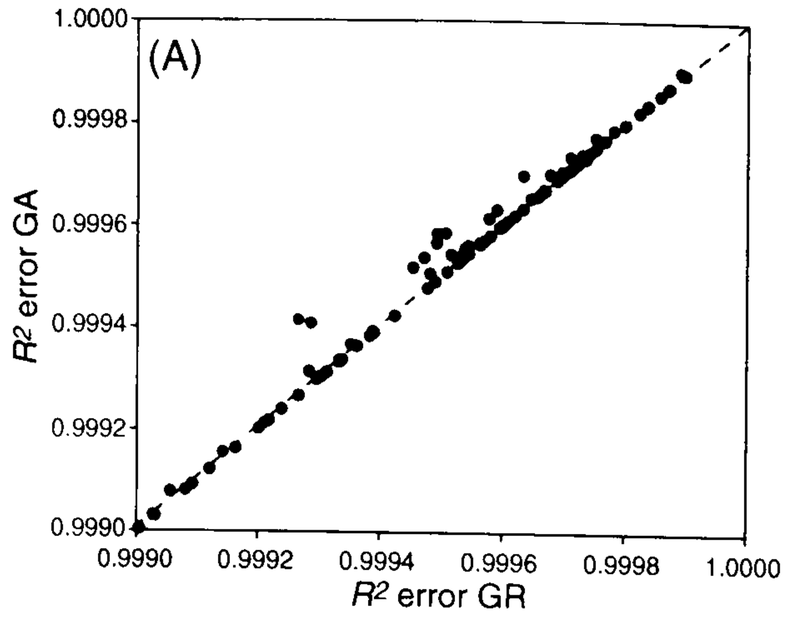


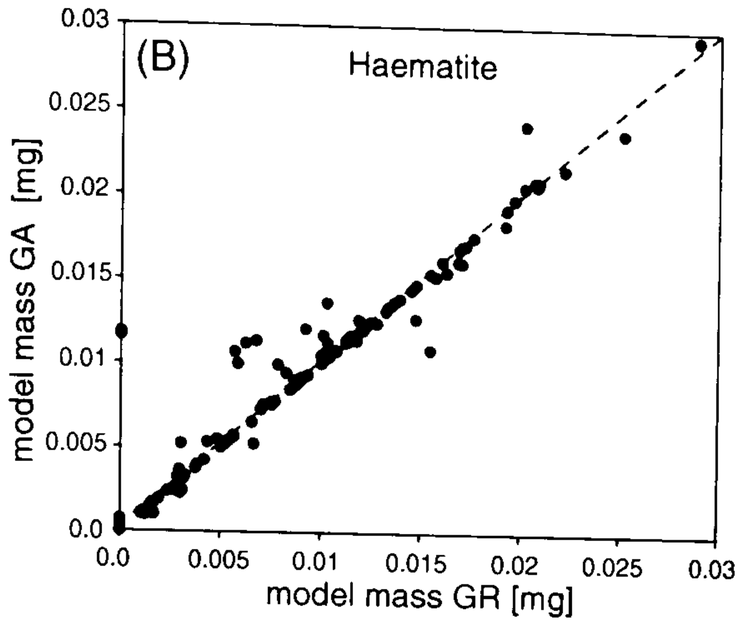


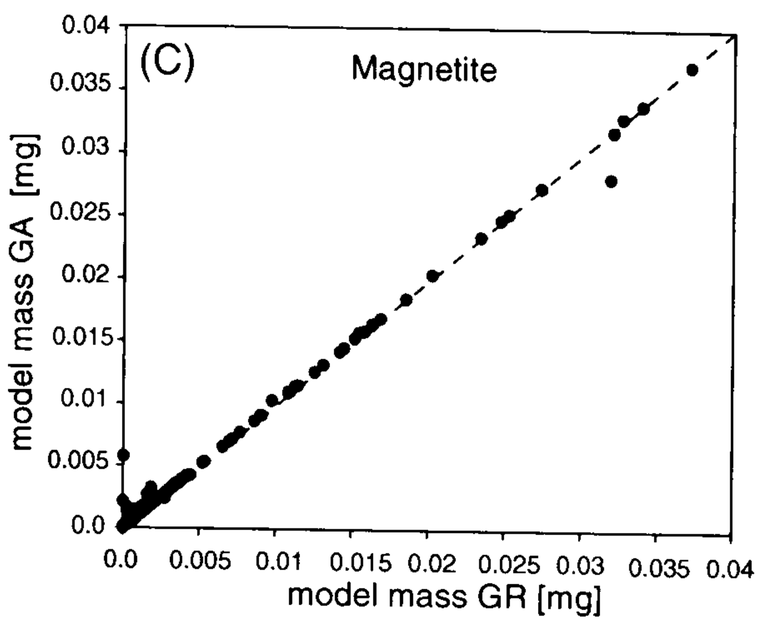


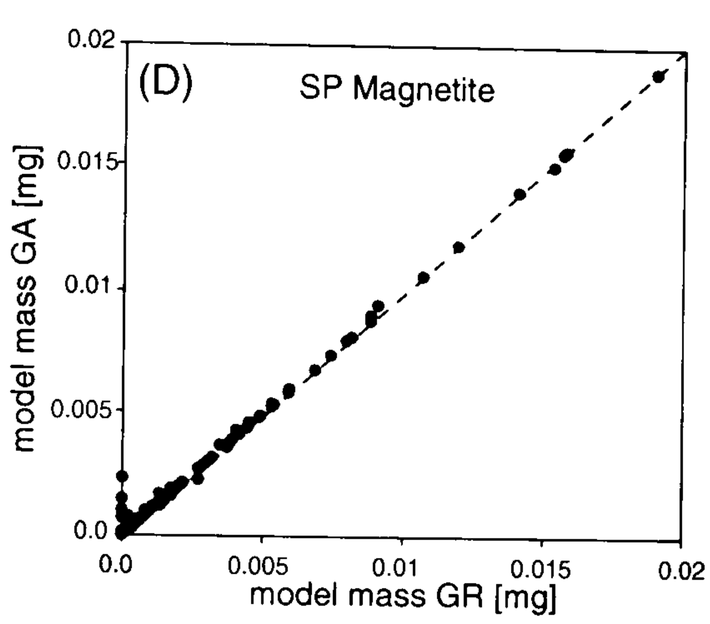


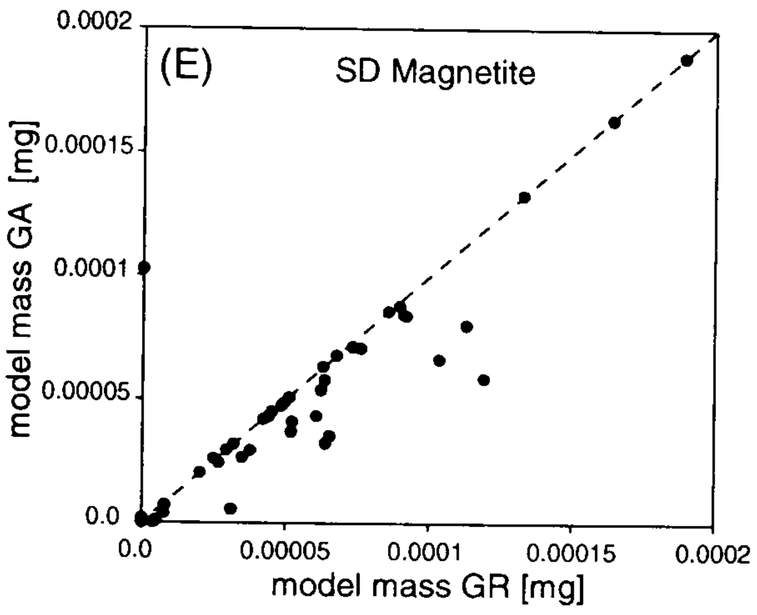


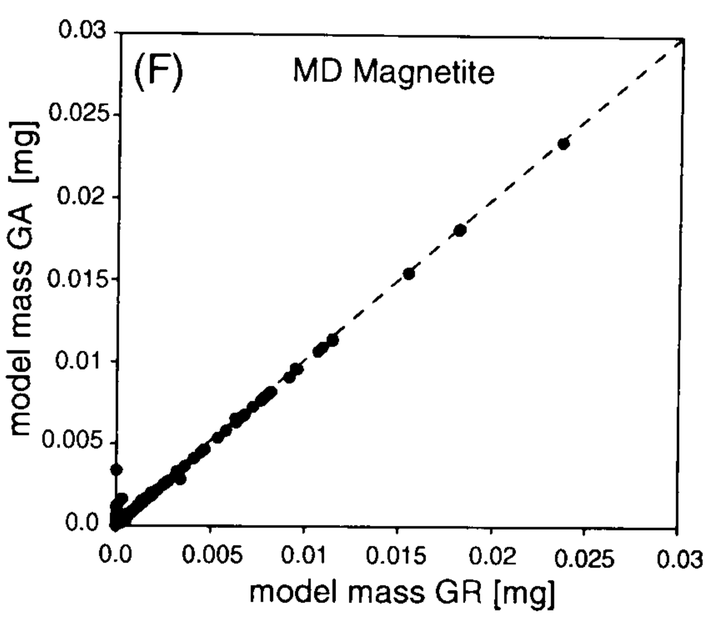


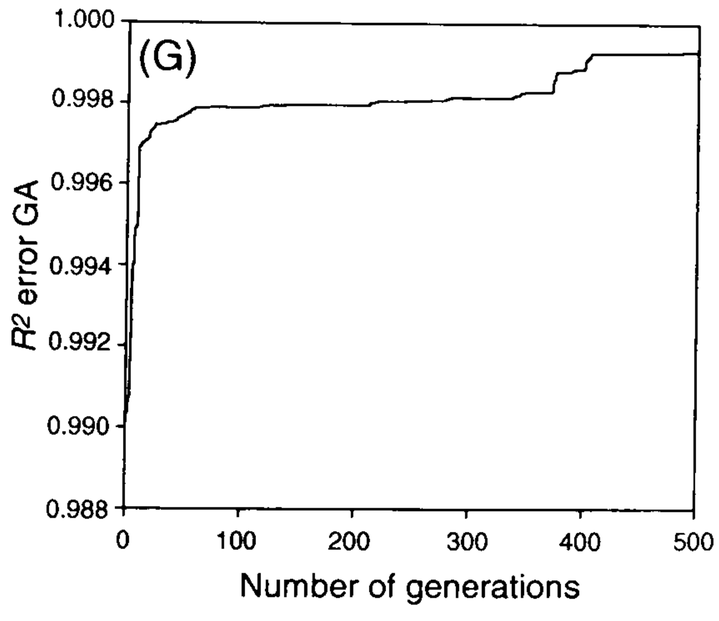


***Figure 6.5*** *(A) Comparison of the final error for IRM acquisition curve unmixing models produced from 170 archaeological samples calculated using genetic (GA) and Golden Rule (GR) optimisation algorithms. Despite a marginal improvement offered by the genetic algorithm, the final solutions are comparable in terms of the predicted concentration of (B) haematite, (C) magnetite and the domain state of the magnetite end-members (D, E and F). The evolution of the genetic algorithm over the first 500 generations is also shown for a typical sample (G) with rapid "jumps" out of local solution space minima.*

the concentration of haematite and magnetite end-members and the relative domain state of magnetite predicted by the optimisation algorithms.

The initial generation of the genetic algorithm was seeded from a random parent solution that was reproduced with subsequent child solutions to produce a total of 1000 solutions per generation. The best fit solutions from each generation were then evolved to seed the next generation through a total of 10000 evolutions. Figure 6.5(G) shows an example of how the error improves between generations for an archaeological sample. Rapid improvement of the initial generations occurs through a series of distinct steps, as the genetic algorithm rejects local minima, until little variation between each evolution is found and the algorithm approaches the global best-fit solution. Analysis of the error curves allows an appropriate number of evolutions to be chosen for the unmixing model. Alternatively, the genetic algorithm may be set to finish when certain constraints regarding either the quality of fit to the data or improvement between evolutions are met.

Compared to the Golden section method, the genetic algorithm required considerably more computational effort resulting in increased processing time. This was not considered to be excessive and becomes even less relevant when the rapidly increasing processor speed of modern computers is considered.

### *6.3.3 Unmixing IRM curves from archaeological samples*

Figure 6.6 shows nine representative IRM unmixing models from the 170 samples analysed in this study. For each dataset the best-fit model IRM curve is shown together with the experimental data and the $R^2$ value indicating the quality of fit between the two. The apparent magnetic mixtures, calculated by both the genetic (GA) and Golden Rule (GR) optimisation algortihms, are also shown as a bar chart beneath the IRM curves.

In general, the models are able to propose an apparent magnetic mixture providing a good quality of fit to the IRM curve data. Obvious areas of misfit do occur with highly viscous samples measured on the VSM that demonstrate a high field IRM "sag" (e.g. PM06 and

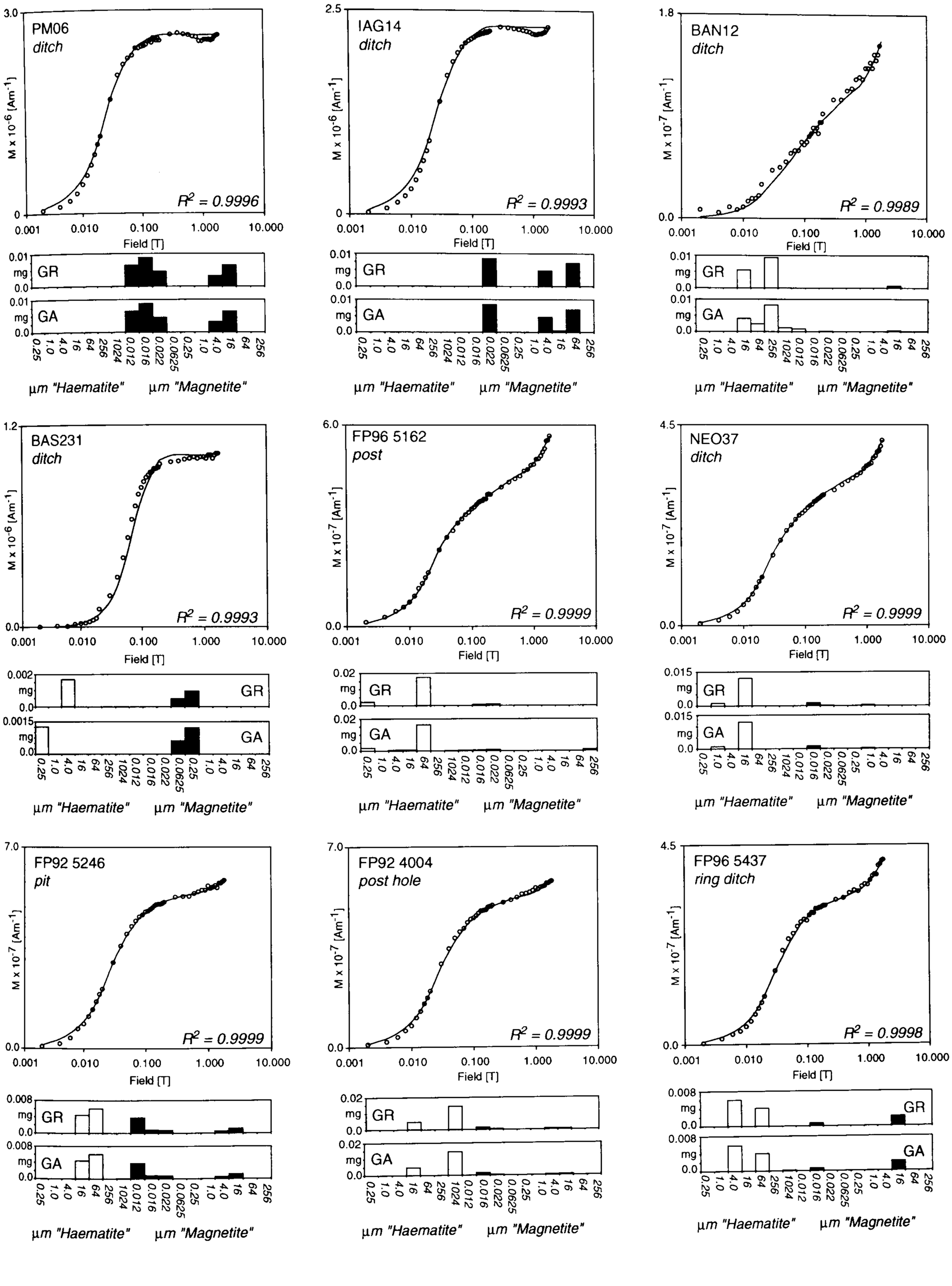


***Figure 6.6*** *Results from the unmixing model based on IRM acquisition curve data showing 9 representative samples from a total of 170. The experimental data (open circles) is shown together with the best-fit model (solid line) including the $R^2$ misfit term. The model solutions, in terms of the predicted concentration of end-member components, are shown as barcharts for both the Golden Rule (GR) and genetic (GA) optimisation algorithms.*

IAG14) and with models fitted to inherently noisy data from weak samples (e.g. BAN12). A bespoke end-member data set measured from known grain-size synthetic samples with the same instrumentation as the archaeological samples would, no doubt, improve the fit to the viscous components. However, despite this misfit, the characteristic increase of IRM between ~10 to 50mT appears to adequately discriminate samples containing a significant viscous component.

The problem of noisy data from weak samples is more difficult to compensate for and it is unlikely that even with a theoretically perfect end-member data set that the misfit between the model and the real data would be greatly improved. Whilst in this case the end-member data does not account for all of the observed sample behaviour, the quality of fit to stronger samples is quite sufficient to support confidence in the proposed models. This suggests the majority of sample behaviour is constrained within the bounds of apparent mixture models and applying such models to noisy data will place appropriate constraints on the resultant model curve. For example, sample BAN12 (Figure 6.6) contains a high degree of noise within the observed IRM acquisition curve, including the apparent loss of magnetisation between successive points magnetised at greater applied fields. The unmixing model provides a smooth curve through this data constrained by the end-member data set applied successfully to stronger samples. It could be argued that such models offer a more pragmatic treatment of noisy data than the application of, for example, a more subjective numerical smoothing algorithm to the experimental data.

### *6.3.4 Unmixing hystersis loops from archaeological samples*

Figure 6.7 shows results of the unmixing model based on hysteresis loop data for the same 9 representative samples previously modeled from the IRM acquisition curve data. In this case both the experimental and end-member hysteresis data were pre-processed to remove any paramagnetic high field slope (§3.3.8). Whilst this might inadverdantly remove high field slope associated with genuine "hard" antiferromagnetic phases, the sensitivity to these components is unlikely to be compromised within hysteresis loops calculated in applied

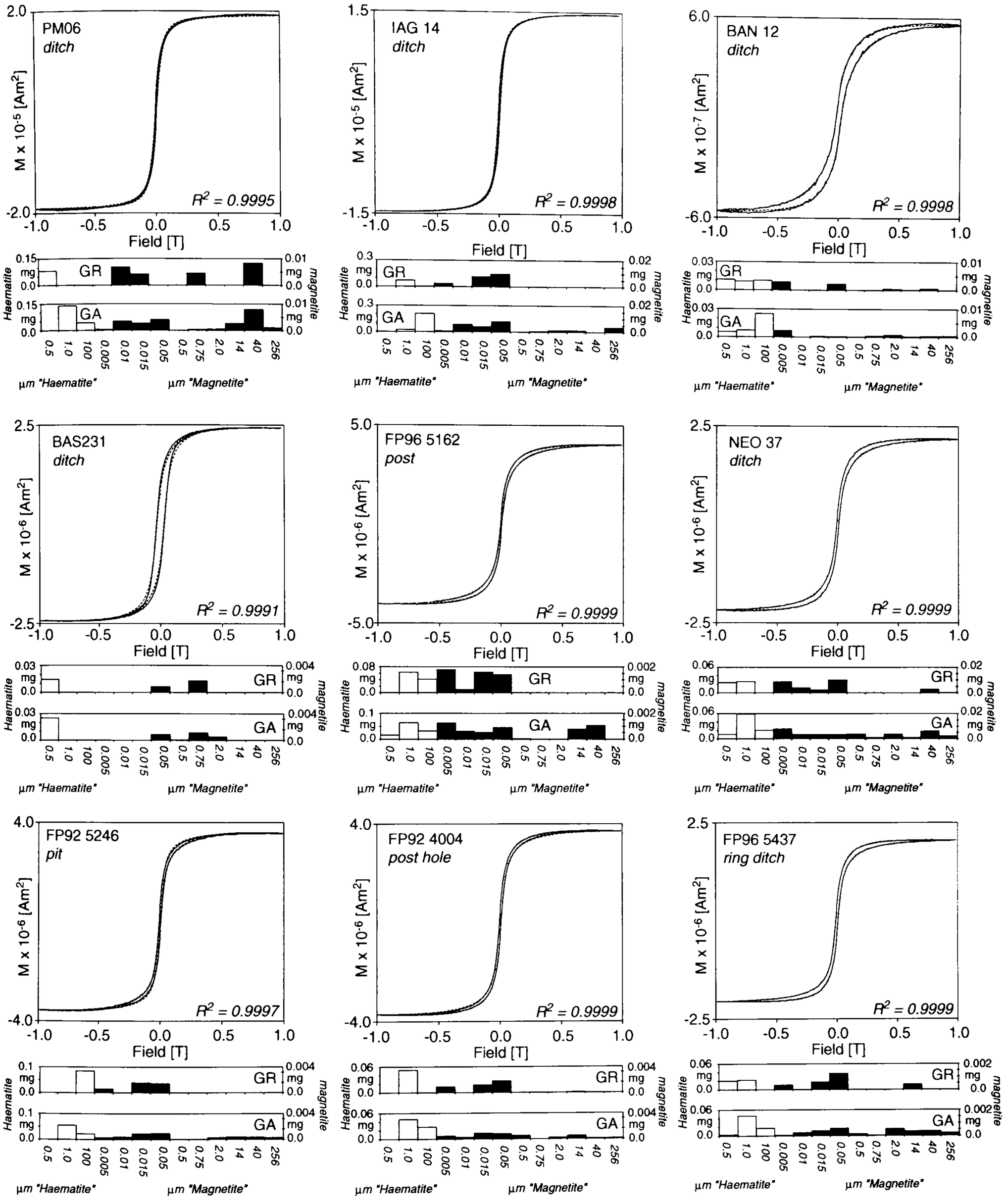


***Figure 6.7*** *Results from the unmixing model based on hysteresis loop data for the same representative samples as shown in Figure 6.6. The best-fit model (dashed line) is superimposed over the experimental hysteresis loop (solid line) including the $R^2$ misfit term. The model solutions, in terms of the predicted concentration of end-member components, are shown as barcharts for both the Golden Rule (GR) and genetic (GA) optimisation algorithms. Where the barcharts are presented with two scale axes the concentration of haematite and magnetite end-members are determined from the left and right hand axes respectively.*

fields of ±1T where a considerable overlap between "hard" and "soft" magnetic phases would be expected.

Despite the reduced number of haematite components within the end-member data set the the final unmixing models produce a good fit to the experimental data. Even the "wasp-waisted" loops are accurately modeled as a mixture of high and low coercivity minerals. In general, the unmixing models based on hysteresis loops broadly agree, in terms of concentration and grain size distribution, with those based on IRM acquisition curves. However, the hysteresis models suggest a greater concentration of high coercivity minerals possibly due to the greater influence such minerals exert at medium applied fields of "wasp waisted" loops.

Sample BAS231 is of interest as it exhibits a greater variation between the two unmixing models in terms of concentration. Both models suggest this sample is dominated by single domain magnetite but a considerable variation in concentration of this component is apparent. Magnetic extracts prepared from similar samples (§5.6.2.6) indicate a mixed mineralogy of magnetite and greigite and as this latter mineral is not represented in the end-member data set a degree of mis-fit between the unmixing models and the experimental data would be expected. Furthermore, the variation in predicted concentration will be influenced by differing $M_{RS}/M_S$ ratios for magnetite and greigite (Snowball 1991) that indicates a weakness of the unmixing model when the end-member data set does not fully describe the dominant magnetic mineralogy of the sample.

The hysteresis model also demonstrates a wider variation between the results generated by the two optimisation algorithms. For a number of samples (e.g. NEO37 and FP92 5246) the genetic algorithm produces a similar quality of fit to the experimental hysteresis data but incorporates a much wider range of magnetite end-members than those selected by the Golden Rule method. This suggests a degree of redundancy within the magnetite end-members due, perhaps, to a greater similarity between the magnetite hysteresis loops to IRM acquisition curves of similar grain-sized material. In this case, the ability of a genetic algorithm to search the entire solution space beyond a local minima has apparently led to

the inclusion of additional end-member components that were not selected by the Golden Rule optimisation algorithm. When this occurs, the genetic algorithm often produces an acceptable but weaker fit to the experimental data suggesting an improved hysteresis unmixing model should, perhaps, include a means for testing a reduced end-member data set against the original model.

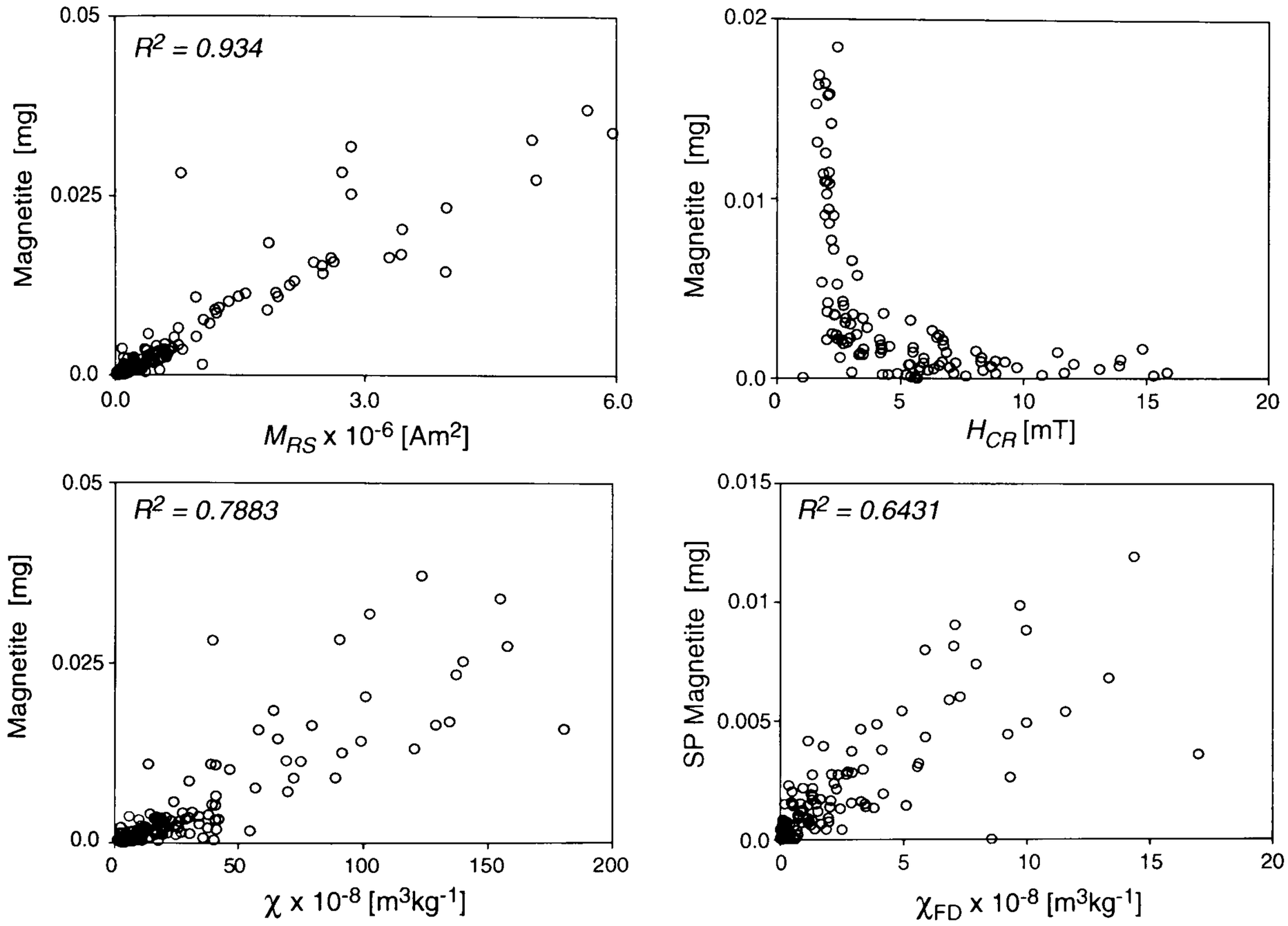


***Figure 6.8*** *Biplots showing the relationship between the total concentration of magnetite predicted by the IRM acquisition curve unmixing model for 170 archaeological samples against magnetic parameters of $M_{RS}$, $\chi$ and $H_{CR}$. The total concentration of superparamagnetic grain-sized magnetite predicted by the model is also shown as a biplot against $\chi_{FD}$. Where appropriate, the quality of a linear least squares regression fit to the data set is indicated by the $R^2$ coefficient.*

### *6.3.5 Physical significance of the unmixing models*

The results of unmixing mixtures of synthetic iron-oxides (§6.3.1) demonstrates the ability of both IRM curves and hysteresis loops to provide a semi-quantitative model of a magnetic mixture. The greatest concern would appear to be estimating the apparent concentration of more weakly magnetic antiferromagnetic minerals within a mixture dominated by soft,

ferrimagnetic material. Despite these reservations unmixing models do provide a simplified mineralogical interpretation of complex hysteresis data that are often (mis)interpreted through the application of highly simplified bi-plots of individual parameters. Whilst such simplified analysis may well be appropriate for distinct mineralogy and grain-size (e.g. Day et al. 1977) it is highly questionable whether these methods are appropriate to the interpretation of complex magnetic mixtures found in environmental samples.

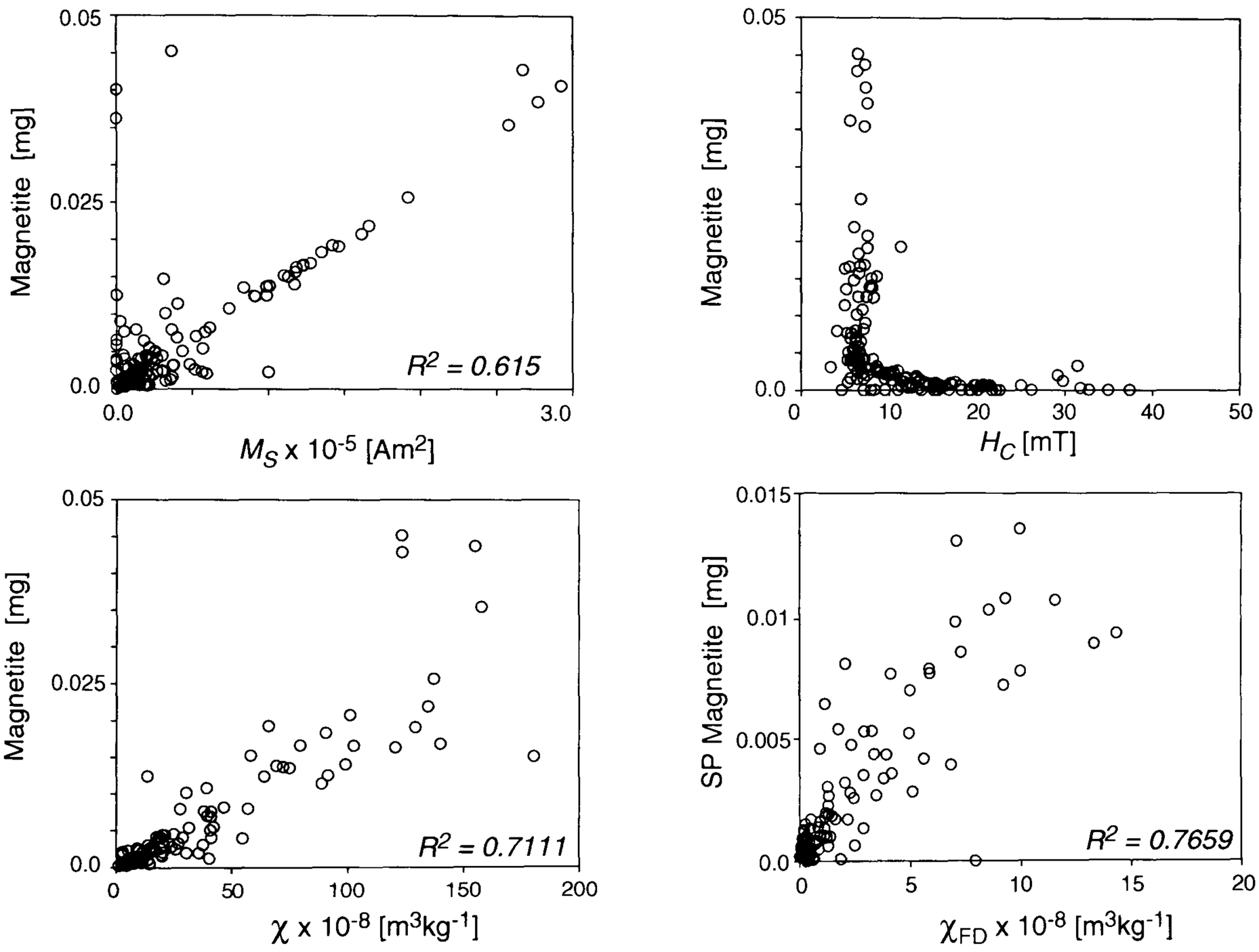


***Figure 6.9*** *Biplots showing the relationship between the total concentration of magnetite predicted by the hysteresis loop unmixing model for 170 archaeological samples against magnetic parameters of $M_S$, $\chi$ and $H_C$. The total concentration of superparamagnetic grain-sized magnetite predicted by the model is also shown as a biplot against $\chi_{FD}$. Where appropriate, the quality of a linear least squares regression fit to the data set is indicated by the $R^2$ coefficient.*

Figure 6.8 shows biplots from the IRM curve unmixing model plotted against more standard magnetic parameters. The results demonstrate a good correlation between the total concentration of magnetite within the apparent magnetic mixtures when plotted against the concentration specific parameters, $M_{RS}$ and $\chi$. The lower value for the linear least mean squares regression coefficient ($R^2$ on Figure 6.8) for the $\chi$ data indicates the sensitivity of this parameter to the grain-size of ferrimagnetic material present. A non-linear relationship between the concentration of magnetite predicted by the model and coercivity of remanence is also evident with high concentrations of these end-members producing $H_{CR} < 5$mT, as might be expected. The SP component also shows a linear correlation against $\chi_{FD}$ although the frequency dependence data from the weaker samples shows a considerable degree of scatter that lowers the regression coefficient.

A similar comparison for the hysteresis unmixing model is shown in Figure 6.9 that again illustrates a linear correlation between the predicted concentration of magnetite with both $M_S$ and $\chi$. The concentration of magnetite is also found to directly influence the coercivity of the sample and concentrations greater than ~0.005mg are found to have $H_C < 10$mT. A good correlation is also found between the concentration of superparamagnetic magnetite predicted by the unmixing model and $\chi_{FD}$. This is apparently stronger than that found for the IRM unmixing model due to the greater sensitivity of the in-field measurements to the superparamagnetic component.

### *6.3.6 Interpreting archaeological samples in terms of the unmixing models*

By providing a description of complex magnetic data in terms of an apparent magnetic mineralogy the influence of specific enhancement mechanisms may be proposed for certain groups of samples. For example, Figure 6.10 illustrates a selection of samples that, from the results of the hysteresis unmixing model, would appear to be dominated by single domain magnetite (calculated from the sum of 0.05, 0.5 and 0.75μm end-members) that may well be derived from a biogenic source. Results from sample BAS232 show a similar unmixing model to an adjacent sample, BAS231, (*cf* Figure 6.7) and the dominant 0.75μm magnetite

component is also found within a magnetic extract of fine grained material <0.38μm (FP97 LT38) from the same section.

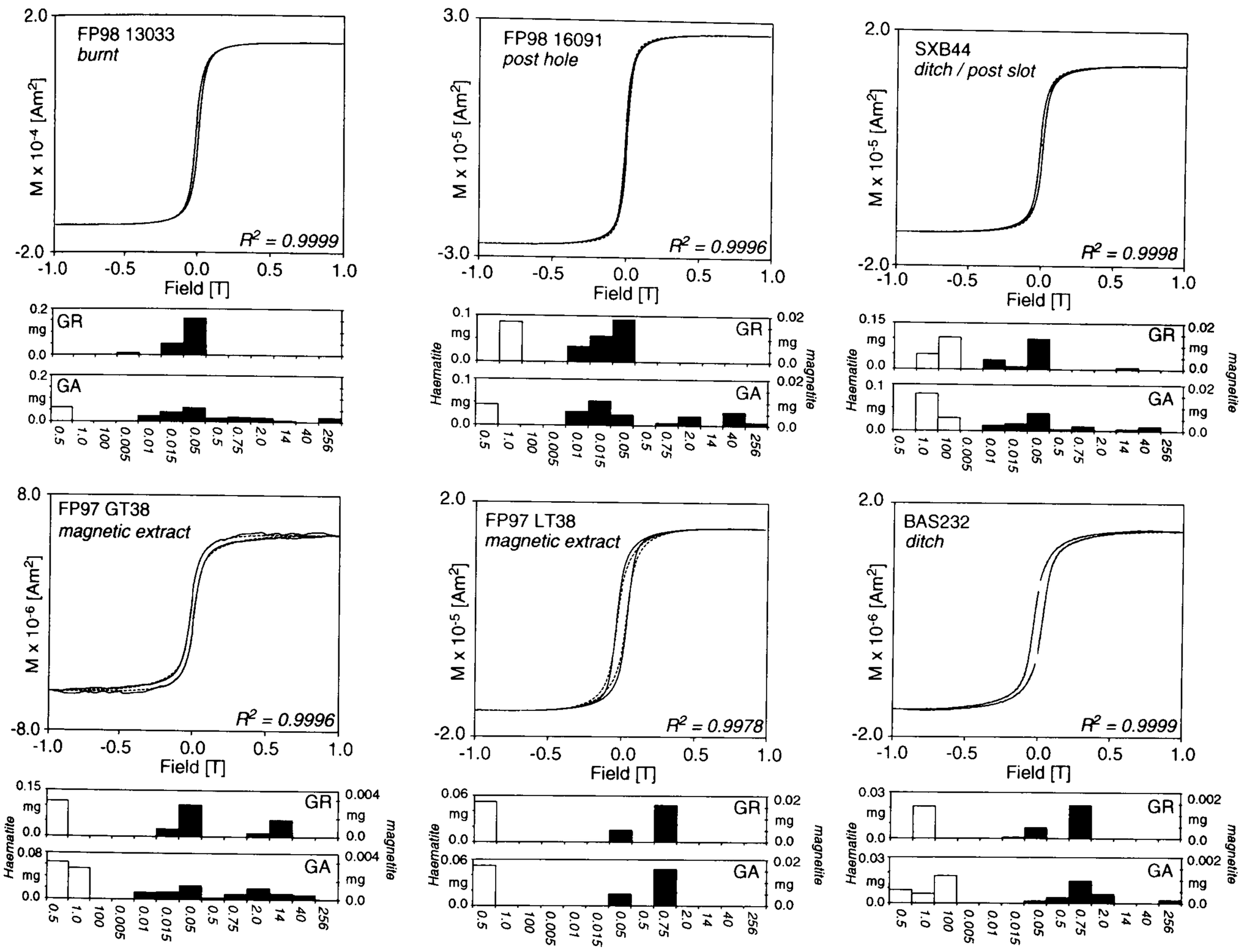


***Figure 6.10*** *Results of the hysteresis loop unmixing model for selected samples apparently dominated by single domain magnetite in a grain size range from 0.05 to 0.75μm. The concentration of individual end-members is shown on separate barcharts for the Golden Rule (GR) and genetic (GA) algorithms. Where the barcharts are presented with two scale axes the concentration of haematite and magnetite end-members are determined from the left and right hand axes respectively.*

Results from the magnetic extract prepared from the coarser 60 to 38μm fraction of the same material (Figure 6.10; FP97 GT38) also contains a significant single domain component. However, this is apparently finer grained (0.05μm) and is found together with a multi domain magnetite phase. It is possible that this finer grained material represents greigite that appeared from the SEM/TEM analysis (Figure 5.39) to be closely associated

with coarser organic remains that would be excluded from the <38μm fraction. The coarser fraction would also be more likely to contain larger detrital minerals suggested by the presence of multi domain magnetite within the unmixing model for FP97 GT38.

Fine grained single domain magnetite (0.05μm) was also found to be a significant end-member component within the unmixing models produced for a number of other samples including FP98 13033, FP98 16091 and SXB44 shown in Figure 6.10. Whilst the features from which these samples were recovered suggest that a similar grain-size of material might be associated with burnt material no evidence for burning was found to be associated with SXB44. As this sample was recovered from the post slot trench of a Saxon timber building it is possible that biogenic enhancement of the decayed timber may have occurred in a manner similar to that reported by Faßbinder and Stanjek (1993).

In an attempt to average inter-sample variation, the results from the unmixing models were classified in terms of the feature type and location (flood plain or raised gravel terrace) to produce a mean apparent magnetic mineralogy for each classification. Due to the inherent sampling bias towards flood plain sites in the study area it has been possible to separate samples from the flood plain into a greater number of classification types. However, results from both the IRM acquisition (Figure 6.11) and hysteresis loop (Figure 6.12) unmixing models allow a semi-quantitative interpretation for the enhancement of archaeological features to be proposed.

Comparison of the apparent magnetic mineralogy of the underlying sand and gravel substrate suggests a broadly similar distribution dominated by high coercivity haematite components between samples from the flood plain and raised gravel terrace. The latter samples apparently contain a slightly higher concentration of magnetite end-members although this classification is drawn from a more limited number of sand and gravel samples than were recovered from the more numerous flood plain sites. A similar concentration of end-members to the sand and gravel samples is also found within the ditch features recovered from the flood plain although an increased significance of single domain magnetite is suggested by the hysteresis loop unmixing model. Samples from the Neolithic enclosure ditch may also be described by a similar concentration of end-members that is

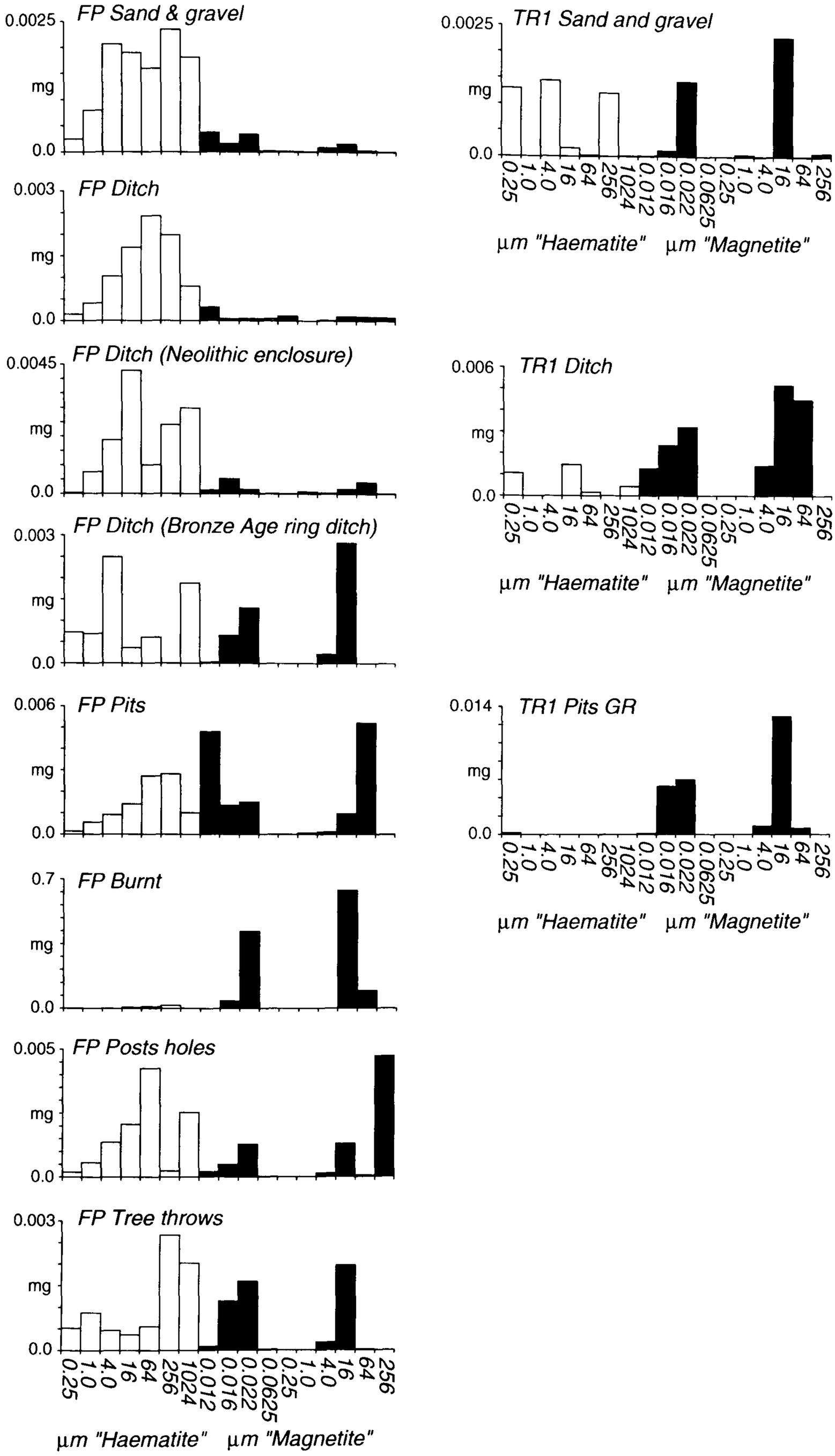


***Figure 6.11*** *Mean IRM acquisition curve unmixing model results for all 170 archaeological samples classified by feature type and origin from either the flood plain (FP) or raised gravel terrace (TR1).*

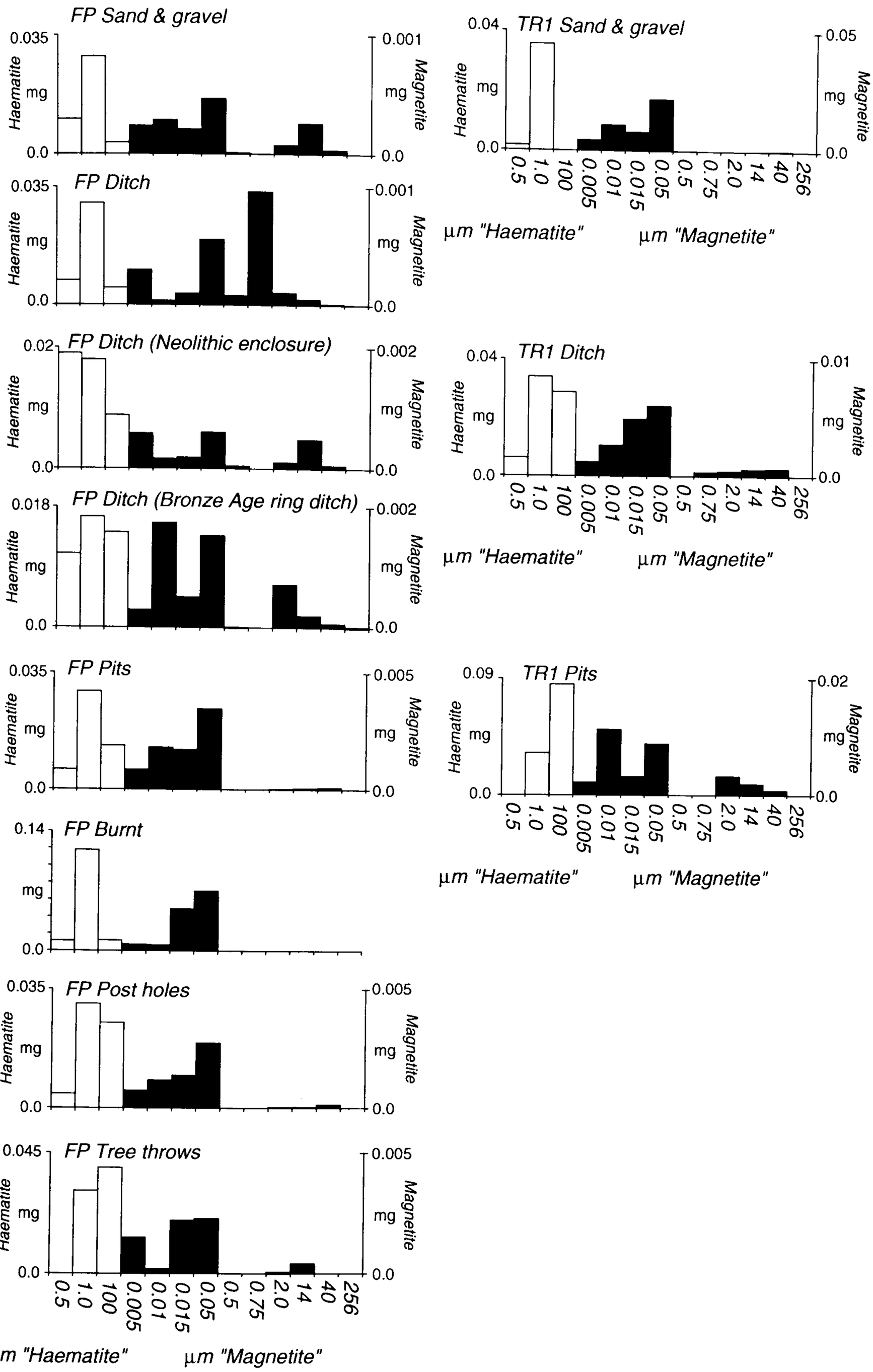


***Figure 6.12*** *Mean hysteresis loop unmixing model results for all 170 archaeological samples classified by feature type and origin from either the flood plain (FP) or raised gravel terrace (TR1). Where the barcharts are presented with two scale axes the concentration of haematite and magnetite end-members are determined from the left and right hand axes respectively.*

surprising as this feature did produce a weak magnetic anomaly that was detected by geophysical survey (§5.5.1).

In contrast, samples recovered from ditch features located on the raised gravel terrace demonstrate a much greater concentration of magnetite end-members than the sand and gravel substrate, particularly superparamagnetic grain-sized material. Unmixing models derived from the IRM acquisition curves also contain a significant multi domain component although it is possible that the superparamagnetic and multi domain end-members are too similar to be distinguished by the model (Figure 6.1). A similar concentration and grain-size distribution of magnetite end-members is found for the pit-type features from the raised gravel terrace that, in common with the ditch type features, were all identified by strong magnetic anomalies during the initial magnetometer survey.

On the flood plain samples recovered from pits, post holes, tree throws and the Bronze Age ring ditch also contain an enhanced concentration of superparamagnetic magnetite. Whilst these concentrations are lower than for similar feature types on the raised gravel terrace they appear to be sufficiently enhanced to generate identifiable magnetic anomalies (§5.3.1).

The most strongly enhanced samples from the entire study area were, unsurprisingly, recovered from obviously burnt features. These contain a high concentration of fine grained magnetite within an apparent grain size range of between ~0.02 to 0.05μm, although the IRM acquisition unmixing model again indicates a significant multi domain component. As this grain size range is also found within the other magnetically enhanced feature classifications, such as tree throws that are often interpreted as deliberate burning pits, it seems likely that the accumulation of burnt material within cut archaeological features represents a significant mechanism for their magnetic enhancement. The presence of finer grained magnetite, <0.02μm, such as that found additionally within the pit-type features or the Bronze Age ring ditch, may therefore represent the influence of pedogenic or biogenic mechanisms favouring the production of such ultra fine grained superparamagnetic material.

## *6.4 Modelling expected magnetic anomalies*

The proceeding section illustrates that despite a considerable variation in the apparent concentration of magnetic minerals between features recovered from the flood plain and the gravel terrace, even quite weakly enhanced features, such as the Neolithic enclosure ditch, were associated with detectable magnetic anomalies. It is therefore of interest to examine why other feature types from the flood plain with a similar concentration of magnetic minerals to the Neolithic enclosure, such as pits and post holes, were not detected by the geophysical survey.

The magnetic anomaly produced by a buried feature will depend upon its physical dimensions, magnetisation (in terms of both induced and any remanent components present) and the depth of burial from the current ground surface. The ability to detect such anomalies is also critically dependent upon the sensitivity of the applied instrumentation and the sample interval used to conduct the geophysical survey. Forward magnetic models based on both the physical dimensions and the magnetic properties of the excavated features allow the geophysical methodology deployed during this study to be tested against theoretical, higher resolution surveys

### *6.4.1 Potential field modelling*

The theory underlying potential field modelling is well developed and many specific references to the magnetic case are available (e.g. Bhattacharyya 1964, Linington 1972, Bhattacharyya and Navalio 1975, Bhattacharyya and Chan 1977, Ku 1977, Blakely 1995, Ivan 1996). The importance of magnetic modelling to aid the interpretation of archaeological surveys has also been recognised through both scale models and numerical methods (e.g. Linington 1965, Bevan 1994) that have become more popular with the increasing availability of powerful computing systems.

In this study, the algorithms employed for the construction of the magnetic model are derived from the triple integration method of Linington (1972). This method begins with

the determination of the magnetisation due to a single dipole and extends this to a series of geometrical bodies (e.g. prism, sphere, etc.) of uniform magnetisation that may be combined to described the more complex geometry of real archaeological features. The algorithm is implemented through the use of an object orientated programming language (C++) to allow the extension of the model through inheritance[3] from basic dipole sources to more complex geometries. Whilst more computationally efficient digital convolution methods are available, some discrepancy between these results and the more intensive triple integration are reported (Bhattacharyya and Navalio 1975).

The current algorithm allows a 3-dimensional model of buried archaeological features to be described in terms of a series of geometrical bodies. These bodies may be subdivided to represent the variation of susceptibility, giving rise to the induced magnetic component, through the feature and may also include a remanent magnetisation in an entirely independent direction to that induced by the Earth's magnetic field. Variations of surface topography, sample interval and sensor configuration may also be fully modelled including the full determination of the resultant three component magnetisation vector. The induced component of magnetisation within the models has been calculated from appropriate current values for the inclination, declination and magnitude of the Earth's magnetic field at the site.

### *6.4.2 Magnetic anomaly models from the raised gravel terrace sites*

Figure 6.13 shows the results of a magnetic model based on the geometry and magnetic properties of a section cut through the ditch of the Anglo-Saxon timber building at Worton 1996 Site B (§4.5.1; Figure 4.15 SXB). The magnetisation of the feature was determined from the measured susceptibility of samples recovered from a section through the ditch section and these values were extended to represent the entire section of the ditch revealed by the geophysical survey and subsequent excavation. No significant natural remanent

---

[3] Object orientated programming languages, such as C++, group code within a series of objects or classes that contain all of the relevant functionality. Inheritance describes the process of deriving a new object from an original class definition, allowing the re-use of common functions, whilst retaining the flexibility to modify the old code if it does not do exactly what is required.

magnetisation was determined during the measurement of these samples or was assumed to be present due to the magnetic viscosity of the soil (*cf* Eder-Hinterleitner et al. 1995).

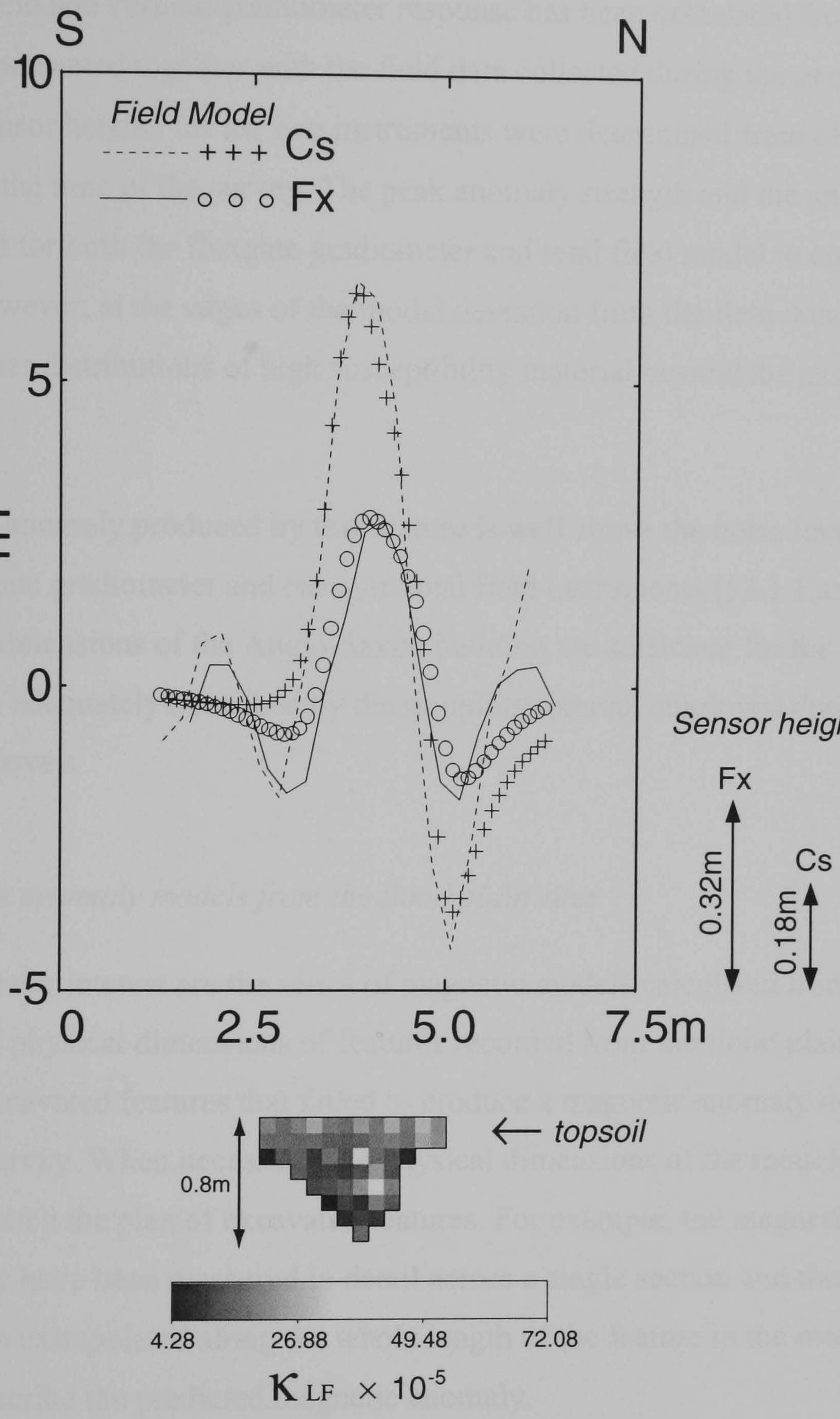


***Figure 6.13*** *Comparison between the field data and numerical model results calculated for a single instrument traverse across a section of the Saxon timber building revealed on the raised gravel terrace. Results for both a total field instrument and vertical gradiometer are shown together with the physical dimensions and distribution of susceptibility recorded through the feature section (lower portion of the figure, scale as indicated).*

Both a total field and vertical gradiometer response has been calculated from the ditch model and is presented together with the field data collected during the geophysical survey of the site. Sensor heights for the two instruments were determined from observations made in the field at the time of the survey. The peak anomaly strength and the anomaly width are well described for both the fluxgate gradiometer and total field model in comparison to the field data. However, at the edges of the model deviation from the field data occurs due, no doubt, to further distributions of high susceptibility material beyond the excavated section of the ditch.

The magnetic anomaly produced by this feature is well above the noise level determined for both the fluxgate gradiometer and caesium total field instruments (§3.1.1 and §3.1.2). In addition, the dimensions of the Anglo-Saxon building are sufficient for the magnetic anomaly to be adequately described by the sampling interval employed during the initial geophysical survey.

### *6.4.3 Magnetic anomaly models from the flood plain sites*

Perhaps of greater interest are the series of magnetic models calculated from the magnetic properties and physical dimensions of features recorded from the flood plain sites, particularly excavated features that failed to produce a magnetic anomaly during the initial geophysical survey. When necessary, the physical dimensions of the models have been extended to match the plan of excavated features. For example, the magnetic properties of a ditch may only have been measured in detail across a single section and these values have, therefore, been extrapolated along the whole length of the feature in the model to adequately describe the predicted magnetic anomaly.

Appropriate levels of Gaussian noise have been added to the data to account for both the stationary instrument noise determined from §3.1 and that due to the overlying topsoil. The degree of topsoil noise was calculated from a numerical model based on the magnetic properties of topsoil recovered from the flood plain sites that suggested appropriated

Gaussian distributions to be added to the model data. No attempt was made to model noise due to either the micro-topography of the ground surface (e.g. plough furrows) or that introduced through the transport of the instrument sensors over the site.

Model results have been calculated for a fluxgate gradiometer (0.5m sensor separation) at sample intervals of 0.25m × 1.0m and 0.25m × 0.5m and for a total field instrument at 0.25m × 0.5m. To enable the fluxgate gradiometer results to be presented in a non-differential form, more comparable to the total field data, the 0.25m × 0.5m vertical gradient data has been transformed to the equivalent total field and downward continued to match the sensor height of the total field instrument (Tabbagh et al. 1997). This process introduces a degree of smoothing to the final data that reduces the dynamic range of the Gaussian noise added to the model.

In contrast to Figure 6.13, the magnetic models for the floodplain features have been calculated over a series of parallel traverses and are presented as greytone images of the data analogous to the display of the field magnetometer results presented in Chapters 4 and 5.

*6.4.3.1 Ditch features*

The results from three magnetic models of excavated ditch features are shown in Figure 6.14 including two examples that were both identified in the initial fluxgate gradiometer survey and a model based on the alluviated Bronze Age boundary ditch that did not produce a detectable anomaly.

The fluxgate gradiometer model of the Neolithic enclosure ditch (§5.5.1) produces results at a sample interval of 0.25m × 1.0m that are very similar to the original field data (*cf* Figure 5.26). A marginal improvement occurs at an increased sample density of 0.25m × 0.5m but even after transformation to the equivalent total field the fluxgate model data does not compare with the clarity suggested by the total field model.

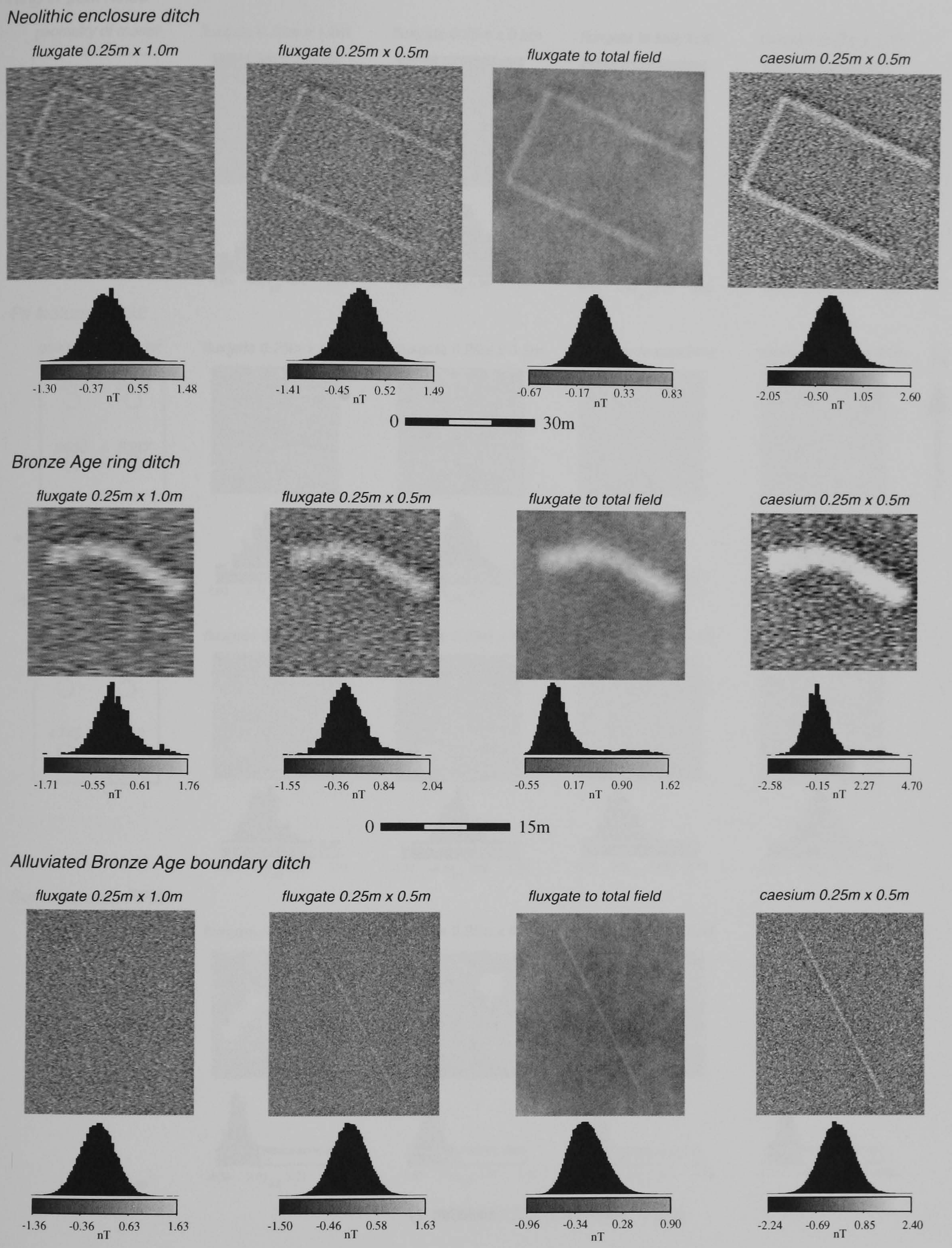


***Figure 6.14*** *Results from numerical models predicting the expected magnetic response constructed from the physical and magnetic properties of three representative ditch-type features excavated on the flood plain. The model response for both a vertical gradiometer (fluxgate) and total field (caesium) instrument has been calculated at varying sample intervals.*

Ring of post holes

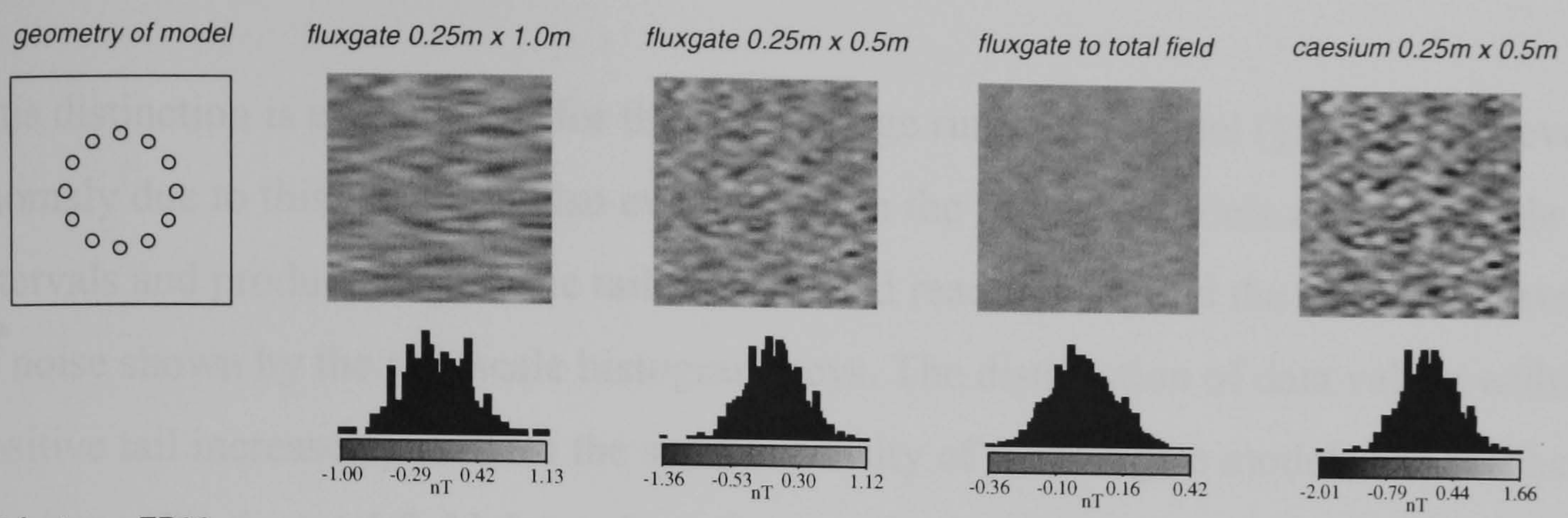


Pit features FP92

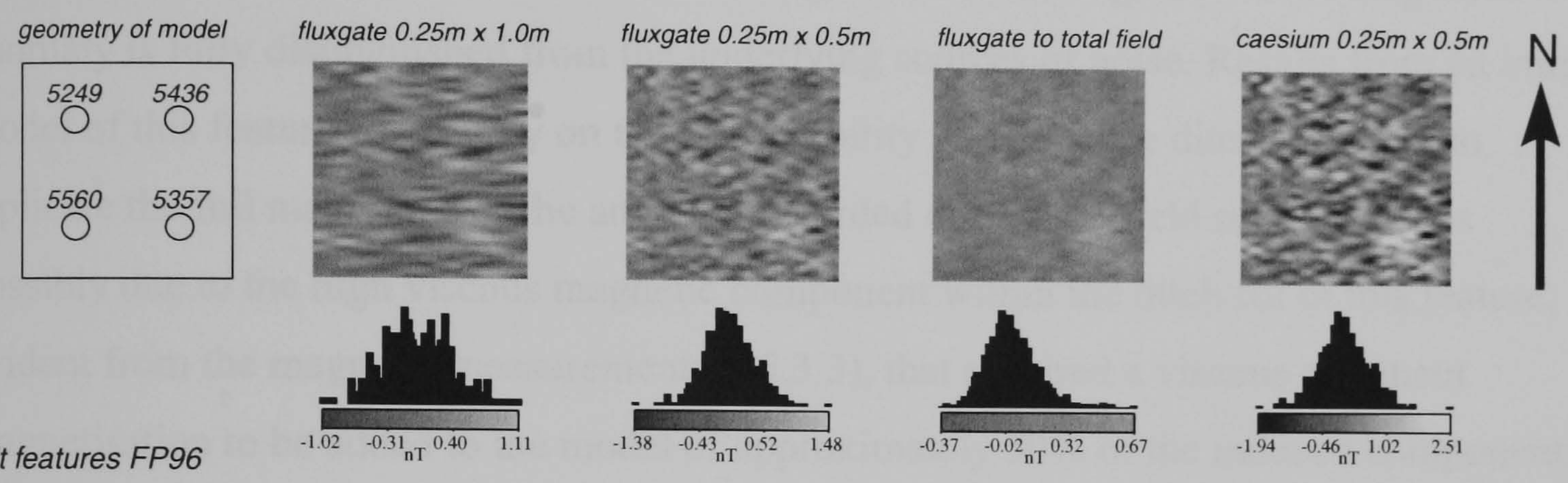


Pit features FP96

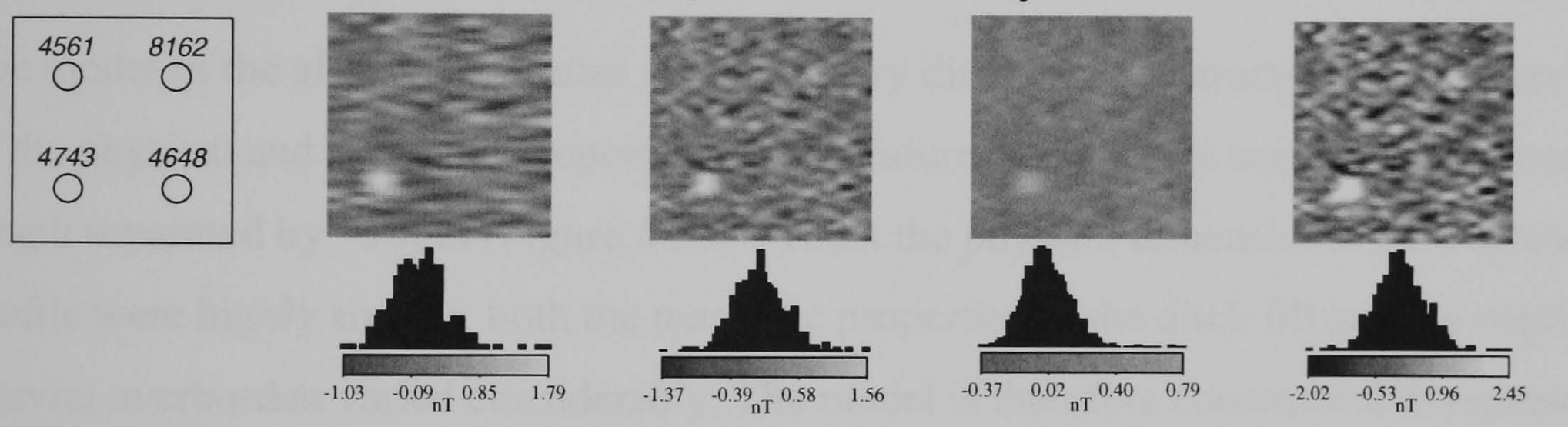


Burnt features FP98

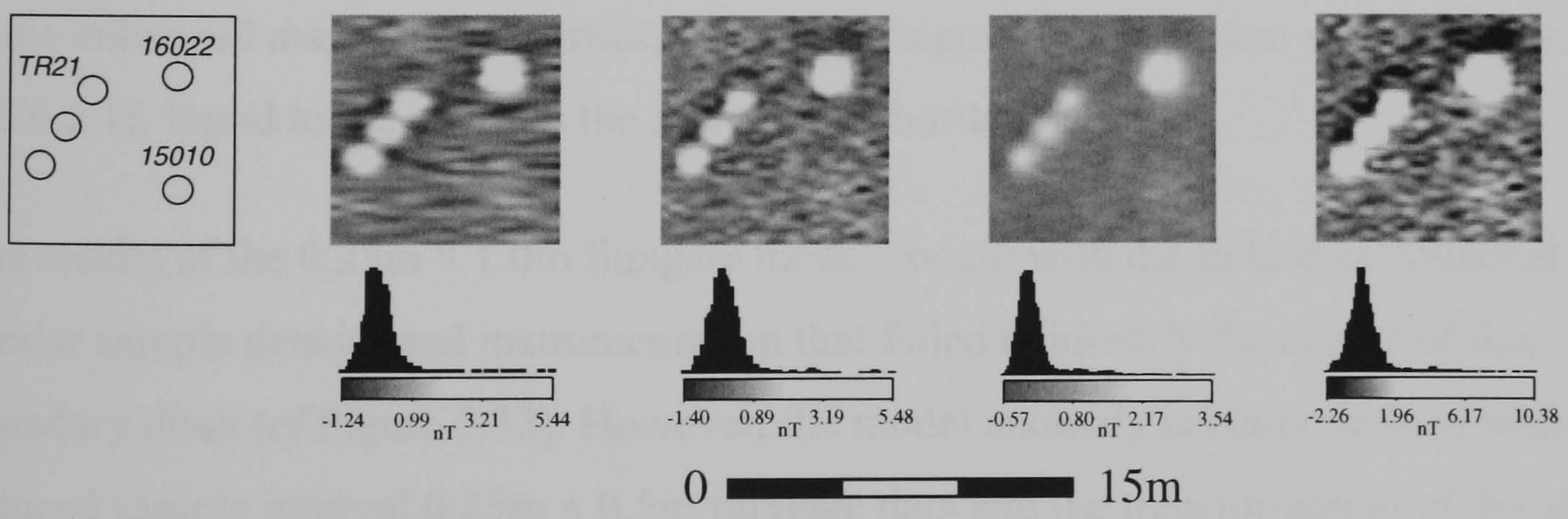


***Figure 6.15*** *Results from numerical models predicting the expected magnetic response constructed from the physical and magnetic properties of representative post, pit and burnt features excavated on the floodplain. The model response for both a vertical gradiometer (fluxgate) and total field (caesium) instrument has been calculated at varying sample intervals. The geometry of the model is also shown together with the appropriate feature number.*

This distinction is even clearer for the Bronze Age ring ditch model (§5.3.1). However, the anomaly due to this feature is also evident within the fluxgate models at both sample intervals and produces a positive tail of enhanced readings beyond the Gaussian distribution of noise shown by the greyscale histogram keys. The distribution of data values within this positive tail increases with both the sample density of the fluxgate models and reaches a maximum for the total field data where the magnitude of readings due to the ring ditch anomaly is fully distinguished from the underlying sources of noise. Results from an initial model of this feature based only on the susceptibility values of the ditch fill failed to replicate the full magnitude of the anomaly recorded during the field survey. This is possibly due to the high viscous magnetic component within the ditch fill of this feature, evident from the magnetic measurements (§5.3.3), that required a viscous remanent magnetisation to be added to the model of approximately 50% of the induced component.

The model of the alluviated Bronze Age boundary ditch was constructed from observations of the physical and magnetic properties of this feature made at two sections cut across its length separated by ~100m (Figure 5.33). Whilst the physical dimensions of the ditch profile were highly similar, both the magnetic properties of the ditch fill and the depth of alluvial overburden varied considerably. The model is therefore constructed to represent this gradation from the shallow, more weakly magnetic properties of the ditch to the north to the enhanced magnetic properties, including a significant remanent magnetisation (§5.6.2.1), found to the south as the alluvial overburden increases.

The results of the 0.25m × 1.0m fluxgate model concur with the field data collected with a similar sample density and instrumentation that failed to identify the course of this boundary ditch (*cf* Figure 5.32). However, the model anomaly is better defined within the reduced sample interval 0.25m × 0.5m fluxgate data and the transformation of this data to the equivalent total field component. It is unclear whether the enhanced resolution of the transformed data is due to the non-differential representation of the fluxgate data or the effective suppression of Gaussian noise, that can be equally well achieved through low-pass filtering of the results. Again the clearest definition of the ditch anomaly is provided by a

total field model that would appear to offer the highest probability of identifying similar features in the field.

*6.4.3.2 Pits and post hole features*

Results from magnetic models based on post hole and pit-type features are shown in Figure 6.15. The post hole model is generic, based on the average dimensions and magnetic properties of 12 such features arranged in a circular distribution similar to those found over many of the flood plain sites (*cf* Figures 5.11 and 5.21). More specific models have been constructed for pit-type features and these are also illustrated in Figure 6.15 by examples from the FP92 and FP96 sites. In each case, a graphical depiction of the model geometry is included indicating the sectioned feature number for each model that can be found on Figures 5.5 and 5.11 for the FP92 and FP96 sites respectively.

It is, perhaps, not surprising that the post-hole features fail to produce an identifiable anomaly even within the high density total field data. Such weakly magnetic, physically slight features produce anomalies that are indistinguishable from the realistic levels of Gaussian noise added to the model data. Only much larger post settings (diameter >0.5m) surviving in a more substantial, deeper post pit or trench are likely to be identifiable under the conditions found on the flood plain.

A greater success is found for the models based on pit-type anomalies, although many of these appear equally elusive as the post holes. Again, the physical dimensions of the features is critical with only the larger pits, such as pit 5357 from site FP92, producing an identifiable anomaly. Exceptions occur when pits, even of quite small physical dimensions, contain a more highly enhanced fill such as 4743 and to a lesser extent 8162 from site FP96. Both these latter features have fills with an average susceptibility $\kappa > 100 \times 10^{-5}$ that suggests the presence, at least in part, of burnt material.

*6.4.3.3 Burnt features*

Figure 6.15 also shows a series of models constructed from the physical dimensions and magnetic properties of obviously burnt features recovered from the FP98 site. These

include two pits, one containing burnt stone (Figure 5.19; Section 15010) and the other ash (Figure 5.21; Section 16022) and a line of three burnt tree throws (Figure 5.19; Section TR21). Given the high volume susceptibility of samples recovered from these features ($\kappa$ $>200 \times 10^{-5}$) it is not surprising that they have produced readily detectable anomalies. Only pit 15010 has failed to produce an identifiable anomaly, possibly due to the mineral magnetic samples being recovered from the interstitial pit fill rather than the larger, individual burnt stones.

In comparison to the results from the ditch, post and unburnt pit features, the total field model, simulating a caesium magnetometer system, has again produced the highest magnitude anomalies, almost double the strength of the fluxgate data. The transformation of the high density fluxgate data, including a realistic noise component, to the equivalent total field component cannot reproduce the same magnitude of anomaly suggesting the application of caesium magnetometers in the field would improve the resolution of weakly magnetic features.

Field trials operating the fluxgate gradiometer at a high density sample interval (0.25m × 0.5m) did not, apparently, produce an improvement in the quality of the recorded data (*cf* Figure 5.16). Comparison with the model data supports this finding and suggests that at a normal sensor height only a marginal increase in the signal to noise ratio would be expected. Models calculated for a fluxgate gradiometer with a reduced sensor height (to the same level as the caesium instrument) did produce an ~25% increase in the magnitude of the anomalies. However, by lowering the fluxgate sensors, the influence of the topsoil noise will increase and the ability to distinguish weakly magnetic anomalies will be more directly influenced by the electronic noise inherent to the instrument itself (Figure 3.1).

## *6.5 Spatial analysis of the geophysical survey and excavation results*

### *6.5.1 Classification by magnetic anomaly strength*

To examine the fidelity of magnetic anomalies recorded during the original geophysical survey compared to subsequently excavated features, a semi-quantitative analysis of the

data was devised through the use of a geographical information system (GIS). The initial analysis was based on reclassifying the geophysical data into areas of "positive" (>0.5nT) and "negative" (<0.5nT) magnetic response, likely to exceed the instrument noise of the fluxgate gradiometer. Table 6.1 shows the spatial correlation of this reclassified fluxgate data with the location of post, pit and ditch type features revealed during the subsequent excavation of 8 sites in the study area where data was available.

***Table 6.1*** *Spatial analysis of the magnetic data in comparison to subsequently excavated features in terms of magnetic anomaly magnitude. Results for the same data following reduction to the pole are shown in parentheses.*

| | *Feature type and anomaly classification* | | | | | |
|---|---|---|---|---|---|---|
| | *Posts* | | *Pits* | | *Ditches* | |
| | *>0.5nT* | *<0.5nT* | *>0.5nT* | *<0.5nT* | *>0.5nT* | *<0.5nT* |
| *Cresswell Field* | 35.2% (34.5%) | 38.2% (35.4%) | 47.6% (47.9%) | 30.5% (27.7%) | 53.0% (54.5%) | 30.0% (25.2%) |
| *Worton 1996B FX* | N/A | N/A | 59.3% (69.5%) | 23.7% (20.3%) | 56.8% (60.3%) | 14.6% (10.0%) |
| *Worton 1996B CS* | N/A | N/A | 64.4% (50.8%) | 28.8% (37.3%) | 68.9% (69.7%) | 19.3% (16.8%) |
| *ARC Stage 4*[1] *(sites 2,3 & 4)* | – | – | 8.1% (11.7%) | 44.7% (45.7%) | 7.9% (4.5%) | 40.1% (45.9%) |
| *Neolithic enclosure* | 22.2% (14.3%) | 20.2% (24.4%) | 17.5% (21.2%) | 24.1% (20.7%) | 35.0% (38.0%) | 11.3% (7.5%) |
| *YFPB 1996*[1] | – | – | 15.7% (11.0%) | 16.2% (26.7%) | 25.8% (22.5%) | 18.9% (28.7%) |
| *YFPB1997*[1] | – | – | 8.2% (13.7%) | 11.1% (12.0%) | 11.1% (22.5%) | 12.1% (10.5%) |
| *YFPB 1998*[1] | – | – | 16.1% (37.2%) | 16.8% (5.6%) | 16.7% (28.9%) | 16.4% (7.8%) |

[1] *pit and post hole features have been amalgamated into a single layer*
*FX = fluxgate gradiometer data, CS = caesium total field data*

The results in Table 6.1 provide statistical confirmation of the improved conditions for magnetic survey on the raised gravel terrace and show a good correlation between positive magnetic response and the location of pit and ditch type features. In general, this correlation is improved (Table 6.1 values in parentheses) if the vertical gradiometer data is first transformed to the equivalent total field component and subsequently reduced to the pole to

correct for the displacement of the magnetic anomalies (Blakely 1995). Results from the flood plain sites are considerably less successful, demonstrating a much lower probability of a positive magnetic response indicating the genuine location of significant archaeological features. In addition, the detection of post hole type features proved particularly difficult throughout the study area supporting the conclusions drawn from the magnetic modelling exercise (§6.4.2).

### *6.5.2 Classification through graphical anomaly interpretation plans*

Magnetic models calculated from the properties of topsoil samples recovered over the study demonstrate a magnitude of anomaly that will generate a number of false classifications, in terms of the positive and negative responses defined above. This is illustrated, for example, by the similar probability of a post hole type feature falling into either a positive or negative classification. To reduce the influence of the topsoil signal, a second spatial analysis was derived reclassifying the geophysical data indirectly through the graphical interpretation diagrams that have been produced for each of the sites. The data was then redefined into categories including: direct correlation between a magnetic anomaly and an excavated feature (True Positive), presence of an anomaly but no underlying feature (False Positive), correct indication of an area devoid of features (True Negative) and areas containing features but no identifiable magnetic anomalies (False Negative).

Table 6.2 provides a summary of this classification scheme and extends the True Positive category to include a 2m buffer zone between the anomalies and subsequently excavated features (Linford and David 2001 provide a more detailed discussion). A graphical representation of this data is also provided (Figure 6.16) showing the distribution by category as a false colour image superimposed over an outline plan of the subsequently excavated features for the Cresswell Field and Neolithic enclosure sites. The results again demonstrate a good correlation between significant anomalies identified from the raised gravel terrace sites and the location of underlying features. High True Positive scores are, however, potentially misleading as they may result from a site with very poor geophysical response where few, if any, anomalies have been identified. In this case consideration of

both the False Positive values and the distribution of True Positive scores across the 2m buffer zone is essential to establish the actual quality of geophysical results from the site.

***Table 6.2*** *Spatial analysis of the magnetometer data in comparison to subsequently excavated features in terms of interpreted significant anomalies. The table also shows the distribution of direct correlation between anomalies and features (True Positive) over the 2m buffer zone used for the analysis.*

| | *True (False) Positive* | | | *True Negative* | *False Negative* |
|---|---|---|---|---|---|
| *Cresswell Field* | 83.3% (16.7%) | *0m* | 30.3% | 61.5% | 20.4% |
| | | *0.5m* | 21.1% | | |
| | | *1.0m* | 16.4% | | |
| | | *1.5m* | 9.8% | | |
| | | *2.0m* | 5.6% | | |
| *Worton 1996B* | 93.6% (6.4%) | *0m* | 69.7% | 70.7% | 3.2% |
| | | *0.5m* | 17.4% | | |
| | | *1.0m* | 3.5% | | |
| | | *1.5m* | 1.6% | | |
| | | *2.0m* | 1.4% | | |
| *ARC Stage 4 (Site 2)* | 78.3% (21.7%) | *0m* | 0% | 0.2% | 99.9% |
| | | *0.5m* | 3.4% | | |
| | | *1.0m* | 2.4% | | |
| | | *1.5m* | 37.9% | | |
| | | *2.0m* | 34.4% | | |
| *ARC Stage 4 (Sites 3 and 4)* | 28.1% (71.9%) | *0m* | 2.4% | 9.6% | 98.0% |
| | | *0.5m* | 2.6% | | |
| | | *1.0m* | 5.7% | | |
| | | *1.5m* | 8.8% | | |
| | | *2.0m* | 8.8% | | |
| *Neolithic enclosure* | 71.6% (28.4%) | *0m* | 52.3% | 57.0% | 21.3% |
| | | *0.5m* | 8.4% | | |
| | | *1.0m* | 5.2% | | |
| | | *1.5m* | 1.6% | | |
| | | *2.0m* | 4.1% | | |
| *YFPB 1996* | 45.2% (54.8%) | *0m* | 24.7% | 21.3% | 89.0% |
| | | *0.5m* | 5.3% | | |
| | | *1.0m* | 5.2% | | |
| | | *1.5m* | 5.1% | | |
| | | *2.0m* | 4.8% | | |
| *YFPB 1997* | 9.2% (90.8%) | *0m* | 0.2% | 14.1% | 99.0% |
| | | *0.5m* | 0.8% | | |
| | | *1.0m* | 1.5% | | |
| | | *1.5m* | 2.7% | | |
| | | *2.0m* | 3.9% | | |
| *YFPB 1998* | 50.4% (49.6%) | *0m* | 6.8% | 78.1% | 70.8% |
| | | *0.5m* | 10.8% | | |
| | | *1.0m* | 11.0% | | |
| | | *1.5m* | 12.1% | | |
| | | *2.0m* | 9.8% | | |

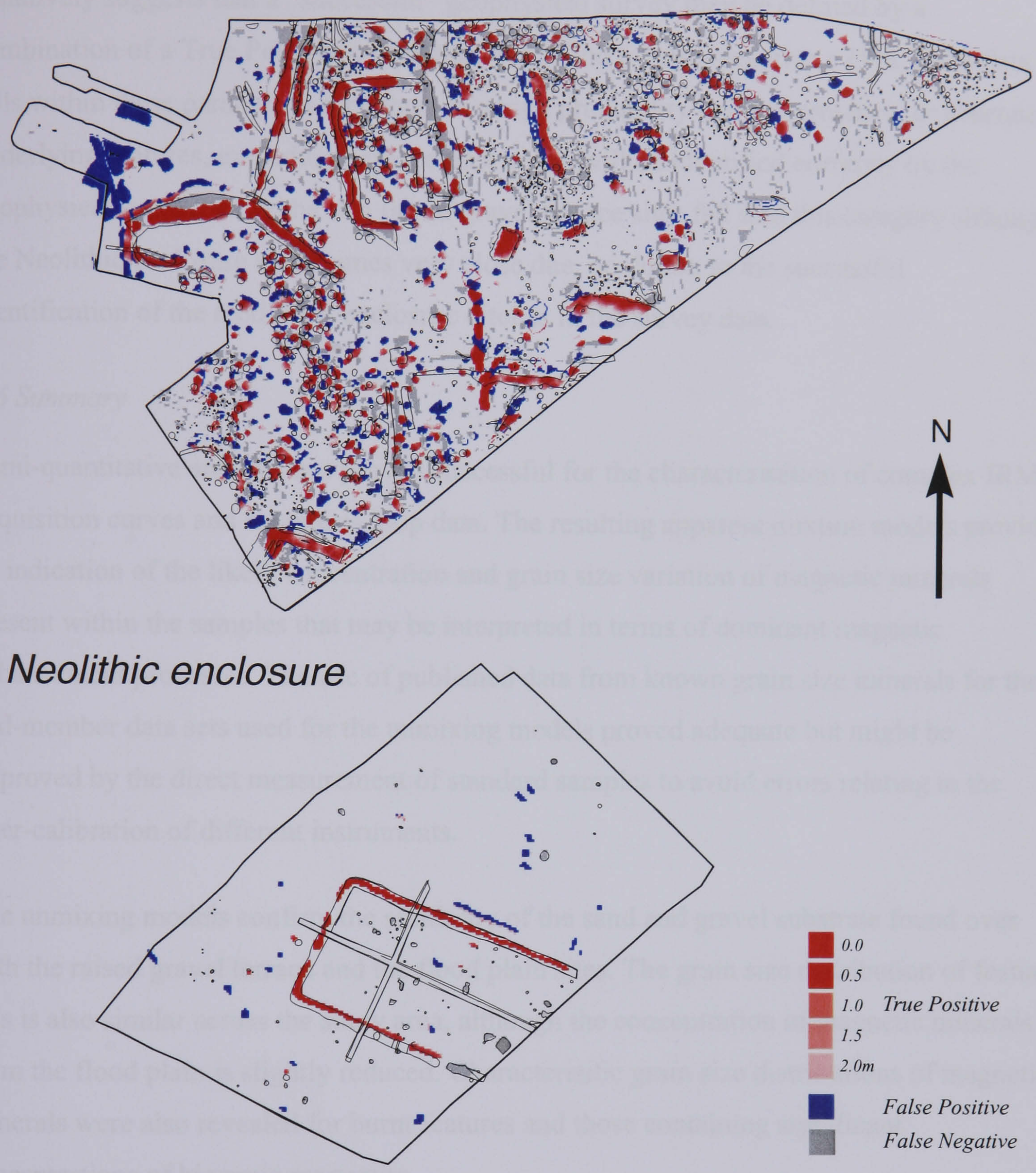


***Figure 6.16*** *Graphical representation of the spatial analysis results presented in Table 6.2 for two representative sites. The correlation between interpreted magnetic anomalies and underlying features is shown as a false colour image superimposed over the excavation plan.*

Comparison with data from a limited number of other sites (Linford and David 2001) tentatively suggests that a "successful" geophysical survey may be defined by a combination of a True Positive correlation >75% and a False Negative <25%. If the data falls within these parameters then there is a high probability that the presence, or absence of underlying features, excluding perhaps post holes, will be identified correctly by the geophysical survey. Only the two raised gravel terrace sites fall into this category although the Neolithic enclosure sites comes very close due, no doubt, to the successful identification of the rectilinear enclosure ditches in the survey data.

*6.6 Summary*

Semi-quantitative analysis has proved successful for the characterisation of complex IRM acquisition curves and hysteresis loop data. The resulting apparent mixture models provide an indication of the likely concentration and grain size variation of magnetic minerals present within the samples that may be interpreted in terms of dominant magnetic enhancement processes. The use of published data from known grain size minerals for the end-member data sets used for the unmixing models proved adequate but might be improved by the direct measurement of standard samples to avoid errors relating to the inter-calibration of different instruments.

The unmixing models confirm the similarity of the sand and gravel substrate found over both the raised gravel terrace and the flood plain sites. The grain size distribution of feature fills is also similar across the study area, although the concentration of magnetic minerals from the flood plain is slightly reduced. Characterisitic grain size distributions of magnetic minerals were also revealed for burnt features and those containing significant concentrations of biogenic magnetite.

The results of the initial geophysical survey were confirmed through consideration of magnetic anomaly models calculated from the magnetic properties and physical dimensions revealed from subsequently excavated archaeological features. These models suggest that even weakly magnetic features may be distinguished from underlying sources of noise and their detection may well be enhanced through the use of high-sensitivity caesium magnetometers applied at a suitable sample interval. Despite obvious success with the

location of well magnetised ditch and larger pit-type features physically slight post hole features appear to be beyond the resolution of geophysical survey techniques under the conditions found on the flood plain sites. This was further confirmed through consideration of both the magnetic anomaly models and the spatial analysis of the geophysical survey data.

# *Chapter 7*

## *7.0 Quantitative evaluation of the effects of fire*

This chapter examines the important role of fire as a magnetic enhancement mechanism in terms of both the thermal alteration of magnetic minerals in sediments and the formation of distinctive geophysical anomalies. Results from a series of actualistic fire experiments are presented together with a comparison with samples heated under controlled laboratory conditions. Particular regard is given to the identification of a diagnostic mineral magnetic signal indicative of the thermal history of a sediment and the findings applied to a number of samples recovered from burnt archaeological features.

## *7.1 Experimental design*

### *7.1.1 Actualistic Fire Experiments*

A series of five experimental fires were conducted over three different soil types found in the study area including the underlying sand and gravel substrate, a water logged clay soil from the floodplain and a sandy loam developed over the raised gravel terrace. Different fuelling regimes and burn times were examined during the experiments and it was hoped that the following objectives might be investigated:

(i) The degree of burning necessary to create discernible magnetic anomalies (in terms of maximum temperature and exposure times)

(ii) The degree of enhancement experienced by soils under typical short duration fires and the volume of enhanced material produced.

(iii) The identification of specific thermal histories through magnetic measurements related to both the length of exposure and maximum temperature attained.

(iv) The ratio between induced and (thermo) remanent components of the resulting magnetic anomaly to be determined for short, camp fire type burning episodes.

In the case of each experiment, both the temperature in the body of the fire and the underlying soil were recorded through a series of thermocouples and soil samples were collected immediately prior to and after the fire was spent. In addition, a magnetometer survey was conducted with a fluxgate gradiometer at a sample interval of 0.25m $\times$ 0.5m both before and after the fire was kindled to establish the residual magnetic anomaly (if any) caused by the burning episode.

For brevity, further experimental details and results are contained within Canti and Linford (2000) and Linford and Canti (2001) produced during the completion of this thesis (Addendum, inside back cover) and the following discussion will concentrate upon aspects of this work not covered within either of these two publications.

*7.2 Laboratory heating experiments*

Additional quantities of the unburnt soil types used for the actualistic fire experiments were recovered for use in a series of laboratory heating experiments. Following air drying five 10g sub-samples of each soil type were heated in a digitally controlled laboratory furnace to a series of maximum temperatures from 50 to 600°C. At each temperature step a sample was removed from the furnace after an exposure time of 10, 30, 60 and 120 minutes had elapsed. The remaining sample from each of the three substrate types was left in the furnace overnight for a period of 24 hours. All heating was conducted in oxygen as experiments conducted in an inert atmosphere did not produce significantly different results. Oldfield (1981) draws attention to a number of additional parameters strongly influencing the magnetic enhancement of sediments including rates of heating and cooling, furnace atmosphere, and the size of the heating crucible. As the current study focused on the differing behaviour of three sediment types it was deemed impractical to repeat such a thorough study of experimental procedure.

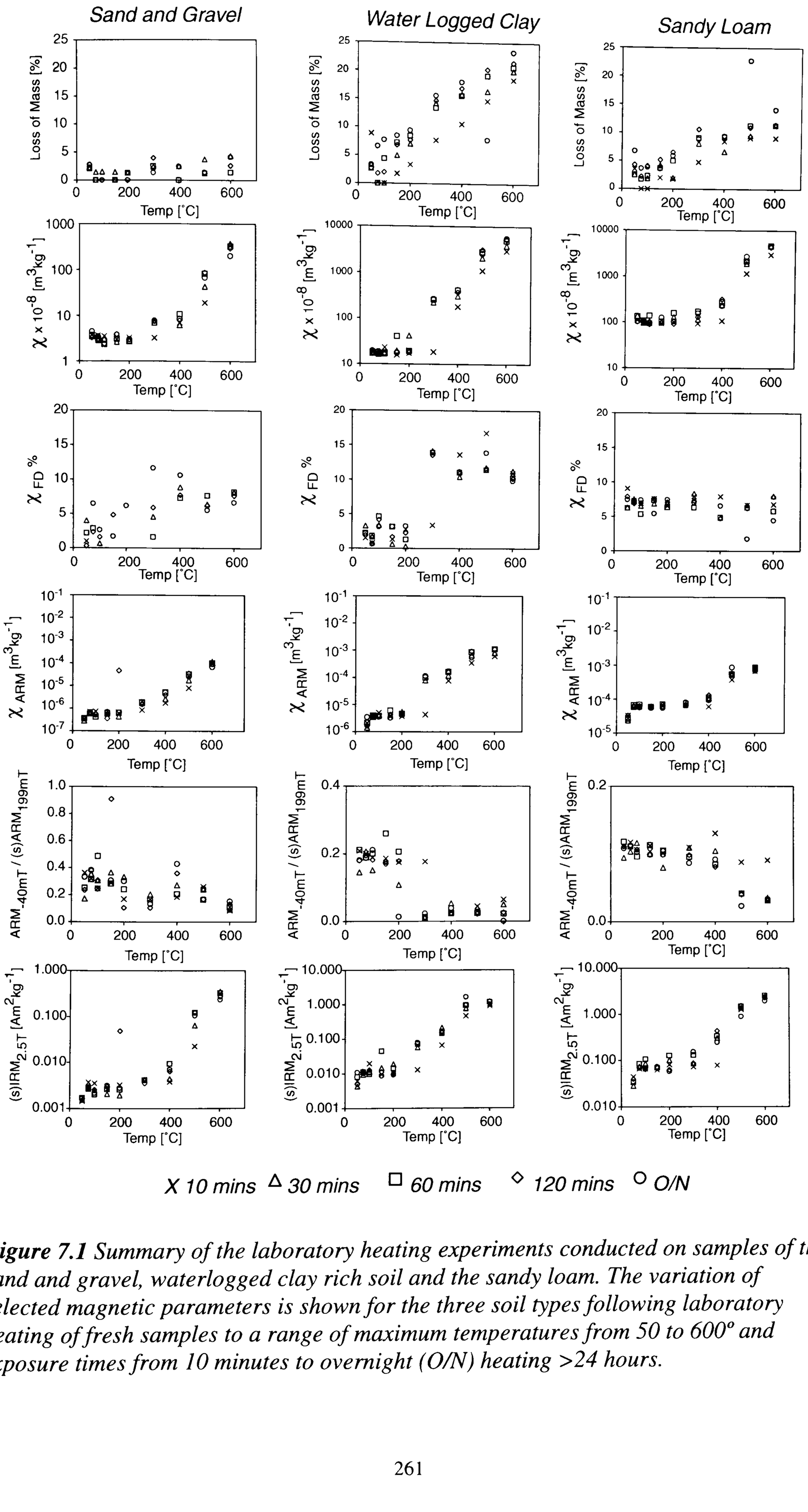


***Figure 7.1*** *Summary of the laboratory heating experiments conducted on samples of the sand and gravel, waterlogged clay rich soil and the sandy loam. The variation of selected magnetic parameters is shown for the three soil types following laboratory heating of fresh samples to a range of maximum temperatures from 50 to 600° and exposure times from 10 minutes to overnight (O/N) heating >24 hours.*

The resulting samples were all measured for loss of mass and a suite of magentic parameters. Selected samples were also subjected to in field hysteresis measurements and low/high temperature thermomagnetic analysis.

### *7.2.1 Results of the laboratory heating experiments*

Figure 7.1 provides a summary of results from the laboratory heating experiments for selected parameters discussed in more detail below.

#### *7.2.1.1 Loss of mass*

The percentage loss of mass after heating shown in Figure 7.1 gradually increases with temperature for both the clay and sandy loam soil types. Loss of mass on heating may be caused by both the evaporation of water or the combustion of constituent organic matter. In this respect it is not surprising that the sand and gravel substrate demonstrates only a marginal (<5%) loss of mass at 600°C compared to the more organic rich water logged clay that shows the greatest variability losing ~20% of its original mass at the same temperature. It is of interest to note the apparent increase in this parameter that occurs for the clay at 300°C and the correlation with the magnetic enhancement discussed below. This possibly represents the ignition of organic matter in the soil resulting in both the dehydroxylation of constituent clay minerals and the onset of strongly reducing conditions for the thermal alteration of weakly magnetic iron oxides.

#### *7.2.1.2 Variation of magnetic susceptibility*

The susceptibility of all three soil types increases by at least two orders of magnitude when heated to the maximum temperature of 600°C. Distinguishable enhancement of $\chi$ occurs at approximately 300°C for the sand and gravel and clay soils but is less evident for the sandy loam at the same temperature. It is of interest to note that at 300°C the degree of enhancement for the sandy loam is directly related to the length of exposure, suggesting thermal alteration begins but is not fully evident until the substrate is heated to 400°C. From this data it would appear that measurements of $\chi$ alone are insufficient to identify burning below a temperature of 400-500°C when the enhancement is seen to increase by order of magnitude for all three substrates.

The variation of $\chi_{FD}\%$ reflects the concentration of fine grained superparamagnetic (SP) material in the sample that is often associated with magnetic enhancement through burning (e.g. Thompson and Oldfield 1986, Dearing et al. 1996a). In this case, both the sand and gravel and clay soils demonstrate a significant increase in $\chi_{FD}\%$ above 400°C. However, this parameter remains almost constant for the sandy loam throughout the entire range of experimental temperatures suggesting either no significant increase in the concentration of SP particles occurs on heating or the degree of grain-grain interaction subdues the magnetic behaviour of this very fine fraction.

*7.2.1.3 Variation of anhysteretic remanent magnetisation (ARM)*

The variation of $\chi_{ARM}$ is similar to magnetic susceptibility and demonstrates little increase with temperature for both the sand and gravel and the clay soils below 300°C and below 400°C for the sandy loam. Above these critical temperatures both the clay and sandy loam soils display an abrupt increase opposed to the more gradual enhancement of the sand and gravel. In all three instances the increase is almost certainly due to the onset of thermal alteration of a more weakly magnetic mineral. It is of interest to note that, unlike the enhancement of $\chi$, the degree of alteration apparently depends more critically on the maximum temperature attained rather than the total length of exposure.

Although $\chi_{ARM}$ is strongly dependent on particle size, the data presented in Figure 7.1 is more likely to reflect an increase in the concentration of enhanced material opposed to real variation in the average grain size present. Normalisation by a strongly concentration dependent parameter such as $\chi$ or (s)$IRM_{2.5T}$ will more readily express alteration of the mineral type or average grain size present.

The stability of $\chi_{ARM}$ to a subsequent 40mT peak AF demagnetising field will indicate the relative coercivity of the material retaining the anhysteretic remanence. This parameter, normalised by the (s)$ARM_{199mT}$ demonstrates a reciprocal behaviour to that of the $\chi_{ARM}$ enhancement suggesting the material developed through thermal alteration has a relatively low coercivity. It is noted that both the unheated and low temperature samples for all three substrates lose over 60% of (s)$ARM_{199mT}$ when demagnetised in the -40mT AF field.

In comparison to the $\chi_{ARM}$ there would appear to be a much greater dependence upon exposure time for the $ARM_{-40mT}$ parameter. This is particularly evident for the sandy loam where the samples heated for only 10 minutes above 400°C appear to be clearly distinguished from those subjected to the same temperatures for a longer period of time. Whilst this may well reflect a temperal dependence of the thermal enhancement (which may be significant for identifying short term exposure to fire), the normalisation of the data may well reveal increased variability by compressing the range of the graph in comparison to the $\chi_{ARM}$ data.

#### *7.2.1.4 Variation of saturation Isothermal Remanence ((s)IRM)*

The variation of the saturation remanence produced in a 2.5T applied field, $(s)IRM_{2.5T}$, with temperature is similar to the variation of $\chi$ for all three soil types, suggesting that both parameters reflect the increased concentration of enhanced magnetic minerals produced through heating. The coercivity of the samples was further investigated by applying a series of reverse fields after saturation in a forward field of 2.5T (not shown on Figure 7.1). Again the results demonstrate the critical enhancement temperatures of 300°C for the sand and gravel and the clay soils and of 400°C for the sandy loam. The coercivity of the enhanced minerals appears to be quite "soft" for both the clay and the sandy loam soils as virtually all of the $(s)IRM_{2.5T}$ is reversed by a comparatively modest –30mT field. Results from the sand and gravel suggest a considerably higher coercivity for the enhanced minerals due, perhaps, to the presence of thermally stable, high coercivity detrital minerals such as haematite.

### *7.3 Discrimination of thermal history through magnetic measurements*

#### *7.3.1 Isothermal parameter biplots*

Figure 7.2 demonstrates the ability to determine the thermal history for the three soil types through the use of isothermal parameters and ratios. Two biplots are presented showing $(s)IRM_{2.5T}$ *vs* $\chi$, that will strongly reflect the concentration of magnetic minerals within the samples and $ARM_{-40mT}$ / $ARM_{199mT}$ *vs* $IRM_{-100mT}$ / $(s)IRM_{2.5T}$, two concentration normalised ratios that reflect the bulk coercivity of the sample. The concentration of magnetic minerals apparently reflects the maximum laboratory heating temperature for all three soil types with a steady increase of both $(s)IRM_{2.5T}$ and

$\chi$. Considering each soil type separately distinguishes the samples by temperature into three distinct groups of <300°C , 300 to 400°C and >500°C. However, considerable overlap between the different soil types exists for these parameters and only the clay and sandy loam samples heated to >500°C remain fully distinct.

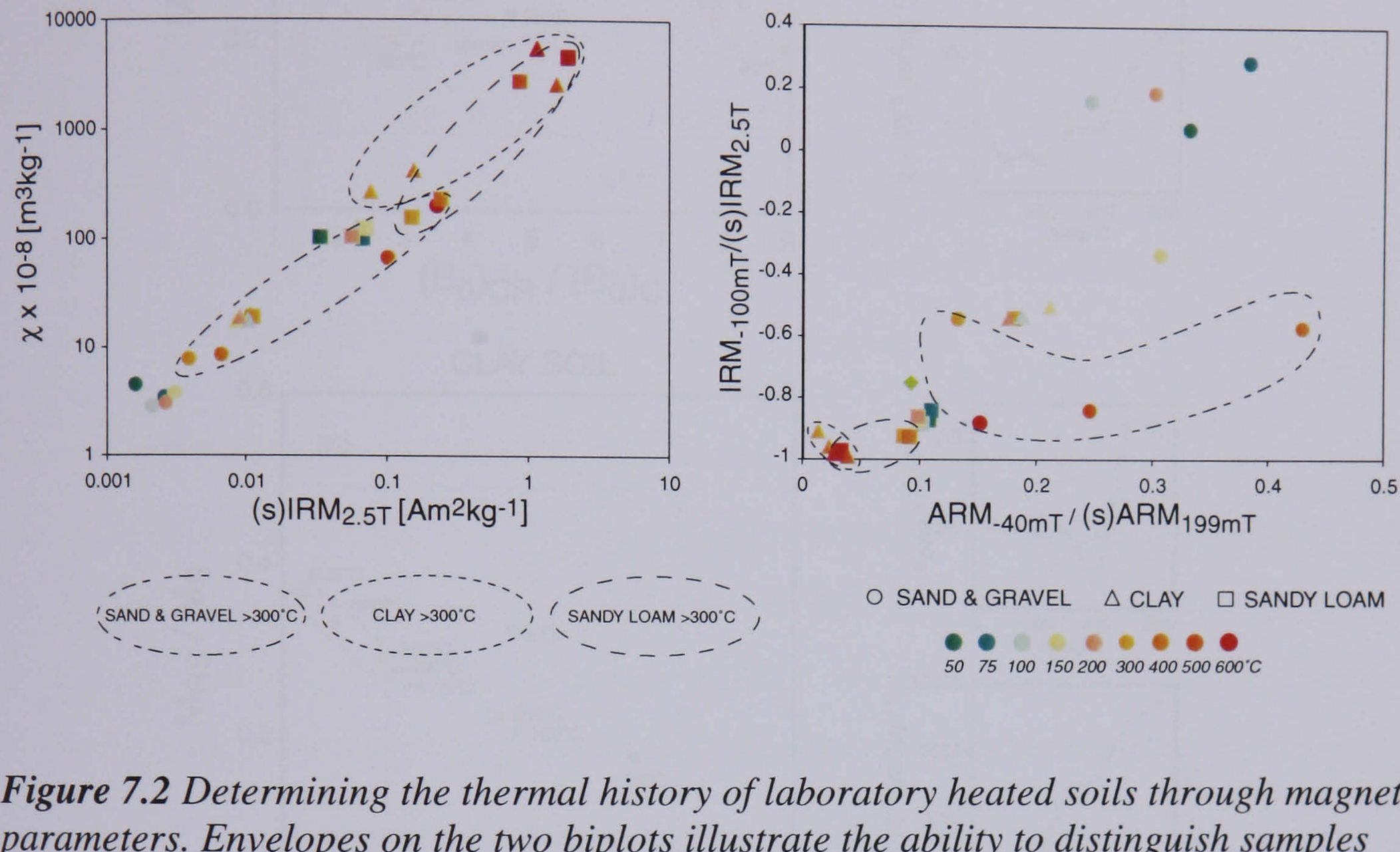


***Figure 7.2*** *Determining the thermal history of laboratory heated soils through magnetic parameters. Envelopes on the two biplots illustrate the ability to distinguish samples heated to 300°C and above.*

The bulk coercivity of the samples is also found to be dominated by increasingly "soft" magnetic minerals with temperature. The clay and sandy loam soil types heated to a maximum temperature >400°C are readily distinguished on a biplot of $ARM_{-40mT}$ / $ARM_{199mT}$ *vs* $IRM_{-100mT}$ / $(s)IRM_{2.5T}$, although this is less successful for samples of sand and gravel with a similar thermal history.

### *7.3.2 Hysteresis parameters*

In field hysteresis parameters also reflect the thermal history of the laboratory heated samples (Figure 7.3), particularly the onset of thermal alteration at low temperatures demonstrated by a loss of $\kappa_{para}$ (calculated from the high field slope of the hysteresis loop) from 50 to ~300°C. This occurs for all three soil types over the same temperature range and is due, perhaps, to the dehydration and dehydroxylation of iron minerals present as colloids within the clay fraction. For the clay soil the loss of $\kappa_{para}$ is mirrored by a corresponding decrease of $\chi$ over the same temperature range

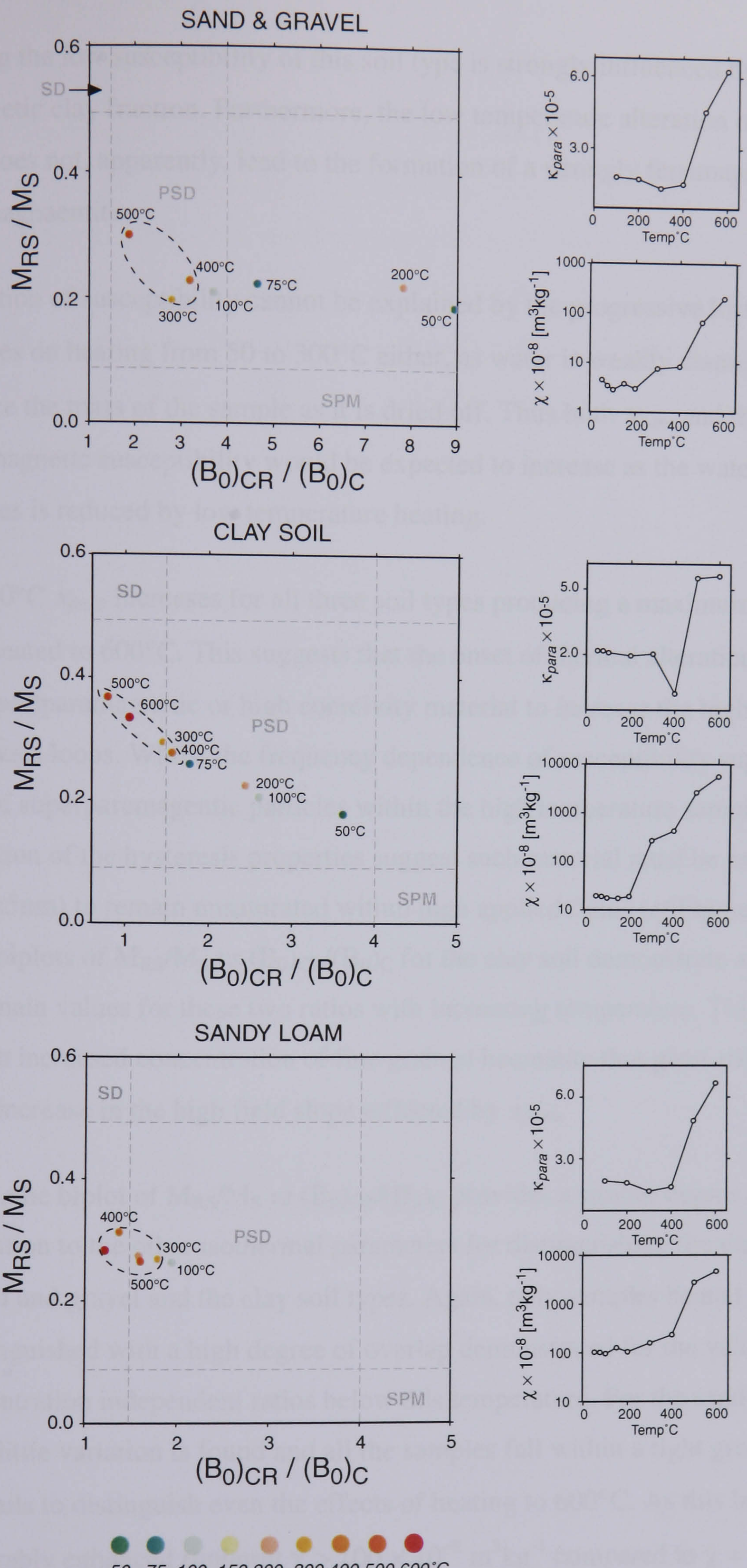


***Figure 7.3*** *Day plot showing the variation of hysteresis parameters for laboratory heated samples of the three soil types. Inset graphs show the corresponding variation of high field ($\kappa_{para}$) and mass specific ($\chi$) magnetic susceptibility.*

suggesting the low susceptibility of this soil type is strongly influenced by the paramagnetic clay fraction. Furthermore, the low temperature alteration of the clay fraction does not, apparently, lead to the formation of a strongly ferrimagnetic mineral such as maghaemite.

The variation of susceptibility cannot be explained by the progressive loss of water from the samples on heating from 50 to 300°C either, as water is weakly diamagnetic and will reduce the mass of the sample as it is dried off. Thus both $\kappa_{para}$ and the mass specific magnetic susceptibility would be expected to increase as the water content of the samples is reduced by low temperature heating.

Above 400°C $\kappa_{para}$ increases for all three soil types producing a maximum value for the samples heated to 600°C. This suggests that the onset of thermal alteration produces either (super)paramagnetic or high coercivity material to increase the high field slope of the hysteresis loops. Whilst the frequency dependence of susceptibility supports the increase of superparamagentic particles within the high temperature samples theoretical consideration of the hysteresis properties suggest such material must be extremely fine grained (<5nm) to remain unsaturated within high applied fields (*cf* Figure 1.3). In addition, biplots of $M_{RS}/M_S$ *vs* $(B_0)_{CR}/(B_0)_C$ for the clay soil demonstrate an increase in single domain values for these two ratios with increasing temperature. This may well indicate an increased concentration of fine grained haematite that gives rise to the observed increase in the high field slope reflected by $\kappa_{para}$.

In general, the biplot of $M_{RS}/M_S$ *vs* $(B_0)_{CR}/(B_0)_C$ provides a similar degree of discrimination to the other isothermal parameters for distinguishing the thermal history of the sand and gravel and the clay soil types. Again, only samples heated to >500°C are fully distinguished with a high degree of overlap demonstrated for the values of these two concentration independent ratios below this temperature. For the sandy loam soil type very little variation is found and all the samples fall within a tight group on the Day plot that fails to distinguish even the effects of heating to 600°C. As this latter soil type is considerably enhanced (unburnt $\chi > 100 \times 10^{-8}$ $m^3kg^{-1}$ compared to $\chi = \sim 10 \times 10^{-8}$ $m^3kg^{-1}$ for the sand and gravel and the clay), it is possible that considerable enhancement has already occurred through either fire or other pedogenic mechanisms producing a similar distribution of magnetic minerals.

### *7.3.3 Variation of high temperature susceptibility*

The magnetic mineralogy and stability to further thermal alteration was investigated through a series of high temperature susceptibility experiments conducted on samples of the three soil types heated over night at temperatures of (100), 150, 200, 300, 400, 500 and 600°C (Figures 7.4, 7.5 and 7.6). Each of the laboratory heated samples was cooled back to room temperature, before measuring the variation of magnetic susceptibility with a Kappabridge (§3.3.3) during heating in air between 40 to 700°C and subsequent cooling back to ambient.

#### *7.3.3.1 Sand and gravel*

Samples of this soil type preheated to 150 or 200°C produce a highly similar result with minor inflections in the heating curve dominated by the thermal alteration of constituent iron minerals to a strongly magnetic phase above 400°C (Figure 7.4). The ~580°C Curie point of this latter phase suggests magnetite that is apparently stable on cooling, although oxidation to maghaemite cannot be entirely dismissed and may account for the loss of susceptibility in the cooling curve between 500°C and room temperature. The final susceptibility of these two samples is considerably enhanced suggesting heating the sand and gravel soil type to a maximum temperature of 200°C is unlikely to produce a discernible magnetic alteration.

The behaviour changes abruptly for samples preheated between 300 and 500°C that demonstrate almost reversible heating and cooling curves with a Curie point of ~580°C. This suggests that the initial annealing has converted the majority of iron minerals to a weakly magnetic, thermally stable phase such as haematite that remains unaltered during subsequent heating to 700°C. The concentration of this stable haematite phase is apparently too low to reveal a discernible Curie point, although the sample preheated to 500°C shows a Curie Point at ~610°C falling between the range of values reported for magnetite (575-585°C) and haematite (675°C).The presence of a low concentration of magnetite may be due to either an original constituent mineral or, perhaps, the incomplete conversion during the initial laboratory preheating. The

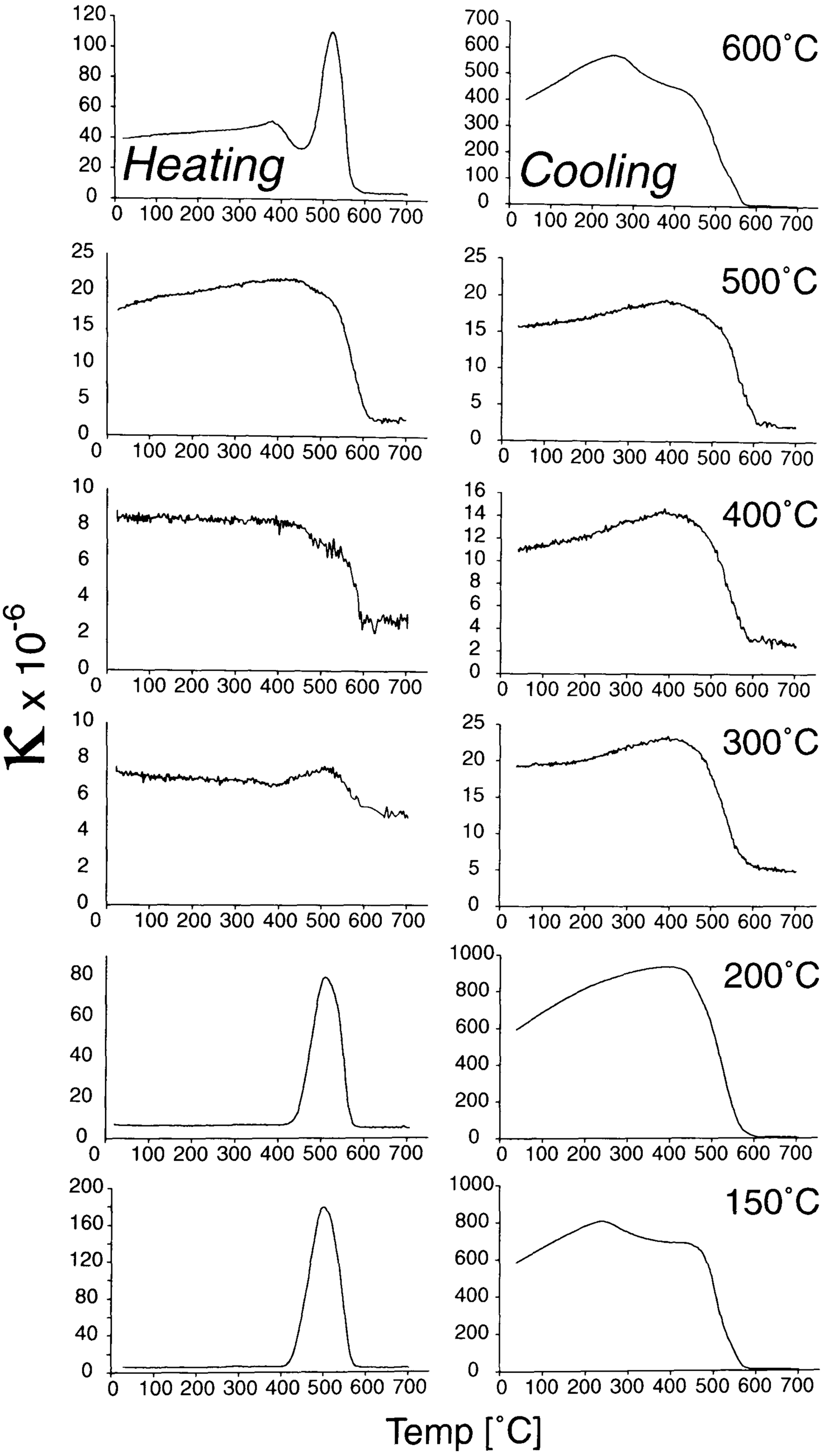


***Figure 7.4*** *Variation of magnetic susceptibility with temperature for samples of the sand and gravel soil type preheated to 150, 200, 300, 400, 500 and 600°C. Both heating(left hand column) and cooling (right hand column) measurements were made in air.*

final susceptibility of these three samples after heating to 700°C demonstrates little or no increase suggesting heating this soil type between 300 to 500°C may actually curtail magnetic enhancement.

The final sample preheated to 600°C has, as would be expected, the highest initial susceptibility ($\kappa = \sim 40 \times 10^{-5}$) and demonstrates an apparent thermal alteration at 400°C. Following this slight peak a gradual decrease in $\kappa$ indicates either an interstitial Curie point or, more likely, a further thermal alteration to a less magnetic form. Beyond 500°C a similar conversion to magnetite peak is found with a corresponding Curie point of ~580°C. On cooling the susceptibility is regained at an identical Curie point and produces a final degree of magnetic enhancement similar to the samples preheated to <300°C.

It would appear from these results that preheating the sand and gravel between 300 to 500°C produces only a slight degree of magnetic enhancement and produces a diagnostic, thermally stable mineralogy. However, it would appear that this stable phase is only created through slow heating to 500°C and cooling under oxidising conditions back to an ambient temperature. Samples preheated to temperatures <300°C and subsequently rapidly heated in the Kappabridge show a much greater degree of volatility and fail to produce the stable magnetic phase.

An explanation for this behaviour may be the slow dehydration of goethite to haematite between 250-400°C (Cornell and Schwertmann 1996; pp352-6) that has recently been further investigated by Özdemir and Dunlop (2000). This latter work found that on heating goethite in air between temperatures of 155-610°C both goethite and haematite remained the dominant magnetic minerals with the exception of samples heated to 500°C and 610°C where only haematite was formed. Furthermore, partially dehydrated goethites created through heating between 238°C to 402°C produced broad peaks or inflections in the low temperature magnetisation curves around 120 K, suggesting the formation of an intermediate spinel phase.

It is possible that a similar intermediate spinel may form the dominant alteration product from goethite during preheating of the sand and gravel samples between 300-500°C. However, if such an intermediate phase does indeed exist it would appear to be highly

sensitive to either the length of exposure to the critical temperature range or immediate cooling in air once the temperature has been attained. This would then explain why a similar alteration does not occur for previously unheated samples of the same soil type heated through a similar critical temperature range during the measurement cycle of the Kappabridge.

Conflicting evidence exists for the alteration products formed from goethite above 500°C with reports of both maghaemite (550°C) and magnetite (>600°C) (Cornell and Schwertmann 1996). In the current experiments the sample heated to 500°C produced the most stable mineral phase although it seems likely that varying heating regimes and atmospheres will have an influence over the final alteration products. When preheated to 600°C the goethite apparently dehydrates to maghaemite, accounting for both the increased initial value of κ and the loss of susceptibility at ~450°C that may be attributed to the conversion of maghaemite to haematite (Dunlop and Özdemir 1997; p59). Reduction of all iron oxides to magnetite subsequently occurs at ~520°C resulting in an apparent Curie point of 580°C.

*7.3.3.2 Clay soil*

Results from the clay soil demonstrate the formation of a similar stable magnetic phase, suppressing further thermal enhancement, but only for the sample preheated to 400°C (Figure 7.5). This latter sample is itself, slightly enhanced compared to the unheated clay soil and apparently contains an additional stable magnetite component that dominates the susceptibility producing reversible heating/cooling curves with a Curie point of 580°C.

The origin of the magnetite may be explained by the samples preheated to 200°C that show a distinctive 'M' shaped heating curve with an initial increase of susceptbility occuring between 240-300°C. This subsequently decays to a local minimum at ~420°C before the production of magnetite occurs at 500°C similar to the peak found in the sand and gravel samples. The 580°C Curie point is reversible on cooling and

# Clay soil

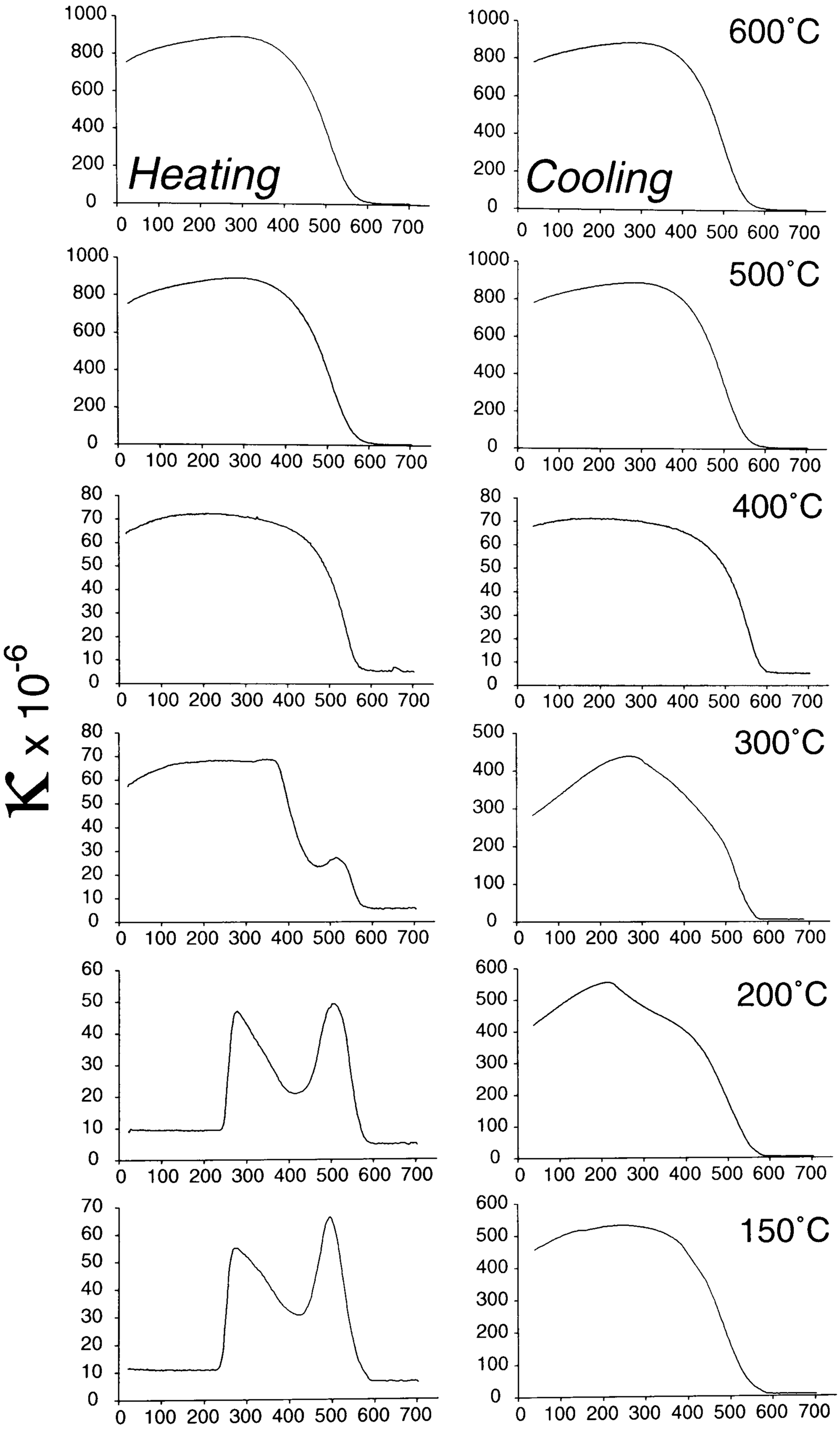


***Figure 7.5*** *Variation of magnetic susceptibility with temperature for samples of the waterlogged clay soil type preheated to 150, 200, 300, 400, 500 and 600°C. Both heating (left hand column) and cooling (right hand column) measurements were made in air.*

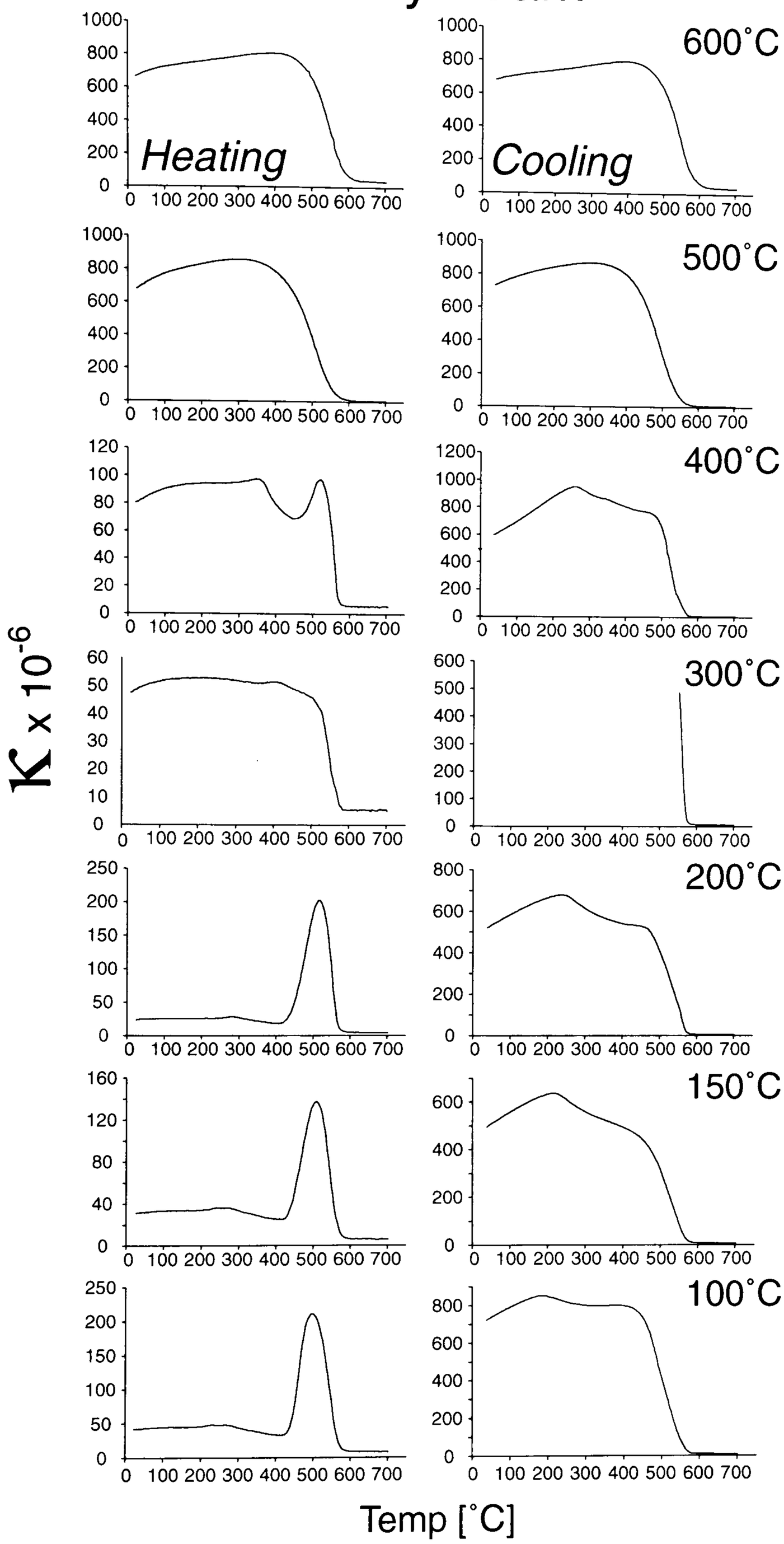


***Figure 7.6*** *Variation of magnetic susceptibility with temperature for samples of the sandy loam soil type preheated to 100, 150, 200, 300, 400, 500 and 600°C. Both heating (left hand column) and cooling (right hand column) measurements were made in air. The sample preheated to 300°C suffered instrument failure during cooling.*

the final susceptibility demonstrates a considerable degree of magnetic enhancement. Samples preheated to 300°C exhibit an intermediary behaviour having already passed through the non-reversible alteration between 240 to 300°C noted above.

Preheating the clay soil above 500°C produces a highly enhanced sample apparently dominated by stable magnetite producing reversible heating/cooling curves and no further thermal ateration.

Results from the clay soil type are similar to the anthropogenically modified soils investigated by Marmet et al. (1999) where the peak in susceptibility at 300°C was explained by the dehydration of lepidocrocite to maghaemite at 220-300°C (Özdemir and Banerjee 1984, Gehring and Hofmeister 1994). Lepidocrocite occurs widely within water logged soils, such as those from the flood plain where the clay soil type was recovered, and is often visible as a bright orange mottling mineral around decayed root fibres. On further heating during the Kappabridge measurement cycle the maghaemite progressively transforms to haematite from ~300°C (e.g. Dunlop and Özdemir 1997; p59), causing the characteristic susceptibility minima at ~400°C and in the presence of organic matter the haematite will subsequently be reduced to magnetite from ~450°C.

Once the organic matter has been exhausted, oxidising conditions will prevail and conversion of the newly formed magnetite to maghaemite may occur through the cooling curve (Eyre and Shaw 1994, Fine et al. 1989). It is also likely that goethite and perhaps haematite present in the original unheated soil will convert through the same mechanism increasing the final susceptibility enhancement.

*7.3.3.3 Sandy loam soil*

Preheating samples of this soil type did not, apparently, reveal a temperature range where the formation of a stable, weakly magnetic phase suppresses any further thermal enhancement. Indeed, samples preheated from 100 to 400°C were all quite considerably enhanced following the Kappabridge measurement cycle to 700°C. Only the two samples preheated to above 400°C failed to show any additional thermal enhancement as the reversible heating/cooling curves and extremely high initial susceptibility ($\kappa > 600 \times 10^{-5}$) suggest heating to these temperatures has already produced the maximum

degree of thermal enhancement possible, apparently through the formation of stable magnetite.

The samples preheated to 100, 150 and 200°C are highly similar and demonstrate an initial increase of susceptibility to ~300°C, then a slight loss immediately above this temperature followed by a increase at 500°C due to the formation of magnetite. This behaviour is similar to that of the clay soil samples, although the initial low temperature alteration peak at 300°C is less evident due to the magnitude of the peak at 500°C. Again, it is likely that the initial alteration results in the formation of both maghaemite and a more weakly magnetic phase that remains thermally stable until conversion to magnetite at ~500°C.

Samples preheated to 300 and 400°C show a far less pronounced thermal alteration when heated to 500°C. This suggests the mineral phase formed through the low temperature annealing is stable to 500°C, above which it apparently inverts to magnetite with a Curie point of 580°C. However, unlike the sand and gravel and clay soil samples preheated to similar temperatures, additional heating to 700°C still produces a considerable degree of magnetic enhancement and suppression of the final susceptibility.

### *7.3.4 Variation of low temperature magnetisation*

Figures 7.7, 7.8 and 7.9 show the variation of low temperature magnetisation for the three soil types. In each case, results from the unheated soil are presented together with laboratory preheated samples in steps of 100°C to a maximum temperature of 600°C. For clarity, the cooling and warming curves are separated and shown with appropriately scaled axes.

The warming curves provide evidence to separate the preheated samples from the original portion of the soil type. A slight variation in the form of both the clay and sandy loam soils preheated to above 200°C is evident as these demonstrate a more rapid decay of (s)$IRM_{2.5T}$ applied between 20 and ~50K, probably due to the unblocking of superparamagnetic particles. The magnitude of (s)$IRM_{2.5T}$ imparted at both room temperature (cooling curve - $M_{300K}$) and at 20K (warming curve - $M_{20K}$) increases for the

heated samples reflecting the greater concentration of enhanced magnetic minerals produced through thermal alteration.

The cooling curves provide the most diagnostic evidence for discriminating samples preheated below 300°C as for all three soil types these demonstrate a gradual increase, as opposed to a loss of, the initial (room temperature) (s)IRM$_{2.5T}$ on cooling to 20K. This increase arises from the variation of $M_S(T)$ as $T \rightarrow 0$K which is controlled by the interaction between the two sublattice magnetisations $M_A$ and $M_B$ (§1.3.4 and §1.3.5) that will vary dependent upon the dominant remanence carrying mineral present.

*7.3.4.1 Sand and Gravel*

Samples of this soil type preheated overnight between 300 and 600°C show an almost linear loss of $M_{300K}$ on cooling between 270 → ~120K, where distinct inflection of the curve occurs. Below 120K these samples recover a small portion of $M_{300K}$ as $T \rightarrow 20$K. The sample preheated to 400°C has inflections at both ~240 and ~120K and shows a gradual increase in $M_{300K}$ between 270 → ~120K rising steeply below 120K. It is of interest to note that whilst all the $M_{300K}$ cooling curves contain a distinct Verwey type transition at ~120K it is not possible to detect a similar inflection in either the $M_{20K}$ warming curves, or the first derivitave of this data ($^{dM}/_{dT}$). This suggests the transition is, perhaps, masked by superparamagnetic unblocking in the $M_{20K}$ curves.

The inflections appearing within the $M_{300K}$ cooling curves at ~120K are similar to those observed by Özdemir and Dunlop (2000) during controlled heating of goethite in air. It seems likely, therefore, that a similar intermediate spinal phase has been created during the preheating of the samples as was suggested by the latter authors. The prevalence of similar Verwey type inflections in all of the $M_{300K}$ samples preheated from 300 to 600°C suggests that this intermediate phase has been created, in this case, through a wider range of temperatures than those reported by Özdemir and Dunlop (2000). In this respect, the length of exposure to the laboratory heating appears to be critical as only samples preheated for longer than 60 minutes produced these inflections.

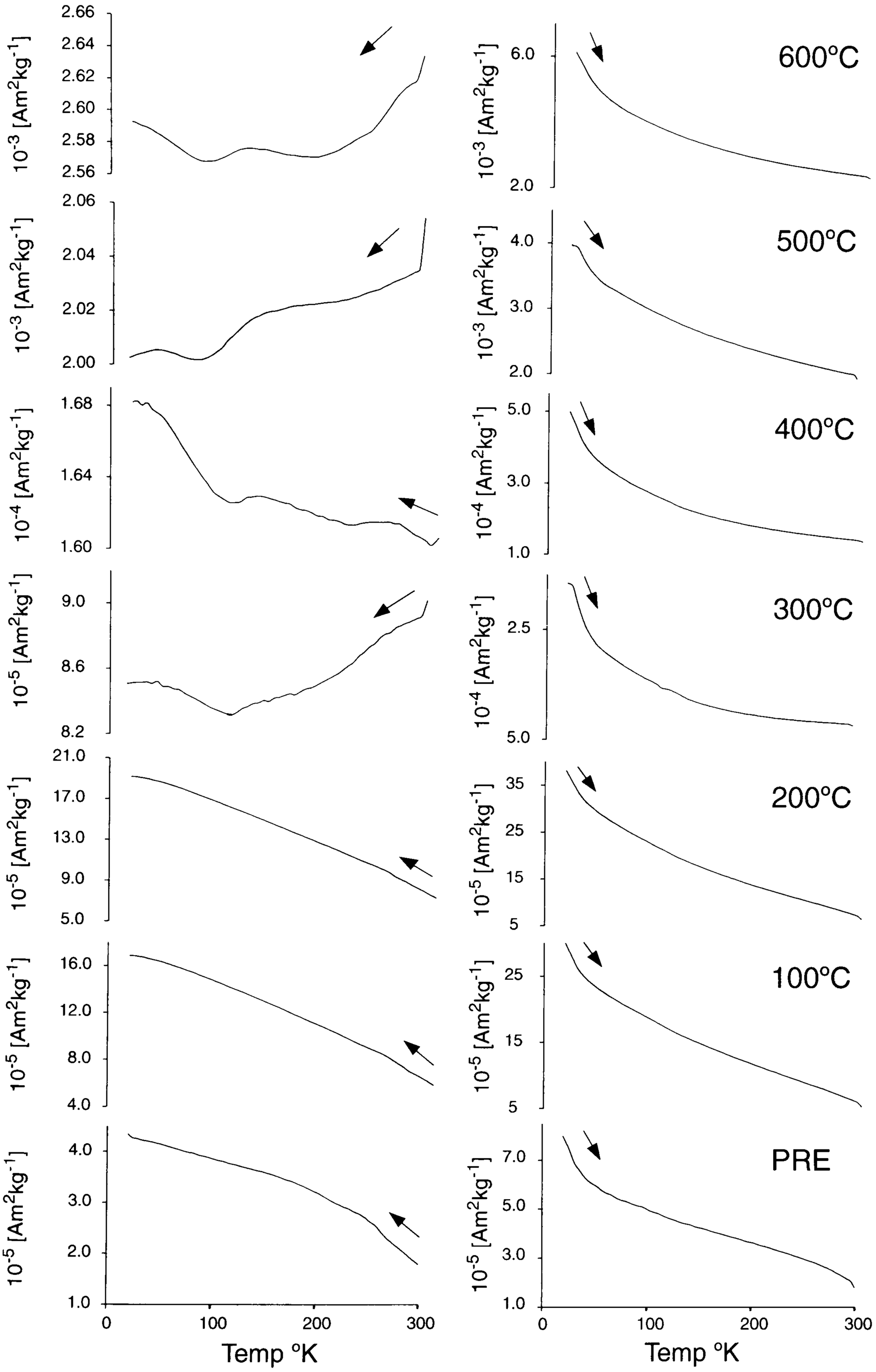


***Figure 7.7*** *Variation of low temperature magnetisation for unheated (PRE) and laboratory heated samples of the sand and gravel soil type. Sharp inflections in the cooling curves (left hand column) between 300 and 273K are due to the formation of ice from moisture present in the samples.*

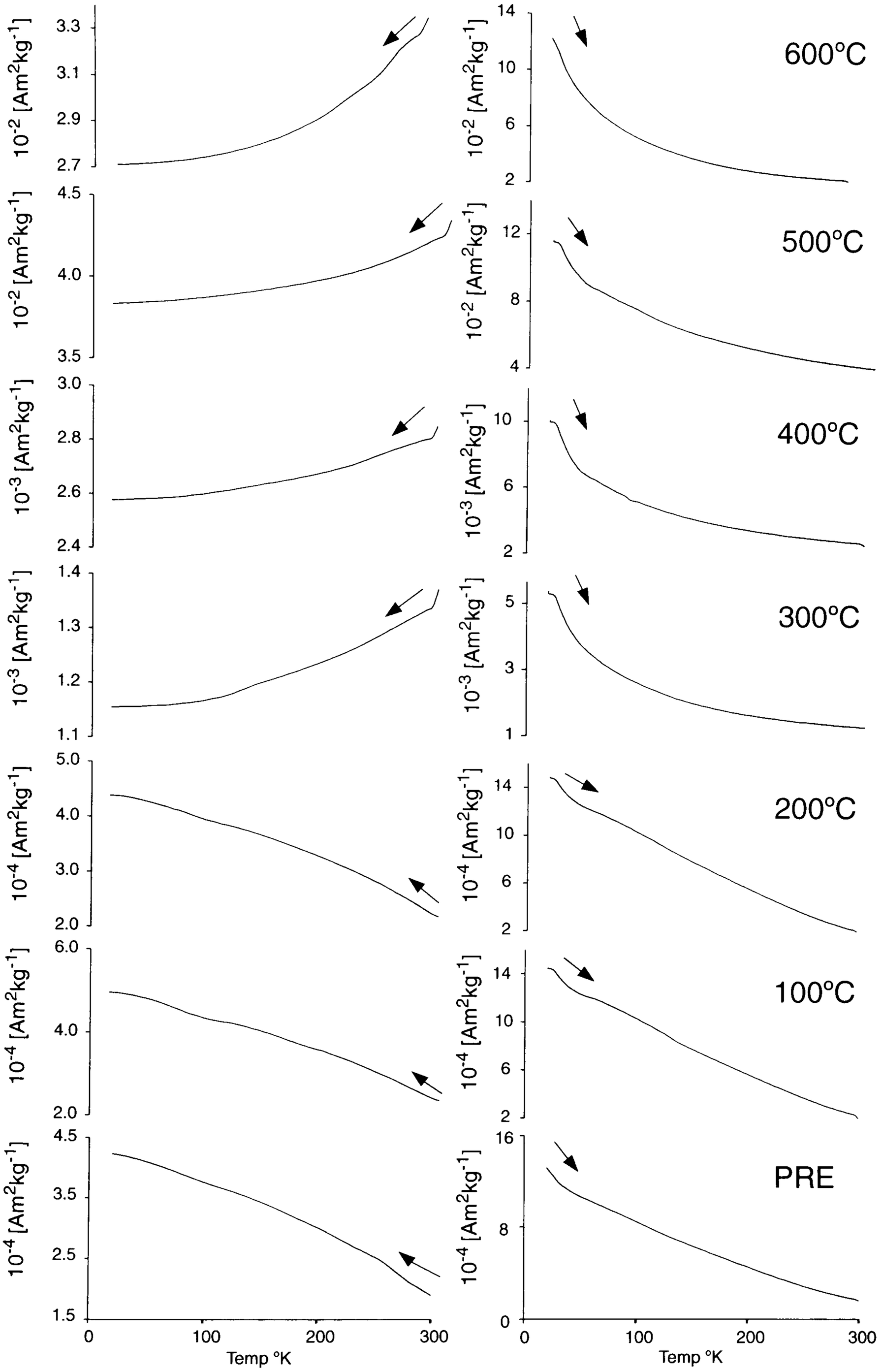


***Figure 7.8*** *Variation of low temperature magnetisation for unheated (PRE) and laboratory heated samples of the waterlogged clay soil type. Sharp inflections in the cooling curves (left hand column) between 300 and 273K are due to the formation of ice from moisture present in the samples.*

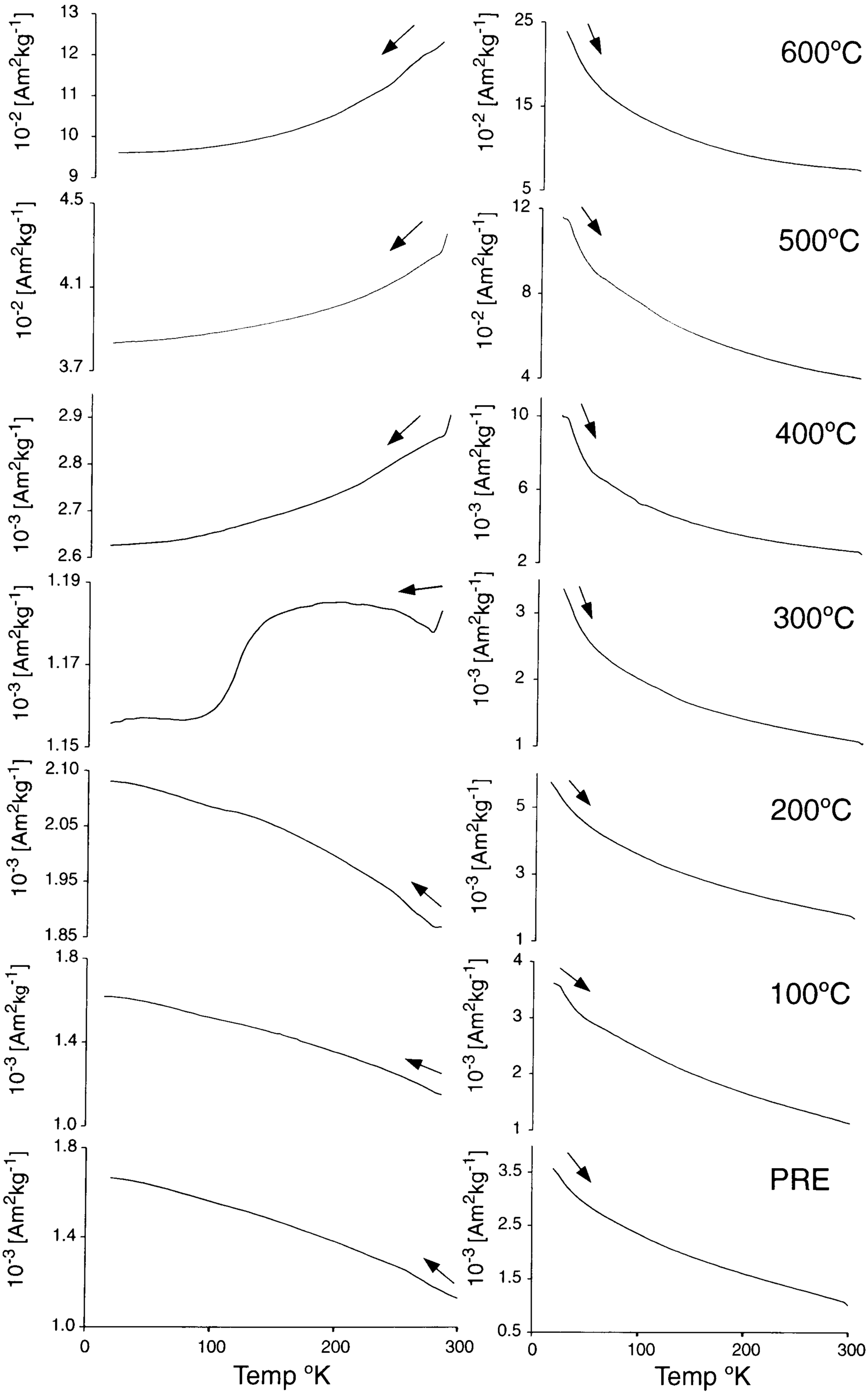


***Figure 7.9*** *Variation of low temperature magnetisation for unheated (PRE) and laboratory heated samples of the sandy loam soil type. Sharp inflections in the cooling curves (left hand column) between 300 and 273K are due to the formation of ice from moisture present in the samples.*

*7.3.4.2 Clay soil*

The clay soil preheated to <200°C demonstrate a diagnostic increase of $M_{300K}$ on cooling from room temperature to 20K that separates them from the samples preheated to above 300°C. Unlike the sand and gravel, no notable inflections are evident with the samples preheated between 300 and 600°C.

*7.3.4.3 Sandy loam*

The cooling of the remanence acquired at room temperature for this soil type is similar to the clay soil with a marked change in polarity for the variation of $M_S(T)$ between the samples preheated above 300°C. No notable inflections are found within the cooling curves with the exception of the sample preheated to 300°C that demonstrates a large loss of magnetisation between 120 and 100K, suggesting the presence of magnetite as the dominant remanence carrying mineral.

Comparison with the variation of high temperature susceptibility data (Figure 7.6) supports this interpretation and suggests that magnetite is the ultimate alteration product formed by heating this soil type to ~300°C. The apparent loss of susceptibility seen on continuous heating of samples preheated between 100 and 200°C suggests either that the initial alteration product is thermally unstable or coexists with an additional mineral phase with a higher alteration temperature. It is possible that the initial thermal alteration proceeds from goethite to maghaemite and that when heated to 300°C in the presence of sufficient organic matter the maghaemite is reduced to magnetite.

*7.3.4.4 Variation due to heating regime*

Figure 7.10 shows the variation of low temperature magnetisation for separate sub-samples of the sandy loam soil type following preheating to 300°C for varying exposure times between 10 and 120 minutes. Whilst the anomalous behaviour of the $M_{300K}$ cooling curve is evident within the sample exposed for only 10 minutes the degree of thermal alteration apparently increases with the length of exposure. Distinct variation may also be seen within the warming curves, with the apparent Verwey transition evident within the 10 and 30 minute exposures slowly smoothed with increased

exposure time due, perhaps, to an increased concentration of superparamagnetic material masking the inflection.

A similar dependence on the length of exposure is also evident for the sand and gravel and clay soil types preheated to 300°C. Again, an exposure of greater than 30 minutes is required to produce the anomalous variation of low temperature magnetisation.

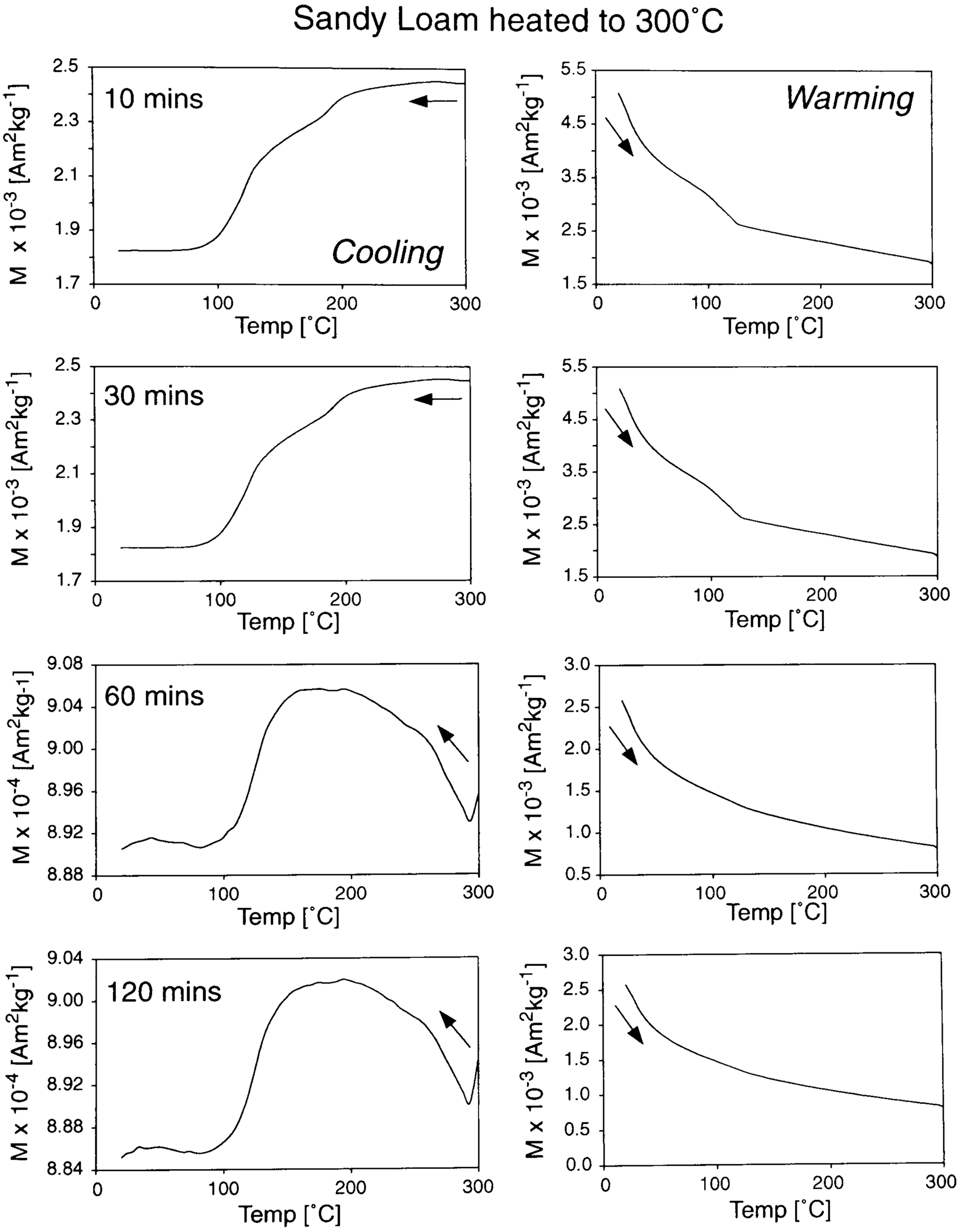


***Figure 7.10*** *Low temperature magnetisation curves for samples of the sandy loam soil type following laboratory heating to 300 ℃ for 10, 30, 60 and 120 minutes.*

*7.4 Unmixing models for burnt samples*

Figures 7.11 and 7.12 show the results of unmixing models calculated from both IRM acquisition curves and hysteresis loops for the laboratory heated samples. In this case, the end-member data sets were the same as those used to evaluate the archaeological samples discussed in §6.2.3. As fresh sub-samples of each of the unburnt soil types were used during the laboratory heating experiments some inter-sample variation would be expected.

In general, the unmixing models based on IRM acquisition curves and in-field hysteresis loops provide similar estimates of both the concentration and grain size distribution of possible end-members present within the sample. Due to the higher applied field used for the measurement of IRM acquisition curves this data is apparently more sensitive to the presence of weakly magnetic, high coercivity components within the samples. However, the ability of the IRM curves to identify increased concentrations of superparamagnetic particles is compromised by the viscous "sag" found at high applied fields that becomes evident for samples of both the clay and sandy loam soils preheated to above 300°C.

The unmixing models suggest the magnetic behaviour of the sand and gravel and the clay rich soil are initially dominated by weakly magnetic, high coercivity components for the unburnt samples. Following laboratory heating, the concentration of fine-grained magnetite-type material increases and dominates the apparent mineralogy from 300 to 400°C where the shape of both the IRM acquisition curves and hysteresis loops changes to reflect the dominance of low coercivity components.

Unheated samples of the sandy loam soil contain a higher initial proportion of magnetite type material of a similar grain size (superparamagnetic) to that apparently produced through the laboratory heating. However, both the concentration and dominance of this material over weakly magnetic haematite components increases rapidly for the samples heated to above 200°C.

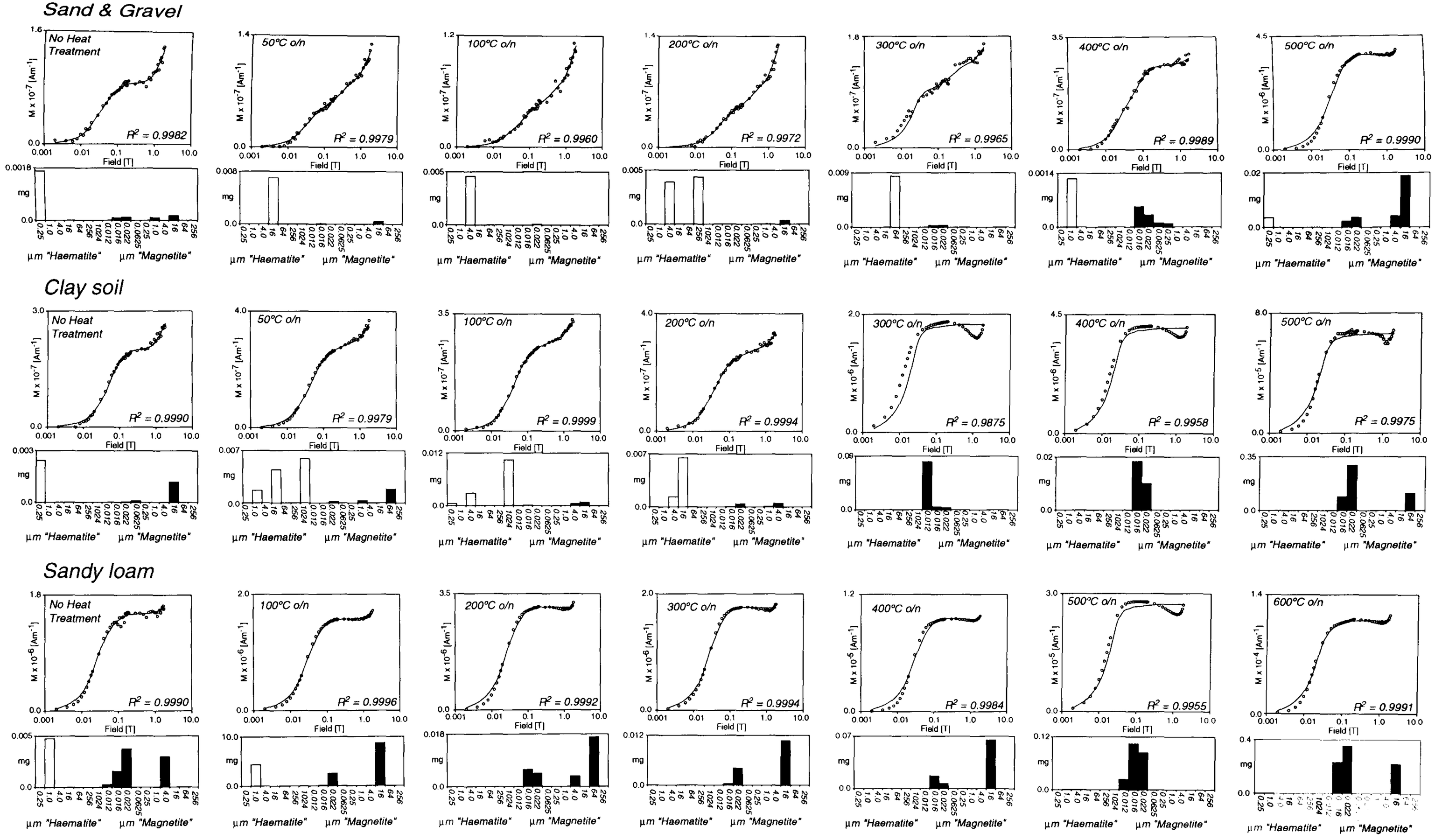


***Figure 7.11*** *Unmixing models calculated from IRM acquisition curves for the unheated and laboratory heated samples of the three soil types. The experimental data (open circles) is shown superimposed over the final model curve (solid line) together with a barchart illustrating the predicted concentration of the end-members.*

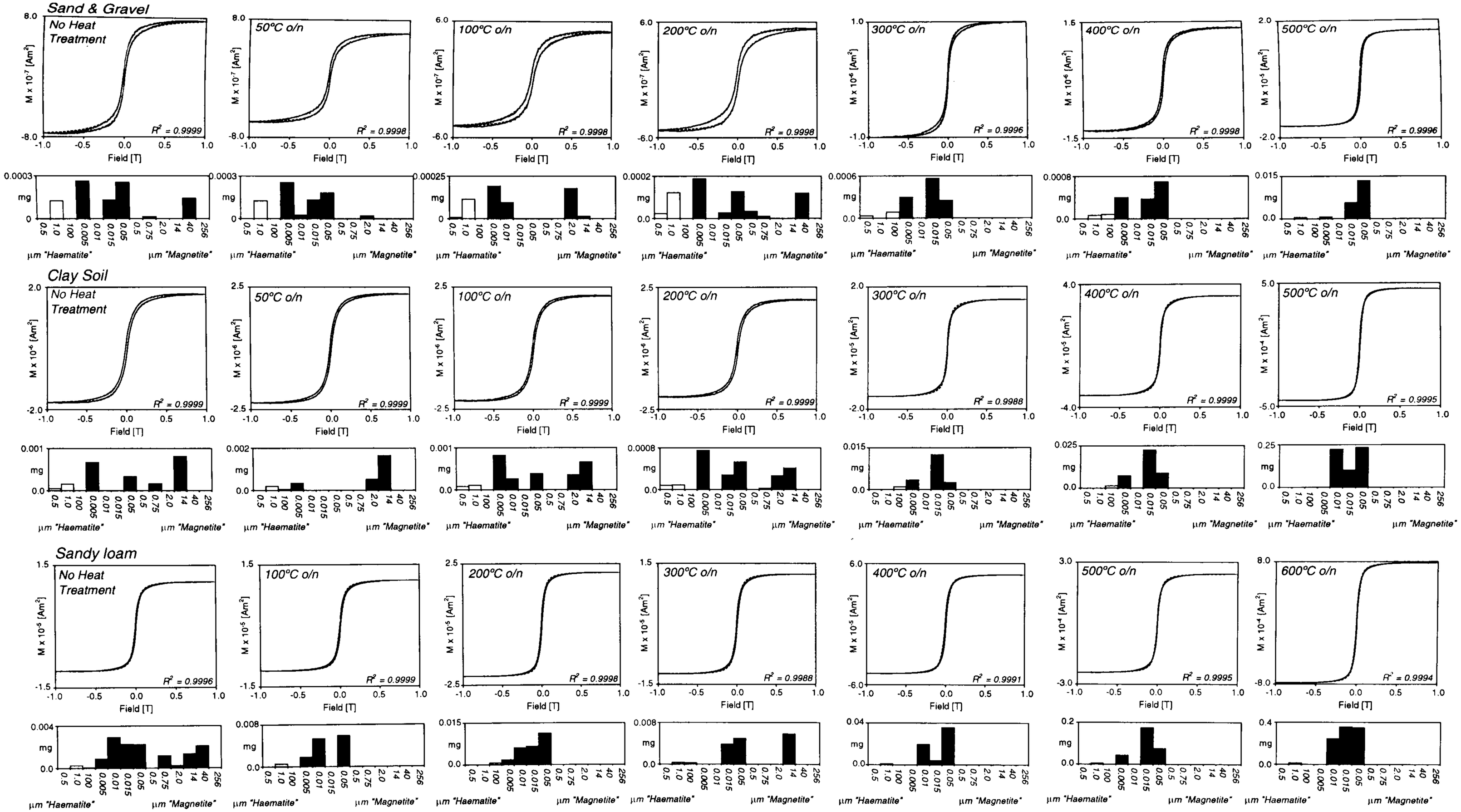


***Figure 7.12*** *Unmixing models calculated from hysteresis loop data for the unheated and laboratory heated samples of the three soil types. The experimental data (solid line) is shown superimposed over the final model curve (dashed line) together with a barchart illustrating the predicted concentration of the end-members.*

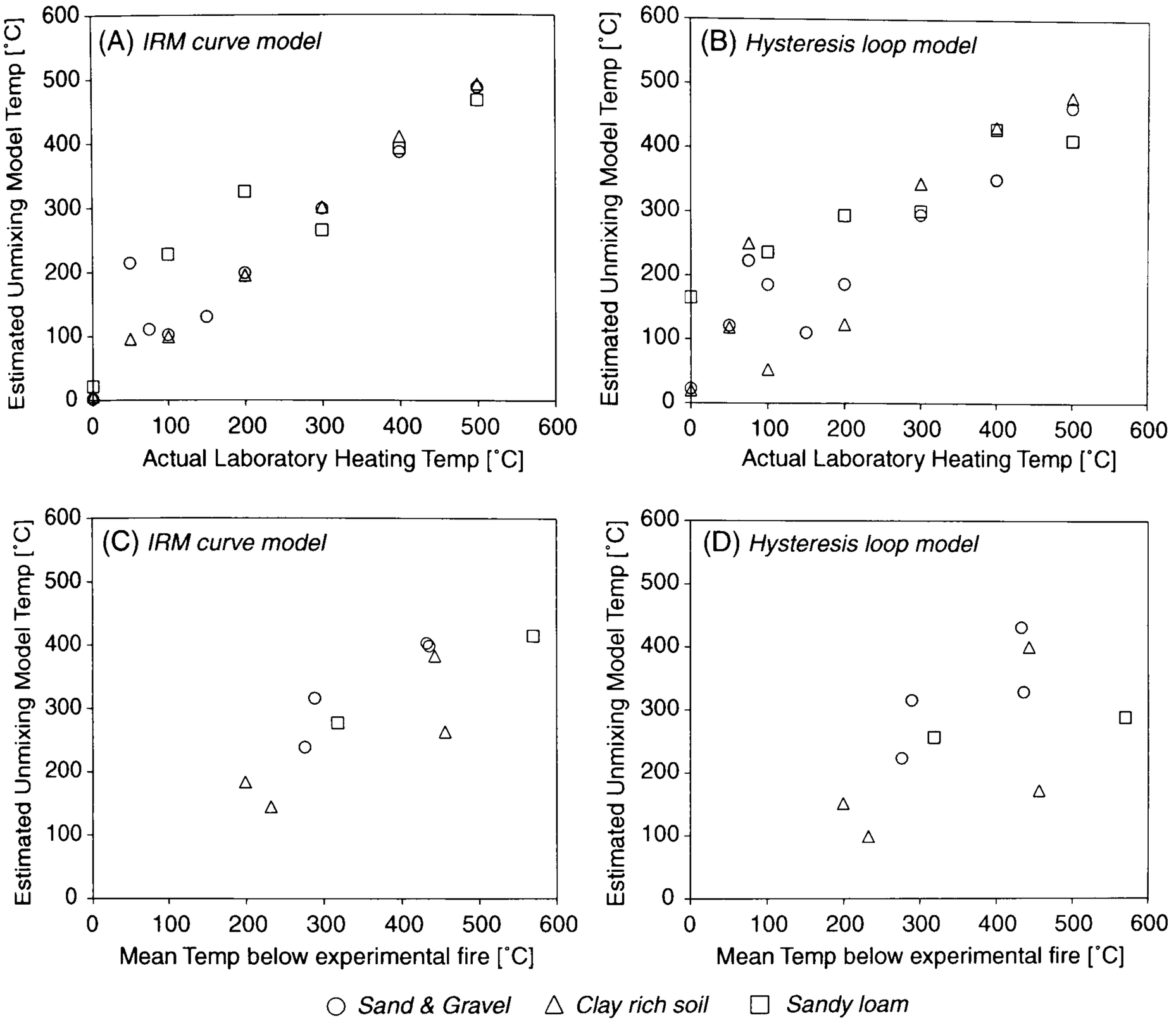


***Figure 7.13*** *Results of unmixing the unheated and laboratory heated soil samples for the three soil types against an end-member data set containing the same components. The results are presented as the known laboratory temperature plotted against that estimated by the unmixing model based on (A) IRM curves and (B) hysteresis loop data. The same end-member data set was then applied to samples recovered from five actualisitc fire experiments where the mean subsurface temperature calculated from a buried thermocouple array is compared with the equivalent temperature estimated from unmixing models based on (C) IRM curve and (D) hysteresis loop data.*

## *7.5 Unmixing models for estimation of thermal history*

### *7.5.1 Uniqueness of thermally induced hysteresis behaviour*

The varying magnetic properties of the three soil types following laboratory heating may, potentially, provide a means for determining the thermal history of a burnt sample. This assumes that burnt samples may adequately be described through some mixture of an end-member data set including the full range of laboratory heated samples. Such an end-member data set was produced for both the IRM acquisition curves and hysteresis

loops of samples heated overnight to maximum temperatures of 100, 200, 300, 400 and 500°C for all three soil types together with data for the initial, unheated soil.

The uniqueness of this end-member data set was initially tested by unmixing against its constituent members and other laboratory heated samples where the maximum temperature of exposure was also known (Figure 7.13 (A) and (B)). The temperature of each sample was estimated from the corresponding unmixing model in terms of an average based on the fraction of each end-member present. For example, an umixing model containing equal concentrations of two end-member components heated to say 100°C and 200°C respectively would be attributed to an average heating episode equivalent to 150°C ((0.5 × 100°C ) + (0.5 × 200°C )).

Figure 7.13 (A) and (B) confirms the strong linear correlation between the known maximum exposure temperature and that estimated through the unmixing model. Obviously, a suitably discrete end-member component would be expected to select itself when it is contained within the end-member data for the unmixing model. This is certainly the case for the samples heated to 300°C and above although the similarity of magnetic behaviour at lower temperatures (particularly for the Sandy loam soil) has produced a wider deviation from the known maximum temperatures.

### *7.5.2 Application to samples from the actualistic fire experiments*

Canti and Linford (2000) and Linford and Canti (2001) describe a series of actualistic fire experiments where the temperature in the soil beneath each of the experimental fires was recorded and samples of the heated soil were subsequently collected. A high degree of local variation was recorded by the subsoil thermocouple array (e.g. Canti and Linford 2000; Figure 5) and it is unrealistic to assume that the precise temperature of each of the recovered soil samples was recorded with the same accuracy as the laboratory heating experiments. However, some correlation might be expected between the maximum temperature recorded in the soil beneath each fire experiment (Canti and Linford 2000; Table 2) and the average temperature estimated by the unmixing model for soil samples recovered from the same depth beneath the ground surface.

Figure 7.13 (C) and (D) does indeed demonstrate a linear correlation between the unmixing model estimates and the maximum soil temperatures recorded by the

thermocouple array. The unmixing model slightly under-estimates the degree of soil heating but this might be expected given the highly ephemeral nature of the maximum temperature peaks recorded by the buried thermocouple array (Canti and Linford 2000; Figure 5).

The most magnetically enhanced samples from the actualistic fire experiments were recovered from the ash layer containing the residue of the spent wood fuel and burnt mineral soil obtained from either the very near surface or that adhering to the fuel itself (Linford and Canti 2001). It seems highly likely that such material would be subjected to quite extreme temperatures >400°C within the body of the fire (e.g. Linford and Canti 2001; Figure 1), although it is difficult to estimate how long this exposure would last. Certainly, maximum exposure temperatures estimated for the recovered ash samples from the unmixing model suggest temperatures of 442, 326 and 414°C for fires conducted over the sand and gravel, clay soil and sandy loam soil respectively.

### *7.5.3 Application to archaeological samples*

Results from unmixing heated soil from the actualistic fire experiments with an end-member data set based on the laboratory heated samples demonstrates a good fit to the experimental data for samples heated to above 300°C (Figure 7.13). As the deliberate use of fire is recognised as an important magnetic enhancement mechanism on archaeological sites, this end-member data set was subsequently used to recalculate unmixing models for all of the IRM acquisition curve and hysteresis loop data recovered from archaeological features (*cf* §6.3.3 and §6.3.4). A number of these samples were recovered with obvious evidence for burning (such as reddened soil or inclusions of charcoal and ash residue) and it was hoped that the unmixing model might indicate the maximum equivalent laboratory temperature to which these burnt features may have been exposed. In addition, the potential importance of fire as an enhancement mechanism may be evaluated in unburnt features, such as ditch fills or pits, where a combination of enhanced burnt material and topsoil would be expected to collect.

In comparison to the synthetic magnetite/haematite end-member data set (§6.2.3) unmixing against the laboratory heated soil produced an improved fit to the experimental data for over 75% of both the IRM acquisition curves and hysteresis loops

of samples recovered from the raised gravel terrace sites. For the flood plain sites a better fit to the experimental data was found for only 57% of the hysteresis loop models and 33% of the IRM acquisition curve models. Much of this improvement will be related to the improved calibration between the end-member and experimental data due to measurement on identical instrumentation. For example, the high field "sag", found for IRM acquisition curves of samples containing viscous material measured on the VSM, is also present within the laboratory heated soil samples (Figure 7.11). This instrumental artefact would not, alone, account for the improved quality of fit and it seems reasonable to suggest that the laboratory heated soil data represents a good analogue for archaeological enhancement mechanisms.

Figures 7.14 and 7.15 show selected results for the archaeological samples unmixed against end-member data sets formed from the laboratory heated soil for IRM acquisition curves and hysteresis loops respectively. Each figure shows the experimental data superimposed over the resulting model together with a bar chart illustrating distribution of end-member components in terms of maximum exposure temperature. A mean, equivalent exposure temperature is also given based on the average of the end-member components. The illustrated samples were selected on the basis of an improved least-mean squares fit to the experimental data and an estimated maximum exposure temperature >300°C.

It is, perhaps, not surprising that a number of samples from obviously burnt features are faithfully reproduced by equivalent mixtures of the laboratory heated soil. Good agreement is found between the IRM acquisition curve and hysteresis loop models for these samples in terms of the maximum predicted exposure temperature that generally exceeds 400°C (e.g. FP96 5485, FP98 13034, FP98 16091). Indeed, a degree of high field mis-fit within some of the model IRM curves (e.g. Figure 7.14; FP98 13033) suggests a more intense degree of thermal magnetic enhancement has occurred than is represented by the maximum 500°C laboratory heated sample within the end-member data set.

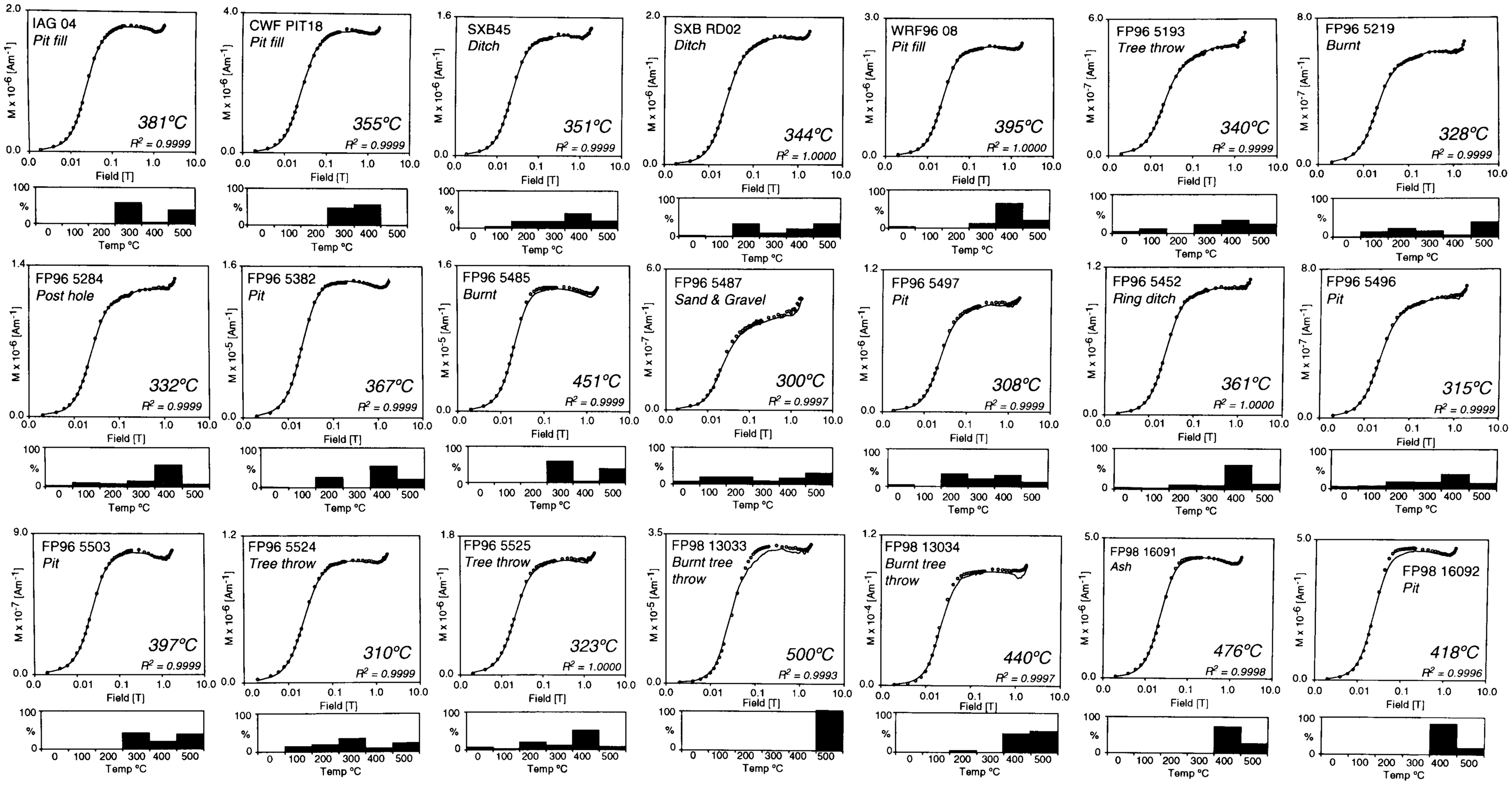


***Figure 7.14*** *Results from selected archaeological samples unmixed against the end-member data set comprising the unheated and laboratory heated soil samples for the three soil types based on IRM acquisition curves. The experimental data (open circles) is shown superimposed over the final model curve (solid line) together with a barchart illustrating the predicted concentration of the end-members in terms of the exposure temperature. An average estimated exposure temperature from the end-member components is also shown.*

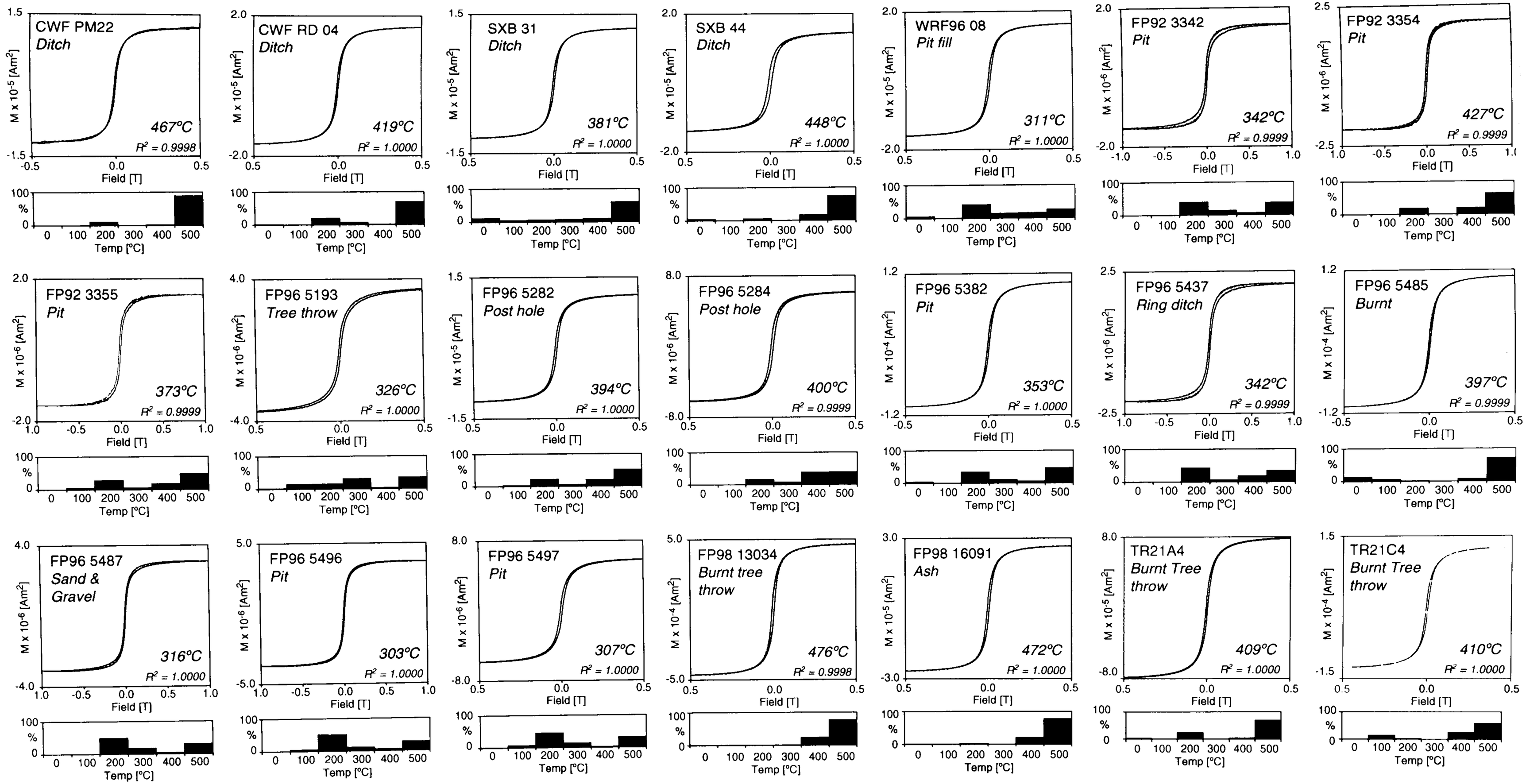


***Figure 7.15*** *Results from selected archaeological samples unmixed against the end-member data set comprising the unheated and laboratory heated soil samples for the three soil types based on hysteresis loop data. The experimental data (solid line) is shown superimposed over the final model curve (dashed line) together with a barchart illustrating the predicted concentration of the end-members in terms of the exposure temperature. An average estimated exposure temperature from the end-member components is also shown.*

### *7.5.4 Significance of burning as an archaeological enhancement mechanism*

Perhaps of greater interest than the successful unmixing models calculated for obviously burnt samples are the positive results suggesting significant quantities of burnt material within features that were not directly associated with the deliberate use of fire. The majority of samples recovered from the raised gravel terrace apparently fall within this category where both ditch and pit-type features apparently contain a quantity of burnt material derived from surrounding anthropogenic activity (e.g. CWF PM22, CWF RD04, SXB44). On the flood plain the apparent distribution of burnt material is more restricted and appears most frequently within pits and tree throw features. It is possible that this activity relates to the deliberate deposition of burnt material within waste pits and the setting of fires within the base of tree throw bowls. These latter, highly enigmatic features are often associated with lithic artefacts and it is suggested that they may have served as either temporary prehistoric shelters or, perhaps, provide evidence for deliberate fire assisted tree clearance for agriculture.

## *7.6 Discussion of the effects of fire*

The results presented in this chapter demonstrate that burnt sediments obtain both a high degree of magnetic enhancement but may also develop a distinctive magnetic behaviour diagnostic of the previous thermal history of the sample. The production of magnetically enhanced material is of obvious importance for the geophysical detection of buried archaeological features where such material has concentrated. However, estimating the thermal history, in terms of the maximum likely temperature of exposure, may well prove to be of equal importance for the interpretation of specific archaeological features.

### *7.6.1 Anomalous low temperature magnetisation curves*

The anomalous behaviour of the low temperature magnetisation curves apparently provide a means for identifying burnt sediments and soils. However, the mechanism controlling the anomalous $M_{300K}$ cooling curves is neither entirely obvious from the current data nor consistent through all the laboratory and field samples. The increase of $M_{300K}$ as $T \rightarrow 0$K for the samples subjected to a laboratory heating to <300°C is

probably explained by the increase in $M_S(T)$ over the same temperature range demonstrated by common Q-type ferrimagnets. In particular, as goethite is close to its Curie temperature at 300K and often shows a reversible increase in $M_S(T)$ during zero field cooling to 77K (Dunlop and Özdemir 1997; p75). This behaviour appears to be so consistent that Dekkers and Linssen (1989) suggest that it may be used as a diagnostic, non-destructive method for identifying the presence of this mineral. The behaviour of samples heated above 300°C are more difficult to explain and the following mechanisms have been considered:

(1) *Conversion of goethite to haematite / maghaemite at 300 °C* it is possible that $M_{300K}$ is dominated by remanence held by goethite within the samples. Preheating to 300°C will progressively increase the conversion of this mineral to an alteration product with a less marked increase of $M_S(T)$ as $T \rightarrow 0K$. However, this mechanism would not directly account for the observed decrease in $M_{300K}$ identified in all three substrates. It is possible that the intermediary spinel identified during the controlled dehydration of goethite in air by Özdemir and Dunlop (2000) may account for the anomalous decrease in $M_{300K}$.

(2) *Formation of a P-type ferrimagnet*[1] *on heating to 300 °C* would explain the decrease in $M_{300K}$ but such behaviour is uncommon within the suspected alteration products created after heating to this temperature. For example, from the measured moment of maghaemite at 0K Weiss and Forrer (1929) predict a saturation magnetisation of 82.5 $Am^2kg^{-1}$ compared to the room temperature value of 74.3 $Am^2kg^{-1}$.

(3) *Formation of a non-saturated ferrimagnet* apparent P-type behaviour can arise from the non-saturation of a mineral phase at low temperature in high coercive force minerals (Dunlop and Özdemir 1997; p33). However, in this case the most likely products of thermal alteration will be magnetite, maghaemite and haematite and it is reasonable to suggest that all of these would be saturated in a 2.5T field.

[1] For ferrimagnets the temperature dependence of the two sublattice magnetisations may vary independently. Diagnostic types of ferrimagnetic behaviour with temperature are recognised with P-type material demonstrating a loss of net saturation magnetisation with falling temperature (O'Reilly 1984; Figure 3.16).

(4) *Reverse remanence from the dehydration of lepidocrocite* the antiferromagnetic Néel point of lepidocrocite is below room temperature and the mineral is thus in capable of carrying a remanence induced at 300K. However, on heating to 250°C lepidocrocite dehydrates to maghaemite that will invert to haematite on further heating to ~400°C. Laboratory investigation of this alteration (Özdemir and Dunlop 1993) revealed the intriguing observation that the final remanence formed in the conversion to haematite could be at an angle of up to 180° from that in the interstitial maghaemite phase. Whilst this mechanism could, in theory, provide an explanation for the anomalous decrease of $M_{300K}$ of the samples preheated to above 300°C, it is questionable as the laboratory heating was conducted on unconsolidated, powdered samples. Thus the mechanism could only be of importance if a mixed phase of maghaemite / haematite was created with opposed easy axes carrying the 300K remanence and differing $M_S(T)$ curves.

(5) *Verwey type transition* there is strong evidence in both the sand and gravel and sandy loam heated above 300°C for a sharp transition in $M_{300K}$ at ~120K. Whilst this would certainly account for a well defined decrease in $M_{300K}$ it does not explain the far smoother decay that occurs for the sandy loam samples preheated between 400 to 600°C and the more irregular behaviour of the sand and gravel samples preheated over a similar temperature range. Certainly, it seems unlikely that the smoother decrease in $M_{300K}$ illustrated by all of the clay soil samples preheated above 300°C could be explained by the smearing of a Verwey type transition over such wide (300 to 20K) temperature range.

(6) *Viscous remanence loss* perhaps the simplest explanation for the smooth decrease of $M_{300K}$ is provided by consideration of the viscous loss of remanence with time over the measurement period (~1 hour) of the low temperature cooling curve. To test this theory the viscous decay of an identical remanence imparted at 300K in a 2.5T field was measured for samples of all three substrates subjected to various degrees of laboratory heating. The normalised results (Figure 7.16) demonstrate that, with the exception of the clay rich soil, there is no consistent increase in magnetic viscosity following laboratory heating over the unheated samples of three all substrates. However, as the degree of laboratory heating progresses the magnetisation of the

sample becomes dominated by fine grained, highly viscous material and the effects of this viscous component will be more evident over the measurement period.

(7) *Complex elastic particle interaction mechanism* a final explanation may be proposed following the increased concentration of viscous particles in the preheated samples. It is possible, if these particles are in close physical contact, that they will form a complex interacting system with a range of unblocking temperatures similar to the model proposed by Stephenson (1975). On exposure to the 2.5T saturating field at 300K all the particles will share a common alignment until individual SP particles gain enough thermal energy, at the current measurement temperature, to overcome the interaction field from their nearest neighbour particles. It is further proposed that at 300K all particles are above their respective blocking temperatures and as an interacting system they will exhibit elastic properties to the degree that the magnetisation of individual particles will rotate to accommodate the thermal excursions of their nearest neighbours. As the measurement temperature is reduced larger particles will become thermally blocked and the elastic properties of the system will be disrupted to the point that thermal demagnetisation, decreasing $M_{300K}$ will occur as $T \rightarrow 0$K.

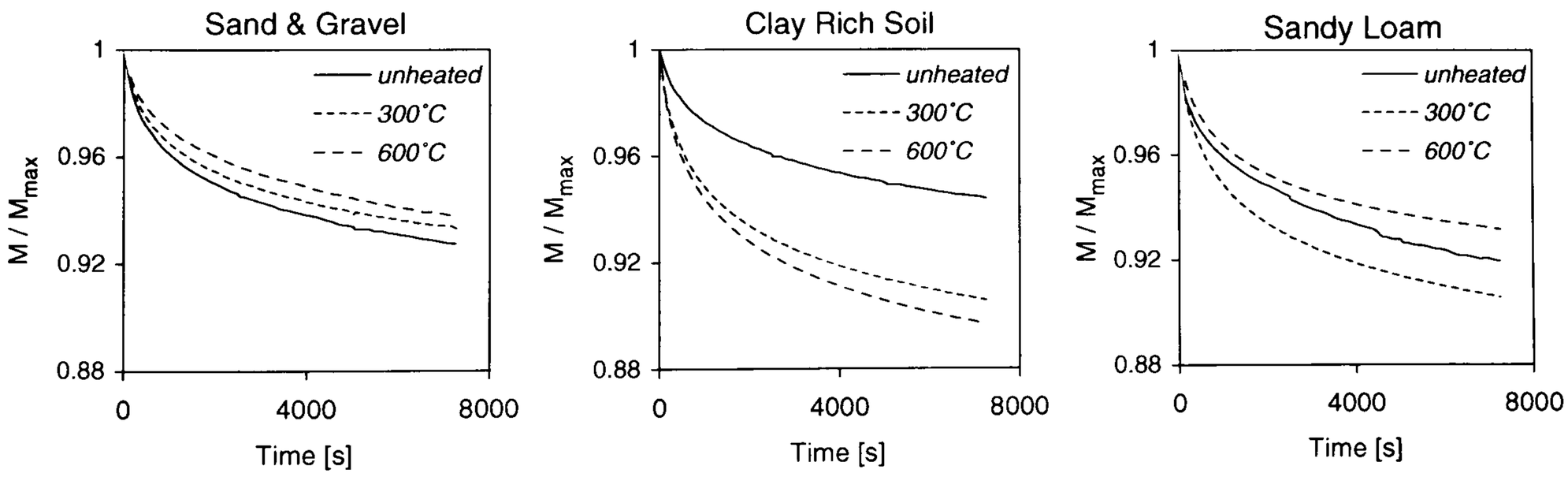


***Figure 7.16*** *Normalised viscous decay of a magnetisation acquired in a 2.5T field at 300K for the three soil types. In each case the unheated soil is compared with samples subjected to overnight laboratory heating to temperatures of 300 and 600°C. All measurements were made in zero field at 300K.*

### *7.6.2 Influence of thermal history on final high temperature alteration products*

The mechanisms discussed in §7.6.1 may also account for the variation of the maximum magnetic susceptibility obtained during the high-temperature measurement of the

laboratory heated samples (§7.3.3). In this case, laboratory heating to ~300°C instigates the thermal alteration of goethite to either maghaemite or haematite via, perhaps, an intermediate spinel form. The production of the final alteration product would appear to be critically dependent on both the soil type and the temperature regime applied during the preheating. Subsequent thermal enhancement of the preheated material reflects the thermal stability of the goethite alteration product formed with certain temperature/soil type combinations retaining an extremely low magnetic susceptibility following subsequent heating to 700°C due, perhaps, to the organic content reducing (mag)haematite to magnetite in the clay and sandy loam soils.

### *7.7 Summary*

The influence of fire as a primary magnetic enhancement mechanism for archaeological sediments and soils has been investigated through a series of actualistic experimental fires and controlled laboratory heating of representative soils from the study area. The effects of heating on the magnetic properties of soils were found to be detectable at relatively low exposure temperatures of ~100°C readily obtained under the experimental fires conducted during this research. However, exposure to temperatures >300°C results in more diagnostic magnetic behaviour that may be identified by thermomagnetic analysis (both low temperature magnetisation and variation of high temperature susceptibility). The results from the laboratory heated soil samples suggest that magnetic enhancement proceeds through the thermal alteration of goethite and lepidocrocite with a strong dependency on the heating regime, in terms of the length and maximum exposure temperature.

Semi-quantitative analysis of both laboratory heated and field samples suggest the final thermal alteration products formed are dominated by fine-grained, viscous material that may be modelled by significant concentrations of superparamagnetic magnetite. In addition, the laboratory heated samples themselves provided a successful end-member data set for describing the magnetic behaviour of many of the archaeological samples recovered for this sample. This confirms the significance of fire for the magnetic enhancement of archaeological sediments and provides a potential means for estimating the equivalent maximum temperature to which a burnt feature may have been exposed.

# *Chapter 8*

## *8.0 Discussion and conclusions*

This study aimed to investigate the variation of magnetic response encountered during the geophysical survey of archaeological remains located on an alluviated, flood plain. Previous studies suggest three main factors may influence this variation, including the depth of alluvial overburden, a shift of settlement activity to higher ground or the post-depositional dissolution of magnetic minerals. Archaeological excavation over the Yarnton flood plain eliminated the depth of alluvium as a controlling factor over the majority of sites and confirmed the continuous occupation of the flood plain from the mid-Neolithic onwards. The variation in magnetic response would, therefore, appear to be related to either the dissolution of magnetic minerals or the perturbation of magnetic enhancement processes under flood plain conditions.

This was investigated through examining the magnetic properties of samples recovered from subsequently excavated archaeological features and comparing these with the magnetic anomalies recorded during the initial magnetometer surveys. To cope with the complex mixtures of magnetic minerals and grain size populations present within environmental samples, unmixing models were developed to provide a more physically significant interpretation of the hysteresis data. This allowed the influence of both magnetic enhancement mechanisms (including the important role of fire) and post-depositional mineral alteration in water logged soils to be evaluated. Finally, forward models of the expected magnetic response from excavated archaeological features were calculated to assess the viability of more highly sensitive caesium vapour field magnetometers over fluxgate gradiometer instruments for the location of the weak magnetic anomalies such features may often produce.

## *8.1 Magnetic survey in a flood plain environment*

Perhaps the most surprising aspect of this study has been the extreme variation encountered within the magnetic response of archaeological features over an area of comparatively uniform geology and soils. Whilst the success of fluxgate gradiometer surveys has certainly been limited on the flood plain, the identification of weak

magnetic anomalies, such as the Neolithic enclosure ditch, encourages the wider use of this technique. The limited trial survey using a caesium magnetometer, augmented by numerical models, suggests high sensitivity instrumentation combined with a close sample interval might enhance the probability of detecting weak magnetic anomalies similar to those encountered over the flood plain sites. Given the recent development of low-noise, multiple sensor, cart-mounted magnetometer systems it does not seem unreasonable to suggest that similar sites would benefit from large area, detailed magnetic survey.

Large scale magnetic surveys conducted with such systems will also provide data sets for the development of spatial analytical techniques extending the limited investigation presented in this thesis (§6.5). The increasing availability of large data sets with minimal instrument or operator derived sources of noise will allow more sophisticated analysis through, perhaps, identifying subtle statistical variations within the apparent "texture" of the background underlying the data. Such variations may become more readily apparent within large-scale data sets where influences due to changes of geology, soil type or land use may be classified. Significant local anomalies within these regional variations might then be identified and related to the presence of archaeological activity.

### *8.2 Magnetic enhancement of archaeological sediments*

Isothermal magnetic measurements have proved a useful, if limited, means of classifying the degree of magnetic enhancement that archaeological sediments have undergone. These limitations are, perhaps, unsurprising given the complex mixtures of magnetic minerals and grain-size distributions present within environmental samples and overlapping magnetic behaviour demonstrated by such material. However, biplots of isothermal parameters and ratios have proved useful in isolating extremes of magnetic behaviour present within the samples, for example clearly identifying burnt sediments found at YFPB98 (Figure 5.22).

The use of more detailed hysteresis and thermomagnetic measurements has afforded a more informed analysis and classification of the underlying magnetic behaviour. For example, the characteristic 'wasp-waisted' shape of hysteresis loops from the samples of

the underlying sand and gravel substrate clearly contrast with the unconstricted loops from the magnetically enhanced archaeological features (e.g. Figure 5.13). Unfortunately, whilst the visual discrimination of such data is readily apparent, classification using hysteresis parameters based on the Day plot proved considerably less successful.

The extreme sensitivity of magnetic parameters to the influence of fire was also demonstrated through a series of laboratory heating experiments. From these experiments it was found that heating to 300°C produced a marked thermal alteration that could be detected through magnetic measurements. However, more subtle thermal alteration was also induced at temperatures below 300°C (e.g. Figures 7.3, 7.7, 7.8 and 7.9). One important aspect of this study was the comparison of the laboratory results with actualistic fire experiments to assess whether the temperatures and heating regimes produced in the laboratory served as a realistic analogue to the archaeological use of fire. The fire experiments confirmed that the critical temperatures required to promote the magnetic enhancement of soils were met. However, the limited depth in the soil profile that such temperatures reach, suggests thermal enhancement requires the continuous, concentrated use of fire to produce sufficient quantities of magnetic enhancement to account for the observed magnetic anomalies recorded over the raised gravel terrace sites.

One surprising observation is the existence of a critical preheating temperature range between 300 and 500°C where further thermal enhancement of the magnetic properties of the sand and gravel and, to a lesser extent, the clay soil, is considerably suppressed (e.g. Figures 7.4 and 7.5). Initial results suggest this may be related to the presence of organic matter within the soil type where a high concentration will result in more highly reductive heating regime due to increased competition for the available oxygen. The archaeological significance of this result is more difficult to quantify although it is possible that this mechanism may, partially, account for the lower degree of magnetic enhancement found on the flood plain. Further actualistic fire experiments should be conducted to test this theory as the current data presented in Linford and Canti (2001) suggests much of the magnetically enhanced material generated through burning is derived from soil particles attached to the fuel exposed to considerably higher temperatures.

*8.3 Semi-quantitative analysis*

The development of a semi-quantitative unmixing model based on hysteresis data to provide an indication of the mineral phase, concentration and grain-size distribution in the samples has proved particularly successful. The models constructed for this study have attempted to use more generic end-member data sets based on previously published results augmented by appropriate phenomenological models. Whilst improved end-member data sets calibrated to the applied instrumentation could, no doubt, be established, the ability of the current models to describe the experimental IRM acquisition curves and hysteresis loops confirms their fidelity (e.g. Figure 6.6 and 6.7). The use of these unmixing models has allowed complex experimental data sets to be reduced to a more readily interpreted form, avoiding the pit-falls inherent in simplified analysis of mixed magnetic systems found, for example, with the traditional Day plot. Evaluation of the optimisation algorithm employed by the unmixing models confirmed the equivalence between the Golden Rule method and the experimental use of a genetic algorithm for the majority of samples. However, the genetic algorithm did prove useful in providing a successful model for a minority of samples, that failed to produce a valid result when the Golden Rule method became trapped in a poorly fitting, local minima.

Perhaps of greater interest is the ability of the unmixing models to identify highly specific magnetic signatures within the hysteresis data, such as a significant concentration of single-domain magnetite derived from magnetotactic bacteria (e.g. Figure 6.10). Given the apparent variability encountered with other suggested magnetic tests for the presence of bacterial magnetite (e.g. Moskowitz et al. 1993, Oldfield 1999), unmixing models may be advanced as an additional means for identifying such material. In addition, the successful application of unmixing models, based on the laboratory heated soil end-member data set, confirms the importance of fire derived material for the enhancement of magnetic properties of archaeological sediments. The ability to estimate an equivalent maximum temperature of exposure from the unmixing model is also of considerable interest and may well find additional application to a range of other archaeological questions. For example, samples collected from a burnt feature for archaeomagnetic dating, such as a hearth, may not all have been exposed to the same maximum temperature when they obtained their magnetisation. The unmixing model

may allow the maximum exposure temperature for such samples to be derived, enabling the fidelity of the recorded magnetisation vector for the sample to be assessed.

Finally, the unmixing models provide a novel means for investigating weak samples that produce data with a high degree of experimental noise. By constraining models to the envelope of behaviour described by the end-member data set, a more realistic determination of hysteresis parameters may be obtained, compared to the application of a numerical smoothing function applied to the original data degraded by noise (e.g. Figure 6.2(A)).

## *8.4 Towards a quantitative model for magnetic enhancement in the study area*

### *8.4.1 Underlying sand and gravel*

A combination of the rock magnetic measurements and the results of the unmixing analysis allows a tentative model for the magnetic enhancement of archaeological sediments in the study area to be proposed. The underlying sand and gravel substrate, from which all the soils and sediments are derived, is relatively invariant across both the flood plain and the raised gravel terrace. It is dominated by weakly magnetic, high coercivity minerals apparently covering quite a wide particle size range but also contains soft, magnetite type component that gives rise to the characteristic "wasp waisted" hysteresis loops that typify this material. Thermomagnetic analysis suggests the high coercivity component is most likely to be goethite and this would account for the failure of these samples to fully saturate in the maximum 1.8T field available during this study.

### *8.4.2 The important role of fire*

Considerable evidence has been presented to support the influence of burning as a primary enhancement mechanism for many of the archaeological features. This results in a significant contribution from a superparamagnetic, magnetite type component combined with an apparently residual, high coercivity phase. Results from the laboratory heating experiments suggest the superparamagnetic phase is derived from the thermal alteration of goethite to either haematite or, more importantly, maghaemite

dependent on the temperature and organic content of the sample. Whilst this largely supports the findings of previous studies (e.g. Tite and Mullins 1971) the thermomagnetic analysis demonstrates that magnetite, as opposed to maghaemite, appears to be the final alteration product formed during laboratory heating experiments. This magnetite persists within the samples following exposure to an oxidising environment on cooling and may be discerned through the presence of a low temperature Verwey transition in both the laboratory heated samples and many of the archaeological sediments.

It seems most likely that the discrepancy between the final alteration product, produced by heating, found in the current study and that suggested by Tite and Mullins (1971), may arise from differing laboratory heating regimes applied during the experiments. The presence of fine-grained magnetite within a soil may, therefore, be due to the action of fire and not to some other pedogenic or microbial enhancement mechanism.

These findings are pertinent to the commonly encountered class of features identified as tree throw bowls. Whilst tree throw bowls often fail to produce any material artefacts there is evidence within this study to support a more common association with burning. Given the prevalence of such features over the flood plain this suggests, perhaps, widespread slash and burn tree clearance of this area to make way for prehistoric agriculture.

### *8.4.3 The influence of a flood plain environment*

Comparison between the magnetic properties of samples from the flood plain and the raised gravel terrace reveals a broadly similar relative particle size distribution for the soft, magnetite type component. However, the overall quantity of magnetic minerals does vary. The majority of (unburnt) samples from archaeological features excavated on the flood plain contain approximately half the concentration of magnetic minerals associated with similar activity on the raised gravel terrace. In addition, the most highly enhanced samples investigated during this study were recovered from burnt, prehistoric tree throw features found on the flood plain.

This, together with the strong magnetic enhancement revealed in samples from a Neolithic enclosure and a Bronze Age ring ditch, questions a universal model based on

the gradual iron mineral dissolution following the onset of flood plain conditions in the late Iron Age. Should such a mechanism dominate then the survival of a very fine-grained magnetic component would be no more expected from prehistoric features, predating the flood plain, than from those formed after these conditions were established.

The influence of the flood plain conditions would, therefore, appear to be through a more complex perturbation of active magnetic enhancement mechanisms combined with the obvious dissolution of iron minerals witnessed by gleyed soil profiles and the presence of lepidocrocite. This may be due to the prevalence of more water retentive, clay rich soils, although the laboratory heating experiments suggest that these are as receptive to thermal enhancement as the other soils in the study area. Perhaps the flood plain instigated a material shift in the intensity and variety of archaeological activity? Heavy winter flooding would discourage permanent settlement on the flood plain encouraging more seasonal occupation and perhaps the transfer of intensive domestic or semi-industrial use of fire to sites on the raised gravel terrace. The archaeological record certainly supports a migration of Anglo-Saxon settlement to the higher ground but also confirms the presence of later, post-medieval occupation on the flood plain. However, these shifts of archaeological activity are not directly reflected in the degree of magnetic enhancement found within contemporary features excavated on the flood plain.

It would seem, from the results of this study, that the lack of interest towards water logged soils expressed by Graham and Scollar (§1.1) may well have been misplaced and a greater archaeological significance cannot be discounted. Certainly, the ongoing threat posed by aggregate extraction to similar sites is quite real and provides a complex challenge for the evaluation of archaeological remains. To this end, the results from Yarnton provide a generally positive outlook suggesting that archaeological activity predating the onset of flood plain conditions will retain a detectable magnetic signature. Thus, for similar sites, determining the approximate date of the environmental change to flood plain conditions will prove critical in assessing the suitability of magnetic survey for the location of archaeological remains.

### *8.4.4 Other magnetic enhancement mechanisms*

The study has also revealed evidence for biogenic enhancement mechanisms that may well prove to be more prevalent under flood plain conditions than has been previously recognised in the limited studies conducted to date. The resulting magnetisation, retained by a combination of biogenic magnetite and an amorphous iron sulphide (most probably greigite), confirms the formation of these minerals under anoxic or micro-aerobic conditions following the onset of flood plain conditions. Whilst the fluxgate gradiometer survey failed to detect an anomaly associated with this magnetisation, models based on more sensitive field instrumentation suggest a similar response may well prove to be detectable, should an appropriate methodology be applied. Indeed, more recent research suggests both waterlogged soils and soils subjected to alternate wet/dry cycles suffer a rapid loss of superparamagnetic material (Dearing et al. 2000) that may account for the difficulty in detecting an anomaly with the fluxgate gradiometer from the biogenically enhanced ditch-section.

Perhaps of greater importance is the recovery of a stable magnetisation vector from the bacterially enhanced sediment that provided a statistically valid date when compared to the archaeomagnetic calibration curve. This date, towards the end of the Iron Age, together with the environmental conditions required for the formation of the magnetisation, allows the onset of environmental change to flood plain conditions to be identified. With this information, the success of further magnetic survey might be gauged, in terms of the likelihood of identifying significant phases of activity pre-dating the environmental change.

## *8.5 Conclusions*

It is, perhaps, naïve to suggest that the complex pedogenic processes resulting in the magnetisation of iron minerals in soils and sediments may be adequately described, even within a comparatively limited study area. Add to this complexity by introducing perturbation due to archaeological activity, post-depositional alteration and recent interference results in a seemingly impossible tangled knot of variables. Despite this apparent complexity the application of the techniques used in this study may certainly claim to have illuminated a number of the individual threads:

- Large scale fluxgate gradiometer survey successfully identified a range of significant magnetic anomalies, including responses associated with archaeological features over flood-plain sites pre-dating the change of environmental conditions. A range of other geophysical techniques failed to produce useful results.

- A marked variation of magnetic response was revealed during the study between adjacent sites on the raised gravel terrace and the flood plain. Following excavation, this variation could not be attributed entirely to the presence of alluvial overburden on the latter sites. This study shows that the variation of magnetic response may well be a consequence of both post-depositional mineral alteration within seasonally waterlogged soils and the perturbation of pedogenic enhancement mechanisms under flood plain conditions.

- Limited surveys conducted with a high sensitivity caesium vapour magnetometer were not comprehensive enough to conclusively determine the advantage of this class of instrument over more commonly applied fluxgate gradiometers. However, a theoretical comparison, based on the modelled response of such instruments, suggests increased instrument sensitivity will improve the identification of weak magnetic anomalies, such as those found over the flood plain sites. The greater availability of both caesium magnetometers and more sensitive fluxgate instruments requires further investigation through comparative survey over similar sites. Such surveys would also be able to take advantage of multi-sensor instrument configurations, increasing both the sample density and cost-effectiveness of magnetic survey compared to that available in this study.

- Isothermal measurements of bulk magnetic parameters, including susceptibility, frequency dependence of susceptibility and laboratory imparted remanences, have proved useful for distinguishing magnetically enhanced soils and sediments from the parent sand and gravel substrate. Further characterisation has been achieved through the application of more detailed hysteresis and thermomagnetic analysis that has successfully distinguished samples recovered from archaeological features. This has shown that more detailed magnetic measurements are often necessary to characterise weakly enhanced samples where (dependent on the available

instrumentation) parameters such as the frequency dependence of susceptibility may produce misleading results.

- Interpreting complex hysteresis data obtained from samples of mixed mineralogy has been greatly assisted through the construction of an unmixing algorithm and suitable end-member data sets. Successful models based on both IRM acquisition curves and in-field hysteresis loops are presented and the concept of an equivalent "apparent magnetic mixture" introduced to describe both the mineral-type and grain size distributions present. The main conclusion of this analysis suggests that, with the exception of obviously burnt sediments and soil, archaeological features, such as pits, ditches and post holes, on the flood plain contain approximately half the concentration of magnetic minerals when compared with equivalent features found on the raised gravel terrace.

- The unmixing models have allowed the influence of varying enhancement mechanisms to be discussed and have provided a means for identifying both the effects of burning and the unique magnetic assemblage associated with biogenic enhancement. The discovery of bacterial magnetite within an archaeological feature is comparatively rare due, perhaps, to the limited number of studies conducted to date. However, it is even more remarkable that a significant archaeomagnetic date carried by this biogenic material could be recovered from this sediment. Further studies are required to determine how common biogenic magnetic enhancement may be within similar, water logged environments.

- Magnetic minerals have also been shown to provide a means for determining the thermal history of particular samples. This has been achieved through both an unmixing model based on hysteresis data and a novel analysis of low temperature magnetisation data. Under controlled laboratory conditions the influence of heating may be detected from comparatively low temperatures (~100°C), although for field samples a more realistic limit of detection is, perhaps, previous heating to above 300°C. In the Yarnton samples analysis of low-temperature cooling curves reveal a diagnostic increase of magnetisation due, apparently, to the presence of goethite. The dehydroxylation of this latter mineral at ~300°C appears to account for both this

diagnostic low temperature behaviour and the suppression of thermal magnetic enhancement (when heated to a maximum temperature of 700°C) found in samples of the flood plain substrates and soils when these are preheated to between ~300 and 400°C.

- The influence of water logged conditions following the onset of the flood plain has proved highly variable and certainly does not preclude the use of magnetic survey techniques over similar sites. Whilst the unmixing models suggest the concentration of magnetic minerals is certainly reduced in samples recovered from the flood plain the distribution of the apparent grain-size population is identical to the more magnetically enhanced material from the raised gravel terrace. Despite showing a migration of Saxon settlement activity to higher ground, the archaeological record confirms the continuous occupation of the flood plain to the late medieval period.

In conclusion, environmental magnetic analysis in conjunction with both actualistic experiments and improved methods of interpretation has proved successful in constraining the processes responsible for the enhancement and concentration of magnetic minerals within archaeological features over the study area. These results correlate well with the initial magnetometer survey data and suggest the potential advantage to be gained from more sensitive instrumentation applied to similar study areas.

# *Acknowledgements*

This thesis originated through my employment with the Archaeometry Branch of the Ancient Monuments Laboratory (AML), English Heritage and was completed during fitful periods of part-time study. Despite bearing only a single author's name, such an undertaking could not have been realised without the continued, often unwitting support, of my colleagues, family and friends. Following the approximate chronology of the project I must begin by thanking my colleagues Emma Bray, Mark Cole, Pete Cotterell, Paul Linford and Andy Payne who all endured periods of inclement weather to assist me with the field work at Yarnton. Andrew David helped cajole me into undertaking this project as a further degree and has provided his continued support and geophysical distraction in roughly equal measure since its conception. The investigation of fire as an enhancement mechanism was conducted in collaboration with Matt Canti, also of the AML, who, through his concurrent doctoral research into the earthworm, convinced me that my own endeavours were not so misguided as my darkest hours often led me to believe. Other contributions to the acquisition of field data were made by Jörg Faβbinder (Cs magnetometer), Andy Brown (GPR) and Adrian Challands (magnetic susceptibility of excavation surfaces).

Additional field assistance was also provided by Steven Fear, Tom Williams and Tim Horsley, to whom my thanks is also duly proffered, during their respective placements with the AML from Bradford University. Louise Martin, a more recent recruit to the Archaeometry Branch, narrowly escaped field work at Yarnton but I am thankful for her assistance with the measurement of misplaced samples during the closing stages of this research.

The English Heritage funded excavation of the Yarnton-Cassington site was conducted most admirably by the Oxford Archaeological Unit, who never failed to offer their assistance in the pursuit of this research. Gill Hey and Chris Bell of the OAU both deserve special mention for their willingness to assist in the field, encouragement with the research and patience for the long awaited results.

I am truly thankful to my principle supervisor, Ellen Platzman (UCL), who took on my magnetometer data, bags of soil and misguided ideas and helped turn them into this thesis. This could not have been achieved without Ellen's continued support and the assistance of my co-supervisors John Milsom (UCL) and Roy Thompson (Edinburgh), who provided plentiful encouragement together with sage academic advice.

Magnetic measurement of the collected samples was greatly enhanced through two visiting travel fellowships awarded by the Institute of Rock Magnetism (IRM), University of Minnesota, Minneapolis. My visits to the IRM always proved both academically and culturally rewarding, that owes as much to staff and students of this venerable institution as it does to the marvellous, magnetic machines they command. Special thanks are due, of course, to that flipping pig. Back in the UK, I am grateful to Mark Hounslow (Lancaster University) for many useful magnetic discussions and his assistance with preparing and analysing magnetic extracts from my samples.

Essential distraction from this project was provided by my family and friends and particularly the "Oxted Crew", who nursed me through much of the production of this thesis. Angus Cox deserves special mention for his seemingly tireless interest in the

current state of my research. I can only hope that when produced in musical form, this thesis is staged with a level of set-dressing to meet with Angus' high expectations.

To close, I wish to reiterate my thanks to my brother Paul who, uniquely, falls within the classification of colleague, family member and friend. Without your inspiration, support and ability to demystify I could never have produced this thesis. But the final vote of thanks must, of course, go to our Mum and Dad for founding and nurturing the Linford geophysical dynasty.

I acknowledge, most gratefully, grants offered in financial support of this thesis provided by the English Heritage Archaeological Commissions Programme (tuition and bench fees at UCL) and the Keck Foundation (Visiting Fellowships to the IRM).

# *Bibliography*


Argyle, K. S. and Dunlop, D. J. (1990). Low-temperature and high-temperature hysteresis of small multidomain magnetites (215–540 nm). *Journal of Geophysical Research B: Solid Earth* **95**: 7069–7083.

Bailey, M. E. and Dunlop, D. J. (1983). Alternating field characterisitics of pseudo-single-domain (2-14μm) and multidomain magnetite. *Earth and Planetary Science Letters* **63**: 335-352.

Banerjee, S. K. (1970). Origin of thermoremanence in goethite. *Earth and Planetary Science Letters* **8**: 197-201.

Banerjee, S. K. (1988). Magnetic soils: magnetite sans microbes. *Nature* **336**: 314.

Banerjee, S. K., King, J. W. and Marvin, J. A. (1981). A rapid method for magnetic granulometry with applications to environmental studies. *Geophysical Research Letters* **8**: 333–336.

Bartlett, A. D. H. (forthcoming). The geophysical survey. in *Excavations at Barrow Hills, Radley, 1983-5*. (eds. E. R. Chambers and E. McAdam). Oxford, Oxford University Committee for Archaeology. The Romano-British cemetery and Anglo-Saxon settlement, Vol. 2.

Batt, C. (1997). The British archaeomagnetic calibration curve: an objective treatment. *Archaeometry* **39**(1): 153-168.

Bauminger, E. R. and Nowik, I. (1989). Magnetism in plant and mammalian ferritin. *Hyperfine Interactions* **50**: 454-498.

Bazylinski, D. A. (1991). Origin of biogenic magnetite and greigite in sediments. In *Handbook from the Environmental Magnetism Workshop*. (ed. C. P. Hunt). Minneapolis, Institute for Rock Magnetism: 181-185.

Bazylinski, D. A., Garratt-Reed, A. J. and Frankel, R. B. (1994). Electron microscopic studies of magnetosomes in magnetotactic bacteria. *Microscopy Research and Technique* **27**: 389–401.

Becker, H. (1995). From nanoTesla to picoTesla - A new window for magnetic prospecting in archaeology. *Archaeological Prospection* **2**: 217-228.

Bell, P. E., Mills, A. L. and Herman , J. S. (1987). Biogeochemical conditions favouring magnetite formation during anaerobic iron reduction. *Applied and Environmental Microbiology* **53**: 2610-2616.

Berner, R. A. (1971). *Principles of Chemical Sedimentology*. New York, McGraw-Hill.

Bevan, B. W. (1994). The magnetic anomaly of a brick foundation. *Archaeological Prospection* **1**(2): 93-104.

Bhattacharyya, B. K. (1964). Magnetic anomalies due to prism shaped bodies with arbitary polarization. *Geophysics* **29**(4): 517-531.

Bhattacharyya, B. K. and Chan, K. C. (1977). Computation of gravity and magnetic anomalies due to inhomogeneous distribution of magnetization and density in a localized region. *Geophysics* **42**(3): 602-609.

Bhattacharyya, B. K. and Navalio, M. E. (1975). Digital convolution for computing gravity anomalies and magnetic anomalies due to arbitary bodies. *Geophysics* **40**(6): 981-992.

Blakely, R. J. (1995). *Potential Theory in Gravity and Magnetic Applications*. Cambridge, Cambridge University Press.

Blakemore, R. P. (1975). Magnetotactic bacteria. *Science* **190**: 377-379.

Blakemore, R. P. and Blakemore, N. A. (1991). Magnetotactic magnetogens. in *Iron Biominerals*. (eds. R. B. Frankel and R. P. Blakemore). New York, Plenum Publishing Corporation: 51-67.

Blanco-Mantecón, M. and O'Grady, K. (1999). Grain size and blocking distributions in fine particle iron oxide nanoparticles. *Journal of Magnetism and Magnetic Materials* **203**: 50-53.

Bleil, U. and Petersen, N. (1982). Magnetische Eigenschaften der Minerale. *Landolt-Börnstein*. G. Angenheister. Berlin, Springer: 308-365.

Bohm, D. (1951). *Quantum Theory*. London, Constable and Company.

Borradaile, G. J. (1994). Magnetic remanence in the chalk of eastern England: an unusually resistant VRM? *Geological Magazine* **131**(5): 593-608.

Borradaile, G. J. (1996). An 1800-year archeological experiment in remagnetization. *Geophysical Research Letters* **23**(13): 1585-1588.

Borradaile, G. J. (1999). Viscous remanent magnetization of high thermal stability in limestone. in *Palaeomagnetism and Diagenesis in Sediments*. (eds. D. H. Tarling and P. Turner). London, Geological Society. **151:** 27-42.

Borradaile, G. J. and Brann, M. (1997). Remagnetization Dating of Roman and Medieval Masonry. *Journal of Archaeological Science* **24**: 813-824.

Borradaile, G. J., Cameron, C., Stewart, J. D. and Start, D. (1999). Magnetization Dating at a Medieval Monastery, (Tupholme, Lincolnshire). *Archaeometry* **41**(1): 175-183.

Boucher, A. R. (1996). Archaeological Feedback in Geophysics. *Archaeological Prospection* **3**(3): 129-140.

van Breemen, N. (1988a). Effects of seasonal redox processes involving iron on the chemistry of periodically reduced soils. in *Iron in Soils and Clay Minerals*. (eds. J. W. Stucki, B. A. Goodman and U. Schwertmann). Reidel Publishing, Dordrecht: 797-809.

van Breemen, N. (1988b). Long-term chemical, mineralogical, and morphological effects of iron-redox processes in periodically flooded soils. in *Iron in Soils and Clay Minerals*. (eds. J. W. Stucki, B. A. Goodman and U. Schwertmann). Reidel Publishing, Dordrecht: 811-823.

Brown, A. P. and O'Reilly, W. (1996). The magnetic hysteresis properties of ball-milled monodomain titanomagnetites, $Fe_{2.4}Ti_{0.6}O_4$. *Geophysical Research Letters* **23**(20): 2863-2866.

Brown, A. P. and O'Reilly, W. (1999). The magnetism and microstructure of pulverized titanomagnetite, $Fe_{2.4}Ti_{0.6}O_4$: the effect of annealing, maghemitization and inversion. *Physics of the Earth and Planetary Interiors* **116**: 19-30.

Brown, W. F. (1963). *Micromagnetics*. New York, Wiley.

Butler, R. F. (1992). *Paleomagnetism: Magnetic Domains to Geological Terranes*. Boston, Blackwell.

Butler, R. F. and Banerjee, S. K. (1975). Theoretical single-domain grain-size range in magnetite and titanomagnetite. *Journal of Geophysical Research* **80**: 252-259.

Canti, M. G. and Linford, N. T. (2000). The Effects of Fire on Archaeological Soils and Sediments: Temperature and Colour Relationships. *Proceedings of the Prehistoric Society* **66**: 385-395.

Carter-Stiglitz, B., Moskowitz, B. and Jackson, M. (2001). Unmixing magnetic assemblages and the magnetic behavior of bimodal mixtures. *Journal of Geophysical Research - Solid Earth* **106**: 26,397.

Challands, A. (1995). Report on the magnetic susceptibility survey at the ARC quarry, Yarnton, Oxfordshire, June 1995: 3.

Challands, A. (1998). Report on the magnetic susceptibility survey at the A.R.C. quarry, Yarnton, Oxfordshire, May 1998.

Chang, S.-B. R., Kirschvink, J. L. and Stolz, J. F. (1987). Biogenic magnetite as a primary remanence carrier in limestone deposits. *Physics of the Earth and Planetary Interiors* **46**: 289–303.

Chantrell, R. W., El-Hilo, M. and O'Grady, K. (1991). Spin-glass behavior in a fine particle system. *IEEE Transactions on Magnetics* **MAG-27**: 3570-3578.

Chester, R., Sharples, E. J., Sanders, G., Oldfield, F. and Saydam, A. C. (1984). The distribution of natural and non-crustal ferrimagnetic minerals in soil-sized particulates from the Mediterranean atmosphere. *Water, Air and Soil Pollution* **23**: 23-35.

Chukrov, F. V., Zvyagin, B. B., Gorshkov, A. I., Ermilova, L. P. and Balashova, V. V. (1973). Ferrihydrite. *Izvestiya Akademii Nauk Seriya Geologicheskaya*, **4**: 23-33.

Cisowski, S. (1981). Interacting vs. non-interacting single-domain behavior in natural and synthetic samples. *Physics of the Earth and Planetary Interiors* **26**: 77–83.

Clark, A. J. (1992). Archaeogeophysical prospecting on alluvium. in *Alluvial Archaeology in Britain*. (eds. S. Needham and M. G. Macklin). Oxford, Oxbow Monograph. **27:** 43-9.

Clark, A. J., Tarling, D. H. and Noel, M. (1988). Developments in Archaeomagnetic Dating in Britain. *Journal of Archaeological Science* (15): 645-667.

Clark, A. J. C. (1990). *Seeing Beneath the Soil*. Batsford, London.

Clark, D. H. (1984). Hysteresis properties of sized dispersed monoclinic pyrrhotite grains. *Geophysical Research Letters* **11**: 173-176.

Coey, J. M. D. (1988). Magnetic properties of iron in soil iron oxides and clay minerals. in *Iron in Soils and Clay Minerals*. (eds. J. W. Stucki, B. A. Goodman and U. Schwertmann). Dordrecht, Reidel Publishing: 397-462.

Coey, J. M. D. and Khalafalla (1972). Superparamagnetic $\gamma$-$Fe_2O_3$. *Physica Status Solidi* **A11**: 229-241.

Cole, M., David, A., Fassbinder, J., Linford, N., Linford, P. and Payne, A. W. (1999). Comparitive high resolution caesium vapour and fluxgate gradiometer survey at a range of archaeological sites in England. *Abstracts of the Archaeological Prospection Conference, Munich, 1999*, Arbeitshefte des Bayerischen Landesamtes Für Denkmalpflege.

Cole, M. A. (1995). Hoe Hills, Dowsby, Lincolnshire. Report on geophysical surveys October 1994 and March 1995, *Ancient Monuments Laboratory Report Series* **17/95**.

Cole, M. A., David, A. E. U., Linford, N. T., Linford , P. K. and Payne, A. W. (1997). Non-destructive techniques in English gardens: geophysical prospecting. *Journal of Garden History* **17**: 26-39.

Cole, M. A., Linford, N. T., Payne, A. P. and Linford, P. K. (1995). Soil Magnetic Susceptibility Measurements and their Application to Archaeological Site Investigation. in *Science and Site: Evaluation and Conservation*, (eds. J. Beavis and K. Barker). Bournemouth University, Bournemouth University.

Collinson, D. W. (1983). *Methods in Rock Magnetism and Palaeomagnetism: Techniques and Instrumentation*. New York, Chapman and Hall.

Cornell, R. M. and Schwertmann, U. (1996). *The Iron Oxides*. Weinham, VCH.

Crangle, J. (1970). *The Magnetic Properties of Solids*. London, Edward Arnold.

Cranshaw, T. E., Dale, B. W., Longworth, G. O. and Johnson, C. E. (1985). *Mössbauer spectroscopy and its applications*. Cambridge, Cambridge University Press.

Creer, K. M. (1962). On the origin of the magnetization of red beds. *Journal of Geomagnetism and Geoelectricity* **13**: 86-100.

Creer, K. M., Tucholka, P. and Barton, C. E., (eds.) (1983). *Geomagnetism of baked clays and recent sediments*. Amsterdam, Elsevier.

Crew, D. C., McCormick, P. G. and Street, R. (1998). Temperature dependence of the magnetic viscosity parameter. *Journal of Magnetism and Magnetic Materials* **177-181**: 987-988.

Crockford, R. H. and Willett, I. R. (1995a). Drying and oxidation effects on the magnetic properties of sulfide material during oxidation. *Soil Chemistry and Mineralogy* **33**: 19-29.

Crockford, R. H. and Willett, I. R. (1995b). Magnetic Properties of Two Soils During Reduction, Drying and Re-Oxidation. *Australian Journal of Soil Research* **33**: 597-609.

Dalan, R. A. and Banerjee, S. K. (1996). Soil magnetism, an approach for examining archeological landscapes. *Geophysical Research Letters* **23**(2): 185-188.

Dankers, P. H. M. (1978). Magnetic properties of dispersed natural iron-oxides of known grain-size, *PhD Thesis, University of Utrecht.*

David, A. (1994). The role of geophysical survey in early medieval archaeology. *Anglo-Saxon studies in archaeology and history*. Oxford. **7**.

David, A. (1995). Geophysical survey in Archaeological Field Evaluation. *Research and Professional Services Guideline*, **1**, English Heritage, London.

David, A. E. U. and Payne, A. W. (1993). Croughton, Northamptonshire, interim report on geophysical surveys 1992-93, *Ancient Monuments Laboratory Report Series* **15/93**.

Davis, P. M. and Evans, M. E. (1974). Interacting single-domain properties of magnetite intergrowths. *Journal of Geophysical Research* **81**: 989-994.

Day, R., Fuller, M. and Schmidt, V. A. (1977). Hysteresis properties of titanomagnetites: grain-size and compositional dependence. *Physics of the Earth and Planetary Interiors* **13**: 260–266.

Dearing, J. A. (1994). *Environmental magnetic susceptibility: using the Bartington MS2 system*. Kenilworth, Chi Publishing.

Dearing, J. A., Dann, R. J. L., Hay, K., Lees, J. A., Loveland, P. J., Maher, B. A. and O'Grady, K. (1996a). Frequency-dependent susceptibility measurements of environmental materials. *Geophysical Journal International* **124**: 228-240.

Dearing, J. A., Hannam, J. A., Anderson, A. S. and Wellington, E. M. H. (2000). Magnetic, geochemical and DNA properties of highly magnetic soils in England. *Geophysical Journal International* **144**: 183-196.

Dearing, J. A., Hay, K. L., Baban, S. M. J., Huddleston, A. S., Wellington, E. M. H. and Loveland, P. J. (1996b). Magnetic susceptibility of soil: an evaluation of conflicting theories using a national data set. *Geophysical Journal International* **127**(3): 728-734.

Dearing, J. A., Lees, J. A. and White, C. (1995). Mineral magnetic properties of acid gleyed soils under oak and Corsican Pine. *Geoderma* **68**: 309-319.

Dearing, J. A., Livingstone, I. and Zhou, L. P. (1996c). A late Quarternary magnetic record of Tunisian loess and its climatic significance. *Geophysical Research Letters* **23**(2): 189-192.

Dekkers, M. J. (1988). Some rock magnetic parameters for natural goethite, pyrrhotite, and fine-grained hematite, *PhD Thesis, University of Utrecht*.

Dekkers, M. J. (1990). Magnetic properties of natural goethite—III. Magnetic behaviour and properties of minerals originating from goethite dehydration during thermal demagnetization. *Geophysical Journal International* **103**: 233–250.

Dekkers, M. J. and Linssen, J. H. (1989). Rock magnetic properties of fine-grained natural low-temperature haematite with reference to remanence acquisition mechanisms in red beds. *Geophysical Journal International* **99**: 1-18.

Del Vecchio, R. M. (1980). An efficient procedure for modeling complex hysteresis processes in ferromagnetic materials. *IEEE Transactions on Magnetics* **16**(5): 809-811.

Dell, C. I. (1972). An occurrence of greigite in Lake Superior sediments. *American Mineralogist* **57**: 1303-1304.

Della Torre, E. and Kadar, G. (1987). Hysteresis modeling II. Accomodation. *IEEE Transactions on Magnetics* **23**(5): 2823-2825.

Diaz Ricci, J. C. and Kirschvink, J. L. (1992). Magnetic domain state and coercivity predictions for biogenic greigite ($Fe_3S_4$): a comparison of theory with magnetosome observations. *Journal of Geophysical Research* **97**: 17309-17315.

Dickinson, D. P. E., Reid, N. M. K., Hunt, C., Williams, H. D., El-Hilo, M. and O'Grady, K. (1993). Determination of $f_0$ for fine magnetic particles. *Journal of Magnetism and Magnetic Particles* **125**: 345-350.

Diebel, C. E., Proksch, R., Green, C. R., Neilson, P. and Walker, M. M. (2000). Magnetite defines a vertebrate magnetoreceptor. *Nature* **406**: 299-302.

von Dobeneck, T. (1996). A systematic analysis of natural magnetic mineral assemblages based on modeling hysteresis loops with coercivity-related hyperbolic basis functions. *Geophysical Journal International* **124**(3): 675-694.

von Dobeneck, T., Fredereichs, T., Bleil, U. and Dekkers, M. (2002). Towards the identification and quantification of sedimentary authigenic minerals such as siderite, vivianite, pyrite and rhodochrosite by their low temperature magnetic properties. *EGS-EGU Joint Assembly, Nice, France, April 2002, Geophysical Research Abstracts*.

Donald, R. and Southam, G. (1999). Low temperature bacterial diagenesis of ferrous monosulfide to pyrite. *Geochimica et Cosmochimica Acta* **63**(13/14): 2019-2023.

Dormann, J. L., Spinu, L., Tronc, E., Jolivet, J. P., Lucari, F., D'Orazio, F. and Fiorani, D. (1998). Effect of interparticle interactions on the dynamical properties of γ-$Fe_2O_3$ nanoparticles. *Journal of Magnetism and Magnetic Materials* **183**: L255-L260.

Dunlop, D. J. (1972). Magnetic mineralogy of unheated and heated red sediments by coercivity spectrum analysis. *Geophysical Journal of the Royal Astronomical Society* **27**: 37–55.

Dunlop, D. J. (1986). Hysteresis poperties of magnetite and their dependence on particle size: A test of pseudo-single domain remanence models. *Journal of Geophysical Research* **91B**: 9569-9584.

Dunlop, D. J. and Argyle, K. S. (1997). Thermoremanence, anhysteretic remanence and susceptibility of submicron magnetites: Nonlinear field dependence and variation with grain size. *Journal of Geophysical Research* **102**(B9): 20199-20210.

Dunlop, D. J. and Özdemir, Ö. (1997). *Rock Magnetism: Fundamentals and Frontiers*. Cambridge University Press, Cambridge.

Eder-Hinterleitner, A., Neubauer, W. and Melichar, P. (1995). Reconstruction of archaeological structures using magnetic prospection. *Interfacing the Past: ComputerApplications and Quantitative methods in Archaeology CAA95, University of Leiden*, Institute of Prehistory, University of Leiden.

Eggleton, R. A., Schulze, D. G. and Stucki, J. W. (1988). Introduction to crystal structures of iron-containing minerals. in *Iron in Soils and Clay Minerals*. (eds. J. W. Stucki, B. A. Goodman and U. Schwertmann). Dordrecht, Reidel Publishing: 141-162.

Ellis, C. and Brown, A. G. (1998). Archaeomagnetic dating and palaeochannel sediments: data from the mediaeval channel fills at Hemington, Leicester. *Journal of Archaeological Science* **25**: 149-163.

Eyre, J. K. (1997). Frequency dependence for populations of single-domain grains. *Geophysical Journal International* **129**: 209-211.

Eyre, J. K. and Shaw, J. (1994). Magnetic enhancement of Chinese loess - the role of γ-$Fe_2O_3$? *Geophysical Journal International* **117**: 265–271.

Fabian, K., Kirchner, A., Williams, W., Heider, F., Leibl, T. and Huber, A. (1996). Three-dimensional micromagnetic calculations for magnetite using FFT. *Geophysical Journal International* **124**: 89-104.

Farina, M., Esquivel, D. M. S. and Lins de Barros, H. G. P. (1990). Magnetic iron-sulphur crystals from a magnetotactic microorganism. *Nature* **343**: 256–258.

Farmer, D. H. (1992). *The Oxford Dictionary of Saints*. Oxford, Oxford University Press.

Faßbinder, J. W. E. (1994). Die magnetischen Eigenschaften und die Genese ferrimagnetischer minerale in boden im Hinblick auf die magnetische prospektion archaologischer bodendenkmaler. *Fakultat Geowissenschaften. Munchen, Ludwig-Maximilians Universitat:* **133**.

Faßbinder, J. W. E. and Stanjek, H. (1993). Occurrence of bacterial magnetite in soils from archaeological sites. *Archaeologia Polona* **31**: 117-128.

Faßbinder, J. W. E., Stanjek, H. and Vali, H. (1990). Occurence of magnetic bacteria in soil. *Nature* **343**: 161–163.

Fearon, M., Chantrell, R. W. and Wohlfarth, E. P. (1990). A theoretical study of interaction effects on the remanence curves of particulate dispersions. *Journal of Magnetism and Magnetic Material* **86**: 197-206.

Featherstone, R. and Dyer, C. (1994). RCHME cropmark plot. in *Yarnton-Cassington evaluation 1993*. G. Hey. London, OAU report for English Heritage**:** 56-9.

Fell, V. and Ward, M. (1998). Iron Sulphides: Corrosion products on artifacts from waterlogged deposits. in *Metals Conservation*, (eds. Mourey, W. and Robbiola, L.), James and James, France.

Fine, P., Singer, M. J., La Ven, R., Verosub, K. L. and Southard, R. J. (1989). Role of pedogenesis in distribution of magnetic susceptibility in two Californian chronosequences. *Geoderma* **44**: 287–306.

Fiorani, D., Dormann, J. L., Lucari, F., D'Orazio, F., Tronc, E., Prene, P., Jolivet, J. P. and Testa, A. M. (1997). Dynamic properties of interacting $\gamma$-$Fe_2O_3$ particles. *Philosophical Magazine B* **76**(4): 457-462.

Fischer, W. R. (1988). Microbiologial reactions of iron in soils. in *Iron in Soils and Clay Minerals*. (eds. J. W. Stucki, B. A. Goodman and U. Schwertmann). Dordrecht, Reidel Publishing**:** 715-748.

Forsythe, G. E., Malcolm, M. A. and Moler, C. B. (1976). *Computer methods for mathematical computations*. Prentice-Hall, Englewood Cliffs.

Foster, I. D. L., Lees, J. A., Owens, P. N. and Walling, D. E. (1998). Mineral magnetic characterization of sediment sources from an analysis of lake and floodplain sediments in the catchments of the old mill reservoir at Slapton Ley, South Devon, U.K. *Earth Surface Processes and Landforms* **23**: 685-703.

France, D. E. (1997). The mineral magnetic characterization of goethite and haematite in soils and sediments. *PhD Thesis, University of Liverpool.*

Frankel, R. B. and Blakemore, R. P., Eds. (1991). *Iron Biominerals*. New York, Plenum Press.

Frederickson, J. K., Zachara, J. M., Kennedy, D. W., Dong, H., Onstott, T. C., Hinman, N. W. and Li, S. (1998). Biogenic iron mineralization accompanying the dissimilatory reduction of hydrous ferric oxide by a ground water bacterium. *Geochimica et Cosmochimica Acta* **62**(19/20): 3239-3257.

Gehring, A. U. and Hofmeister, A. M. (1994). The transformation of lepidocrocite during heating: a magnetic and spectroscopic study. *Clays and Clay Minerals* **42**: 409-415.

Geonics (1992). Geonics EM38 ground conductivity meter operating manual. Geonics, Ontario.

Geosoft (1997). *MAGMAP (FFT-2D) 2-D Frequency Domain Processing of Potential Field Data*. Geosoft, Toronto.

Gibbs-Eggar, Z., Jude, B., Dominik, J., Loizeau, J.-L. and Oldfield, F. (1999). Possible evidence for dissimilatory bacterial magnetite dominating the magnetic properties of recent lake sediments. *Earth and Planetary Science Letters* **168**: 1-6.

Gillingham, D. E. W. and Stacey, F. D. (1971). Anhysteretic Remanent Magnetization (ARM) in Magnetite Grains. *Pure and Applied Geophysics* **91**: 160-165.

Godhino, M., Carvalho, A., Noguès, M., Dormann, J. L. and Seqqat, M. (1994). Field and temperature dependence of magnetic viscosity in randomly canted Li-Ti ferrite. *Journal of Magnetism and Magnetic Materials* **133**: 457-459.

Goldberg, D. (1989). *Genetic Algorithms in Search, Optimization, and Machine Learning*, Addison-Wesley, New York.

Graham, I. and Scollar, I. (1976). Limitatons on magnetic prospection in archaeology imposed by soil properties. *Archaeo-Physika* **6**: 1–125.

Grodzicki, M. and Amthauer , G. (2000). Electronic and magnetic structure of vivianite: cluster molecular orbital calculations. *Physics and Chemistry of Minerals* **27**: 694-702.

Hallam, D. F. and Maher, B. A. (1994). A record of reversed polarity carried by the iron sulphide greigite in British Early Pleistocene sediments. *Earth and Planetary Science Letters* **121**: 71–80.

Hamilton, A. C., Magowan, W. and Taylor, D. (1986). Use of the Bartington meter to determine the magnetic susceptibility of organic-rich sediments from western Uganda. *Physics of the Earth and Planetary Interiors* **42**: 5-9.

Hartstra, R. L. (1982). Grain-size dependence of initial susceptibility and saturation magnetization-related parameters of four natural magnetites in the PSD-MD range. *Geophysical Journal of the Royal Astronomical Society* **71**: 477-495.

Hayashi, M., Masahiro, S. and Nagat, K. (1997). Magnetic interaction between magnetite particles dispersed in calcium-silicate glasses. *Journal of Magnetism and Magnetic Materials* **171**: 170-178.

Hejda, P., Petrovsky, E. and Zelinka, T. (1994). The Preisach diagram, Wohlfarth's remanence formula and magnetic interactions. *IEEE Transactions on Magnetics* **MAG-30**: 896–898.

Hejda, P. and Zelinka, T. (1990). Modelling of hysteresis processes in magnetic rock samples using the Preisach diagram. *Physics of the Earth and Planetary Interiors* **63**: 32–40.

Heller, F. and Market, H. (1973). The age of Viscous Remanent Magnetization of Hadrian's Wall (Northern England). *Geophysical Journal of the Royal Astronomical Society* **31**: 395-406.

Hesse, P. and Stolz, J. F. (1999). Bacterial magnetite and the Quarternary record. in *Quarternary Climates, Environments and Magnetism*. (eds. B. A. Maher and R. Thompson). Cambridge University Press, Cambridge**:** 163-198.

Hesse, P. P. (1994). Evidence for bacterial palaeoecological origin of mineral cycles in oxic and sub-oxic Tasman Sea sediments. *Marine Geology* **117**: 1-17.

Hey, G. (1991). Yarnton and Cassington Worton Rectory Farm; 1990/1 assessments., Oxford Archaeological Unit, Oxford.

Hey, G. (1993a). Yarnton Floodplain 1992 post excavation assessment. Oxford Archaeological Unit, Oxford.

Hey, G. (1993b). Yarnton Worton Rectory Farm: post excavation assessment and research design. Oxford Archaeological Unit, Oxford.

Heywood, B. R., Bazylinski, D. A., Garratt-Reed, A., Mann, S. and Frankel, R. B. (1990). Controlled biosynthesis of greigite ($Fe_3S_4$) in magnetotactic bacteria. *Naturwissenschaften* **77**: 536-538.

Hilgenfeldt, K. (2000). Diagenetic Dissolution of Biogenic Magnetite in Surface Sediments of the Benguela Upwelling System. *International Journal of Earth Sciences* **88**: 630-640.

Hilton, J. (1990). Greigite and the magnetic properties of sediments. *Limnology and Oceanography* **35**: 509–520.

Hoffman, V. (1992). Greigite ($Fe_3S_4$): magnetic properties and first domain observations. *Physics of the Earth and Planetary Interiors* **70**: 288-301.

Houck, C., Joines, J. and Kay, M. (1995). A Genetic Algorithm for Function Optimization: A Matlab Implementation, Report No. 96-03, North Carolina State University: 14.

Hounslow, M. and Maher, B. (1999). Laboratory procedures for the quantitative extraction and analysis of magnetic minerals from sediments. in *Environmental Magnetism: a practical guide*. (eds. J. Walden, F. Oldfield and J. Smith). Quarternary Research Association, London. **6:** 139-184.

Hounslow, M. W. and Maher, B. A. (1996). Quantitative extraction and analysis of carriers of magnetization in sediments. *Geophysical Journal International* **124**: 57-74.

Hrouda, F., Jelinek, V. and Zapletal, K. (1997). Refined technique for susceptibility resolution into ferromagnetic and paramagnetic components based on susceptibility temperature-variation measurement. *Geophysical Journal International* **129**(3): 715-719.

Hunt, A., Jones, J. and Oldfield, F. (1984). Magnetic measurements and heavy metals in atmospheric particulates of anthropogenic origin. *The Science of the Total Environment* **33**: 129-139.

Hunt, C. P., Singer, M. J., Kletetschka, G., TenPas, J. and Verosub, K. L. (1995). Effect of citrate-bicarbonate-dithionite treatment on fine-grained magnetite and maghemite. *Earth and Planetary Science Letters* **130**: 87–94.

Institute of Geological Sciences (1972). *Geological Survey of Great Britain*, Sheet 236, Witney.

Ivan, M. (1996). Optimum expression for computation of the magnetic field of a homogeneous polyhedral body. *Geophysics* **44**: 279-288.

Jackson, M. and Marvin, J. (1998). New Low Temperature Measurement Capabilities. *The IRM Quarterly* **8**(4): 1, 7-8.

Jackson, M., Moskowitz, B., Rosenbaum, J. and Kissel, C. (1998). Field-dependence of AC susceptibility in titanomagnetites. *Earth and Planetary Science Letters* **157**: 129-139.

Jakubovics, J. P. (1994). *Magnetism and Magnetic Materials*. The Institute of Materials, Ashgate Publishing, London.

Jiles, D. C. and Atherton, D. L. (1986). Theory of ferromagnetic hysteresis. *Journal of Magnetism and Magnetic Materials* **61**: 48-60.

Johnson, H. P., Lowrie, W. and Kent, D. V. (1975). Stability of anhysteretic remanent magnetization in fine and coarse magnetite and maghemite particles. *Geophysical Journal of the Royal Astronomical Society* **41**: 1–10.

Jolivet, J. P. and Tronc, E. (1988). Interfacial electron transfer in colloidal spinel iron oxide. Conversion of $Fe_2O_3$ to $\gamma$-$Fe_2O_3$ in aqueous medium. *Journal of Colloid Interface Science* **125**: 688-701.

Kadar, G. and Della Torre, E. (1987). Hysteresis modeling I. Noncongruency. *IEEE Transactions on Magnetics* **23**(5): 2820-2822.

Keller, R. and Schmidbauer, E. (1999). Magnetic hysteresis properties and rotational hysteresis losses of synthetic stress-controlled titanomagnetite ($Fe_{2.4}Ti_{0.6}O_4$) particles - I. Magnetic and hysteresis properties. *Geophysical Journal International* **138**: 319-333.

King, J. W., Banerjee, S. K., Marvin, J. A. and Özdemir, Ö. (1982). A comparison of different magnetic methods for determining the relative grain size of magnetite in natural materials: some results from lake sediments. *Earth and Planetary Science Letters* **59**: 404–419.

Kirschvink, J. L. and Chang, S.-B. R. (1984). Ultrafine-grained magnetite in deep sea sediments, possible bacterial magnetofossils. *Geology* **12**: 559-562.

Kirschvink, J. L., Jones, D. S. and MacFadden, B. J. (1985). *Magnetite Biomineralization and Magnetoreception in Organisms: A New Biomagnetism.* Plenum press, New York.

Kittel, C. (1976). *Introduction to solid state physics*. John Wiley, New York.

Kletetschka, G. and Banerjee, S. K. (1995). Magnetic stratigraphy of Chinese loess as a record of natural fires. *Geophysical Research Letters* **22**: 1341–1343.

Kletetschka, G. and Wasilewski, P. J. (2002). Grain size limit for SD hematite. *Physics of the Earth and Planetary Interiors* **129**: 173-179.

Kostka, J. E., Wu, J., Nealson, K. H. and Stucki, J. W. (1999). The impact of structural Fe(III) reduction by bacteria on the surface chemistry of smectite clay minerals. *Geochimica et Cosmochimica Acta* **63**(22): 3705-3713.

Krs, M., Krsová, M., Pruner, P., Zeman, A., Novàk, F. and Jansa, J. (1990). A petromagnetic study of Miocene rocks bearing micro-organic material and the magnetic mineral greigite (Sokolov and Cheb basins, Czechoslovakia). *Physics of the Earth and Planetary Interiors* **63**: 98–112.

Krs, M., Krsová, M., Prunner, P. and Kouklikova, L. (1991). On the detailed magnetostratigraphy of greigite - (smythite) mineralization, Sokolov brown-coal basin, Bohemia. *Studia Geophysica et Geodaedica* **35**: 267-284.

Krs, M., Novak, F., Krsová, M., Prunner, P., Kouklikova, L. and Jansa, J. (1992). magnetic properties and metastability of greigite-smythite mineralization in brown-coal basins of the Krusnehory Piedmont, Bohemia. *Physics of the Earth and Planetary Interiors* **70**: 273-287.

Kruiver, P., Dekkers, M. and Heslop, D. (2001). Quantification of magnetic coercivity components by the analysis of acquisition curves of isothermal remanent magnetisation. *Earth and Planetary Science Letters* **189**: 269-276.

Ku, C. C. (1977). A direct computation of gravity and magnetic anomalies caused by 2- and 3-dimensional bodies of srbitary shape and arbitary magnetic polarization by equivalent- point method and a simplified cubic spline. *Geophysics* **42**(3): 610-622.

Laulhere, J.-P. and Briat, J.-F. (1993). Iron release and uptake by plant ferritin: effects of pH, reduction and chelation. *Biochemical Journal* **290**: 693-699.

LeBorgne, E. (1955). Susceptibilité magnétique anormale du sol superficiel. *Annales de Géophysique* **11**: 399–419.

LeBorgne, E. (1960a). Êtude expérimental du trainage magnétique dans le cas d'un ensemble de grains magnétiques très fins disperses dans une substance non magnétique. *Annales de Géophysique* **16**: 445-493.

LeBorgne, E. (1960b). Influence de feu sur les propriétés magnétique anormale du sol et du granite. *Annales de Géophysique* **16**: 159-195.

Lecoanet, H., Lévêque, F. and Segura, S. (1999). Magnetic susceptibility in environmental applications: comparison of field probes. *Physics of the Earth and Planetary Interiors* **115**: 191-204.

Lees, J. (1999). Evaluating magnetic parameters for use in source identification, classification and modelling of natural and environmental materials. in *Environmental Magnetism: A practical guide*. (eds. J. Walden, F. Oldfield and J. Smith). Quarternary Research Association, London, **6:** 113-138.

Lees, J. A. (1997). Mineral magnetic properties of mixtures of environmental and synthetic materials: linear additivity and interaction effects. *Geophysical Journal International* **131**(2): 335-46.

Levi, S. and Banerjee, S. K. (1990). On the origin of inclination shallowing in redeposited sediments. *Journal of Geophysical Research B: Solid Earth* **95**: 4383–4390.

Linford, N. (1994). Mineral magnetic profiling of archaeological sediments. *Archaeological Prospection* **1**: 37-52.

Linford, N. and David, A. (2001). Study of geophysical surveys. in *Evaluation of archaeological decision-making processes and sampling strategies*. (eds. G. Hey and M. Lacey). Kent County Council, Canterbury**:** 76-89.

Linford, N. T. (1998). Geophysical Survey at Boden Vean, Cornwall, Including an assessment of the Microgravity Technique for the Location of Suspected Archaeological Void Features. *Archaeometry* **40**: 187-216.

Linford, N. T. and Canti, M. G. (2001). Geophysical Evidence for Fires in Antiquity: Preliminary Results from an Experimental Study. *Archaeological Prospection* **8**: 211-225.

Linington, R. E. (1965). The use of simplified anomalies in magnetic surveying. *Archaeometry* **7**: 3-13.

Linington, R. E. (1972). A summary of simple theory applicable to magnetic prospecting in archaeology. *Prospezioni Archeologiche* **7**: 9-60.

Liu, H., Hihara, T., Sumiyama, K. and Suzuki, K. (1998). Magnetic Viscosity of Fine Maghemite Clusters Prepared by Electrochemical Method. *Physica Status Solidi* **169**: 153-160.

Liu, X. M., Hesse, P., Rolph, T. and Begét, J. E. (1999). Properties of magnetic mineralogy of Alaskan loess: evidence for pedogenesis. *Quarternary International* **62**: 93-102.

Loke, M. H. and Barker, R. D. (1996a). Practical techniques for 3D resistivity surveys and data inversion. *Geophysical Prospecting* **44**: 499-523.

Loke, M. H. and Barker, R. D. (1996b). Rapid least-squares inversion of apparent resistivity pseudosections by a quasi-Newton method. *Geophysical Prospecting* **44**: 131-152.

Longworth, G., Becker, L. W., Thompson, R., Oldfield, F., Dearing, J. A. and Rummery, T. A. (1979). Mössbauer and magnetic studies of secondary iron oxides in soils. *Journal of Soil Science* **30**: 93–110.

Longworth, G. and Tite, M. S. (1977). Mössbauer and magnetic susceptibility studies of iron oxides in soils from archaeological sites. *Archaeometry* **19**(1): 3-14.

Lovley, D. R. (1987). Organic matter mineralisation with the reduction of ferric iron: a review. *Geomicrobiology Journal* **5**: 375-399.

Lovley, D. R. (1991). Magnetite formation during dissimilatory iron reduction. in *Iron Biominerals*. (eds. R. B. Frankel and R. P. Blakemore). Plenum Publishing Corporation, New York**:** 151-166.

Lovley, D. R., Stolz, J. F., Nord, G. L., Jr. and Phillips, E. J. P. (1987). Anaerobic production of magnetite by a dissimilatory iron-reducing microorganism. *Nature* **330**: 252–254.

Lowenstam, H. A. (1962). Magnetite in denticle capping in recent chitons (polyplacophora). *Science* **156**: 1373-1375.

Lowenstam, H. A. (1981). Minerals formed by organisms. *Science* **211**: 1126-1131.

Lowrie, W. (1990). Identification of ferromagnetic minerals in a rock by coercivity and unblocking temperature properties. *Geophysical Research Letters* **17**: 159–162.

Lowrie, W. and Fuller, M. (1971). On the alternating field demagnetization characteristics of multidomain thermoremanent magnetization in magnetite. *Journal of Geophysical Research* **76**: 6339–6349.

Lowrie, W. and Heller, F. (1982). Magnetic properties of marine limestones. *Reviews of Geophysics and Space Physics* **20**: 171-192.

Maher, B. (1999). Comments on "Origin of the magnetic susceptibility signal in Chinese loess". *Quarternary Science Reviews* **18**: 865-869.

Maher, B., Thompson, R. and Hounslow, M. (1999). Introduction. in *Quarternary Climates, Environments and Magnetism*. (eds. B. A. Maher and R. Thompson). Cambridge University Press, Cambridge: 1-48.

Maher, B. A. (1988). Magnetic properties of some synthetic submicron magnetites. *Geophysical Journal* **94**: 83–96.

Maher, B. A. and Hounslow, M. W. (1999). The significance of magnetotactic bacteria for the palaeomagnetic and rock magnetic record of Quarternary sediments and soils. in *Palaeomagnetism and Diagenesis in Sediments*. (eds. D. H. Tarling and P. Turner). Geological Society, London. **151:** 43-46.

Maher, B. A. and Taylor, R. M. (1988). Formation of ultrafine-grained magnetite in soils. *Nature* **336**: 368–371.

Maher, B. A. and Thompson, R. (1995). Paleorainfall reconstructions from pedogenic magnetic susceptibility. *Quarternary Research* **44**: 383-391.

Mann, S., Sparks, N. H. C., Frankel, R. B., Bazylinski, D. A. and Jannasch, H. W. (1990). Biomineralization of ferrimagnetic greigite ($Fe_3S_4$) and iron pyrite ($FeS_2$) in a magnetotactic bacterium. *Nature* **343**: 258-261.

Marmet, E., Bina, M., Fedoroff, N. and Tabbagh, A. (1999). Relationships between Human Activity and the Magnetic Properties of Soils: A Case Study in the Medieval Site of Roissy-en-France. *Archaeological Prospection* **6**: 161-170.

Marshall, A. (1998). Visualising Burnt Areas: Patterns of Magnetic Susceptibility at Guiting Power 1 Round Barrow (Glos., UK). *Archaeological Prospection* **5**(3): 159-177.

Maxwell, L. R., Smart , J. S. and Brunaver, S. (1949). Dependence of the intensity of magnetization and the Curie point of certain iron oxides upon the ratio of $Fe^{2+}/Fe^{3+}$. *Physical Review* **76**: 459-460.

Mayer, R. and Heinrichs, H. (1980). Flüssebilanzen und aktuelle Änderungsraten der Schwermetall-Vorräte in Wald-Ökosystemen des Solling. *Zeitschrift für Pflanzenernahrung und Bodenkunde* **143**: 232-246.

Mayergoyz, I. D. (1986). Mathematical models of hysteresis. *Physical Review Letters* **56**(15): 1518-1521.

McClean, R. G. and Kean, W. F. (1993). Contributions of wood ash magnetism to archaeomagnetic properties of fire pits and hearths. *Earth and Planetary Science Letters* **119**: 387–394.

McClelland, E. (1996). Theory of CRM acquired by grain growth, and its implications for TRM discrimination and paleointensity determination in igneous rocks. *Geophysical Journal International* **126**(1): 271-280.

Meng, X., Derbyshire, E. and Kemp, R. A. (1997). Origin of the magnetic susceptibility signal in Chinese loess. *Quarternary Science Review* **16**: 833-839.

Meng, X., Derbyshire, E. and Kemp, R. A. (1999). Reply to Comments on "Origin of the magnetic susceptibility signal in Chinese loess". *Quarternary Science Reviews* **18**: 871-875.

Menyeh, A. and O'Reilly, W. (1991). The magnetization process in monoclinic pyrrhotite ($Fe_7S_8$) particles containing few domains. *Geophysical Journal International* **104**: 387-399.

Michel, A., Chaudron, G. and Bénard, J. (1951). Propriétés des composés ferromagnetiqués non métalliques. *Journal de Physique* **12**: 189-201.

Morin, J. (1950). Magnetic susceptibility of $\alpha Fe_20_3$ and $Fe_20_3$ with added titanium. *Physics Reports*. **78**: 819-820.

Morinaga, H., Inokuchi, H., Yamashita, H., Ono, A. and Inada, T. (1999). Magnetic Detection of Heated Soils at Palaeolithic Sites in Japan. *Geoarchaeology* **14**(5): 377-399.

Mørup, S., Dumesic, A. and Topsøe, H. (1980). Magnetic microcrystals. *Applications of Mössbauer spectroscopy*. R. L. Cohen, Academic Press, New York**:** 1-53.

Moskowitz, B., Jackson, M. and Kissel, C. (1998). Low temperature magnetic behaviour of titanomagnetites. *Earth and Planetary Science Letters* **157**: 141-149.

Moskowitz, B. M., Frankel, R. and Bazylinski, D. (1993). Rock magnetic criteria for the detection of biogenic magnetite. *Earth and Planetary Science Letters* **120**: 283–300.

Mullins, C. E. (1974). The magnetic properties of the soil and their application to archaeological prospecting. *Archaeo-Physika* **5**: 143–347.

Mullins, C. E. (1977). Magnetic susceptibility of the soil and its significance in soil science - a review. *Journal of Soil Science* **28**: 223–246.

Murad, E. (1988). Properties and behaviour of iron oxides as determined by Mössbauer spectroscopy. in *Iron in Soils and Clay Minerals*. (eds. J. W. Stucki, B. A. Goodman and U. Schwertmann). Reidel Publishing, Dordrecht**:** 309-350.

Murad, E. and Fischer, W. R. (1988). The Geobiochemical Cycle of Iron. in *Iron in Soils and Clay Minerals*. (eds. J. W. Stucki, B. A. Goodman and U. Schwertmann). Reidel Publishing, Dordrecht**:** 1-18.

Murad, E. and Johnston, J. H. (1987). Iron oxides and oxyhydroxides. in *Mössbauer spectroscopy applied to inorganic chemistry*. (ed. G. Long). Plenum Publishing Corporation, New York**:** 507-582.

Murad, E. and Schwertmann, U. (1984). The influence of crystallinity on the Mössbauer spectrum of lepidocrocite. *Mineralogical Magazine*. **48**: 507-511.

Muttoni, G. (1995). "Wasp-waisted" hysteresis loops from pyrrhotite and magnetite-bearing remagnetized Triassic limestone. *Geophysical Research Letters* **22**(23): 3167-3170.

Muxworthy, A. R. (1999). Low-temperature susceptibility and hysteresis of magnetite. *Earth and Planetary Science Letters* **169**: 51-58.

Nagata, T. (1961). *Rock Magnetism*. Maruzen, Tokyo.

Nawrocki, J., Wojcik, A. and Bogucki, A. (1996). The magnetic susceptibility record in the Polish and western Ukranian loess-palaeosol sequences conditioned by palaeoclimate. *Boreas* **25**: 161-169.

Néel, L. (1949). Théorie du traînage magnétique des ferromagnétiques en grains fins avec applications aux terres cuites. *Annales Géophysique* **5**: 99-136.

Nöel, M. and Thistlewood, L. (1989). Developements in cave sediment paleomagnetism. in *Geomagnetism and Paleomagnetism*. (eds. F. J. Lowes, D. W. Collinson, J. H. Parry, S. K. Runcorn, D. C. Tozer and A. Soward). Kluwer Academic Publishers, Dordrecht: 91-106.

Oldfield, F. (1991). Sediment magnetism: soil erosion, bushfires, or bacteria? *Geology* **19**: 1153–1156.

Oldfield, F. (1994). Toward the discrimination of fine grained ferrimagnets by magnetic measurements in lake and near-shore marine sediments. *Journal of Geophysical Research* **99**(B5): 9045-9050.

Oldfield, F. (1999). The rock magnetic identification of magnetic mineral and grain size assemblages. in *Environmental Magnetism: A practical guide*. (eds. J. Walden, F. Oldfield and J. Smith). Quarternary Research Association, London. **6:** 243.

Oldfield, F., Dickson, D. P. E. and Thompson, R. (1981). Artificial magnetic enhancement of stream bedload: a hydrological application of superparamagnetism. *Physics of the Earth and Planetary Interiors* **26**: 107–124.

Oorschot, I. H. M. and Dekkers, M. J. (1999). Dissolution behavior of fine-grained magnetite and maghemite in the citrate-bicarbonate-dithionite extraction method. *Earth and Planetary Science Letters* **167**: 283-295.

O'Reilly, W. (1984). *Rock and Mineral Magnetism*. Blackie, Glasgow.

Orlicky, O. (1990). Detection of magnetic carriers in rocks: results of susceptibility changes in powdered rock samples induced by temperature. *Physics of the Earth and Planetary Interiors* **63**: 66-70.

Ottow, J. C. G. and Glathe, H. (1971). Isolation and identification of iron-reducing bacteria from gley soils. *Soil Biology and Biochemistry* **3**: 43-55.

Özdemir, Ö. and Banerjee, S. K. (1984). High temperature stability of maghemite. *Geophysical Research Letters* **11**(3): 161-164.

Özdemir, Ö. and Dunlop, D. J. (2000). Intermediate magnetite formation during dehydration of goethite. *Earth and Planetary Science Letters* **177**: 59-67.

Özdemir, Ö. and Dunlop, D. J. (1993). Chemical remanent magnetization during γFeOOH phase transformations. *Journal of Geophysical Research* **98**: 4191-4198.

Özdemir, Ö., Dunlop, D. J. and Moskowitz, B. M. (1993). Effect of oxidation on the Verwey transition in magnetite. *Geophysical Research Letters* **20**: 1671-1674.

Parfitt, R. L., Childs, C. W. and Eden, D. N. (1988). Ferrihydrite and allophane in four Andepts from Hawaii and implications for their classification. *Geoderma* **41**: 223-241.

Parry, L. G. (1965). Magnetic properties of dispersed magnetite powders. *Philosophical Magazine* **11**: 303-312.

Parry, L. G. (1981). The influence of fine structures on the remanence of multidomain particles of magnetite and titanomagnetite. *Physics of the Earth and Planetary Interiors* **26**: 63-71.

Peters, C. (1995). Unravelling magnetic mixtures in sediments, soils and rocks. Department of Geophysics. *PhD Thesis, University of Edinburgh.*

Peters, C., Church, M. J. and Coles, G. (1999a). Mineral Magnetism and Archaeology at Galson on the Isle of Lewis, Scotland. *Poster displayed at Magnetic Moments Conference, Oxford, January 1999.*

Peters, C., Church, M. J. and Mitchell, C. (1999b). Investigation of Hearth Fuel Sources on Lewis using Mineral Magnetism. *Abstracts of the Archaeological Prospection Conference, Munich, 1999*, Arbeitshefte des Bayerischen Landesamtes Für Denkmalpflege.

Peters, C. and Thompson, R. (1998). Magnetic identification of selected natural iron oxides and sulphides. *Journal of Magnetism and Magnetic Materials* **183**: 365-374.

Peters, C. and Thompson, R. (1999). Superparamagnetic Enhancement, Superparamagnetism, and Archaeological Soils. *Geoarchaeology* **14**(5): 401-413.

Petersen, N., von Dobeneck, T. and Vali, H. (1986). Fossil bacterial magnetite in deep-sea sediments from the South Atlantic Ocean. *Nature* **320**: 611–615.

Pick, T. and Tauxe, L. (1991). Chemical remanent magnetization in synthetic magnetite. *Journal of Geophysical Research B: Solid Earth* **96**: 9925–9936.

Popa, R. and Nealson, K. H. Microbial Magnetite Formation: Interaction of biotic and abiotic factors. *EGS-AGU-EGU Joint Assembly, Nice, France, 06-11 April 2003, Geophysical Research Abstracts*.

PPG16 (1990). Planning Policy Guidance - Archaeology and Planning, Department of the Environment, London.

Press, W. H., Flannery, B. P., Teukolsky, S. A. and Vetterling, W. T. (1988). *Numerical Recipes in C; The Art of Scientific Computing*. Cambridge University Press, Cambridge.

Rahman, A. A., Duncan, A. D. and Parry, L. G. (1973). Magnetization of multidomain magnetite particles. *Rivista Italiana di Geofisica* **22**: 259-266.

Ralph, E. K., Morrison, F. and O'Brien, D. (1968). Archaeological surveying utilizing a high-sensitivity difference magnetometer. *Geoexploration* **6**: 109-122.

Ratcliffe, J. A., (1970). *Sun, Earth and Radio*, World University Library, London.

Rees, A. I. (1961). The effect of water currents on the magnetic remanence and anisotropy of susceptibility of some sediments. *Geophysical Journal of the Royal Astronomical Society* **5**: 235–251.

Richardson, L., Arkell, W. J. and Dines, H. G. (1946,). *Geology of the Country around Witney*. Her Majesty's Stationery Office, London.

Richter, C. and van der Pluijm, B. A. (1994). Separation of paramagnetic and ferrimagnetic susceptibilities using low temperature magnetic susceptibilities and comparison with high field methods. *Physics of the Earth and Planetary Interiors* **82**: 111–121.

Rivas, J., Zamarro, J. M., Martín, E. and Pereira, C. (1981). Simple approximation for magnetization curves and hysteresis loops. *IEEE Transactions on Magnetics* **MAG-17**: 1498-1502.

Roberts, A. P. (1995). Magnetic properties of sedimentary greigite ($Fe_3S_4$). *Earth and Planetary Science Letters* **134**: 227-236.

Roberts, A. P., Cui, Y.-L. and Verosub, K. L. (1995). Wasp-waisted hysteresis loops: mineral magnetic characteristics and discrimination of components in mixed magnetic systems. *Journal of Geophysical Research B: Solid Earth* **100**: 17,909-17,924.

Roberts, A. P., Pike, C. R. and Verosub, K. L. (2000a). First-order reversal curve diagrams: A new tool for characterizing the magnetic properties of natural samples. *Journal of Geophysical Research* **105**(B12): 28461-28475.

Roberts, A. P., Pike, C. R. and Verosub, K. L. (2000b). FORC diagrams: A new tool for characterizing the magnetic properties of natural samples. *Journal of Geophysical Research* **102**: 28,461-28,475.

Roberts, A. P., Reynolds, R. L., Verosub, K. L. and Adam, D. P. (1996). Environmental magnetic implications of greigite ($Fe_3S_4$) formation in a 3 m.y. lake sediment record from Butte Valley, northern California. *Geophysical Research Letters* **23**(20): 2859-2862.

Roberts, A. P. and Turner, G. M. (1993). Diagenetic formation of ferrimagnetic iron sulphide minerals in rapidly deposited marine sediments, South Island, New Zealand. *Earth and Planetary Science Letters* **115**: 257–273.

Robertson, D. J. and France, D. E. (1994). Discrimination of remanence-carrying minerals in mixtures, using isothermal remanent magnetization acquisition curves. *Physics of the Earth and Planetary Interiors* **82**: 223-234.

Roy, J. L. and Park, J. K. (1972). Red beds: DRM or CRM? *Earth and Planetary Science Letters* **17**: 211-216.

Rummery, T. A. (1983). The use of magnetic measurements in interpreting the fire histories of lake drainage basins. *Hydrobilogica* **103**: 53-58.

Rummery, T. A., Bloemendal, J., Dearing, J. A., Oldfield, F. and Thompson, R. (1979). The persistence of fire-induced magnetic oxides in soils and sediments. *Annales de Géophysique* **35**: 103–107.

Saarinen, T. (1999). Palaeomagnetic dating of Late Holocene sediments in Fennoscandia. *Quarternary Science Reviews* **18**: 889-897.

Sandford, K. S. (1924). The River Gravels of the Oxford District, Quaternary. *Journal of the Geological Society* **lxxx**: 113.

Sawolowicz, Z. (1993). Pyrite framboids and their development: a new conceptual mechanism. *Geolgische Rundschau* **82**: 148-156.

Schmidbauer, E. and Schembera, N. (1987). Magnetic hysteresis properties and anhysteretic remanent magnetization of spherical $Fe_3O_4$ particles in the grain size range 60–160 nm. *Physics of the Earth and Planetary Interiors* **46**: 77–83.

Schmidt, A. and Marshall, A. (1995). Impact of resolution on the interpretation of archaeological prospection data. *Archaeological Sciences 1995, Liverpool*, Oxbow Books, Oxford.

Schumann, R. and Jahn, L. (1995). Influence of texture on the magnetic viscosity. *Journal of Magnetism and Magnetic Materials* **149**: 318-330.

Schwarz, E. J. (1975). Magnetic properties of pyrrhotite and their use in applied geology and geophysics. *Geological Survey of Canada Professional Paper* **74-59**: 1-24.

Schwertmann, U. (1988). Occurrence and formation of iron oxides in various pedoenvironments. in *Iron in Soils and Clay Minerals*. (eds. J. W. Stucki, B. A. Goodman and U. Schwertmann). Reidel Publishing, Dordrecht: 267-302.

Schwertmann, U. and Heinmann, B. (1959). Über das Vorkommen and die Entstehung von Maghemit in nordwestdeutschen Böden. *Neues Jahrbuch fur Mineralogie-Monatshefte.* **8**: 174-181.

Schwertmann, U., Kodama, H. and Fischer, W. R. (1986). Mutual interactions between organics and iron oxides. in *Interactions of soil minerals with natural organics and microbes*. (eds. P. M. Huang and M. Schnitzer). Soil Science Society of America Special Publication, Madison, WI. **17:** 223-250.

Schwertmann, U. and Taylor, R. M. (1972). The transformation of lepidocrocite to goethite. *Clay and Clay Minerals* **20**: 151-158.

Schwertmann, U. and Taylor, R. M. (1977). Iron Oxides. in *Minerals in Soil Environments*. (ed. J. B. Dixon)**:** 45-50.

Schwertmann, U. and Taylor, R. M. (1979). Natural and synthetic purely crystallized lepidocrocite. *Clay and Clay Minerals* **14**: 285-293.

Scintrex (1996). SMARTMAG SM-4/4G Operations Manual.

Scollar, I., Tabbagh, A., Hesse, A. and Herzog, I. (1990). *Archaeological Prospecting and Remote Sensing*. Cambridge University Press, Cambridge.

Shankar, R., Thompson, R. and Galloway, R. B. (1994). Sediment source modelling: Unmixing of artificial magnetisation and natural radioactivity measurements. *Earth and Planetary Science Letters* **126**: 411-420.

Shcherbakov, V. P. and Shcherbakova, V. V. (1987). On the physics of post-depositional remanent magnetization. *Physics of the Earth and Planetary Interiors* **46**: 64–70.

Singer, M. J., Bowen, L. H., Verosub, K. L., Fine, P. and TenPas, J. (1995). Mössbauer spectroscopic evidence for citrate-bicarbonate-dithionate extraction of maghemite from soils. *Clays and Clay Minerals* **43**(1): 1-7.

Singer, M. J. and Fine, P. (1989). Pedeogenic factors affecting magnetic susceptibility of northern Californian soils. *Soil Science Society of America Journal* **53**: 1119-1127.

Skinner, B. J., Erd, R. C. and Grimaldi, F. S. (1964). Greigite, the thio-spinel of iron; a new mineral. *American Mineralogist* **49**: 543–553.

Snowball, I. and Thompson, R. (1992). A mineral magnetic study of Holocene sediment yields and deposition patterns in the Llyn Geirionydd catchment, north Wales. *The Holocene* **2**(3): 238-248.

Snowball, I. and Torii, M. (1999). Incidence and significance of magnetic iron sulphides in Quarternary sediments and soils. in *Quarternary Climates, Environments and Magnetism*. (eds. B. A. Maher and R. Thompson). Cambridge University Press, Cambridge**:** 199-230.

Snowball, I., Zillen, L. and Sandgren, P. (2002). Bacterial magnetite in Swedish varved lake-sediments: a potential bio-marker of environmental change. *Quaternary International* **188**(1): 14-19.

Snowball, I. F. (1991). Magnetic hysteresis properties of greigite ($Fe_3S_4$) and a new occurrence in Holocene sediments from Swedish Lapland. *Physics of the Earth and Planetary Interiors* **68**: 32–40.

Snowball, I. F. (1994). Bacterial magnetite and the magnetic properties of sediments in a Swedish lake. *Earth and Planetary Science Letters* **126**: 129–142.

Snowball, I. F. (1997a). The detection of single-domain greigite ($Fe_3S_4$) using rotational remanent magnetisation (RRM) and the effective gyro field (BG): mineral magnetic and palaeomagnetic applications. *Geophysical Journal International* **130**: 704-706.

Snowball, I. F. (1997b). Gyroremanent magnetization and the magnetic properties of greigite-bearing clays in southern Sweden. *Geophysical Journal International* **129**(3): 624-636.

Snowball, I. F. and Thompson, R. (1988). An occurrence of greigite in the sediments of Loch Lomond. *Journal of Quarternary Science* **4**: 121-125.

Snowball, I. F. and Thompson, R. (1990). A stable chemical remanence in Holocene sediments. *Journal of Geophysical Research B: Solid Earth* **95**: 4471–4479.

Soil Survey of England and Wales (1983). Soils of England and Wales, Sheet 6, South East England.

Solheid, P. and Jackson, M. (2001). The Rock Magnetic Bestiary. *The IRM Quarterly* **11**(3): 1, 7-10.

Sparks, S. (1991). Structural and morphological characterization of biogenic magnetite crystals. in *Handbook from the Environmental Magnetism Workshop*. (ed. C. P. Hunt). Institute for Rock Magnetism, Minneapolis: 181-185.

Spender, M. R., Coey, J. M. D. and Morrish, A. H. (1972). The magnetic properties and Mössbauer spectra of synthetic samples of $Fe_3S_4$. *Canadian Journal of Physics* **50**: 2313-2326.

Stacey, F. D. and Banerjee, S. K. (1974). *The Physical Principles of Rock Magnetism*. Elsevier, Amsterdam.

Stanjek, H. (1987). The formation of maghemite and hematite from lepidocrocite and goethite in a Cambisol from Corsica. *Zeitschrift fur Pflanzerernahung und Bodenkunde* **150**: 314-318.

Stanjek, H., Faßbinder, J. W. E., Vali, H., Wagele, H. and Graf, W. (1994). Evidence for biogenic greigite (ferrimagnetic $Fe_3S_4$) in soil. *European Journal of Soil Science* **45**: 97-103.

Stephenson, A. (1971). Single domain grain distributions I. A method for the determination of single domain grain distributions. *Physics of the Earth and Planetary Interiors* **4**: 353–360.

Stephenson, A. (1975). The observed moment of a magnetized inclusion of high Curie point within a titanomagnetite particle of lower Curie point. *Geophysical Journal of the Royal Astronomical Society* **40**: 29-36.

Stober, J. C. and Thompson, R. (1979). Magnetic remanence acquisition in Finnish Lake sediments. *Geophysical Journal of the Royal Astronomical Society* **57**: 727-739.

Stockhausen, H. (1998). Some new aspects for the modelling of isothermal remanent magnetization aquisition curves by cumulative log Gaussian functions. *Geophysical Research Letters* **25**(12): 2217-2220.

Stolz, J. F., Lovley, D. R. and Haggerty, S. E. (1990). Biogenic magnetite and the magnetization of sediments. *Journal of Geophysical Research B: Solid Earth* **95**: 4355–4361.

Stoner, E. C. and Wohlfarth, E. P. (1948). A mechanism of magnetic hysteresis in heterogeneous alloys. *Philosophical Transactions of the Royal Society of London, Series A* **240**: 599–602.

Stott, A. P. (1986). Sediment tracing in a reservoir-catchment system using a magnetic mixing model. *Physics of the Earth and Planetary Interiors* **42**: 105-112.

Tabbagh, A., Desvignes, G. and Dabas, M. (1997). Processing of Z gradiometer magnetic data using linear transforms and analytical signal. *Archaeological Prospection* **4**: 1-13.

Tamaura, Y., Ita, K. and Katsua, T. (1983). Transformation of γ-FeOOH to $Fe_3S_4$ by adsorption of iron(II) ion on FeO(OH). *Journal of the Chemical Society Dalton Transactions*: 189-194.

Tarling, D. H. (1983). *Palaeomagnetism: Principles and Applications in Geology, Geophysics and Archaeology*. Chapman and Hall, London.

Tauxe, L., Pick, T. and Constable, C. (1996). Wasp-waists, pot-bellies, and superparamagnetism. *Journal of Geophysical Research B: Solid Earth* **101**: 571-583.

Taylor, C. (1975). *Fields in the English Landscape*. Aldine Press, London.

Taylor, R. M. (1984). Influence of chloride on the formation of iron oxides from Fe(II) chloride. I Effect of (Cl)/(Fe) on the formation of magnetite. *Clays and Clay Minerals* **32**: 167-174.

Taylor, R. M. and McKenzie, M. (1980). The influence of aluminium on iron oxides VI. The formation of Fe(II)-Al(III) hydroxy-chlorides, -sulfates, and -carbonates as new members of the pyraurites group and their significance in soils. *Clays and Clay Minerals* **28**: 179-187.

Tejada, J., Balcells, L. and Zhang, X. X. (1993). Dependence of magnetic viscosity on temperature and external magnetic fields in very thin films (5Å) deposited onto crystalline Cu(111). *Journal of Magnetism and Magnetic Materials* **118**: 65-69.

Telford, W. M., Geldart, L. P., Sheriff, R. E. and Keys, D. A. (1976). *Applied Geophysics*. Cambridge University Press, Cambridge.

Thompson, R. (1986). Modelling magnetization data using SIMPLEX. *Physics of the Earth and Planetary Interiors* **42**: 113–127.

Thompson, R. and Oldfield, F. (1986). *Environmental Magnetism*. Allen and Unwin, London.

Tite, M. S. and Linington, R. E. (1975). Effect of climate on the magnetic susceptibility of soils. *Nature* **256**: 565–566.

Tite, M. S. and Mullins, C. E. (1971). Enhancement of the magnetic susceptibility of soils on archaeological sites. *Archaeometry* **13(2)**: 209–219.

Topping, J. (1972). *Errors of observation and their treatment*. Chapman and Hall, London.

Towe, K. M. and Moench, T. T. (1981). Electron-optical characterization of bacterial magnetite. *Earth Planetary Science Letters* **52**: 213-220.

Vali, H., Forster, O., Amarantidis, G. and Petersen, N. (1987). Magnetotactic bacteria and their magnetofossils in sediments. *Earth and Planetary Science Letters* **86**: 389–400.

Van der Marel, H. W. (1951). γ-ferric oxide in sediments. *Journal of Sedimentary Petrology* **21**: 12-21.

Vandenberghe, R. E., De Grave, E., de Bakker, P. M. A., Krs, M. and Hus, J. J. (1991). Mössbauer effect study of natural greigite. *Hyperfine Interactions* **68**: 319-322.

Verosub, K. L. (1977). Depositional and post-depositional processes in the magnetization of sediments. *Reviews of Geophysics and Space Physics,* **15**: 129-143.

Verosub, K. L. and Roberts, A. P. (1995). Environmental magnetism: past, present, and future. *Journal of Geophysical Research B: Solid Earth* **100**: 2175–2192.

Verwey, E. J. W. and Haayman, P. W. (1941). Electronic conductivity and transition point in magnetite. *Physics* **8**: 979-982.

Walden, J. (1999). Sample collection and preparation. in *Environmental Magnetism: A practical guide*. (eds. J. Walden, F. Oldfield and J. Smith). Quarternary Research Association, London. **6:** 26-34.

Walden, J., Oldfield, F. and Smith, J. P., (eds.) (1999). *Environmental Magnetism: a practical guide*. Technical Guide. Quarternary Research Association, London.

de Wall, H. and Worm, H.-U. (1999). A cautionary note on interpreting frequency-dependence of susceptibility solely in terms of superparamagnetism or two ways to be wrong. *The IRM Quarterly* **10**(4): p1+6.

Weiss, P. and Forrer, R. (1929). Absolute Saturation of Ferromagnetic Substances and the Law of Approach as a Function of the Field and of the Temperature. *Annalen der Physik* **12**(10): 279-374.

Westcott-Lewis, M. F. and Parry, L. G. (1971). Magnetism in rhombohedral iron-titanium oxides. *Australian Journal of Physics* **24**: 719-734.

Williams, R. J. P. (1990). Biomineralization: iron and the origin of life. *Nature* **343**: 213-214.

Williams, W. and Dunlop, D. J. (1995). Simulation of magnetic hysteresis in pseudo-single-domain grains of magnetite. *Journal of Geophysical Research B: Solid Earth* **100**: 3859–3871.

Winklhofer, M., Fabian, K. and Heider, F. (1997). Magnetic blocking temperatures of magnetite calculated with a three-dimensional micromagnetic model. *Journal of Geophysical Research* **102**(B10): 22,695-22,709.

Wohlfarth, E. P. (1958). Relations between different modes of acquisition of the remanent magnetization of ferromagnetic particles. *Journal of Applied Physics* **29**: 595–596.

Wong, K. K. W., Douglas, T., Gider, S., Awschalom, D. D. and Mann, S. (1998). Biomimetic Synthesis and Characterization of Magnetic Proteins (Magnetoferritin). *Chemistry of Materials* **10**: 279-285.

Worm, H.-U. (1998). On the superparamagnetic-stable single domain transition for magnetite, and frequency dependence of susceptibility. *Geophysical Journal International* **133**: 201-206.

Worm, H.-U. and Markert, H. (1987). Magnetic hysteresis properties of fine particle titanomagnetites precipitated in a silicate matrix. *Physics of the Earth and Planetary Interiors* **46**: 84–93.

Yu, L. and Oldfield, F. (1989). A multivariate mixing model for identifying sediment source from magnetic measurements. *Quaternary Research* **32**: 168–181.

# MISSING PAGES REMOVED ON INSTRUCTION FROM THE UNIVERSITY